UNIVERSITAT DE BARCELONA

Post-Hercynian tectonic and paleogeographic evolution of SW Iberia and the Gulf of Cadiz

Adrià Ramos Ordoño

Institut de Recerca Geomodels
Departament de Dinàmica de la Terra i de l'Oceà
Universitat de Barcelona

Post-Hercynian tectonic and paleogeographic evolution of SW Iberia and the Gulf of Cadiz

Memòria presentada per Adrià Ramos Ordoño per optar al grau de Doctor en Geologia. Aquesta memòria s'ha realitzat dins del Programa de Doctorat de Ciències de la Terra i sota la direcció del Dr. Josep Anton Muñoz i del Dr. Oscar Fernández

Adrià Ramos Ordoño
Barcelona, Maig de 2017

Dr. Josep Anton Muñoz

Dr. Oscar Fernández

The cover photograph shows the Praia do Telheiro, located in Cabo São Vicente, SW corner of Portugal. It is represented by the angular unconformity between the folded Carboniferous basement and the Triassic, the youngest Mesozoic unit of the Algarve Basin

This PhD thesis has been carried out in the “Departament de Dinàmica de la Terra i de l’Oceà”, specifically in the “Institut de Recerca Geomodels”, which is funded by the “Generalitat de Catalunya” and other private entities. This thesis has been funded by Repsol Exploración and partially supported by the SALTECRES project (CGL2014-54118-C2-1-R). We also wish to thank Midland Valley, Schlumberger and Oasis Montaj for providing academic licenses of the respective softwares used during the course of this thesis, and Repsol, Partex Oil and Gas, and TGS for providing and allowing publication of seismic data.

A mind is like parachute, it doesn't work unless it's open

Frank Zappa

Als meus pares, Joaquim i Estrella
A Cris

Agraïments

Quan vaig començar la tesi tenia la sensació que encarava un repte brutal, i més després del primer dia d'arribar a Repsol (Madrid). Aquell mateix dia acudeixo a una reunió on geòlegs d'exploració discuteixen sobre l'Algarve, tot posant-se les mans al cap mentre un geòleg intenta explicar l'evolució del marge del SW d'Ibèria. "This is too much complex! Who is going to unravel this stuff?" – va comentar un – "He will..." – va dir el que seria el meu supervisor a Repsol mirant-me a mi, qui tenia cara d'haver acabat de baixar de l'AVE. L'aventura començava, i l'aprenentatge prenia empenta per els quatre anys més meravellosos i intensos de la meva vida.

Durant aquest viatge, primer de tot voldria agrair als tres directors de tesi, Oscar Fernández, Josep Anton Muñoz i Pedro Terrinha, ja que han format part de la tesi de manera activa durant aquests anys, a distància o reunits, discutint, interpretant la sísmica, anant al camp, en fi, fent tesi. A tots tres els hi dec tot el que he après.

Aquesta tesi no seria la mateixa sense les sessions interminables de discussió sobre geologia i altres matèries amb l'Oscar. Sento que aquesta tesi és tant teva com meva. Encara avui em fascina que tinguis temps a discutir extensament sobre els infinits reptes que han aparegut durant la tesi! T'agraeixo el suport en els moments crítics, i haver-me donat empentetes per a que m'espavili, però sempre amb el pal i la pastanaga. A encoratjar-me a ser productiu i a acompanyar-me al camp tot gaudint la geologia i alguna cataplana i/o arròs de tamboril, tot s'ha de dir. A enviar-me a Strasbourg, a tenir la oportunitat de treballar a Repsol, i a fer aquesta tesi. He après com un animal treballant al teu costat.

A l'Anton per la teva supervisió i sessions de discussió. Amb tu un se n'adona que 5 minuts teus interpretant són 3 mesos mínim per a mi, si és que arribo a la mateixa conclusió. Gràcies a tu, aquesta tesi també ha estat possible i ha pres forma amb el seu coneixement brutal sobre sistemes extensius, contractius, tectònica salina... mmmh, de tot??

Y Pedro, el mayor experto sobre el Algarve! Aunque la distancia nos haya separado durante estos años, siempre has estado ahí supervisando, dando soporte al campo y como no, aportando la puntilla en momentos clave que han aportado ideas tremendas.

En mi etapa de Repsol (poco más de dos años), aprendí mucho más allá que pura geología, y eso se lo debo a toda la gente con la que he tenido el placer de trabajar. A Álvaro por recibirme con los brazos abiertos e integrarme como uno más en el grupo de exploración de Portugal, y brindarme la oportunidad de aprender cómo funciona este "mundillo" de la empresa que me era desconocido hasta el momento, pudiendo acudir como parte activa a data rooms y sesiones con consultores externos e internos. Siempre nos ha acompañado el eterno debate: ¿la sal de Esperança es alóctona o autóctona? Espero que con esta tesis se te resuelva la duda ;) . A Carlos Rosales por las discusiones sobre la interpretación (a veces imposible) del cubo 3D. A Begoña por las eternas discusiones sobre todo lo que nos rodea. También agradecer al resto del grupo, Abdul, Ylva y Ángel por facilitarme el camino en más de una ocasión.

Carlos Giraldo "chamo" me tendiste más de una mano sobre el Golfo de Cádiz, y también te debo alguna que otra sesión con el Geoframe. Agradecer también al antiguo grupo de regionales, Núria, Consuelo, Wilber y Juan.

Al grupo de Métodos Geofísicos no Sísmicos: Lorenzo, Adriana, Antonio y Almudena, por haberme permitido trabajar con vosotros y tener los primeros contactos sobre modelización gravimétrica.

Al grupo de soporte de geología por ayudarme en tantas ocasiones y saber ahora un poco más sobre ArcGIS: Julio, Lídia, Manuel, Marcela, Cristina y Ana. Si no fuera por vosotros, aún estaría haciendo polígonos y polilíneas en el sistema geográfico de Saturno.

A todo el resto de personas que no han colaborado de manera directa en la tesis pero que no sería la misma sin su compañía durante el tiempo en Repsol: Elisenda, Sílvia, Sandra, Áxel, Luz, David. A Zulema, simplemente la mejor organizándolo todo. A Tomás, por preocuparse del "okupa". I cannot close the Repsol phase without naming Gail Soberman, without you I could have not discover the nooks of Geoframe.

My stay in Strasbourg was possible thanks to the implication of Gianreto Manatschal. Thank you Gianreto for such good discussion sessions about hyper-extension and lot more things, and for your enthusiasm. It was also a privilege to share "tarte flambée" with you Nico, we still pending a home-made beer in a braserie discussing on how to finish our theses without die trying. I also wish to thank Michael and Pauline for their welcoming in the office of the department. També a tu Irene, per compartir alguna que altra bierre per Strasbourg.

La tornada a Barcelona va ser més agraïda gràcies als companys de departament: Pablo, Núria, Mireia, Frede, Ester, Oriol, Lluís, Oscar, Oskar, Pau, Marco, Uri, Maria, Dani, Joana, David, Rubén. I com no Marina, gràcies per tot i per ajudar-me a maquetejar la tesi en temps rècord!! També vull donar les gràcies a les persones que s'han encarregat de la part administrativa i logística: Ana Romera i Teresa, la vostra col·laboració no apareix directament al volum de la tesi, però sense ella no la podria haver dut a terme, imprescindibles!!

Gràcies també a Montserrat Torné per la inestimable col·laboració amb l'elaboració dels models gravimètrics. La naturalitat i intensitat amb la que comparteixes els teus coneixements i habilitats m'ha ajudat molt. A Maria Carolina por darme alguna que otra mano con los perfiles gravimétricos.

A la meva família que tants bons moments hem passat i passem junts. Vull agrair especialment als meus pares, Joaquim i Estrella que, gràcies al seu suport, energia, amor i a l'educació que m'han donat, he pogut arribar fins aquí, essent conscient que la vida no té límits. A mi avi, que tanto me enseñaste y que hoy estarías más contento y orgulloso que yo. A la meva iaia, perquè t'ho mereixes.

A Oto, porque has aparecido en el camino y sin tus lametones y cariños durante la realización de artículos y volumen, esta tesis no sería la misma.

A mi reproductor de música, por acompañar con banda sonora tantas horas interminables de interpretación símica y escritura.

A Cris. Me topé contigo al principio de esta aventura, acompañándome y dándome soporte en todo momento. A ti te debo muchas otras cosas que van más allá de las "rocas". Gracias por apoyarme, por hacerme feliz y hacerme sentir que podría hacer cualquier cosa a tu lado. Esta tesis también lleva tu nombre. Te quiero.

Contents

ABSTRACT

ABSTRACT

This thesis addresses the tectonic and paleogeographic evolution of the SW Iberia Margin from the Mesozoic rifting stage to the post-rifting collision of Late Cretaceous through Miocene times and transpressive stages of Pliocene and Quaternary. The study is based on onshore field work, and analysis of well logs, a large set of 2D and 3D seismic reflection profiles and gravity data of the offshore.

The main contribution of this thesis is to provide an integrated model for the Mesozoic evolution of the Algarve Basin taking into account the main factors that affected the its configuration, such as the stratigraphic record, crustal structure, salt tectonics, rifting and compressional deformation.

At present, the SW Iberian margin is located along the convergent Nubia-Iberia plate boundary. In Mesozoic times, this passive margin was located to the northeast of the triple junction of the Ligurian Tethys, Central Atlantic and Northern Atlantic. Seismic interpretation and gravity modelling shows the possible presence of Ligurian Tethys oceanic crust under the Gulf of Cadiz and the existence of anomalous density bodies at lower crustal levels interpreted either as pieces of exhumed sub-continental mantle or underplated material. Tapering of Iberian crust is characterized by rapid changes in the thickness of the upper and lower crust. Gravity modelling also allows the characterization of the Cenozoic contractional overprint experienced by this Mesozoic oblique margin.

The presence of evaporites and the tectonic pulses that triggered their mobilization through diapirism in the Algarve Basin also controlled the paleogeographic configuration of the margin. From north to south, in the onshore, the evaporite unit, Hettangian in age and source for the salt tectonics, is observed to thicken basinward, in fault-controlled depocenters. Salt-related structures are only present in areas of thick initial evaporites. In the offshore, multiple salt-structures cored by the Lower Jurassic evaporites are documented by seismic reflection data and exploratory drilling. Offshore salt structures include the allochthonous Esperança salt nappe, which extends over an area roughly 40x60 km. The amount of salt-related structures and their typology is observed to be controlled by the distribution of evaporite facies, which is in turn controlled by the structure of rift-related faulting. The study of salt tectonics of the Algarve Basin contributed on better constraining the paleogeography during the Hettangian and the units that were affected by diapirism. The comprehensive image of salt tectonics over the SW Iberian passive margin presented in this thesis covers all aspects from initial evaporite facies and thickness to the evolution of salt-related structures through Mesozoic extension and Cenozoic basin inversion.

The SW of Iberia has undergone compression during the Late Cretaceous-Cenozoic, up to present-day, due to the convergence between Africa and Eurasia. Multiple contractional features and their seismic activity have been documented immediately west of the Gulf of Cadiz, in the Atlantic domain. East of the Gulf of Cadiz, the Betic-Rif orogen and its active contractional and extensional structures are well known. Significant seismic activity reflecting a dominantly compressive stress state has been observed between these two domains. The seismic activity spans the entire Gulf of Cadiz, but the features associated with this seismicity have remained elusive.

During Late Cretaceous-Cenozoic compression, basement discontinuities such as Variscan foliation and thrusts were reactivated forming south-verging monoclines. The monoclines, along with deep seawater currents, controlled the deposition of the Upper Cretaceous and Cenozoic sediments. Compression also lead to the reactivation of other basement structures (e.g., Guadalquivir Bank), which are responsible for the present-day seismicity and bathymetry in the area. The compressional phase also reactivated the salt tectonics.

In conclusion, the SW Iberian margin was firstly affected by an extensional phase during the Mesozoic that resulted into a highly-extended margin the formation of oceanic crust at its deepest part. The different extensional tectonic phases that took place in the margin controlled the thickness and depositional environments of the Mesozoic sediments. Initial rifting also contributed to the evaporite basin configuration, which, together with the basement structure, triggered diapirism in the SW Iberian margin.

CHAPTER 1. INTRODUCTION

CHAPTER 1. INTRODUCTION

The Gulf of Cadiz is the oceanographic domain surrounded to the north by the SW Iberian coast, to the south by the NW African coast, to the east by the Gibraltar Arc and to the west it extends to deep waters, represented by large seamounts and deep abyssal plains. The SW Iberian margin is the southwesternmost geological province of Portugal and Spain, which comprises the onshore and offshore Algarve Basin and its basin margin. The basin is represented by Mesozoic and Cenozoic sediments lying over the Hercynian Iberian Massif. The Mesozoic stratigraphic record started due to the breakup of Pangea, followed by Jurassic-Early Cretaceous extension and Late Cretaceous-Cenozoic compression.

The SW Iberian Margin has been the objective of study of several authors during the past decades. Besides of scientific publications, several PhD theses have been resulted from the research conducted in the area. Rocha (1976) is probably the first complete study of the palaeontology, stratigraphy and sedimentology of the Jurassic in the Algarve Basin, being a reference nowadays. The exploration of hydrocarbons in the Algarve Basin since the 1974 was initiated with the acquisition of seismic profiles. This allowed to work the offshore portion of the basin (Mougenot 1989). Onshore Algarve Basin was mapped by Manuppella (1992) and later enhanced by Terrinha (1998), integrating also seismic data from offshore. As a result, Terrinha (1998) is the most complete work about the Algarve Basin from a structural geology and tectonics points of view. Later, several studies were carried out in the offshore basin to improve the knowledge about the structure of the basin (Lopes, 2002; Roque, 2007). The hydrocarbon potential of the offshore Algarve Basin was studied by Matias (2007), who published a complete scientific paper about the salt tectonics in the basin years later (Matias et al., 2011).

Many other authors have contributed to the geological knowledge the Gulf of Cadiz, as the structure in the area and the tectonic evolution (Medialdea, 2005), the Cenozoic structure (Duarte, 2011; Iribarren et al., 2007), active structures and the nature of the basement (Martínez-Loriente, 2013; Martínez-Loriente et al., 2016, 2014). However, the 3D comprehension of the deposition and the evolution of the margin, together with its mapping, have remained elusive. The main objective of the thesis was to establish the structural evolution of the margin during the Mesozoic and Cenozoic and predict its related depositional environments.

Part of the interest on the SW Iberian Margin is that during the Mesozoic it was located at the junction of the Tethys and Central and North Atlantic realms. In addition, it represents the present-day boundary between Nubia and Iberia tectonic plates. Moreover, the margin lies west of the Gibraltar Arc, which is the westernmost termination of the Alpine orogen.

The Mesozoic paleogeographic configuration of the SW Iberian margin remained elusive from previous works, given the lack of agreement in the scientific community about how this margin has been configured.

In order to achieve the main objective of the thesis, the Tethys or Atlantic affinity of the margin becomes crucial. The complexity of the margin brings other conditioning factors that were not fully studied and

had to be solved. These are the crustal structure, the salt tectonics and the inversion tectonics.

Overall, the thesis focuses on the regional comprehension of the SW Iberian margin and its Mesozoic and Cenozoic evolution. The achievement of these goals was possible due to the access to a private large data set from an oil and gas company (Repsol) and a seismic acquisition company (TGS). Several studies of different topics have been integrated in this thesis in order to obtain a complete understanding of the geological processes that have configured the margin since Mesozoic times.

1.1. GEOLOGICAL SETTING

The Algarve Basin lies along the SW Iberian margin, a tectonically complex area located north of the eastern termination of the Fault Zone of Azores-Gibraltar (AGFZ). At present, the AGFZ is a diffuse transpressional plate boundary between the Nubian and Iberian plates (Sartori et al., 1994; Fig. 1.1.1a). The margin lies over the Iberian Paleozoic massif (Fig. 1.1.1), which crops out to the north (Fig. 1.1.1b). To the south and west the margin opens to the Atlantic Ocean, and to the east, the margin is overthrusted by the Betic-Rif orogen.

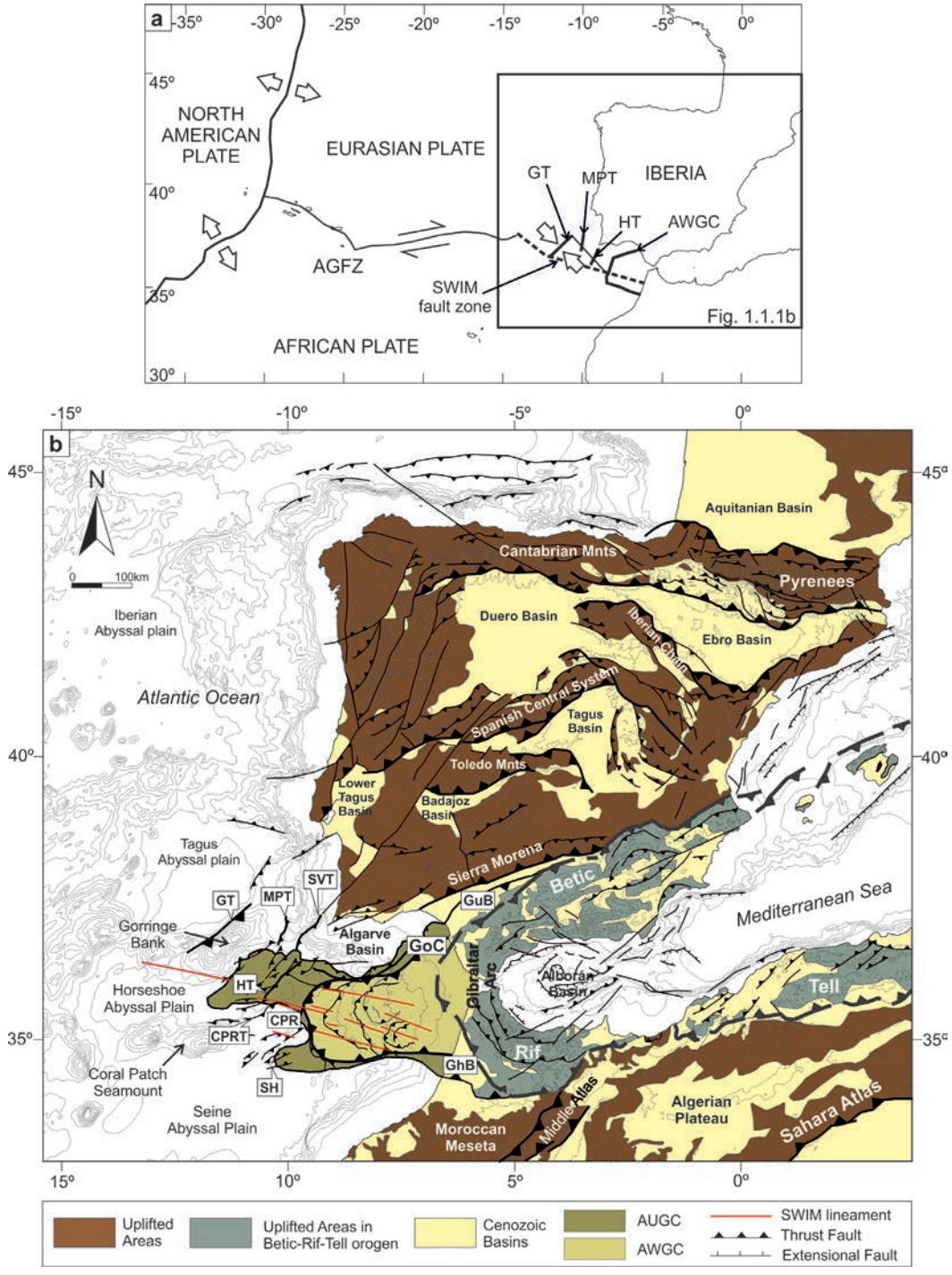

Figure 1.1.1. (a) Main elements of plate boundaries and relative plate kinematics. (b) Map showing location of Cenozoic contractional structures in Iberia and surrounding areas related to the Nuabian-Iberian plate boundary. AGFZ: Azores-Gibraltar fracture zone; AUGC: Allochthonous Unit of the Gulf of Cadiz; AWGC: Allochthonous Wedge of the Gulf of Cadiz; CPR: Coral Patch Ridge; CPRT: Coral Patch Ridge Thrust; GuB: Guadalquivir Basin; GhB: Gharb Basin; GoC: Gulf of Cadiz; GT: Gorringe Thrust; HT: Horseshoe Thrust; MPT: Marquês de Pombal Thrust; SH: Seine Hills; SVT: São Vicente Thrust. Adapted using data from: Gomez et al., (2000), Michard et al. (2008), De Vicente and Vegas (2009), Gutscher et al. (2009), Medialdea et al. (2009), Zitellini et al. (2009), De Vicente and Muñoz-Martín (2013), Duarte et al., (2013) and Martínez-Loriente et al. (2013).

1.1.1. Tectonic evolution

Over the last two decades several models have been proposed for the regional geodynamic evolution of the Gulf of Cadiz (e.g., Gràcia et al., 2003; Gutscher et al., 2002; Maldonado et al., 1999; Terrinha et al., 2009; Tortella et al., 1997) that generally agree to define two main phases of evolution. The first phase is dominated by extensional tectonics during the Mesozoic, and the second phase is dominated by contractional tectonics related to the collision between Iberia and Africa from the Late Cretaceous to present-day.

1.1.1.1. Mesozoic extension

Part of the extensional structure of the Algarve Basin is related to Pangea breakup (Dewey et al., 1989; Srivastava et al., 1990a, 1990b; Ziegler, 1988). From the beginning of the Algarve Basin formation, the basin was affected by stretching and fracturing due to differential displacement between the African and American plates, and the Eurasian and American plates. This phase resulted in Triassic rifting and the development of the margins of southern Iberia and northern Africa (Heyman, 1989). The boundary between the Eurasian and African plates in the region of Iberia began to take shape at Triassic times as a transtensive sinistral limit, due to the movement of roughly E-W orientation between Eurasia and America and NW-SE between Africa and America (present-day coordinates; Fig. 1.1.2; Dewey et al., 1989; Schettino and Turco, 2011; Srivastava et al., 1990a, 1990b). The inherited Hercynian fault system of the South Portuguese Margin accommodated these two rifting components (Terrinha et al., 2002).

The differential movement between Eurasia and America led the aperture of Atlantic Ocean (Bird et al., 2007; Labails et al., 2010; Manatschal, 2004; Schettino and Turco, 2011; Srivastava et al., 1990a, 1990b; Srivastava and Verhoef, 1992; Vissers et al., 2013; Fig. 1.1.2). The main extensional fault orientations, accommodating the stretching component, were N-S and NW-SE in the westernmost parts of the basin. Meanwhile, the transtensive stretching due to the differential movement between Eurasia and Africa, resulted in the formation of faults with E-W to ENE – WSW orientation. These faults are distributed from the High Atlas to the Pyrenees, being the Algarve Basin the testimony of the stretched continental margin of Eurasia, associated with propagation of the Tethys Ocean to the west (Fourcade et al., 1991). The fault systems were active during extension in the SW Iberian margin. The variation of facies and thickness increasing from W to E (Terrinha, 1998; Terrinha et al., 2013) is respond to the presence of the current N-S fault path, which played a greater role in the Basin subdivision. These fault system,during the

Jurassic, prior to rotation of Iberia, had a roughly NE-SW to ENE-WSW orientation.

The extensional phase that underwent the margin was a prolonged multi-stage extensional period that started in the Triassic and continued up to the Early Cretaceous. The first extensional phase starts in the Triassic and ends in the Sinemurian, and is followed by a short period of marine transgression and tectonic quiescence. This was followed by a subsidence phase which ended at the transition to the Middle Jurassic (Terrinha et al., 2002). Middle Jurassic reactivation of older extensional basins triggered an initial phase of salt tectonics (driven by Hettangian evaporites in the deepest parts of the basin). Salt tectonics resulted into the development of diapirs and salt walls onshore (Afonso, 1983; Davison et al., 2016; Manuppella, 1992; Terrinha, 1998; Terrinha et al., 1990). In the offshore, salt structures were documented given the availability of MCS data (Fernández-Puga et al., 2007; Lopes et al., 2006; Maestro et al., 2003; Matias, 2007; Terrinha, 1998).

Extension during Middle Jurassic is dominated by E-W to ENE-WSW trending extensional faults and NW-SE to NNW-SSE trending relay or transfer zones. Extensional and salt tectonics continued through the Middle and Late Jurassic. This phase culminated in the formation of oceanic crust to the south (Sallarès et al., 2011; Fig. 1.1.3). Thickness of the Middle to Upper Jurassic sediments is highly variable on account of both salt tectonism and extensional faulting related to the main phase of rifting between Iberia and Africa.

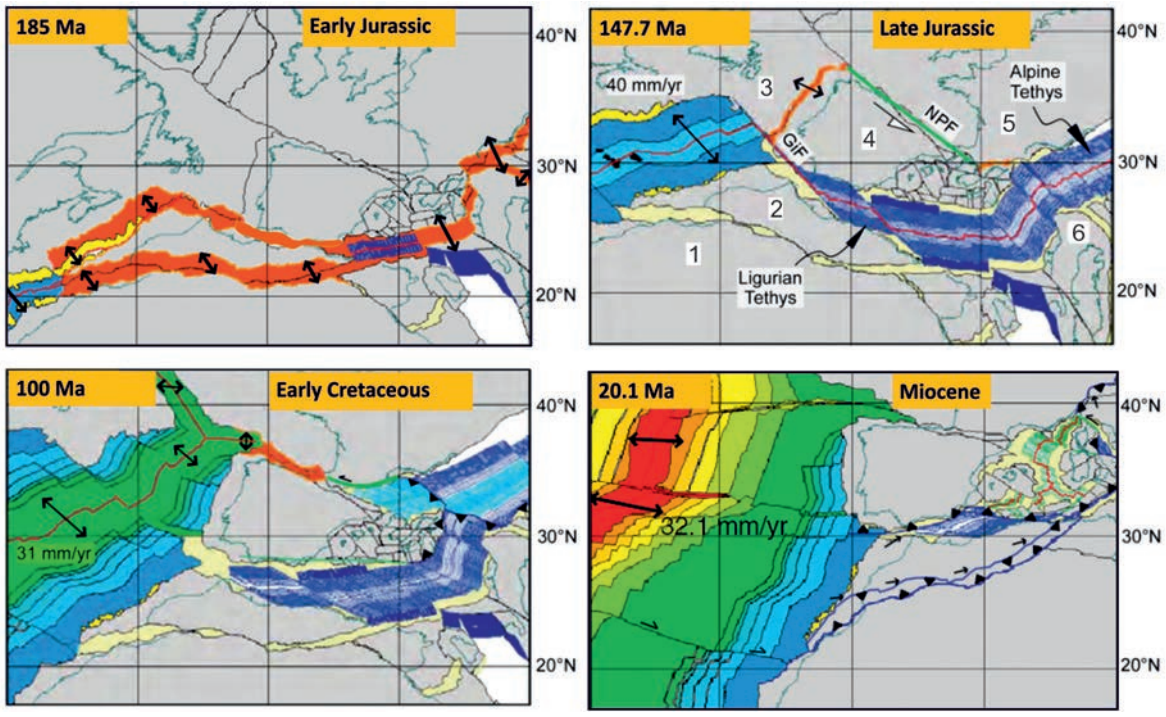

Figure 1.1.2. Early Jurassic to Miocene plate reconstruction of the triple junction formed by the Tethys, Central and Northern Atlantic oceans. 1: North Africa; 2: Morocco; 3: North America; 4: Iberia; 5: Eurasia; 6: Adria. Modified from Schettino and Turco (2011).

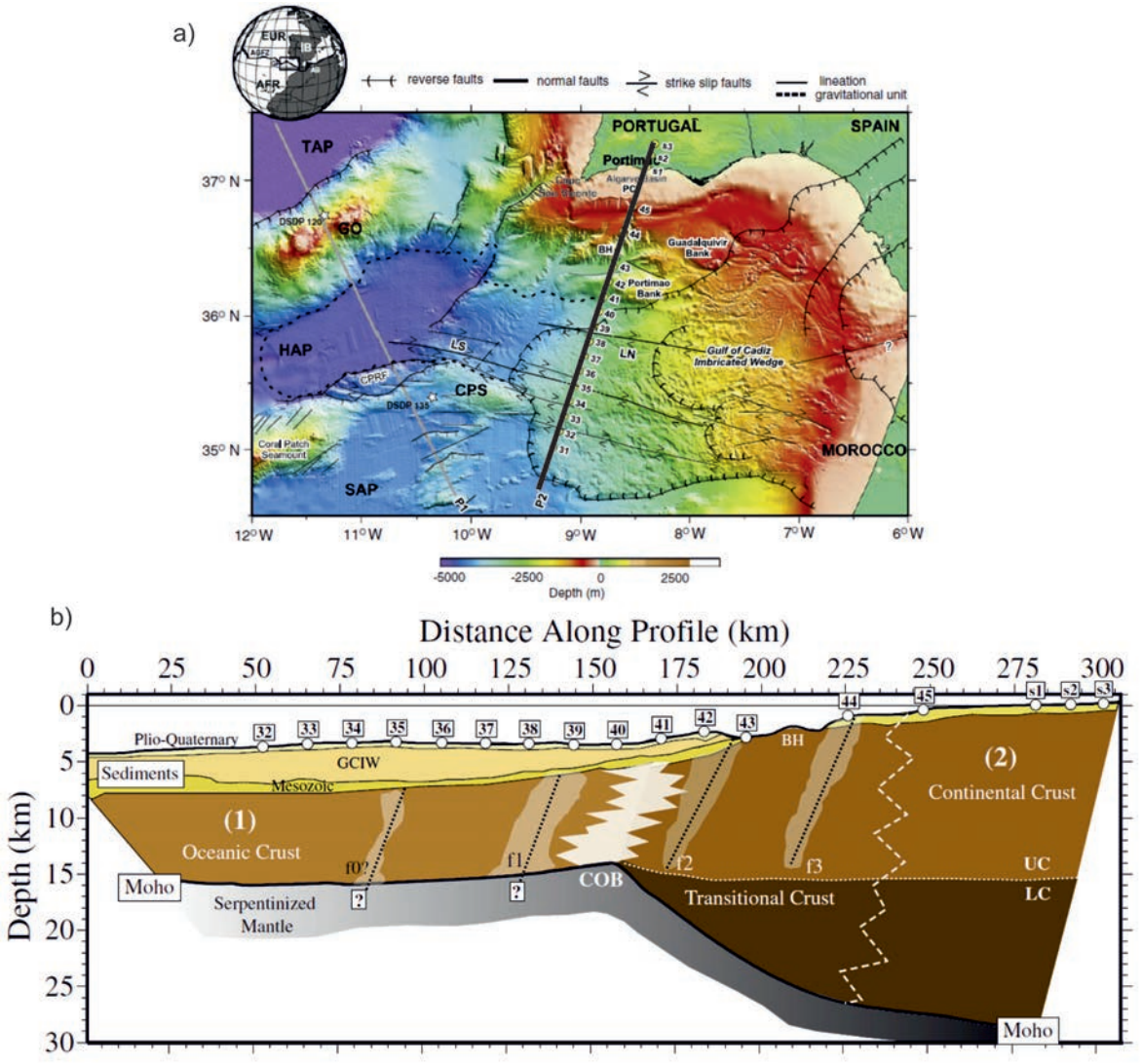

Figure 1.1.3. (a)Location map of the (b) interpretative crustal cross-section of the SW Iberian margin. Taken from Sallarès et al. (2011).

Five main extensional episodes can be identified during this period of time, separated by regional unconformities or hiatuses (Manuppella et al., 1988; Terrinha et al., 2002). These episodes are associated with five sedimentary mega-cycles bounded by episodes of inversion or non-deposition (Terrinha et al., 2002). The most representative unconformities took place between Middle and Late Jurassic, documented onshore (Terrinha et al., 2002). The unconformities correspond to the Toarcian-Aalenian, the Callovian-Oxfordian, and the Tithonian-Berriasian transition. These episodes of tectonic inversion resulted in the partial reactivation of syn-sedimentary extensional faults, and the development of small amplitude folds and unconformities. The Lower Cretaceous succession, representing a thermal subsidence phase, is capped onshore by a sedimentary hiatus, related to a marine regression, during the Valanginian-Hautevirian or Valanginian-Berriasian (Correia, 1989).

Lower Cretaceous sediments mostly drape over the entire basin and they only locally exhibit

variations in thickness related to ongoing salt tectonism or extensional faulting. This prolonged Jurassic to Early Cretaceous extension was related with the opening of the Tethys and North-Atlantic oceans (Schettino and Turco, 2011; Fig. 1.1.2). The rapid eastward drifting of the African plate while Iberia was fixed during the opening of the Central Atlantic, controlled the spreading of the south Portuguese margin, and thus the locus of a new wide plate boundary between both plates. This extensional event was responsible for the development of the SW passive margin and the Algarve Basin.

Middle Jurassic to Early Cretaceous extension was responsible for the main phase of salt tectonism documented in the area (Lopes et al., 2006; Matias, 2007; Matias et al., 2011; Terrinha et al., 2009). Extrusive salt diapirs in the onshore occur; the Espiche, Loulé, Albufeira, and Faro diapirs (Terrinha, 1998; Terrinha et al., 1990), associated with the main E-W striking extensional faults. The diapirs and salt structures of the onshore Algarve basin have all been reactivated during tectonic inversion (Davison et al., 2016).

1.1.1.2. Late Cretaceous-Cenozoic compression

At Santonian times (84 Ma), Iberia was coupled to the African plate (e.g., Dewey et al., 1989) and the plate boundary with Eurasia jumped to the Bay of Biscay (Srivastava et al., 1990a, 1990b) while Africa was moving northward. This new geodynamic setting resulted in inversion of the northern Iberian margin, where the convergence was accommodated, causing the northward subduction of the Iberian lithosphere underneath the European plate (Muñoz, 1992) and forming the Pyrenees (Fig. 1.1.1b). The inversion of the SW Iberian margin also initiated during the Late Cretaceous (Terrinha, 1998).

Since the Oligocene, the ongoing compressional deformation was transferred to the interior of the Iberian plate, while compression in the Pyrenees ceased. The plate boundary jumped again to the SW Iberian margin, along the AGFZ (Fig. 1.1.1a), with a N-S convergence between Africa and Eurasia. The pronounced topography of Iberia was the result of several episodes of compression during the Alpine Orogeny, and extension, as a back-arc extension in the western Mediterranean domain through most of the Miocene times (Vergés and Fernàndez, 2012). The building of the intraplate Iberian Chain and the deformation of the Iberian Massif can be recognized through basement highs, and its associated depressions (Fig. 1.1.1b). The Late Cretaceous-Cenozoic compression led to the formation of new contractional structures, the reactivation and deformation of other previous Mesozoic features, such as extensional faults and salt tectonics (Terrinha, 1998).

To the west of the Gibraltar Arc formation, this was accompanied by the emplacement of a giant chaotic unit emplaced synchronously with the development of the Betic-Rif orogen (Medialdea et al., 2004) during the Late Tortonian (Flinch and Vail, 1998; Maldonado et al., 1999; Perconig, 1962; Torelli et al., 1997; Tortella et al., 1997). This chaotic unit is divided into two sub-units (Iribarren et al., 2007; Torelli et al., 1997): one of tectonic origin (Accretionary Wedge of the Gulf of Cadiz; AWGC; Figs. 1.1.1b and 1.1.4) and a second one related to gravitational collapse of the first one (Allochthonous Unit of the Gulf of Cadiz; AUGC; Fig. 1.1.1b.

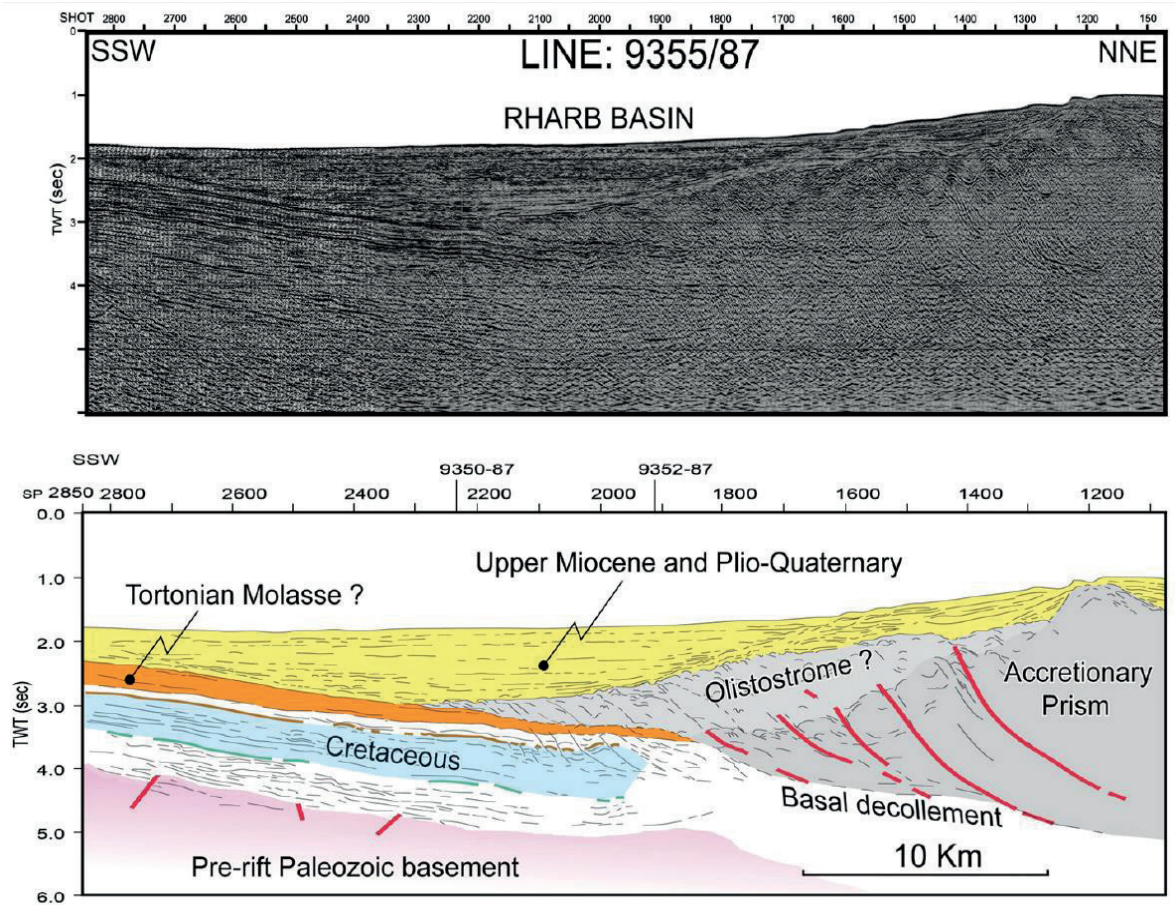

Figure 1.1.4. Multi-channel seismic (MCS) line showing the AWGC (accretionary prism) and the AUGC (olistostrome) at the Rharb Valley, in the Moroccan offshore. Taken from Zitellini et al. (2009).

The east-dipping thrusts within the AWGC root into a décollement and occasionally reach up the seafloor, exhibiting a geometry compatible with ongoing eastward B-type subduction beneath the Gibraltar Arc (Duarte et al., 2013; Gutscher et al., 2002). According to Gutscher et al. (2002) and (2009), this movement is a consequence of the active roll back of the east dipping oceanic slab that still exists between Iberia and Africa and beneath the Gibraltar Arc (Fig. 1.1.5). The existence of Tethyan oceanic lithosphere in the Gulf of Cadiz beneath the accretionary wedge was recently confirmed using seismic refraction data (Martínez-Loriente et al., 2014; Sallarès et al., 2011).

The AWGC/AUGC partially overlies a regional unconformity that defines the base of the Betic foredeep deposits, the Basal Foredeep Unconformity (BFU; Ledesma, 2000; Maldonado et al., 1999). The BFU is roughly equivalent to the base Miocene unconformity in the area of the Algarve Basin and is a key marker as it records Miocene and younger deformation.

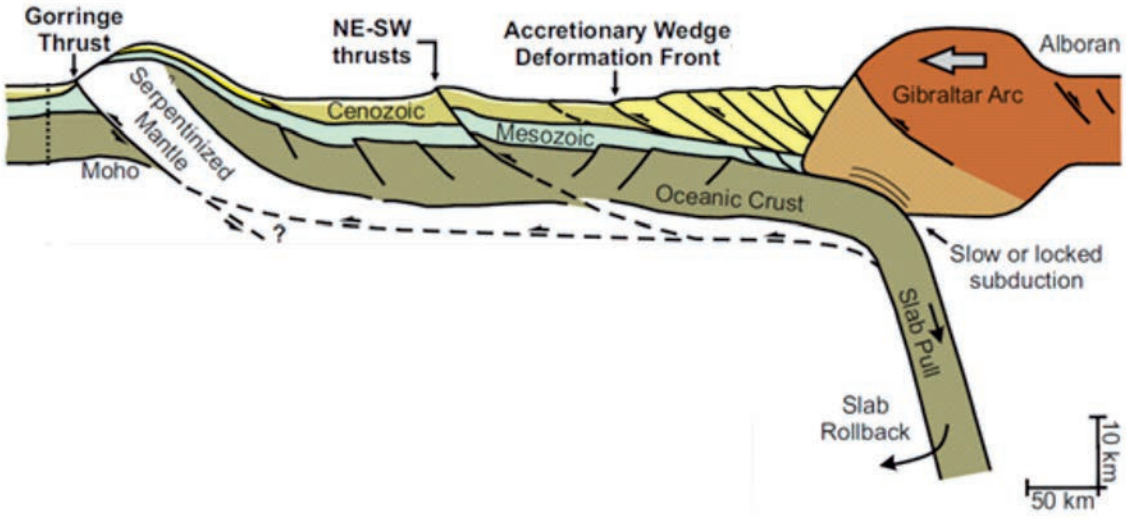

Figure 1.1.5. Schematic crustal section across Gibraltar-Arc-SW Iberian margin region. Taken from Duarte et al. (2013).

1.1.1.3. Present-day configuration

The Atlantic-Mediterranean transition region consists of two main large-scale tectonic domains: the Betic-Rif arcuate orogeny and the Atlas Mountains (Middle, High and Anti Atlas; Fig. 1.1.1b). The Betic-Rif orogenic system along the southern Iberian margin has associated Neogene basins (Alborán back-arc basin, Guadalquivir and Gharb foreland basins, and intermountain basins; Fig. 1.1.1b). The tectonic units that form the Betics are roughly continuous to the Rif belt across the Gibraltar Strait, producing an arcuate shape that has been referred to as the Gibraltar Arc system (e.g., Maldonado et al., 1999). This arcuate shape is the result of the southwestward drifting of the Alborán terrane that led to its collision with the SE Iberia and NW Africa in the Middle Miocene. The foreland basins, called Guadalquivir and Gharb basins, were formed by the flexure of the lithosphere in response to the load of the Betic and Rif thrust belts (Crespo-Blanc, 2007; Flinch, 1994; Garcia-Castellanos et al., 2002). The infill of the distal parts of both the Guadalquivir and Gharb basins started in middle Miocene.

Despite the recent collapse of the Betic range in the Alboran Sea, geodetic data show that the Gibraltar Arc region is moving westward at a rate of 3.5 mm/yr relatively to Iberia (e.g., Asensio et al., 2014; Stich et al., 2006; Fig. 1.1.6). The Iberian-African boundary is interpreted to still undergoing collision, as demonstrated by the dominance of reverse fault earthquake mechanisms (e.g., Ribeiro et al., 1996; Zitellini et al., 2009), the evidence of recent inversion of Mesozoic basins and high-angle faulting in the deeper portions of the Gulf of Cadiz, south and southwest of the Algarve Basin (Terrinha et al., 2009; Fig. 1.1.1b). Stress strain maps also show compression in the area (Olaiz et al., 2009; Zitellini et al., 2009; Fig. 1.1.6). Zitellini et al. (2009) describe a set of almost linear and subparallel, WNW–ESE trending vertical dextral strike-slip faults, according to Rosas et al. (2009), the SWIM Faults (Fig. 1.1.1b). These faults affect the seafloor, which form a narrow band of deformation over a length of 600 km connecting the Gloria Fault (the central part of the AGFZ) to the Rif–Tell Fault Zone. The SWIM Fault Zone forms the

southern boundary of the main tectonically and seismically active area of the Gulf of Cadiz (Fig. 1.1.6). To the south of the fault zone, earthquake activity is minor and tectonic shortening negligible. Zitellini et al. (2009) interpreted the SWIM Fault Zone as a precursor to the formation of a new transcurrent plate boundary controlling the present-day plate interaction between Nubia and Iberia (Fig. 1.1.6).

Further west, it has also been proposed that the southwest Iberia may also be the locus of the initiation of closure of the Atlantic Ocean along NE-SW trending structures, namely the Gorringe Bank (Fig. 1.1.5), the Marquês de Pombal Thrust (Fig. 1.1.5) or the Horseshoe Thrust (Fig. 1.1.1; Duarte, 2011; Duarte et al., 2013; Martínez-Loriente et al., 2016; Ribeiro et al., 1996). These contractional structures are deeply rooted into the basement, which some of them root into mantle (e.g., Martínez-Loriente et al., 2014), showing prominent escarpments in the bathymetry (e.g., Cunha et al., 2012; Terrinha et al., 2009; Fig. 1.1.1).

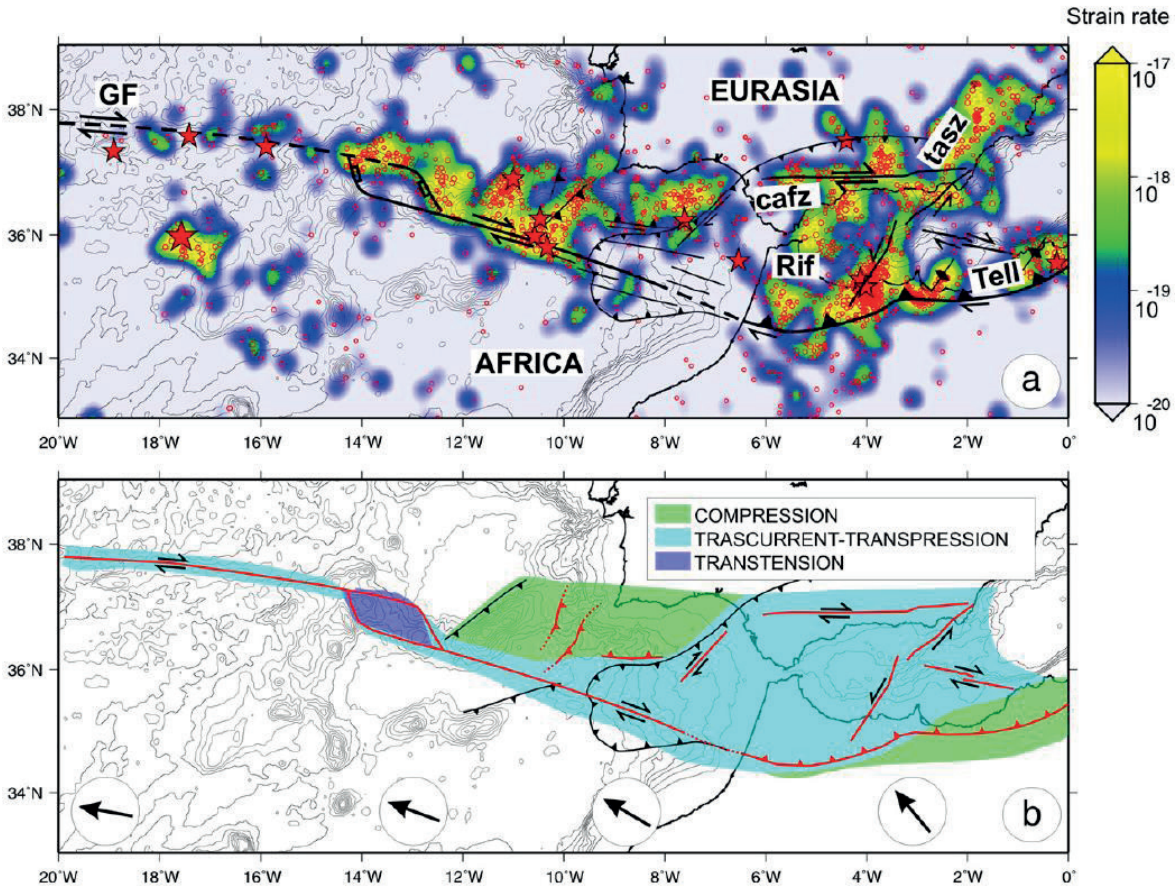

Figure 1.1.6. (a) Proposed NW Nubia - SW Iberiaplate boundary coincident with the SWIM Fault Zone. Open circles and stars represent seismic epicentres of different magnitude. (b) Simplified tectonic sketch of the area. Arrows represent the relative motion of Africa respect to Eurasia. Taken from Zitellini et al. (2009).

1.1.1.4. Oblique structures

Up to the Early Cretaceous, the structural style was dominated by E-W to ENE-WSW trending extensional faults (Maldonado et al., 1999; Moulin et al., 2005; Terrinha, 1998). The extensional fault system is segmented by N-S to NW-SE trending faults (Aljezur, Portimão and São Marcos-Quarteira faults; Fig. 2.1.1.B). These faults are parallel to the Late Hercynian thrusts documented in the Carboniferous basement in the South Portuguese Zone and the Iberian Pyrite Belt (Arthaud and Matte, 1977; Manuppella, 1992; Terrinha, 1998). The N-S to NW-SE trending faults acted mainly as transfer faults compartmentalizing the Algarve Basin during Mesozoic extension, controlling changes in the deposition of the Mesozoic units, which thicken eastwards across these faults (Terrinha, 1998). Manuppella (1988) and Manuppella et al. (1988) used these faults to define three sub-basins: the Western, the Budens-Lagoa/Algoz (Central) and the Eastern sub-basins. During Upper Cretaceous-Cenozoic inversion, many of these faults were reactivated as strike-slip features (e.g., Barreto et al., 2015).

The Portimão Fault separates the Algarve Basin into two sub-basins, the Western and the Central-Eastern sub-basins, each of which has extensional faults with different trends. The two sub-basins are also characterized by having different depositional environments and thickness of sediments throughout the Jurassic and the Lower Cretaceous units (Correia, 1989; Manuppella, 1988; Terrinha, 1998). Present-day activity is also observed on the Aljezur Fault, a N-S trending left-lateral strike-slip fault in the Western sub-basin that also controls the position of a submarine canyon across the continental shelf and slope. The Aljezur Fault controls the formation of Miocene grabens (Terrinha et al., 2009). However, there is no evidence that this fault was active during Mesozoic extension. The São Marcos Quarteira Fault (SMQF) was active since Triassic through Quaternary times, i.e., during extensional and compressional tectonics, affecting the deposition of sediments in both blocks (Terrinha, 1998).

1.1.2. Stratigraphy

The stratigraphy of the Algarve Basin presented here (Fig. 1.1.7) is defined onshore and offshore by Manuppella et al. (1988), Terrinha (1998) and Matias (2007). Mesozoic sedimentation starts with red continental alluvial clastics (conglomerates, sandstones and shales) in the Late Triassic (Rhaetian). Triassic rocks unconformably rest on low grade metamorphosed Carboniferous flysch sediments and Permian rocks that were involved in Hercynian deformation. The overlying Hettangian pelite-evaporitic unit is made up of alluvial to shallow lacustrine red shales (Fig. 1.1.7), a thin layer of shallow water dolomites and an evaporitic sequence constituted by halite, anhydrite and gypsum. At the Hettangian-Sinemurian transition, these units are capped by a volcano-sedimentary complex, consisting of basaltic lavas and pyroclastic rocks intercalated with clays and dolomites (Fig. 1.1.7). This volcanic event is associated with the Central Atlantic Magmatic Province (CAMP; documented onshore by Martins et al., 2008 and Verati et al., 2007) and the ending of the first extensional episode in the Algarve Basin (Terrinha et al., 2002). This unit has not been identified in any well in the entire SW Iberian margin.

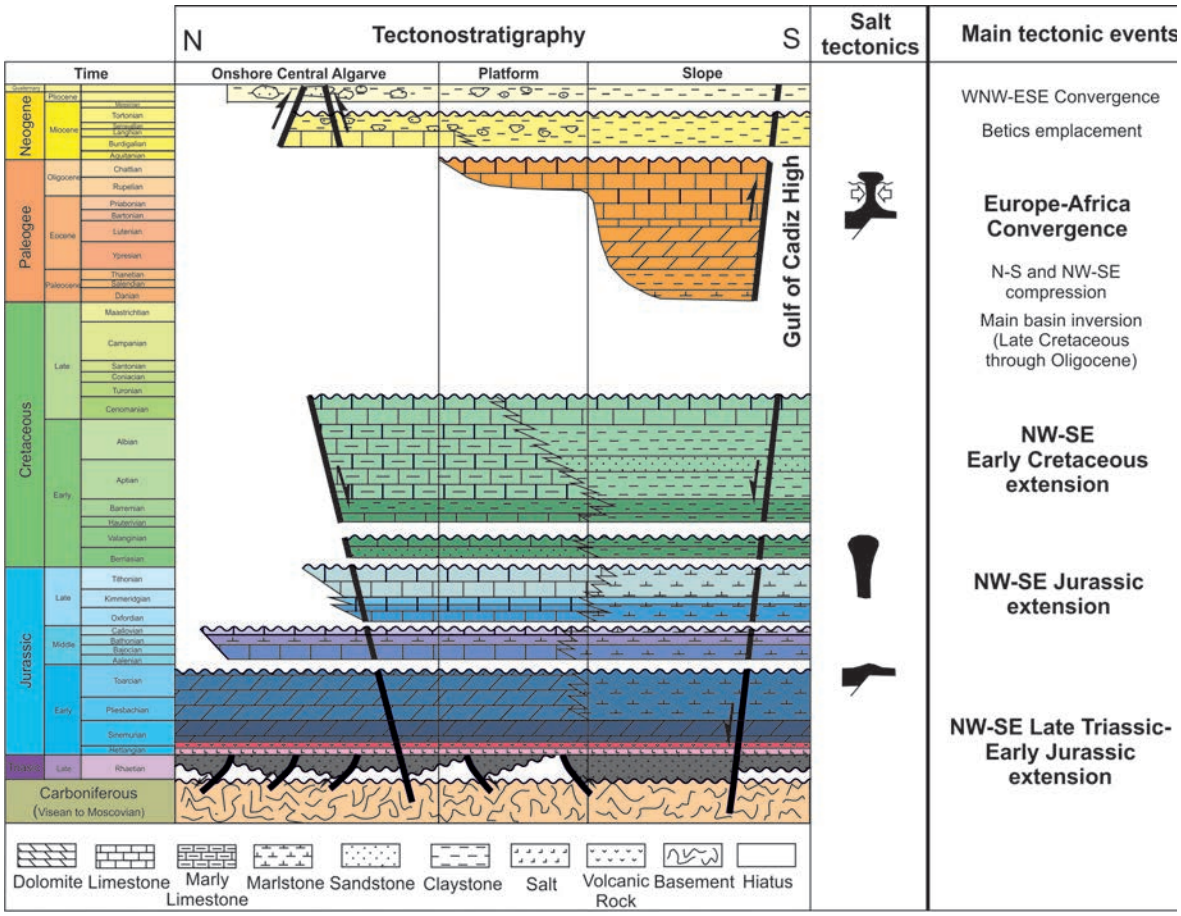

Figure 1.1.7. Simplified stratigraphy of the Algarve Basin with main stratigraphic units and main tectonic events. Bold type represents the major tectonic events (adapted from Fernandes et al., 2013; Matias et al., 2011; Terrinha, 1998).

The Lower Jurassic succession is well exposed in the onshore Western sub-basin in the Algarve. It is made up of dolomitic limestones and dolomites (shallow marine water conditions) in the Sinemurian, limestones and marls in the Pliensbachian, and pelagic marls in the Lower Toarcian (Terrinha, 1998; Fig. 1.1.7). Offshore, Lower Jurassic sediments are only penetrated by two wells in the eastern Algarve Basin, the wells GCB-1 and GC6Y-1BIS (Fig. 1.1.8). At the beginning of the Early Jurassic a generalized transgression occurred that resulted into the deposition of neritic and pelagic sediments with a thickness varying from 150 to 600 m.

In the Western Sub-Basin, the Middle Jurassic is represented by a deepening carbonate cycle, while in the Central-Eastern Sub-Basin is also represented by carbonates (marly limestones and marls; Fig. 1.1.7), only cropping out in the cores of regional anticlines north of Faro (Borges et al., 2012; Marques and Rocha, 1988a, 1988b). The Middle Jurassic succession is truncated by the Callovian-Oxfordian erosional unconformity, known as the "Callovian regression" (Manuppella et al., 1988; Mouterde, 1971; Rocha, 1976), well documented in all the Iberian Mesozoic basins and also affected the neighbouring Lusitanian and Betic basins (Alves et al., 2009; García-Hernández et al., 1989; Montenat et al., 1988; Pereira and Alves, 2012; Vera, 1988; Wilson, 1988), other Iberian basins (Hiscott et al., 1990; Stapel et al.,

1996), and the Atlas and External Rif basins of northwest Africa (Aïfa and Zaagane, 2014; Flinch, 1994; Zizi, 1996). The thickness of the Middle Jurassic sediments is variable, ranging from ~300 m onshore to ~1300 m offshore (Corvina-1 well; carbonate facies; Fig. 1.1.8). Roque (2007) suggested a change of the depositional environment from neritic in the western part of the basin to bathyal eastwards.

The Jurassic extension ends up with an Upper Jurassic carbonate platform. Onshore, the Upper Jurassic show different facies due to sub-basin differentiation and is affected by basin-wide events: Oxfordian-Kimmeridgian transgression, Kimmeridgian-Valanginian regression and intra-Tithonian transgression event (Terrinha, 1998). Thickness varies from 200 m in the west to more than 1600 in the east (Terrinha, 1998), while offshore ranges from ~125m (Imperador-1 well) to 550 m (Algarve-1 well; Fig. 1.1.8). The carbonate platform facies that characterizes the Upper Jurassic succession changes to a more bathyal conditions towards the east.

The Lower Cretaceous unit was deposited during the thermal subsidence of the margin, also dominated by salt tectonics, after a brief hiatus (the base of this formation is absent; Fig. 1.1.7). Lower Cretaceous is represented by a mixed carbonate and siliciclastic succession (Rey, 2009, 2006, 1983), with thickness ranging from 500 m to ~1500 m. This unit is characterized by a series of transgressive and regressive cycles (Correia, 1989). According to Roque (2007), the Lower Cretaceous succession changes from neritic in the west to marginal marine/inner neritic in the central area and neritic to east.

The Upper Cretaceous succession is almost absent onshore due to uplift during the main phase inversion of the Algarve Basin. Some authors postulate that this unit is restricted to thin remnants of Cenomanian reefal limestones in the Algarve Basin (Manuppella, 1988), however its existence is still under dispute. Upper Cretaceous rocks are only represented in the onshore Algarve Basin locally by volcanic products such as dikes and sills (Martins and Munhá, 1993; Martins, 1999) associated with the emplacement of the Monchique alkaline laccolith complex (Miranda et al. 2009). The emplacement age is well constrained to 72 ± 2 Ma by several whole rock K-Ar and Rb-Sr data (e.g., Bernard-Griffiths et al., 1997; Macintyre and Berger, 1982). In the eastern extent of the Algarve Basin, the offshore wells drilled up to 360 m (Atlantida-2) of a clastic dominated Upper Cretaceous (Fig. 1.1.8). Roque (2007) suggest neritic depositional environment for this unit.

Figure 1.1.8. Stratigraphic correlation of the Mesozoic and Paleocene successions along the northern portion of the margin. The correlation panel is flattened to the BFU. Note that the Neogene to Quaternary thickness is not drawn to scale. Both Mesozoic and Cenozoic strata thicken towards the Algarve-1 well, located in the central part of the shelf of the Algarve Basin. Depositional environment for all Mesozoic and Paleogene units is neritic, excepting for well Algarve-1 where the Middle and Upper Jurassic were deposited in a bathyal environment. The deposition of Mesozoic sediments is affected by the Portimão and the São Marcos Quarteira (SMQF) faults, Jurassic-Lower Cretaceous diapiric activity (Ruivo-1 well) and Paleogene thrusts (GC6Y-1BIS well). Well stratigraphic composites of the Algarve Basin were taken from Lanaja (1987) and Terrinha (1998). Stratigraphic chart from Terrinha (1998) and depositional environments were interpreted by Roque (2007) and well reports. Map location in the bottom left of the figure.

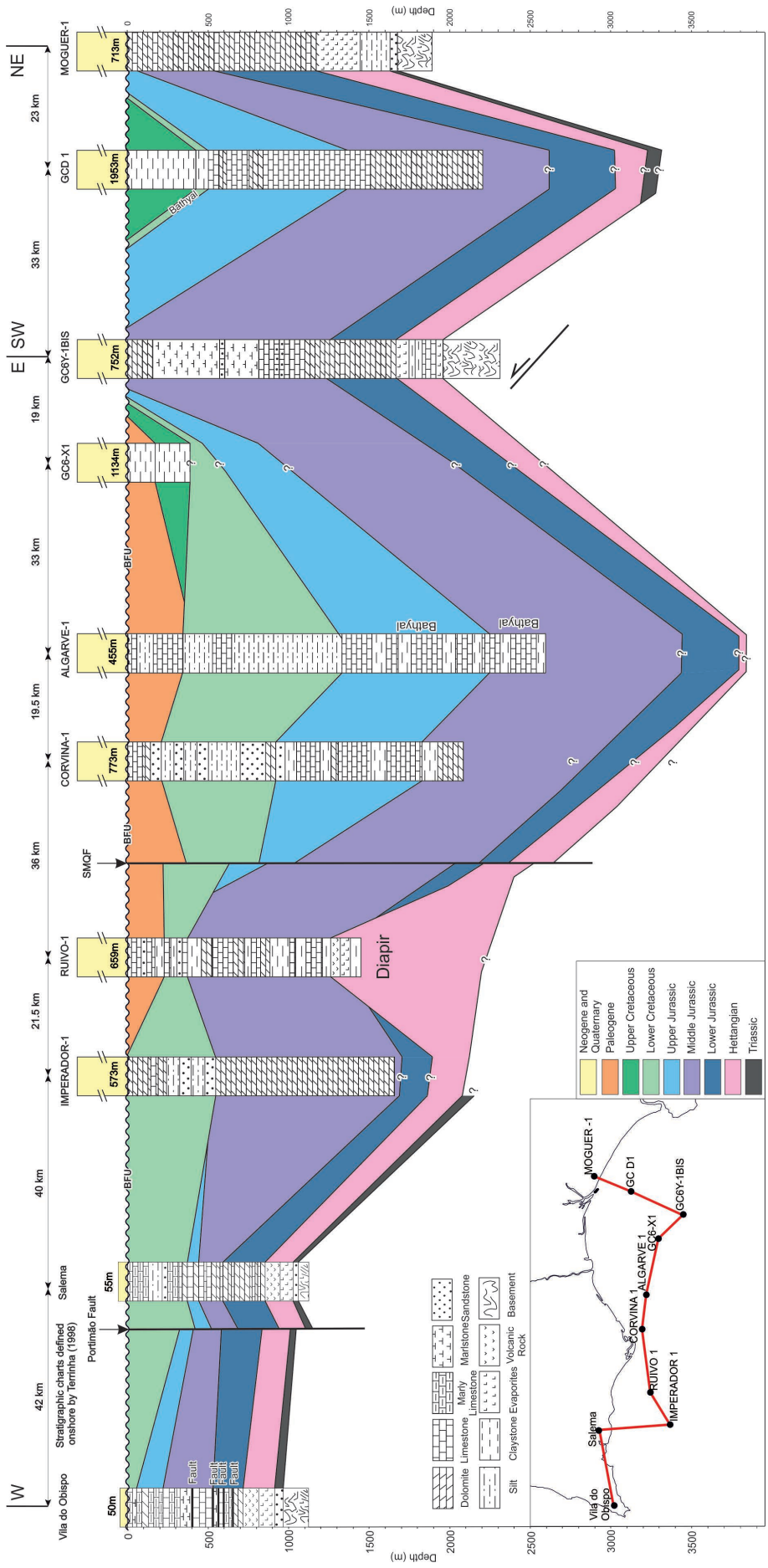
W
E
SW
NE
Vila do Obispo
Stratigraphic charts defined onshore by Terrinha (1998)
Salema
Portimão Fault
IMPERADOR-1
RUIVO-1
SMQF
CORVINA-1
ALGARVE-1
GC6-X1
GC6Y-1BIS
GCD 1
MOGUER-1
42 km
40 km
21.5 km
36 km
19.5 km
33 km
19 km
33 km
23 km
50m
55m
573m
659m
773m
455m
1134m
752m
1953m
713m
BFU
Batnyal
Diapir
Fault
Depth (m)
Neogene and Quaternary
Paleogene
Upper Cretaceous
Lower Cretaceous
Upper Jurassic
Middle Jurassic
Lower Jurassic
Hettangian
Triassic
Dolomite
Limestone
Marly Limestone
Marlstone
Sandstone
Silt
Claystone
Evaporites
Volcanic Rock
Basement
MOGUER -1
GC D1
GC6Y-1BIS
GC6-X1
ALGARVE 1
CORVINA 1
RUIVO 1
IMPERADOR 1
Salema
Vila do Obispo

The first Cenozoic sediments, represented by the Paleogene, have not been found in the onshore portion of the Algarve Basin. Clastic and carbonate sediments of Paleogene age have only been described in offshore wells, reaching thickness values of ~1400 m (Gulf of Cadiz D-1; Fig. 1.1.8). The depositional environment is described as neritic through the margin, according to well data from Roque (2007).

The Mesozoic and Paleogene rocks of the Algarve Basin are bounded by a regional erosional unconformity, the BFU (Fig. 1.1.8), overlain by Neogene strata. Locally, the entire Mesozoic sequence is eroded, setting the Miocene succession directly on top of the Paleozoic basement. The Miocene succession is represented by limestones, turbidites and other clastic material that grade upwards into siltstones and fine sandstones (Pais et al., 2010). These units were karstified and covered by Pliocene to Pleistocene fluvial/marine detrital sediments onshore. Pliocene to Present sedimentation is dominated by the Mediterranean Outflow Water (MOW), whose activity started with the opening of the Strait of Gibraltar (Hernández-Molina et al., 2014). The current resulted in the deposition of fine-grained contourite drifts; strongly controlling the present-day seafloor geometry. In general, the Neogene-Quaternary succession is represented by a clastic dominated unit, with intercalations of carbonates, and represented by varied thickness, ranging from hundreds of meters up to ~2400 m (Gulf of Cadiz B-1). The youngest sediments Algarve Basin are lithified Holocene beach sand and dunes, influenced by frequent climatic oscillations and sea-level fluctuations (Moura et al., 2007).

1.2. WORK PROCESS

Some aspects of the margin have been elusive up to now and needed to be reviewed, revaluated and newly documented. This allowed to obtain the crustal structure in both onshore and offshore portions of the margin and reconstruct the initial Mesozoic geometry of the margin, and decipher the extensional and compressional structural evolution as well as the role of the salt tectonics in the final configuration of the margin.

Onshore gives the best opportunity to get a close look to the structures that controlled the evolution of, at least, the northern margin of the Algarve Basin. An accurate field work can help to better understand the main trend, geometries and timing of faults, the inversion of these features during the Cenozoic, the role of the evaporites in controlling the tectonic styles, and their relationship with regional events (opening of Tethys and Atlantic oceans). To accomplish these objectives, several field campaigns were carried out, taking measurements through all the onshore Algarve Basin, leading to construct a geological map and four regional cross-sections. The comprehension of the tectonic structures and phases that occurred in onshore can be extrapolated offshore. All these results will be addressed in the Chapter 2.1, which is based on the article: Ramos, A., Fernández, O., Terrinha, P., Muñoz, J.A., 2016. Extension and inversion structures in the Tethys–Atlantic linkage zone, Algarve Basin, Portugal. Int. J. Earth Sci. 105, 1663–1679. doi:10.1007/s00531-015-1280-1.

Compression is documented to be present in the margin since the Late Cretaceous to present-day (Terrinha, 1998). Offshore, the presence of contractional structures (e.g., thrust faults) is not obvious on seismic. A complete analysis of the tectonosedimentary relationships between the syn-compressional sedimentary strata and the inversion structures is needed to address new insights of the features responsible for the margin inversion, in terms of timing and kinematics. Offshore tectonic processes must be integrated with those occurring onshore. The Chapter 2.2 tries to explain the mechanisms of compression in this margin, and it is based on the article: Ramos, A., Fernández, O., Terrinha, P., Muñoz, J.A., 2017. Neogene to recent contraction and basin inversion along the Nubia-Iberia boundary in SW Iberia. Tectonics 36, 257-286. doi:10.1002/2016TC004262.

The paleogeography of the margin through the Mesozoic was highly affected by salt tectonism. Salt structures are quite obvious on seismic and they have been documented in several works through the Algarve Basin (Lopes et al., 2006; Matias et al., 2011), but none of these works have studied how the distribution of the evaporites facies controlled the salt structures style. New 3D seismic data and other 2D seismic surveys allowed for a better understanding of the salt tectonics in the margin, along with its evolution during Mesozoic and Cenozoic, including the mechanisms of emplacement for the Esperança salt sheet. Distribution of the Hettangian evaporite unit is interpreted to be the responsible for the thin-tectonic deformation during compression. Unravelling salt tectonics is indispensable for comprehending the thick-skinned tectonic deformation in the basement below. The Chapter 2.3 deals with the salt tectonism and is based on the article: Ramos, A., Fernández, O., Terrinha, P., Muñoz, J.A. Impact of basin structure and evaporite distribution on salt tectonics in the Gulf of Cadiz, Southwest Iberian margin (submitted in Marine and Petroleum Geology).

Once the thin- and thick-skinned tectonics are well studied, there are more aspects of the margin to be solved, such as the structure of the distal part, and the extension of the sedimentary basin beyond the Guadalquivir and Portimão Banks. Several studies have been carried out to investigate the deep structure of the SW Iberian margin (González et al., 1996; Gràcia et al., 2003a; Gutscher et al., 2009, 2002; Zeyen et al., 2005). The results show a crustal thinning from the proximal margin to the deepest parts (from 30-32km o 15km). However up to now, there are no studies contributing to the geological explanation for the crustal structure of the margin.

The interpretation of seismic data was also useful to obtain the preliminary basement structure and basin architecture. The acquired seismic data are commercial and were recorded down to 12 seconds. It is essential then to take into account other geophysical data, such as the gravity, for better defining the deepest structure of the crust. The integration between seismic and gravity data can constrain the structure of the transition from a normal thick continental crust to the north of the margin to an oceanic crust to the south, (Gutscher et al., 2002; Martínez-Loriente et al., 2014; Sallarès et al., 2011). This allows understanding the tectonic and paleogeographic evolution of the margin. The Chapter 2.4 will be focus on this subject and is based on the article: Ramos, A., Fernández, O., Torne, M., Sánchez de la Muela, A., Muñoz, J.A., Terrinha, P., Manatschal, G., Salas, M.C. Crustal structure of the SW Iberian passive margin: The westernmost remnant of the Ligurian Tethys? Tectonophysics 705, 42-62. doi:10.1016/j.tecto.2017.03.012.

The comprehension of the crustal structure is the key for obtaining the paleogeographic evolution of the SW Iberian margin from the Mesozoic extension to the Late Cretaceous-Cenozoic inversion. The regional paleogeographic maps, obtained from the integration of the previous information, help to better understand how the tectonic processes affected the margin during each period of evolution. The Chapter 2.5 deals with this part of the thesis and is based on the article: Ramos, A., Fernández, O., Terrinha, P., Muñoz, J.A., Arnaiz, A. Paleogeographic evolution of a segmented oblique passive margin: the case of the SW Iberian margin (this paper will be submitted to the Journal of Geological Society).

1.3. METHODOLOGY

The interpretation of the structure of SW Iberia and the Algarve Basin presented in this thesis are based on geological mapping of onshore Portugal and the interpretation of seismic data, well data and gravity and magnetic data. Data interpretation has been integrated with regional geological understanding, in order to ensure that the obtained conclusions are coherent with the history of Mesozoic extension and Cenozoic compression experienced by SW Iberia.

The data required an initial quality control to homogenize the essential data taken from different sources into one unified file. The georeferentation of the outcrop measurements, the geological map, cross-sections, wells, seismic and gravity data were set using the UTM projection, zone 29 and European Datum 50, using the ArcGIS software when necessary.

1.3.1. Field data

Onshore fieldwork was carried out in several campaigns covering the entire onshore Algarve Basin. During these campaigns 398 outcrop data were taken (dip data, fault contact, stratigraphic traces…; Appendix Table) in an area of roughly 2000 km2 (Fig. 1.3.3). This led to the building of a revised geological map of the onshore Algarve Basin and several cross-sections across the basin, in order to synthetize the Mesozoic and Cenozoic evolution of the basin margin, as well as to review and redefine the geological map done by Manuppella (1992) and Terrinha (1998). Geological mapping was mainly supported by 1:25.000 ortophotographs from Bing Maps (https://www.bing.com/mapspreview) and 1:25.000 topographic cartography maps from Instituto Geográfico do Exército.

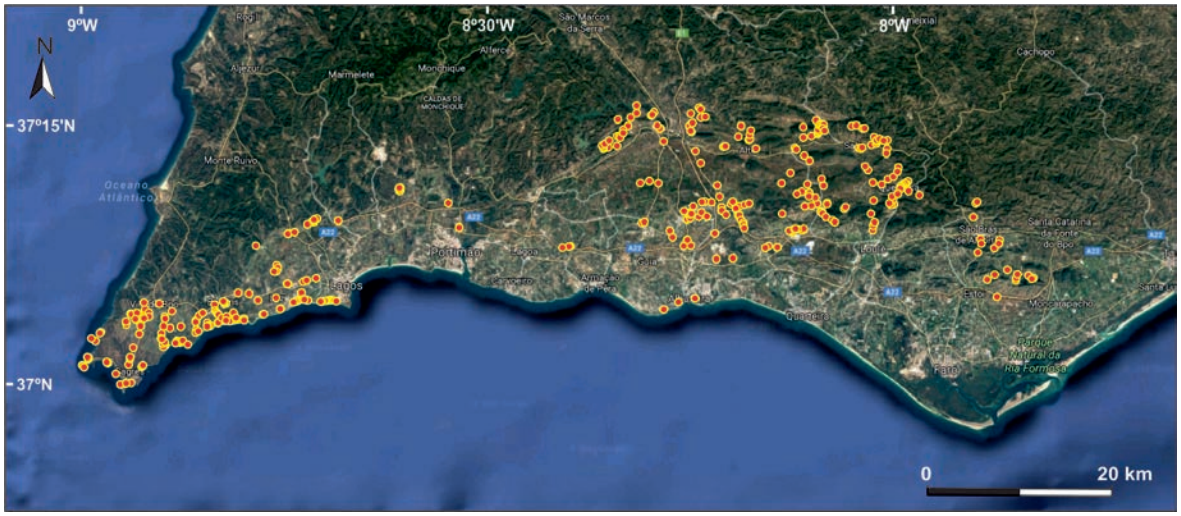

Figure 1.3.1. Map from the onshore Algarve Basin with the overprinted location of the outcrop data taken for this thesis. Satellite image from Google Maps.

1.3.2. Seismic data

Vintage 2D seismic surveys of the Algarve Basin and a more recent 2D regional seismic reflection survey (acquired by TGS in 2001 during the PDT00 and PD000 cruises, TGS, 2005) have been used to interpret the offshore structure in the Algarve Basin (Fig. 3). The PDT00-PD00 regional survey consists of a set of 58 lines of 2D multichannel reflection seismic data (Fig. 1.3.1). This seismic survey consists of NNW-SSE lines spaced every 4 km and ENE-WSW lines spaced every 8 km, and it has a shotpoint interval of 12.5 and 15 m. Recording length was 12 s two-way travel time (TWTT). The seismic survey was acquired with an streamer length of 6km (TGS, 2005). The interpretation on this survey was performed on the migrated stack in time.

A 3D seismic cube was acquired in 2012 by Repsol in the central part of the offshore margin, from south of Faro to the Portuguese-Spanish border (Fig. 1.3.1). The 3D seismic cube covers an extension of 1500 km2 and it consists of 151 shot lines oriented NNW-SSE and spaced every 375 m, with a recording length of 7.2 s TWTT. This 3D cube has also been interpreted, using the pre-stack time and depth migrated versions. All seismic data have been unified using UTM projection, zone 29 and European Datum 50 and interpreted using Petrel and Geoframe (by Schlumberger).

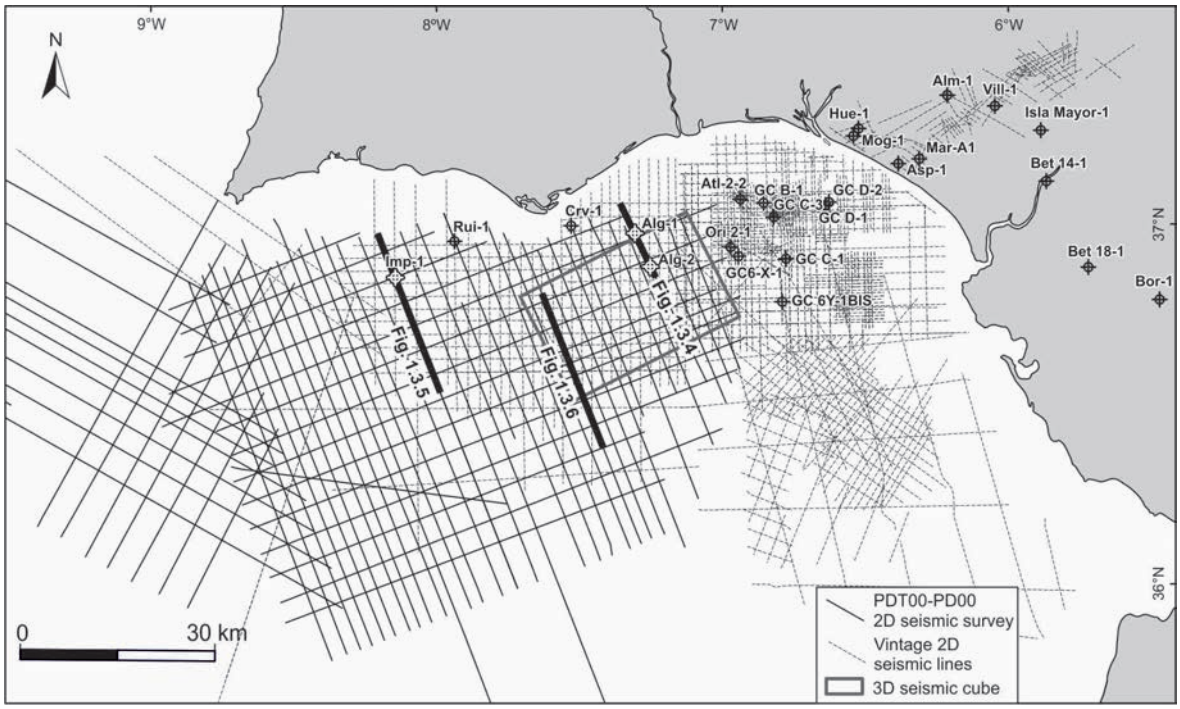

Figure 1.3.2. Available data in the Algarve Basin used in this thesis. Black lines: PD00 2D seismic survey; dashed black lines: 2D vintage seismic; grey line: seismic cube. Most representative wells: Alg-1: Algarve-1; Alg-2; Algarve-2; Alm-1: Almonte-1; Asp-1: Asperillo-1; Atl-2-2: Atlantida-2-2; Bet 14-1: Betica 14-1; Bet 18-1: Betica 18-1; Bor-1: Bornos-1; Crv-1: Corvina-1; GC B-1: Gulf of Cadiz B-1; GC B-6: Gulf of Cadiz B-6; GB D-1: Gulf of Cadiz D-2; GB D-2: Gulf of Cadiz D-2; GB C-3: Gulf of Cadiz C-3; GB 6Y-1bis: Gulf of Cadiz 6Y-1bis; Hue-1: Huelva-1; Imp-1: Imperador-1; Mog-1: Moguer-1; Ori 2-1: Orion 2-1; Rui-1: Ruivo-1.

Seismic correlation has been based on the interpretation of unconformity bounded sequences (Terrinha, 1998; Roque, 2007), which were useful to correlate the reflectors between the MSC seismic profiles. Seismic profiles have been interpreted using Petrel (by Schlumberger). Conversion of interpreted 2D seismic profiles to depth has been performed where necessary using Move 2014.2 (by Midland Valley Exploration). Depth conversion has been performed by using an average time-depth relationship established from wells along the basin margin (Algarve-1, Algarve-2, Corvina-1, Imperador-1 and Ruivo-1; Fig. 1.3.1). As a result, three stratigraphic intervals with an average P-wave velocity were used in the conversion (Neogene-Quaternary, Paleogene to Middle Jurassic and Middle Jurassic to Basement; Fig. 1.3.2). The time-depth relationship has been calibrated using the depth image of the depth migrated 3D seismic cube to make it meaningful for the parts of the basin away from wells.

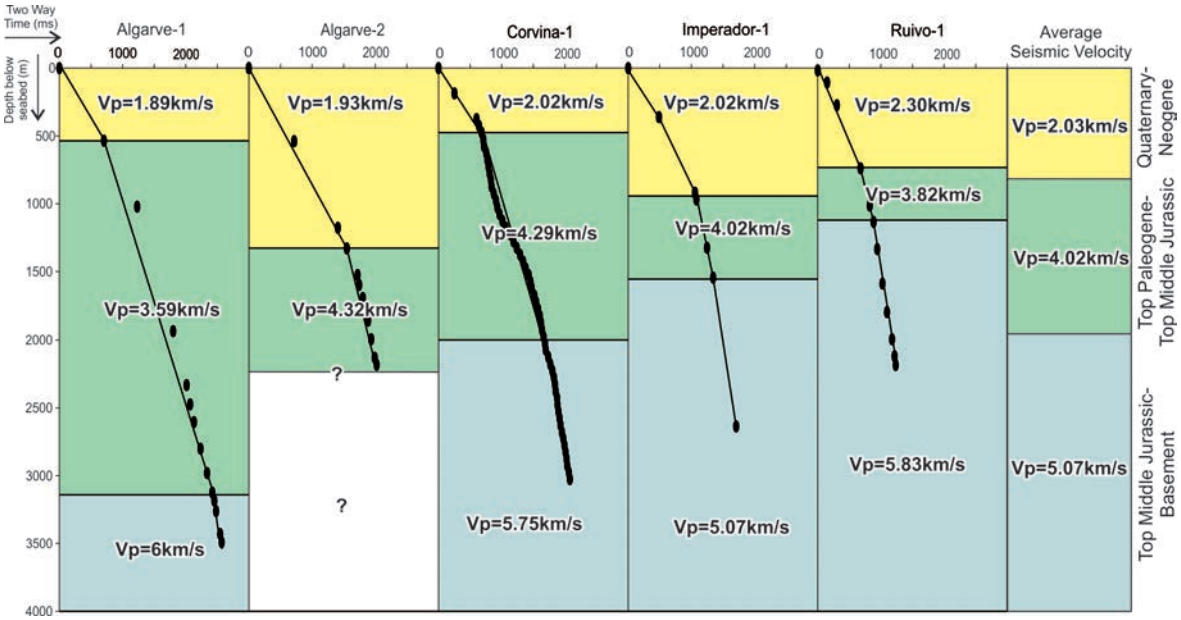

Figure 1.3.3. Checkshot data from the 5 wells in the Portuguese Algarve Basin. The time-depth relationships from Algarve Basin of the 5 wells have been used to define 3 velocity intervals: Neogene-Quaternary (yellow), top Paleogene to top Middle Jurassic (green) and top Middle Jurassic to top of Basement (blue). See Fig. 1.3.1 for location.

1.3.3. Well data

Seismic interpretation was constrained by the calibration with five wells in offshore Portugal (Roque, 2007), along with 67 wells in the eastern Algarve Basin and Guadalquivir Basin Lanaja, 1987 (the most relevant are illustrated in Figure 1.3.1).

All well data were obtained by oil companies from the 1950' to 1980'. Well data were provided by Repsol Exploración in pdf and image files. The formation tops were obtained from reviewing the Portuguese wells and from previous works (Matias, 2007; Roque, 2007; Terrinha, 1998; Fig. 1.1.8), and from wells of the eastern Algarve Basin (Lanaja, 1987).

1.3.4. Gravity data

Gravity modelling has been used to constrain the interpretation of deeper seismic horizons (pre-Jurassic picks, mainly the top of basement) and the crustal scale structure. Gravity modelling was performed using offshore free-air gravity anomalies acquired from the global satellite altimetry data model V16.1 (Smith and Sandwell, 1997, updated 2007), given that they imaged lateral density contrasts within the earth's crust, but these data are very sensitive to bathymetry. Bouguer anomaly is only imaged in the onshore margin and is calculated from the free-air anomaly to reduce the topographic contribution to the gravity signal. These gravity anomalies were taken from a recent compilation of gravity data on Iberia (Ayala et al., 2016).

The forward modelling has been performed using GM-SYS (modelling application of Oasis Montaj, Geosoft software), which calculates the gravity response of the density models built using the methods of Talwani (1965) and Talwani et al. (1959).

While these regional data covered the entire SW Iberian margin, another more detailed set of gravity data were used in the 3D seismic cube, which was acquired by Repsol during the same campaign as the seismic data.

1.3.5. Seismic interpretation

Seismic interpretation has been based on the assumption that each stratigraphic unit has a unique seismic response across the entire SW Iberian margin. From top to bottom, the first unit is the Cenozoic, which is represented by high frequency continuous bright reflectors, and multiple wedge and onlap geometries. Internally, the Cenozoic is subdivided into Neogene and Paleogene, which are separated by the BFU, represented by a strong reflector truncating the underlying units (Fig. 1.3.4). To the south, within the Cenozoic unit, the AWGC/AUGC is displayed by internally chaotic or transparent seismic facies. Its top is represented by a sharp transition to layered seismic facies above and below. Cenozoic was deposited above this unit forming mini-basins bounded by shale positive structures (e.g., Hernández-Molina et al., 2016; Medialdea et al., 2009). In some parts of the basin, the base of the AWGC/AUGC truncates or is parallel to the underlying sediments.

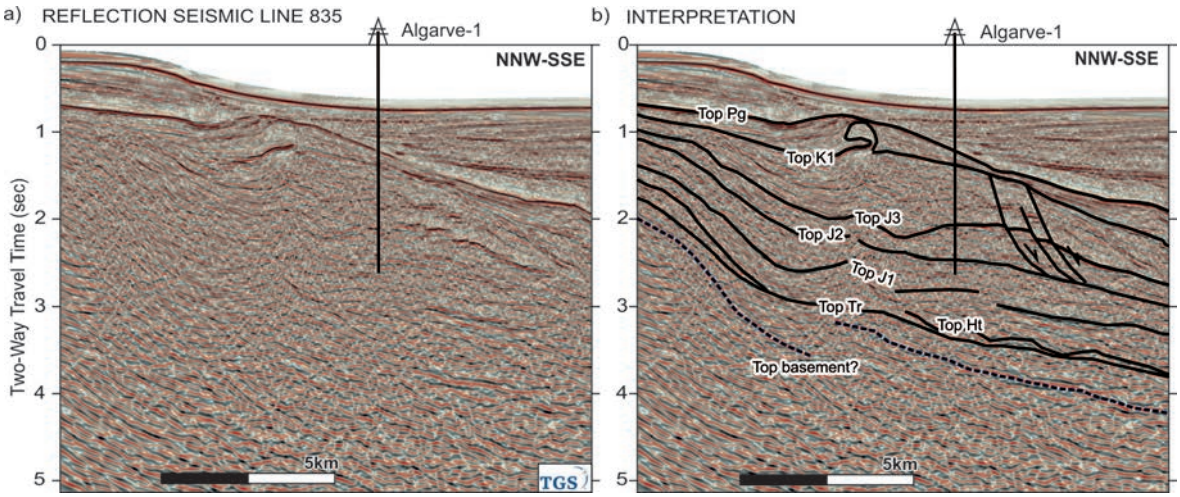

Figure 1.3.4. Portion of seismic line 835 across wells Algarve-1 and Algarve-2, in time (a) and seismic interpretation (b). BFU: base foredeep unconformity; K1: Lower Cretaceous; J3: Upper Jurassic; J2: Middle Jurassic; J1: Upper Jurassic; Tr: Triassic; Ht: Hettangian. The allochthonous Esperança salt unit (Matias et al., 2011) is also identified (Es). See Fig. 1.3.2 for location.

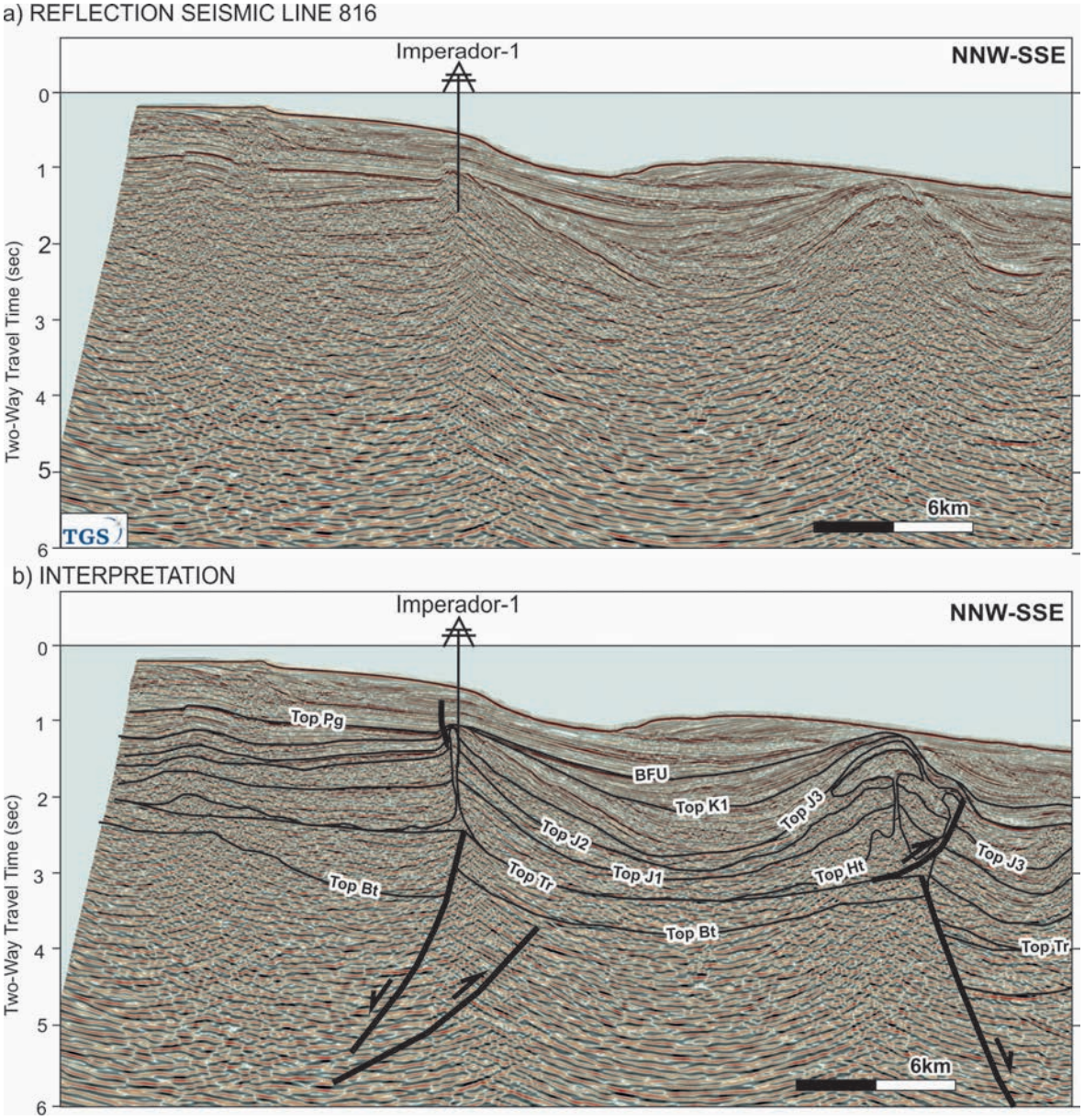

Figure 1.3.5. Portion of seismic line 816 across the well Imperador-1, in time (a) and seismic interpretation (b). See Fig. 1.3.2 for location and Fig. 1.3.4 for acronyms. Data courtesy of TGS.

The base of the Cenozoic succession consists on another unconformity, which locally truncates the units below (Fig. 1.3.5). The Upper Cretaceous succession is not represented in most of the Algarve Basin. The Lower Cretaceous sediments instead, are widely preserved. This unit is characterized by bright and continuous reflectors, and its depocenters and internal unconformities are related to halokinesis.

The Jurassic tends to lie conformably beneath the Lower Cretaceous. Jurassic is represented by bright but short reflectors of low frequency. The boundaries of the Upper, Middle and Lower Jurassic are depicted by regional angular unconformities related to rifting phases (Terrinha, 1998), also controlled by halokinetic processes. Changes in thickness are interpreted to be controlled by salt tectonics and extensional faulting (Fig. 1.3.5).

The base of the Jurassic succession is deformed by diapirs and salt walls sourced from the underlying Hettangian unit. Both top and base are frequently depicted as bright reflectors, while its internal facies are chaotic to transparent. This unit marks the base of the halokinetic growth strata and therefore is probably the deepest unit that is relatively easy to pick on seismic. Locally, the Hettangian evaporite unit extrudes to form parautochthonous and allochthonous salt bodies (Figs. 1.3.5 and 1.3.6). The Esperança salt sheet (Matias et al., 2011) is one of this salt bodies and it has been emplaced mostly within the Jurassic (Fig. 1.3.6). Above this salt sheet, the Middle Jurassic to Lower Cretaceous mini-basins are represented by fanning geometries and strongly tilted and folded reflectors. Although the image is poor beneath the salt sheet on seismic, the structure was supported by the surrounding areas.

The base of the Hettangian succession corresponds to the top of the Triassic one, which is irregularly distributed through the basin. Triassic sediments were deposited in fault-bounded grabens or half-grabens (Figs. 1.3.5 and 1.3.6), according to the analogy with the onshore Algarve Basin. This unit is represented by mid-high frequency and high amplitude reflectors. The base of the Triassic rocks correspond to the top of the basement as a bright reflector segmented by extensional faults (Fig. 1.3.6). However, this reflector is sometimes ambiguous on seismic image due to the limited impedance contrast of the shallower units of the basement (Hercynian foreland flysch) with the overlying Triassic clastics. Offshore, the basement is only constrained by the well GC6Y-1BIS and by a dredge along the Guadalquivir Bank (Vegas et al., 2004). The offset of Mesozoic units by extensional faults is interpreted to affect also the basement, which helps to carry out the final interpretation of the top basement (Fig. 1.3.6).

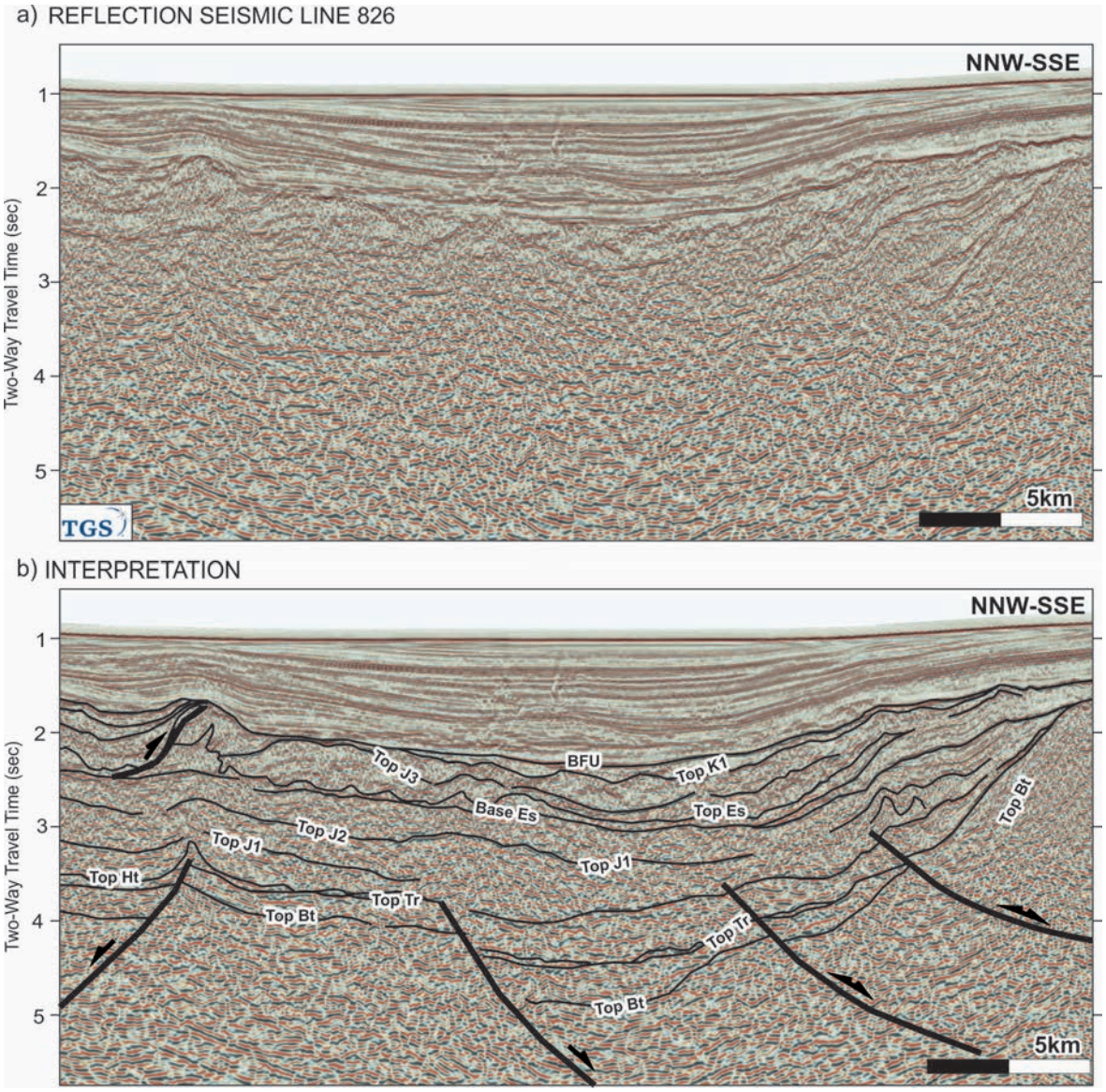

Figure 1.3.6. Portion of seismic line 826 in the central part of the Algarve Basin, in time (a) and seismic interpretation (b) in the central part of the basin, north of Guadalquivir Bank. Es: Esperança salt sheet. See Fig. 1.3.2 for location and Fig. 1.3.4 for acronyms. Data courtesy of TGS.

1.3.6. Model-driven interpretation

Regional seismic interpretation of the areas, with not much control (located away from the wells in the deepest parts of the margin), was carried out based on a few concepts. These consist on the integration of all the regional knowledge of the previous works in the SW Iberian margin and other oblique passive margins, possibly hyper-extended.

Along with the majority of the eastern margin of the Atlantic Ocean (Peron-Pinvidic et al., 2013; Reston and Manatschal, 2011), the surrounding margins of the SW Iberian margin were defined as hyper-extended, such as the Western Iberia margin (Manatschal, 2004), the Atlantic Moroccan margin (Contrucci et al., 2004) and the Ligurian Tethys (Masini et al., 2014; Mohn et al., 2012).. The implications

on considering the SW Iberian margin as a hyper-extended margin are relevant and some definitions need to be addressed.

In the hyper-extended margins, extreme crustal thinning occurs, from 30 to 35 km thick to a few km in most cases over a distance of 100-200 km (e.g., Reston and Manatschal, 2011; Fig. 1.3.7). Thinning of the crust occurs most rapidly in a necking zone between about 10-20 km wide (Fig. 1.3.7). Other characteristic of this type of rifted margins is that at their outer parts, a high velocity, high gradient zone beneath thinned crust can be largely serpentinized mantle and there are not thick basalt sequences. They are defined as hyper-extended margins.

The seismic image quality is chaotic in the distal parts of the margin, due to the obscuring of the overlying AUGC/AWGC. The crustal thinning towards the south and the presence of oceanic crust in the deepest parts of the Gulf of Cadiz (e.g., Sallarès et al., 2011) beneath the AUGC/AWGC, along with the proximity of hyper-extended margins (W Iberian margin), makes the SW Iberian margin a potential candidate of an hyper-extended margin. The model of passive margin evolution of Peron-Pinvidic et al. (2013) is proposed to interpret on seismic these areas of uncertainty.

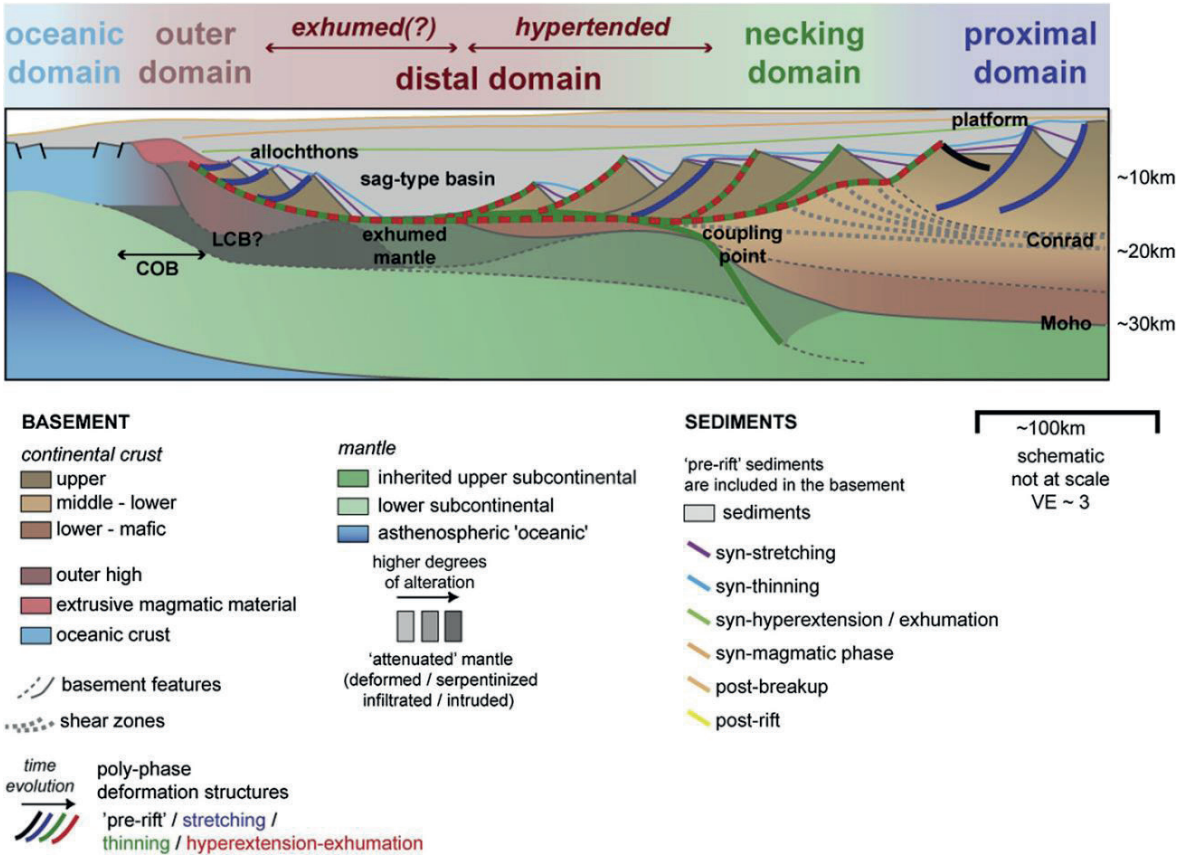

Figure 1.3.7. Schematic section of a typical hyper-extended margin. Taken from Peron-Pinvidic et al. (2013).

Peron-Pinvidic et al. (2013) define several phases of evolution. The first phase corresponds to the initial stretching phase, which defines the proximal domain. During this phase the extensional structures sole out at mid-crustal level, and it does not explain the crustal thinning (Fig. 1.3.7). The following phase is defined by the thinning and coupling of the continental crust in the necking domain (Fig. 1.3.7). Once the continental crust is <~10 km thick, it becomes brittle and the upper and lower crustal conjugate structures couple. When the deformation migrates progressively oceanward, the continental crust becomes hyperextended (by downward concave detachment faults; Fig. 1.3.7). This phase can led to serpentinized mantle exhumation, defining the distal domain along with the hyperextended sub-domain (Fig. 1.3.7). The lithospheric breakup is the latest rifting phase of these margins, and marks the onset of seafloor spreading and therefore the formation of oceanic crust, observable in the outer and oceanic domains (Fig. 1.3.7).

Moreover, seismic interpretation was also influenced by the concept of oblique passive margin. Most of the plate reconstructions of the SW Iberian margin during the Mesozoic, considered this margin as an oblique passive margin bounded by transfer faults, located in the linkage between the Ligurian Tethys and the Atlantic domain (Frizon de Lamotte et al., 2011; Gràcia et al., 2003; Stampfli and Borel, 2002; Vergés and Fernàndez, 2012). Transfer zones are important structural elements in oblique rift systems, allowing the accommodation of extension between individual fault and basin segments along the zone of deformation (Gawthorpe and Hurst, 1993). Some examples can be found in Rio Grande rift (Mack and Seager, 1995) or in the Atlantic margin of southeastern Brazil (e.g., Meisling et al., 2001). The presence of transfer zones in the margin affects the distribution and geometry of the main tectonic features and stratigraphic units.

1.3.7. Gravity modelling and potential field maps

The interpretation of the offshore structure has been an iterative process involving well-seismic correlation, seismic interpretation and gravity modelling.

The 2D gravity modelling results shown in the section 2.4 helped to better constrain the structure of the margin, such as the basement geometry and the thickness of the Triassic basins. The crustal structure obtained from gravity modelling and the comprehension of salt tectonics, led to complete a coherent seismic interpretation of the SW Iberian margin.

Local gravity anomaly maps were also helpful to interpret in detail the basement extensional faults in the area covered by the 3D seismic cube, beneath the Esperança salt structure (Fig. 1.3.8). Residual gravity was used in the 3D seismic cube in order to constrain the seismic interpretation. Enhancement or filtering is a way to separate signals of different wavelength to isolate and hence enhance anomalous features with a certain wavelength. Filtering can be used to enhance anomalies produced by features in a given depth range. In the 3D cube, the first vertical derivative (Repsol data) was very helpful to interpret the structure above and beneath the Esperança salt structure (Fig. 1.3.8). The enhancement sharpens anomalies over bodies and tends to reduce anomaly complexity, allowing a clearer imaging of the basement structure.

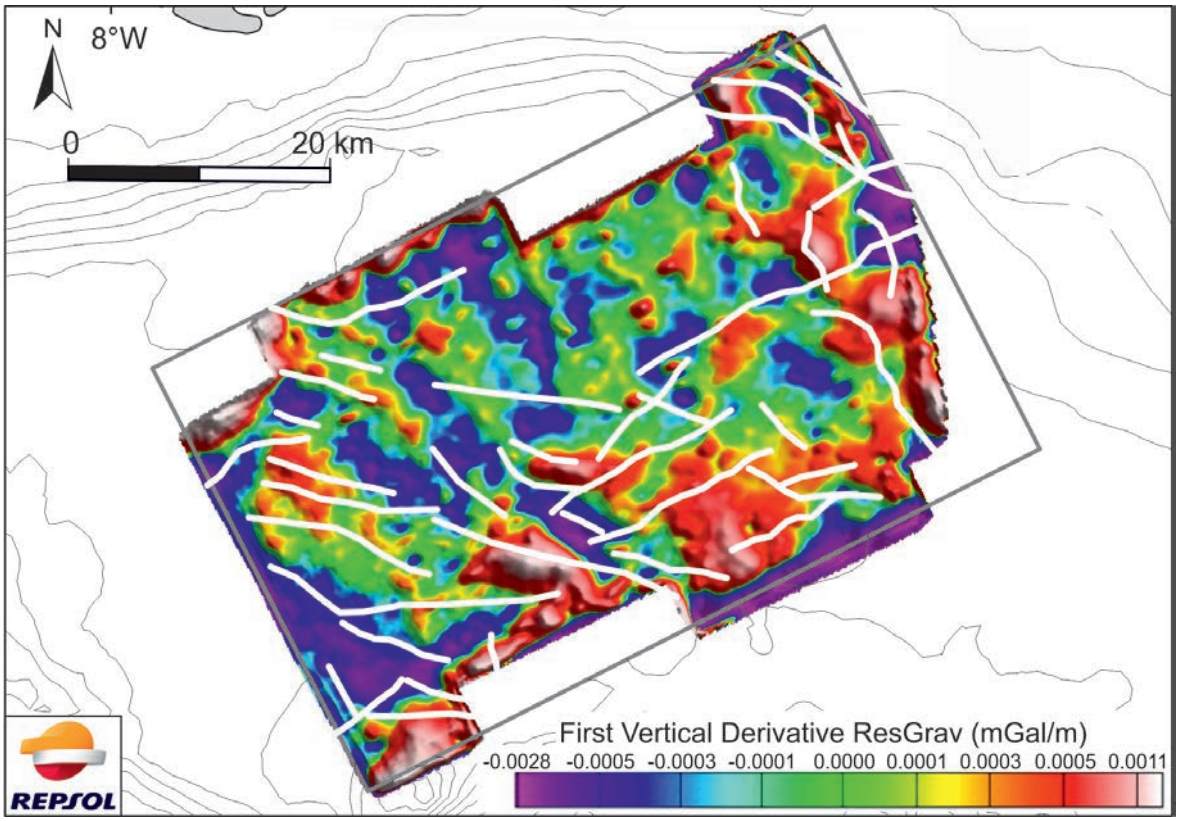

Fig. 1.3.8. Basement extensional faults on a map of the first vertical derivative of the residual gravity anomaly covering the area of the 3D seismic cube. See Fig. 1.3.1 for location. Data courtesy of Repsol.

CHAPTER 2. RESULTS

CHAPTER 2. RESULTS

The main results are presented in this section as a result from the interpretation of the onshore and offshore structure, after analysing field and geophysical data and integrated with the regional knowledge of the SW Iberian margin.

2.1. ONSHORE ALGARVE BASIN

The field work carried out in the onshore portion of the Algarve Basin resulted in a revised geological map of the basin and the construction of cross-sections. The map shows the orientation and distribution of extensional and contractional structures, and the different stratigraphic units (Fig. 2.1.1). The extensional faults are north-dipping, strike E-W to WNW-ESE and involve basement. They have displacements of tens of meters, juxtaposing Upper Triassic and Lower Jurassic sediments with Carboniferous basement (Fig. 2.1.1).

The paper titled "Extension and inversion structures in the Tethys-Atlantic linkage zone, Algarve Basin, Portugal", included in the appendix 1.1, explains in more details the results of the onshore structural study.

The presence of Middle Jurassic depocenters to the south is controlled by a set of E-W trending basin-scale faults. The Algibre Fault and its western continuation, the Espiche Fault (Fig. 2.1.1b), are interpreted as southward dipping extensional faults, with a roughly E-W orientation, overprinted by the Algibre and Espiche thrusts respectively. These faults mark the northern limit of the Upper Jurassic and Lower Cretaceous outcrops, along with the observed salt-related structures. To the east, the Faro-Tavira Fault trends ENE-WSW and is parallel to the eastern coastline of Faro, acting as the northern limit for the Lower Cretaceous and uppermost Upper Jurassic sediments (Fig. 2.1.1b). The ENE-WSW trending Carcavai Fault is interpreted to have formed as a relaying structure between the Algibre and the Faro-Tavira faults (Fig. 2.1.1b).

In contrast to the dominant E-W trend of extensional faults in the central and eastern parts of the basin, the general structural pattern of the western part is dominated by NNE-SSW to N-S trending extensional faults (Fig. 2.1.1). Nonetheless, E-W to NE-SW normal faults, which are more common further east, are still present (such as the Espiche Fault).

East of the São Marcos Quarteira Fault (SMQF), the Querença margin acted as an extensional transfer zone during the Mesozoic (Fig. 2.1.1b) connecting the Algibre and the Faro-Tavira faults. The present-day basement-contact geometry along the Querença transfer zone (Fig. 2.1.1b) responds to the reactivation of this structure onto a lateral ramp structure in the inversion system, relaying the basin margin basement monocline.

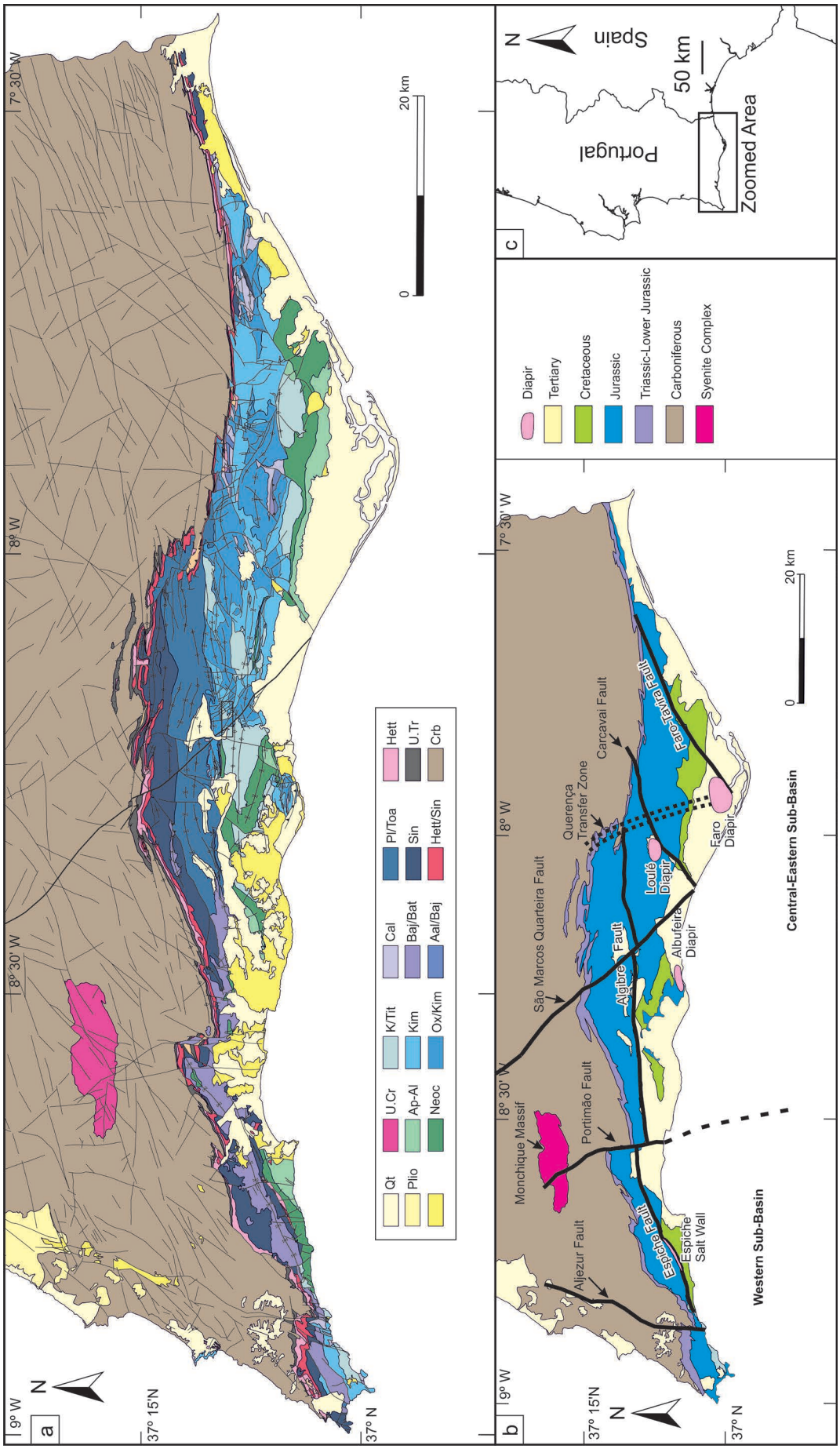
a
b
c
9º W
8º 30' W
8º W
7º 30' W
37º 15'N
37º N
N
0
20 km
Qt
Plio
U.Cr
Ap-Al
Neoc
K/Tit
Kim
Ox/Kim
Cal
Baj/Bat
Aal/Baj
Pl/Toa
Sin
Hett/Sin
Hett
U.Tr
Crb
Diapir
Tertiary
Cretaceous
Jurassic
Triassic-Lower Jurassic
Carboniferous
Syenite Complex
Portugal
Spain
50 km
Zoomed Area
São Marcos Quarteira Fault
Querença Transfer Zone
Carcavai Fault
Faro Tavira Fault
Algibre Fault
Louié Diapir
Albufeira Diapir
Faro Diapir
Monchique Massif
Portimão Fault
Aljezur Fault
Espiche Fault
Espiche Salt Wall
Western Sub-Basin
Central-Eastern Sub-Basin

Figure 2.1.1. (a) Study area location and geological map of the Algarve Basin (modified after Davison et al., 2016; Manuppella, 1992; Terrinha, 1998). Qt: Quaternary; Plio: Piocene; Mc: Miocene; U. Cr: Upper Cretaceous; Ap-Al: Aptian-Albian; Neoc: Neocomian; K/Tit: Kimmeridgian/Tithonian; Kim: Kimmeridgian; Ox/Kim: Oxfordian/Kimmeridgian; Cal: Callovian; Baj/Bat: Bajonian/Batonian; Aal/Baj: Aalenian/Bajocian; Pl/Toa: Pliensbaquian/Toarcian; Sin: Sinemurian; Hett/Sin: Hettangian/Sinemurian; Hett: Hettangian; U. Tr: Upper Triassic; Crb: Carboniferous. (b) Simplified map showing major tectonic features, which have had different behaviour since the Late Triassic. (c) Location of the study area.

The faults changed from being mainly north-dipping in the Triassic-Early Jurassic to south-dipping (basinward dipping) in Middle Jurassic-Early Cretaceous (Fig. 2.1.2b,c). Furthermore, a significant change in style occurred. The initial extensional phase from Triassic to Early Jurassic triggered the formation of closely spaced faults with a limited throw (tens to few hundreds of meters). On the contrary, from Pliensbachian onwards, the extension was accommodated along major extensional faults with a greater throw (many hundreds of meters) and spacing, cross-cutting the basement weakness surfaces.

At a more local scale, a number of thrusts and contractional structures have been reinterpreted. These include the Algibre Thrust (Fig. 2.1.2b), short-cuts that affect the Triassic half-grabens along the northern margin of the basin (Fig. 2.1.2), and multiple buttressing related structures along the Algibre Fault (Fig. 2.1.2b).

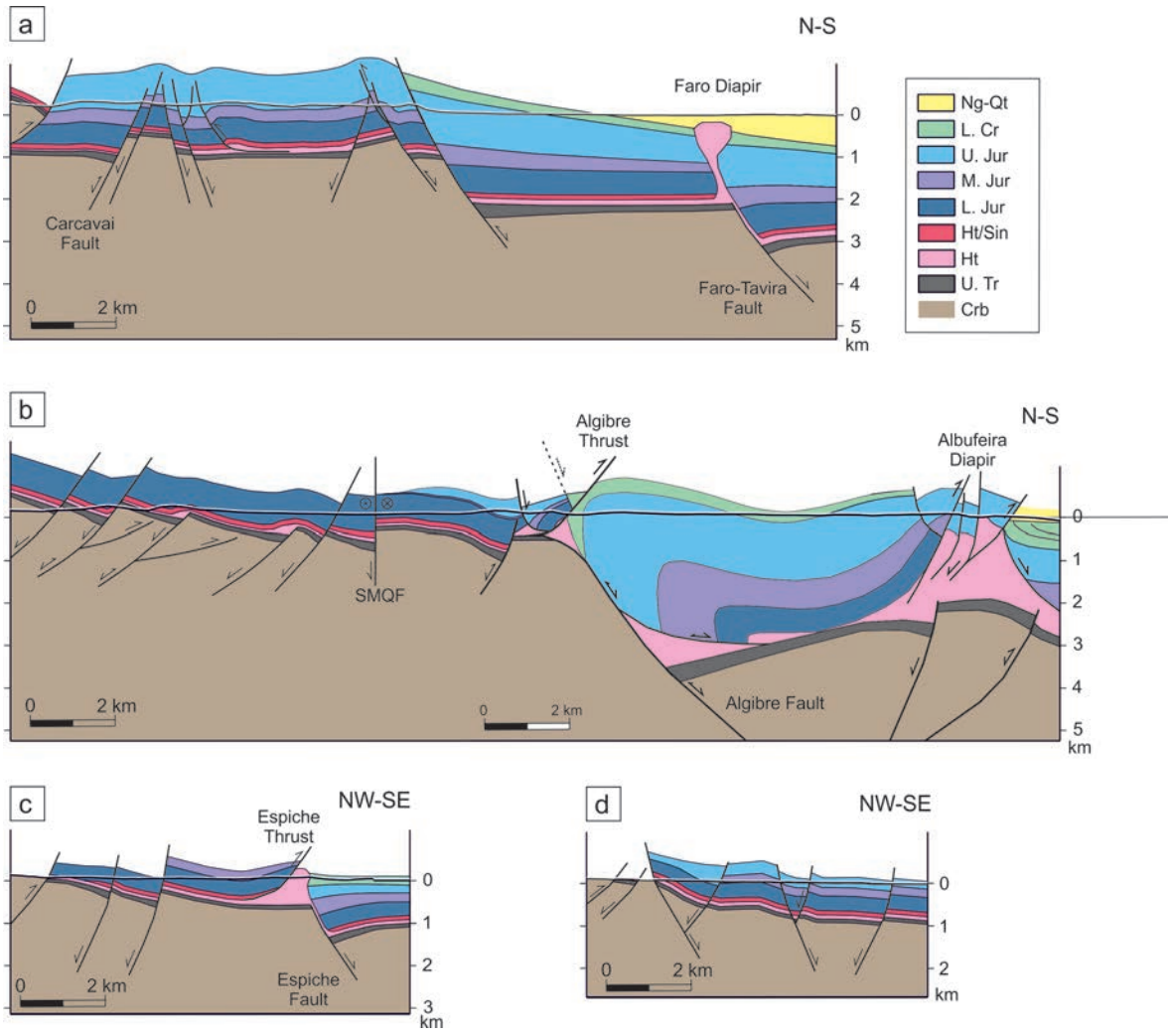

Figure 2.1.2. Cross-sections along the Algarve Basin. Ng-Qt: Neogene-Quaternary; L. Cr: Lower Cretaceous; U. Jur: Upper Jurassic; M. Jur: Middle Jurassic; L. Jur: Lower Jurassic; Ht/Sin: Hettangian/Sinemurian; Ht: Hettangian; U. Tr: Upper Triassic; Crb: Carboniferous basement. See Fig. 2.1.1a map for location.

The Algibre Fault marks the northern limit for the presence of the salt structures (Fig. 2.1.1), and the change in thickness of Mesozoic strata towards the south, indicating that the Espiche-Algibre-Faro-Tavira corridor was a relevant basin boundary since the deposition of the evaporites, acting as the northern boundary for thick evaporite sequences. During the Late Cretaceous-Cenozoic tectonic inversion two different structural styles resulted into the Algarve Basin related to the amount of evaporites across this corridor. To the north, where the evaporites are thin, the deformation was accommodated by basement-involved thrusts, whereas to the south of the corridor, the Mesozoic cover is affected by structures detaching on the Hettangian evaporites. The hangingwall of the Algibre Fault was detached above the Hettangian evaporites. This resulted into folding by buttressing against the Algibre Fault footwall, producing E-W trending tight detachment folds (Fig. 2.1.2b) and tightening and overturning the Algibre roll-over. The inversion structure is further complicated by the presence, locally, of a south-directed thrust that places Lower and Mid-Lower Jurassic rocks on top of the Lower Cretaceous sediments (Fig. 2.1.2b), rooting into the salt of the Algibre Thrust footwall.

The main effect of shortening and basin inversion in the onshore Algarve Basin is the broad southward tilt of the basin (Fig. 2.1.2). This regional tilt is related to basin-scale deformation and uplift of the basement during the Cenozoic, most probably associated with the presence of a south-directed basin-scale thrust, rooting into the basement. Tilting and uplift related to this thrust is responsible for the regional southward dip of Mesozoic beds and the complete absence of Neogene and Quaternary deposits over most of the onshore Algarve Basin. There is also evidence for at least one other contraction-related monocline in the basin, which causes a step in the offshore bathymetry in the west (along offshore segment of the Carcavai fault), and controls the location of the present-day coastline further to the east (Fig. 2.2.1). This basement-involved monocline was probably located along a basement-step of extensional origin that focussed the folding during the Alpine contraction.

2.2. CENOZOIC CONTRACTION AND BASIN INVERSION

The SW Iberian margin is surrounded by the Gorringe Bank to the west (Sallarès et al., 2013) and the Betic fold and thrust belt to the east (e.g., Crespo-Blanc, 2007; Pedrera et al., 2012; Fig. 1.1.1), which represent regional structures that concentrate a significant amount of contractional deformation. However, the structures responsible for the seismic activity and Neogene deformation in the Algarve Basin have remained elusive. This chapter deals with the documentation of the contractional structures linking the AGFZ to the west with the Gibraltar Arc to the east across the Algarve Basin. The observations derived from seismic and onshore data interpretation show regional contractional structures responsible for the Late Cretaceous-Cenozoic margin inversion. This helps to better document the contractional structures that link the Gorringe Bank and the Betics for the first time.

The paper titled "Neogene to recent contraction and basin inversion along the Africa-Iberia boundary in SW Iberia" included in the appendix 1.2 summarizes the work done for the detailed understanding of the compressional configuration of the margin during the Late Cretaceous and Cenozoic.

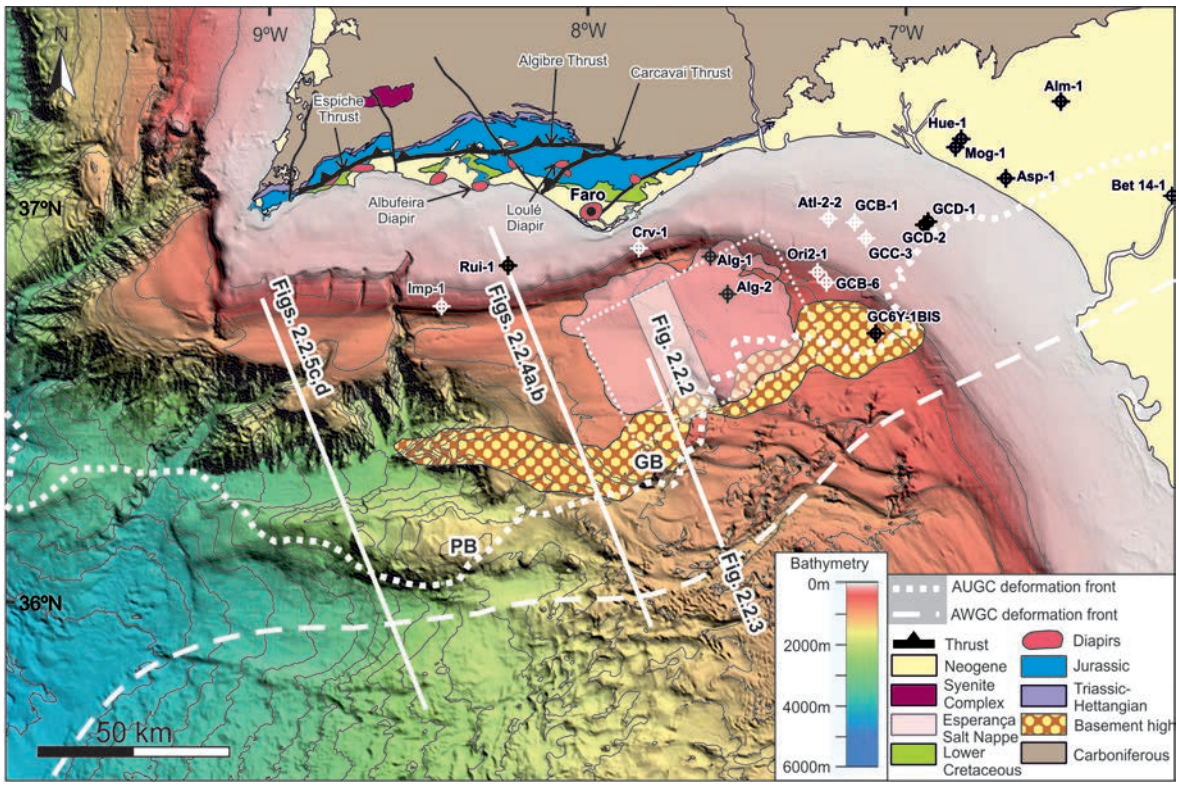

Figure 2.2.1. Map showing the available data in the SW Iberian margin with bathymetry coloured for depth, and the location of the figures described below in this paper. GB: Guadalquivir Bank; PB: Portimão Bank. High resolution bathymetry is taken from the General Bathymetric Chart of Oceans (GEBCO) digital atlas (IOC et al., 2003). The most representative wells are also depicted in this figure. See figure 1.3.2 for wells nomenclature.

The most evident contractional structures on seismic in the offshore Algarve Basin are those related with the reactivation of pre-existing salt structures, in particular those associated with the allochthonous Esperança salt sheet (Figs. 2.2.1 and 2.2.2). In the central portion of the Esperança salt sheet south-directed thrusts, active since the Paleogene, resulted from the reactivation of WSW-ENE trending salt walls (Fig. 2.2.2). Towards the south, another set of south-directed thrusts detached on the allochthonous Esperança salt sheet is interpreted to be the toe-thrust system. However, this contractional system is associated with the allochthonous emplacement and gravitationally-driven deformation of the Esperança salt sheet in Middle to Late Jurassic times, although it was reactivated during the Cenozoic (Fig. 2.2.2). The southern part of the Esperança salt sheet is tilted towards the north due to the uplift of the Guadalquivir Bank (Fig. 2.2.2).

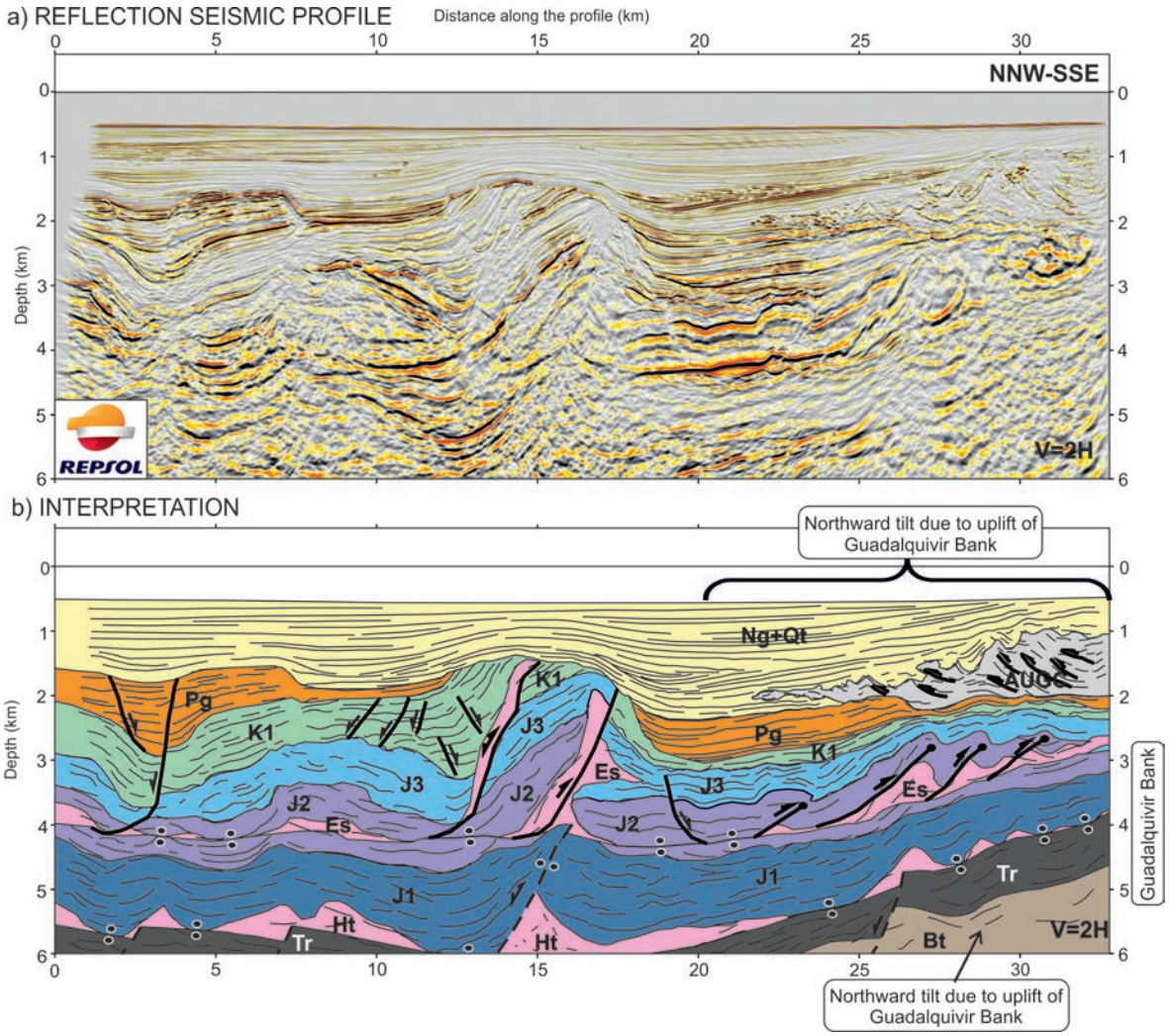

Figure 2.2.2. Seismic section across the Esperança salt sheet. (a) Reflection seismic profile (extracted from a proprietary 3D seismic cube migrated in depth). (b) Interpretation of (a). Ht: autochthonous evaporitic layer; Es: Esperança salt structure. The section is a NNW-SSE trending section through the Esperança salt structure shown in Figure 2.2.1 (the precise location is not shown due to confidentiality). Data courtesy of Repsol.

All the unconformities observable above and around the Guadalquivir Bank are clear indications of uplift of this basement high from Paleogene to Present-day. The uplift can be resumed in at least two distinct stages: a Late Paleogene (or Early Miocene?) stage, accounting for the erosional truncation below the BFU (and acting as a physical barrier for the progression of the AWGC during the Miocene), and a Late Pliocene to Quaternary stage that accounts for tilting and truncation at the seabed of Late Pliocene and older sediments. Recent uplift accounts for the noticeable drop in bathymetry that occurs across the Bank (Figs. 2.2.1 and 2.2.3). Uplift and tilting of the northern flank of the Guadalquivir Bank extends up to 10 km north of the Bank, indicating a deep source for the tilt (Fig. 2.2.3). Although no thrust responsible for this tilt or uplift has been identified on seismic, a southward vergent basement-involved thrust is the simplest way to account for the gentle northward tilt of beds north of the Bank and the steep drop observed to the south (Fig. 2.2.3). This thrust would also be responsible for the tilting of the AUGC and Miocene sediments, along with the differences on Miocene thickness in both sides of the Bank (Fig. 2.2.3). In the northern limb of the Bank north-directed back-thrusts accommodate part of the compression triggered by the basal regional thrust.

Most of major extensional faults are not inverted nor affected by the contractional structures. Where basement thrusts do actually coincide with a pre-existing extensional fault, they steepen it or cross-cut it. Although the Guadalquivir Bank is interpreted to be uplifted during the Late Cretaceous-Cenozoic inversion, the differences in depth of Mesozoic sediments across the bank is, in part, the result of the presence of a Mesozoic extensional fault pre-dating thrusting (Fig. 2.2.3e). The Guadalquivir Bank basement high initially originated as the uplifted footwall of a major (possibly crustal-scale) south-dipping Mesozoic extensional fault (Fig. 2.2.3).

Towards the west, the bathymetric expression of the Guadalquivir Bank connects with the Portimão Bank (Fig. 2.2.1d), which has been interpreted as an inverted Mesozoic fault-bounded basin by Terrinha et al. (2009). Thinning of Mesozoic sediments towards the southern extent of the Portimão Bank and the steeper bathymetry on the northern flank of the bank (Fig. 2.2.4d) indicate that this is an inverted Mesozoic half-graben developed on a south dipping extensional fault. Inversion occurred from Neogene to Recent times. As in the case of the Guadalquivir Bank, faults cannot be traced unambiguously on seismic, but the interpreted geometry requires the presence of both north- and south-directed thrusts underneath the Portimão Bank (Fig. 2.2.4d).

Along the margin, the basement deepens towards the south (Fig. 2.2.4), consistent with a passive margin geometry facing to the south. However, the BFU deepening southward describes a stair-steeped geometry, interpreted to be limiting the Neogene-Quaternary depocenters (Fig. 2.2.4). At least, three steps have been identified in the margin, related to the Late Cretaceous-Cenozoic inversion (Fig. 2.2.4).

Figure 2.2.3. Seismic section across the Guadalquivir Bank. (a) Reflection seismic profile in time. (b) Interpretation of the same profile. (c) Depth version of profile in (a). (d) Restoration at Oligocene time (prior to the emplacement of the AUGC). (e) Restoration at Early Cretaceous time. The interpretation beneath the depth of 3-4 seconds is based on the 3D seismic image north of the Guadalquivir Bank and inferred to its south due to the poor seismic image. See Figure 2.2.1 for location and Figure 2.2.2 for legend. Data courtesy of TGS.

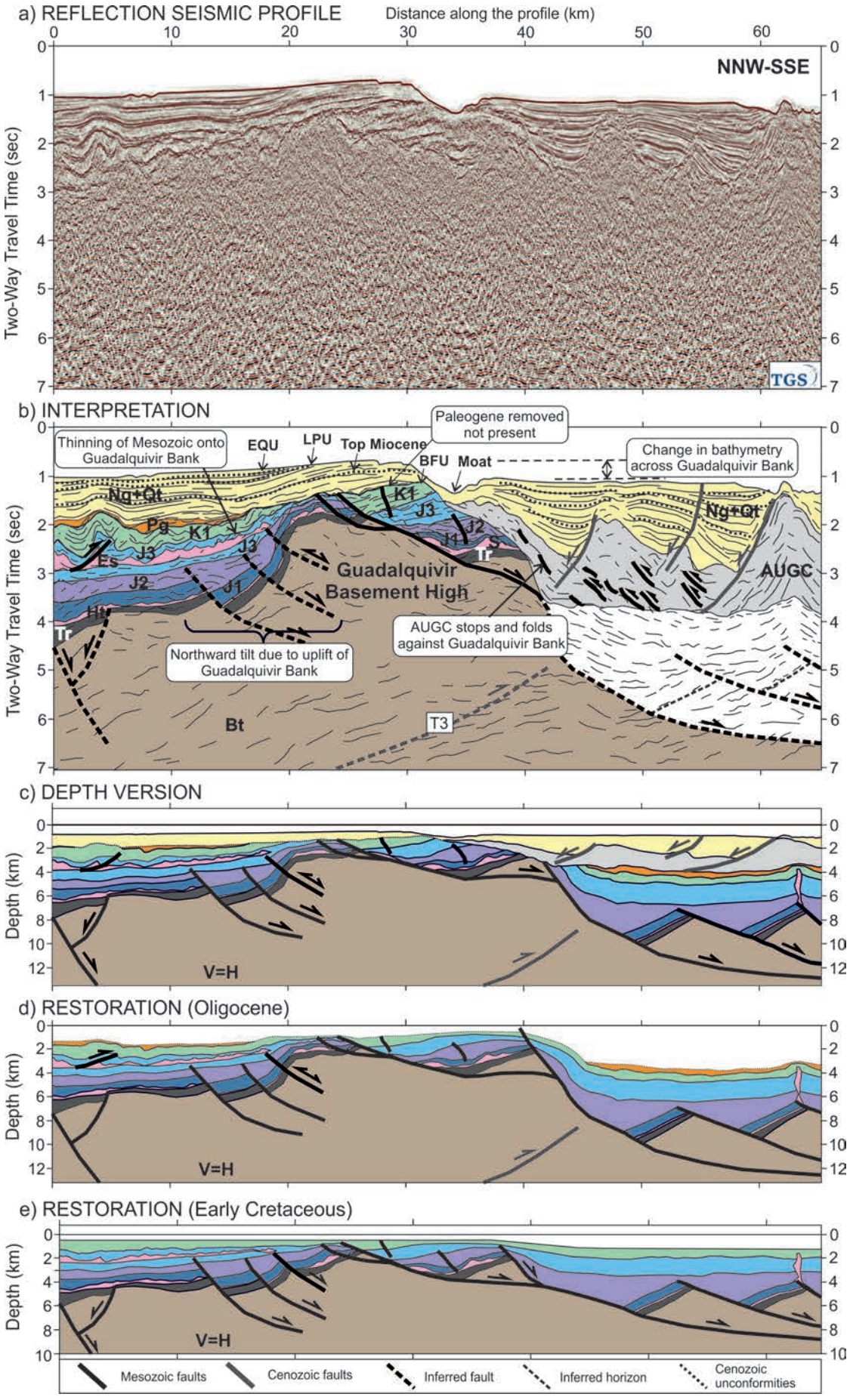
a) REFLECTION SEISMIC PROFILE
Distance along the profile (km)
NNW-SSE
Two-Way Travel Time (sec)
TGS
b) INTERPRETATION
Thinning of Mesozoic onto Guadalquivir Bank
EQU
LPU
Top Miocene
BFU
Moat
Paleogene removed not present
Change in bathymetry across Guadalquivir Bank
Ng+Qt
Pg
K1
J3
J2
J1
Es
Tr
Guadalquivir Basement High
AUGC
AUGC stops and folds against Guadalquivir Bank
Northward tilt due to uplift of Guadalquivir Bank
Bt
T3
c) DEPTH VERSION
Depth (km)
V=H
d) RESTORATION (Oligocene)
e) RESTORATION (Early Cretaceous)
Mesozoic faults
Cenozoic faults
Inferred fault
Inferred horizon
Cenozoic unconformities

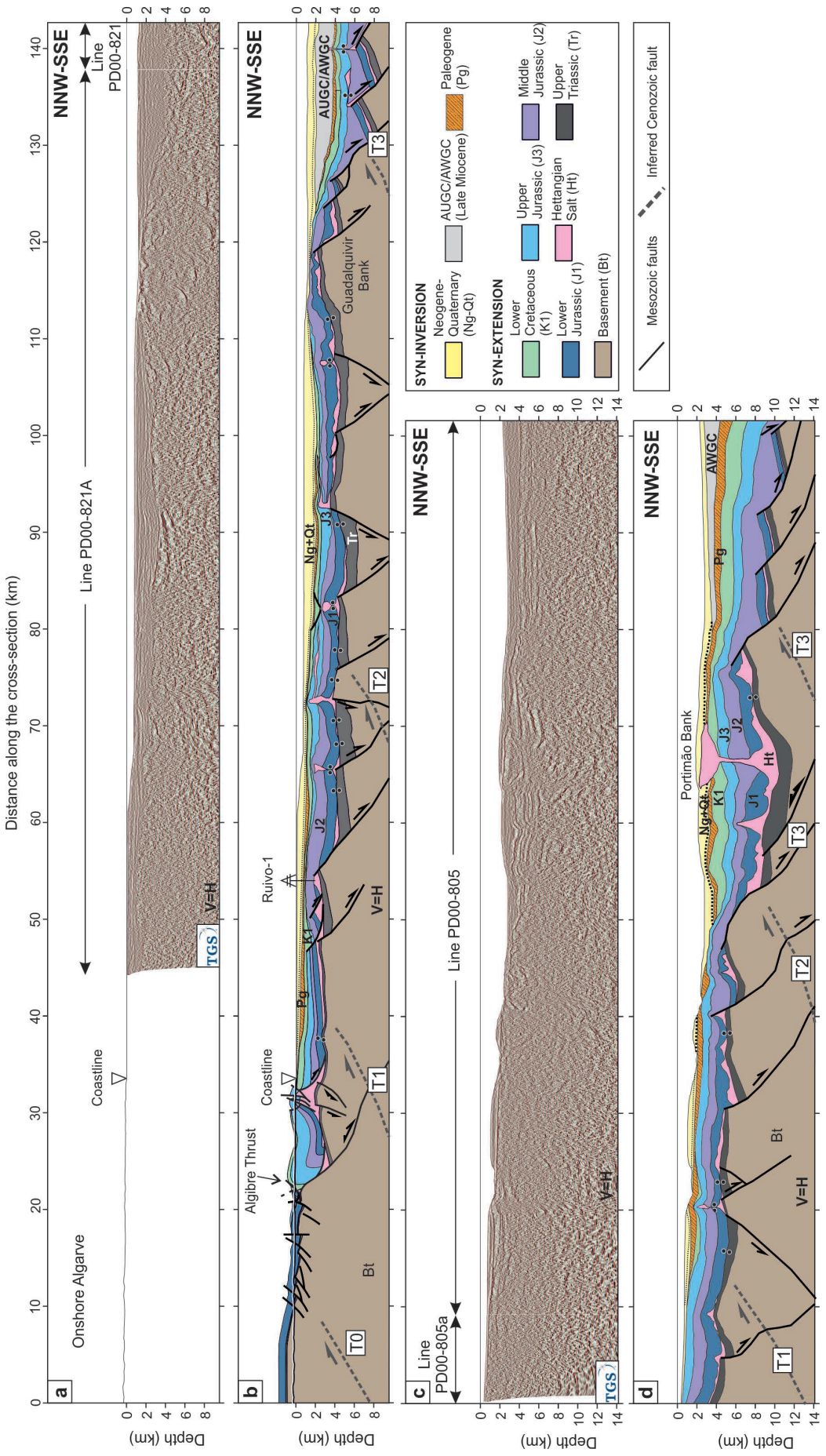
Distance along the cross-section (km)
a
NNW-SSE
Onshore Algarve
Coastline
Line PD00-821A
Line PD00-821
TGS
V=H
b
NNW-SSE
Algibre Thrust
Coastline
Ruivo-1
T0
T1
T2
T3
Bt
Pg
K1
J2
J1
J3
Tr
Ng+Qt
AUGC/AWGC
Guadalquivir Bank
V=H
c
NNW-SSE
Line PD00-805a
Line PD00-805
TGS
V=H
d
NNW-SSE
Portimão Bank
AWGC
Ng+Qt
Pg
K1
J3
J2
J1
Ht
T1
T2
T3
Bt
V=H
SYN-INVERSION
Neogene-Quaternary (Ng-Qt)
AUGC/AWGC (Late Miocene)
Paleogene (Pg)
SYN-EXTENSION
Lower Cretaceous (K1)
Upper Jurassic (J3)
Middle Jurassic (J2)
Lower Jurassic (J1)
Hettangian Salt (Ht)
Upper Triassic (Tr)
Basement (Bt)
Mesozoic faults
Inferred Cenozoic fault
Depth (km)

Figure 2.2.4. Cross-sections through the Algarve Basin showing the major contractional structures identified. (a) Composite seismic section through the central Algarve Basin. (b) Interpretation of the seismic in (a), with interpretation extended onshore and complemented with outcrop data. (c) Seismic section through the western Algarve Basin. (d) Interpretation of seismic in (c). Pairs of black dots represent salt welds. See Figure 2.2.1 for location. Seismic data courtesy of TGS.

Major steps of the basement, such as that south of the Portimão Bank (Fig. 2.2.2d), which coincide with a step in the BFU, have been interpreted to indicate a post-Mesozoic uplift. The BFU surface records Miocene and younger contractional deformation. (Fig. 2.2.4). To correlate the steps in basement at the scale of the basin, the BFU surface has been mapped in 3D (Fig. 2.2.5). The combination between the available seismic and the outcrop data allowed to define 4 WSW-ENE trending main steps in the regional elevation of the BFU and the basement (Fig. 2.2.5). These steps have been related to Cenozoic to Recent shortening. As mentioned above, uplift along the Guadalquivir Bank and the onshore northern limit of the basin are interpreted to be related with underlying south-verging basement-involved thrusts. These two fault structures, labelled T0 and T3 in Figures 2.2.4 and 2.2.5, bound the domain of contractional structures documented here. In between these two structures, two other main steps can be identified: i) a monocline shown in the Figure 2.2.4, labelled T2; ii) the T1, which corresponds to the Carcavai fault zone, a ENE-WSW contractional fault (e.g., Carvalho et al., 2012). The four main thrusts identified in the Algarve Basin locally deviate from their dominant WSW-ENE trend, forming a set of oblique ramps of the thrust system with NW-SE orientation (Fig. 2.2.5). In the offshore, thrusts T1, T2 and T3 and the above commented oblique structures liking them, also exert a control on the Neogene-Quaternary depocenters (Fig. 2.2.5).

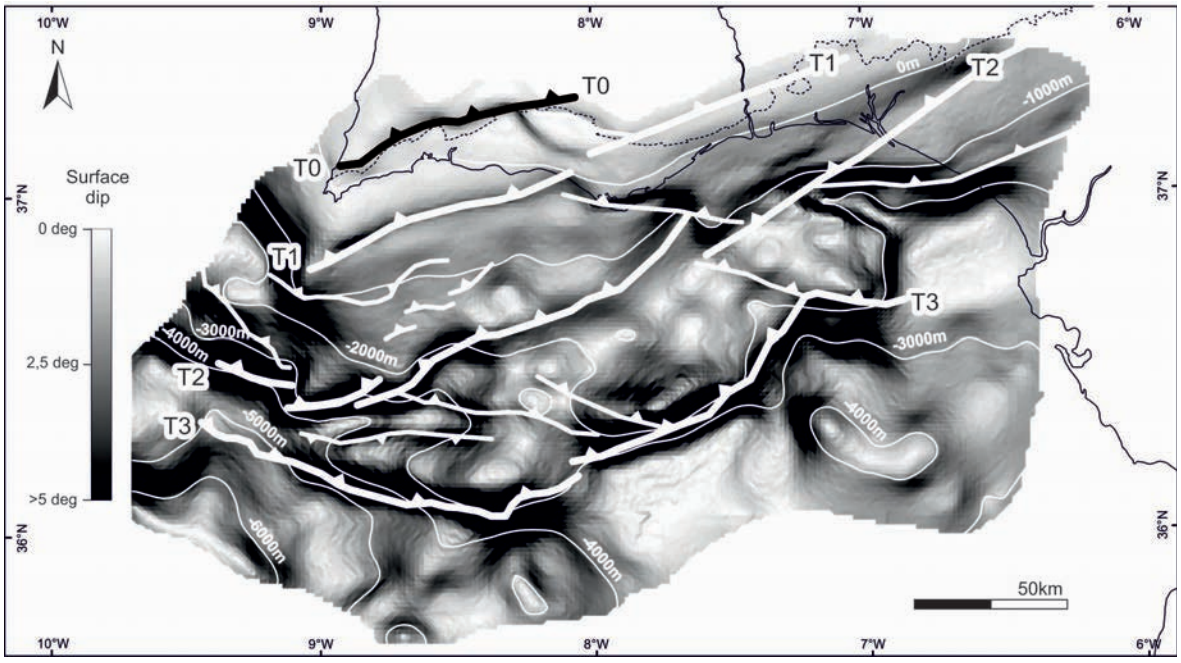

Figure 2.2.5. Map of the BFU coloured for dip, with white contours indicating depth below sea-level. Steeper parts of the surface indicate steps in the surface, interpreted to be related to erosional geometries or to the presence of underlying basement-involved blind thrusts (traces of the thrust tips shown in white lines).

The basement-involved thrusts control locally the present-day bathymetry, indicating neotectonic activity. Moreover, instrumental seismic activity and focal mechanisms in the area coincide with the location of these thrusts, along with other surrounding basement thrusts (e.g., Horseshoe Thrusts; Fig. 2.2.6).

Finally, the results obtained in this section show four main stages of contractional deformation identified in the Algarve Basin, consistent with those defined by Terrinha (1998) and Roque (2007): 1) Late Cretaceous to Paleogene; 2) Late Oligocene; 3) Middle to Late Miocene; and 4) Late Pliocene to Present.

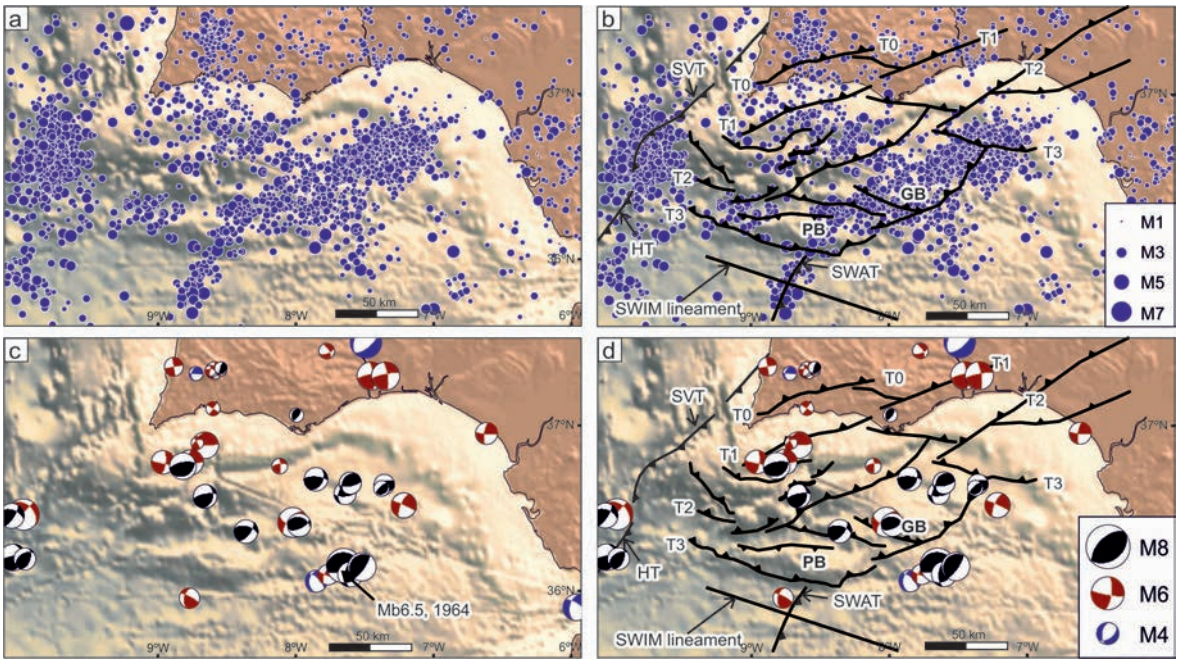

Figure 2.2.6. (a) Earthquake epicentres in SW Iberia, sized as a function of magnitude (modified after Palano et al. 2013). The earthquakes were recorded between 1951 and 2010, with magnitudes between 2.0 and 8.0 and depths down to ~30 km. (b) Location of the earthquake epicentres relative to the thrusts described in this paper. (c) Lower hemisphere, equal area projection for fault plane solutions, complied from several earthquakes; red for strike-slip faulting, black for thrust faulting and blue for normal faulting, modified after Palano et al. (2013). (d) Location of the focal mechanisms relative to the thrust faults described in the paper. GB: Guadalquivir Bank; PB: Portimão Bank; HT: Horseshoe Thrust; SVT: São Vicente Thrust; SWAT: South West Algarve Thrust.

2.3. SALT TECTONICS

The availability of regional 2D seismic surveys and high-resolution 3D seismic, along with well and gravity data, allowed to unravel the structural evolution related to salt tectonics (including the emplacement of a large allochthonous salt body) and the initial configuration of the evaporite basin,

The paper titled "Impact of basin structure and evaporite distribution on salt tectonics in the Gulf of Cadiz, Southwest Iberian margin" and included in the appendix 1.3 deals with detail of the salt structures and the evaporite basin configuration.

The Algarve Basin is characterized by a wide variety of salt structures, such as diapirs, salt walls and allochthonous salt bodies (Fig. 2.3.1). Along the northern onshore part of the margin, they only appear south of the Algibre Fault, where the salt-related structures relate to major thickness changes in the surrounding Jurassic sediments and, locally, in the Lower Cretaceous.

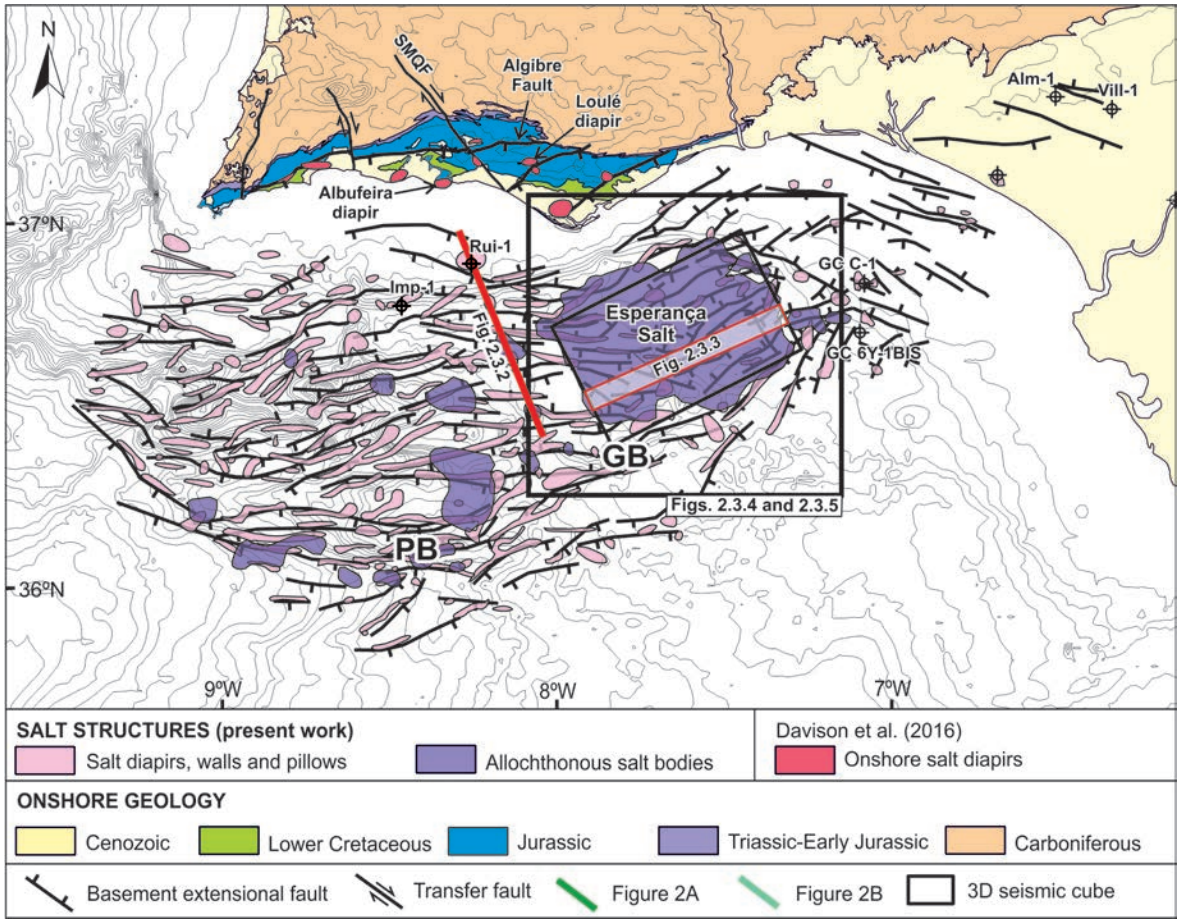

Figure 2.3.1. Map of salt structures and the extensional fault system of the basement in the Algarve Basin on the SW Iberian margin. Salt structures mapped in this paper are depicted by pink polygons, their area defined by the cut-off of the top of the Lower Jurassic succession. Allochthonous units are shown by lilac polygons, mapped according to their greatest lateral extent. Onshore diapirs are taken from Davison et al. (2016). GB: Guadalquivir Bank; PB: Portimão Bank. Notice the same orientation and location between the basement extensional faults and the salt structures through the margin, from onshore to offshore. The precise location of Figures 2.1.2 and 2.1.3 that cross the 3D seismic survey is not shown due to confidentiality issues; the outline of the 3D seismic cube is shown nonetheless.

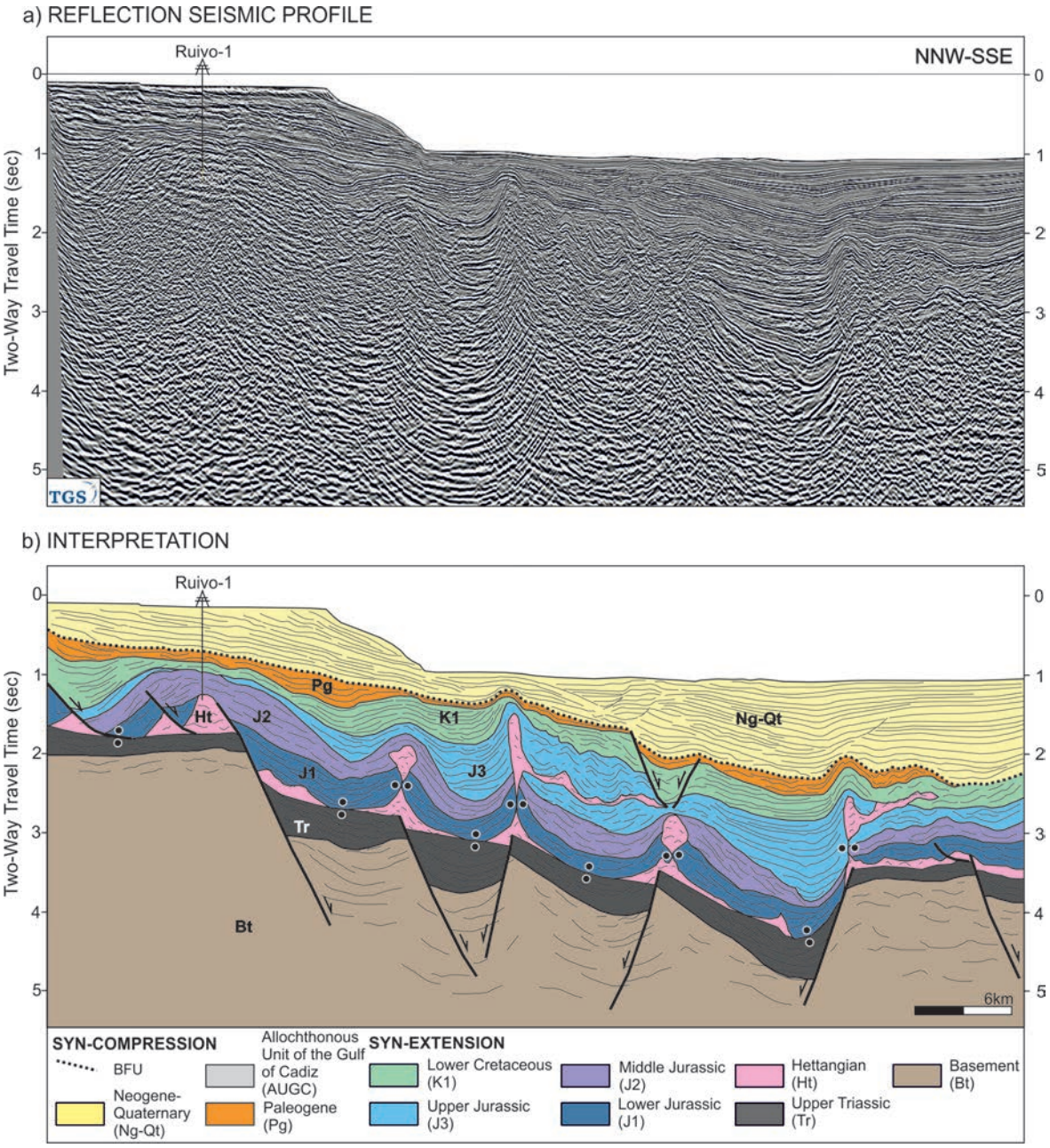

Figure 2.3.2. (a) Seismic section in time. (b) Interpreted section illustrating various salt-related structures and their link to underlying basement structures. See Figure 2.3.1 for location. Data courtesy of TGS.

To the south, offshore, salt structures are more prominent than onshore, with well-developed Jurassic salt withdrawal mini-basins (Fig. 2.3.2). To the west, the salt bulbs are more evident and the presence of allochthonous bodies increases (Fig. 2.3.1 and 2.3.2).

Salt structures tend to be located in the footwall of basement extensional faults. The BFU is in most of the cases folded above the diapirs (Fig. 2.3.2) and truncates the underlying Jurassic, Lower and Upper Cretaceous, and Paleogene sediments. The Miocene sediments onlap the salt-related positive relief of the BFU (Fig. 2.3.2).

Salt structures were triggered by extensional deformation at Early Juraais times and continued growing by downbuilding of Mesozoic layers from Early Jurassic to Early Cretaceous (Fig. 2.3.2). Paleogene sediments also show thickness variations into mini-basins in the westernmost part of the basin. Cenozoic compression during Late Paleogene and Neogene caused the reactivation and squeezing of the salt structures.

The most remarkable allochthonous salt body in the margin is the Esperança salt sheet (e.g., Matias et al., 2011), consisting of a highly deformed evaporite unit (Fig. 2.3.3) covering an area roughly 40x60 km (Figs. 2.3.1 and 2.3.4). The Esperança salt sheet is considered to be the largest allochthonous salt body in the basin (Fig. 2.3.1).

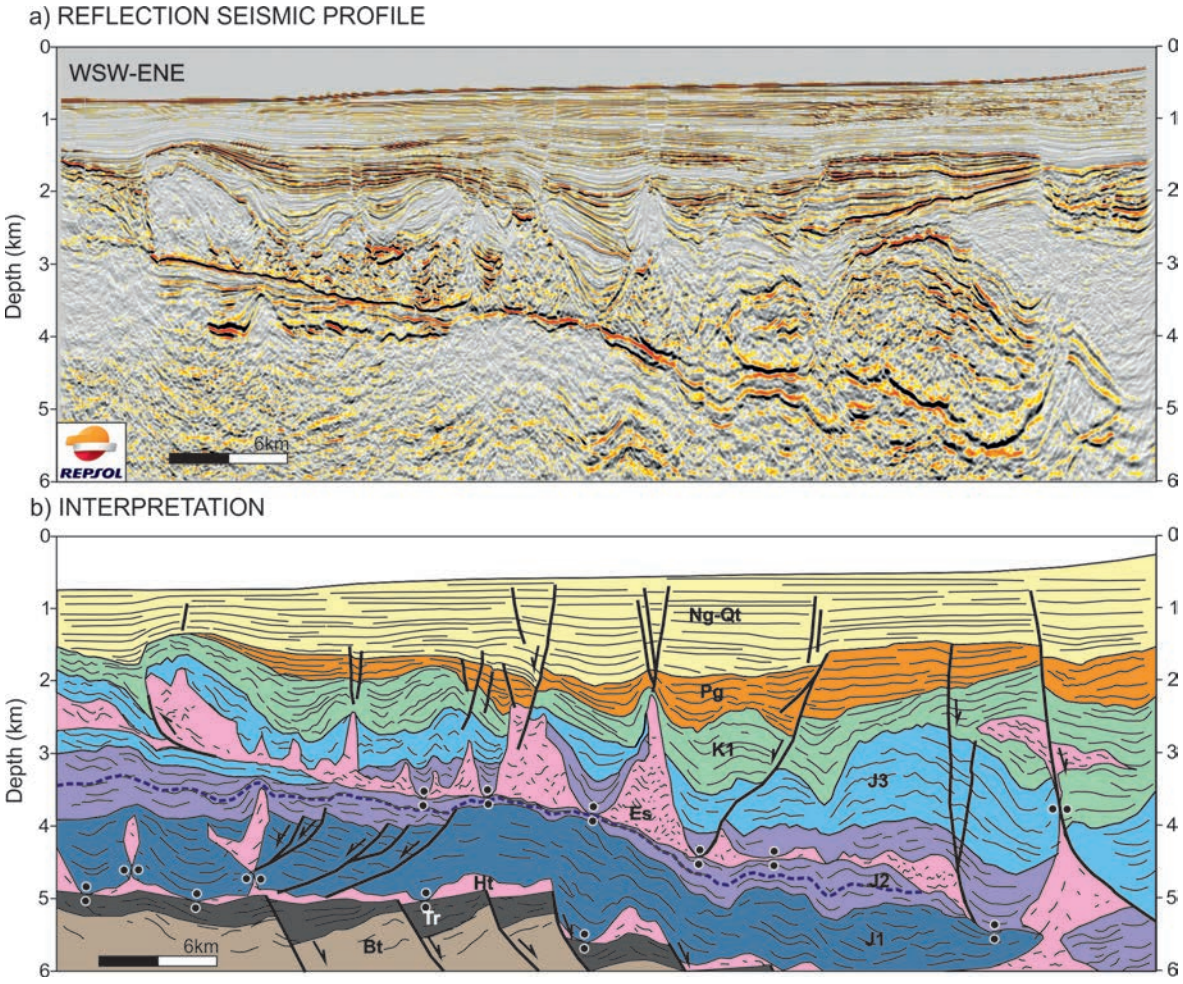

Figure 2.3.3. (a) Seismic section in depth across the Esperança salt sheet. (b) Interpretation of the seismic section. The section shows how the base of the Esperança salt sheet truncates progressively younger sediments towards the west. The section also illustrates the contrast between the strong control of halokinetics on sediments above the allochthonous Esperança salt sheet, and the limited amount of salt-related deformation observed below the Esperança salt sheet. The dashed line within the Middle Jurassic is the unconformity mapped to generate the map in Figure 2.3.4. See Figure 2.3.1 for location and Figure 2.2.2 for legend. Es: Esperança salt sheet. Data courtesy of Repsol.

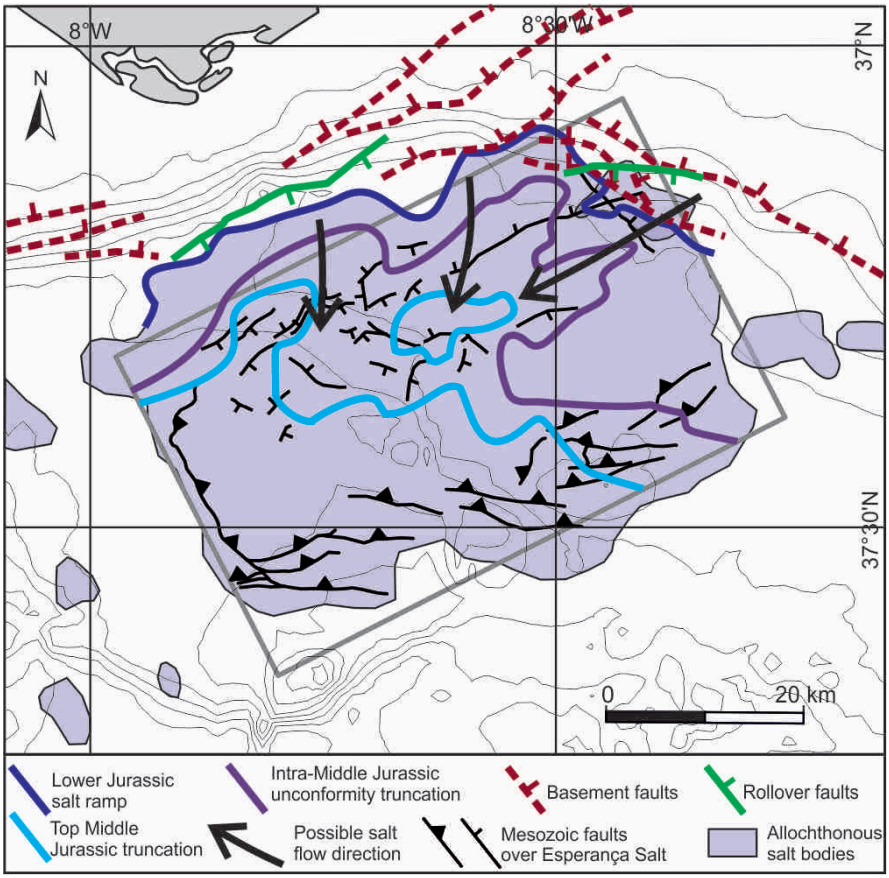

Figure 2.3.4. Map of features associated with the emplacement of the Esperança salt sheet. The intersection of the base of the Esperança salt sheet with 3 underlying Jurassic horizons indicates south and west directed emplacement, consistent with supra-salt deformation features indicating extension in the north and contraction along the southern and western edge of the allochthonous salt. The L-shaped trace of the feeder ramp for the Esperança salt sheet is related to the configuration of basement faults that controlled evaporite deposition (in this map only a selection of basement faults is shown; a more complete map can be seen in the Fig. 2.3.5). See Fig. 2.3.1 for location.

Mapping of the Jurassic ramp beneath the Esperança salt sheet has allowed to define the L-shaped trace of its source in map view (Fig. 2.3.4). This shape is the result of two trends of basement faults striking WSW-ENE and NW-SE. Expulsion rollover anticlines are seen over these basement faults (Fig. 2.3.2).

The Esperança salt sheet was emplaced over a feeder ramp climbing up to the south and west. The transport of the allochthonous salt triggers the formation of WSW-ESE and NW-SE extensional faults detaching on the Esperança salt structure in the northern part (Figs. 2.3.4 and 2.3.5c), with associate Mesozoic depocenters. To the south, the frontal contractional structures formed a linked system with the extensional ones to the north. Contractional structures at the front consist of NW-SE and WSW-ENE thrusts (Fig. 2.3.4), which have folded the overlying sediments. These thrusts were reactivated during the Late Cretaceous-Cenozoic contractional event. To the south, the Esperança salt sheet is bounded by the Guadalquivir Bank, acting as a backstop for its southward progression. Extension under Esperança salt

sheet was firstly accommodated by ENE-WSW to WSW-ENE basement extensional faults during Triassic and Early Jurassic (Figs. 2.3.3 and 2.3.5a). During the Jurassic, the extensionwas also accommodated by minor-scale extensional faults, mostly dipping towards the north and northwest (Figs. 2.3.3 and 2.3.5a), affecting Lower and Middle Jurassic sediments and detaching on the autochthonous Hettangian evaporite unit (Fig. 2.3.3). The signal of this complex system of Mesozoic and Cenozoic faults is also observable on gravity anomaly maps (Fig. 2.3.5b,d).

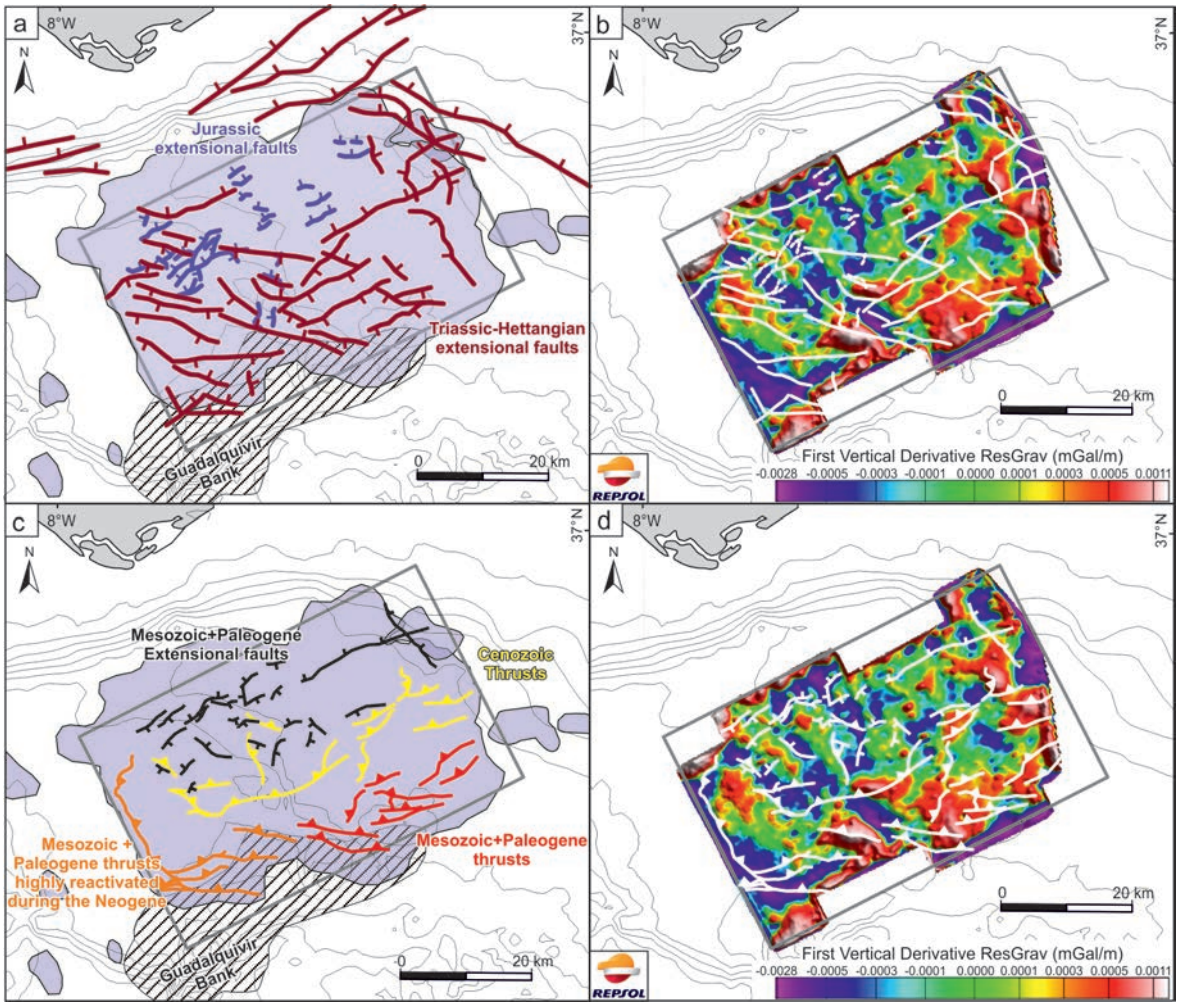

Figure 2.3.5. Maps of sub- and supra-Esperança structures and their gravimetric signal. (a) Sub-Esperança structures: Mesozoic-age extensional faults affecting the basement (brown) and shallow detachment faults causing tilting of Jurassic fault blocks (purple). (b) Overlay of the structures in (a) on a map of the first vertical derivative of the second-order residual Bouguer anomaly. (c) Supra-Esperança structures: Extensional faults (black) and thrusts (red and orange) related to the emplacement of the Esperança salt sheet in the Mesozoic, and Cenozoic-age thrusts detached in the Esperança salt sheet formed during contraction (yellow), including the reactivation of Mesozoic and Paleogene thrusts during the Neogene (orange). (d) Overlay of the structures in (c) on a map of the first vertical derivative of the second-order residual Bouguer anomaly. See Fig. 2.3.1 for location. Data courtesy of Repsol.

The Esperança Salt structure was interpreted as a Roho system (Matias et al., 2011). New data show more detailed features of the nappe that suggest a more complex interpretation of its emplacement., The Esperança salt sheet is interpreted to be emplaced over a domain of reduced evaporite thickness and possibly more rich in anhydrite, interpreted to be a relative basement high during the Mesozoic. North of the Esperança salt sheet, a great sediment influx from the margin allowed for the development of thick Jurassic depocenters above the Hettangian evaporites that led to the expulsion of the allochthonous salt to the south. The L-shaped trend of the allochthonous feeder is interpreted as a variant of a plug-fed extrusion (Hudec and Jackson, 2006) in which the feeder is linear, initially a Lower Jurassic salt wall. Salt extrusion started in Early Jurassic or in Middle Jurassic. Once the initial canopy was emplaced, it was remobilized by roof sedimentation and extensional faults leading to its frontal advacne (Diegel et al., 1995; Peel et al., 1995; Schuster, 1995). Thus, the basal ramp of the allochthonous body gradually truncated the underlying stratigraphy during its emplacement, similar to the case documented by Ings and Shimeld (2006) (Fig. 2.3.6).

The velocity of emplacement of this salt body is estimated to be less than 1mm/yr, comparable to those for the Sigsbee Salt in the Gulf of Mexico (e.g., Peel et al., 1995). Nevertheless, the irregularity of the intersections between some Jurassic unconformities and the Esperança salt sheet is an indicative of the variability in the direction and velocity of salt emplacement.

Figure 2.3.6. Conceptual model for the development and evolution of the Esperança salt structure. (a) Evaporite depocenters formed during the Hettangian in fault-bounded half-grabens are capped by Sinemurian units during a period of tectonic quiescence. (b) Reactivation of basement faults during the latter part of the Early Jurassic causes initial development of salt rollers due to extension of the overburden. (c) Continued extensional faulting of the basement during the Middle Jurassic caused basement fault blocks to tilt further basinward, facilitating the development of listric extensional faults and salt evacuation basinward above a relative basement high. (d) Welding in the feeder area coincides with the final stages of extension in the Late Jurassic. A Roho system developed above the salt sheet with a linked contractional system at the toe. (e) During the Early Cretaceous, basement faulting had ceased and evolution of the Esperança salt sheet was controlled by sediment-driven salt evacuation. See Figure 7 for legend. Horizontal scale is approximate, vertically exaggerated.

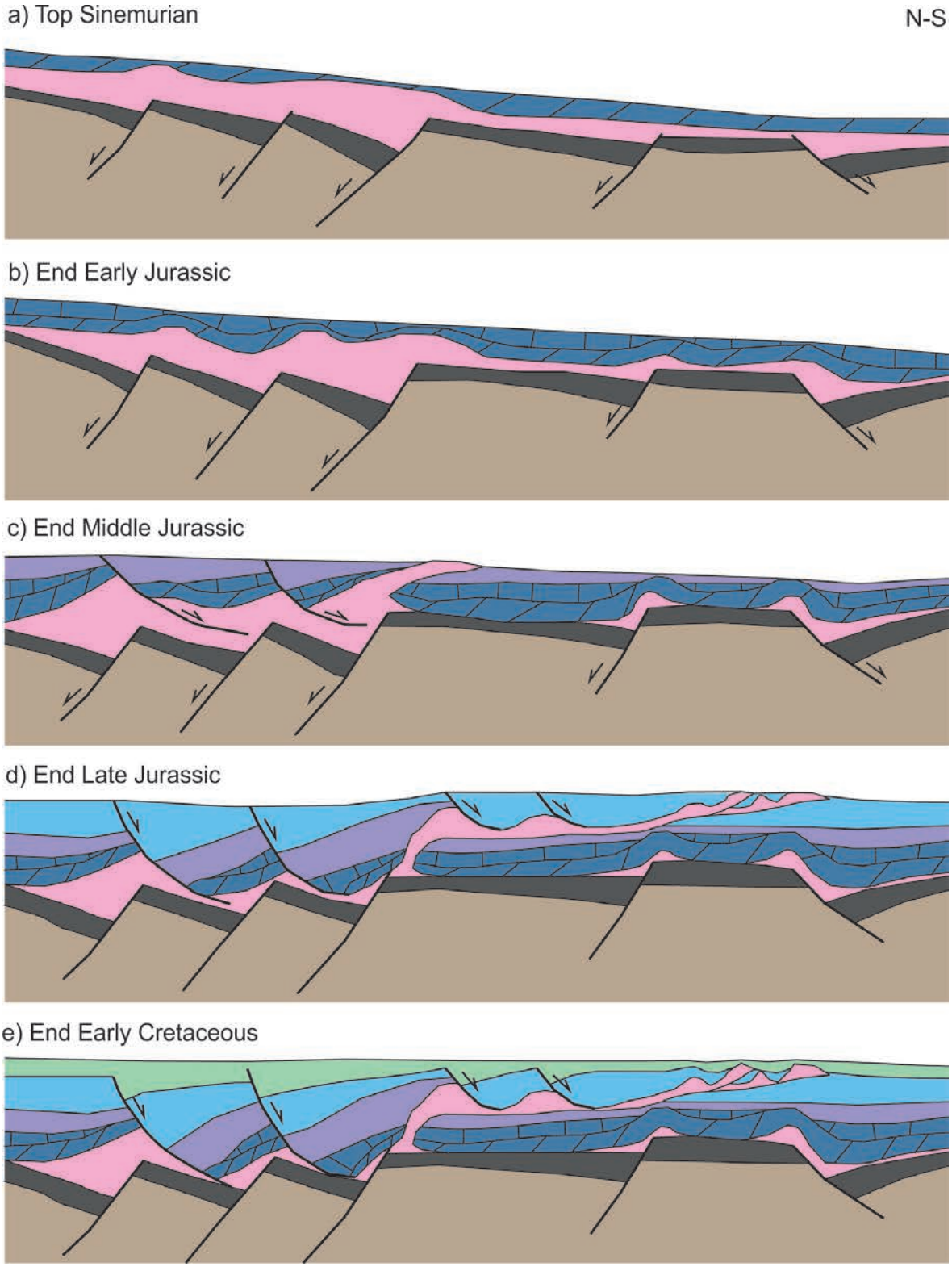
a) Top Sinemurian
N-S
b) End Early Jurassic
c) End Middle Jurassic
d) End Late Jurassic
e) End Early Cretaceous

2.4. CRUSTAL STRUCTURE OF THE SW IBERIAN MARGIN

The interpretation of the crustal structure of the SW Iberian margin has been integrated with the previous works in the Gulf of Cadiz during the past decades. The first study that documented the crustal thinning in the margin concluded that the crust underwent continuous thinning towards the southwest (González et al., 1996). Later, a series of geophysical studies were carried out to better define the deep structure of the margin. These studies concluded that the crust thins from 30-32 km in the mainland to 25 km in the central part of the Algarve Basin and to 15 km in the most western parts (Dañobeitia et al., 1999; Gràcia et al., 2003; Gutscher et al., 2002, 2009; Zeyen et al., 2005).

Interpretation of seismic reflection profiles can shed some light on the processes and domains that configured rifted margins. Nevertheless, the depth and accuracy of reflection profiles are not enough to interpret the deepest parts of a passive margin. Gravimetric modelling has been carried out in order to constrain the crustal configuration of the SW Iberian margin based on the seismic interpretation. Other authors used similar techniques to study other rifted margins (Korenaga et al., 2001; Kvarven et al., 2014; Mjelde et al., 1998; Nirrengarten et al., 2014; Wilson et al., 2003). Gravity modelling was performed in four 2D transects across the SW Iberian margin (Fig. 2.4.1).

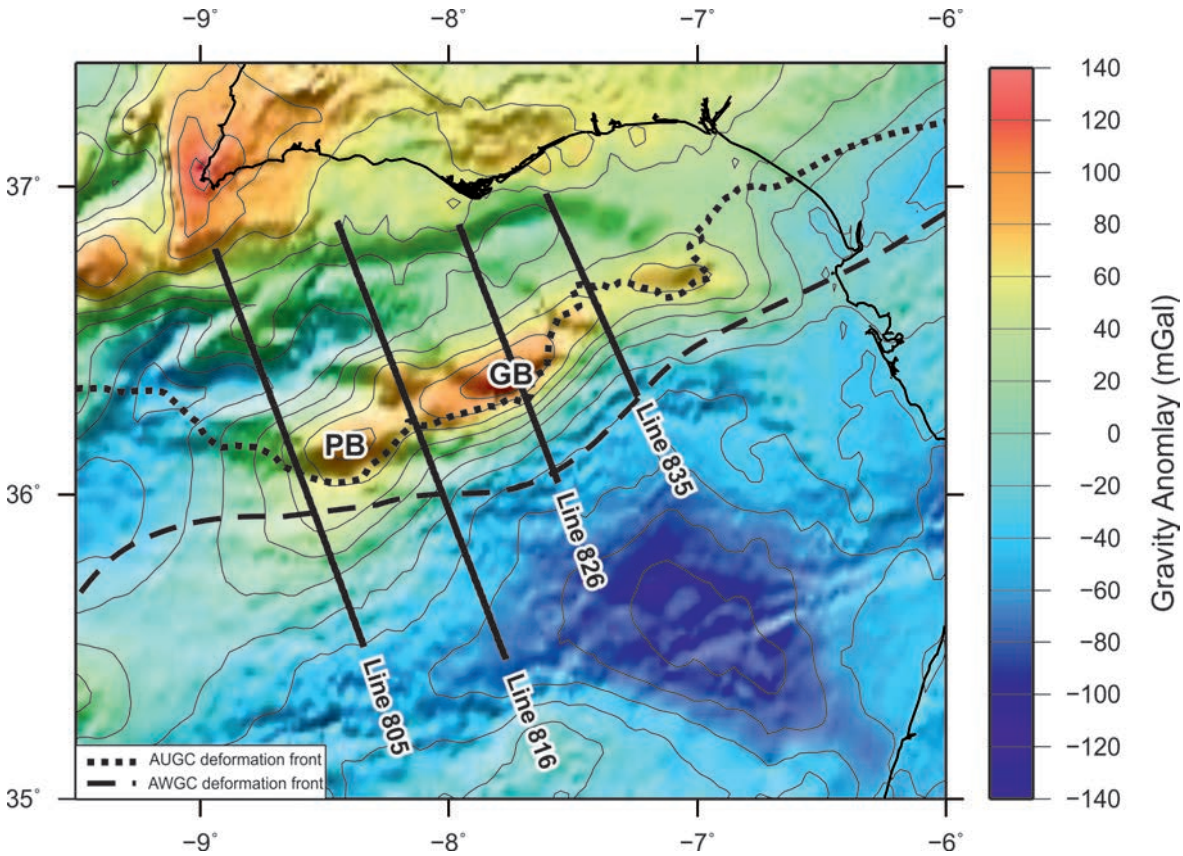

Figure 2.4.1. Map of free-air gravity anomaly offshore and Bouguer anomaly onshore. Black lines show the location of the 2D gravimetric profiles presented in this study. Note the ENE-WSW trending positive gravity anomaly located offshore (> 40 mGal), and the negative gravity anomaly (<-60 mGal) to the SE. GB: Guadalquivir Bank; PB: Portimão Bank.

The paper titled “Crustal structure of the SW Iberian passive margin: The westernmost remnant of the Ligurian Tethys?”, included in the appendix 1.4 is an attempt at understanding the crustal structure of this margin. Four regional 2D lines striking NNW-SSE (Figs. 2.4.2 and 2.4.3), perpendicular to the main extensional trend, were interpreted. Crustal thicknesses from previous works (Palomeras et al., 2009; Sallarès et al., 2011; Simancas et al., 2003) were used as initial input.2D seismic quality is good enough to interpret almost the shallow stratigraphic units, nevertheless, the interpretation was hindered to the south of Guadalquivir-Portimão Bank due to the poor image quality under the AUGC/AWGC.

The structure of the margin as interpreted on the 4 profiles (Figs. 2.4.2 and 2.4.3) is characterized by both south and north dipping extensional faults, with growth from Triassic to Middle Jurassic. The main trend of these Mesozoic extensional faults is ENE-WSW to E-W, relayed by NNW-SSE to NW-SE trending transfer zones.

Throw of the extensional faults and thickness of Jurassic depocenters increases southwards. The geometry of basement faults in the highly extended domain was based on the location and tilt of Jurassic depocenters. In the highly extended domain the basement faults tend to be low-angle extensional faults, indicating larger magnitude of crustal stretching and thinning. Uplift in the Miocene of the Guadalquivir and Portimão banks accentuates the apparent throw of the extensional faults.

The geometry of the seismic interpretation, information from all available seismic data and previous 2D geophysical modelling (González et al., 1998; Gutscher et al., 2002; Sallarès et al., 2011), were useful to build the four gravity models made in this study (Figs. 2.4.2 and 2.4.3).

Gravity modelling validated the top of basement, with little changes on the Triassic depocenters. At the crustal scale, the most evident feature resulting from gravimetric modelling is the change in crustal thickness from north to south, and four key domains were defined. The northern domain (proximal domain) is characterized by crust of a 26-30 km thick (Figs. 2.4.2 and 2.4.3). The incensement of the gravity signal to the south is due to the crustal thinning (Figs. 2.4.2 and 2.4.3). The thinning domain is wider to the west (Figs. 2.4.2 and 2.4.3).

In the eastern part of the margin (over the Guadalquivir Bank), the stretching factor (β) increases rapidly, while to the west (over the Portimão Bank) the transition is more gradual spreading across a broader area. However, the transition in stretching factors from the inner to outer portions of the margin is the same.

In the case of Portimão Bank (Fig. 2.4.2a) the gravity anomaly is broad due to the greater width of the necking domain. Crustal thinning further east (Fig. 2.4.3b) is more abrupt on account of the initial extensional geometry (one major extensional fault) and coincides with an uplifted basement (Guadalquivir Bank: Vegas et al., 2004), which explains the narrower and greater positive anomaly.

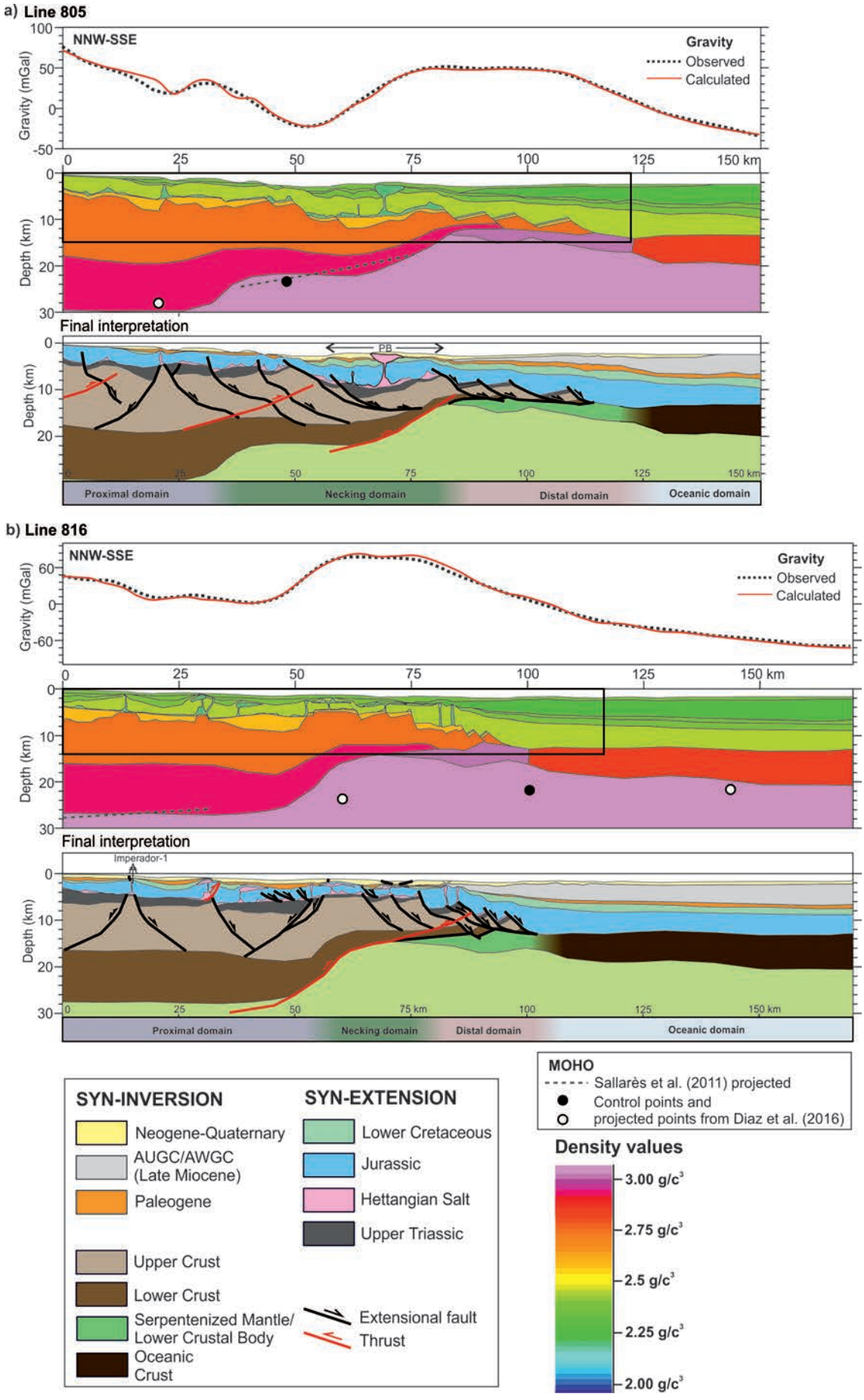
a) Line 805
NNW-SSE
Gravity
Observed
Calculated
Gravity (mGal)
Depth (km)
Final interpretation
PB
Proximal domain
Necking domain
Distal domain
Oceanic domain
b) Line 816
NNW-SSE
Gravity
Observed
Calculated
Gravity (mGal)
Depth (km)
Final interpretation
Imperador-1
Proximal domain
Necking domain
Distal domain
Oceanic domain
SYN-INVERSION
Neogene-Quaternary
AUGC/AWGC (Late Miocene)
Paleogene
Upper Crust
Lower Crust
Serpentenized Mantle/ Lower Crustal Body
Oceanic Crust
SYN-EXTENSION
Lower Cretaceous
Jurassic
Hettangian Salt
Upper Triassic
Extensional fault
Thrust
MOHO
Sallarès et al. (2011) projected
Control points and
projected points from Diaz et al. (2016)
Density values
3.00 g/c3
2.75 g/c3
2.5 g/c3
2.25 g/c3
2.00 g/c3

Figure 2.4.2. Composition of observed and forward modelled gravity, density model and final interpretation for profiles along lines 805 (a) and 816 (b). The geometry of the sedimentary layers, from Triassic to Quaternary, has been derived from the interpretation of MCS data. Extent of the seismic profiles is represented by a black box on the density model. The Moho from the profile of Sallarès et al. (2011) has been projected onto the density models over the pertinent segments. Points from the compilation by Diaz et al. (2016) lying on the modelled profiles (black) and projected from nearby locations (white) are also shown on the density model. On the final interpretation note the combination of Mesozoic extensional and Cenozoic contractional features. See text for a discussion of the defined crustal domains. PB: Portimão Bank. See Fig. 2.4.1 for location.

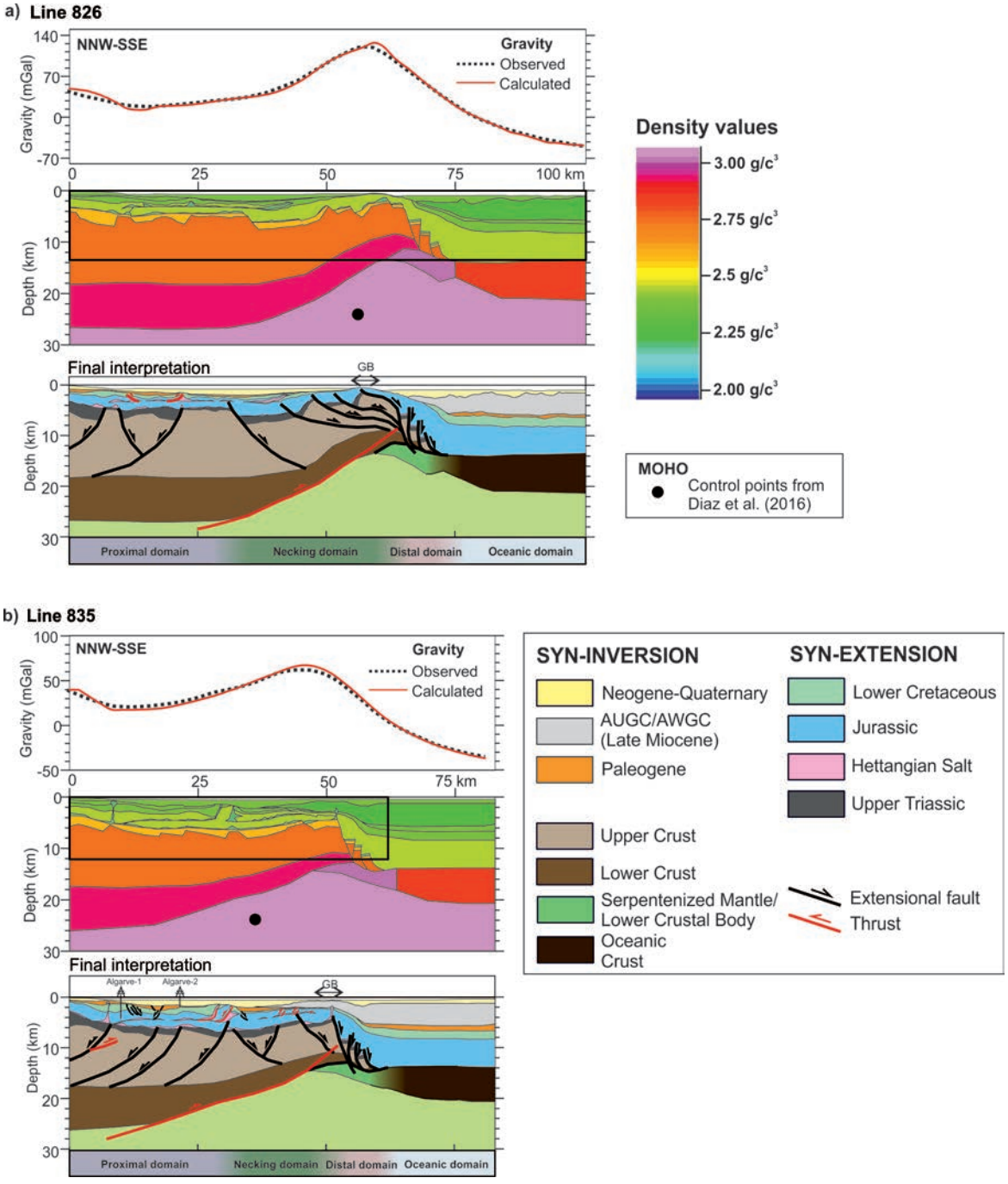

Figure 2.4.3. Composition of observed and forward modelled gravity, density model and final interpretation for profiles along lines 826 (a) and 835 (b). The geometry of the sedimentary layers, from Triassic to Quaternary, has been derived from the interpretation of MCS data. Extent of the seismic profiles is represented by a black box on the density model. The Moho control points from Diaz et al. (2016) are shown on the density model. On the final interpretation note the combination of Mesozoic extensional and Cenozoic contractional features. See text for a discussion of the defined crustal domains. GB: Guadalquivir Bank. See Fig. 2.4.1 for location.

It is interpreted that fragments of continental crust are still present for some distance south of the Guadalquivir-Portimão Bank (Figs. 2.4.2 and 2.4.3). In between the thicker continental crust and true oceanic crust, it is therefore inferred the presence of a domain of highly thinned and fragmented continental crust underlain by mantle at very shallow depths (12 km depth, Figs. 2.4.2 and 2.4.3). A shallow unit of low density mantle material has been interpreted forming the distal domain and best fit the gravity anomaly accordingly to the geological setting. The material forming the basement could correspond to serpentinized mantle (Figs. 2.4.2 and 2.4.3). To the south, the extent of the distal domain remains uncertain, given that the AWGC/AUGC masks the image in the transition to distal domain.

Gravity modelling shows a Moho rising southeastward (and the crustal thinning at the same direction, perpendicular to the margin; Fig. 2.4.4), consistent with the data from Diaz et al. (2016). Towards the west, the control points for the Moho, taken from González et al. (1996) and Sallarès et al. (2011), show the Moho rising towards the southwest (Fig. 2.4.4). This SW direction of the Moho rising coincides with the transition from continental to oceanic crust (González et al., 1996; Sallarès et al., 2011), and with the presence of extensional faults dipping to the southwest (Fig. 2.3.1). In this part of the margin, the abrupt continent-oceanic crust transition (Fig. 1.1.3; Sallarès et al., 2011) is interpreted to correspond to a major transfer zone linking the exhumed mantle of the Gorringe Bank and the proposed exhumed mantle of the Portimão Bank (Gorringe-Gulf of Cadiz transfer zone; Fig. 2.4.4). To the east, the lateral continuity of the passive margin is also interrupted. The eastwards thinning of Mesozoic ends under the foreland Guadalquivir basin (Lanaja, 1987). Moreover, the basement rises up to the east, affected by NW-SE extensional faults. This is interpreted to respond to the presence of another major feature, the NW-SE Gulf of Cadiz-Betics transfer zone (Fig. 2.4.4).

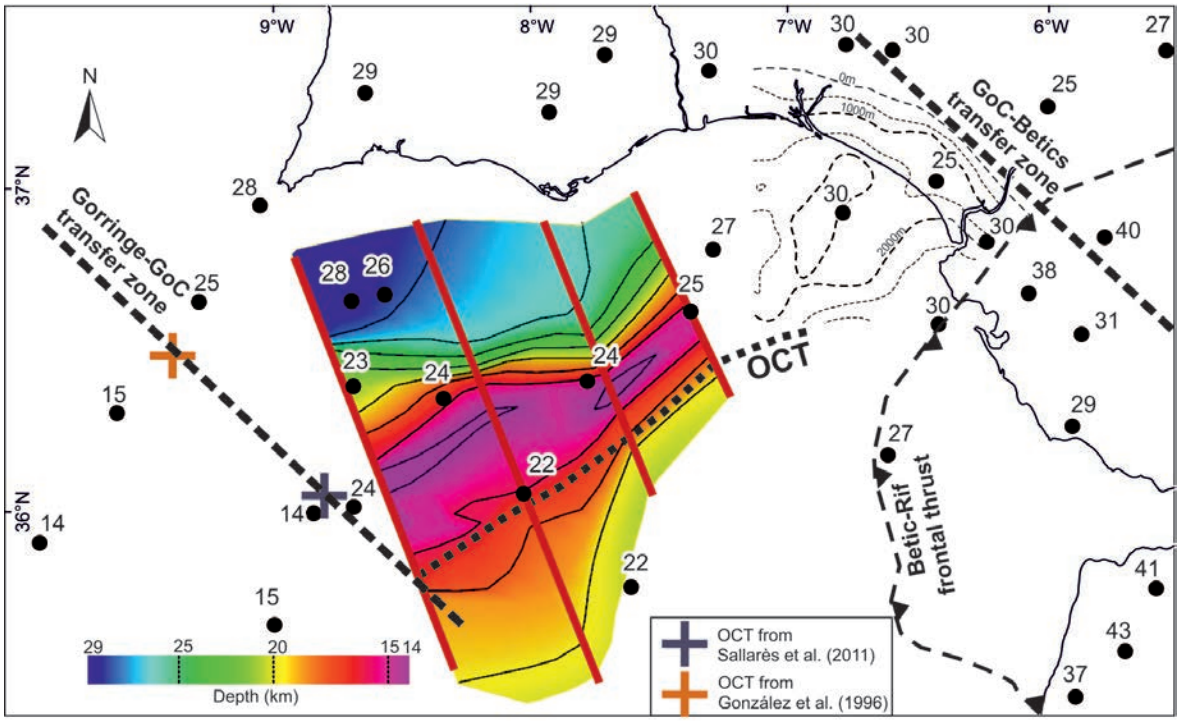

Figure. 2.4.4. Map of the base of the crust derived from seismic interpretation and gravimetric modelling. The OCT (ocean-continent transition) derived from gravimetric modelling is shown by the bold dashed line. Points with numbers indicate the depth to the base of the crust from the compilation of Diaz et al. (2016). The western limit of the Gulf of Cadiz (GoC) segment of the margin is marked by the Gorringe-GoC transfer zone along the transition from ocean to continental domains defined by González et al. (1996) and Sallarès et al. (2011). The eastern limit of the margin segment is located along the GoC-Betic transfer zone, across which Mesozoic thickness drops (dashed contours indicate Mesozoic thickness in this area).

2.5. PALEOGEOGRAPHY

This chapter documents the regional geologic and paleogeographic evolution of the SW Iberian passive margin, from the Mesozoic extension to the Late Cretaceous-Cenozoic inversion, as a segment of a passive margin.

The paper titled “Paleogeographic evolution of a segmented oblique passive margin: the case of the SW Iberian margin” and included in the appendix 1.5 explain in more detail the evolution of this margin. Geophysical data, well data and onshore data were integrated to build paleogeographic reconstructions for the margin for eight periods: 1) Late Triassic, 2) Hettangian, 3) Early Jurassic, 4) Middle Jurassic, 5) Late Jurassic, 6) Early Cretaceous, 7) Late Cretaceous and 8) Paleogene.

The initial stages of extension in the margin are Triassic in age. The extensional faults controlled the deposition of alluvial to fluvial facies along the entire basin margin, based on outcrop and well data. Towards the south, the Triassic unit thickens in order to define two broad and thick depocenters, both up to 1000 m thick (Fig. 2.5.1a). The orientation of these depocenters is almost opposite: NE-SW in the central basin vs. WNW-ESE to the west (Fig. 2.5.1a). The sedimentation in these depocenters may have been dominated by fine grained deposits.

Hettangian evaporites are involved in diapiric structures at present-day. Where deformation of the Hettangian unit is significant, particularly in the distal Algarve Basin, the initial thickness has been estimated based on the total cross-sectional area of the Hettangian interpreted at present-day, assuming the preservation of area on each section and no loss of evaporite through time.. As Triassic, Hettangian evaporites also thicken towards the south, up to 600 m thick (Fig. 2.5.1b), to the north and south of the Guadalquivir Bank. The trend of the initial Hettangian evaporite thickness coincides with the distribution of the evaporite facies, along with outcrops and wells (Fig. 2.5.1b). This trend describes the model of bulls-eye pattern, with the most soluble salts (halite) in the basin centre (Nichols, 2009; Rouchy and Caruso, 2006).

The Lower Jurassic succession is affected by the initial rifting phase, which causes an irregular thickness distribution (Fig. 2.5.1c), due to the basement extensional fault activity and the salt tectonics initiated during this period. Thickness tends to increase towards the south, up to 1000 m thick (Fig. 2.5.1c). Major thickness is localized in two major depocenters, one E-W oriented to the east, and another one NNW-SSE to the west (Fig. 2.5.1c). This unit is composed by carbonates deposited in neritic environments in the northern margin. To the south, bathyal conditions are interpreted in the higher subsidence areas (Fig. 2.5.1c).

Triassic, Hettangian and Lower Jurassic basins are limited to the west by the Gorringe-Gulf of Cadiz transfer zone at present day (Fig. 2.5.1a,b,c). This transfer zone lies parallel to the western depocenter of these maps (Fig. 2.5.1a,b,c). To the east, these basins extend to the Betic Basin across the Gulf of Cadiz-Betics transfer zone. The Lower Jurassic map shows how the São Vicente transfer zone limits the two main depocenters (Fig. 2.5.1c).

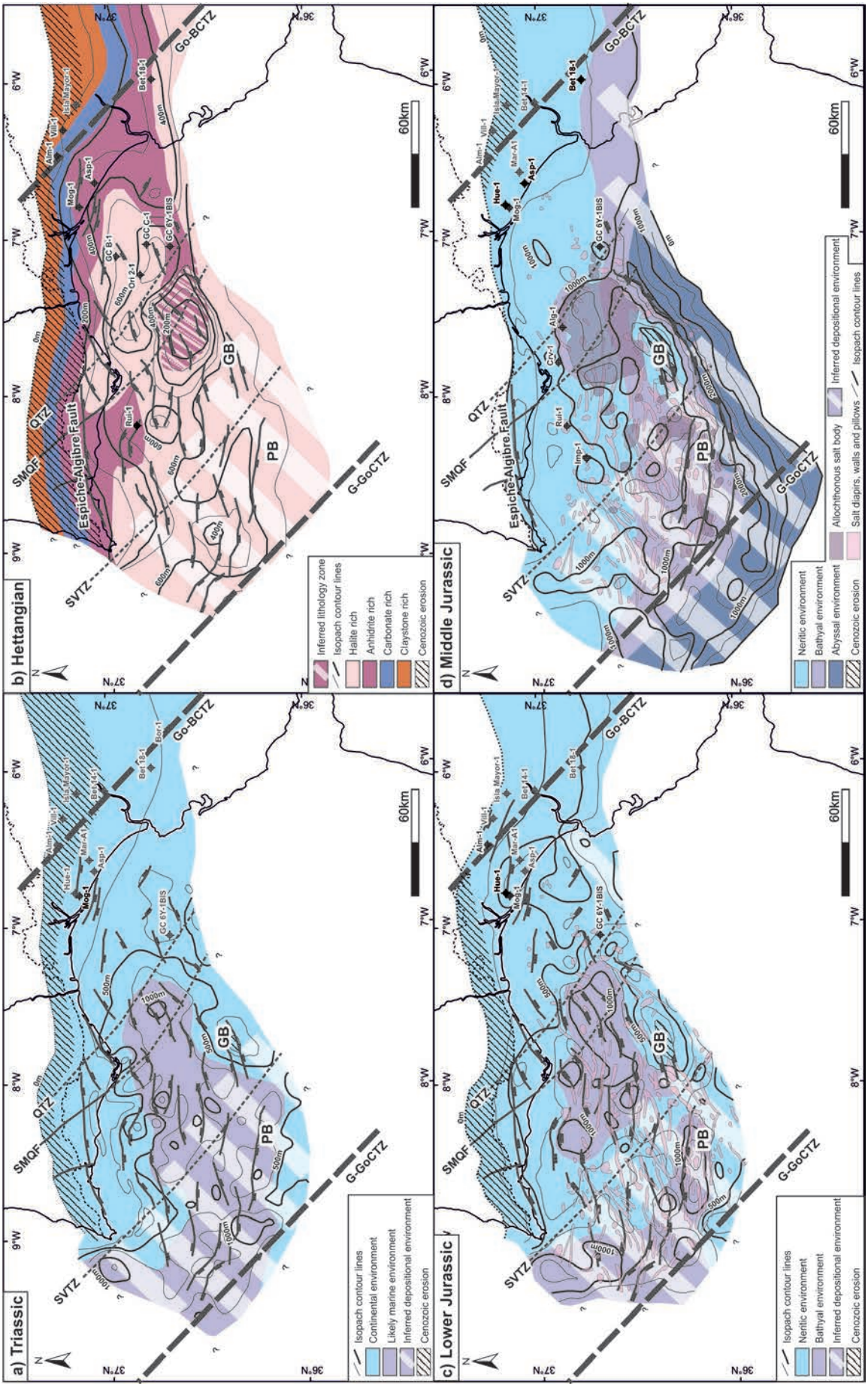
a) Triassic
b) Hettangian
c) Lower Jurassic
d) Middle Jurassic
SMQF
QTZ
SVTZ
G-GoCTZ
Go-BCTZ
Espiche-Algibre Fault
GB
PB
Aim-1
Vill-1
Isla Mayor-1
Mar-A1
Asp-1
Mog-1
Hue-1
Bej-14-1
Bet 18-1
Bor-1
GC 6Y-1BIS
GC C-1
CC B-1
Ort 2-1
Rui-1
Imp-1
Alg-1
CC-1
60km
Isopach contour lines
Continental environment
Likely marine environment
Inferred depositional environment
Cenozoic erosion
Inferred lithology zone
Halite rich
Anhidrite rich
Carbonate rich
Claystone rich
Neritic environment
Bathyal environment
Abyssal environment
Allochthonous salt body
Salt diapirs, walls and pillows

Figure 2.5.1. Isopach maps of Triassic to Middle Jurassic units of the SW Iberian margin with interpreted paleogeographic water depths. (a) Triassic. (b) Hettangian map, with the distribution of evaporitic facies. (c) Early Jurassic. (d) Middle Jurassic. See text for a full description of each map. GB: Guadalquivir Bank. G-GoCTZ: Gorringe-Gulf of Cadiz transfer zone; GoC-BTZ: Gulf of Cadiz-Betics transfer zone; PB: Portimão Bank; QTZ: Querença transfer zone; SMQF: São Marcos Quarteira Fault; SVTZ: São Vicente transfer zone.

The Middle Jurassic succession, limited to the north by the Algibre-Espiche extensional fault, thickens to the south, up to 2000 m thick south of the Guadalquivir and Portimão Banks (Fig. 2.5.1d). The orientation of the depocenters (NW-SE) is highly affected by the presence of the WNW-ESE transfer zones (Fig. 2.5.1d). The Middle Jurassic carbonates were deposited in shallow environments to the north. The depositional conditions deepen to the south, attested by the Algarve-1 well (Fig. 2.5.1d; Roque, 2007).

The Upper Jurassic succession is also controlled to the north by Algibre-Espiche fault, thickening towards the south as well (Fig. 2.5.2a). Upper Jurassic presents the largest thickness south of the Guadalquivir and Portimão Banks, up to 2500 m thick (Fig. 2.5.2a). These are the first sediments that lie on the oceanic crust generated during the Late Jurassic, as was interpreted to occur in the southeastern Iberian margin (García-Hernández et al., 1989; Vera et al., 2004), as a post-rift unit. The Upper Jurassic succession presents neritic environments in the northern margin, whereas bathyal environments dominate the deepest parts of the margin (Fig. 2.5.2a). The Upper Jurassic and the following units extend south beyond the reach of earlier units.

The Lower Cretaceous sediments reach thickness values up to 1000 m south of the present-day shelf-break, with the presence of bathyal environments. The thickening (up to more than 2000 m) and deepening of environmental conditions of this unit continue south of the Guadalquivir Bank (Fig. 2.5.2b). This is interpreted to act as a post-rift unit, as the Upper Jurassic. The NNW-SSE eroded areas are interpreted to be related to the inversion of NW-SE transfer features (Fig. 2.5.2b).

The Upper Cretaceous unit is only found offshore and is restricted in an area of roughly 40x70 km, controlled by the contractional structures described above (Fig. 2.5.2c) and by salt tectonism. This unit reaches thickness up to 600 m and was deposited in a neritic environment (Fig. 2.5.2c).

Paleogene presents thickness up to 1000 m in the distal parts of the basin, with neritic conditions in the shallow part of the basin and bathyal conditions interpreted towards the distal parts (Fig. 2.5.2d). The deposition of this unit is controlled by the initial development of the contractional structures documented in the Algarve Basin (Fig. 2.5.2d). The Paleogene represents the final stage prior to the generalized and more intense inversion of the margin.

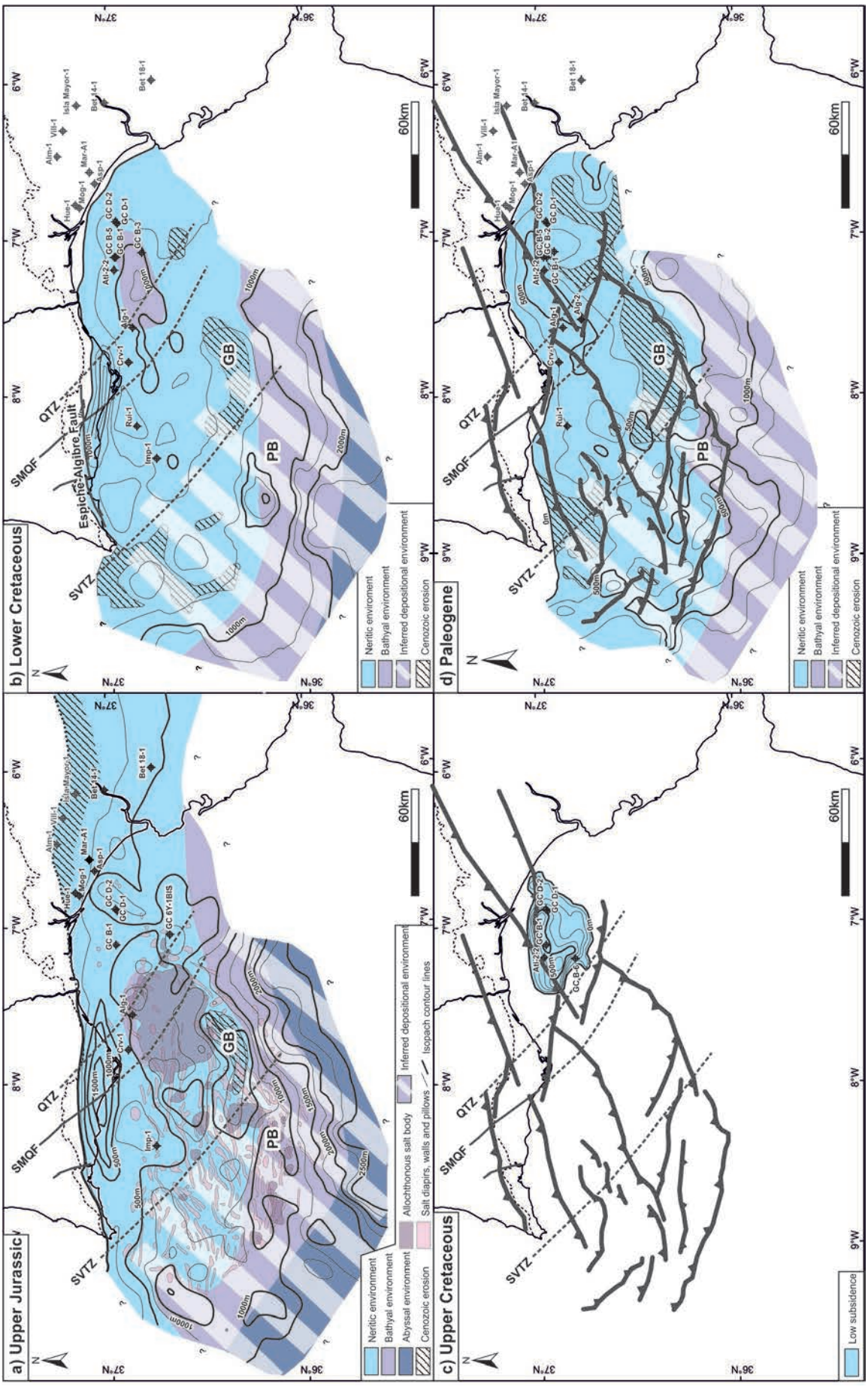
a) Upper Jurassic
b) Lower Cretaceous
c) Upper Cretaceous
d) Paleogene
SVTZ
QTZ
SMQF
Espichel-Algibre Fault
GB
PB
Neritic environment
Bathyal environment
Abyssal environment
Allochthonous salt body
Inferred depositional environment
Salt diapirs, walls and pillows
Isopach contour lines
Cenozoic erosion
Low subsidence
60km

Figure 2.5.2. Isopach maps of Late Jurassic to Paleogene units of the SW Iberian margin with interpreted paleogeographic water depths. (a) Late Jurassic. (b) Early Cretaceous. Note an increase in the number of the eroded areas, mostly towards the west. c) Late Cretaceous. (d) Paleogene map. See text for a full description of each map. GB: Guadalquivir Bank; PB: Portimão Bank; QTZ: Querença transfer zone; SMQF: São Marcos Quarteira Fault; SVTZ: São Vicente transfer zone.

CHAPTER 3. DISCUSSION

CHAPTER 3. DISCUSSION

This chapter deals with the global discussion derived from the results of this thesis in order to provide a complete overview of the evolution of the SW Iberian margin and its regional implications.

3.1. CRUSTAL STRUCTURE AND REGIONAL FRAMEWORK

The SW Iberian margin was configured as an ENE-WSW trending Mesozoic passive margin that opened southward (Fig. 3.1.1). The margin orientation and opening are consistent with it being part of the westernmost part of the Ligurian Tethys (Schettino and Turco, 2011), in contrast with the N-S to NE-SW trending Atlantic margins.

The transition from continental to oceanic crust is interpreted to also trend ENE-WSW, consistent with the regional trend of the margin. During the Jurassic, the SW Iberian margin was separated from the Central Atlantic to the west, and the Betic Basin to the east, by the NW-SE regional transfer fault zones (Fig. 3.1.1).

I have interpreted the SW Iberian margin as a hyper-extended margin. This is based on: 1) the rapid thinning of the continental crust (in about 150 km wide), before reaching the oceanic crust in the deepest part of the Gulf of Cadiz (Fig. 3.1.1); 2) the absence of important volcanism (with the exception of the CAMP volcanics) and 3) the possible presence of exhumed mantle based on gravity modelling. The crustal domains of the margin were defined based on the crustal thicknesses. The domains were assimilated to those defined by Manatschal et al. (2010), in order to define the crustal structure of margin (Fig. 3.1.1). These domains are defined in the results section, from north to south: proximal, necking, distal and oceanic domain.

The width of the necking domain and Cenozoic uplift of basement are the factors that control the width and amplitude of the prominent ENE-WSW trending positive gravity anomaly of the Gulf of Cadiz (Fig. 3.1.1).

The ocean-continental transition obtained here is gradual towards the southeast. This transition is sharpest towards the southwest due to the presence of a NW-SE transform fault (Fig. 3.1.1), consistent with the transfer faults of the same orientation documented onshore. The presence of NW-SE transfer faults has also been documented in neighbouring basins, such as the Betics (Vera, 1988) and the Atlas (Frizon de Lamotte et al., 2008).

The mentioned ocean-continent transition south of the Algarve Basin was imaged by the a seismic refraction profile of Sallarès et al. (2011) and it seem to extend westwards possibly cutting across the Gorringe Bank. This transfer fault zone separates the Upper Jurassic exhumed mantle in the Gorringe Bank and the southwestern distal domain of the SW Iberian margin. To the east, the Ocean Continent Transition (OCT) is offset by a major transfer fault under the Internal Betics, called Gulf of Cadiz-Betics transfer zone (Fig. 3.1.1).

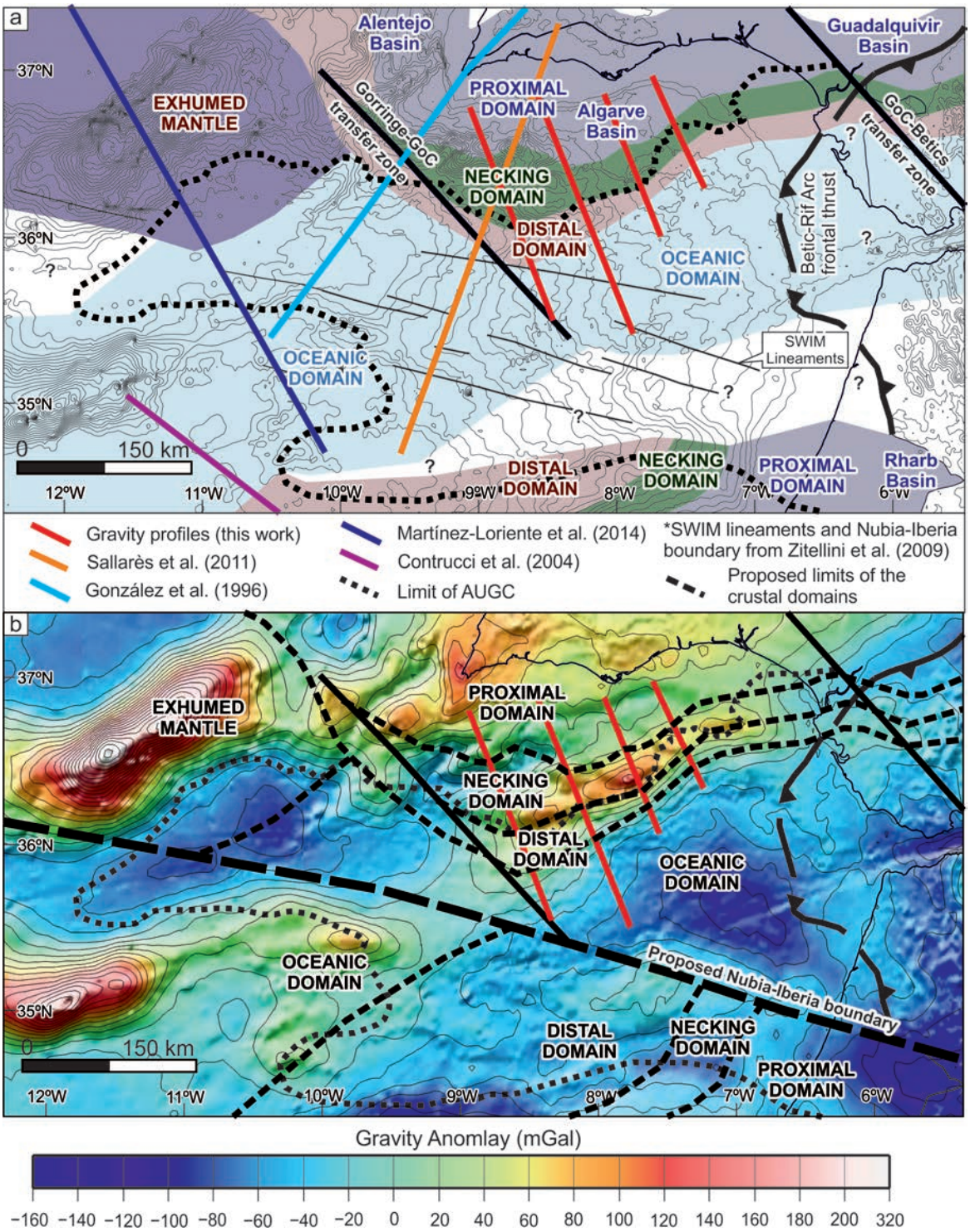

Figure 3.1.1. (a) Map of the main crustal domains of the Gulf of Cadiz and surrounding areas. Bathymetry is shown in the background (contours every 200 m). The location of published profiles is shown. The domains defined for the Morocco margin are derived by projecting the domains defined by Contrucci et al. (2004). (b) Map of the free-air gravity anomaly map (offshore) and Bouguer gravity anomaly (onshore) of the SW Iberian margin with the crustal domain distribution based on integrated regional 2D seismic data and gravimetric modelling. Thin dashed black lines: crustal domain boundaries.

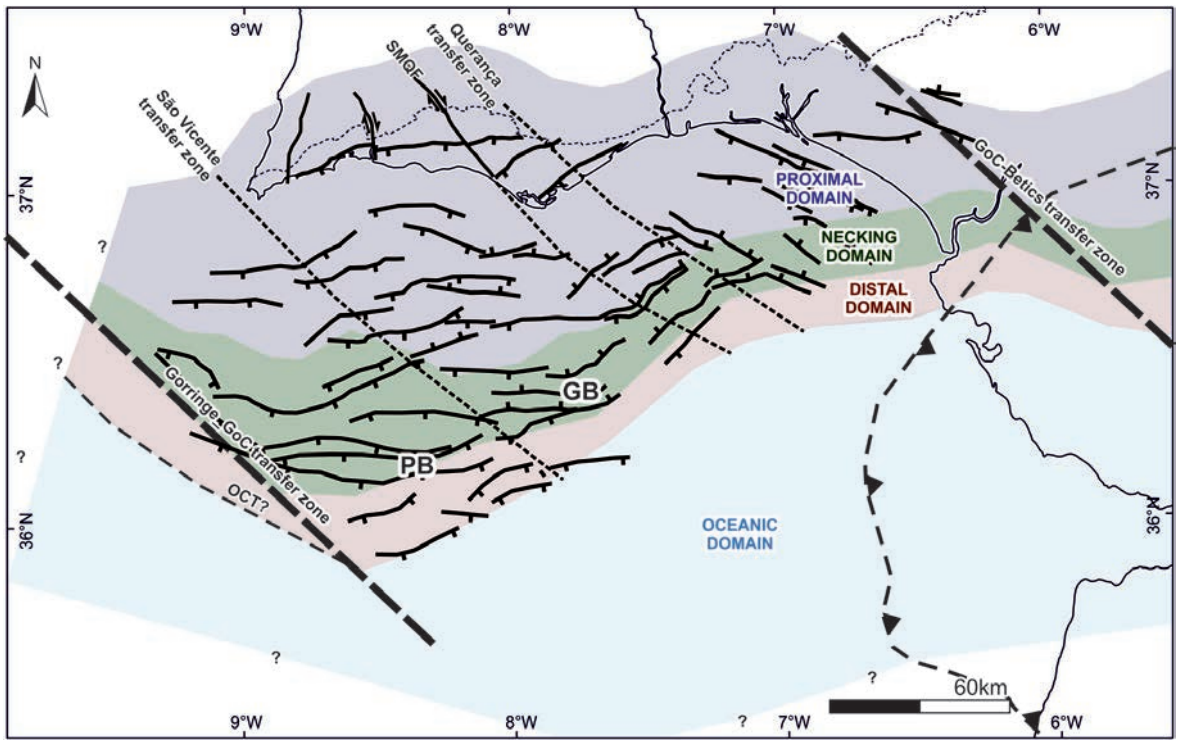

Figure 3.1.2. Map of the SW Iberian margin showing the crustal domains, the main extensional faults and the transfer faults. GB: Guadalquivir Bank; PB: Portimão Bank; SMQF: São Marcos Quarteira Fault.

NW-SE trending transfer fault zones in the Algarve Basin (Fig. 3.1.5) exert some control on the orientation of the Mesozoic and Cenozoic depocenters previously described. The Querença transfer zone controlled the evaporite depocenter from which the Esperança salt sheet was sourced (Fig. 3.1.3). The control on the depocenters is observable from Triassic to the Upper Jurassic (Figs. 2.5.1 and 2.5.2). The difference on the structural style between the Guadalquivir and Portimão Banks is controlled by the inferred São Vicente transfer zone (SVTZ; Fig. 3.1.2). The width of the necking domain also seems to be controlled by the inferred SVTZ (Fig. 3.1.2).

The continental crust of the Iberian margin and the Betics foreland experienced thinning towards the southeast, accommodated by ENE-WSW extensional faults and dissected by NW-SE transfer faults (Vera, 1988; Fig. 3.1.3). The conditions and the margin configuration during the rifting phase of the Betics foreland is similar to the SW Iberian margin: initial rifting phase with the deposition of Triassic clastics, Upper Triassic evaporites and Lower Jurassic shallow carbonates, followed by a differentiation in shallow (Prebetic Zone) and deep (Subbetic Zone) parts of the margin during the Middle Jurassic rift climax (e.g., Vera, 1988). The Upper Jurassic oceanization marks the post-rift deposition of Upper Jurassic-Lower Cretaceous sediments, which show deepening of sedimentary environments towards the southeast.

The margin orientation, crustal structure, polarity of syn- and post-rift sediments, and the timing of the main rifting episodes in the southeastern margin (Betics) are similar to those documented in the SW Iberian margin. The Betics are therefore interpreted to be the continuation of the Algarve Basin to the east, separated by the Gulf of Cadiz-Betics transfer zone (Fig. 3.1.3).

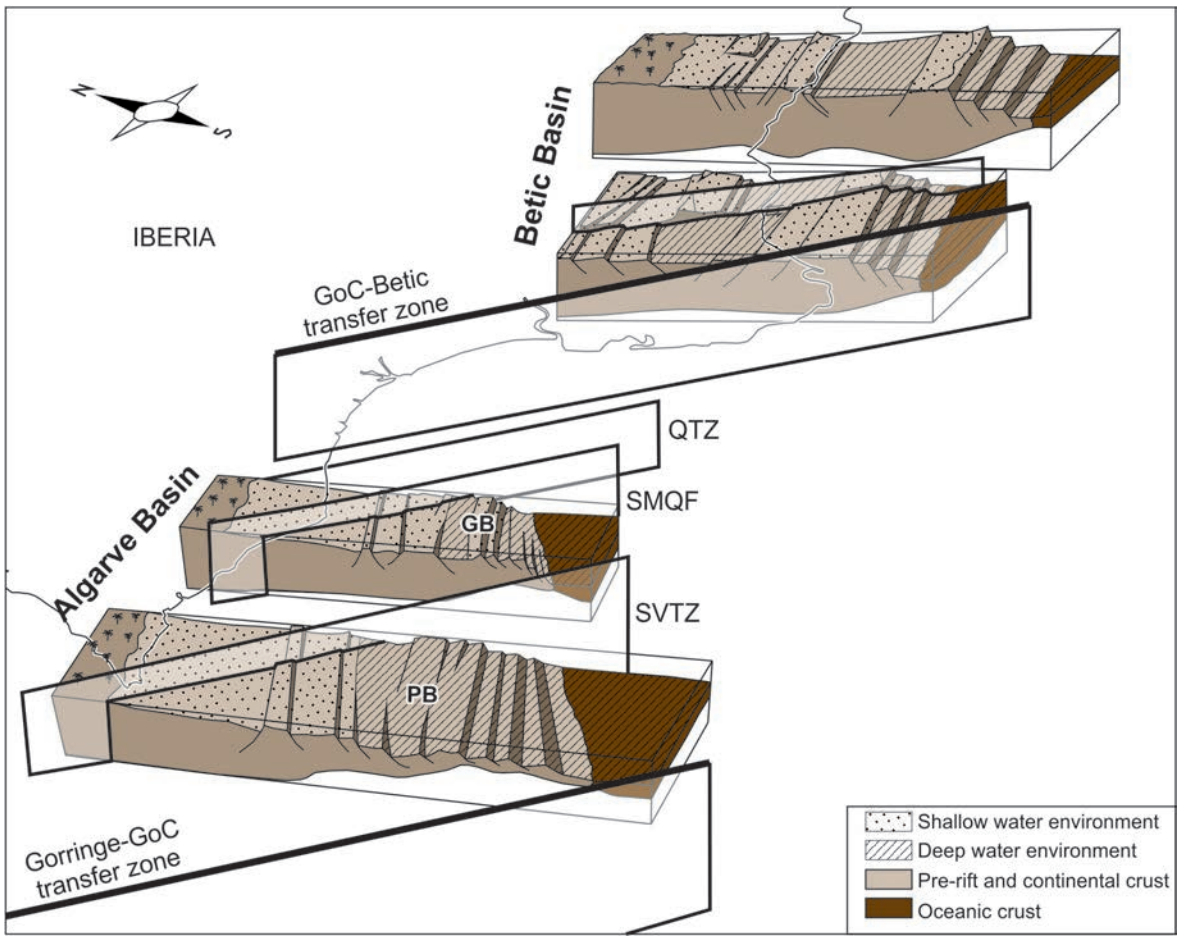

Figure 3.1.3. Three-dimensional sketch of the South Iberian margin comprising the Algarve Basin to the west and the Betic Basin to the east at the beginning of the oceanization at the beginning of the Late Jurassic. Notice the swells and troughs formed by extensional faulting and the presence of transfer faults that differentiate the PB and the GB (SVTZ), and the Gulf of Cadiz from the Betic Basin (GoC-Betic transfer zone). Sketches from the Betic Basin are modified from Vera (1988), while those of the Algarve Basin were constructed from the sections presented in this thesis.

According to kinematic reconstructions from oceanic magnetic anomalies for the Ligurian Tethys-Atlantic triple junction (e.g., Schettino and Turco, 2011), the conjugate margin during the Jurassic of SW Iberia is the NW African margin. The Jurassic conjugate margin would present a shallowing, in terms of facies and thickness, to the south, asymmetric to the SW Iberian margin. Notwithstanding, the NW African margin is expected to present structures (e.g., extensional faults, transfer zones) parallel to the ones in the SW Iberian margin.

The observed structural asymmetry of rifted margins was better explained by the concept of the upper plate-lower plate (Lister et al., 1986). Their model proposed that rifting is governed by a major low angle detachment fault system which separates an “upper plate margin” in the hanging wall of the detachment fault from a “lower plate margin” in the footwall of the same fault. The lower plate is represented by ocean-ward tilted crustal blocks and extensional rafts overlying highly structured exhumed rocks, while the upper plate is less structured (Peron-Pinvidic et al., 2015). The upper plate margins are narrower than

the lower plate margins, showing a sharp crustal taper and no well-developed hyper-extended domain (e.g., Faleide et al., 2010). Therefore, it is interpreted that the SW Iberian margin crustal architecture (Figs. 2.4.2 and 2.4.3) responds to this geometry and can be defined as an upper crust margin., On the other side, the NW African margin conjugate margin is expected to be classified as the lower plate.

The correlation between both margins is not easy to determine at present-day. The transition between the Iberian and the Nubian plates (displaced ~500 km from each other compared with the Mesozoic scenario; Schettino and Turco, 2011) is disrupted by the diffuse plate boundary, interpreted to be located along the South West Iberian Margin (SWIM) lineaments (Zitellini et al., 2009). This feature coincides with a roughly E-W lineament in the free-air gravity anomaly map (Fig. 3.1.1).

3.1.1. Timing of oceanization

Several authors proposed the presence of Jurassic oceanic crust in the deepest part of the Gulf of Cadiz (Gutscher et al., 2002; Martínez-Loriente et al., 2014; Sallarès et al., 2011). Some works suggest the oceanization of the margin to have occurred in the Late Jurassic (Bortolotti and Principi, 2005; García-Hernández et al., 1989; Vera et al., 2004). The oceanization is consistent with the presence of an oceanic crust located between the Iberian and African conjugate margins, at the westernmost part of the Ligurian Tethys. However a more precise timing for oceanization has remained elusive due to the absence of magnetic anomalies or well data from the oceanic crust.

In the Southern Iberian margin, several studies have documented submarine volcanic rocks interbedded between Middle-Upper Jurassic pelagic sediments. These materials form part of one of the deepest units of the Betic Basin (Vera et al., 1997). The volcanic rocks are very rich in potassium, generated in the upper mantle and extruded in the seafloor through a thick continental crust (Vera et al., 1997) as pillow lava flows, hydroclastites and pillow-breccias, and sills, dykes and small laccoliths (Molina and Vera, 2001). The age of these rocks would be between 170 Ma and 157 Ma (Bajocian-Oxfordian; Portugal-Ferreira et al., 1995; Vera et al., 1997).

An important plutonic and volcanic event also occurred in the Central and Eastern High Atlas during almost the same period of time (175-155±5 Ma; Amrhar et al., 1997; Frizon de Lamotte et al., 2008), represented by gabbro intrusions and basalt lava flows.

The break-up of the continental crust between Iberia and Africa should have been a tectonic event with regional impact, affecting nearby margins. The most characteristic Jurassic unconformity in the External Zones of the Betic Cordillera is the Middle-Upper Jurassic unconformity, documented at the end of the Bajocian (García-Hernández et al., 1989). This unconformity is controlled by a drop of the sea level, followed by transgression phases culminating in the “Middle Oxfordian transgression.

The Lusitanian Basin, a nearby Meso-Cenozoic basin is located in the West Portuguese margin and also records the unconformity between the Middle and Late Jurassic, in this case Callovian/Oxfordian boundary (Montenat et al., 1988). Lower and Middle Jurassic show evidences for block tilting and salt extrusion, along a series of west-northwest Jurassic extensional faults (among other orientations). This

fault system is fossilized by the unfaulted Oxfordian. This boundary is also represented by an erosional unconformity in the Algarve Basin (e.g., Terrinha et al., 2002).

These observations support the possibility that the oceanization of the SW Iberian margin took place at the transition between the Middle Jurassic and the Late Jurassic, also coincident with the opening of the western Ligurian Tethys (e.g., Bortolotti and Principi, 2005).

3.2. MESO-CENOZOIC EVOLUTION OF THE SW IBERIAN MARGIN

Based on the results, the overall tectonic evolution of the SW Iberian margin can be summarized in four different stages: 1) Triassic-Early Jurassic early rifting; 2) Middle Jurassic rift climax; 3) Late Jurassic-Early Cretaceous post-rift; 4) Late Cretaceous-Cenozoic inversion. These stages are represented in the restoration of a NNW-SSE regional 2D section (Fig. 3.2.1), perpendicular to the main extensional and contractional structures.

3.2.1. Mesozoic tectonic and paleogeographic evolution

The most evident structures formed during the Triassic-Early Jurassic early-rift are located in the onshore Algarve Basin. They consist on extensional faults oriented E-W to NE-SW (Fig. 3.2.2), affecting almost the whole onshore basin, and are interpreted to be active since the Triassic to Early Jurassic (Fig. 3.2.1a,b). These extensional faults extend offshore (Fig. 3.1.2). The orientation and timing are coherent with the Jurassic westernmost Ligurian Tethys rifting phase.

The basement extensional faults controlled the deposition of sediments through the margin from Triassic to Early Jurassic (Figs. 2.5.1a-c and Fig. 3.2.1). The depocenters of Triassic, Hettangian and Lower Jurassic succession describe a ENE-WSW regional axial system in response to the initial rifting phase of the margin. The oblique structures (parallel to Hercynian thrusts) slightly conditioned the orientation of depocenters (Fig. 2.5.1a-c).

The southward thickening of the Middle Jurassic sediment is due to the migration of the fault activity to the south during the rift climax. This is represented by thick packages and deep sedimentary environments in the distal domain, south of the Guadalquivir and Portimão Banks (Fig. 2.5.1d). The Gorringe-GoC transfer zone controlled the western part of the margin during this period (Fig. 2.5.1d).y

Figure 3.2.1. Restoration of a WNW-ESE regional cross-section during its evolution from the Triassic to present-day (a-g). Thicker lines with arrows represent active faults for each period. GB: Guadalquivir Bank. (a) Triassic clastics were deposited during the initial rifting phase in fault-bound grabens and half-grabens. (b) The Hettangian evaporites deposited during ongoing rifting, with greater thickness basinward. The remaining Lower Jurassic sediments deposited in salt withdrawal minibasins, marking the onset of salt tectonics. (c) The Middle Jurassic marks the rift climax, with the Guadalquivir Bank acting as an intra-basinal high and the development of a highly-extended domain in the distal part of the margin (right end of the section). Initial oceanic crust may have formed at the latest Middle or the early Late Jurassic. (d) and (e) represent the stages of post-rift (Late Jurassic and Early Cretaceous), with major thickening only in the distal part of the margin. Diapirism continued to be active. (f) During the Paleogene, initial inversion occurred mainly along the northern margin of the basin and in the Guadalquivir Bank. (g) During the Neogene-Quaternary, inversion extended through the entire margin. The AUGC/AWGC was emplaced over the distal domain in Miocene times. During the Cenozoic, salt structures were reactivated in compression.

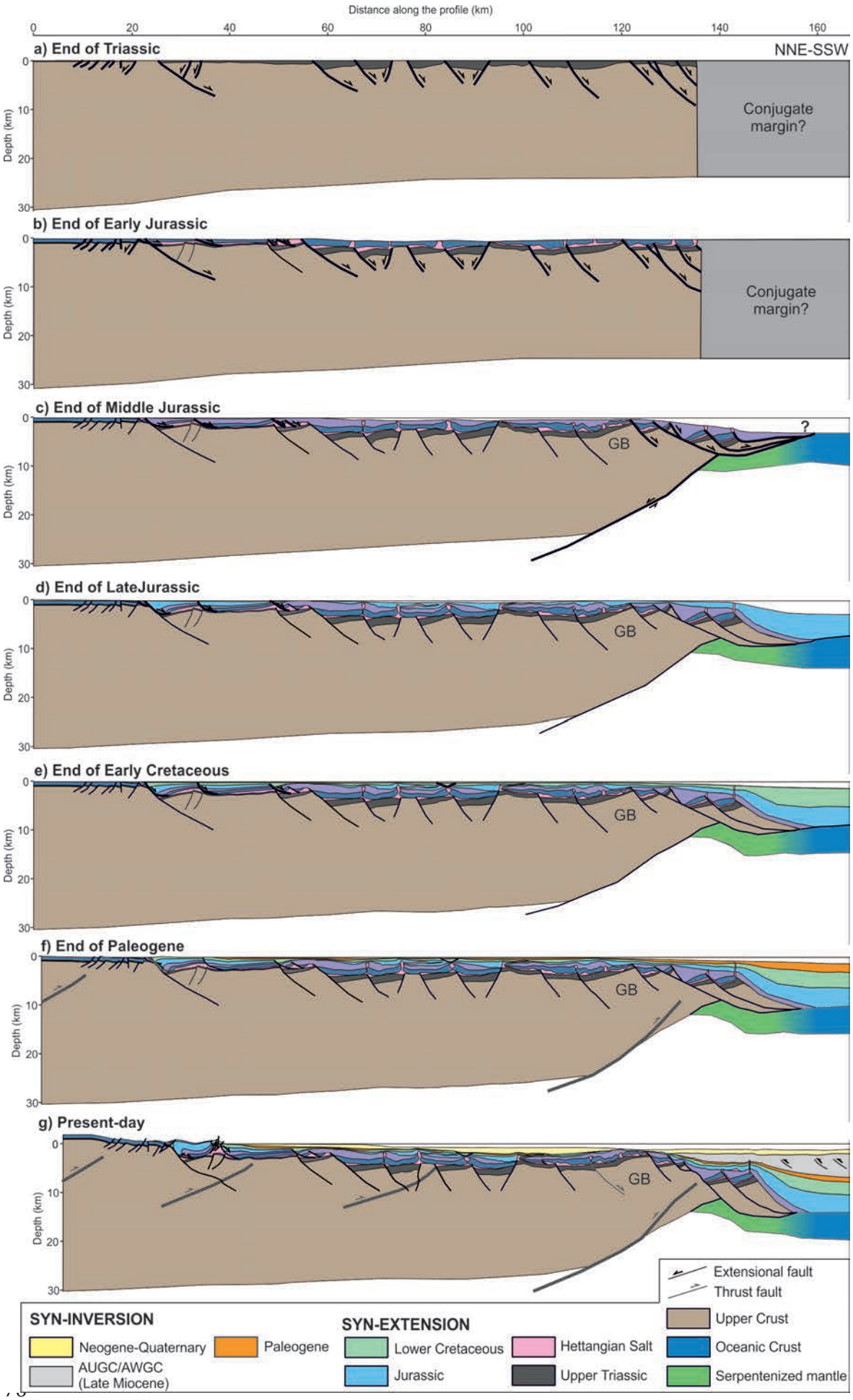
Distance along the profile (km)
0
20
40
60
80
100
120
140
160
a) End of Triassic
NNE-SSW
Conjugate margin?
b) End of Early Jurassic
Conjugate margin?
c) End of Middle Jurassic
GB
?
d) End of LateJurassic
GB
e) End of Early Cretaceous
GB
f) End of Paleogene
GB
g) Present-day
GB
Depth (km)
0
10
20
30
Extensional fault
Thrust fault
SYN-INVERSION
Neogene-Quaternary
Paleogene
AUGC/AWGC (Late Miocene)
SYN-EXTENSION
Lower Cretaceous
Hettangian Salt
Jurassic
Upper Triassic
Upper Crust
Oceanic Crust
Serpentenized mantle

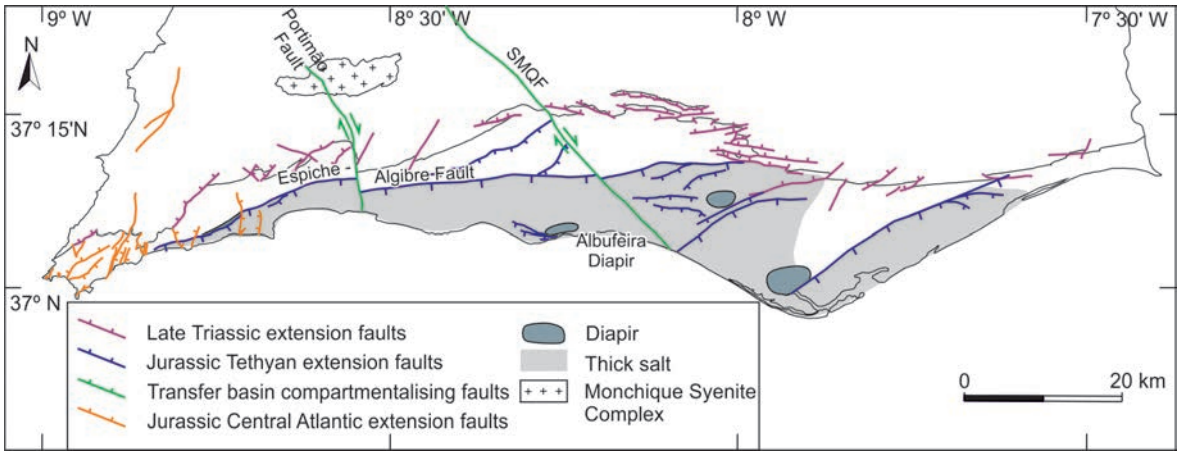

Figure 3.2.2. Mesozoic extensional fault system of the Algarve Basin and the salt distribution. West of the Portimão fault, along the Espiche fault the outcrop is "shaly diapir"; At Albufeira the outcropping diapir rock is gypsum; east of the SMQF the diapirs are halite. It seems there is a gradient towards the east from shale through gypsum/anhydrite to halite; this is also compatible with deepening eastwards.

Another set of faults N-S oriented were formed in the westernmost part of the onshore Algarve Basin during Jurassic rifting (Fig. 3.2.2). These faults are dated to be active from the Early to Late Jurassic, and respond to the Atlantic rifting, consistent with the faults observed along the western Portuguese margin (Alves et al., 2002; Montenat et al., 1988; Soto et al., 2012).

3.2.2. Salt tectonics implications

The Algarve Basin can be subdivided into three main domains based on the deformation style of salt-related structures (Fig. 3.2.3). The northern and eastern onshore parts of the margin represent the domain with no salt tectonics, given by the reduced thickness of Hettangian evaporites (<100 m). To the south and west, the autochthonous evaporite layer thickens and led to the formation of a domain of diapirs, including the Esperança salt sheet. The central and southwest portion of the Algarve Basin is represented by a domain of pervasive salt tectonism, with well-developed salt structures.

The evaporite unit thickens towards the south and west (Fig. 3.2.3a), coinciding with a domain of isolated diapirs, salt rollers and salt pillows development (Fig. 2.3.1). Further south, the OCT marks the southern limit of the evaporite basin (Fig. 3.2.3b).

The general trend is a northern and eastern basin dominated by claystone and dolomite, while to the south the basin is dominated by anhydrite and halite (Fig. 3.2.3a). The distribution is disrupted by the presence of the Guadalquivir Bank (Fig. 3.2.3a), as assumed to present anhydritic facies (e.g., well CG 6Y-1BIS). Assuming that mineralogy of evaporites play a major role in the mobility of evaporites and hence in the style of deformation (e.g., Stewart, 2007), the evaporite facies distribution beyond the wells and outcrops (Fig. 3.2.3) was inferred based on the distribution of salt-related structures.

The original evaporite basin is interpreted to show a bulls-eye pattern with the most soluble evaporites

(halite) in the basin centre (Fig. 3.2.3b). The initial thickness of Hettangian evaporites increases towards the south and west. The transition from 400 to 600 m marks the limit between the anhydrite and halite, and the domain of isolated diapirs and pervasive salt diapirism (Fig. 3.2.3b). Thickness decreases and facies of the evaporites shallow towards the Guadalquivir Bank (Fig. 3.2.3), given that the bank acted as an intra-basinal high. Salt structures and evaporitic facies distribution follow the same trend as the ENE-WSW basement extensional faults (Fig. 3.2.3).

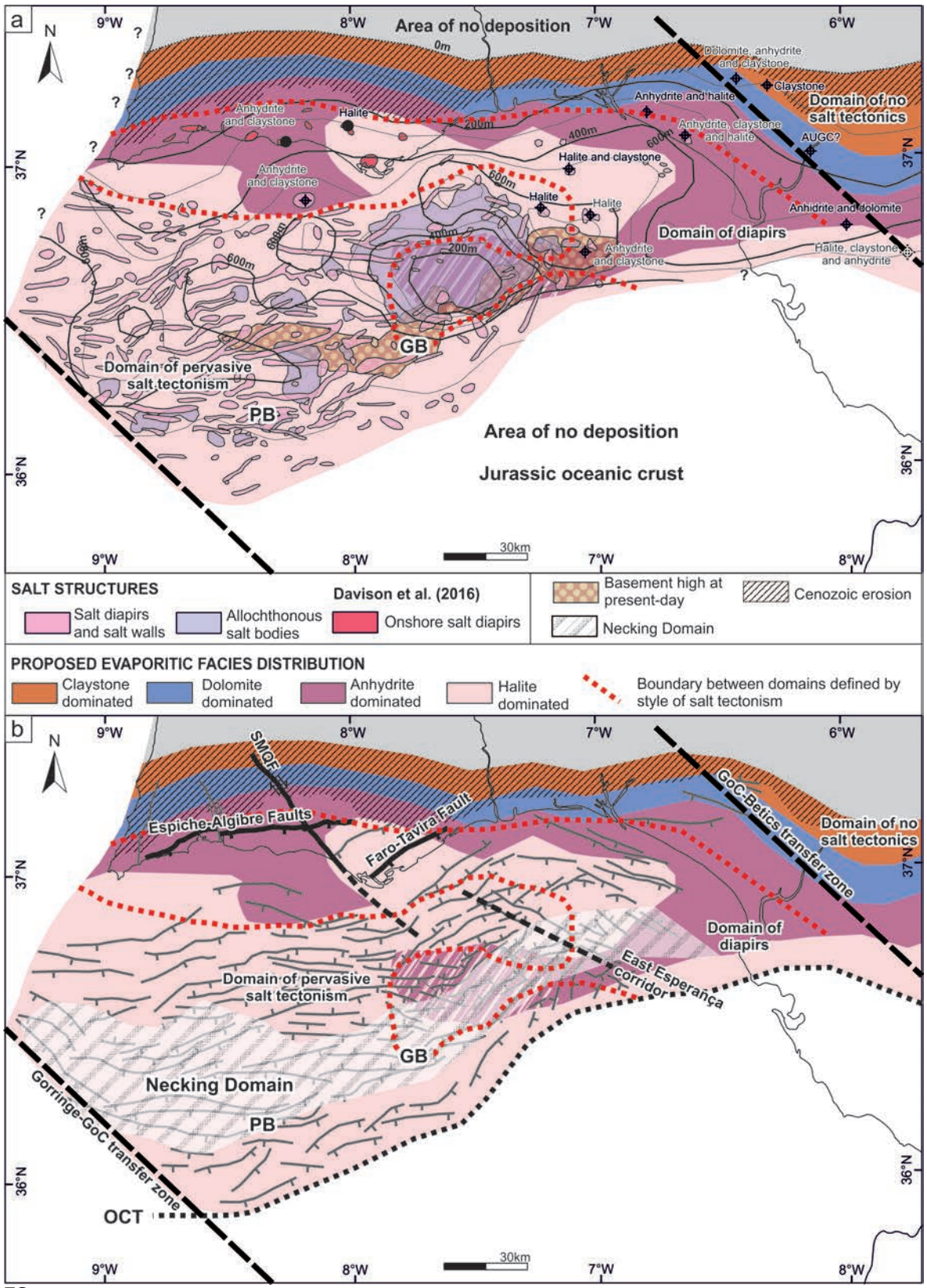

Figure 3.2.3. (a) Map of Hettangian evaporite facies (in colour) and thickness (isopach contours) across the Algarve Basin. The map is based on well and outcrop data, interpreted seismic sections, and the salt tectonic style. Overlain is the map of salt-related structures and the boundaries between domains defined based on style of salt tectonism. GB: Guadalquivir Bank; PB: Portimão Bank; SMQF: São Marcos Quarteira Fault. (b) Basement extensional faults, necking domain and Ocean-Continent Transition (OCT) overlain on the Hettangian evaporite facies distribution. Note the coincidence between basement trends and evaporite facies limits and domains of salt tectonism.

3.3. LATE CRETACEOUS-CENOZOIC CONTRACTION

The offshore SW Iberian margin shows a widespread tectonic inversion. The timing for the contractional deformation in the SW Iberia has been determined by tectonosedimentary relationships between the Mesozoic and Cenozoic sediments, the BFU geometry and the basement structure.

The Esperança salt sheet records the four main Cenozoic contractional deformation phases Onlap of Paleogene onto the two most evolved salt walls in the Esperança salt sheet, indicates that deformation started in Late Cretaceous or Paleogene. Thinning or absence of Paleogene over the salt sheet also indicates uplift in Late Paleogene or Early Miocene previous to the BFU. The third stage of deformation is related to the emplacement of the AWGC and AUGC in the area from Middle to Late Miocene times. The last one is dated in Late Pliocene to Present supported by onlap relationships and neotectonic activity. These stages of deformation are coherent with those defined by other authors in the area (Roque, 2007; Terrinha, 1998).

In the Algarve Basin, the restricted presence of the Upper Cretaceous succession (Fig. 2.5.2c) indicates the early inversion of the margin. The Paleogene is better preserved (Fig. 2.5.2d), indicating a possible relative quiescence period.

Late Cretaceous and Cenozoic inversion in the onshore Algarve Basin led to the partial reactivation of extensional faults, the formation of shortcut structures in the northern part of the basin and basement monoclines with ENE-WSW trend and dipping to the south (Fig. 3.3.1). Onshore, the northern monocline is responsible for the south-dipping of the basin-boundary (Fig. 3.3.1). Contractional structures are interpreted to be formed by reactivating pre-existing discontinuities in the Carboniferous basement, with similar orientation and dip (Vegas, 1980), as has been documented within the South-Portuguese Zone and the Algarve Basin (Soriano, 1996; Terrinha, 1998).

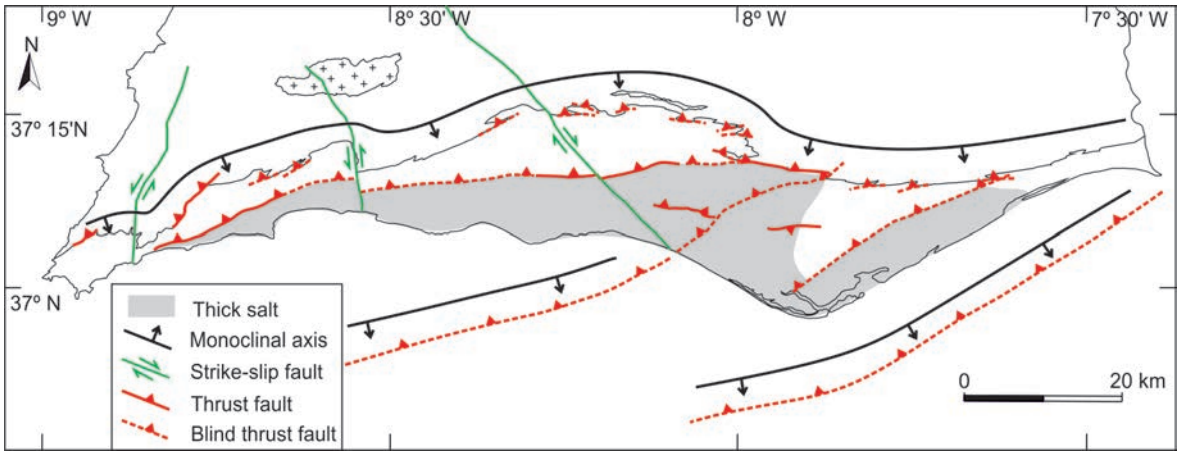

Figure 3.3.1. Late Cretaceous-Cenozoic contractional structures of the Algarve Basin.

One of the most peculiar aspects of the inversion experienced in the Algarve Basin is the opposing dip of Upper Cretaceous-Cenozoic thrusts and Mesozoic extensional faults (Fig. 3.3.2), as has been documented in the onshore Algarve Basin. This is interpreted by firstly, the formation of south-dipping extensional faults accommodating increasing extension in the margin during the Mesozoic. The Late Cretaceous-Cenozoic compression led to the reactivation of north-dipping low-angle thrusts and foliation within the Carboniferous and deeper units (e.g., Díaz Azpiazu et al., 2004; Soriano, 1996; Fig. 3.3.2). This led to the anomalous inversion style of the SW Iberian margin, in which basement trusts cross-cut previous extensional faults (Fig. 3.3.2).

Basement thrusts cross-cutting extensional faults have also been documented in the Moroccan Atlas (Domènech, 2015; Teixell et al., 2003), with geometries very similar to those observed in the Algarve Basin, in the Cordillera Oriental of the Argentine Andes (Carrera and Muñoz, 2013), and in the northern Iberian margin (Tugend et al., 2014). The tectonic uplift of basement structures (likely monoclines) is also described in several mountain ranges within the Iberian plate (Casas-Sainz and Gil-Imaz, 1998; De Vicente et al., 2007; Fernández-Lozano, 2012; Stapel, 1999). In the eastern Guadalquivir Basin, there are NE-SW trending monoclines deforming the overlying Jurassic (Pedrera et al., 2013) in a manner very similar to the monoclines described in the Algarve Basin.

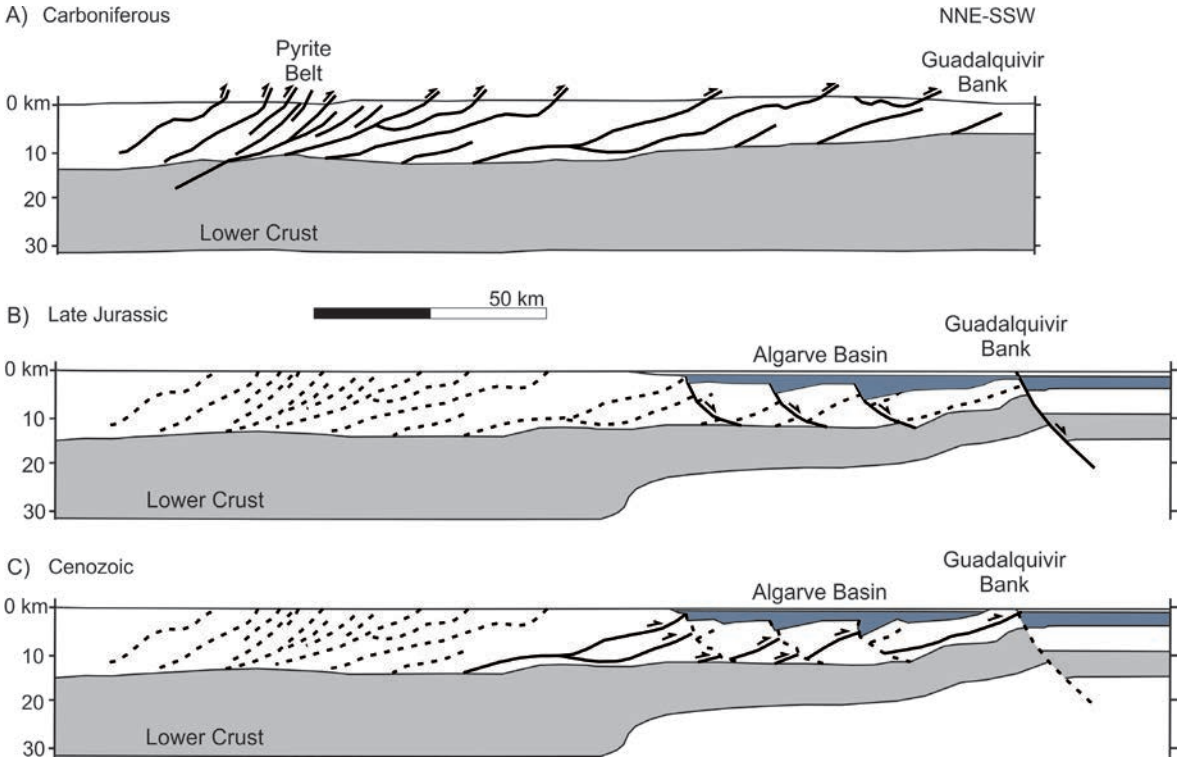

Figure 3.3.2. Synthetic crustal cross-section of the SW Iberian Margin at key time steps. (a) At the end of Hercynian thrusting (Carboniferous). (b) At the end of Jurassic extension. (c) During Cenozoic thrusting. Black lines show faults active at each time step. Dashed black lines show inactive faults. Modified after Vegas et al. (2004).

The main inversion structure of the SW Iberian margin is the T3, coinciding with the location and trend of the necking zone (Fig. 3.3.3). This basement thrust is responsible for the reactivation of the Guadalquivir and Portimão Banks. In inverted passive margins, the inversion normally initiates in the most distal domain (Mohn et al., 2012; Peron-Pinvidic et al., 2008; Tugend et al., 2014). In the SW Iberian margin, basement heterogeneities could have played a key role for the inversion. I have interpreted that the T3 takes advantage of the tilting of the lower crust and Moho induced during extensional necking (Figs. 2.4.2 and 2.4.3).

To the west, the Algarve Basin relays with contractional structures NE-SW oriented and mainly NW directed (e.g., Marquês de Pombal Thrust, Gorringe Thrust, Horseshoe Thrust; Fig. 1.1.1). The amount of shortening and the age of deformation in the Algarve Basin is consistent with the deformation of the Gorringe Bank. This structure is considered the main contractional structure west of the Algarve Basin (Galindo-Zaldívar, 2003; Jiménez-Munt et al., 2010).

East of the Algarve Basin, the structures responsible for the uplift of the Sierra Morena (Stapel, 1999) are likely the continuation of contractional basement structures described in the Algarve Basin, which are still active nowadays (Herraiz et al., 1996; Stich et al., 2006; Vázquez-Vílchez et al., 2015). This is consistent with the interpretation for the Sierra Morena as an upper crust antiform associated with the presence of a south-directed crustal-scale blind thrust (De Vicente et al., 2007). This thrust is interpreted to be the eastern continuation of the T1 and T2 described in the Algarve Basin.

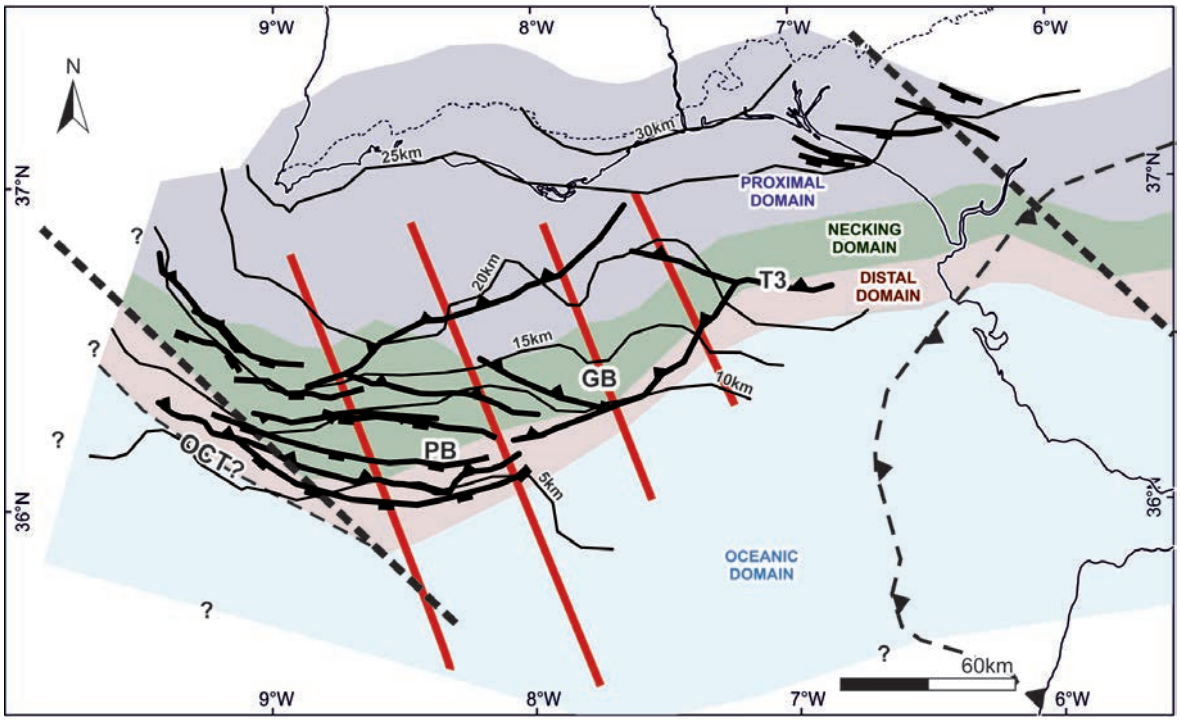

Figure. 3.3.3. Map of crustal thickness of SW Iberia with crustal domains (proximal, necking, and distal) defined through gravimetric modelling and from crustal thickness. Thrusts relevant to the discussion and relevant extensional faults are superimposed.

In the offshore Algarve Basin, post-Paleogene deposits were controlled by the basement monoclines related with crustal-scale thrusts (T1, T2 and T3; Fig. 3.3.4). Above the BFU, high reflective wedge-shaped set of reflectors could correspond to contourite deposits. The contourites are related with the circulation of Mediterranean Outflow Water (MOW) from the Gibraltar strait to the Gulf of Cadiz since Pliocene times (Llave et al., 2011). These sediments were channelled between the AUGC, the Guadalquivir Bank and the growing antiform. Contourite deposits are dominated by sheeted drifts and mostly constant thickness other than around tectonically active structures (Hernández-Molina et al., 2016). The system of basement-involved thrusts (T0 through T3 and oblique branches) identified in this study are observed to locally control the present-day bathymetry and contourite currents of the MOW (Figure 3.3.4).

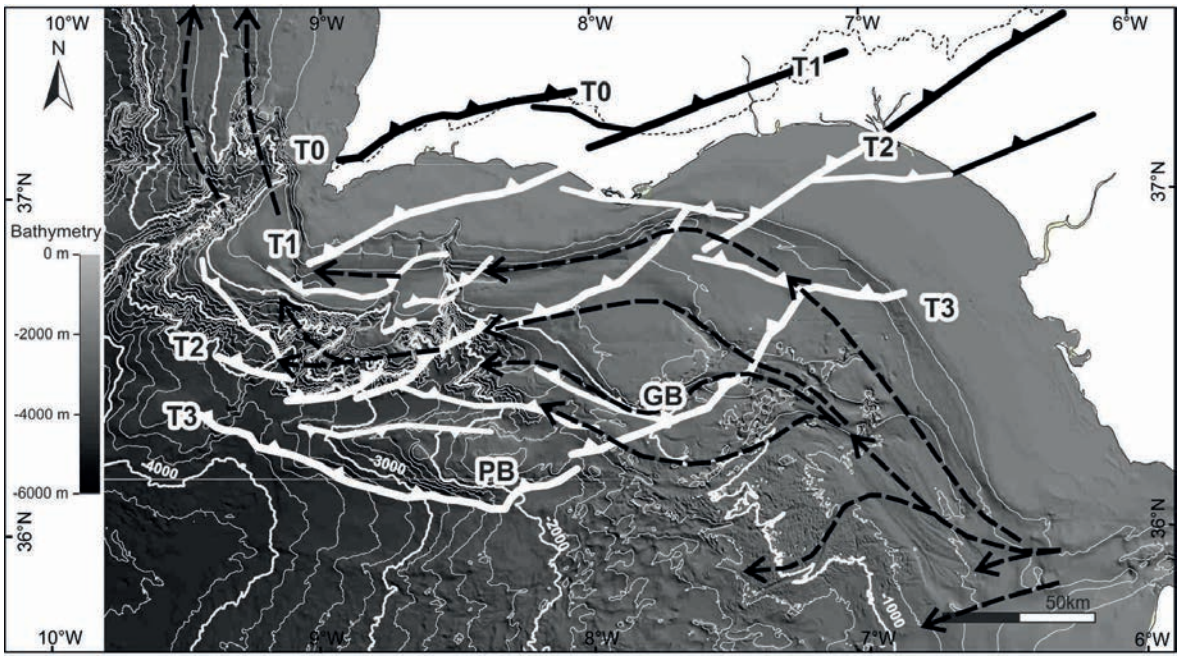

Figure 3.3.4. Seabed bathymetry and location of basement thrusts. Black dashed arrows indicate MOW currents taken from Hernández-Molina et al. (2016). Note the control exerted locally by thrusts T2, T3 and their lateral ramps on the trajectories of the MOW currents.

In a plate scale, south of the Sierra Morena, the subducting lithospheric slab underneath the Betics (Vergés and Fernàndez, 2012) is interpreted to be segmented into three parts further to the east, under the Algerian Sea (Fichtner and Villaseñor, 2015; Fig. 3.3.5). The tearing of the slab coincides with the location of the Gulf of Cadiz-Betic transfer zone, interpreted to be the locus of initiation for the tearing event. The segments of the slab identified to the east can be delimited by faults with the same trend as the NW-SE transfer faults previously documented (Fig. 3.3.5). It is here suggested that the transfer fault zones offset realms of oceanic lithosphere or of OCT that later were subducted.

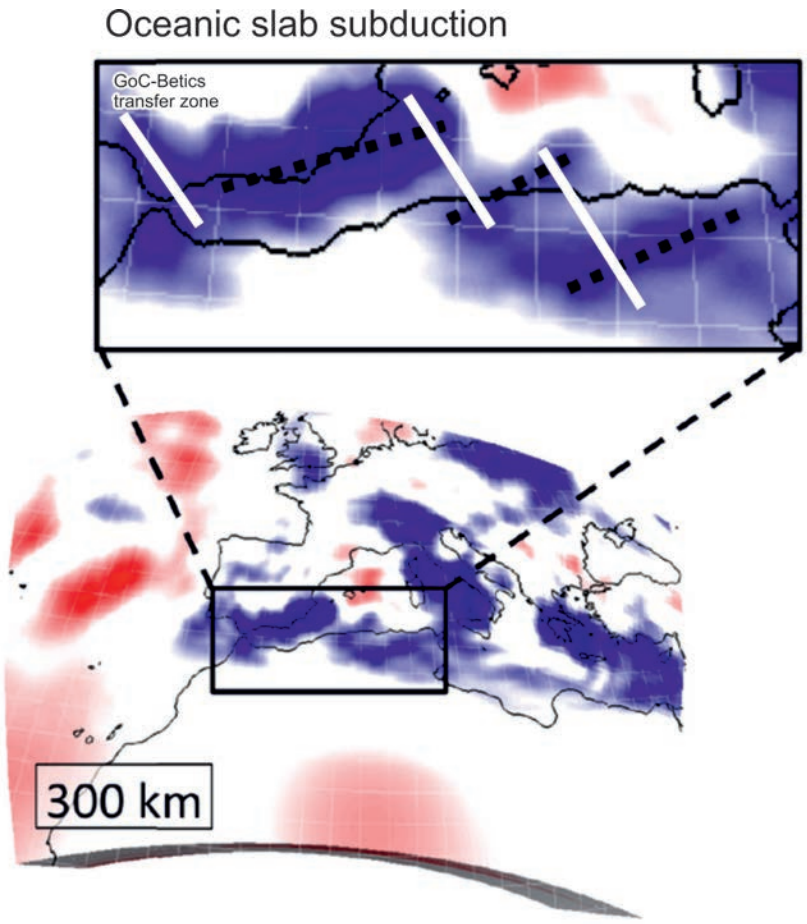

Fig. 3.3.5. Illustration of the possible impact of NW-SE transfer zones in the present-day subduction geometry under the Alboran Sea. A horizontal slice at 300 km depth coloured for the absolute variations of isotropic S velocity (modified from Fichtner and Villaseñor, 2015) reveals a possible segmentation in the subducting oceanic slab. Features drawn in the enlarged panel are described as follows: dotted black line: possible segments of the Tethyan oceanic slab; white lines: possible transfer faults.

CHAPTER 4. CONCLUSIONS

CHAPTER 4. CONCLUSIONS

The SW Iberian margin is a segmented Jurassic passive margin inverted from the Late Cretaceous to the present-day. The Algarve Basin is the continuation of the Betic Basin and both correspond to the westernmost remnant of the Ligurian Tethys.

The SW Iberian margin underwent four main tectonic phases: 1) Triassic-Early Jurassic initial rifting, 2) Middle Jurassic rifting climax, 3) Late Jurassic-Early Cretaceous post-rift and 4) Late Cretaceous-Present-day inversion.

Extensional faulting ENE-WSW trending was initially set in the whole margin, rooting into the basement and controlling the deposition of the syn-rift sequences (Triassic and Lower Jurassic). Salt tectonics was triggered during the first Early Jurassic extensional pulses.

The second phase of rifting caused the southward crustal thinning through major extensional faults increasing their throw towards the south. Salt tectonics activity increased during this phase and controlled the depocenters in the proximal domain. The oceanization of the margin took place most likely in the Middle to Late Jurassic transition. The oceanic crust was covered by deep and thick sediments during the Late Jurassic and Early Cretaceous. During this period the extensional faulting ceased but the salt tectonics was still active.

As a result, the SW Iberian margin was configured during the Mesozoic as a hyper-extended margin facing towards the SE and culminating in an oceanic crust, configured from north to south by a proximal, necking, distal and oceanic domain. The crustal thinning towards the southeast was responsible for the increase of the depositional space towards the same direction, and thus, the deepening of the depositional environments and thicker sequences. However, this trend was disturbed by the Guadalquivir Bank, an intra-basinal high during the Mesozoic. The regional E-W trend on the depositional environments is also affected by a NW-SE orientation, corresponding to intra-marginal transfer zones.

To the east and to the west, the margin was limited by two NW-SE transfer zones connecting with the Ligurian Tethys to the east and the Central Atlantic to the west.

Four main basement contractional structures are E-W to NE-SW oriented and are responsible for the inversion of the margin, which are parallel to the Mesozoic extensional fault system but with an opposite vergence. These contractional structures, which were originated from the reactivation of foliation and thrust faults within the Hercynian basement, controlled the deposition of the Upper Cretaceous and Cenozoic sediments, along with the MOW currents (contourite deposits), were responsible for the seismicity in the Gulf of Cadiz, and reactivated the salt tectonics and the Guadalquivir and Portimão Banks.

The inversion is controlled by the passive margin structure, attested by the main shortening in the necking domain. The contractional structures documented in the SW Iberian margin link the shortening in Gorringe Bank in the west to the Betics in the east, thus outlining the inversion tectonics structure of the SW Iberian margin.

REFERENCES

Afonso, A.R.A., 1983. O problema inverso linear em prospecção gravimétrica. Algumas considerações sobre os jazigos de sal-gema di Algarve. Dep Física Fac Ciênc. Univ Lisb. 59.

Aïfa, T., Zaagane, M., 2014. Brittle tectonics within the Jurassic formations of the Ouarsenis culminating area, northwestern Algeria. J. Afr. Earth Sci. 96, 39–50. doi:10.1016/j.jafrearsci.2014.03.020

Alves, T.M., Gawthorpe, R.L., Hunt, D.W., Monteiro, J.H., 2002. Jurassic tectono-sedimentary evolution of the Northern Lusitanian Basin (offshore Portugal). Mar. Pet. Geol. 19, 727–754. doi:10.1016/S0264-8172(02)00036-3

Alves, T.M., Moita, C., Cunha, T., Ullnaess, M., Myklebust, R., Monteiro, J.H., Manuppella, G., 2009. Diachronous evolution of Late Jurassic-Cretaceous continental rifting in the northeast Atlantic (west Iberian margin). Tectonics 28, n/a-n/a. doi:10.1029/2008TC002337

Amrhar, M., Bouabdelli, M., Pique, A., 1997. Les marqueurs structuraux et magmatiques de l'extension crustale dans le Haut-Atlas occidental (Maroc) au Dogger, témoins de l'évolution de la marge orientale de l'Atlantique central. Comptes Rendus Académie Sci. Sér. 2 Sci. Terre Planètes 324, 119–126.

Arthaud, F., Matte, P., 1977. Late Paleozoic strike-slip faulting in southern Europe and northern Africa: Result of a right-lateral shear zone between the Appalachians and the Urals. Geol. Soc. Am. Bull. 88, 1305–1320. doi:10.1130/0016-7606(1977)88<1305:LPSFIS>2.0.CO;2

Asensio, E., Khazaradze, G., Echeverria, A., 2014. Block Kinematics of the Iberia-Maghrebian region from inversion of geodetic data. Presented at the Resúmenes de la 2a Reunión Ibérica sobre Fallas Activas y Paleosismología, Lorca, España.

Ayala, C., Bohoyo, F., Maestro, A., Reguera, M.I., Torne, M., Rubio, F., Fernàndez, M., García-Lobón, J.L., 2016. Updated Bouguer anomalies of the Iberian Peninsula: a new perspective to interpret the regional geology. J. Maps 1–4. doi:10.1080/17445647.2015.1126538

Barreto, P., Silva, C., Leonardo, P., Sousa, J., Caeiro, M.H., Maciel, C., Guerreiro, L., 2015. The relationship between the onshore and offshore structure of São Marcos-Quarteira Fault System, Algarve Basin, Portugal. Presented at the AAPG European Regional Conference and Exhibition, Lisbon.

Bernard-Griffiths, J., Gruau, G., Cornen, G., Azambre, B., Macé, J., 1997. Continental Lithospheric Contribution to Alkaline Magmatism: Isotopic (Nd, Sr, Pb) and Geochemical (REE) Evidence from Serra de Monchique and Mount Ormonde Complexes. J. Petrol. 38, 115–132. doi:10.1093/petroj/38.1.115

Bird, D.E., Hall, S.A., Burke, K., Casey, J.F., Sawyer, D.S., 2007. Early Central Atlantic Ocean seafloor spreading history. Geosphere 3, 282–298. doi:10.1130/GES00047.1

Bortolotti, V., Principi, G., 2005. Tethyan ophiolites and Pangea break-up. Isl. Arc 14, 442–470. doi:10.1111/j.1440-1738.2005.00478.x

Carrera, N., Muñoz, J.A., 2013. Thick-skinned tectonic style resulting from the inversion of previous structures in the southern Cordillera Oriental (NW Argentine Andes). Geol. Soc. Lond. Spec. Publ. 377, 77–100. doi:10.1144/SP377.2

Carvalho, J., Matias, H., Rabeh, T., Menezes, P.T.L., Barbosa, V.C.F., Dias, R., Carrilho, F., 2012. Connecting onshore structures in the Algarve with the southern Portuguese continental margin: The Carcavai fault zone. Tectonophysics 570–571, 151–162. doi:10.1016/j.tecto.2012.08.011

Casas-Sainz, A.M., Gil-Imaz, A., 1998. Extensional subsidence, contractional folding and thrust inversion of the eastern Cameros basin, northern Spain. Geol. Rundsch. 86, 802–818. doi:10.1007/s005310050178

Contrucci, I., Klingelhöfer, F., Perrot, J., Bartolome, R., Gutscher, M.-A., Sahabi, M., Malod, J., Rehault, J.-P., 2004. The crustal structure of the NW Moroccan continental margin from wide-angle and reflection seismic data. Geophys. J. Int. 159, 117–128. doi:10.1111/j.1365-246X.2004.02391.x

Correia, F., 1989. Estudo biostratigráfico e microfácies do Cretácico carbonatado da bacia sedimentar meridional portuguesa (Algarve). Faculdade de Ciências da Universidade Nova de Lisboa.

Crespo-Blanc, A., 2007. Superimposed folding and oblique structures in the palaeomargin-derived units of the Central Betics (SW Spain). J. Geol. Soc. 164, 621–636. doi:10.1144/0016-76492006-084

Cunha, T.A., Matias, L.M., Terrinha, P., Negredo, A.M., Rosas, F., Fernandes, R.M.S., Pinheiro, L.M., 2012. Neotectonics of the SW Iberia margin, Gulf of Cadiz and Alboran Sea: a reassessment including recent structural, seismic and geodetic data: Neotectonics SW Iberia-Gulf of Cadiz-Alboran. Geophys. J. Int. 188, 850–872. doi:10.1111/j.1365-246X.2011.05328.x

Dañobeitia, J.J., Bartolomé, R., Checa, A., Maldonado, A., Slootweg, A.P., 1999. An interpretation of a prominent magnetic anomaly near the boundary between the Eurasian and African plates (Gulf of Cadiz, SW margin of Iberia). Mar. Geol. 155, 45–62. doi:10.1016/S0025-3227(98)00140-6

Davison, I., Barreto, P., Andrade, A.J.M., 2016. Loulé: the anatomy of a squeezed diapir, Algarve Basin, southern Portugal. J. Geol. Soc. jgs2016-035. doi:10.1144/jgs2016-035

De Vicente, G., Muñoz-Martín, A., 2013. The Madrid Basin and the Central System: A tectonostratigraphic analysis from 2D seismic lines. Tectonophysics 602, 259–285. doi:10.1016/j.tecto.2012.04.003

De Vicente, G., Vegas, R., 2009. Large-scale distributed deformation controlled topography along the western Africa–Eurasia limit: Tectonic constraints. Tectonophysics 474, 124–143. doi:10.1016/j.tecto.2008.11.026

De Vicente, G., Vegas, R., Muñoz-Martín, A., Silva, P., Andriessen, P., Cloetingh, S., Gonzalezcasado, J., Vanwees, J., Alvarez, J., Carbo, A., 2007. Cenozoic thick-skinned deformation and topography evolution of the Spanish Central System. Glob. Planet. Change 58, 335–381. doi:10.1016/j.gloplacha.2006.11.042

Dewey, J.F., Helman, M.L., Knott, S.D., Turco, E., Hutton, D.H.W., 1989. Kinematics of the western Mediterranean. Geol. Soc. Lond. Spec. Publ. 45, 265–283. doi:10.1144/GSL.SP.1989.045.01.15

Diaz, J., Gallart, J., Carbonell, R., 2016. Moho topography beneath the Iberian-Western Mediterranean region mapped from controlled-source and natural seismicity surveys. Tectonophysics. doi:10.1016/j.tecto.2016.08.023

Díaz Azpiazu, M., Castro, A., Fernández, C., López, S., Fernández Caliani, J.C., Moreno-Ventas, I., 2004. The contact between the Ossa Morena and the South Portuguese zones: characteristics and significance of the Aracena metamorphic belt, in its central sector between Aroche and Aracena (Huelva). J. Iber. Geol. 23–52.

Diegel, F.A., Karlo, J.F., Schuster, D.C., Shoup, R.C., Tauvers, and P.R., 1995. Cenozoic Structural Evolution and Tectono-Stratigraphic Framework of the Northern Gulf Coast Continental Margin, in: M. P. A. Jackson, D. G. Roberts, and S. Snelson, Eds., Salt Tectonics: A Global Perspective: AAPG Memoir 65. pp. 109–151.

Domènech, M., 2015. Rift opening and inversion in the Marrakech High Atlas: integrated structural and thermochronologic study. PhD Thesis, Universitat Autònoma de Barcelona (157 pp).

Duarte, J.C., 2011. Tectonics of the Gulf of Cadiz: the role of the Gibraltar Arc in the reactivation of the SW Iberia Margin. PhD Thesis, Universidade de Lisboa (304 pp).

Duarte, J.C., Rosas, F.M., Terrinha, P., Schellart, W.P., Boutelier, D., Gutscher, M.-A., Ribeiro, A., 2013. Are subduction zones invading the Atlantic? Evidence from the southwest Iberia margin. Geology 41, 839–842. doi:10.1130/G34100.1

Faleide, J.I., Bjørlykke, K., Gabrielsen, R.H., 2010. Geology of the Norwegian Continental Shelf, in: Petroleum Geoscience. Springer Berlin Heidelberg, pp. 467–499.

Fernandes, P., Rodrigues, B., Borges, M., Matos, V., Clayton, G., 2013. Organic maturation of the Algarve Basin (southern Portugal) and its bearing on thermal history and hydrocarbon exploration. Mar. Pet. Geol. 46, 210–233. doi:10.1016/j.marpetgeo.2013.06.015

Fernández-Lozano, J., 2012. Cainozoic deformation of Iberia: a model for intraplate mountain building and basin development based on analogue modelling. PhD Thesis, Utretcht University (173 pp).

Fernández-Puga, M.C., Vázquez, J.T., Somoza, L., Rio, V.D. del, Medialdea, T., Mata, M.P., León, R., 2007. Gas-related morphologies and diapirism in the Gulf of Cádiz. Geo-Mar. Lett. 27, 213–221. doi:10.1007/s00367-007-0076-0

Fichtner, A., Villaseñor, A., 2015. Crust and upper mantle of the western Mediterranean – Constraints from full-waveform inversion. Earth Planet. Sci. Lett. 428, 52–62. doi:10.1016/j.epsl.2015.07.038

Flinch, J.F., 1994. Tectonic evolution of the Gibraltar Arc. PhD Thesis. Rice University (811 pp).

Flinch, J.F., Vail, P.R., 1998. Plio-Pleistocene Sequence Stratigraphy and Tectonics of the Gibralter Arc, in: De Graciansky, P.C., Hardenbol, J., Thierry, J., Vail, P.R. (Eds.), Mesozoic and Cenozoic Sequence Stratigraphy of European Basins. SEPM Spec. Publ, Tulsa. pp. 199– 208.

Fourcade, E., Azema, J., Cecca, F., Bonneau, M., Peybernes, B., Dercourt, J., 1991. Essai de reconstitution cartographique de la paléogéographique et des paléoenvironnements de la Téthys au Tithonique supérieur (138 à 135 Ma). Bull Soc Géol Fr. 162, 1197–1208.

Frizon de Lamotte, D., Raulin, C., Mouchot, N., Wrobel-Daveau, J.-C., Blanpied, C., Ringenbach, J.-C., 2011. The southernmost margin of the Tethys realm during the Mesozoic and Cenozoic: Initial geometry and timing of the inversion processes: TETHYS SOUTHERNMOST MARGIN. Tectonics 30, n/a-n/a. doi:10.1029/2010TC002691

Frizon de Lamotte, D., Zizi, M., Missenard, Y., Hafid, M., Azzouzi, M.E., Maury, R.C., Charrière, A., Taki, Z., Benammi, M., Michard, A., 2008. The Atlas System, in: Michard, A., Saddiqi, O., Chalouan, A., Lamotte, D.F. de (Eds.), Continental Evolution: The Geology of Morocco, Lecture Notes in Earth Sciences. Springer Berlin Heidelberg, pp. 133–202.

Galindo-Zaldívar, J., 2003. Active faulting in the internal zones of the central Betic Cordilleras (SE, Spain). J. Geodyn. 36, 239–250. doi:10.1016/S0264-3707(03)00049-8

Garcia-Castellanos, D., Fernàndez, M., Torne, M., 2002. Modeling the evolution of the Guadalquivir foreland basin (southern Spain). Tectonics 21, 9–1. doi:10.1029/2001TC001339

García-Hernández, M., López-Garrido, Á.C., Martín-Algarra, A., Cámara, J.M., Ruiz-Ortiz, P.A., Vera, J.A., 1989. Las discontinuidades mayores del Jurásico de las Zonas Externas de las Cordilleras Béticas: análisis e interpretación de los ciclos sedimentarios. J. Iber. Geol. 35–52.

Gawthorpe, R.L., Hurst, J.M., 1993. Transfer zones in extensional basins: their structural style and influence on drainage development and stratigraphy. J. Geol. Soc. 150, 1137–1152. doi:10.1144/gsjgs.150.6.1137

Gomez, F., Beauchamp, W., Barazangi, M., 2000. Role of the Atlas Mountains (northwest Africa) within the African-Eurasian plate-boundary zone. Geology 28, 775–778. doi:10.1130/0091-7613(2000)28<775:ROTAMN>2.0.CO;2

González, A., Córdoba Barba, D., Vegas, R., Matías, L.M., González Fernández, A., Córdoba Barba, D., Vegas, R., Matías, L.M., 1998. Seismic crustal structure in the southwest of the Iberian Peninsula and the Gulf of Cadiz. Tectonophysics 296, 317–331.

González, A., Torne, M., Córdoba, D., Vidal, N., Matias, L.M., Díaz, J., 1996. Crustal thinning in the Southwestern Iberia Margin. Geophys. Res. Lett. 23, 2477–2480. doi:10.1029/96GL02299

Gràcia, E., Dañobeitia, J., Vergés, J., Bartolomé, R., Córdoba, D., 2003. Crustal architecture and tectonic evolution of the Gulf of Cadiz (SW Iberian margin) at the convergence of the Eurasian and African plates. Tectonics 22, 1033. doi:10.1029/2001TC901045

Gutscher, M.-A., Dominguez, S., Westbrook, G.K., Leroy, P., 2009. Deep structure, recent deformation and analog modeling of the Gulf of Cadiz accretionary wedge: Implications for the 1755 Lisbon earthquake. Tectonophysics 475, 85–97. doi:10.1016/j.tecto.2008.11.031

Gutscher, M.-A., Malod, J., Rehault, J.-P., Contrucci, I., Klingelhoefer, F., Mendes-Victor, L., Spakman, W., 2002. Evidence for active subduction beneath Gibraltar. Geology 30, 1071. doi:10.1130/0091-7613(2002)030<1071:EFASBG>2.0.CO;2

Hernández-Molina, F.J., Sierro, F.J., Llave, E., Roque, C., Stow, D.A.V., Williams, T., Lofi, J., Van der Schee, M., Arnáiz, A., Ledesma, S., Rosales, C., Rodríguez-Tovar, F.J., Pardo-Igúzquiza, E., Brackenridge, R.E., 2016. Evolution of the gulf of Cadiz margin and southwest Portugal contourite depositional system: Tectonic, sedimentary and paleoceanographic implications from IODP expedition 339. Mar. Geol. 377, 7–39. doi:10.1016/j.margeo.2015.09.013

Hernández-Molina, F.J., Stow, D.A.V., Alvarez-Zarikian, C.A., Acton, G., Bahr, A., Balestra, B., Ducassou, E., Flood, R., Flores, J.-A., Furota, S., Grunert, P., Hodell, D., Jimenez-Espejo, F., Kim, J.K., Krissek, L., Kuroda, J., Li, B., Llave, E., Lofi, J., Lourens, L., Miller, M., Nanayama, F., Nishida, N., Richter, C., Roque, C., Pereira, H., Sanchez Goni, M.F., Sierro, F.J., Singh, A.D., Sloss, C., Takashimizu, Y., Tzanova, A., Voelker, A., Williams, T., Xuan, C., 2014. Onset of Mediterranean outflow into the North Atlantic. Science 344, 1244–1250. doi:10.1126/science.1251306

Herraiz, M., de Vicente, G., Lindo, R., Sánchez-Caba~nero, J.G., 1996. Seismotectonics of the Sierra Albarrana area (southern Spain). Constraints for a regional model of the Sierra Morena-Guadalquivir Basin limit. Tectonophysics, Dynamics of Extensional Basins and Inversion Tectonics 266, 425–442. doi:10.1016/S0040-1951(96)00201-6

Heyman, M.A., 1989. Tectonic and Depositional History of the Moroccan Continental Margin. Tankard AJ Balkwill HR Eds Extensional Tecton. Stratigr. North. Atl. Margins Am Assoc Pet Geol Can Geol Found AAPG Mem 46 323–340.

Hiscott, R.N., Wilson, R.C.L., Gradstein, F.M., (5), V.P., (5), J.G.-M., (6), R.R.B., (6), H. a. W., 1990. Comparative Stratigraphy and Subsidence History of Mesozoic Rift Basins of North Atlantic (1). AAPG Bull. 74, 60–76.

Hudec, M.R., Jackson, M.P.A., 2006. Advance of allochthonous salt sheets in passive margins and orogens. AAPG Bull. 90, 1535–1564. doi:10.1306/05080605143

Ings, S.J., Shimeld, J.W., 2006. A new conceptual model for the structural evolution of a regional salt detachment on the northeast Scotian margin, offshore eastern Canada. AAPG Bull. 90, 1407–1423. doi:10.1306/04050605159

IOC, IHO, BODC, 2003. Centenary Edition of the GEBCO Digital Atlas, published on CDROM on behalf of the Intergovernmental Oceanographic Commission and the International Hydrographic Organization as part of the General Bathymetric Chart of the Oceans, British Oceanographic Data Centre, Liverpool, UK.

Iribarren, L., Vergés, J., Camurri, F., Fullea, J., Fernàndez, M., 2007. The structure of the Atlantic–Mediterranean transition zone from the Alboran Sea to the Horseshoe Abyssal Plain (Iberia–Africa plate boundary). Mar. Geol. 243, 97–119. doi:10.1016/j.margeo.2007.05.011

Jiménez-Munt, I., Fernàndez, M., Vergés, J., Afonso, J.C., Garcia-Castellanos, D., Fullea, J., 2010. Lithospheric structure of the Gorringe Bank: Insights into its origin and tectonic evolution. Tectonics 29, n/a-n/a. doi:10.1029/2009TC002458

Korenaga, J., Holbrook, W.S., Detrick, R.S., Kelemen, P.B., 2001. Gravity anomalies and crustal structure at the southeast Greenland margin. J. Geophys. Res. Solid Earth 106, 8853–8870. doi:10.1029/2000JB900416

Kvarven, T., Ebbing, J., Mjelde, R., Faleide, J.I., Libak, A., Thybo, H., Flueh, E.R., Murai, Y., 2014. Crustal structure across the Møre margin, mid-Norway, from wide-angle seismic and gravity data. Tectonophysics 626, 21–40.

Labails, C., Olivet, J.-L., Aslanian, D., Roest, W.R., 2010. An alternative early opening scenario for the Central Atlantic Ocean. Earth Planet. Sci. Lett. 297, 355–368. doi:10.1016/j.epsl.2010.06.024

Lanaja, J.M., 1987. Contribución de la exploración petrolífera al conocimiento de la geología de España. IGME, Madrid.

Ledesma, S.M., 2000. Astrobiocronología y estratigrafía de alta resolución del Neógeno de la Cuenca del Guadalquivir-Golfo de Cádiz. PhD Thesis. Universidad de Salamanca (464 pp).

Lister, G.S., Etheridge, M.A., Symonds, P.A., 1986. Detachment faulting and the evolution of passive continental margins. Geology 14, 246–250.

Llave, E., Matias, H., Hernández-Molina, F.J., Ercilla, G., Stow, D.A.V., Medialdea, T., 2011. Pliocene–Quaternary contourites along the northern Gulf of Cadiz margin: sedimentary stacking pattern and regional distribution. Geo-Mar. Lett. 31, 377–390. doi:10.1007/s00367-011-0241-3

Lopes, C.M., 2002. Análise e modelação da bacia do Algarve. PhD Thesis, Faculdade de Ciências da Universidade Nova de Lisboa (173 pp).

Lopes, F.C., Cunha, P.P., Le Gall, B., 2006. Cenozoic seismic stratigraphy and tectonic evolution of the Algarve margin (offshore Portugal, southwestern Iberian Peninsula). Mar. Geol. 231, 1–36. doi:10.1016/j.margeo.2006.05.007

Macintyre, R.M., Berger, G.W., 1982. A note on the geochronology of the Iberian Alkaline Province. Lithos 15, 133–136. doi:10.1016/0024-4937(82)90005-6

Mack, G.H., Seager, W.R., 1995. Transfer zones in the southern Rio Grande rift. J. Geol. Soc. 152, 551–560. doi:10.1144/gsjgs.152.3.0551

Maestro, A., Somoza, L., Medialdea, T., Talbot, C.J., Lowrie, A., Vazquez, J.T., Diaz-del-Rio, V., 2003. Large-scale slope failure involving Triassic and Middle Miocene salt and shale in the Gulf of Cadiz (Atlantic Iberian Margin). Terra Nova 15, 380–391. doi:10.1046/j.1365-3121.2003.00513.x

Maldonado, A., Somoza, L., Pallarés, L., 1999. The Betic orogen and the Iberian–African boundary in the Gulf of Cadiz: geological evolution (central North Atlantic). Mar. Geol. 155, 9–43. doi:10.1016/S0025-3227(98)00139-X

Manatschal, G., 2004. New models for evolution of magma-poor rifted margins based on a review of data and concepts from West Iberia and the Alps. Int. J. Earth Sci. 93. doi:10.1007/s00531-004-0394-7

Manatschal, G., Sutra, E., Peron-Pinvidic, G., 2010. The lesson from the Iberia-Newfoundland rifted margins: how applicable is it to other rifted margins? CM 2010-Abstr. 2, 27–37.

Manuppella, G., 1992. Carta geológica da região do Algarve. Noticia explicativa da Carta Geologica da regiao do Algarve. Serviços geológicos de Portugal.

Manuppella, G., 1988. Litoestratigrafia e tectónica da Bacia Algarvia. Geonovas 10, 67–71.

Manuppella, G., Marques, B., Rocha, R.B., 1988. Évolution tectono-sédimentaire du bassin de l'Algarve pendant le Jurassique, in: 2nd International Symposium on Jurassic Stratigraphy, Lisboa. pp. 1031–1046.

Martínez-Loriente, S., 2013. Geophysical and geological characterization of the active structures and of the nature of the basement in the Eurasia-Africa plate boundary (SW Iberian Margin): Implications for regional geodynamics and seismic hazard assessment. PhD Thesis, Universitat de Barcelona (353 pp).

Martínez-Loriente, S., Gràcia, E., Bartolome, R., Perea, H., Klaeschen, D., Dañobeitia, J.J., Zitellini, N., Wynn, R.B., Masson, D.G., 2016. Morphostructure, tectono-sedimentary evolution and seismic potential of the Horseshoe Fault, SW Iberian Margin. Basin Res. doi:10.1111/bre.12225

Martínez-Loriente, S., Gràcia, E., Bartolome, R., Sallarès, V., Connors, C., Perea, H., Lo Iacono, C., Klaeschen, D., Terrinha, P., Dañobeitia, J.J., Zitellini, N., 2013. Active deformation in old oceanic lithosphere and significance for earthquake hazard: Seismic imaging of the Coral Patch Ridge area and neighboring abyssal plains (SW Iberian Margin): Active Deformation Coral Patch Ridge. Geochem. Geophys. Geosystems 14, 2206–2231. doi:10.1002/ggge.20173

Martínez-Loriente, S., Sallarès, V., Gràcia, E., Bartolome, R., Dañobeitia, J.J., Zitellini, N., 2014. Seismic and gravity constraints on the nature of the basement in the Africa-Eurasia plate boundary: New insights for the geodynamic evolution of the SW Iberian margin: Thin oceanic crust at the CPR and SH. J. Geophys. Res. Solid Earth 119, 127–149. doi:10.1002/2013JB010476

Martins, I., Munhá, J., 1993. Magmatismo cretácico do Algarve litoral: zonamento inverso em clinopiroxenas e suas implicações petrogenéticas. Mem Mus Lab Min Geol Fac Ciênc Univ Porto 3, 102–124.

Martins, L.T., 1999. Cretaceous Alkaline Magmatism in Algarve Littoral (South Portugal): a Basanite-Lamprophyre Rock Suite. Magmat. Rift Basin Evol. Int. Geol. Correl. Programme Liblice Czech Repub. Sept. 7-11 1998 84.

Martins, L.T., Madeira, J., Youbi, N., Munhá, J., Mata, J., Kerrich, R., 2008. Rift-related magmatism of the Central Atlantic magmatic province in Algarve, Southern Portugal. Lithos 101, 102–124. doi:10.1016/j.lithos.2007.07.010

Masini, E., Manatschal, G., Tugend, J., Mohn, G., Flament, J.-M., 2014. The tectono-sedimentary evolution of a hyper-extended rift basin: The example of the Arzacq–Mauléon rift system (Western Pyrenees, SW France). Int. J. Earth Sci. 103, 1569–1596.

Matias, H., 2007. Hydrocarbon potential of the offshore Algarve Basin. PhD Thesis, Faculdade de Ciências da Universidade Nova de Lisboa (324 pp).

Matias, H., Kress, P., Terrinha, P., Mohriak, W., Menezes, P.T.L., Matias, L., Santos, F., Sandnes, F., 2011. Salt tectonics in the western Gulf of Cadiz, southwest Iberia. AAPG Bull. 95, 1667–1698. doi:10.1306/01271110032

Medialdea, T., 2005. Estructura y evolución tectónica del Golfo de Cádiz. PhD Thesis, Universidad Complutense (318 pp).

Medialdea, T., Somoza, L., Pinheiro, L.M., Fernández-Puga, M.C., Vázquez, J.T., León, R., Ivanov, M.K., Magalhaes, V., Díaz-del-Río, V., Vegas, R., 2009. Tectonics and mud volcano development in the Gulf of Cádiz. Mar. Geol., EUROMARGINS: Imaging, monitoring, and modelling the physical, chemical and biological processes in the European passive continental margins 261, 48–63. doi:10.1016/j.margeo.2008.10.007

Medialdea, T., Vegas, R., Somoza, L., Vázquez, J.T., Maldonado, A., Díaz-del-Río, V., Maestro, A., Córdoba, D., Fernández-Puga, M.C., 2004. Structure and evolution of the "Olistostrome" complex of the Gibraltar Arc in the Gulf of Cádiz (eastern Central Atlantic): evidence from two long seismic cross-sections. Mar. Geol. 209, 173–198. doi:10.1016/j.margeo.2004.05.029

Meisling, K., Cobbold, P., Mount, V.S., 2001. Segmentation of an obliquely rifted margin, Campos and Santos basins, southeastern Brazil. AAPG Bull. 85, 1925–1944.

Michard, A., Saddiqi, O., Chalouan, A., de Lamotte, D.F., 2008. Continental evolution: The geology of Morocco: Structure, stratigraphy, and tectonics of the Africa-Atlantic-Mediterranean triple junction, (eds A. Michard, A. Chalouan & O. Saddiqi), p. 33–64. Lecture Notes in Earth Sciences, 116. Springer–Verlag. ed.

Mjelde, R., Digranes, P., Shimamura, H., Shiobara, H., Kodaira, S., Brekke, H., Egebjerg, T., Sørenes, N., Thorbjørnsen, S., 1998. Crustal structure of the northern part of the Vøring Basin, mid-Norway margin, from wide-angle seismic and gravity data. Tectonophysics 293, 175–205.

Mohn, G., Manatschal, G., Beltrando, M., Masini, E., Kusznir, N., 2012. Necking of continental crust in magma-poor rifted margins: Evidence from the fossil Alpine Tethys margins. Tectonics 31, TC1012. doi:10.1029/2011TC002961

Molina, J.M., Vera, J.A., 2001. Interaction between sedimentation and submarine volcanism (Jurassic, Subbetic, Southern Spain). Geogaceta 29, 142–145.

Montenat, C.H., Guery, F., Jamet, M., Berthou, P.Y., 1988. Mesozoic evolution of the Lusitanian Basin: comparison with the adjacent margin, in: Proceedings of the Ocean Drilling Program, Scientific Results. pp. 757–775.

Mougenot, D., 1989. Geologia da margem portuguesa. PhD Thesis, Univer. Pierre et Marie Curie, Paris VI (259 pp).

Moulin, M., Aslanian, D., Olivet, J.-L., Contrucci, I., Matias, L., Géli, L., Klingelhoefer, F., Nouzé, H., Réhault, J.-P., Unternehr, P., 2005. Geological constraints on the evolution of the Angolan margin based on reflection and refraction seismic data (ZaïAngo project). Geophys. J. Int. 162, 793–810. doi:10.1111/j.1365-246X.2005.02668.x

Moura, D., Veiga-Pires, C., Albardeiro, L., Boski, T., Rodrigues, A.L., Tareco, H., 2007. Holocene sea level fluctuations and coastal evolution in the central Algarve (southern Portugal). Mar. Geol. 237, 127–142. doi:10.1016/j.margeo.2006.10.026

Mouterde, R., 1971. Esquisse de l'e´volution biostratigraphique de la Pe´ninsule Ibe´ rique au Jurassique. Cuad. Geol. Ibérica 2, 21–31.

Muñoz, J.A., 1992. Evolution of a continental collision belt: ECORS-Pyrenees crustal. Thrust Tecton. 235.

Nichols, G., 2009. Sedimentology and stratigraphy, 2nd ed. ed. Wiley-Blackwell, Chichester, UK ; Hoboken, NJ.

Nirrengarten, M., Gernigon, L., Manatschal, G., 2014. Lower crustal bodies in the Møre volcanic rifted margin: Geophysical determination and geological implications. Tectonophysics 636, 143–157. doi:10.1016/j.tecto.2014.08.004

Olaiz, A.J., Muñoz-Martín, A., De Vicente, G., Vegas, R., Cloetingh, S., 2009. European continuous active tectonic strain–stress map. Tectonophysics 474, 33–40. doi:10.1016/j.tecto.2008.06.023

Pais, J., Legoinha, P., Elderfield, H., Sousa, L., Estevens, M., 2010. The Neogene of Algarve (Portugal). Ciênc. Terra UNL 14, 277–288.

Palano, M., González, P.J., Fernández, J., 2013. Strain and stress fields along the Gibraltar Orogenic Arc: Constraints on active geodynamics. Gondwana Res. 23, 1071–1088. doi:10.1016/j.gr.2012.05.021

Palomeras, I., Carbonell, R., Flecha, I., Simancas, F., Ayarza, P., Matas, J., Martínez Poyatos, D., Azor, A., González Lodeiro, F., Pérez-Estaún, A., 2009. Nature of the lithosphere across the Variscan orogen of SW Iberia: Dense wide-angle seismic reflection data. J. Geophys. Res. 114. doi:10.1029/2007JB005050

Pedrera, A., Galindo-Zaldívar, J., Marín-Lechado, C., García-Tortosa, F.J., Ruano, P., López Garrido, A.C., Azañón, J.M., Peláez, J.A., Giaconia, F., 2012. Recent and active faults and folds in the central-eastern Internal Zones of the Betic Cordillera. J. Iber. Geol. 38. doi:10.5209/rev_JIGE.2012.v38.n1.39213

Pedrera, A., Ruiz-Constán, A., Marín-Lechado, C., Galindo-Zaldívar, J., González, A., Peláez, J.A., 2013. Seismic transpressive basement faults and monocline development in a foreland basin (Eastern Guadalquivir, SE Spain). Tectonics 32, 1571–1586. doi:10.1002/2013TC003397

Peel, F.J., Travis, C.J., Hossack, J.R., 1995. Genetic structural provinces and salt tectonics of the Cenozoic offshore US Gulf of Mexico: a preliminary analysis, in: M. P. A. Jackson, D. G. Roberts, and S. Snelson, Eds., Salt Tectonics: A Global Perspective: AAPG Memoir 65. pp. 153–175.

Perconig, E., 1962. Sur la constitution géologique de l'Andalousie occidentale en particulier du bassin du Guadalquivir (Espagne méridionale) Livre Mémoire du Professeur Paul Fallot. Mem. Hors-Ser. Soc. Geol. Fr. 1, 229–256.

Pereira, R., Alves, T.M., 2012. Tectono-stratigraphic signature of multiphased rifting on divergent margins (deep-offshore southwest Iberia, North Atlantic): TECTONIC SIGNATURE OF MULTIPHASED RIFTS. Tectonics 31, n/a-n/a. doi:10.1029/2011TC003001

Peron-Pinvidic, G., Manatschal, G., Dean, S.M., Minshull, T.A., 2008. Compressional structures on the West Iberia rifted margin: controls on their distribution. Geol. Soc. Lond. Spec. Publ. 306, 169–183. doi:10.1144/SP306.8

Peron-Pinvidic, G., Manatschal, G., Masini, E., Sutra, E., Flament, J.M., Haupert, I., Unternehr, P., 2015. Unravelling the along-strike variability of the Angola-Gabon rifted margin: a mapping approach. Geol. Soc. Lond. Spec. Publ. doi:10.1144/SP438.1

Peron-Pinvidic, G., Manatschal, G., Osmundsen, P.T., 2013. Structural comparison of archetypal Atlantic rifted margins: A review of observations and concepts. Mar. Pet. Geol. 43, 21–47. doi:10.1016/j.marpetgeo.2013.02.002

Portugal-Ferreira, M., Morata, D., Puga, E., Demant, A., Aguirre, L., 1995. Evolución geoquímica y temporal del magmatismo básico mesozoico en las Zonas Externas de las Cordilleras Béticas. Estud. Geológicos 51. doi:10.3989/egeol.95513-4289

Reston, T., Manatschal, G., 2011. Rifted Margins: Building Blocks of Later Collision, in: Arc-Continent Collision, Frontiers in Earth Sciences. Springer Berlin Heidelberg, pp. 3–21.

Rey, J., 2009. Les Formations Crétacées de l'Algarve Oriental. Comun. Geológicas 19–38.

Rey, J., 2006. Les formations Crétacées de l'Algarve occidental et central. Comun. Geológicas 93, 39–80.

Rey, J., 1983. Le Cretacé de l'Algarve: essay de synthèse. Com Ser Geol Port 69, 87–101.

Ribeiro, A., Cabral, J., Baptista, R., Matias, L., 1996. Stress pattern in Portugal mainland and the adjacent Atlantic region, West Iberia. Tectonics 15, 641–659. doi:10.1029/95TC03683

Rocha, R.B., 1976. Estudo estratigráfico e paleontológico do jurássico do Algarve Ocidental. PhD Thesis, Universidade Nova de Lisboa, Lisboa (178 pp).

Roque, C., 2007. Tectonostratigrafia do cenozóico das margens continentais sul e sudoeaste portuguesas: um modelo de correlação sismostratigráfica. PhD Thesis, Universidade de Lisboa (310 pp).

Rosas, F.M., Duarte, J.C., Terrinha, P., Valadares, V., Matias, L., 2009. Morphotectonic characterization of major bathymetric lineaments in Gulf of Cadiz (Africa–Iberia plate boundary): Insights from analogue modelling experiments. Mar. Geol. 261, 33–47. doi:10.1016/j.margeo.2008.08.002

Rouchy, J.M., Caruso, A., 2006. The Messinian salinity crisis in the Mediterranean basin: A reassessment of the data and an integrated scenario. Sediment. Geol. 188–189, 35–67. doi:10.1016/j.sedgeo.2006.02.005

Sallarès, V., Gailler, A., Gutscher, M.-A., Graindorge, D., Bartolomé, R., Gràcia, E., Díaz, J., Dañobeitia, J.J., Zitellini, N., 2011. Seismic evidence for the presence of Jurassic oceanic crust in the central Gulf of Cadiz (SW Iberian margin). Earth Planet. Sci. Lett. 311, 112–123. doi:10.1016/j.epsl.2011.09.003

Sallarès, V., Martínez-Loriente, S., Prada, M., Gràcia, E., Ranero, C., Gutscher, M.-A., Bartolome, R., Gailler, A., Dañobeitia, J.J., Zitellini, N., 2013. Seismic evidence of exhumed mantle rock basement at the Gorringe Bank and the adjacent Horseshoe and Tagus abyssal plains (SW Iberia). Earth Planet. Sci. Lett. 365, 120–131. doi:10.1016/j.epsl.2013.01.021

Sartori, R., Torelli, L., Zitellini, N., Peis, D., Lodolo, E., 1994. Eastern segment of the Azores-Gibraltar line (central-eastern Atlantic): An oceanic plate boundary with diffuse compressional deformation. Geology 22, 555–558.

Schettino, A., Turco, E., 2011. Tectonic history of the western Tethys since the Late Triassic. Geol. Soc. Am. Bull. 123, 89–105.

Schuster, D.C., 1995. Deformation of allochthonous salt and evolution of related salt-structural systems, eastern Louisiana Gulf Coast, in: M. P. A. Jackson, D. G. Roberts, and S. Snelson, Eds., Salt Tectonics: A Global Perspective: AAPG Memoir 65. pp. 177–198.

Simancas, J.F., Carbonell, R., González Lodeiro, F., Pérez Estaún, A., Juhlin, C., Ayarza, P., Kashubin, A., Azor, A., Martínez Poyatos, D., Almodóvar, G.R., Pascual, E., Sáez, R., Expósito, I., 2003. Crustal structure of the transpressional Variscan orogen of SW Iberia: SW Iberia deep seismic reflection profile (IBERSEIS). Tectonics 22, 1062. doi:10.1029/2002TC001479

Smith, W.H., Sandwell, D.T., 1997. Global sea floor topography from satellite altimetry and ship depth soundings. Science 277, 1956–1962.

Soriano, C., 1996. Tectónica de cabalgamientos en la Faja Pirítica Ibérica (Zona Sur Portuguesa): el Antiforme de la Puebla de Guzmán, y la lámina de cabalgamiento de Sanlúcar de Guadiana. Geogaceta 20, 786–788.

Soto, R., Kullberg, J.C., Oliva-Urcia, B., Casas-Sainz, A.M., Villalaín, J.J., 2012. Switch of Mesozoic extensional tectonic style in the Lusitanian basin (Portugal): Insights from magnetic fabrics. Tectonophysics 536–537, 122–135. doi:10.1016/j.tecto.2012.03.010

Srivastava, S.P., Roest, W.R., Kovacs, L.C., Oakey, G., Levesque, S., Verhoef, J., Macnab, R., 1990a. Motion of Iberia since the Late Jurassic: results from detailed aeromagnetic measurements in the Newfoundland Basin. Tectonophysics 184, 229–260.

Srivastava, S.P., Schouten, H., Roest, W.R., Klitgord, K.D., Kovacs, L.C., Verhoef, J., Macnab, R., 1990b. Iberian plate kinematics: a jumping plate boundary between Eurasia and Africa. Nature 344, 756–759. doi:10.1038/344756a0

Srivastava, S.P., Verhoef, J., 1992. Evolution of Mesozoic sedimentary basins around the North Central Atlantic: a preliminary plate kinematic solution. Geol. Soc. Lond. Spec. Publ. 62, 397–420. doi:10.1144/GSL.SP.1992.062.01.30

Stampfli, G.M., Borel, G.D., 2002. A plate tectonic model for the Paleozoic and Mesozoic constrained by dynamic plate boundaries and restored synthetic oceanic isochrons. Earth Planet. Sci. Lett. 196, 17–33.

Stapel, G., 1999. The Nature of Isostasy in West Iberia and Its Bearing on Mesozoic and Cenozoic Regional Tectonics PhD Thesis, Vrije Universiteit (148 pp).

Stapel, G., Cloetingh, S., Pronk, B., 1996. Quantitative subsidence analysis of the Mesozoic evolution of the Lusitanian basin (western Iberian margin). Tectonophysics, Dynamics of Extensional Basins and Inversion Tectonics 266, 493–507. doi:10.1016/S0040-1951(96)00203-X

Stewart, S.A., 2007. Salt tectonics in the North Sea Basin: a structural style template for seismic interpreters. Geol. Soc. Lond. Spec. Publ. 272, 361–396. doi:10.1144/GSL.SP.2007.272.01.19

Stich, D., Serpelloni, E., de Lis Mancilla, F., Morales, J., 2006. Kinematics of the Iberia–Maghreb plate contact from seismic moment tensors and GPS observations. Tectonophysics 426, 295–317. doi:10.1016/j.tecto.2006.08.004

Talwani, M., 1965. Computation with the help of a digital computer of magnetic anomalies caused by bodies of arbitrary shape. Geophysics 30, 797–817. doi:10.1190/1.1439654

Talwani, M., Worzel, J.L., Landisman, M., 1959. Rapid gravity computations for two-dimensional bodies with application to the Mendocino submarine fracture zone. J. Geophys. Res. 64, 49–59. doi:10.1029/JZ064i001p00049

Teixell, A., Arboleya, M.-L., Julivert, M., Charroud, M., 2003. Tectonic shortening and topography in the central High Atlas (Morocco). Tectonics 22, 1051. doi:10.1029/2002TC001460

Terrinha, P., 1998. Structural geology and tectonic evolution of the Algarve Basin, South Portugal. PhD Thesis, Imperial College, London (430 pp).

Terrinha, P., Coward, M., Ribeiro, A., 1990. Salt tectonics in the Algarve Basin: The Loulé diapir. Comun. Serviços Geológicos Port. 76, 33–40.

Terrinha, P., Matias, L., Vicente, J., Duarte, J., Luís, J., Pinheiro, L., Lourenço, N., Diez, S., Rosas, F., Magalhães, V., Valadares, V., Zitellini, N., Roque, C., Víctor, L.M., 2009. Morphotectonics and strain partitioning at the Iberia–Africa plate boundary from multibeam and seismic reflection data. Mar. Geol. 267, 156–174. doi:10.1016/j.margeo.2009.09.012

Terrinha, P., Ribeiro, C., Kullberg, J.C., Lopes, C., Rocha, R., Ribeiro, A., 2002. Compressive episodes and faunal isolation during rifting, Southwest Iberia. J. Geol. 110, 101–113.

Terrinha, P., Rocha, R.B., Rey, J., Cachão, M., Moura, D., Roque, C., Martins, L., Valadares, V., Cabral, J., Azevedo, M.R., Barbero, L., Clavijo, E., Dias, R.P., Gafeira, J., Matias, H., Matias, L., Madeira, C.M.S., Munhã, J., Rebêlo, L.P., Ribeiro, C., Vicente, J., Noiva, J., Youbi, N., Bensalah, M.K., 2013. A Bacia do Algarve: Estratigrafia, Paleogeografia e Tectónica. In: Geologia de Portugal, Vol. II: Geologia Meso-cenozóica de Portugal. Eds. Rui Dias, Alexandre Araújo, Pedro Terrinha, José Carlos Kullberg. Lisboa : Livraria Escolar Editora, Cap III: p. 29-166.

TGS, 2005. PD00: non-exclusive 2D Survey, TGS online data zone. (http://www.tgs.com/TGS/specsheets/PD-00_Spec.pdf).

Torelli, L., Sartori, R., Zitellini, N., 1997. The giant chaotic body in the Atlantic Ocean off Gibraltar: new results from a deep seismic reflection survey. Mar. Pet. Geol. 14, 125–138. doi:10.1016/S0264-8172(96)00060-8

Tortella, D., Torne, M., Pérez-Estaún, A., 1997. Geodynamic evolution of the eastern segment of the Azores-Gibraltar zone: the Gorringe Bank and the Gulf of Cadiz region. Mar. Geophys. Res. 19, 211–230.

Tugend, J., Manatschal, G., Kusznir, N.J., Masini, E., Mohn, G., Thinon, I., 2014. Formation and deformation of hyperextended rift systems: Insights from rift domain mapping in the Bay of Biscay-Pyrenees. Tectonics 33, 1239–1276. doi:10.1002/2014TC003529

Vázquez-Vílchez, M., Jabaloy-Sánchez, A., Azor, A., Stuart, F., Persano, C., Alonso-Chaves, F.M., Martín-Parra, L.M., Matas, J., García-Navarro, E., 2015. Mesozoic and Cenozoic exhumation history of the SW Iberian Variscides inferred from low-temperature thermochronology. Tectonophysics 663, 110–121. doi:10.1016/j.tecto.2015.06.034

Vegas, R., 1980. Carboniferous subduction complex in the south portuguese zone coeval with basament reactivation and uplift in the Iberian massif. Cad. Lab. Xeol. Laxe Rev. Xeoloxía Galega E Hercínico Penins. 187–204.

Vegas, R., Medialdea, T., Muñoz García, M., Díaz del Río, V., Somoza, L., 2004. Nature and tectonic setting of the Guadalquivier Bank (Gulf of Cadiz, SW Iberian Peninsula). Rev. Soc. Geológica Esp. 17, 49–60.

Vera, J.A., 1988. Evolución de los sistemas de depósito en el margen ibérico de la Cordillera Bética. Rev. Soc. Geológica Esp. 1, 373–391.

Vera, J.A., Molina, J.M., Aguado, R., 2004. Calcarenitas de Microcodium (Formación Majalcorón, Paleoceno, Subbético): descripción, bioestratigrafía y significado en el Terciario de la Cordillera Bética. Bol. Geológico Min. Esp. 115, 453–468.

Vera, J.A., Molina, J.M., Montero, P., Bea, F., 1997. Jurassic guyots on the Southern Iberian Continental Margin: a model of isolated carbonate platforms on volcanic submarine edifices. Terra Nova 9, 163–166. doi:10.1046/j.1365-3121.1997.d01-22.x

Verati, C., Rapaille, C., Féraud, G., Marzoli, A., Bertrand, H., Youbi, N., 2007. 40Ar/39Ar ages and duration of the Central Atlantic Magmatic Province volcanism in Morocco and Portugal and its relation to the Triassic–Jurassic boundary. Palaeogeogr. Palaeoclimatol. Palaeoecol. 244, 308–325. doi:10.1016/j.palaeo.2006.06.033

Vergés, J., Fernàndez, M., 2012. Tethys–Atlantic interaction along the Iberia–Africa plate boundary: The Betic–Rif orogenic system. Tectonophysics 579, 144–172. doi:10.1016/j.tecto.2012.08.032

Vissers, R.L.M., van Hinsbergen, D.J.J., Meijer, P.T., Piccardo, G.B., 2013. Kinematics of Jurassic ultra-slow spreading in the Piemonte Ligurian ocean. Earth Planet. Sci. Lett. 380, 138–150. doi:10.1016/j.epsl.2013.08.033

Wilson, P.G., Turner, J.P., Westbrook, G.K., 2003. Structural architecture of the ocean–continent boundary at an oblique transform margin through deep-imaging seismic interpretation and gravity modelling: Equatorial Guinea, West Africa. Tectonophysics 374, 19–40. doi:10.1016/S0040-1951(03)00326-3

Wilson, R.C.L., 1988. Mesozoic development of the Lusitanian basin, Portugal. Rev. Soc. Geológica Esp. 1, 393–407.

Zeyen, H., Ayarza, P., Fernàndez, M., Rimi, A., 2005. Lithospheric structure under the western African-European plate boundary: A transect across the Atlas Mountains and the Gulf of Cadiz. Tectonics 24, TC2001. doi:10.1029/2004TC001639

Ziegler, P.A., 1988. Evolution of the Arctic-North Atlantic and the Western Tethys, AAPG Memoir 43 edition. ed. Amer Assn of Petroleum Geologists, Tulsa, Okla., U.S.A.

Zitellini, N., Gràcia, E., Matias, L., Terrinha, P., Abreu, M.A., DeAlteriis, G., Henriet, J.P., Dañobeitia, J.J., Masson, D.G., Mulder, T., 2009. The quest for the Africa–Eurasia plate boundary west of the Strait of Gibraltar. Earth Planet. Sci. Lett. 280, 13–50. doi:10.1016/j.epsl.2008.12.005

Zizi, M., 1996. Triassic-Jurassic extensional systems and their Neogene reactivation in northern Morocco (the Rides Prerifaines and Guercif Basin). PhD thesis, Rice University (574 pp).

APPENDIX 1.1

Extension and inversion structures in the Tethys–Atlantic linkage zone, Algarve Basin, Portugal.

Fernández, O., Terrinha, P., Muñoz, J.A., 2016. International Journal of Earth Sciences. 105, 1663–1679. doi:10.1007/s00531-015-1280-1.

Int J Earth Sci (Geol Rundsch)
DOI 10.1007/s00531-015-1280-1

ORIGINAL PAPER

Extension and inversion structures in the Tethys–Atlantic linkage zone, Algarve Basin, Portugal

Adrià Ramos[1] · Oscar Fernández[2] · Pedro Terrinha[3] · Josep Anton Muñoz[1]

Received: 28 July 2015 / Accepted: 22 November 2015

Abstract The Algarve Basin is a Meso-Cenozoic sedimentary basin overlying Carboniferous basement, located in the southwestern margin of the Iberian Peninsula. Its structure reveals a protracted tectonic history comprising various pulses of Mesozoic extension followed by Cenozoic compression. This work deals with the structure along the northern margin, where the Mesozoic extensional structures and Cenozoic inversion structures crop out. The strike of the extensional structures ranges from E–W to N–S, as controlled by a shift from Tethyan-dominated extension in the east to Atlantic-dominated extension in the west. Contractional structures are inverted extensional structures, following their same trends. It is argued that the thickness of the Hettangian evaporite layer exerts a strong control on the structural style throughout the basin during the extensional and inversion episodes. The basin is affected by thick-skinned deformation along the northern margin, where salt is thin or absent, basement involved fault systems and short-cut structures. Basinward, as the Hettangian salt thickens, the margin is affected by thin-skinned deformation, with listric and down-to-the-basin growth faults, diapirism and salt-cored detachment folds. The aim was to discuss the key tectonic features, the relevance of salt, and understand the nature, timing, and significance of all these structures in the regional tectonic evolution.

✉ Adrià Ramos
adriaramos@ub.edu

[1] Departament de Geodinàmica i Geofísica, Facultat de Geologia, Institut Geomodels, Universitat de Barcelona, Barcelona, Spain

[2] Repsol Exploración, Dirección de Geología, Madrid, Spain

[3] Divisão de Geologia e Georecursos Marinhos, Instituto Português do Mar e da Atmosfera, Lisbon, Portugal

Keywords Algarve Basin · Extensional tectonics · Inversion tectonics

Introduction

The Algarve Basin in the Gulf of Cadiz is a Meso-Cenozoic sedimentary basin located on the southwestern margin of the Iberian Peninsula, north of the Africa–Iberia plate boundary (Fig. 1). Rifting occurred during the breakup of Pangea, associated with the opening of the North-Central Atlantic and Tethys oceans. The Mesozoic sedimentary record of the basin spans from the Late Triassic to the Early Cretaceous, with the main depocenter located in the central part of the offshore Algarve Basin. The basin extends to the offshore as far as 100 km south, as recognized on several seismic surveys. The southern margin of the basin is defined by the Gulf of Cadiz Basement High (GoCBH), a ENE–WSW trending structure with bathymetric relief (Fig. 1). Oceanic lithosphere extends beyond the GoCBH (Sallarès et al. 2011), interpreted to be the westernmost part of the Tethys Ocean (Martínez-Loriente et al. 2013), which has partially been subducted under the Gibraltar Arc (Gutscher et al. 2002).

Two main tectonic phases have been documented for the Gulf of Cadiz and the Algarve basins: a Mesozoic phase dominated by extensional tectonics, and a compressional phase from Late Cretaceous to Quaternary (mainly during Cenozoic), related to the collision between Iberia and Africa (Tortella et al. 1997; Terrinha 1998; Maldonado et al. 1999; Gutscher et al. 2002; Gràcia et al. 2003; Terrinha et al. 2009). Terrinha (1998) developed a detailed tectonic model for the Mesozoic basin onshore, along with a kinematic model for the offshore Cenozoic basin, linked to the geodynamic evolution of the Gulf of Cadiz and the Betic Cordillera. However, the relationship between the onshore Mesozoic basin

Published online: 10 December 2015

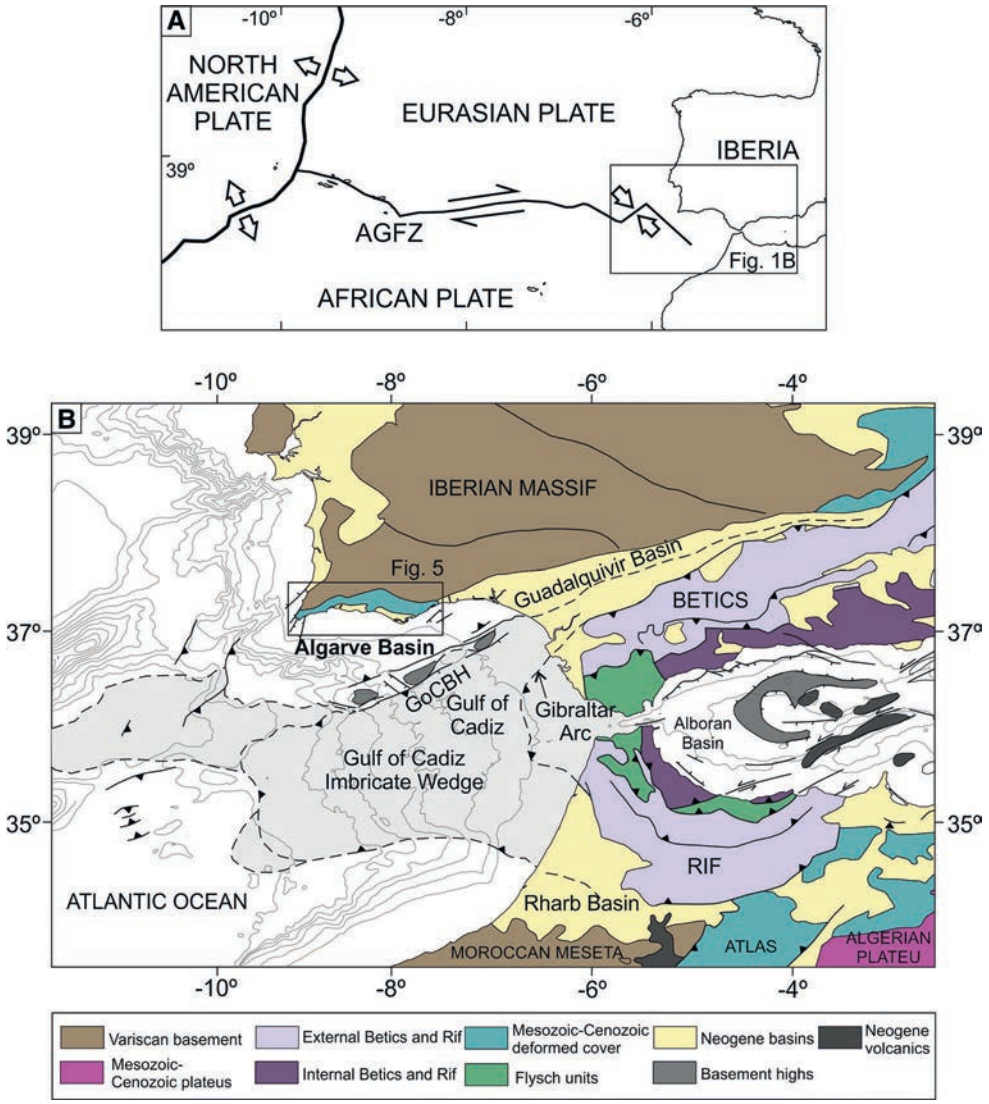

Fig. 1 **a** Main elements of plate boundaries and relative plate kinematics. *AGFZ* Azores–Gibraltar fracture zone. **b** Geologic map of the Betic–Rif system showing the principal tectonic units and associated Neogene basins (modified from Iribarren et al. 2007). *GoCBH* Gulf of Cadiz Basement High

and its deeper counterparts, in the Gulf of Cadiz and west toward the Atlantic Ocean, has not been fully resolved.

This paper presents a revision of the interpretation of the tectonic architecture of the onshore, northern margin of the Algarve Basin, and its significance in defining the transition between the Tethys and the Atlantic extensional domain. An improved understanding of the Mesozoic extensional systems also sheds light on the relationship between Mesozoic extension and Cenozoic contraction, and the role of the salt in the structural evolution of the Algarve Basin.

Geological setting

Stratigraphy

The stratigraphy of the Algarve Basin presented here (Fig. 2) is defined onshore and offshore by Manuppella (1988), Terrinha (1998), and Matias (2007). Mesozoic sedimentation starts with red continental alluvial clastics in the Late Triassic (Rhaetian; Fig. 3d). Triassic rocks unconformably rest on low-grade metamorphosed Carboniferous flysch sediments and Permian rocks that were involved in Variscan deformation (Fig. 4). The overlying Hettangian pelite–evaporitic unit is made up of alluvial to shallow lacustrine red shales (Fig. 2), a thin layer of shallow water dolomites, and an evaporitic sequence constituted by halite, anhydrite, and gypsum. At the Hettangian–Sinemurian transition, these units are capped by a volcano-sedimentary complex consisting of basaltic lavas and pyroclastic rocks intercalated with clays and dolomites (Fig. 2). This volcanic event is associated with the Central Atlantic Magmatic Province (CAMP; Martins et al. 2008; Verati et al. 2007) and the ending of the first extensional episode in the Algarve Basin (Terrinha et al. 2002).

Limestones and dolomitic limestones of the Early Jurassic give way gradually to more marly units during the

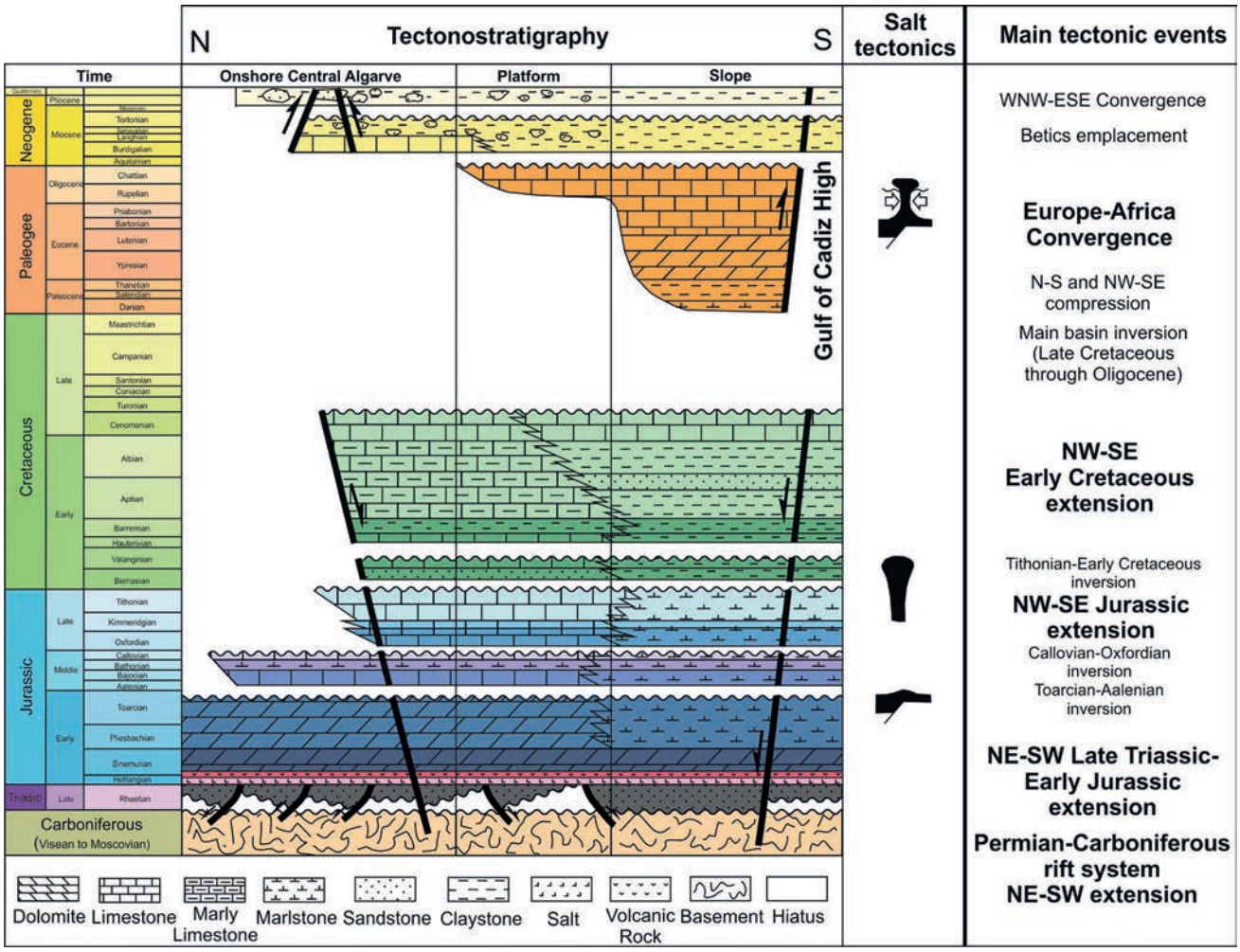

Fig. 2 Simplified stratigraphy of the Algarve Basin with main stratigraphic units and main tectonic events. *Bold type* represents the major tectonic events (adapted from Terrinha 1998; Matias et al. 2011; Fernandes et al. 2013)

Middle Jurassic, and the Late Jurassic consists of limestones (Fig. 2).

The Lower Cretaceous was deposited during the latest phase of extension, after a brief hiatus, and is represented by a mixed carbonate and siliciclastic succession (Rey 1983, 2006, 2009; Fig. 2). The Upper Cretaceous and Paleogene are absent due to uplift during the main phase of basin inversion. Upper Cretaceous rocks are only represented locally by volcanic products such as dikes and sills (Martins 1999; Martins and Munhá 1993) associated with the emplacement of the Monchique alkaline laccolith complex (Miranda et al. 2009). The emplacement age is well constrained to 72 ± 2 Ma by several whole-rock K–Ar and Rb–Sr data (e.g., McIntyre and Berger 1982; Bernard-Griffiths et al. 1997). Sedimentary rocks of Late Cretaceous and Paleogene age have only been described in offshore wells. The Mesozoic rocks of the Algarve Basin are bounded by a regional erosional unconformity, overlain by Neogene strata (Fig. 3f). Locally, the entire Mesozoic sequence is eroded, setting the Miocene directly on top of the Paleozoic basement. The Miocene is represented by limestones that grade upwards into siltstones and fine sandstones (Pais et al. 2000). These units were karstified and covered by Pliocene to Pleistocene fluvial/marine detrital sediments. The youngest sediments Algarve Basin are lithified Holocene beach sand and dunes, influenced by frequent climatic oscillations and sea level fluctuations (Moura et al. 2007).

Structure and evolution

The extensional evolution of the Algarve Basin starts with rifting in the Mid–Late Triassic along the sinistral transtensional boundary between Iberia and Africa. The relative motion of both plates was controlled by the differential movement of Africa with respect to Eurasia and North America, associated with the breakup of Pangea and the


A
N-S
Tithonian
B
W-E
Tithonian
Kimmeridgian
C
SW-NE
Bathonian
Bajocian
D
N-S
Triassic
Triassic
E
S-N
Detrital
Lower Cretaceous
F
S-N
Miocene
Lower
Cretaceous
G
NW-SE
Kimmeridgian
Oxfordian
Callovian

◀ **Fig. 3** Outcrops of the Algarve Basin. **a** Upper Jurassic rollover, located in the hanging-wall of the Algibre Thrust. Normal polarity toward the north. It corresponds to the minor rollover of Fig. 12b. An equivalent image of the outcrop can be explored here: https://goo.gl/maps/iBnr9Z6NdZJ2; latitude and longitude: 37.169755N, −8.2552556W. **b** N–S extensional fault affecting the Upper Jurassic in the western sub-basin. Latitude and longitude: 37.063481N, −8.792303W. **c** Bajocian SW-dipping extensional faults fossilized by Bathonian sediments. 37.003903, −8.942807. **d** South-directed thrust affecting the Triassic unit in the margin of the basin. It is analogous to the thrusts in Fig. 10c. An equivalent image of the outcrop can be explored here: https://goo.gl/maps/rM6USoYiSLM2; latitude and longitude: 37.2631981N, −8.2932982W. **e** Highly steeped flank of Lower Cretaceous below the Algibre Thrust. See Fig. 12b. Latitude and longitude: 37.164728N, −8247658W. **f** Erosional unconformity between the Lower Cretaceous and the Miocene, south of the Albufeira diapir. See Fig. 12b. Latitude and longitude: 37.080496N, −8.261459W. **g** Praia do Cilheta outcrop: Oxfordian faulting and an inverted Middle/Upper Jurassic rollover during the Cenozoic. *Red line* faults, *dashed red line* interpreted fault, *white line* bedding plane, *dotted white line* unconformity. Latitude and longitude: 37.008546N, −8.948964W

development of the westernmost Neo-Tethys (Srivastava et al. 1990; Dewey et al. 1989). As a result, a new ENE–WSW trend extensional fault system dominated the basin. Extension lasted into the Early Cretaceous. During this time the structural style of the basin was dominated by extensional faulting and diapirism (Terrinha 1998; Maldonado et al. 1999; Matias et al. 2005).

Four main unconformities or hiatuses can be identified in the Jurassic to Early Cretaceous succession, defining five sedimentary mega-cycles (Fig. 2, Manuppella 1988; Terrinha et al. 2002). These unconformities have been interpreted as episodes of inversion or non-deposition between extensional episodes, based on inversion structures identified onshore and offshore (Terrinha 1998; Lopes 2002) and later defined by Terrinha et al. (2002). The first extensional phase starts in the Triassic and ends in the Sinemurian and is followed by a short period of marine transgression and tectonic quiescence. Subsequent extension is punctuated by three episodes of inversion that occurred in the Toarcian–Aalenian, the Callovian–Oxfordian, and the Tithonian–Berriasian transition. These episodes of tectonic inversion resulted in the partial reactivation of syn-sedimentary extensional faults and the development of small amplitude folds and unconformities. Terrinha et al. (2002) proposed three kinematic models for the inversion episodes: reversal of the shear movement of the Iberia–Africa plate boundary, ridge push, and compression induced by thermal collapse. The last extensional phase took place in the Early Cretaceous and lasted until the Cenomanian. Within this phase there is the presence of a major unconformity, related to a marine regression (Correia 1989), during the Valanginian–Hauteirian in the central-eastern sub-basin, or during the Valanginian–Berriasian in the western sub-basin.

The extensional fault system is compartmentalized by N–S to NW–SE trending faults (Aljezur, Portimão and São Marcos-Quarteira faults, Fig. 5b). These faults controlled changes in the deposition of the Mesozoic units, which thicken eastwards across these faults (Terrinha 1998).

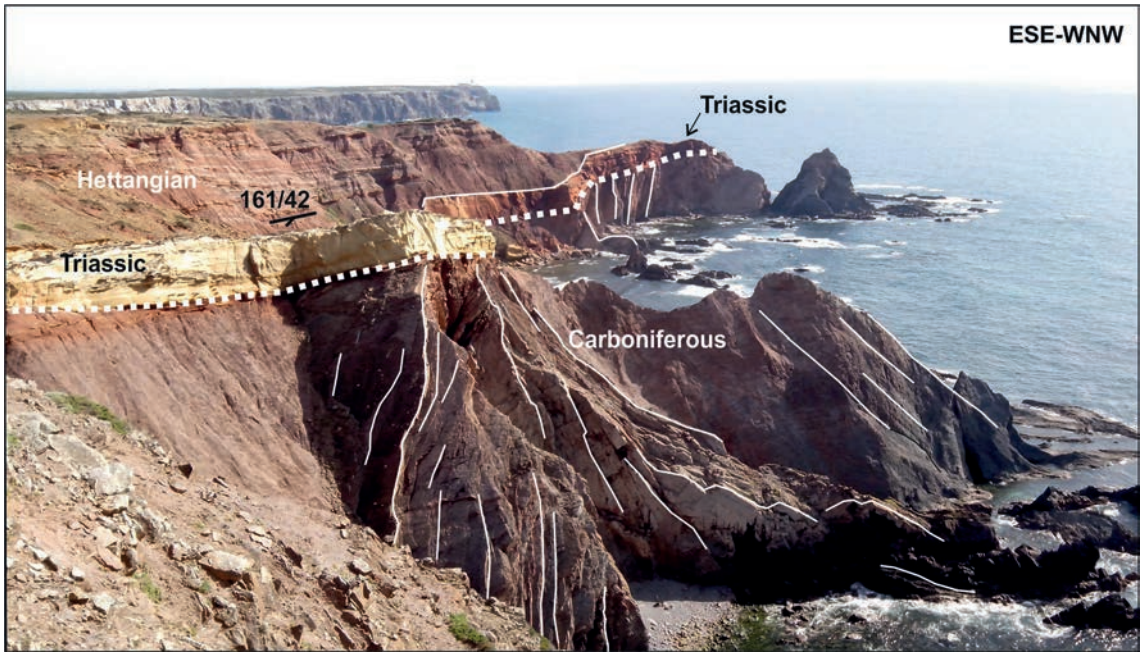

Fig. 4 Praia do Telheiro landscape. Triassic unconformably on *top* of Carboniferous *vertical* layers. Notice the south-dipping of the basin margin. *White line* bedding plane, *dotted white line* unconformity. Latitude and longitude: 37.051607N, −8.980471W

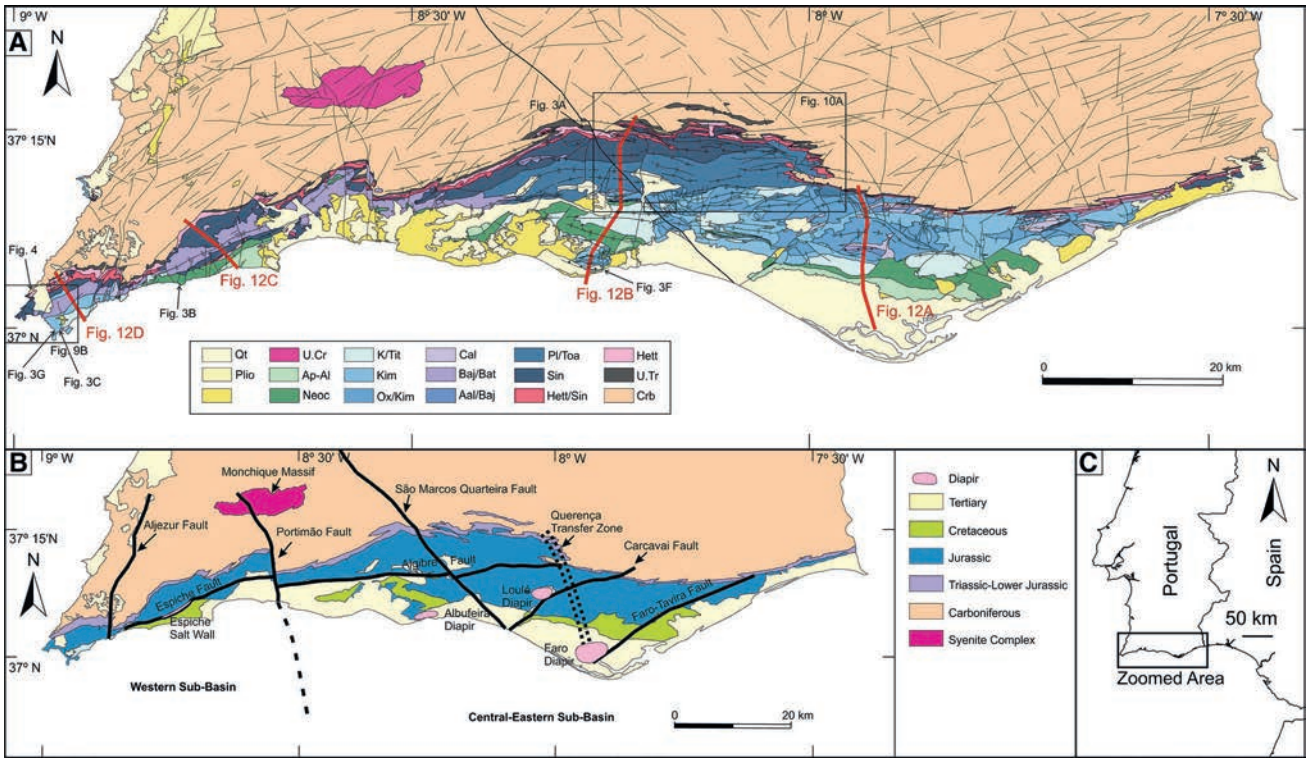

Fig. 5 **a** Study area location and geological map of the Algarve Basin (modified from Manuppella 1992; Terrinha 1998 and Davison et al. 2015). *Qt* Quaternary, *Plio* Piocene, *Mc* Miocene, *U. Cr* Upper Cretaceous, *Ap–Al* Aptian–Albian, *Neoc* Neocomian, *K/Tit* Kimmeridgian/Tithonian, *Kim* Kimmeridgian, *Ox/Kim* Oxfordian/Kimmeridgian, *Cal* Callovian, *Baj/Bat* Bajonian/Batonian, *Aal/Baj* Aalenian/Bajocian, *Pl/Toa* Pliensbaquian/Toarcian, *Sin* Sinemurian, *Hett/Sin* Hettangian/Sinemurian, *Hett* Hettangian, *U. Tr* Upper Triassic, *Crb* Carboniferous. **b** Simplified map showing major tectonic features, which have had different behavior since the Late Triassic. **c** Location of the study area

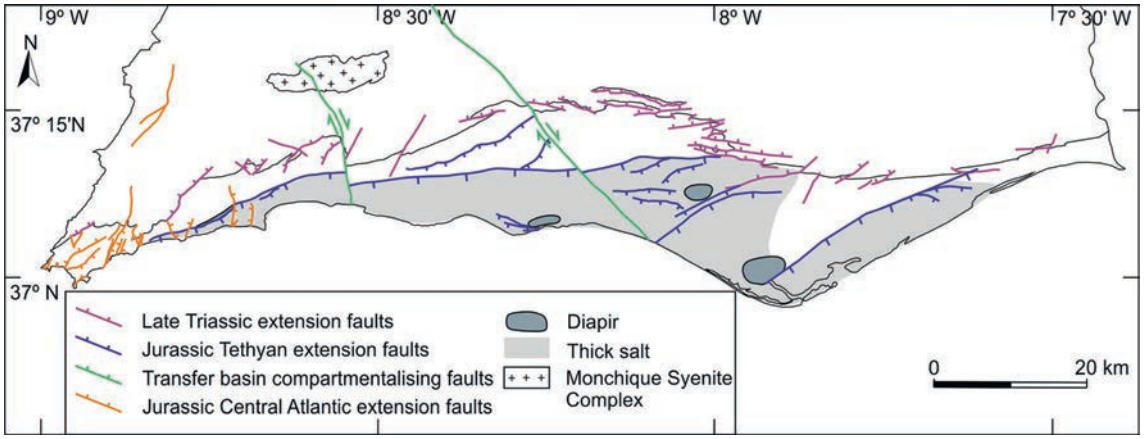

Fig. 6 Mesozoic extensional fault system of the Algarve Basin and the salt distribution. West of the Portimão fault, along the Espiche fault the outcrop is "slay diapir"; At Albufeira the outcropping diapir rock is gypsum; east of the SMQF the diapirs are halite. It seems there is a gradient toward the east from shale thru gypsum/anhydrite to halite; This is also compatible with deepening eastwards

Manuppella (1988) and Manuppella et al. (1988) used the Portimão and São Marco Quarteira faults to define three sub-basins: the western, the Budens-Lagoa/Algoz (central) and the eastern sub-basins. Nevertheless, in this article, we propose a simpler subdivision into only two sub-basins based on the dominant structural features. We will refer to

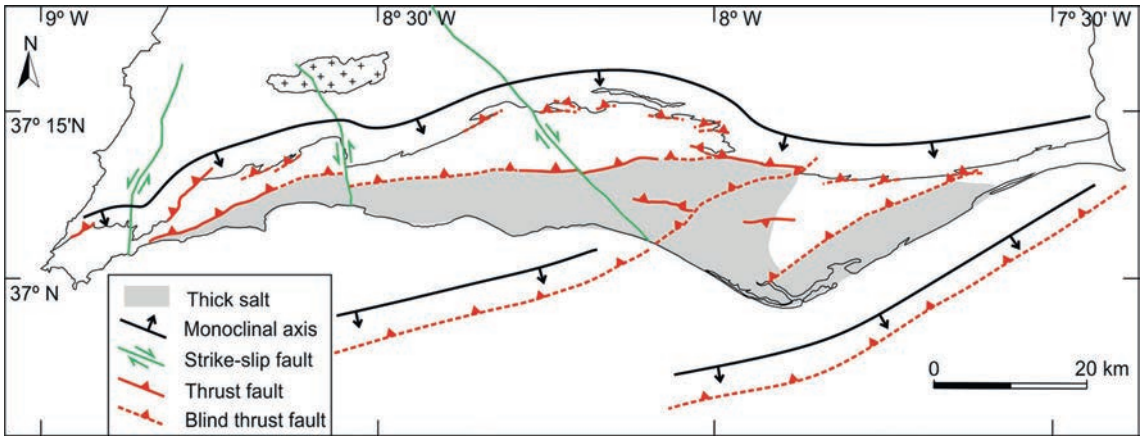

Fig. 7 Late Cretaceous–Cenozoic contractional structures of the Algarve Basin

the western and the central-eastern sub-basins, separated by the Portimão Fault (Fig. 5b). The central-eastern sub-basin is dominated by E–W to ENE–WSW trending extensional faults (Fig. 6), a trend inherited from the Variscan structural grain of the South Portuguese Zone (Terrinha 1998). In the western sub-basin, extensional fault orientation is N–S to NE–SW, parallel to the Atlantic margin of Iberia, cross-cutting some E–W structures that extend from the central-eastern sub-basin. The central-eastern basin and the offshore Algarve Basin are also characterized by Mesozoic salt tectonism of varying intensity (Terrinha 1998; Maldonado et al. 1999; Matias et al. 2005; Figs. 3, 4).

From Late Cretaceous to Quaternary, the basin underwent tectonic inversion due to the convergence between Africa and Iberia. East of the Algarve Basin, convergence led to the formation of the arcuate Betic–Rif mountain belt and the formation of an eastward subduction under the Gibraltar Arc (e.g., Royden 1993; Lonergan and White 1997; Gutscher et al. 2002; Duarte et al. 2011). Basin inversion is characterized by the deformation of ENE–WSW to E–W trending Mesozoic extensional faults (Terrinha 1998; Lopes et al. 2006) and the truncation of these faults by thrusts (Figs. 10b, 11a). Shortening was mainly accommodated by E–W-oriented folds formed by buttressing against extensional faults (Fig. 12b) and south-directed short-cutting of partially reactivated extensional faults. Basin inversion has resulted as well in the reactivation of previously developed salt structures. Diapirs were squeezed against extensional faults to form thrusts (Loulé and Albufeira diapirs, Fig. 12a; Davison et al. 2015). Inversion is also expressed along the basin margin by the general southward dip of the onshore Mesozoic basin. The uplift of the Iberian Peninsula, including the SW Iberian margin, is related to the Cenozoic convergence between Africa and Iberia, which favored the formation of intra-plate mountain ranges (Fernández-Lozano 2012). The recent uplift and south tilting of the margin basin are registered in the coast by an erosional unconformity between Lower Cretaceous and the overlying south-dipping Miocene (Fig. 3f; Terrinha 1998).

Multi-phase deformation of the Algarve Basin: from extension to inversion

The multi-stage tectonic history of the Algarve Basin presented above has resulted in a complex superposition of extensional and contractional structures (Fig. 6). Firstly, the structural fabric is heterogeneous as it varies with the different extensional phases. This is further complicated by the fact that the Algarve Basin formed as an E–W trending rift basin in the vicinity of the N–S trending north-central Atlantic Ocean rift margin. Tectonic inversion due to the N–S convergence between Iberia and Africa later strongly overprinted many of the extensional structures of the basin (Fig. 7). In this section we aim to discuss the different generations of extensional structures that have been observed in the basin and their role in the extensional history of the basin. In order to do this, we will simplify the history of rifting into two main stages, an early rift stage (Late Triassic to Early Jurassic) and the main rift stage (Early Jurassic to Early Cretaceous), and describe the associated structures prior to inversion (Fig. 6).

Late Triassic to Early Jurassic extension

The present-day northern limit of the Algarve Basin is marked by the outcrop of Carboniferous basement unconformably underlying a generally southward dipping Triassic to Lower Jurassic sequence. This basement–basin unconformity is roughly E–W trending (Fig. 5). Along this margin, extensional faults are preserved (Fig. 6). These faults

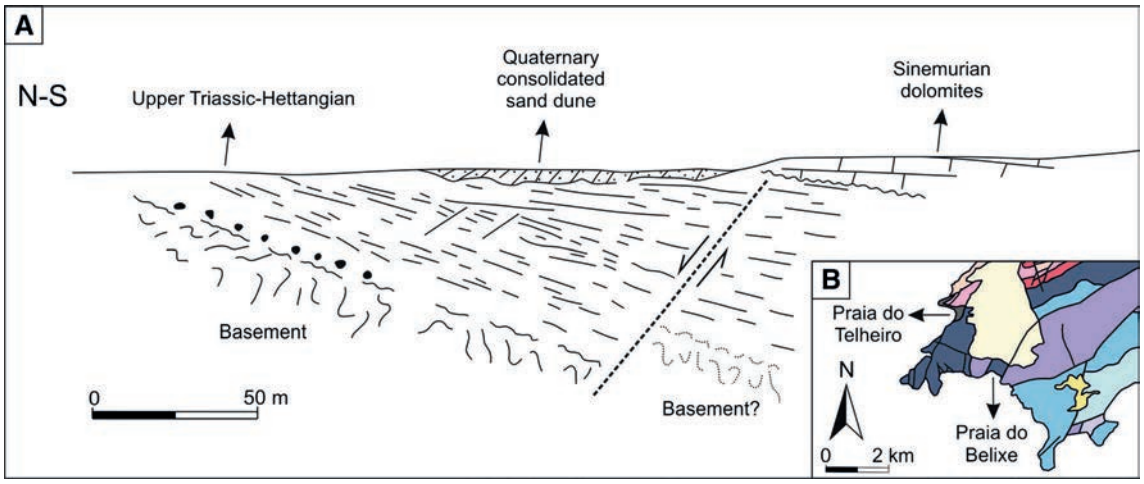

Fig. 8 **a** Triassic–Hettangian growth faults in Praia do Telheiro outcrop. The onlaps of Sinemurian carbonates cover the blind extensional fault and the sedimentary complex of Hettangian age. *Dashed black line* interpreted fault, *dotted black line* interpreted basement (modified after Terrinha 1998). **b** Location of Praia do Telheiro and Praia do Belixe outcrops. See Fig. 5a for location and legend. Latitude and longitude: 37.051607N, −8.980471W

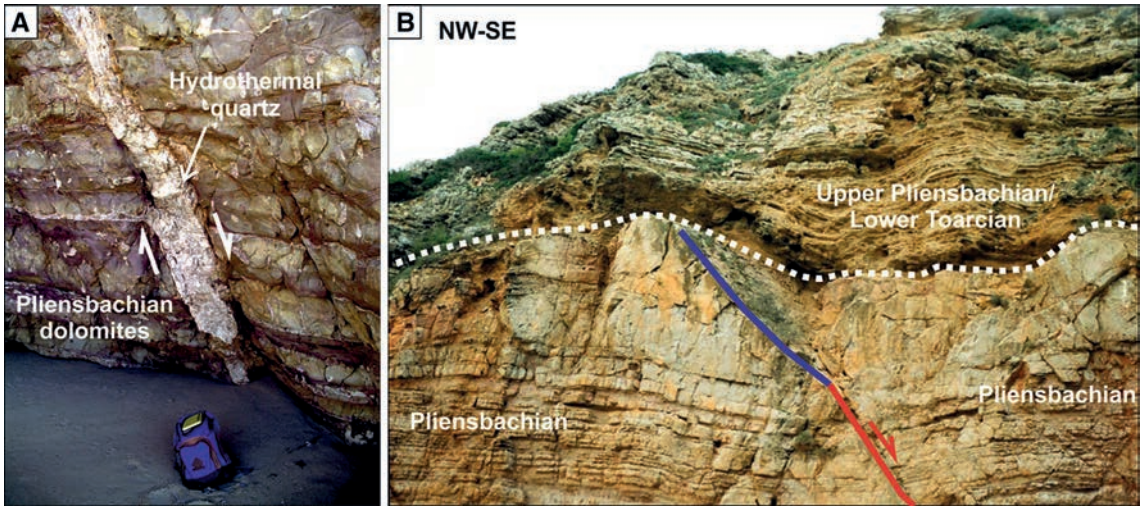

Fig. 9 Praia do Belixe outcrop interpreted photographs. **a** Pliensbachian extensional faults filled with hydrothermal quartz. **b** Extensional faults eroded by intra-Pliensbachian and Early Toarcian unconformities. *Blue line* outcrop splay, *red line* extensional fault. See Fig. 9a for location

are north-dipping, strike E–W to WNW–ESE, and involve basement. They have displacements of tens of meters, juxtaposing Upper Triassic and Lower Jurassic sediments with Carboniferous basement (Figs. 6, 7). This extensional system was active from the Late Triassic to Early Jurassic. The age of the end of deformation can be inferred from the outcrops in Telheiro beach, in the western sub-basin (Fig. 8). Here, a north-dipping fault and its associated half-graben filled with Upper Triassic—Hettangian rocks are covered by Sinemurian sediments. A similar relationship is also seen at an outcrop of Pliensbachian age located at Praia do Belixe (Fig. 9), where syn-sedimentary extensional faults are filled with hydrothermal quartz (Ribeiro and Terrinha 2007). These syn-sedimentary faults are eroded by intra-Pliensbachian and Early Toarcian unconformities (Fig. 9), attesting for syn-rifitng vertical movements of the basin.

These early rifting extensional faults extend a few kilometers north of the present-day limit of Jurassic outcrop, as observed in isolated outcrops of Upper Triassic within the Carboniferous basement (Manuppella 1992, one such example seen in Fig. 10A). This indicates that the present-day northern limit of Jurassic outcrops is not the original limit of the extensional basin; uplift of the basin margin during Cenozoic

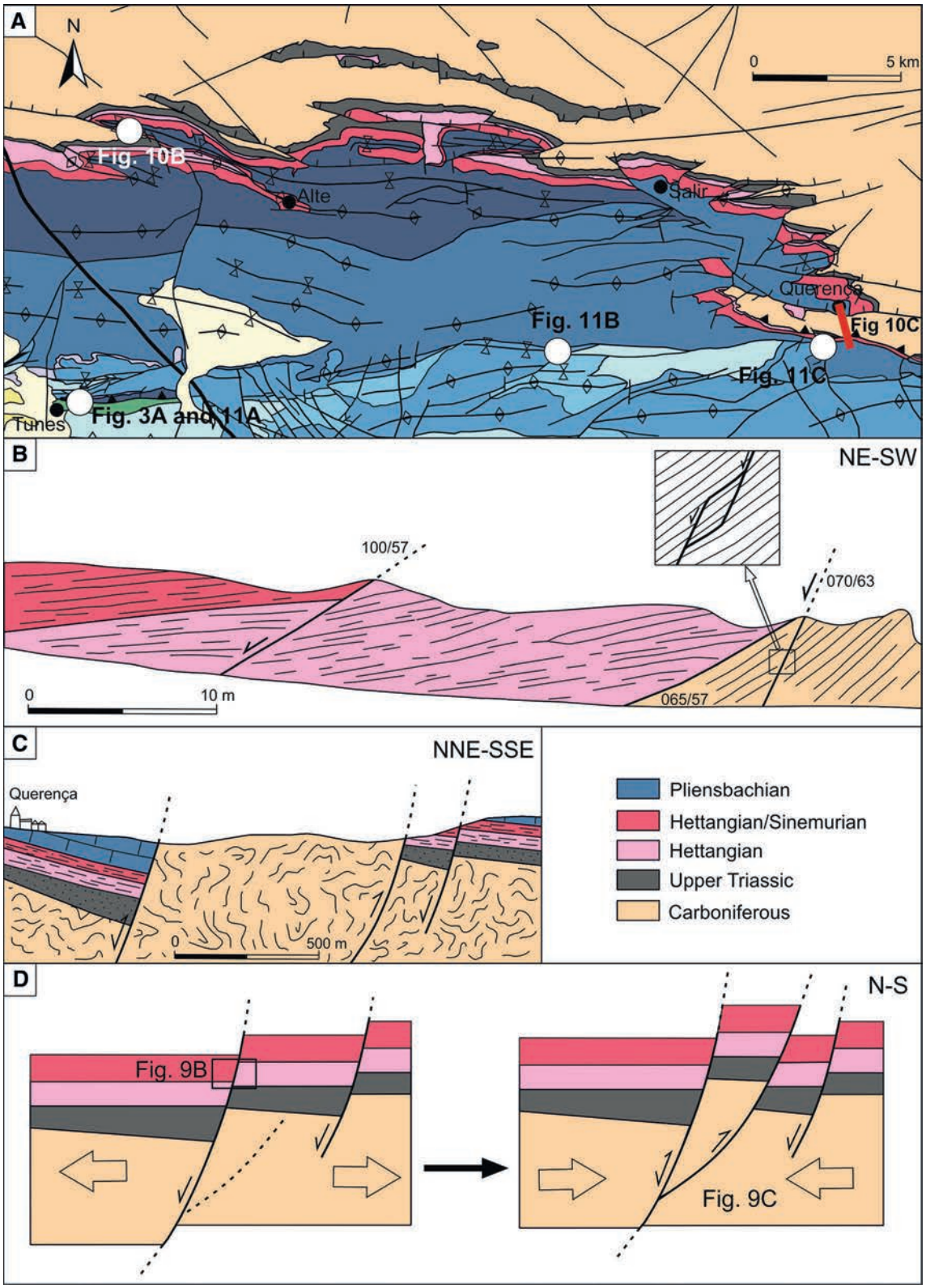

Fig. 10 **a** Geological map with location of outcrops. See Fig. 5a for location and legend. **b** Pico Alto outcrop. An equivalent image of the outcrop can be explored here: https://goo.gl/maps/GgeYcPvmz2n. Latitude and longitude: 37.2604932N, −8.2332851W. **c** Querença cross section. Detail of the extensional fault to the right of the cross section can be explored here: https://goo.gl/maps/7xf6NRiC2kE2; latitude and longitude: 37.1832447N, −7.9656067W. **d** Schematic evolution of the basin-basement contact

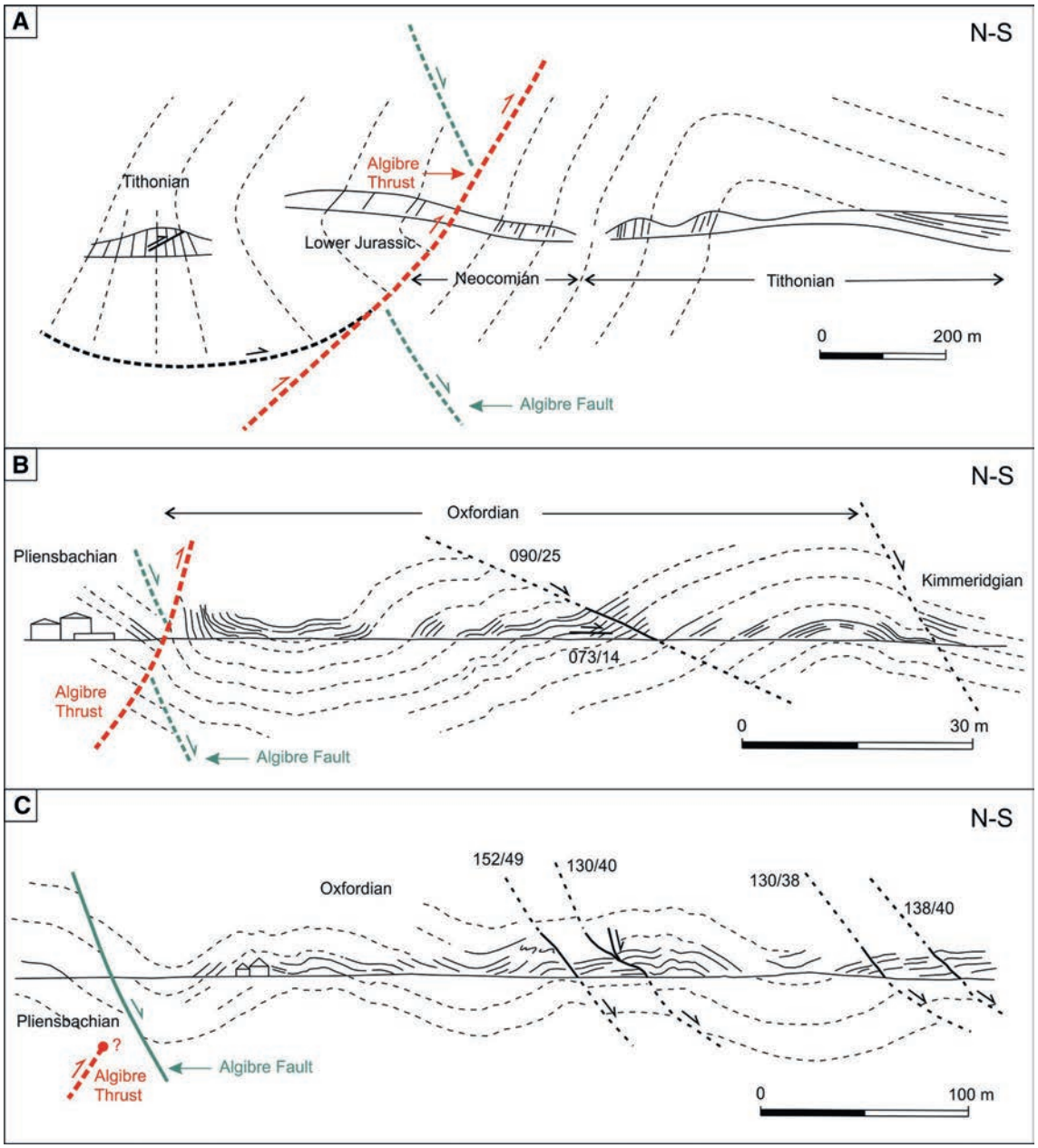

Fig. 11 Key outcrops from W to E showing the Algibre. See Fig. 5a for location. *Solid lines* represents observed outcrop and *dashed lines* represents interpreted bedding and faults. **a** Tunes outcrop. See Fig. 3e for more detail about the rollover structure on the *left* of the figure. Detail of the highly steeped Tithonian can be explored here: https://goo.gl/maps/pLdZNp8Dv5x; latitude and longitude: 37.1621192N, −8.25151W. **b** Ribera de Algibre outcrop. Detail of the highly deformed Oxfordian in the footwall of the Algibre Thrusts can be explored here: https://goo.gl/maps/f5XaNB7mmiH2; latitude and longitude: 37.1830056, −8.0842423. **c** Penedos Altos outcrop. Extensional fault affecting the Oxfordian can be explored here: https://goo.gl/maps/1phYa221f2m; latitude and longitude: 37.183179N, −7.9901272W

inversion has removed Jurassic strata to the north of the present outcrop limit.

Uplift of the basin margin imposes a southward regional dip on the Algarve Basin, which means that the Late Triassic—Early Jurassic fault system does not crop out basinward (to the south), as it is covered by the post-faulting Sinemurian carbonates. However, it is interpreted that this fault system extends south over the entire onshore Algarve Basin. Proof of this is the change in thickness and facies of Hettangian units to the south. Along the northern margin of the basin, this unit is only a few meters thick and dominated by pelites. To the south and to the east, it

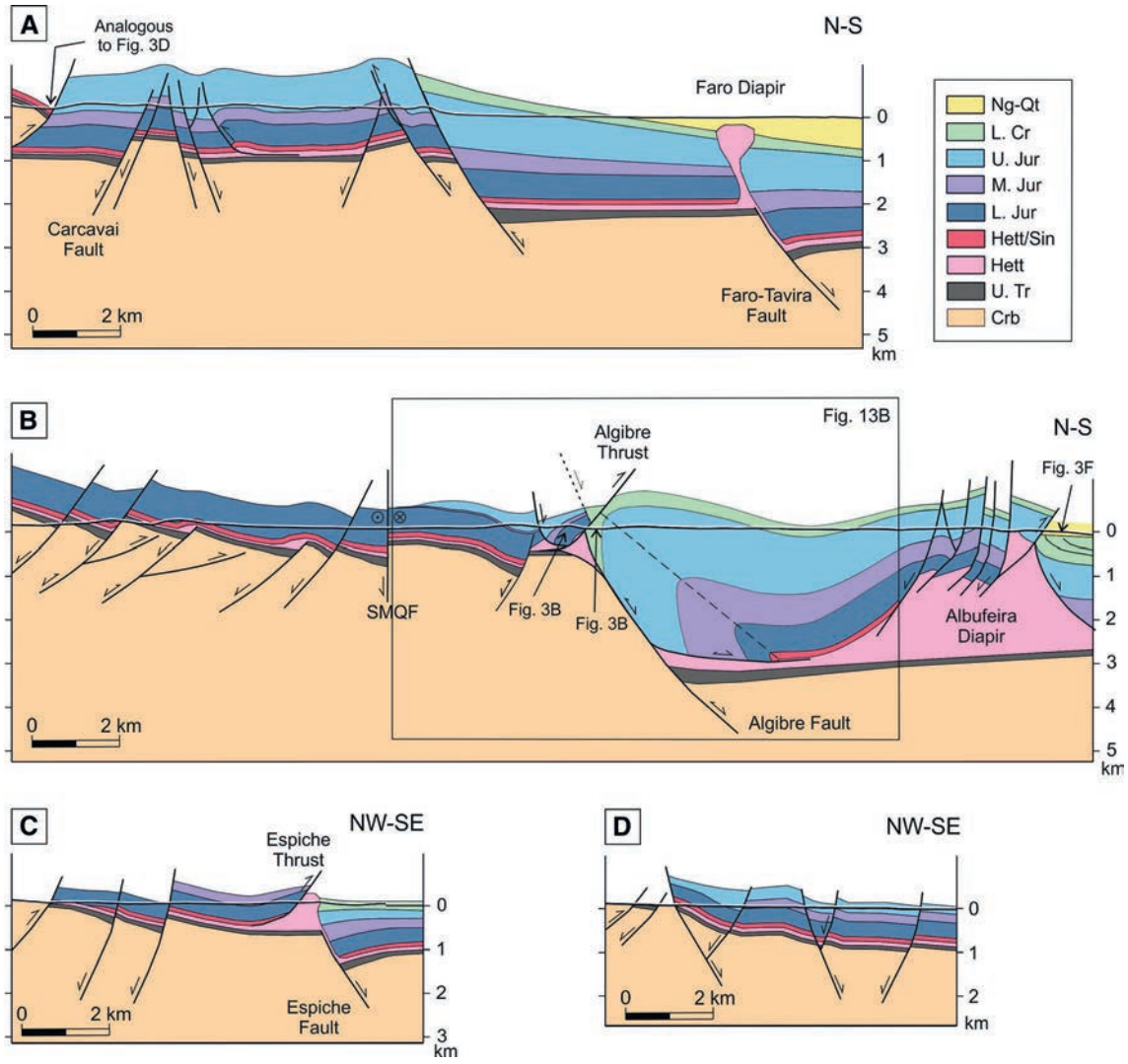

Fig. 12 Cross sections along the Algarve Basin. *Ng-Qt* Neogene–Quaternary, *L. Cr* Lower Cretaceous, *U. Jur* Upper Jurassic, *M. Jur* Middle Jurassic, *L. Jur* Lower Jurassic, *Hett/Sin* Hettangian/Sinemurian, *Hett* Hettangian, *U. Tr* Upper Triassic, *Crb* Carboniferous. See Fig. 5a map for location

becomes thick enough and rich enough in evaporites to feed the Loulé, Albufeira (Figs. 5b, 12b), and Faro diapirs (Figs. 5b, 12a; Terrinha et al. 1990, 1998), or even the allochthonous Esperança salt nappe (Matias et al. 2011). It is interpreted that the increase in subsidence toward the southeast was related to a greater amount of extensional fault activity.

Early Jurassic to Early Cretaceous extension

After a period of tectonic quiescence with regional thermal subsidence during the Sinemurian, extension was recommenced in the Pliensbachian. During this stage there was a clear basinward migration of deformation. This second phase of extension also brought along a change in the dominant vergence of faults, which changed from being mainly north-dipping in the Triassic–Early Jurassic to south-dipping (basinward dipping) faults. Furthermore, a significant change in style occurred. The initial extensional phase from Triassic to Early Jurassic triggered the formation of closely spaced faults with a limited throw (tens to few hundreds of meters). The orientation and spacing of these faults is interpreted to be related to the reactivation of the north-dipping basement foliation (Vegas 1980). From Pliensbachian, the extension was accommodated along major extensional faults with a greater throw (many hundreds of meters) and spacing, cross-cutting the basement weakness surfaces.

Extension during the Jurassic also led to a focalization of deformation away from the basin margin. Along the

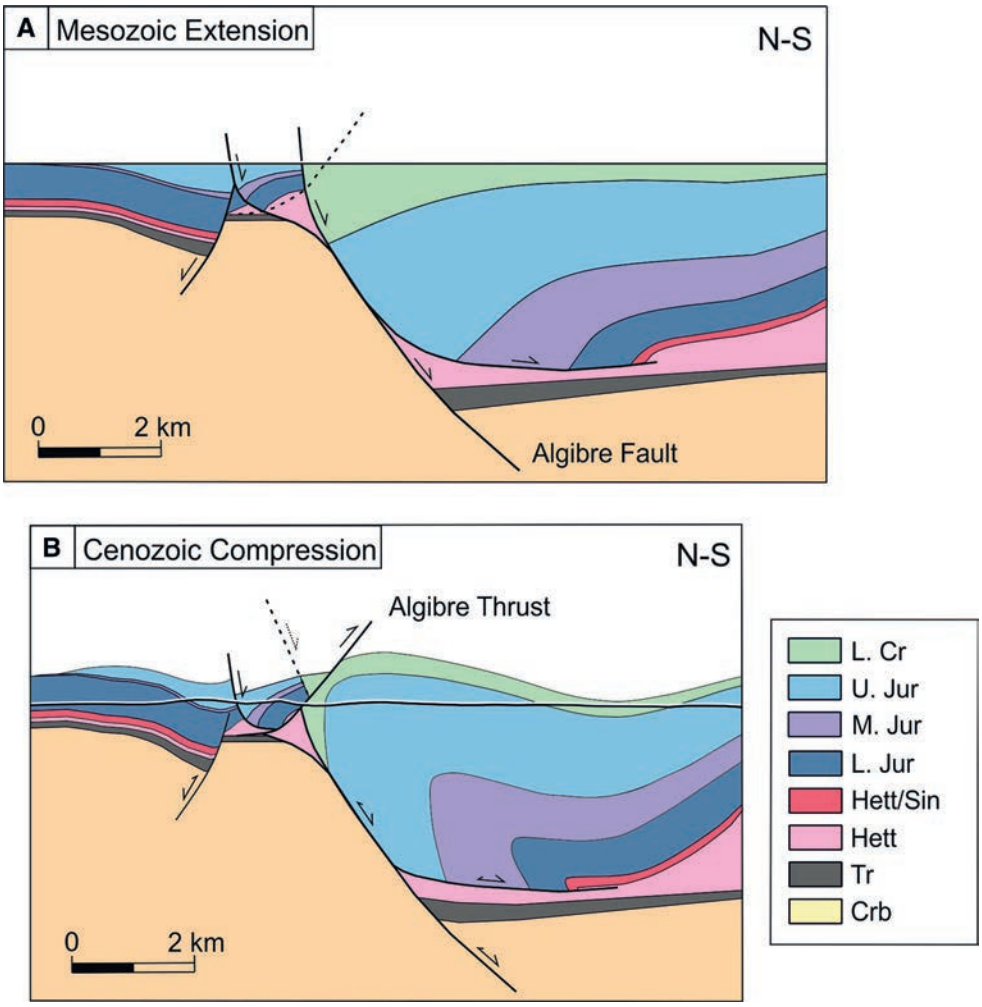

Fig. 13 **a** Restitution of the rollover structure at the end of the Mesozoic extensional phase, in the Early Cretaceous, and **b** the reconstruction of the same structure inverted during the Cenozoic compressional phase. *Ng-Qt* Neogene–Quaternary, *L. Cr* Lower Cretaceous, *U. Jur* Upper Jurassic, *M. Jur* Middle Jurassic, *L. Jur* Lower Jurassic, *Hett/Sin* Hettangian/Sinemurian, *Hett* Hettangian, *U. Tr* Upper Triassic, *Crb* Carboniferous. See Fig. 12 for location

northern margin of the basin, no post-Sinemurian extensional faults can be observed, whereas to the south, significant depocenters of Middle and Late Jurassic are present. The presence of these depocenters is controlled by a set of E–W trending basin-scale faults. These extensional structures are named the Algibre, Espiche, Carcavai, and the Faro-Tavira faults (Fig. 5b).

The Algibre Fault (Figs. 10b, 11) marks the northern limit of the Upper Jurassic and Lower Cretaceous outcrops. To the north of this fault, the Lower Jurassic carbonates crop out extensively, with pervasive karstification and brecciation inferred to reflect a prolonged phase of subaerial exposure and tectonic quiescence prior to the Mid-Jurassic (which is not karstified). The Algibre Fault is also the northern limit of the observed salt-related structures. Manuppella (1992), Terrinha (1998), and other authors interpreted the main feature in this area to be the Algibre Thrust, an E–W regional south-directed thrust, extending from Portimão to Querença (Fig. 5). However, detailed fieldwork and observations of changes in stratigraphy and structural style across the Algibre Fault indicate that this is actually a complex zone with at least two features: an extensional Algibre Fault and a reverse fault, the Algibre Thrust.

The Algibre Fault is interpreted to be a south-dipping extensional fault bounding a half-graben to the north (Fig. 12b). It is interpreted that the Algibre Fault initiated its activity at Late Triassic times, defining the boundary between an area of greater subsidence to the north and an area of thicker evaporite deposition during the Hettangian to the south. When extension restarted in the Middle Jurassic, this fault continued to grow, with faulting and evacuation of Hettangian evaporites resulting in a rollover geometry of Jurassic and Cretaceous beds that thickened against the fault (Fig. 13a). At present, within the hanging-wall of the Algibre Fault, the Upper Jurassic and Lower Cretaceous layers form an overturned anticline with northward vergence due to Cenozoic inversion (Figs. 3f, 12b).

The Espiche Fault (Figs. 5b, 9c) is a WSW–ENE structural feature that is also a northern limit for outcrops of Upper Jurassic and thick Lower Cretaceous sediments. It is interpreted as a southeastwards dipping normal fault, overprinted by a southeast vergent thrust, the Espiche Thrust

(Fig. 12c), in which the Lower Jurassic rocks thrust over the Lower Cretaceous sediments. The presence of pelites and evaporites along the fault and their relationships with the adjacent sediments suggest that a salt wall developed along the extensional fault that was subsequently reactivated and squeezed to form a thrust during the pre-Miocene basin inversion (Terrinha 1998). The Espiche Fault is the western continuation of the Algibre Fault (Figs. 5b, 10), partly offset by the Portimão Fault. The presence of Middle Jurassic and limited Lower Cretaceous outcrops in the footwall (to the north) of the Espiche Fault indicates that this extensional boundary was not as prominent as the Algibre Fault.

The Faro-Tavira fault is an ENE–WSW trending, south-dipping regional extensional fault, parallel to the coast (Figs. 5b, 9a). The Faro-Tavira Fault controls the geometry of the eastern coastline of Faro and marks the northern limit of lower Cretaceous and the uppermost Jurassic (Tithonian) outcrops in the easternmost portion of the basin. Inversion of this fault led to a greater amount of uplift and erosion of this part of the basin (as evident in the greater amount of basement uplift and the vitrinite reflectance data (Fernandes et al. 2013). There is only one documented salt structure north of the Faro-Tavira fault, the Faro diapir. This diapir is interpreted to have developed in the footwall of the Faro-Tavira fault by evacuation of salt in its hanging-wall depocenter (Fig. 11a).

The last of the major extensional faults in the onshore basin is the Carcavai Fault zone. It is an ENE–WSW trending structure extending from the basement outcrop NE of the Loulé diapir, and at least 150 km into the offshore, south of Portimão (Fig. 5b; Noiva 2009; Carvalho et al. 2012). During the Upper Jurassic this fault acted as an extensional fault down throwing to the SE, while in its northeast termination, it is a NW dipping extensional fault (Terrinha 1998; Fig. 12a). This fault is not a major paleogeographical boundary, and it is interpreted to have formed as a structure relaying throw between the Algibre and the Faro-Tavira faults and acting as locus of growth for the Loulé diapir. During basin inversion, the fault was reactivated in contraction, and the Loulé diapir was squeezed (Terrinha et al. 1990 and Terrinha et al. 1994b; Davison et al. 2015).

In contrast to the dominant E–W trend of extensional faults in the central-eastern sub-basin, the general structural pattern of the western sub-basin is dominated by NNE–SSW to N–S trending normal faults (Figs. 2f, 6). Nonetheless, E–W to NE–SW normal faults, which are more common further east, are still present (such as the Espiche Fault). The presence of these two, almost perpendicular sets of faults indicates the interference of two different regional extensional systems. On the one hand, E–W-to-NE–SW faults are related to Tethyan rifting. N–S to NE–SW faults, on the other hand, are associated with extension along the proto-Atlantic rift from Early to Late Jurassic, an orientation consistent with that observed further north along the western Portuguese margin (Alves et al. 2002; Montenat et al. 1998; Soto et al. 2012). Extension on these two differently oriented fault systems also seems to have shifted in time from the Tethyan domain system in the Early Jurassic to the Atlantic domain system in the Late Jurassic (Terrinha 1998).

Middle Jurassic to Early Cretaceous extension was responsible for the main phase of salt tectonism documented in the area (Lopes et al. 2006; Matias 2007; Terrinha et al. 2009; Matias et al. 2011). Other than the evidence for salt movement in the footwall of the Algibre Fault, extrusive salt diapirs in the onshore also occur; the Espiche, Loulé, Albufeira, and Faro diapirs (Terrinha et al. 1990; Terrinha 1998), associated with the main E–W-striking extensional faults. Salt diapirism is not reported north of the Algibre Fault due to the almost complete absence of evaporites in the Hettangian, which highlights the relevance of the Algibre Fault as a relevant paleogeographical basin boundary since the Late Triassic. The diapirs and salt structures of the onshore Algarve basin have all been reactivated during tectonic inversion (Davison et al. 2015).

Oblique, basin compartmentalizing faults

The Algarve Basin is dissected by several regional-scale faults (Portimão, SMQF, Aljezur; Terrinha 1998), which are parallel to the Late Variscan thrusts documented in the Carboniferous basement in the South Portuguese Zone and the Iberian Pyrite Belt (Arthaud and Matte 1977; Manuppella 1992; Terrinha 1998) and acted mainly as transfer faults compartmentalizing the Algarve Basin during Mesozoic extension. During Cenozoic inversion, many of these faults were reactivated as strike-slip features (Fig. 5b; Barreto et al. 2015).

The Portimão Fault strikes roughly N–S (Fig. 5b). This fault is interpreted to have acted as transfer fault during the Mesozoic. As mentioned above, the Portimão Fault separates the Algarve Basin into two sub-basins, the western and the central-eastern sub-basins, each of which has extensional faults with different trends. The two sub-basins are also characterized by having different depositional environments and thickness of sediments throughout the Jurassic and the Lower Cretaceous (Manuppella et al. 1988; Correia 1989 and Terrinha 1998). During the Early to Middle Jurassic, both sub-basins are dominated by hemipelagic sedimentation. The main difference between both basins during this time is a greater sediment thickness in the central-eastern sub-basin which is in excess of 1000 m in contrast with less than 500 m in the western sub-basin. The central-eastern sub-basin also records intervals of more

confined sedimentation and even an event of uplift and subaerial erosion, represented by a Callovian erosion unconformity and depositional hiatus that lasted until the Late and Middle Oxfordian in the Algarve and Lusitanian basins (Terrinha et al. 2002).

During the Late Jurassic, the differentiation on sedimentation between the two sub-basins increased, with thicknesses varying from 200 m in the west to more than 1600 m in the east. Despite the larger amount of subsidence, the eastern sub-basin developed internal compartments and important lateral facies differentiation, especially in the Late Oxfordian to Early Kimmeridgian. From the upper Kimmeridgian and through the Lower Cretaceous, the sedimentary environment becomes uniform throughout the sub-basin with the generalized development of internal platform facies. In contrast with the western sub-basin, where the Lower Cretaceous presents a marine-like facies and a thickness up to 500 m, it presents continental and littoral facies, reaching a thickness of roughly 1500 m (Terrinha 1998).

Present-day activity is also observed on the Aljezur Fault (Fig. 5b), a N–S trending left-lateral strike-slip fault in the western sub-basin that also controls the position of a submarine canyon across the continental shelf and slope. The Aljezur Fault extends around 60 km northwards into the Variscan basement where it controls the formation of Miocene grabens (Terrinha et al. 2009). However, there is no evidence that this fault was active during Mesozoic extension.

The SMQF is the third of the major compartmentalizing faults of the Algarve Basin (Fig. 5b). This fault extends from the non-rifted Paleozoic basement into and across the Algarve rift and post-rift Basin. Inspection of the geological maps and field work shows that the SMQF was active since Triassic through Quaternary times, i.e., during extensional and compressional tectonics. Palain (1976) showed how this fault affected the distribution of the clastic Triassic–Hettangian facies and thickness. It has also been reported that the onshore occurrence of salt diapirs is common on the hanging-wall of the SMQF (e.g. Terrinha et al. 1999). Various works (e.g., Manuppella 1988 and Manuppella 1992) showed that the thickness of the Jurassic and Cretaceous hanging-wall (i.e., northeast of the fault) are considerably thicker than the foot-wall sequences.

This argues in favor of the role of a transfer fault for the SMQF during rifting (Fig. 6), creating a hanging-wall block with higher subsidence and sub-basin development, important salt basins, and thicker sedimentary sequences.

While in the non-rifted basement and Triassic clastics the SMQF is mapped as a discrete fault, in the Jurassic carbonate sequences of the hanging-wall, the SMQF forms a diffuse deformation corridor that materializes as a series of dextral strike-slip transpressive duplexes, some of them deeply rooted in the pelite–evaporite complex, as shown by sheared gypsum mylonites squeezed out along faults parallel to the SMQF. At the Triassic–basement contact the discrete dextral offset is visible (Fig. 5a) as well as the up-thrown displacement of the northeastern hanging-wall block.

Finally, east of the SMQF, the Querença margin would have acted as an extensional transfer zone during the Mesozoic (Fig. 5b) along with the Carcavai fault zone, connecting the Algibre and the Faro–Tavira faults. The Querença zone was later reactivated as a lateral ramp structure in the inversion system, relaying the basin margin basement monocline (Fig. 7).

Late cretaceous to Quaternary inversion and shortening

The main effect of shortening and basin inversion in the onshore Algarve Basin is the broad southward tilt of the basin. This regional tilt is related to basin-scale deformation and uplift of the basement during the Cenozoic (Fernández-Lozano 2012), most probably associated with the presence of a south-directed basin-scale thrust, rooting into the basement. Tilting and uplift related to this structure are responsible for the regional southward dip of Mesozoic beds and the complete absence of Neogene and Quaternary deposits over most of the onshore Algarve Basin. There is also evidence for at least one other contraction-related monocline in the basin, which causes a step in the offshore bathymetry in the west (along offshore segment of the Carcavai fault) and controls the location of the present-day coastline further to the east (Fig. 7). This basement-involved monocline was probably located along a basement step of extensional origin which focussed the folding during the Alpine contraction.

It is interpreted that at this basin-scale, and along the northern margin of the basin where Hettangian evaporites are almost absent, Cenozoic inversion reactivated pre-existing discontinuities in the Carboniferous basement. As a result, the regional thrusts formed with ENE–WSW trend and dipping to the north. This trend is related to the reactivated fabric, which is probably the pervasive Variscan-age foliation of the meta-sedimentary basement, which is known regionally to dip toward the north and crops out along the northern margin of the basin (Vegas 1980). The foliation is documented to be reactivated in multiple south-directed thrusts within the outcrop of the South Portuguese Zone and the northern margin of the Algarve Basin (Soriano Clemente 1996; Terrinha 1998). In some cases, this caused the partial reactivation of pre-existing Triassic faults and the formation of shortcuts (Fig. 10d), and in others it led to the formation of monoclines with no evident rupture (Fig. 7), but completely deforming the overlying Mesozoic cover and its associated faults.

At a more local scale, a number of thrusts and contractional structures have been unambiguously documented in the area. These include the Algibre Thrust (Fig. 12b), shortcuts that affect the Triassic half-grabens along the northern margin of the basin (Figs. 7, 10), and multiple buttressing structures along the Algibre Fault (Fig. 12b).

Perhaps the best defined contractional structure is the inversion of the Algibre fault and its associated thrust. During Cenozoic inversion, the hanging-wall of the Algibre Fault was detached above the Hettangian evaporites and folded by buttressing against the Algibre Fault footwall, producing E–W trending tight detachment folds (Fig. 11) and tightening and overturning the Algibre rollover (Figs. 12b, 13b). The inversion structure is further complicated by the presence, locally, of a south-directed thrust that places Lower and Mid-Jurassic rocks on top of the Early Cretaceous (Figs. 11a, 12b), rooting into the salt of the footwall.

The example of the Algibre Fault illustrates how the pattern of basin inversion was influenced by the presence of a thick Hettangian salt unit. This unit only presents thicknesses in excess of a few tens of meters to the south of the Espiche–Algibre–Faro–Tavira corridor. To the south of this corridor, deformation during shortening was dominated by decoupling between basement deformation and deformation of the Mesozoic cover. This decoupling is evident for both the abundant buttressing structures in the hanging-wall of the Algibre Fault (Figs. 11, 13b), which detach within the Hettangian evaporites, and in the reactivation of diapirs throughout the basin. On the other hand, north of the Espiche–Algibre–Faro–Tavira corridor, shortening structures propagate from the basement through the Mesozoic units above without any decoupling (Figs. 11, 12). In summary, evaporites played a key role in defining two different structural styles during inversion of the basin: one dominated by thick-skinned thrusts where salt is very thin and one dominated by decoupling of the Mesozoic cover above the basement where salt deposits were originally thicker.

Conclusions

1. The Algarve Basin is interpreted to have formed mainly as the consequence of N–S-to-NW–SE-directed extension (in present-day orientation) that is consistent with extension along the westernmost end of the Tethys. The related E–W to ENE–WSW fault trend dominates the central-eastern sub-basin.
2. The influence of Atlantic domain extension is observed in the western sub-basin of the Algarve Basin. In this sub-basin, the dominant trend of extensional faults is NE–SW to N–S.
3. The Algarve Basin is the result of the interaction between two major phases of Mesozoic extension (Triassic–Early Sinemurian and Pliensbachian–Early Cretaceous) and one phase of Alpine compression (mainly Cenozoic). Minor extension prevailed through the earliest extensional phase, which is characterized by north-dipping faults, whereas faults with greater throw generated during the second extensional phase are predominantly southward dipping. Extensional structures were inverted during the Cenozoic as south to southeast-directed structures throughout the basin accompanied by buttressing on the major extensional faults.
4. Extension played a key role in defining the location of evaporite deposition, which was greater to the south of the Algibre–Espiche and Faro–Tavira faults. In turn, evaporites played a key role in differentiating two structural styles during basin inversion from north to south. The northern margin of the basin (evaporite poor) is dominated by thick-skinned deformation in both extension and inversion. Southward, the basin records thin-skinned deformation above the evaporites in both extension and inversion, decoupled above the deeper basement-rooted structures.
5. This basin is a great example of reactivation of structures: Both extensional faults and basin compartmentalizing faults formed along previously existing Variscan structures. These structures were in turn reactivated during inversion of the basin, which also caused the reactivation of Variscan-age fabrics in contraction.

Acknowledgments This study was funded by Repsol Exploración (Madrid) and partially financially supported by the SALTECRES project (CGL2014-54118-C2-1-R). Adrià Ramos thanks Repsol Exploración for his PhD grant. The authors thank Ian Davison and an anonymous reviewer for thorough and helpful suggestions and comments. We also acknowledge Midland Valley for the academic software license used for cross-sectional construction.

References

Alves TM, Gawthorpe RL, Hunt DW, Monteiro JH (2002) Jurassic tectono-sedimentary evolution of the Northern Lusitanian Basin (offshore Portugal). Mar Pet Geol 6:727–754

Arthaud F, Matte P (1977) Late Paleozoic strike-slip faulting in southern Europe and Northern Africa: result of a right-lateral shear zone between the Appalachians and the Urals. Geol Soc Am Bull 88:1305–1320

Barreto P, Silvia C, Leonardo P. Sousa J, Caeiro MH, Maciel C, Guerreiro L (2015) The relationship between the onshore and offshore structure of São Marcos-Quarteira Fault System, Algarve Basin, Portugal. AAPG European Regional Conference and Exhibition, Lisbon, 18–19th May 2015

Bernard-Griffiths J, Gruau G, Cornen G, Azambre B, Mac J (1997) Continental lithospheric contribution to alkaline magmatism: isotopic (Nd. Sr. Pb) and geochemical (REE) evidence from Serra de Monchique and Mount Ormonde complexes. J Pet 38(1):115–132

Carvalho J, Matias H, Rabeh T, Menezes PTL, Barbosa VCF, Dias R, Carrilho F (2012) Connecting onshore structures in the Algarve with the southern Portuguese continental margin: the Carcavai fault zone. Tectonophysics 570–571:151–162

Correia FMC (1989) Estudo biostratigrafico e microfacies do Cretacico carbonatado da Bacia Sedimentar Meridional Portuguesa (Algarve), PhD Thesis. Faculdade de Ciencias da Universidade de Lisboa, pp 1–377

Davison I, Barreto P, Andrade A, Terrinha P (2015) Loulé: a shunted diapir affected by Late Cretaceous dyke intrusions and Alpine inversion, Algarve Basin, Portugal. AAPG European Regional Conference and Exhibition, Lisbon, 18–19th May 2015

Dewey JF, Helman ML, Turco E, Hutton DHW, Knott SD (1989) Kinematics of the Western Mediterranean. In: Coward MP, Dietrich D, Park RG (eds) Alpine tectonics. Geol Soc, London. Spec Publ 45, pp 265–283

Duarte JC, Rosas FM, Terrinha P, Gutscher M-A, Malavieille J, Silva S, Matias L (2011) Thrust-wrench interference tectonics in the Gulf of Cadiz (Africa-Iberia plate boundary in the North-East Atlantic): insights from analog models. Mar Geol 289:135–149

Fernandes P, Rodrigues B, Borges M, Matos V, Clayton G (2013) Organic maturation of the Algarve Basin (southern Portugal) and its bearing on thermal history and hydrocarbon exploration. Mar Petrol Geol 46:210–233

Fernández-Lozano J (2012) Cainozoic deformation of Iberia: a model for intraplate mountain building and basin development based on analogue modelling. PhD Thesis, Utretcht University, pp 1–186

Gràcia E, Dañobeitia J, Vergés J, Bartolomé R, Córdoba D (2003) Crustal architecture and tectonic evolution of the Gulf of Cádiz (SW Iberian margin) at the convergence of the Eurasian and African plates. Tectonics 22(4):1033–1051

Gutscher M-A, Malod J, Rehault JP, Contrucci I, Klingelhoefer F, Spakman W, Mendes-Victor L (2002) Evidence for active subduction beneath Gibraltar. Geology 30:1071–1074

Iribarren L, Vergés J, Camurri F, Fullea J, Fernàndez M (2007) The structure of the Atlantic-Mediterranean transition zone from the Alboran Sea to the Horseshoe Abyssal Plain (Iberia–Africa plate boundary). Mar Geol 243:97–119

Lonergan L, White N (1997) Origin of the Betic-Rif mountain belt. Tectonics 16(3):504–522

Lopes C (2002) Análise e Modelação da Bacia do Algarve, PhD Thesis, Faculdade de Ciências e Tecnologia da Universidade Nova de Lisboa, p 173

Lopes F, Cunha PP, Le Gall B (2006) Cenozoic seismic stratigraphy and tectonic evolution of the Algarve margin (offshore Portugal, southwest Iberian Peninsula). Mar Geol 231:1–36

Maldonado A, Somoza L, Pallarés L (1999) The Betic orogen and the Iberian-African boundary in the Gulf of Cadiz: geological evolution (central North Atlantic). Mar Geol 155:9–43

Manuppella G (1988) Litoestratigrafia e tectónica da Bacia Algarvia. Geonovas 10:67–71

Manuppella G (1992) Carta geologica da regiao do Algarve, escala 1/100,000. Noticia explicativa da Carta Geologica da regiao do Algarve. Serv Geol Portugal, Lisboa, 15p

Manuppella G, Marques B, Rocha RB (1988) Évolution tectonosédimentaire du bassin de l'Algarve pendant le Jurassique. In: 2nd international symposium on jurassic stratigraphy, Lisboa, pp 1031–1046

Martínez-Loriente S, Gràcia E, Bartolome R, Sallarès V, Connors C, Perea H, Lo Iacono C, Klaeschen D, Terrinha P, Dañobeitia JJ, Zitellini N (2013) Active deformation in old oceanic lithosphere and significance for earthquake hazard: seismic imaging of the Coral Patch Ridge area and neighboring abyssal plains (SW Iberian Margin). Geochem Geophys Geosyst 14:2206–2231

Martins L (1999) Cretaceous alkaline magmatism in Algarve litoral (South Portugal): a basanite e lamprophyre suite. Geolines 9:84–91

Martins L, Munhá J (1993) Magmatismo cretácico do Algarve litoral: zonamento inverso em clinopiroxenas e suas implicações petrogenéticas. Mem Mus Lab Min Geol Fac Ciênc Univ Porto 3:105–106

Martins L, Madeira J, Youbi N, Munhá J, Mata J, Kerrich R (2008) Rift-related magmatism of the Central Atlantic magmatic province in Algarve, southern Portugal. Lithos 101:102–124

Matias H (2007) Hydrocarbon potential of the offshore Algarve Basin: PhD Thesis, Faculdade de Ciências da Universidade Nova de Lisboa, pp 1–324

Matias H, Mohriak WU, Menezes P, Sandnes F, Barbosa VCF, Matias L, Santos F (2005) Salt distribution and morphology in the offshore Algarve Basin. In: Post P, Rosen N (eds) Petroleum systems of divergent continental margin basins. Proceedings of the 25th Annual Bob F. Perkins Research Conference, Gulf Coast Section SEPM, pp 481–509

Matias H, Kress P, Terrinha P, Mohriak W, Menezes P, Matias L, Santos F, Sandnes F (2011) Salt tectonics in the western Gulf of Cadiz, southwest Iberia. AAPG Bull 95(10):1667–1698

McIntyre RM, Berger GW (1982) A note on the geochronology of the Iberian Alkaline Province. Lithos 15:133–136

Miranda R, Valadares V, Terrinha P, Mata J, Azevedo MR, Gaspar M, Kullberg J, Ribeiro C (2009) Age constraints on the Late Cretaceous alkaline magmatism on the West Iberian Margin. Cretac Res 30:575–586

Montenat C, Guery F, Jamet M (1998) Mesozoic evolution of the Lusitanian basin: comparison with the adjacent margin. Proc Ocean Drill Program Sci Result 103:757–775

Moura D, Veiga Pires L, Albardeiro T, Boski T, Rodrigues AL, Tareco H (2007) Holocene sea level fluctuations and coastal evolution in the central Algarve (southern Portugal). Mar Geol 237:127–142

Noiva J (2009) Caracterização das estruturas tectónicas activas da região sul de Portugal com recurso a ferramentas SIG: O caso da falha de São Marcos-Quarteira. MSc Thesis, Universidade Nova de Lisboa pp 1–112

Pais J, Legoinha P, Elderfield H, Sousa L, Estevens M (2000) The Neogene of Algarve (Portugal). Ciências da Terra 14:277–288

Palain C (1976) Una serie detritique terrigene, les "Gras de Silves": Trias et Uas lnferieur du Portugal, Sar. Geol. Portugal, Memoria n° 25, Usboa, p 377

Rey J (1983) Le Cretacé de l'Algarve: essay de synthèse. Com Ser Geol Port 69(1):87–101

Rey J (2006) Les formations Crétacées de l'Algarve occidental et central. Com Ser Geol Port 93:39–80

Rey J (2009) Les formations Crétacées de l'Algarve oriental. Com Ser Geol Port 96:19–38

Ribeiro C, Terrinha P (2007) Formation, deformation and chertification of systematic clastic dykes in a differentially lithified carbonate multilayer. SW Iberia, Algarve Basin, Lower Jurassic. Sediment Geol 196:201–215

Royden LH (1993) Evolution of retreating subduction boundaries formed during continental collision. Tectonics 12(3):629–638

Sallarès V, Gailler A, Gutscher MA, Graindorge D, Bartolomé R, Gràcia E, Díaz J, Dañobeitia JJ, Zitellini N (2011) Seismic evidence for the presence of Jurassic oceanic crust in the central Gulf of Cadiz (SW Iberian margin). Earth Planet Sci Lett 311:112–123

Soriano Clemente C (1996) Tectónica de cabalgamientos en la Faja Pirítica Ibérica (Zona Sur Portuguesa): el Antiforme de la Puebla de Guzmán, y la lámina de cabalgamiento de Sanlúcar de Guadiana. Geogaceta 20(4):786–788

Soto R, Kullberg JC, Oliva-Urcia B, Casas-Sainz AM, Villalaín JJ (2012) Switch of Mesozoic extensional tectonic style in the

Lusitanian basin (Portugal): insights from magnetic fabrics. Tectonophysics 236–537:122–135

Srivastava S, Roest W, Kovacs L, Oakey G, Levesque S, Verhoef J, Macnab R (1990) Motion of Iberia since the Late Jurassic: results from detailed aeromagnetic measurements in the Newfoundland Basin. Tectonophysics 184:229–260

Terrinha P (1998) Structural geology and tectonic evolution of the Algarve Basin, South Portugal. PhD thesis, Imperial College of London, London pp 1–430

Terrinha P, Coward MP, Ribeiro A (1990) Salt tectonics in the Algarve Basin: the Loulé diapir. Commun Serv Geol Port 76:33–40

Terrinha P, Ribeiro A, Coward MP (1994) Salt tectonics in the Meso-Cenozoic Lusitanian and Algarve Basins, Portugal. Salt Tectonics, 14–15th September 1994, Programme and Abstracts

Terrinha P, Dias RP, Ribeiro A, Cabral J (1999) The Portimão Fault, Algarve Basin, South Portugal. Comun Inst Geol Miner 86:107–120

Terrinha P, Ribeiro C, Kullberg JC, Rocha R, Ribeiro A (2002) Compression episodes during rifting and faunal isolation in the Algarve Basin, southwest Iberia. J Geol 110:101–113

Terrinha P, Matias L, Vicente J, Duarte J, Luis J, Pinheiro L, Lourenço N, Diez S, Rosas F, Maglhães V, Valadares V, Zitellini N, Roque C, Mendes-Victor L, MATESPRO Team (2009) Morphotectonics and strain partitioning at the Iberia-Africa plate boundary from multibeam and seismic reflection data. Mar Geol 267:156–174

Tortella D, Torné M, Pérez-Estaún A (1997) Geodynamic evolution of the eastern segment of the Azores-Gibraltar zone: Gorringe Bank and the Gulf of Cádiz Region. Mar Geophys Res 19:211–230

Vegas R (1980) Carboniferous subduction complex in the South Portuguesa zone Coeval with basement reactivation and uplift in the Iberian Massif. Cuad Lab Xe 1:187–202

Verati C, Rapaille C, Féraud G, Marzoli A, Bertrand H, Youbi N (2007) 40Ar/39Ar ages and duration of the Central Atlantic Magmatic Province volcanism in Morocco and Portugal and its relation to the Triassic-Jurassic boundary. Palaeogeogr Palaeoclimatol 344:308–325

APPENDIX 1.2

Neogene to recent contraction and basin inversion along the Nubia-Iberia boundary in SW Iberia

Ramos, A., Fernández, O., Terrinha, P., Muñoz, J.A., 2017.
Tectonics 36, 257-286. doi:10.1002/2016TC004262

AGU PUBLICATIONS

Tectonics

RESEARCH ARTICLE
10.1002/2016TC004262

Neogene to recent contraction and basin inversion along the Nubia-Iberia boundary in SW Iberia

Adrià Ramos[1], Oscar Fernández[2], Pedro Terrinha[3], and Josep Anton Muñoz[1]

[1]Institut de Recerca Geomodels, Departament de Dinámica de la Terra i de l'Oceá, Facultat de Ciéncies de la Terra, Universitat de Barcelona, Barcelona, Spain, [2]Dirección de Geociencias, Repsol Exploración, Madrid, Spain, [3]Divisão de Geologia e Georecursos Marinhos, Instituto Português do Mar e da Atmosfera, Lisboa, Portugal

Key Points:
- The Gulf of Cadiz links shortening across Africa-Iberia boundary from the Atlantic to the Betics
- Four main south directed thrusts responsible for uplift of SW Iberia in the Cenozoic are documented
- Cenozoic thrusting overprints and inverts the Mesozoic passive margin structures

Correspondence to:
A. Ramos,
adriaramos@ub.edu;
adria_ramos@outlook.com

Citation:
Ramos, A., O. Fernández, P. Terrinha, and J. A. Muñoz (2017), Neogene to recent contraction and basin inversion along the Nubia-Iberia boundary in SW Iberia, *Tectonics*, *36*, doi:10.1002/2016TC004262.

Received 4 JUN 2016
Accepted 23 JAN 2017
Accepted article online 25 JAN 2017

Abstract The SW of Iberia is currently undergoing compression related to the convergence between Nubia and Iberia. Multiple compressive structures, and their related seismic activity, have been documented along the diffuse Nubia-Iberia plate boundary, including the Gorringe bank west of the Gulf of Cadiz, and the Betic-Rif orogen to the east. Despite seismic activity indicating a dominant compressive stress along the Algarve margin in the Gulf of Cadiz, the structures at the origin of this seismicity remain elusive. This paper documents the contractional structures that provide linkage across the Gulf of Cadiz and play a major role in defining the present-day seismicity and bathymetry of this area. The structures described in this paper caused the Neogene inversion of the Jurassic oblique passive margin that formed between the central Atlantic and the Ligurian Tethys. This example of a partially inverted margin provides insights into the factors that condition the inversion of passive margins.

1. Introduction

Since the end of the Mesozoic, the Iberian microplate has been trapped between the converging African and Eurasian plates [*Dewey et al*., 1989; *Rosenbaum et al*., 2002]. As a consequence, the paleogeographic and tectonic evolution of Iberia as well as their surrounding margins during the Cenozoic have been strongly linked to the Alpine orogeny and to the closing of the Tethys Ocean [e.g., *Ziegler*, 1988; *Dewey et al*., 1989]. Cenozoic N-S convergence between Africa and Eurasia is thus the cause of the development of a number of mountain chains in the internal parts of the Iberian microplate and along its northern and southern margins (the Pyrenean-Cantabrian chain, the Spanish Central System, the Sierra Morena, and the Betic-Rif chain; Figure 1b) [*De Vicente et al*., 2004; *Vergés and Fernàndez*, 2012]. These mountain chains are interpreted to represent the westernmost termination of the Alpine-Himalayan orogenic system [*Dewey et al*., 1973; *Şengör*, 1984; *Dercourt et al*., 1986].

From the Late Cretaceous and throughout the Cenozoic, deformation in Iberia migrated from north to south, as the Iberian microplate progressively welded with the Eurasian plate. Orogenic deformation in the Iberian plate initiated along the Pyrenean-Cantabrian chain along its northern border in Late Cretaceous. By the early Miocene, orogenic deformation, and the Nubia-Iberia boundary, had migrated to the south of Iberia, to the Betic-Rif system [*Srivastava et al*., 1990a, 1990b]. West of Iberia, the Azores-Gibraltar Fracture Zone (AGFZ), and its eastern continuation along the Southwest Iberian Margin lineaments [*Zitellini et al*., 2009] in the southern Gulf of Cadiz, is interpreted as the current Nubia-Iberia plate boundary in the Atlantic Ocean (Figure 1a) by some authors [e.g., *Maldonado et al*., 1999; *Zitellini et al*., 2009].

The present-day Nubia-Iberia plate boundary between the AGFZ and the Gibraltar Arc (the link between the Rif and Betic orogens) has been described as a diffuse plate boundary by *Sartori et al*. [1994]. The transition from the AGFZ, which originates as a transform in the mid-Atlantic, into the contractional systems of Iberia has been the subject of study in recent years [e.g., *Maldonado et al*., 1999; *Zitellini et al*., 2009]. This has led to the identification of multiple contractional features with neotectonic activity (and potential tsunamigenic hazard) at the eastern termination of the AGFZ immediately west of the Gulf of Cadiz, namely, the Gorringe Thrust, Horseshoe Thrust, Marquês de Pombal Thrust, and the Coral Patch Ridge (Figure 1) [*Gràcia et al*., 2003a; *Terrinha et al*., 2003; *Zitellini et al*., 2004; *Jiménez-Munt et al*., 2010; *Sallarès et al*., 2013, *Martínez-Loriente et al*., 2014, 2016].

Previous structural interpretations of the Gulf of Cadiz have concentrated on the Algarve Basin as part of the SW Iberian passive margin [e.g., *Terrinha*, 1998; *Matias et al*., 2011]. Thus, the structures responsible for the seismic activity and Neogene deformation in the Gulf of Cadiz remained elusive [*Carrilho et al*., 2004]. In

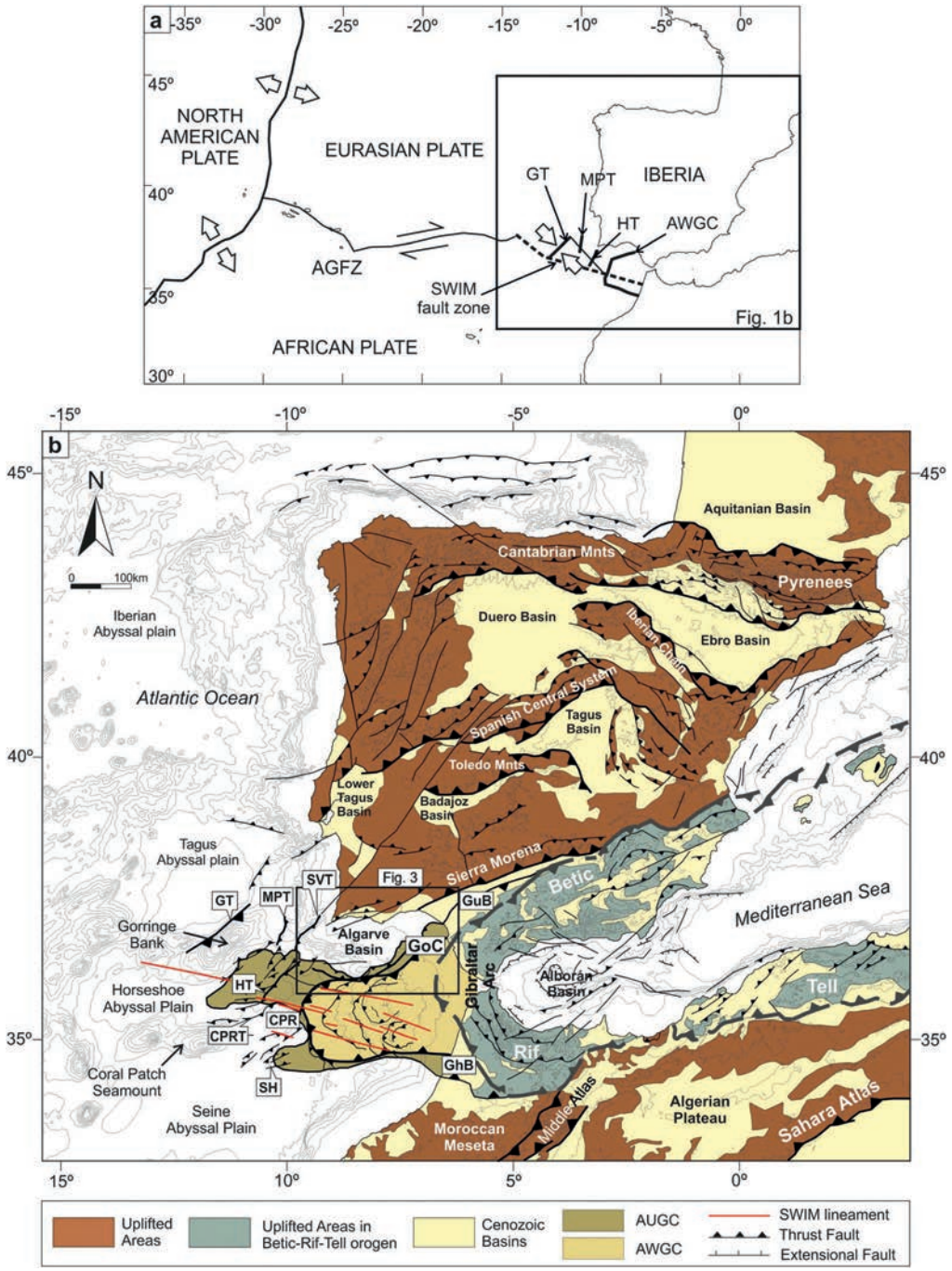

Figure 1. (a) Main elements of plate boundaries and relative plate kinematics. (b) Map showing the location of Cenozoic contractional structures in Iberia and surrounding areas related to the Nubia-Iberia plate boundary. AGFZ: Azores-Gibraltar Fracture Zone, AUGC: Allochthonous Unit of the Gulf of Cadiz, AWGC: Allochthonous Wedge of the Gulf of Cadiz, CPR: Coral Patch Ridge, CPRT: Coral Patch Ridge Thrust, GuB: Guadalquivir Basin, GhB: Gharb Basin, GoC: Gulf of Cadiz, GT: Gorringe Thrust, HT: Horseshoe Thrust, MPT: Marquês de Pombal Thrust, SH: Seine Hills, SVT: São Vicente Thrust. Adapted using data from *Gomez et al.* [2000], *Michard et al.* [2008], *De Vicente and Vegas* [2009], *Gutscher et al.* [2009], *Medialdea et al.* [2009], *Zitellini et al.* [2009], *De Vicente and Muñoz-Martín* [2013], *Duarte et al.* [2013], and *Martínez-Loriente et al.* [2013].

this paper we aim to document the contractional structures that link the AGFZ and the Gibraltar Arc across the Algarve Basin and are the locus of major instrumental seismic activity. We will demonstrate that these features are, at least in part, responsible for the deformation and uplift of the SW Iberian margin from Oligocene to present.

The partial inversion of passive margins, similar to that documented here for the SW Iberian margin, is a common feature to the western and northern Iberian margins [*Peron-Pinvidic et al*., 2008; *Duarte et al*., 2013; *Tugend et al*., 2014; *Druet*, 2016]. Partial inversion has also been documented in other parts of the Tethyan domain [e.g., *Gardosh and Druckman*, 2006; *Arsenikos et al*., 2013] and the North Atlantic [e.g., *Boldreel and Andersen*, 1993; *Vågnes et al*., 1998; *Lundin and Doré*, 2002; *Johnson et al*., 2005; *Doré et al*., 2008]. The inversion of oblique to transform margins has even been explored in areas such as the Svalbard-West Barents margin of Norway [e.g., *Faleide et al*., 2008; *Indrevær et al*., 2016], the Otway Basin of Australia [*Hill et al*., 1994], or the Santos Basin of Brazil [*Cobbold et al*., 2001]. In recent years there have been an increasing interest in the geological evolution of passive margins, mainly since new concepts on hyperextended margins were proposed [*Peron-Pinvidic and Manatschal*, 2009; *Brune et al*., 2016]. As a result, the influence of the rift inheritance, particularly the distribution of the different rifts domains and the rift architecture, has been proposed to play a significant role on margin inversion and subsequent continental collision [*Roca et al*., 2011; *Tugend et al*., 2014]. However, a problem arises when considering the relative role that other factors may have contributed to the compressional deformation of margins other than the rift inheritance, such as prerift inheritance or obliquity of the deformation axis during the subsequent tectonic events.

Within this context, the example presented here of the SW Iberian margin provides key insight into the elements that control the initial stages of inversion of a passive margin. In particular, inherited heterogeneities at different scale and of different nature appear to be the main controlling factor in the configuration of the inverted margin. We will propose that the pattern of inversion observed in this margin is the consequence of crustal heterogeneities inherited from the (prerifting) Paleozoic Variscan orogeny, the structure of the rifted margin, and its Mesozoic mechanical stratigraphy.

2. Geological Setting

2.1. Tectonic and Geodynamic History of the Algarve Margin Since the Mesozoic

The evolution of southern Iberia during the Mesozoic was dominated by rifting associated to the westward propagation of the Tethys and to the opening of central and North Atlantic [*Handy et al*., 2010; *Schettino and Turco*, 2011]. The southern margin of Iberia developed during this time as a transtensional rift margin connecting the central Atlantic with the Ligurian Tethys [*Handy et al*., 2010]. Rifting of southern Iberia led to the development of a thick Mesozoic sequence of sediments in fault-controlled depocenters unconformably overlying a Paleozoic basement. Mesozoic extension in the Algarve Basin was dominated by the development of roughly E-W trending extensional faults and the presence of NW-SE trending transfer zones or faults [*Terrinha*, 1998; *Ramos et al*., 2016].

The Algarve Basin is the only remnant of the southern Iberian rift margin that was not overprinted by the Betic orogenic system in the Cenozoic. At the time of the opening of the North Atlantic in the Early Cretaceous, Iberia was an isolated microplate, separated from Eurasia by the Bay of Biscay-Pyrenean rift system and from Africa by a transcurrent oceanic ridge-transform system [*Sallarès et al*., 2011].

Evolution of southern Iberia since Late Cretaceous has been dominated by the convergence between Africa and Eurasia and the progressive southward migration of deformation and orogeny across the Iberian plate previously discussed. Deformation in the Late Cretaceous to Cenozoic intraplate mountain chains of Iberia is deep rooted, involving basement and, where present, inverting preexisting Mesozoic rift basins. In addition to the generation of intraplate relief, the relative motion of Africa, Iberia-Eurasia, and the western Mediterranean also led to the development of the Betic-Rif orogen from late Oligocene to middle Miocene [*Lonergan and White*, 1997].

2.2. Stratigraphy

The Algarve Basin started to develop during the Triassic, with the deposition of siliciclastic continental sediments unconformably overlying the Carboniferous flysch deformed in the foreland of the Variscan foreland and infilling roughly E-W trending half-grabens [*Terrinha*, 1998; *Ramos et al*., 2016] (Figure 2). Triassic

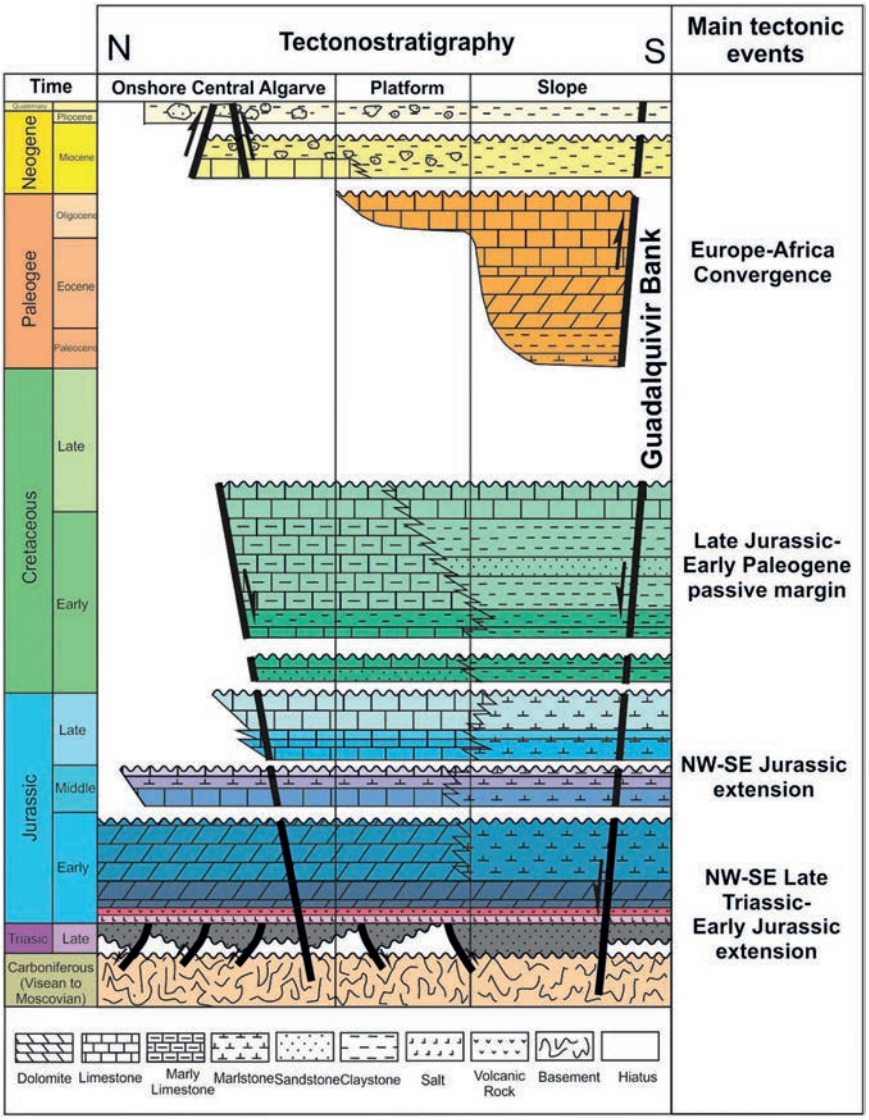

Figure 2. Synthetic stratigraphy of the Algarve Basin with the main tectonic events and the seismic character for each stratigraphic unit interpreted in this work.

sediments are covered by Hettangian evaporites and terrigenous clastics (Figure 2), which are capped in turn by a volcanic-sedimentary complex, Hettangian-Sinemurian in age, and associated with the central Atlantic Magmatic Province [e.g., *Martins et al*., 2008]. During a period of Sinemurian tectonic quiescence, shallow water limestones and dolomites were deposited in the basin (Figure 2). From Pliensbachian to Toarcian (at the transition to the Middle Jurassic), the basin recorded progressive deepening with the development of marly facies with abundant ammonoid fauna [*Terrinha et al*., 2002].

Extensional and salt tectonics controlled the basin configuration during the Middle and Late Jurassic, affecting sediment distribution and thickness. During this time, deposition was dominated by carbonates [*Terrinha*, 1998; *Ramos et al*., 2016] (Figure 2). An allochthonous salt body (the Esperança Salt) sourced from the lowermost Lower Jurassic (Hettangian) evaporite layer was emplaced progressively from mid-Jurassic up to Miocene times in the eastern half of the Algarve Basin [*Matias*, 2007].

The Lower Cretaceous, represented by siliciclastics and carbonates (Figure 2), shows variations in thickness related to the ongoing salt tectonism and locally to basement-involved extensional faulting. Overall,

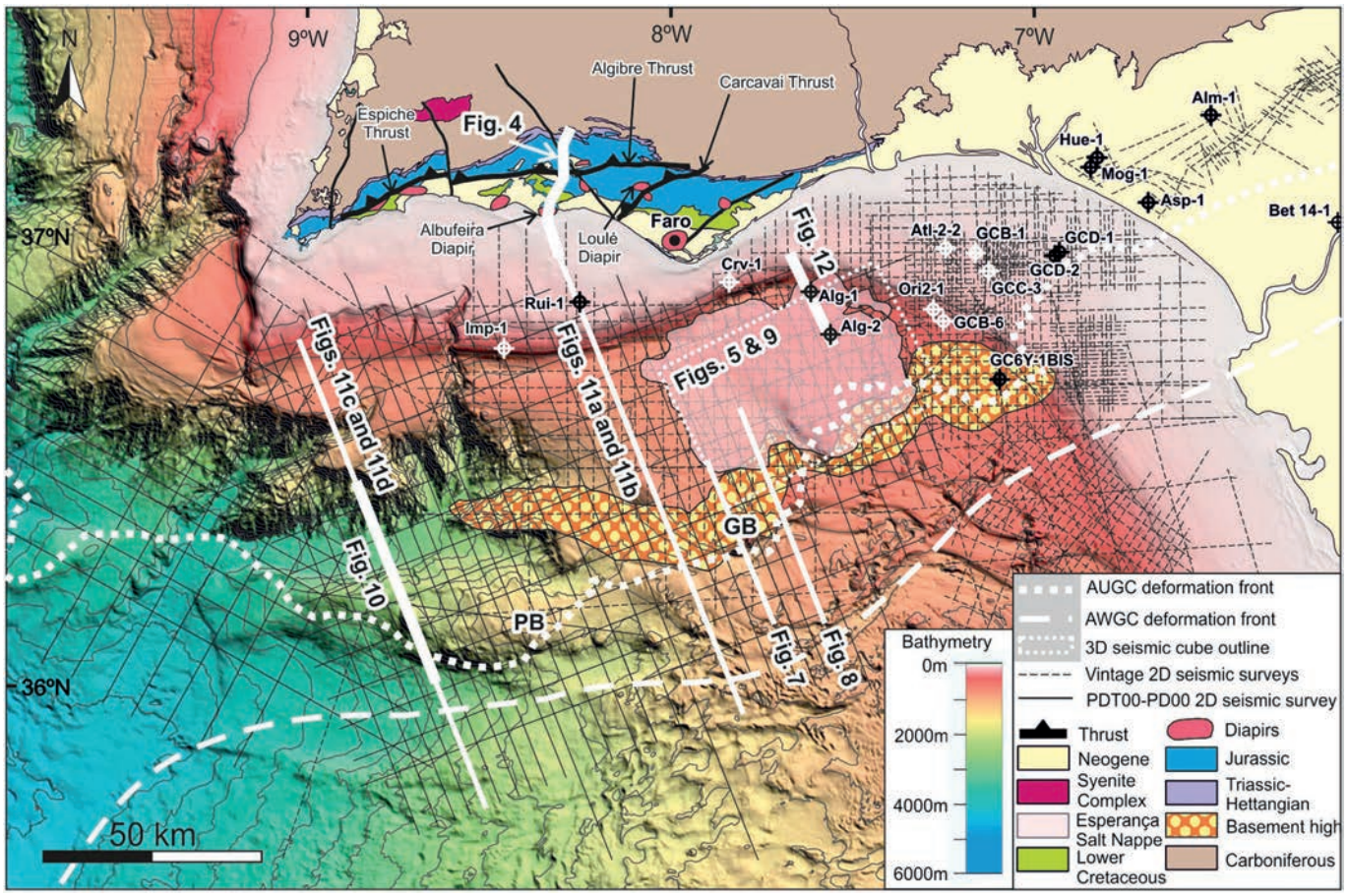

Figure 3. Map showing the available data in the SW Iberian margin with bathymetry colored for depth and the location of the figures described below in this paper. GB: Guadalquivir Bank, PB: Portimão Bank. High-resolution bathymetry is taken from the General Bathymetric Chart of Oceans (GEBCO) digital atlas [*IOC et al.*, 2003]. The most representative wells are also depicted in this figure as follows: Alg-1: Algarve-1, Alg-2: Algarve-2, Alm-1: Almonte-1, Asp-1: Asperillo-1, Atl-2-2: Atlantida-2-2, Bet 14-1: Betica 14-1, Crv-1: Corvina-1, GCB-1: Gulf of Cadiz B-1, GCB-6: Gulf of CadizB-6, GCD-1: Gulf of CadizD-1, GCD-2: Gulf of CadizD-2, GCD-2: Gulf of CadizC-3, GC 6Y-1Bis: Gulf of Cadiz6Y-1Bis, Hue-1: Huelva-1, Imp-1: Imperador-1, Mog-1: Moguer-1, Ori 2-1: Orion 2-1, Rui-1: Ruivo-1. See Figure 1b for the location.

Cretaceous sediments reflect a shallowing of the basin and a reduction in accommodation space. The Lower Cretaceous sediments are followed by a very condensed Upper Cretaceous succession or an equivalent sedimentary hiatus and/or an angular unconformity at the base of the Paleogene, reflecting regional uplift during this time. The Paleogene is partially preserved in the offshore, represented by shallow water carbonates (Figure 2). Above the Paleogene, Miocene deposits overlie the Basal Foredeep Unconformity (BFU) (Figure 2 [*Ledesma*, 2000; *Maldonado et al.*, 1999]) and are a mix of siliciclastics and carbonates in the proximal areas of the basin and turbidite-dominated clastics in the deeper parts. The BFU is a key marker as it records Miocene and younger deformation.

Finally, the Pliocene-Quaternary succession consists of siliciclastics (Figure 2). Pliocene to Present sedimentation in the Gulf of Cadiz is controlled by the Mediterranean Outflow Water (MOW), whose activity started with the opening of the Strait of Gibraltar in Pliocene times [*Hernández-Molina et al.*, 2014]. This current resulted in the deposition of fine-grained contourite drifts, strongly controlling the present-day seafloor geometry.

2.3. Shortening Structures

To date, the contractional deformation and basin inversion experienced elsewhere in Iberia have only been documented to affect the Algarve Basin to a small extent as mostly isolated features in the onshore and the offshore.

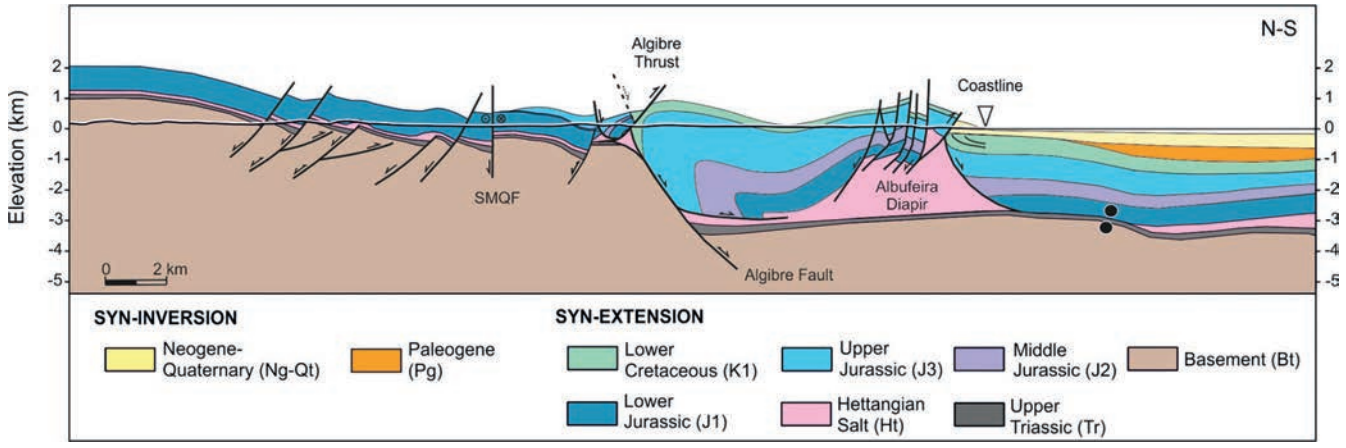

Figure 4. Cross section along the onshore central Algarve Basin. Extensional motion on the southward dipping Algibre fault from Jurassic to Cretaceous times was responsible for the formation of the rollover structure, later inverted during Cenozoic compression. Inversion also led to the formation shortcuts and inversion of extensional faults in the northern sector of the figure. Notice the Algibre Thrust detaching on the Hettangian evaporite unit in the footwall of the Algibre fault. Modified after *Ramos et al.* [2016]. See Figure 3 for the location.

2.3.1. Onshore Structures

Contractional structures are mainly observed along the northern margin of the basin, which crops out due to approximately 350 m of Plio-Pleistocene uplift of southern Portugal [*Feio*, 1951; *Dias and Cabral*, 1997; *Terrinha*, 1998]. This uplift causes southward tilting of the Paleozoic basement and the overlying Mesozoic along the northern outcrop limit of the Algarve Basin (Figure 4). Dips of Mesozoic beds are as high as 32° toward the south and form a continuous monocline along the entire northern outcrop margin of the Algarve Basin. This southward tilt of beds has led to the presence of a clear break in topography, such that the basin is flanked to the north by a sudden rise of topographic relief in the order of up to 200 m (Figure 4). In addition to the regional southward tilt, the basin margin is also characterized by south directed shortcut structures that developed in the footwall of E-W trending extensional faults that bound Triassic half-grabens (Figure 4) [*Terrinha*, 1998; *Ramos et al*., 2016].

Further basinward, the Algibre Thrust (Figures 3 and 4), described by *Manuppella* [1992] and *Terrinha* [1998], is a laterally continuous E-W trending, southward directed thrust that can be correlated to the west with the Espiche Thrust [*Ramos et al*., 2016] (Figure 3). The Algibre Thrust detaches on the regionally ubiquitous Early Jurassic evaporite level [*Ramos et al*., 2016] (Figure 4). In its footwall, Mesozoic beds are characterized by multiple E-W trending tight folds, produced by buttressing against a southward dipping Mesozoic extensional fault (Figure 4) [*Ramos et al*., 2016]. Age for the Algibre thrust cannot be constrained precisely, but the youngest materials in its footwall are Early Cretaceous in age.

Throughout the onshore portion of the basin, isolated salt structures also record shortening and reactivation. The Loulé Salt diapir (Figure 3) displays various pulses of shortening, associated to progressive exhumation of the diapir [*Terrinha et al*., 1990]. The Albufeira Diapir (Figures 3 and 4) also shows two phases of contractional deformation [*Terrinha et al*., 2013; *Ramos et al*., 2016], attested by the deformed and thrusted Miocene overlying isoclinal folds of the Lower Cretaceous.

2.3.2. Offshore Structures

In the offshore, the Portimão Bank (Figure 3) was documented by *Roque* [2007] and *Terrinha et al*. [2009] to be a Mesozoic graben inverted from Neogene times to present day. To the east of the Portimão Bank, the Guadalquivir Bank (Figure 3) is a prominent bathymetric high, but its precise nature has remained elusive. Other than the Portimão Bank, no contractional structures have been documented within the offshore Algarve Basin.

The most evident Cenozoic contractional feature in the Gulf of Cadiz lies to the south of the Algarve Basin but provides key timing relationships discussed in this paper. It is a giant chaotic unit emplaced synchronously with the development of the Betic-Rif orogen. This chaotic unit is divided into two subunits: one of tectonic origin and a second one related to gravitational collapse of the first one. The first one is the Accretionary

Wedge of the Gulf of Cadiz (AWGC), also labeled GCIW, Gulf of Cadiz Imbricated Wedge, by some authors), and the second one is the Allochthonous Unit of the Gulf of Cadiz (AUGC), labeled HGU, Horseshow Gravitational Unit, by some authors) [*Torelli et al*., 1997; *Iribarren et al*., 2007]. The Accretionary Wedge of the Gulf of Cadiz (AWGC) consists of a thick chaotic, mélange-like assemblage of Mesozoic to Cenozoic rocks affected by west migrating thrust system. The AWGC developed as the outermost structure of the Betic-Rif orogen during the Miocene as the orogenic arc progressed westward driven by the roll back of the Gibraltar subducted oceanic slab [*Gutscher et al*., 2002]. Disagreement exists as to the ongoing activity of the accretionary wedge [*Gutscher et al*., 2002, 2009; *Medialdea et al*., 2004; *Iribarren et al*., 2007]. The AUGC is an olistostrome, gravitationally emplaced submarine debris flows sourced from the AWGC [*Iribarren et al*., 2007; *Gutscher et al*., 2009]. It buried the front of the AWGC along the entire front of the Betic and Rif, over the Guadalquivir and Gharb forelands and their extension toward offshore. To the west, the lack of a shallow continental mass allowed the AUGC to spread downslope into the deep ocean [*Torelli et al*., 1997]. Locally, the AUGC is seen to be incorporated into the accretionary wedge [*Thiebot and Gutscher*, 2006]. There is general agreement that the AUGC was emplaced by Late Tortonian [*Perconig*, 1962; *Torelli et al*., 1997; *Tortella et al*., 1997; *Flinch and Vail*, 1998; *Maldonado et al*., 1999]. It overlies a regional unconformity that defines the base of the Betic foredeep deposits (BFU) [*Maldonado et al*., 1999; *Ledesma*, 2000].

2.4. Present-Day Configuration

The Mesozoic to Cenozoic Algarve Basin sits between the Atlantic oceanic thrusts (Gorringe, Marquês de Pombal, and Horseshoe Thrusts) and the Betic-Rif orogen (Figure 1b), areas of known Miocene to present contractional deformation. This area is dominated at present day by transpressional to compressional stress due to its location relative to the plate boundary between the Nubian and Iberian plates [*Zitellini et al*., 2009; *DeMets et al*., 2010]. The Algarve Basin, and the broader Gulf of Cadiz, has been documented as a tectonically active domain by many authors [*Gràcia et al*., 2003a, 2003b; *Duarte et al*., 2009, 2010; *Terrinha et al*., 2009; *Zitellini et al*., 2009; *Duarte*, 2011; *Martínez-Loriente et al*., 2013, 2014]. Seismicity, as indicated by focal mechanisms, is coherent with N-S to NW-SE directed shortening across the Gulf of Cadiz [*Zitellini et al*., 2009; *Palano et al*., 2013; *Custódio et al*., 2015, 2016]. The Guadalquivir and Portimão Banks, which define the southern boundary of the Algarve Basin (Figure 3), have been identified as tectonically active features since the Neogene [*Ribeiro et al*., 1979; *Mougenot*, 1989; *Terrinha*, 1998; *Gràcia et al*., 2003a; *Zitellini et al*., 2004; *Terrinha et al*., 2009].

3. Data and Methods

The observations and interpretation of the structure of SW Iberia and the Algarve Basin presented in this paper are based on interpretation of seismic data, well data, geological mapping of onshore Portugal, and gravity and magnetic data. Data have been integrated with regional geological understanding to ensure that the interpretation is coherent with the history of Mesozoic extension and Cenozoic compression experienced by SW Iberia.

Vintage 2-D seismic surveys of the Gulf of Cadiz and a more recent 2-D regional seismic reflection survey (acquired by TGS in 2001 during the PDT00 and PD000 cruises [*TGS*, 2005]) have been used to interpret the offshore structure in the Gulf of Cadiz (Figure 3). The PDT00-PD00 regional survey consists of a set of 58 lines of 2-D multichannel reflection seismic data. This seismic survey consists of NNW-SSE lines spaced every 4 km and ENE-WSW lines spaced every 8 km, and it has a shot point interval of 12.5 and 15 m. Recording length was 12 s two-way travel time (TWTT). The interpretation on this survey was performed on the migrated stack in time.

A 3-D seismic cube was acquired in 2012 by Repsol in the central part of the offshore margin, from south of Faro to the Portuguese-Spanish border (Figure 3). It covers an area of 1500 km^2 and it consists of 151 shot lines oriented NNW-SSE and spaced every 375 m, with a recording length of 7.2 s TWTT. This 3-D cube has also been interpreted, using the prestack time and prestack depth migrated versions.

Seismic interpretation was constrained by the calibration with 5 wells in offshore Portugal [*Roque*, 2007] along with 67 wells in the Gulf of Cadiz and Guadalquivir Basin [*Lanaja*, 1987] (the location of the most relevant wells is shown in Figure 3). Portuguese wells have been tied to seismic using their individual check shot data or average interval velocities (Figure 2) when check shot data was of poor quality or not available. The interval velocities have been calibrated using the depth image of the depth-migrated 3-D seismic cube to

make it meaningful for the deeper portions of the basin where no wells are available. Seismic profiles have been interpreted using Petrel (by Schlumberger). Conversion of 2-D seismic profiles to depth has been performed where necessary using Move 2014.2 (by Midland Valley Exploration).

Seismic correlation has been based on the interpretation of unconformity-bounded sequences [*Terrinha*, 1998; *Roque*, 2007]. The seismic response is different in every stratigraphic unit. Paleozoic is represented by transparent and chaotic seismic facies, sometimes stratified (e.g., Figure 8). The basement is followed by the first Mesozoic sediments, the Triassic, represented by middle-to-high-frequency and high-amplitude reflectors (e.g., Figure 9). The roof of this section coincides with the base of the Hettangian evaporites, describing a strong reflector (Figure 9). Evaporite seismic facies are made of chaotic and transparent reflectors. Salt tectonic structures are typically represented by positive and irregular strong reflectors, deforming the overlying and surrounding sediments (Figure 8). The seismic image shows a poor quality beneath salt structures (Figure 10).

Lower Jurassic shows low-frequency and high-amplitude reflectors (e.g., Figure 5). Middle and Upper Jurassic show similar seismic response (e.g., Figures 5 and 9) and present some unconformities, such as the Bajocian-Bathonian and the Callovian-Oxfordian among the most representative. The Lower Cretaceous, represented by middle-to-high-frequency and medium-amplitude reflectors, tends to onlap the Upper Jurassic (e.g., Figure 5). The Upper Cretaceous and the Paleogene, where present, lay over an erosional unconformity over the last unit. They are represented by strong middle-amplitude and middle-frequency reflectors (e.g., Figure 6). Neogene and Quaternary are depicted by high-frequency and low-amplitude continuous reflectors, and onlap the BFU, while its roof represented the seafloor (e.g., Figure 6).

The AUGC is depicted by a highly irregular roof and an erosional flat base, with chaotic and transparent internal facies (e.g., Figure 6). The AWGC has a similar seismic response, although the southward dipping reflectors suggest the presence of imbricated thrusting (Figure 10) [*Gutscher et al*., 2002]. To the south and southeast the image beneath is obscured by both bodies (AUGC and AWGC).

Seismic interpretation has also been integrated with published onshore data [*Ramos et al*., 2016]. Finally, gravity and magnetic modeling [*Ramos et al*., 2015] have been used to constrain the deeper seismic horizons (pre-Jurassic picks, mainly the top of basement) and the crustal-scale structure.

4. Contractional Structures of the Algarve Basin

The preservation of the overall Mesozoic age rift architecture of the Algarve Basin gives a false impression that the basin has not experienced major inversion and merely subsided in the Cenozoic as the foredeep to the Betic-Rif orogen. In this section we aim to demonstrate that contractional structures of Cenozoic age are more common in the area than previously documented. To do this we will provide an overview of known and newly documented contractional structures, from the onshore basin margin to the offshore.

Multiple scales of contractional deformation features in the offshore Algarve Basin can be observed on 2-D and 3-D reflection seismic data. On one hand, there are thrusts detaching within the Mesozoic sediments that can be clearly identified on seismic activity, and their activity dated is based on stratigraphic unconformities. On the other hand, there are angular relationships and observations which cannot be tied down to specific structures visible on seismic but can be ascribed to basement-involving structures, possibly thick-skinned blind thrusts.

4.1.1. Reactivated Salt Structures in the Eastern Algarve Basin

The contractional structures most evident on seismic in the offshore Algarve Basin are those associated with the deformation of salt bodies, mainly in the allochthonous Esperança Salt (Figures 3 and 5), which shows squeezing of salt structures in its central part (Figure 5). Salt accumulations related with the salt structures that formed during the rifting stage of the Algarve Basin were the weakest parts of the basin and the areas prone to localize and record the subsequent contractional deformation.

In the central part of the profile of Figure 5, an antiform cored by imbricated Lower Cretaceous and Jurassic sediments can be observed (Figures 5 and 6). Structural relief related with this contractional structure is of 1.7 km. Unfolding of the top of Cretaceous to a restored geometry (Figure 5c) indicates that shortening on this structure was in the order of 2.5 km. Onlap of the Paleogene onto the Lower Cretaceous and the thinning of Quaternary sediments over this structure demonstrate that this antiform grew from Paleogene until recent

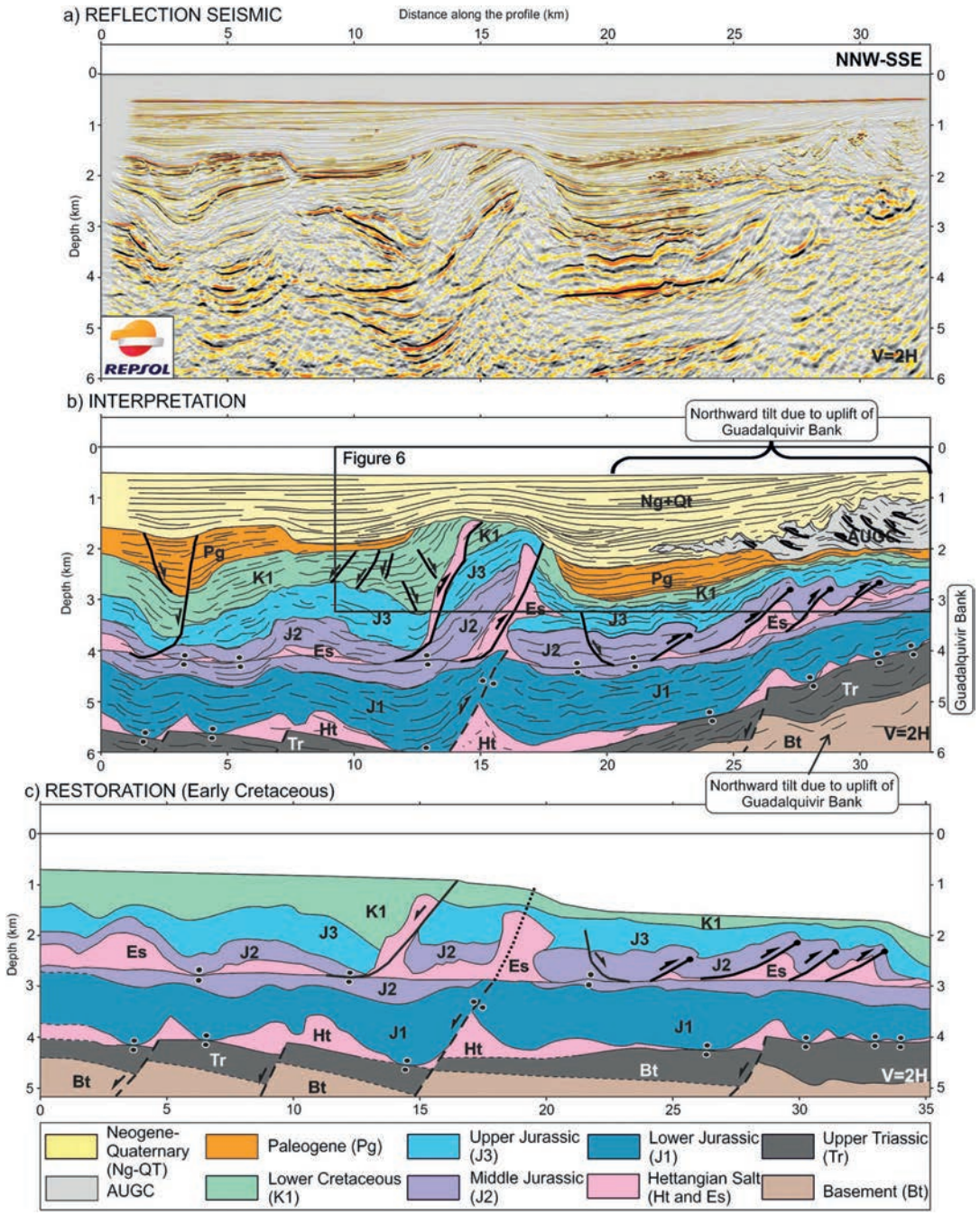

Figure 5. Seismic section across the Esperança Salt. (a) Reflection seismic profile (extracted from a proprietary 3-D seismic cube migrated in depth). (b) Interpretation of Figure 5a. (c) Restoration at Early Cretaceous time. Black dashed line: inferred fault and horizon, Ht: autochthonous evaporitic layer, Es: Esperança Salt. The section is a NNW-SSE trending section through the 3-D seismic survey shown in Figure 3 (the precise location is not shown due to confidentiality). Data courtesy of Repsol.

times. Different stages of growing are emphasized by the three main unconformities observed in the growth package (Figure 6). Paleogene sediments onlap the Lower Cretaceous unit on the southern limb of the antiform, evidencing the earliest stages of folding. Above, the BFU unconformity truncates the imbricated Jurassic to Paleogene sediments in the core of the antiform, revealing a period of more intense shortening and erosion. It is worth noting that the BFU connects with the basal surface of the AUGC (Figure 6), demonstrating the synchronicity between antiformal growing and the emplacement of the AUGC.

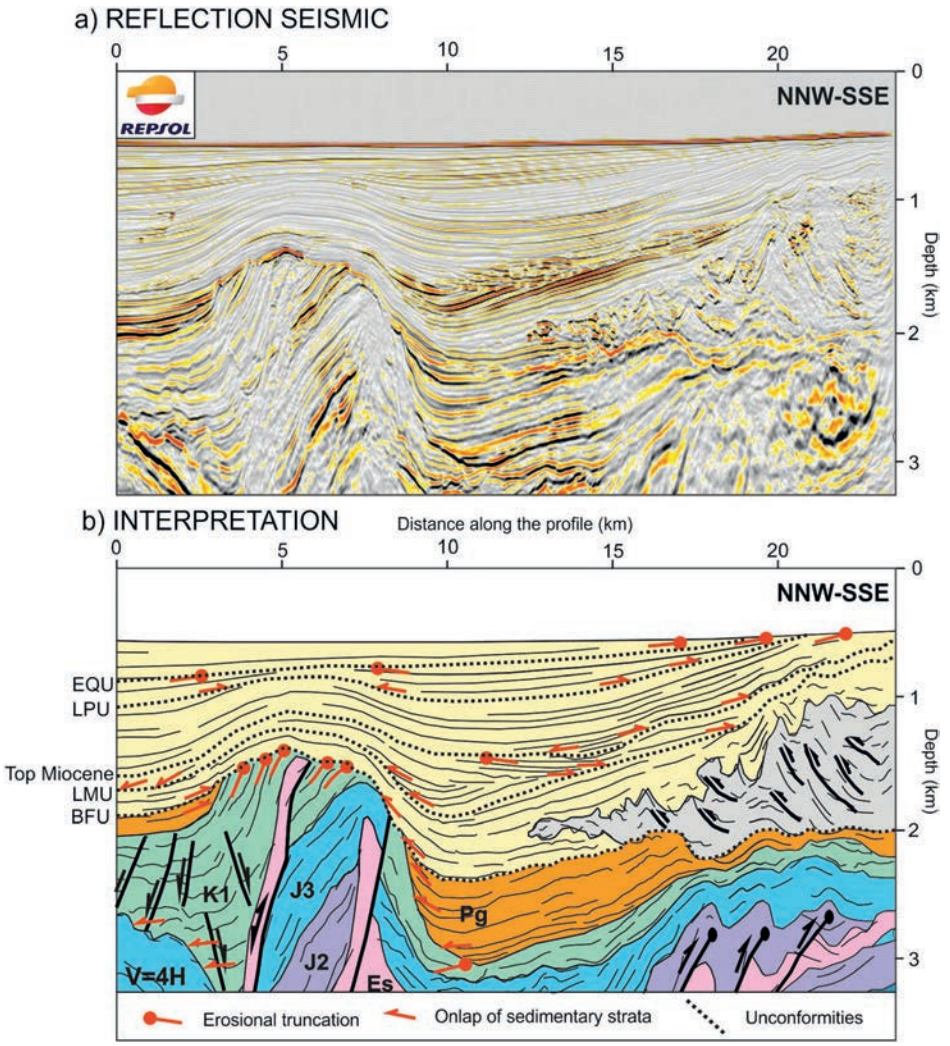

Figure 6. (a) Seismic section of the detailed Cenozoic unit over the Esperança Salt in Figure 5b. (b) Seismic interpretation showing the main unconformities within the Cenozoic sediments described by *Hernández-Molina et al*. [2016], along with the onlaps and erosional truncations resulting from different tectonic pulses. See Figure 5 for the legend. BFU = Basal Foredeep Unconformity, LMU = Late Miocene Unconformity, LPU = Late Pliocene Unconformity, EQU = Early Quaternary Unconformity.

The AUGC is sandwiched between its basal contact and an unconformity within the late Miocene (labeled LMU on Figure 6), which truncates Miocene growth sediments and is folded by the antiform (Figure 6). Above the LMU, a highly reflective wedge-shaped set of reflectors could correspond to contourite deposits related with the circulation of Mediterranean Outflow Water from the Gibraltar strait to the Gulf of Cadiz since Pliocene times [*Llave et al*., 2011], channeled between the AUGC and the Guadalquivir Bank and the growing antiform. These sediments, as well as the younger succession above, show a growth geometry at both sides of the anticline. They also have experience a regional northward tilting and moderate deformation by the reactivation of the internal structures of the AUGC (Figure 6). Despite Pliocene sediments being dominated by contouritic deposits, onlap onto the late Pliocene unconformity [*Hernández-Molina et al.*, 2016] and truncation below the Early Quaternary Unconformity [*Hernández-Molina et al.*, 2016] observed in this section are interpreted to respond to tectonic causes and not primary sedimentary geometry [see also *Hernández-Molina et al.*, 2016]. The symmetrical arrangement of the Pliocene-Quaternary sedimentary growth wedges at both sides of the antiform demonstrates the progressive tilting of their limbs. This geometry significantly differs from the wedge-shaped contourite drifts deposited in the adjacent structural lows (Figure 6). Contourite

deposits are dominated by sheeted drifts and mostly constant thickness other than around tectonically active structures [*Hernández-Molina et al*., 2016].

The internal structure of the antiform consists of two thrusts involving the Jurassic and Lower Cretaceous sediments. However, normal throw of the Jurassic across the northern thrust and the presence of a localized, thick Upper Jurassic/Lower Cretaceous depocenter strongly affected by extensional faults demonstrate extensional faulting, downbuilding, and salt evacuation, indicating the existence of a salt wall that has been subsequently squeezed to form a thrust weld. The southern thrust would also correspond to a thrust weld formed by shortening of a salt wall (Figure 5c). This salt wall could correspond to a feeder connecting the autochthonous Hettangian Salt horizon with the allochthonous Esperança Salt nappe. The reconstructed geometry of the section in Figure 5 at Early Cretaceous time (Figure 5c) shows that none of the salt walls accommodated any shortening prior to the Late Cretaceous.

The section in Figure 5 also contains two other sets of contractional features. For one, Figure 5c shows a set of shortening structures already present at Early Cretaceous times along the southern end of the section. These are part of a south directed fold-and-thrust system detached on the allochthonous Esperança Salt. This system is interpreted to be the toe-thrust system associated to the allochthonous emplacement and gravitationally driven deformation of the Esperança Salt in Middle to Late Jurassic times. Folds and thrusts record syntectonic thinning and thickening of Middle to Upper Jurassic sediments, defining a pre-Cretaceous age for the thrusting. Folding of overlying units is interpreted to relate to a later reactivation.

The last set of contractional features observed on this section (Figure 5) is related to the AUGC. The base of the AUGC is seen to tectonically erode Paleogene sediments and climb up stratigraphically toward the north. The chaotic facies of this body are in response to highly deformed sediments due to intense thrusting and sedimentary reworking during transport. The top of this body is highly irregular due to postemplacement mobilization of sediments, probably driven by shale tectonism (documented by the abundant shale diapirs in the Gulf of Cadiz) [*Medialdea et al*., 2009]. The resulting minibasins are infilled by late Miocene sediments.

4.1.2. Guadalquivir Bank

The Guadalquivir Bank is an elongated ENE-WSE seamount 50 km long and 30 km wide (Figure 3) constituted by a core of Paleozoic basement that locally crops out at the seafloor as testified by dredging [*Malod and Mougenot*, 1979; *Gràcia et al*., 2003a, 2003b]. To the SW, this bathymetric high links with another positive bathymetric structure, the Portimão Bank (Figure 3).

Figure 5 ends short of the crest of the Guadalquivir Bank (note outline of 3-D seismic survey in Figure 3). The basement that can be seen on the southern end of the section rising up toward the south is the northern flank of the Guadalquivir Bank. Just as the basement is tilted to the north, overlying Mesozoic and Cenozoic sediments (ranging from Paleogene to Quaternary, including the base of the AUGC) are dipping to the north. Within the Cenozoic package, late Miocene to late Pliocene age sediments that onlap and blanket the AUGC are dipping north and truncated at the seabed above the Guadalquivir Bank (above the AUGC at the right end of the section; Figure 6). These sediments are in turn onlapped by sediments of latest Pliocene to Quaternary age (Figure 6), which are truncated by the seabed and are the same sediments involved in the antiform resulting from the reactivation of salt walls in the center of the section (Figure 6).

The northward dip of Mesozoic to Cenozoic sediments on the northern limb of the Guadalquivir Bank is observed also on 2-D seismic lines (Figures 7–9 and 11). It is also associated to truncation of the most recent sediments at the seabed observed in the Figures 6 and 9 and by contouritic moats in Figures 7 and 8. Likewise, erosion associated to the BFU is seen to locally remove the entire Paleogene and truncate the top of the Lower Cretaceous over the Guadalquivir Bank (Figures 8 and 9) before being draped by Miocene sediments. As in the case of Figure 6, late Pliocene sediments are clearly tilted and erosionally truncated at the seabed above the Guadalquivir Bank in the sections in Figures 8b and 9b. Quaternary sediments are also observed to onlap tilted Pliocene sediments in Figure 8b. All these geometries are clear indications of uplift of the Guadalquivir Bank from Paleogene to Present, in at least two distinct stages: a late Paleogene (or early Miocene?) stage, accounting for the erosional truncation below the BFU, and a late Pliocene to Quaternary stage that accounts for tilting and truncation at the seabed of late Pliocene and older sediments.

Paleogene or early Miocene uplift of the Guadalquivir Bank explains why the bank acted as a barrier to the progression during the middle to late Miocene of the AUGC in its southern flank (Figures 3, 7, 8, and 11). The AUGC was only capable of overcoming this physiographical barrier locally (e.g., Figure 5) in areas of

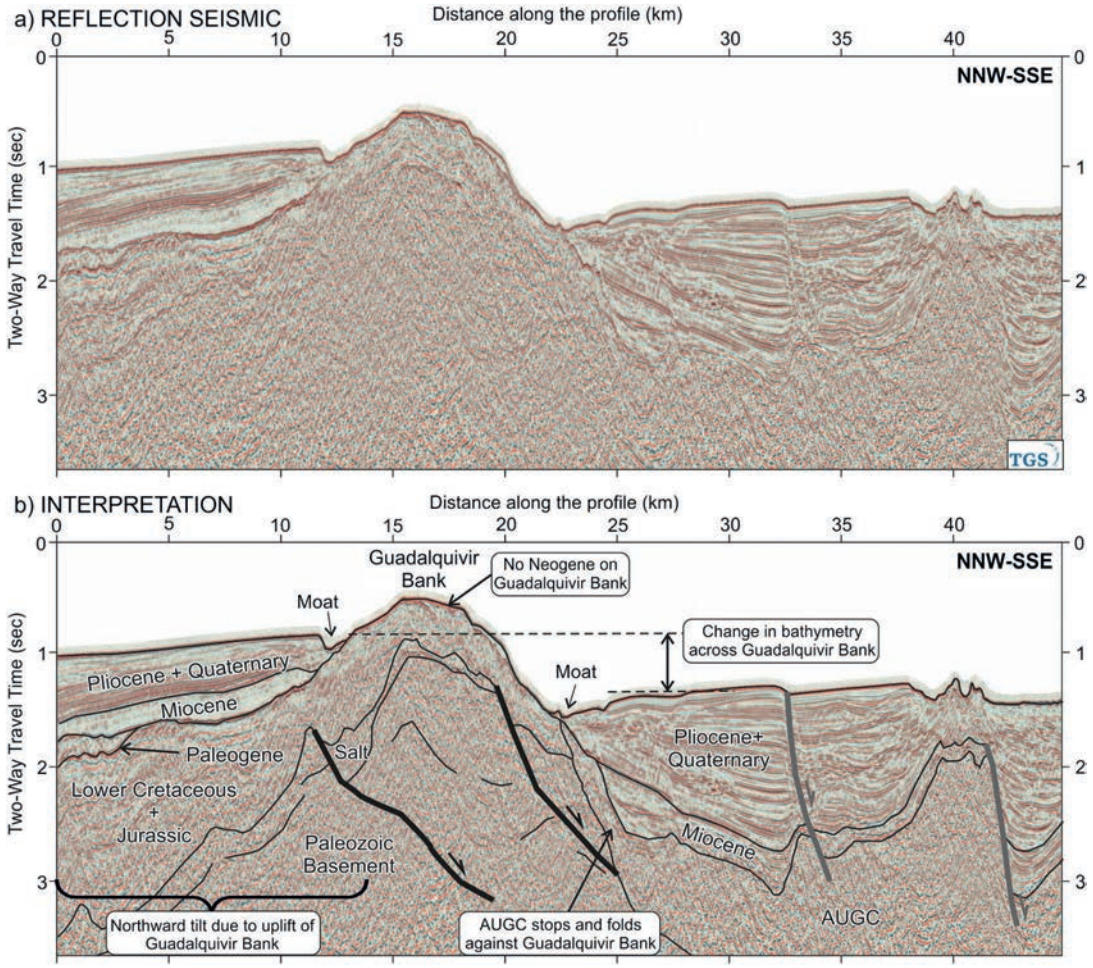

Figure 7. (a) Seismic section across the Guadalquivir Bank in TWTT and (b) its interpretation. Note the bathymetric relief of the Guadalquivir Bank and its lack of inner reflectivity. The onlap of Miocene to Quaternary sediments on both flanks indicates the presence of pre-Miocene sediments at seabed on the Guadalquivir Bank. Note also the northward tilt of sediments on the north of the Bank and the southward steepening of the AUGC and Miocene sediments on the south. See Figure 3 for the location. Data courtesy of TGS.

lesser uplift of the bank. Recent uplift also accounts for the noticeable drop in bathymetry (in the order of 200–400 m) that occurs across the bank (Figures 7 and 8) and that conditions present-day sea bottom contouritic currents (MOW) and erosion (note the localization of contouritic moats on both flanks of the bank in Figure 7 and on the southern flank of the Bank in Figure 8).

The 3-D seismic cube reveals the presence of north directed thrusts in the northern flank of the Guadalquivir Bank, affecting the sediments ranging from basement to Early Cretaceous (Figure 9). These are interpreted as back thrusts accommodating part of the contractional deformation due to the uplift of the Guadalquivir Bank by the basal regional thrust. In some cases, based on the thickening of pre-Cretaceous sediments in their hanging wall, they seem to reactivate previous Triassic-Jurassic extensional faults.

Beyond the geometries that are related to Cenozoic shortening and uplift, some geometries observed on the seismic profiles already discussed prove the relevance of the Guadalquivir Bank as a structural high during basin extension in the Mesozoic. The section in Figure 8, for instance, shows that the basement high under the Guadalquivir Bank can be interpreted as the footwall of a major extensional fault dipping toward the south/southeast. In this case, the hanging wall of the extensional fault has been uplifted by approximately 2 km by Cenozoic thrusting (see Figures 8c and 8d) and deeply eroded by the BFU before being "onlapped" by the AUGC and later sediments. The equivalent Mesozoic in the footwall of the thrust responsible for uplift

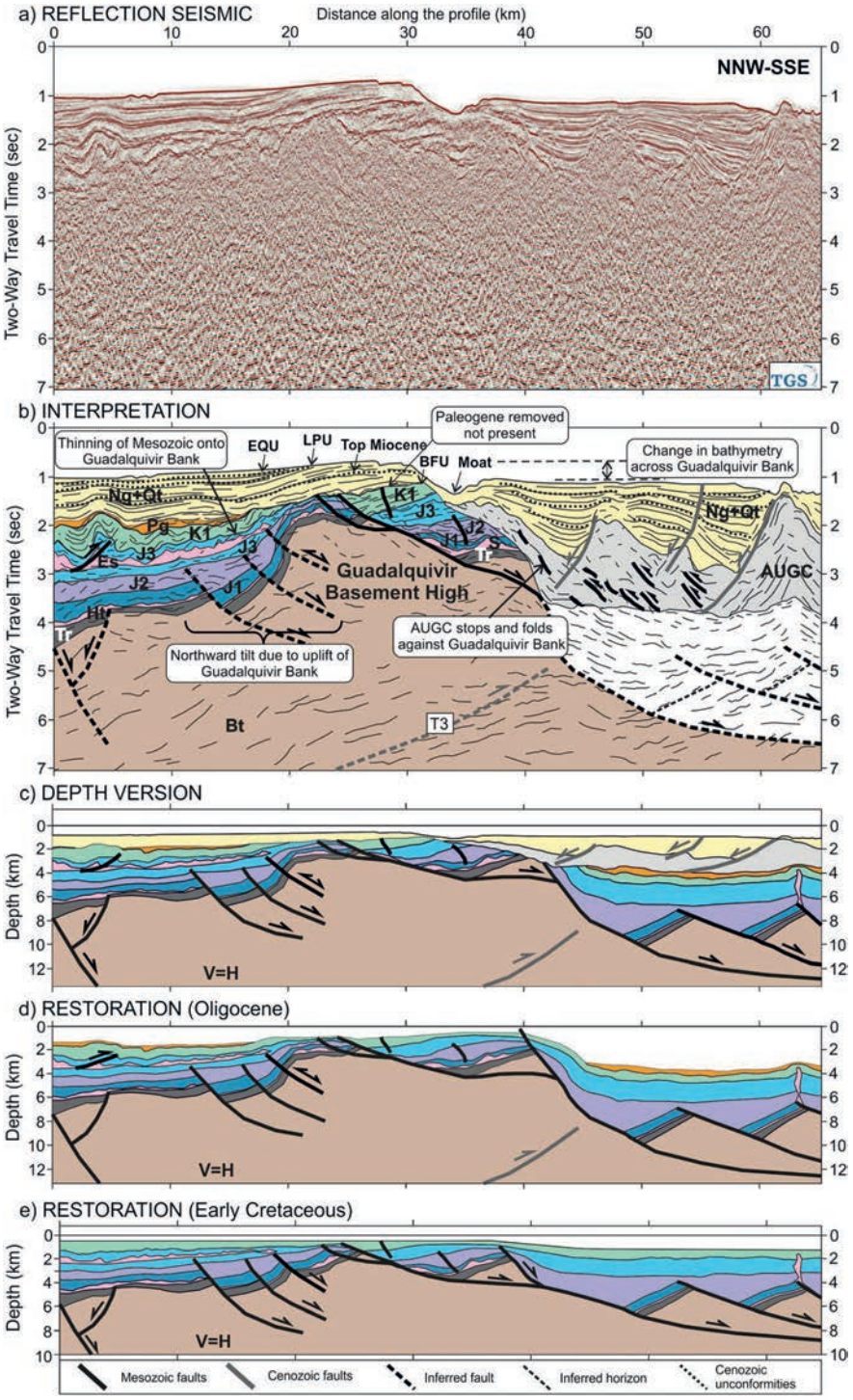

Figure 8. Seismic section across the Guadalquivir Bank. (a) Reflection seismic profile in time. (b) Interpretation of the same profile. (c) Depth version of profile in Figure 8a. (d) Restoration at Oligocene time (prior to the emplacement of the AUGC). (e) Restoration at Early Cretaceous time. The interpretation beneath the depth of 3–4 s is based on the 3-D seismic image north of the Guadalquivir Bank and inferred to its south due to the poor seismic image. Extensional faults interpreted north of the Guadalquivir Bank are projected from 3-D seismic interpretation (see Figure 9). See Figure 3 for the location and Figure 5 for the legend. BFU = Basal Foredeep Unconformity, LPU = Late Pliocene Unconformity, EQU = Early Quaternary Unconformity. Data courtesy of TGS.

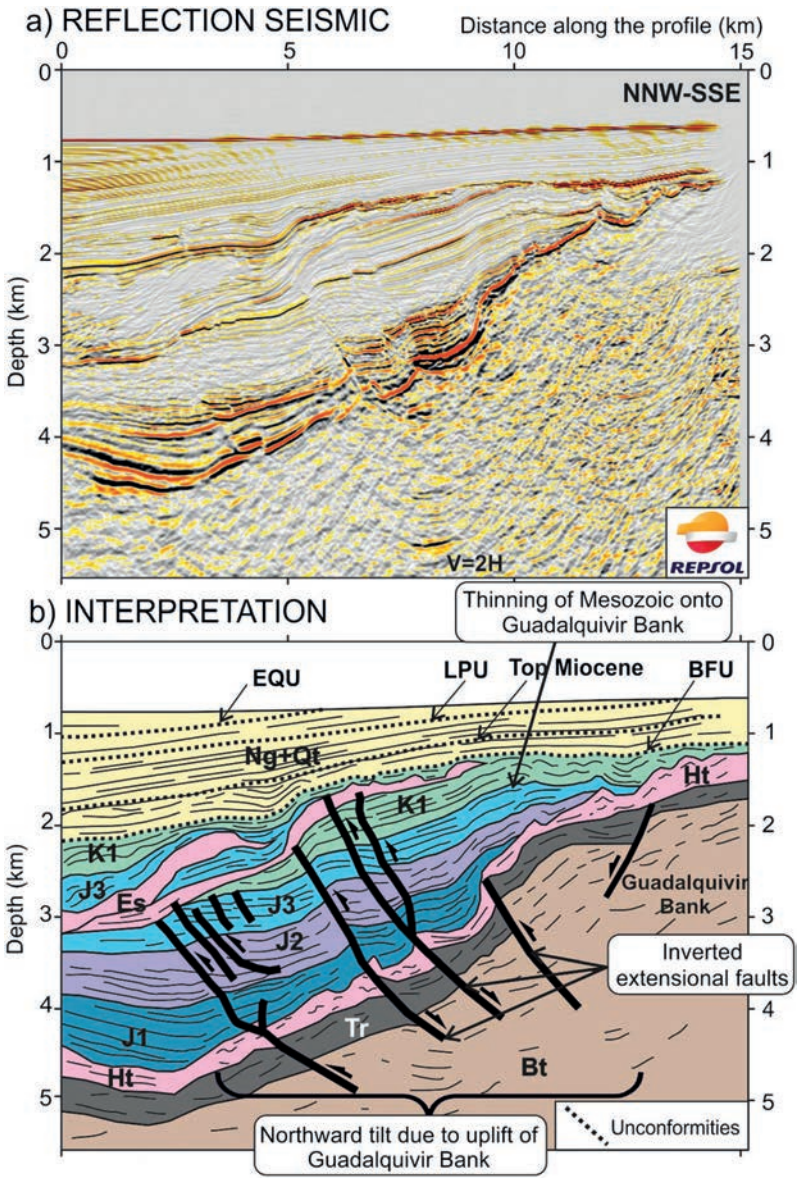

Figure 9. (a) Reflection seismic profile in depth across the northern flank of the Guadalquivir Bank and the southwestern portion of the Esperança Salt and (b) its corresponding interpretation. See Figure 5 for the legend. The section is the southern portion of a NNW-SSE trending section through the 3-D seismic survey shown in Figure 3 (the precise location is not shown due to confidentiality). BFU = Basal Foredeep Unconformity, LPU = Late Pliocene Unconformity, EQU = Early Quaternary Unconformity. Data courtesy of Repsol.

of the bank is interpreted to be in the order of 4 to 6 km deeper than that in the hanging wall of the thrust (the base of the AUGC that is assumed to lie over Paleogene and Mesozoic sediments, as in Figure 5, is at a depth of nearly 4 km). This difference in depth of Mesozoic sediments across the Guadalquivir Bank can also be seen on other sections through the area (e.g., Figures 7 and 11b if the Mesozoic south of the bank is also inferred to lie under the base of the AUGC). It is difficult to account for this throw merely by Cenozoic uplift; we interpret that Mesozoic extensional faulting predating thrusting can account for part of this vertical offset (Figures 8d and 8e).

The relationship of the Guadalquivir Bank basement high with Mesozoic sediments to the north is not as clear on seismic due to poor image quality. Locally, where image is good enough, onlap and thinning of

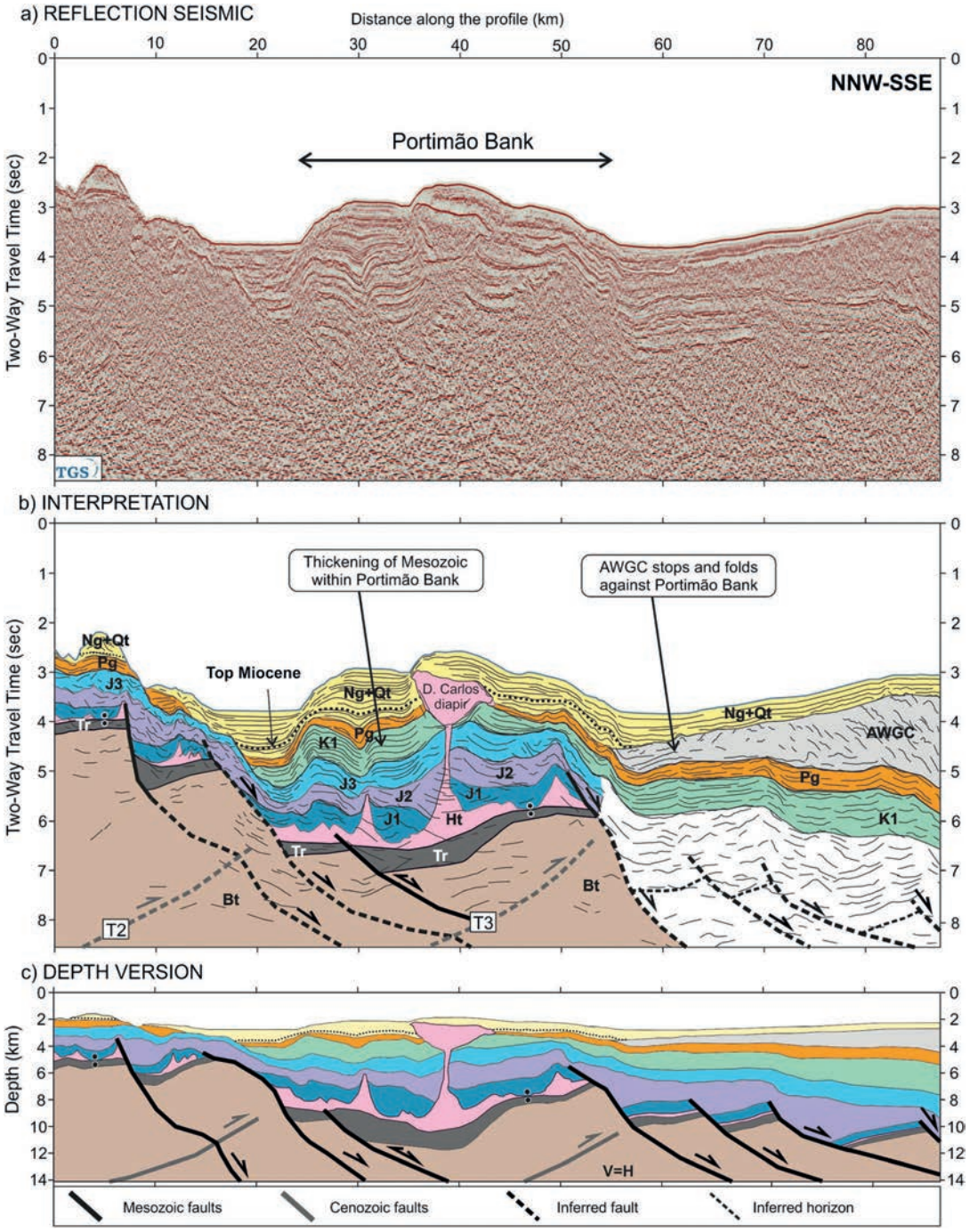

Figure 10. Representative section across the Portimão Bank. (a) Reflection seismic profile in time. (b) Interpretation of the profile in Figure 10a. (c) Depth version of the profile. See Figure 3 for the location and Figure 5 for the legend. The interpretation of the deep section south of the Portimão Bank is inferred. Data courtesy of TGS.

Cretaceous and Jurassic sediments onto the basement high can be seen, inferred to represent infill of a basin flanking a basement high (Figure 8e). In other cases, progressive depositional thinning of the Jurassic and Lower Cretaceous sediments toward the Guadalquivir Bank (Figures 5 and 9) indicate that the basement under the Guadalquivir Bank was already dipping gently to the north prior to Cenozoic deformation. This is consistent with the interpretation of the Guadalquivir Banks as a basement high during Mesozoic

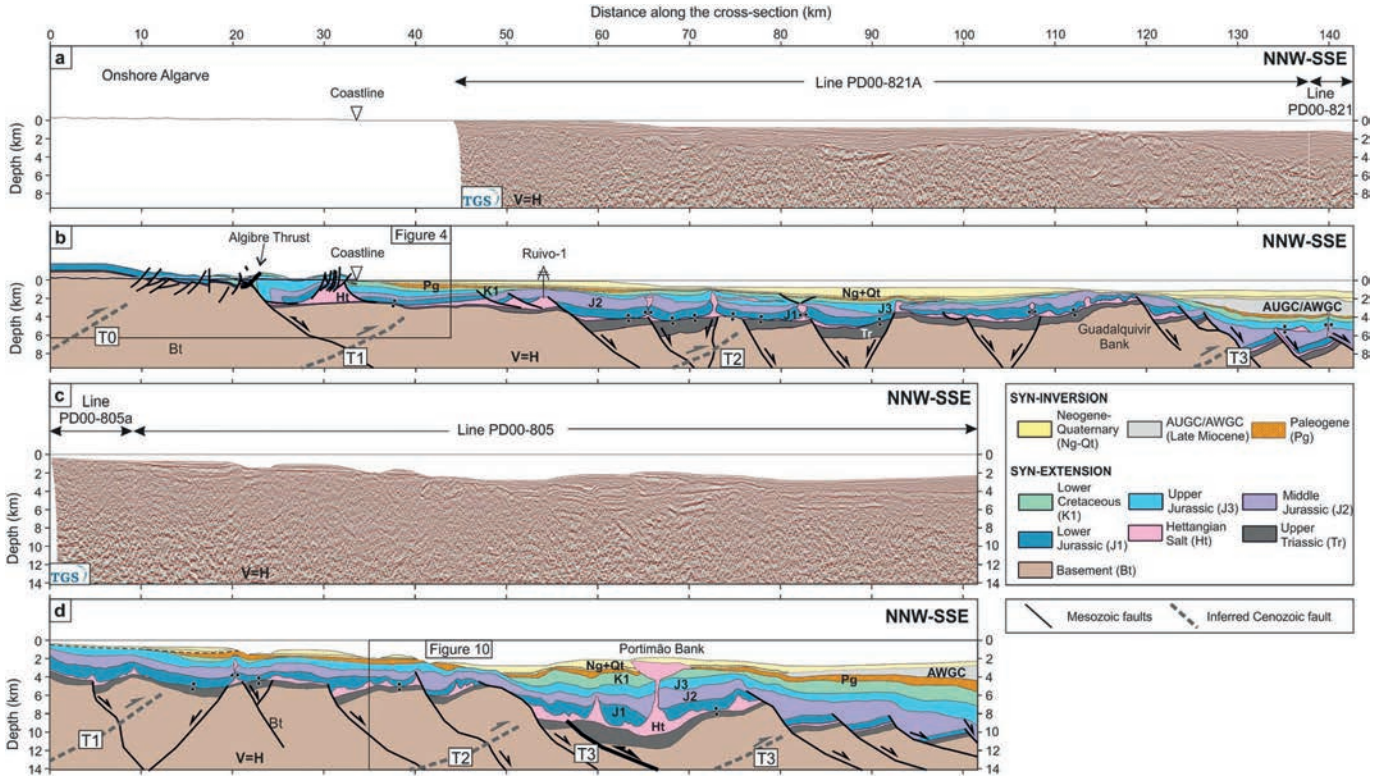

Figure 11. Cross sections through the Algarve Basin showing the major contractional structures identified. (a) Composite seismic section through the central Algarve Basin. (b) Interpretation of the seismic in Figure 11a, with interpretation extended onshore and complemented with outcrop data. (c) Seismic section through the western Algarve Basin. (d) Interpretation of seismic in Figure 11c. The black dots represent the salt welds. See Figure 3 for the location. BFU = Basal Foredeep Unconformity, LPU = Late Pliocene Unconformity, EQU = Early Quaternary Unconformity. Seismic data courtesy of TGS.

extension by previous authors [*Terrinha*, 1998; *Matias*, 2007]. Our observations indicate that the Guadalquivir Bank basement high initially originated as the uplifted footwall of a major (possibly crustal scale) south dipping Mesozoic extensional fault (Figure 7d). This structure was later inverted by a south verging thrust that caused further uplift of the Guadalquivir Bank from Paleogene to Present.

4.1.3. Portimão Bank

In contrast to the Guadalquivir Bank, which is a basement-cored structure, the Portimão Bank (Figures 3, 10, and 11d) has been interpreted as an inverted Mesozoic fault-bounded basin by *Terrinha et al*. [2009]. The Mesozoic nature of sediments in the half-graben is supported by the presence of the Dom Carlos diapir (Figure 10), evident on bathymetry as a dome structure, and interpreted to be constituted by Early Jurassic Salt (the only evaporitic unit known in the region) [*Terrinha et al*., 2009]. At the core of the bank, wedging of Mesozoic sediments toward the south and the steeper bathymetry on the northern flank of the bank (Figure 10) indicate that this is an inverted Mesozoic half-graben developed on a south dipping extensional fault. Inversion is of Neogene to recent times, as inferred from the folding of constant-thickness Paleogene strata, thickness variations observed in Miocene and younger sediments, and present-day bathymetry (Figure 10). As with the Guadalquivir Bank, its uplift from late Paleogene or early Miocene times is recorded by the tipping of the AWGC along the southern flank of the bank (Figure 10). To the south, the Mesozoic and Paleogene units beneath the AWGC are deformed in monoclines (Figure 10), suggesting compaction folding over basement rotated blocks. The Neogene-Quaternary sediments and the seabed also show deformation in the Portimão Bank, coherent with the monocline geometry affecting the sediments below (Figure 10), suggesting a recent reactivation for these thrust faults. The continuous growth of the Dom Carlos diapir through Neogene times to present day was probably partly driven by contractional reactivation.

Inversion of the Portimão Bank Mesozoic half-graben is consistent with N-S to NW-SE shortening and with present-day seismic activity that indicates NNW-SSE directed compression [*Dewey et al*., 1989; *Srivastava*

et al., 1990b; *Roest and Srivastava*, 1991; *Maldonado et al*., 1999; *Zitellini et al*., 2001, 2009; *Rosenbaum et al*., 2002; *Muñoz-Martín et al*., 2012; *Palano et al*., 2013; *Custódio et al*., 2015]. Faults cannot be traced unambiguously on seismicity, but present-day positive bathymetry and the rapid thickening of Jurassic and Cretaceous sediments into the Portimão Bank cannot be accounted for only by salt tectonics but can be better explained as an inverted Mesozoic fault-bounded graben (Figure 10). Unlike the Guadalquivir Bank, there is no change in the regional level of bathymetry on both sides of the Portimão Bank. Major bathymetric changes occur toward the north of the bank (Figure 10) and are associated with southward steepening of Jurassic sediments and the localization of contouritic moats (Figure 10). To the south of the Portimão Bank there is an increase in depositional space for the Neogene-Quaternary (this space includes the AUGC and the AWGC).

5. Discussion

5.1. Regional Basement Uplift

Significant Neogene to Recent uplift of the basement along the northern margin of the Algarve Basin has been documented by inspection of the Pliocene marine unconformity [*Feio*, 1951; *Dias and Cabral*, 1997]. Likewise, uplift of the basement at the edge of the southern part of the Algarve Basin (which coincides with the southern limit of SW-Iberia continental crust) is occurring at Present across the Guadalquivir Bank (as discussed above; Figure 7). The uplift of basement at both locations trends WSW-ENE, parallel to the trend of the inherited Mesozoic extensional faults and perpendicular to the dominant direction of present-day convergence between Africa and Eurasia [*Olaiz et al*., 2009; *Pérez-Peña et al*., 2010; *Muñoz-Martín et al*., 2012].

The origin of the basement uplift at these and other locations cannot be identified on seismic or in the field as no major basement thrusts are observed on either. However, there are multiple indications that uplift is being caused by southward verging, deep-rooted blind thrusts. For instance, the uplift observed along the northern margin of the basin is regional, causing an elevated topography to the north. This regional uplift and the southward tilt of Mesozoic units along the basin margin can be consistent with uplift generated by a southward directed contractional structure of crustal scale (along the style of deformation discussed by *Fernández-Lozano* [2012]; between 0 km and 10 km in Figure 11b). This interpretation is also compatible with the interpretation of *Terrinha* [1998] that the tilting at the basin margin is related to broad antiformal folding during the Cenozoic.

Likewise, uplift and tilting of the northern flank of the Guadalquivir Bank extend up to 10 km north of the bank, indicating a deep source for the tilt. Although no thrust responsible for this tilt or uplift has been identified on seismicity, a southward vergent basement involving thrust is the simplest way to account for the gentle northward tilt of beds north of the bank and the steep drop observed to the south. This thrust would be equivalent in nature to that proposed before for the northern outcrop margin of the basin (between 0 km and 10 km in Figure 11b). A southward vergence of thrusting is also supported by the fact that the tilt of the AUGC and Miocene sediments on the southern limb of the bank is much greater than that on the northern limb (Figures 7 and 8). Likewise, Miocene to Recent depositional space (including the space taken by the AUGC, emplaced in the Miocene) south of the bank is considerably greater (2000 m or more).

The northern basin margin and the Guadalquivir Bank are in the order of 100 km apart. Over this distance, the basement must rise from approximately 5 km depth just north of the Guadalquivir Bank to hundreds of meters above sea level along the northern basin margin (Figure 11b). Southward deepening of the basement is consistent with the expected passive margin geometry (deepening oceanward). However, documented Plio-Pleistocene uplift of the basin margin [*Feio*, 1951; *Dias and Cabral*, 1997; *Terrinha*, 1998] along with the geometry of the BFU and overlying Neogene sediments in the offshore indicates that at least part of this difference in depth of the basement is related to Cenozoic deformation. The geometry of the BFU is characterized by deepening southward across relatively rapid steps. At least three of these steps can be identified in outcrop and subsurface.

As has already been discussed, the northernmost step in the BFU occurs across the northern outcrop limit of the basin (Figures 4 and 11). This step in the BFU is related to a relatively narrow southward verging monocline, less than 5 km wide, for which a south directed blind thrust is the most likely culprit.

A similar monocline geometry can be seen locally on some seismic profiles, close the coast. Figure 12, for instance, was shot across one of these monoclines (although incompletely). Basement, which lies at

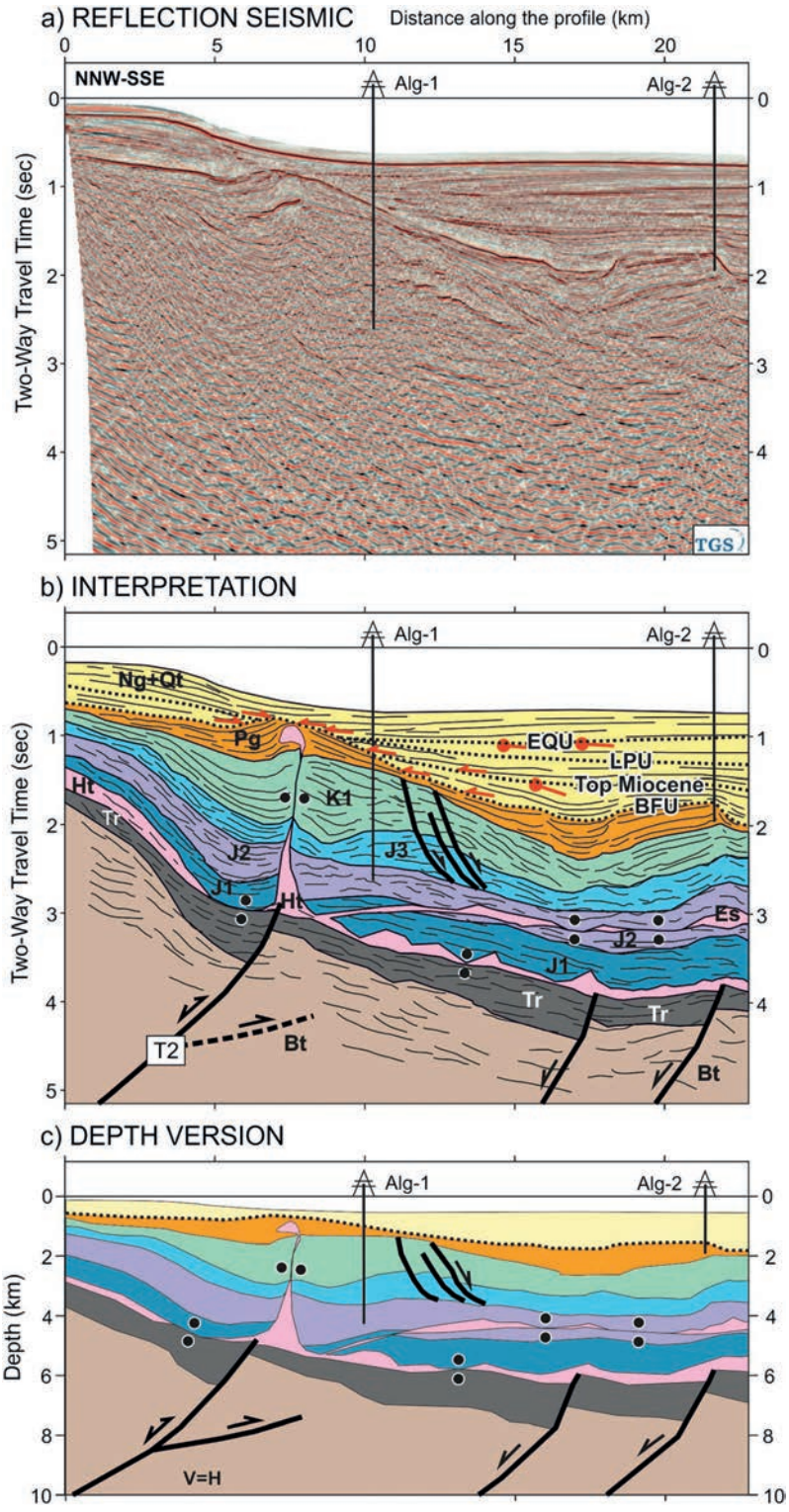

Figure 12. Seismic section across the shelf break in the proximal margin of the Algarve Basin and the underlying thrust T2. (a) Reflection seismic profile. (b) Interpretation of the same seismic profile. (c) Depth version of profile in Figure 12b. Black dashed line: inferred fault. See Figure 3 for the location and Figures 5 and 6 for the legend. Data courtesy of TGS.

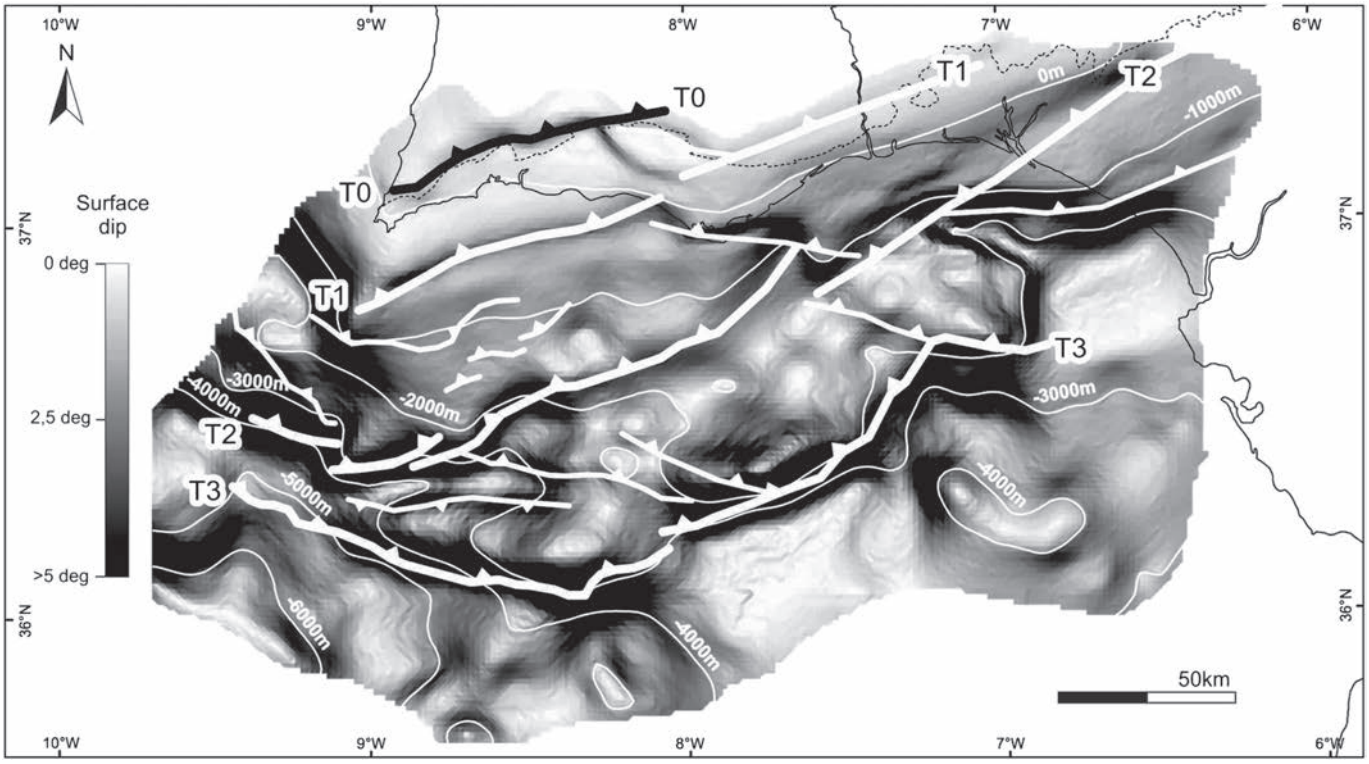

Figure 13. Map of the BFU colored for dip, with white contours indicating depth below sea level. Steeper parts of the surface indicate the steps in the surface, interpreted to be related to erosional geometries or to the presence of underlying basement-involving blind thrusts (traces of the thrust tips shown in white lines).

roughly 7 km in depth on the southern end of the image, rises progressively, in a broad monocline, over a distance of approximately 25 km to a depth of around 4 km (an uplift of roughly 3 km). Part of the change in depth of the basement is linked to extension, as can be seen by the thinning of the Mesozoic from 5 km on the south to less than 3 km in the north. This Mesozoic thinning is interpreted to be linked to the configuration of extensional faults and half-grabens. However, not the entire geometry is Mesozoic in origin; of the 3 km of uplift, only 2 km can be accounted for by Mesozoic extension based on the change of thickness of the Mesozoic. The remaining 1 km of uplift is of post-Paleogene times. In Figure 12, the BFU (or top Paleogene) is seen to rise by approximately 1 km from south to north. This uplift is accompanied by a significant northward onlap of Miocene and Pliocene sediments and overall thinning of the Miocene-Quaternary sediments by nearly 1 km. Furthermore, the present-day shelf break (possibly controlled by contourite currents) is located exactly above the step in the basement and slightly offset relative to the step in the BFU, indicating a possible neotectonic control. All these elements indicate that at least 1 km of uplift is accommodated at this location during the Neogene to Present across a step less than 10 km wide.

The Guadalquivir Bank is the location of the third monoclinal step in the basement and in the BFU (Figures 8 and 11b). The Guadalquivir Bank also has a combined origin for the basement high. On one hand, the entire Mesozoic section is seen to thin southward onto the Guadalquivir Bank (Figure 8), indicating that the Guadalquivir Bank was relative high during this time. Above this, Neogene to Quaternary sediments are seen to also thin onto the bank as well as being uplifted and truncated at the seafloor (Figure 8), related to Cenozoic contraction and uplift.

The geometry in these three well-documented locations (the basin outcrop margin, the northern end of Figure 12, and the Guadalquivir Bank) indicates that the uplift of the basement, related to Cenozoic shortening, occurs at discrete locations, few kilometers across, separated by long intervening segments (tens of kilometers) with relatively constant basement depth. Across these narrow areas both the basement and BFU are uplifted by southward verging monoclinal structures.

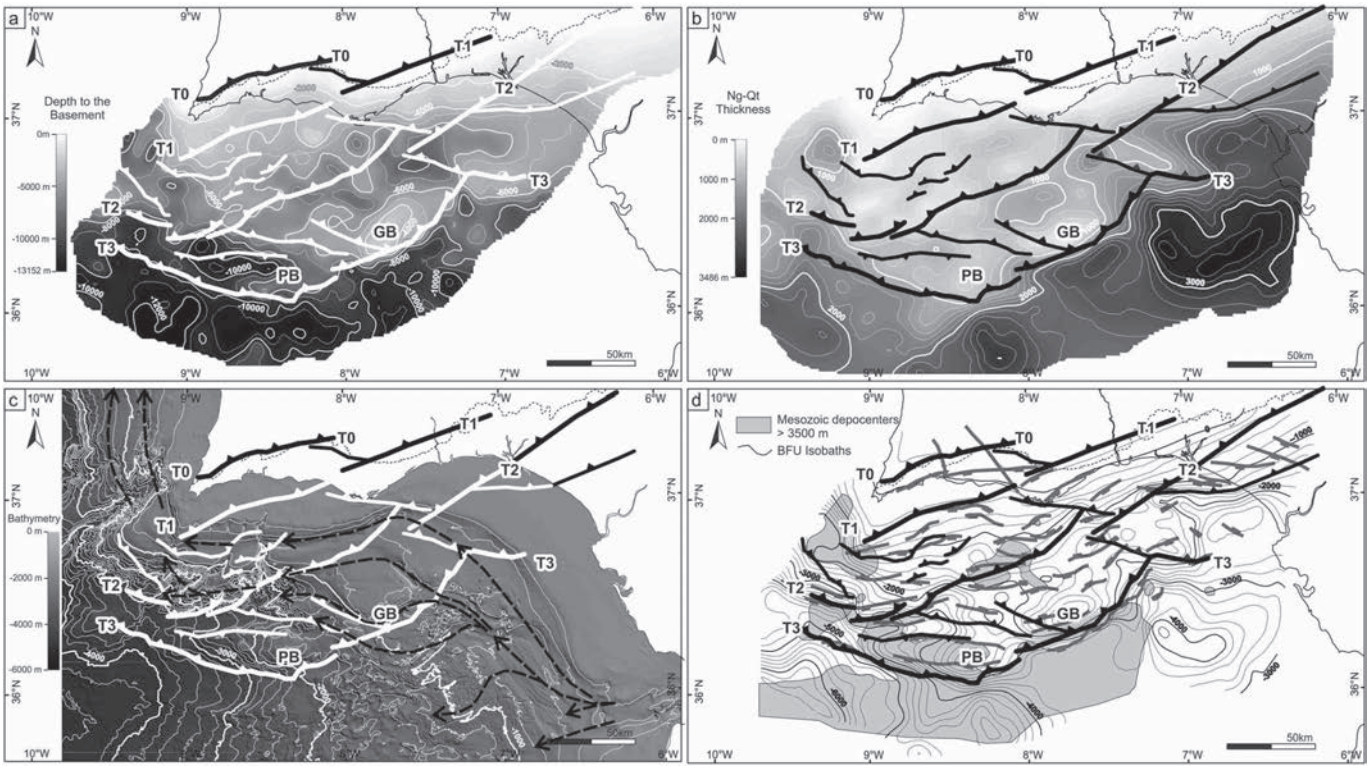

Figure 14. Structural maps of SW Iberian margin. (a) Depth map of the top of basement and location of the main thrust faults responsible for its uplift in Cenozoic times. (b) True vertical thickness (TVT) of the Neogene/Quaternary succession and location of basement thrusts. Note the impact of thrusts on the location of post-Oligocene depocenters. (c) Seabed bathymetry and location of basement thrusts. The black dashed arrows indicate the MOW currents taken from *Hernández-Molina et al*. [2016]. Note the control exerted locally by thrusts T2, T3, and their lateral ramps on the trajectories of the MOW currents. (d) Depth map of the BFU and basement thrust traces, with an overlay of Mesozoic age extensional faults in grey and Mesozoic depocenters greater than 3500 m thick in grey shade. See discussion in text.

The timing of the BFU relative to the basement uplift structures mentioned above makes the BFU an ideal surface to discriminate structures that have uplifted due to basement uplift in the Cenozoic. Note, for instance, that a major step in the basement seen south of the Ruivo well (Figure 11b) that is interpreted to respond to a major Mesozoic extensional fault has no major impact on the BFU geometry, whereas other major steps such as that south of the Portimão Bank (Figure 11d) does coincide with a step in the BFU, indicating a post-Mesozoic uplift.

To correlate the steps in basement at the scale of the basin, the BFU surface has been mapped in 3-D (Figure 13). This map shows a number of WSW-ENE trending steps, which, in combination with the available seismic and outcrop data, have been used to define four main steps in the regional elevation of the BFU and of the basement (Figure 14a) related to Cenozoic to recent shortening. Uplift along the Guadalquivir Bank and the onshore northern limit of the basin are interpreted to be related to underlying south verging basement-involving thrusts. These two fault structures, labeled T0 and T3 in Figures 11 and 13, bound the domain of contractional structures documented in this paper. In between these two structures two other main steps can be identified. One is the monocline in Figure 10, labeled T2. The fourth structure is T1 (Figures 11b and 11d). Toward the west T1 corresponds to the Carcavai fault zone, an ENE-WSW compressional fault [e.g., *Carvalho et al*., 2012].

The four main thrusts identified in the Algarve Basin locally deviate from their dominant WSW-ENE trend, forming a set of oblique ramps of the thrust system with NW-SE orientation (Figure 13). One of the most prominent of these is that formed onshore, where the northern thrust (T0) merges with thrust T1 (Figure 13). This oblique ramp is responsible for the jog in the map expression of the northern outcrop margin of the basin. Other oblique ramps are also visible between T2 and T3, at the western end of the Guadalquivir

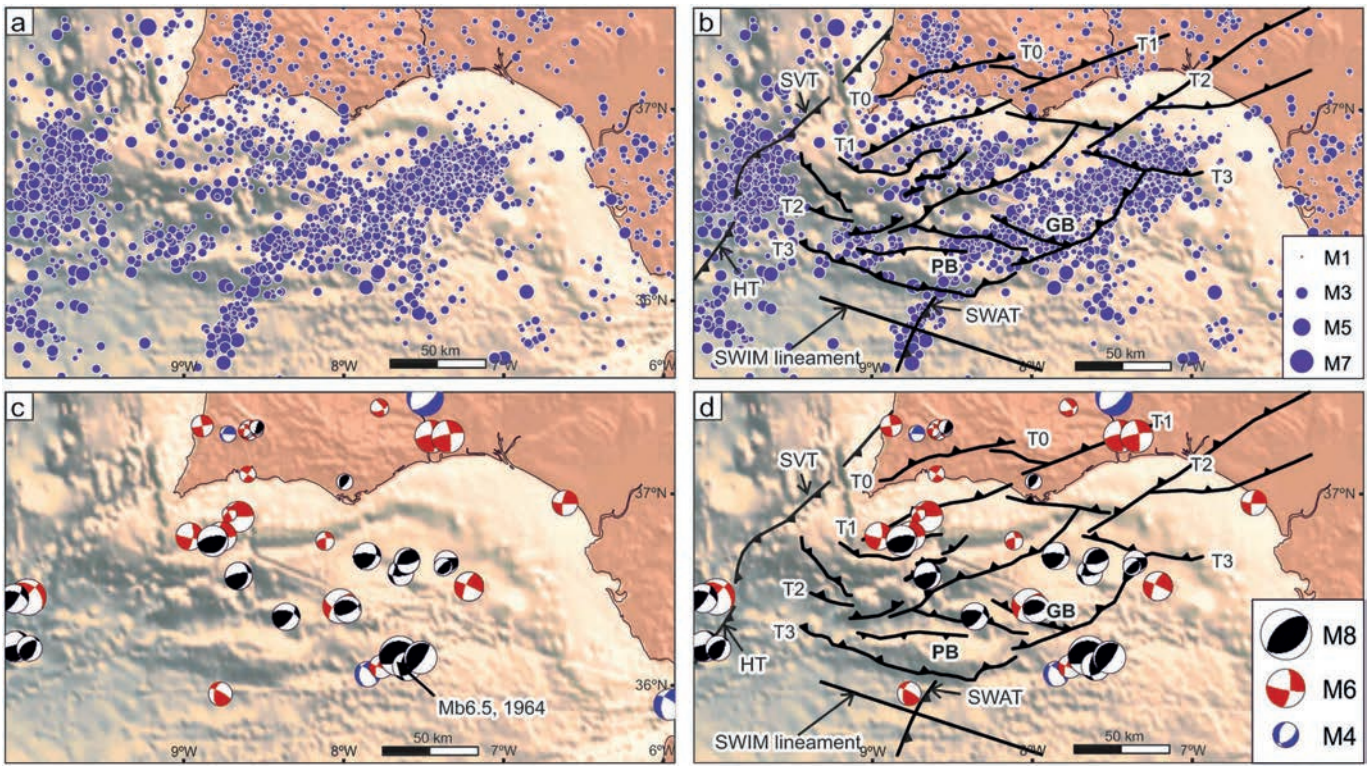

Figure 15. (a) Earthquake epicenters in SW Iberia, sized as a function of magnitude (modified after *Palano et al.* [2013]). The earthquakes were recorded between 1951 and 2010, with magnitudes between 2.0 and 8.0 down to ~30 km depth. (b) Location of the earthquake epicenters relative to the thrusts described in this paper. (c) Lower hemisphere, equal area projection for fault-plane solutions, complied from several earthquakes: red for strike-slip faulting, black for thrust faulting, and blue for normal faulting, modified after *Palano et al.* [2013]. (d) Location of the focal mechanisms relative to the thrust faults described in the paper. GB: Guadalquivir Bank, PB: Portimão Bank, HT: Horseshoe Thrust, SVT: São Vicente Thrust, SWAT: Southwest Algarve Thrust.

Bank (Figure 13). The western margin of the Algarve Basin is also characterized by a swing in the strike of basement thrusts to a NW-SE strike (Figure 13).

Thrust T2 runs south of the present-day southern Portuguese coastline and parallel to it east of Faro. T1 also runs roughly parallel to the coast east of Faro up to the Spanish border (in the order of 50 km) and accounts for the basement uplift that brings the outcrop margin of the basin some 20 km south in the eastern Algarve. At least in this eastern sector, it appears that both T1 and T2 probably exert a control on the present-day coastline.

In the offshore, thrusts T1, T2, and T3 also exert a control on the Neogene-Quaternary depocenters (Figure 14 b) and the present-day bathymetry and contouritic moats (Figures 7, 8, and 14c). Whereas the correlation between individual thrusts and Neogene-Quaternary depocenters or bathymetry is not one to one, it is evident that thrusts T2 and T3 exert a strong control on the thickness of Neogene-Quaternary sediments (Figure 14b) and bathymetry locally follows the trend of the main thrusts (particularly T3 and the western part of T2; Figure 14c). The oblique structures linking the main thrusts also have a marked impact on the trace of the basement outcrop (as discussed above) and in controlling some Neogene-Quaternary depocenters (for structures linking T3 and T2) and bathymetry in the central part of the basin and along its western limit.

5.2. Neotectonics

The system of basement-involving thrusts (T0 through T3 and oblique branches) identified in this study are observed to locally control the present-day bathymetry and contourite currents of the MOW (Figure 14c). This correlation may indicate neotectonic activity of these thrusts, but it could also result from present-day currents and seabed adapting to an inherited (pre-Quaternary) bathymetry (Figure 14). However, when overlying the map of thrusts identified in this study on maps of instrumental seismicity [*Ribeiro et al.*, 1996;

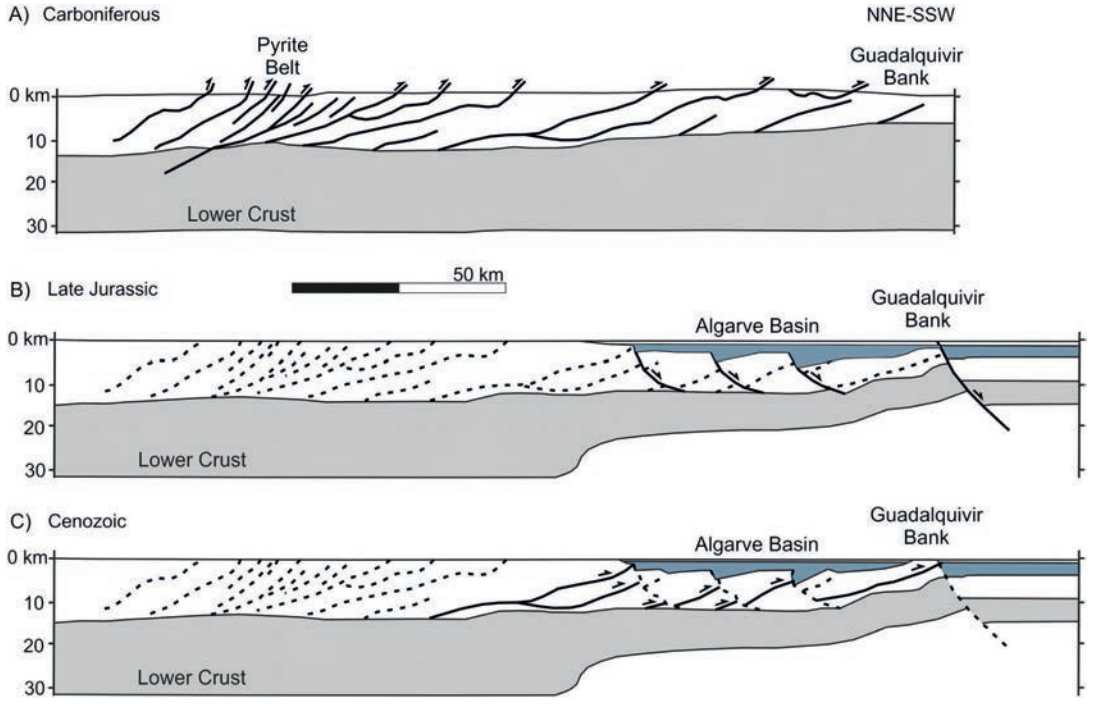

Figure 16. Synthetic crustal cross section of the SW Iberian Margin at key time steps. (a) At the end of Variscan thrusting (Carboniferous). (b) At the end of Jurassic extension. (c) During Cenozoic thrusting. The black lines show the faults active at each time step. The dashed black lines show the inactive faults. Modified after *Vegas et al.* [2004].

Pedrera et al., 2011], it can be seen that the main cluster of seismic events in the Gulf of Cadiz sits immediately north of the Guadalquivir and Portimão Banks and associated thrust T3 (Figure 15b). This thrust is the one that has the strongest imprint on bathymetry, hence indicating that bathymetric expression of the thrusts can be related to neotectonic activity. Furthermore, thrusting on T3 is supported by the fact that focal mechanisms estimated in this area are compatible with an E-W to WSW-ENE trending thrust (Figures 15c and 15d) and the location of the epicenters is consistent with a northward dipping T3, as surface dipping to the north mapped from epicenters by *Palano et al.* [2016]. A similar relationship can be observed between minor clusters further north and the T2 thrust and for the minor oblique thrusts between T2 and T1 (Figure 15b). The fact that the other focal mechanisms derived for the Algarve Basin indicate strike slip along N-S and E-W conjugates or NW-SE and NE-SW conjugates (Figure 15d) is taken to respond to the presence of NW-SE to N-S trending tear faults and lateral ramps in the main thrust system defined by T0–T3 (Figure 13). The intermediate depth of these earthquakes [*Palano et al.*, 2013], ranging from crust to mantle, supports the idea that these events are linked to basement or crustal faults. We therefore consider that the basement thrust system described in this paper and their associated structures (tear faults and lateral ramps) are the most likely culprits for the seismic activity recorded in the Algarve Basin.

The two other evident clusters of seismic activity that can be seen in the vicinity of the Algarve Basin lie in the area of the Horseshoe, Marquês de Pombal, and São Vicente Thrusts to the west (Figures 15a and 15b) and south of the Portimão Bank and the T3 Thrust. The cluster south of the Portimão Bank runs along a NE-SW trend that cannot be correlated to any known structure (Figures 15a and 15b) but is parallel to the thrusts further west (Gorringe, Horseshoe, Marquês de Pombal, and São Vicente) and is therefore interpreted to be associated to a structure not yet identified on seismic and proposed here as the Southwest Algarve Thrust (Figure 15b). This structure has not been documented on seismic as it lies under the AWGC and poor seismic image precludes its identification.

The generalized absence of seismic activity to the south of the Algarve Basin, in the domain nowadays covered by the AUGC and AWGC (Figure 16), coincides with the area that could potentially be interpreted to be oceanic crust [*Sallarès et al.*, 2011; *Martínez-Loriente et al.*, 2014] and indicates that deformation

within the AUGC and the AWGC is reduced at present, or nonseismic and shallow and dominated by deformation related to shale and evaporite mobility [*Medialdea et al*., 2004].

5.3. Timing

The tectono-sedimentary relationships observed so far in the Algarve Basin are consistent with two main broad stages of basin evolution: one lasting from Triassic to Early Cretaceous dominated by extensional tectonics and one lasting from possibly Late Cretaceous, and certainly from Oligocene, to Present dominated by compressional tectonics. These two stages are in turn coherent in the framework of Mesozoic opening of the Tethys and Atlantic Oceans and the mainly Cenozoic convergence between Africa and Eurasia [*Schettino and Turco*, 2011].

As discussed above, multiple unconformities in the Miocene to Recent sediments in the Algarve Basin record the contractional deformation of the offshore structures (e.g., Figure 6) [*Hernández-Molina et al*., 2016]. The oldest Cenozoic contractional deformation is that related to the reactivation of salt walls documented in the Esperança Salt area of Paleogene age (Figure 5). A similar magnitude of Paleogene deformation has not been recognized for other structures in the area with the available data. Nonetheless, the Paleogene is observed to thin (depositionally) onto some of the offshore thrusts (for instance, onto the monocline related to T2; on the northern end of Figure 10), indicating that basement uplift might have started as early as Paleogene. Thrusting on T2 and tilting and folding north of the Esperança Salt in the Paleogene could tentatively be the source of the shortening absorbed by the salt walls on the Esperança Salt.

The Paleogene is also observed to thin or be absent over the other two basement thrusts in the offshore (as occurs above the Guadalquivir Bank in Figure 8 or above all the thrusts in Figures 11b and 11d). However, in some cases this thinning or absence of the Paleogene can be interpreted to be either depositional (recording Paleogene age uplift) or erosional (implying late Paleogene or early Miocene uplift prior to incision by the BFU). In many cases, the case for late Paleogene or early Miocene pre-BFU uplift and truncation of the Paleogene or even Cretaceous is evident (Figure 8).

For the remainder of the Neogene to Quaternary two main stages of deformation are observed in the area. For one, emplacement of the AWGC and AUGC in the area is of middle to late Miocene age. Sediments that seal movement of these units are later folded in late Pliocene times and onlapped by latest Pliocene and Quaternary sediments (consistent with the tectonic control on contourite deposits proposed by *Hernández-Molina et al*. [2016]). More recent deformation has not been documented based on seismic interpretation, but evidence of neotectonic activity discussed above indicates that one final stage of deformation is currently active.

The stages of deformation documented in the offshore Algarve Basin are consistent with those defined by other authors in the area [*Terrinha*, 1998; *Roque*, 2007] who interpret four main stages of contractional deformation: (1) Late Cretaceous to Paleogene, (2) late Oligocene, (3) middle to late Miocene, and (4) late Pliocene to Present.

5.4. Tectonic Inheritance and Basin Inversion of the Algarve Basin

Extension during the Mesozoic in southern Iberia led to the development of E-W to WSW-ENE trending extensional faults [*Terrinha*, 1998; *Vera*, 1998; *Martínez del Olmo*, 2002; *Ramos et al*., 2016] that controlled Triassic-Jurassic depocenters (units synchronous with the main stage of extension). This trend is strongly coincident with the strike of Cenozoic contractional structures (thrusts and monoclines of the BFU) and roughly perpendicular to present-day maximum shortening directions [*Olaiz et al*., 2009; *Pérez-Peña et al*., 2010; *Muñoz-Martín et al*., 2012]. The strike of the extensional faults, perpendicular to shortening, coupled with the fact that some faults are interpreted to have had low angle of dip prior to Cenozoic shortening (e.g., faults south of the Guadalquivir Bank; Figure 7), makes them good candidates for reactivation [*Letouzey*, 1990]. However, there appears to be no direct correlation between inversion and preexisting extensional structures (Figure 14d). Only the Portimão Bank has been documented as an inverted half-graben (Figure 10) [*Terrinha et al*., 2009]. For the rest, onshore extensional faults have been observed to accommodate buttressing but no fault reactivation [*Ramos et al*., 2016]. And in the offshore the only contractional structure that coincides with a major basin-bounding extensional fault is thrust T3, whose trace coincides with the northern limit of a major Mesozoic depocenter. However, as opposed to reactivating the fault responsible for the depocenter, thrust T3 dips in the opposite direction and causes inversion by steepening the extensional fault.

This opposing dip of Cenozoic thrusts and Mesozoic extensional faults is one of the most peculiar aspects of the inversion experienced by the Algarve Basin. Throughout the basin, thrusts are north dipping (south directed), while the extensional faults are dominantly south dipping (Figures 5, 9, 11, and 14). This style has already been documented at outcrop scale in the Algibre Thrust by *Ramos et al*. [2016]. Also, in a context equivalent to the offshore Algarve Basin, inversion in the NW Iberian passive margin shows similar contractional structures, where major extensional faults are inverted by a thrust fault with opposing dip [*Tugend et al*., 2014].

A possible origin for this anomalous inversion style in the SW Iberian margin is the impact of basement fabrics on structural development. SW Iberia was located in the foreland fold-and-thrust belt of the Variscan orogen. Basement in the area is dominated by strongly deformed Carboniferous flysch sediments affected by northward dipping, southward directed thrusts and by regional cleavage dipping to the N/NE (Figure 16a) [*Vegas*, 1980; *Soriano*, 1996; *Díaz Azpiazu et al*., 2004; *Marques et al*., 2010; *Pereira et al*., 2012]. During Mesozoic extension, initial extension (in the Triassic) probably reactivated this fabric leading to small-displacement, northward dipping normal faults with relatively shallow detachments [*Terrinha*, 1998; *Ramos et al*., 2016]. As extension progressed, southward dipping regional-scale faults became more efficient at accommodating increasing extension, leading to the regional pattern of WSW-ENE striking, southward dipping faults (Figure 1 b). Finally, basin inversion during the Cenozoic led to the reactivation of the low-angle thrusts and cleavage within the Carboniferous and deeper units (now near midcrustal depths; Figure 16c).

A similar style of inversion has been documented in the Moroccan Atlas. *Teixell et al*. [2003] and *Domènech* [2015] have documented multiple examples where thrusts steepen or crosscut preexisting extensional faults dipping in the opposite direction. The result is geometries very similar to those observed in the Algarve Basin (Figure 17a). *Teixell et al*. [2003] and *Domènech* [2015] have not proposed a cause for this style of inversion, but a similar basement and the location of the High Atlas in a context similar to the Algarve with respect to the Variscan orogen (southern foreland [*Simancas et al*., 2005]) provide support to the analogy in the deformation style.

Carrera and Muñoz [2013] also describe a similar example of tectonic inversion in the Cordillera Oriental of the Argentine Andes. There, the basement fabrics in the Precambrian sedimentary rocks caused the Andean contractional structures to develop differently from the Cretaceous extensional system.

5.5. Thick-Skinned Cenozoic Deformation in the Iberian Plate

The tectonic style of broad basement uplifts described in this paper for the Algarve Basin is not unique in the Iberian plate. The mountain ranges found in the interior of the Iberian plate (Figure 1b) are also characterized by thick-skinned contractional features.

These mountain ranges also display structures that in detail are analogous to those described in the Algarve Basin. For instance, in the eastern Guadalquivir Basin, immediately south of the eastern termination of the Sierra Morena, *Pedrera et al*. [2013] describe NE-SW trending monoclines deforming the overlying Jurassic in a manner very similar to the stair-stepped geometry seen in the Algarve Basin, also of late Miocene age (Figure 17b).

The southern border thrust of the eastern segment of the Spanish Central System is also similar to the Algarve structures. It is a blind thrust and is expressed at surface by a large NE-SW fold propagation fault (Figure 17c) [*De Vicente et al*., 2007]. The basement in the hanging wall of this thrust (of granitic composition) is cut by two north directed back thrusts (Figure 17c) [*De Vicente et al*., 2007], as occurs in the Guadalquivir Bank (Figures 7 and 8). Along the northern margin of the chain, the subhorizontal schistosity of the Variscan basement (metasediments) favors the formation of thrusts that generate a sequence of monoclines and tight anticlines with barely any fault displacement in the sedimentary cover similar to the nature of thrusts T0 to T3 (Figure 17d) [*De Vicente et al*., 2007]. The difference in tectonic styles between north and south resides in the different basement lithology [*De Vicente and Muñoz-Martín*, 2013].

5.6. Shortening Estimates and Correlation to Other Structures

Shortening is accommodated in the SW Iberian margin by thrusts or zones of distributed basement shearing. The uplift caused by these structures can range from 1 km (e.g., monoclines in Figure 11) to 3 km (Guadalquivir Bank in Figure 8). At the highest spot of the Guadalquivir Bank, at its western end, the uplift caused by thrusting has been estimated to be in excess of 5 km, probably related to the intersection of a

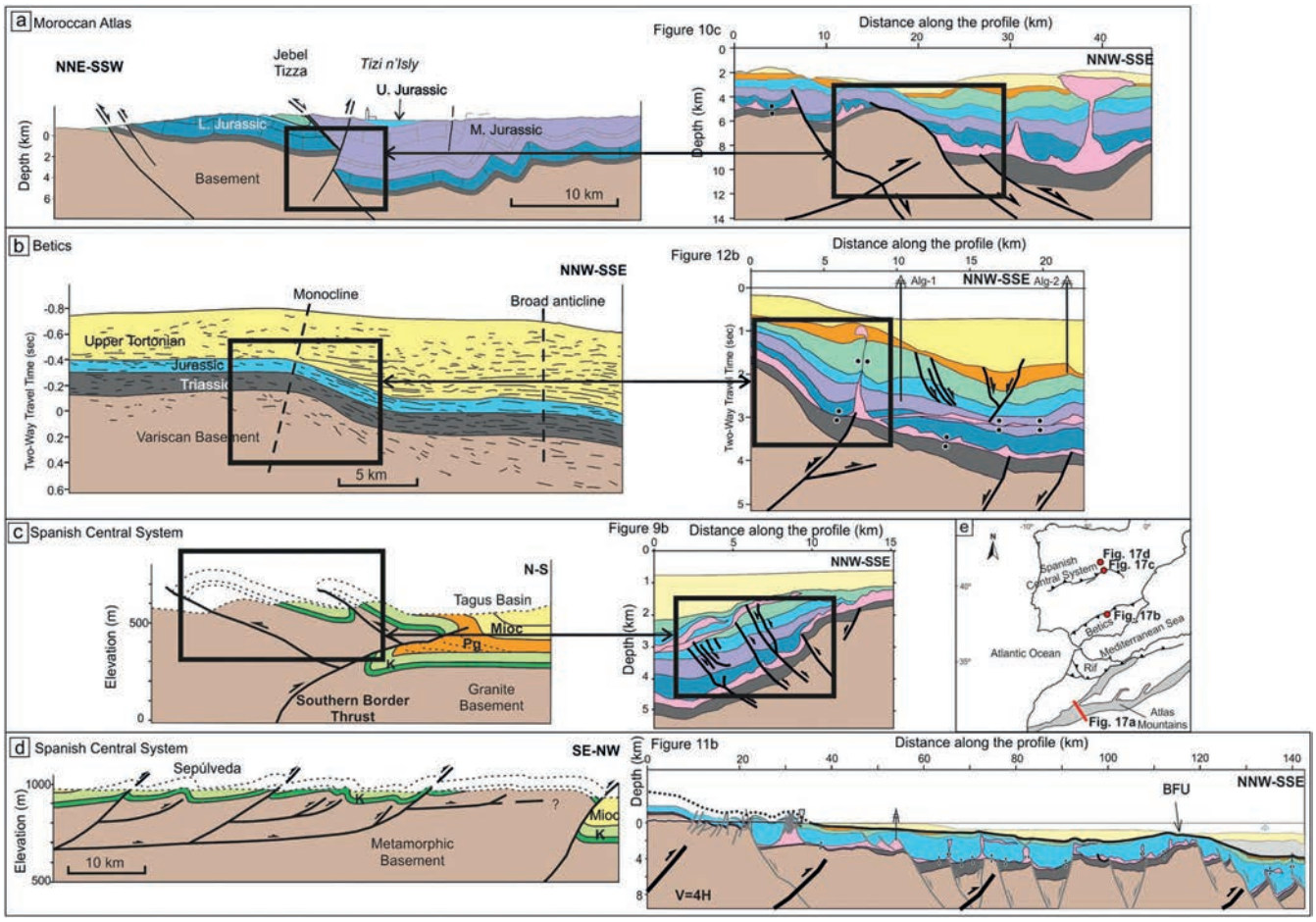

Figure 17. Analogue examples for the basement-involved tectonic style in SW Iberia. (a) Cross section through the high Atlas of Morocco, modified after *Teixell et al.* [2003], and the Portimão Bank (Figure 9). (b) South directed monocline in the Betics, modified after *Pedrera et al.* [2013], and the monocline above T2 (Figure 12). (c) Simplified cross section of the Tortuero back thrusting system and the back thrusts on the Guadalquivir Bank (Figure 9). (d) Sepúlveda imbricate thrust system (Mioc: Miocene, K: Cretaceous) and section across the Algarve Basin (Figure 11b). Both sections are vertically exaggerated. (Figures 17c and 17d) The examples are cross sections across the Spanish Central System, modified after *De Vicente et al.* [2007]. (e) Small inset location map for the sections presented in this figure. L., M., and U. Jurassic: Lower, Middle, and Upper Jurassic respectively; Mioc: Miocene; Pg: Paleogene.

frontal and lateral ramp of thrust T3 (Figure 13). The horizontal shortening required to generate these magnitudes of uplift is difficult to estimate and depends greatly on the estimates of depth to detachment. Restoration of some key profiles (e.g., Figure 8) and estimates of the unfolded (or untilted) length of the preinversion units allow us to estimate a horizontal shortening for the entire margin of roughly 5–10 km. This represents a shortening of less than 10% of the entire SW Iberian margin in the Algarve Basin, which is roughly 150 km wide at present day [e.g., *Terrinha*, 1998].

The amount of shortening estimated for the Algarve Basin can therefore be considered to be consistent with the approximately 20 km of NW-SE shortening estimated for the Gorringe Bank (the main contractional structure west of the Algarve Basin on the Nubia-Iberia boundary) [*Galindo-Zaldívar*, 2003; *Jiménez-Munt et al.*, 2010]. The age of deformation for the Gorringe Bank (Oligocene to Miocene; according to *Jiménez-Munt et al.* [2010]) is also broadly consistent with the earliest stages of deformation documented here for the Algarve Basin.

Estimates of basement shortening to the east along the Nubia-Iberia boundary are hindered by the presence of the allochthonous units of the Betic-Rif orogen that mask the basement structure. Furthermore, the presence of subduction processes east of the Gibraltar Arc [*Pedrera et al.*, 2011; *Vergés and Fernàndez*, 2012]

implies that the magnitude of Africa-Eurasia convergence is greater eastward and that it is absorbed by other mechanisms not seen west of the Gibraltar Arc. Nonetheless, Neogene deformation under the Guadalquivir foreland basin such as that documented by *Pedrera et al*. [2013] or the structures responsible for the uplift of the Sierra Morena [*Stapel*, 1999] are the likely continuation of the Cenozoic thrusts described in the Algarve Basin. In particular, T2 and T1 can be correlated to the east with the southern limit of the Sierra Morena (Figure 1b). The Sierra Morena is a currently tectonically active mountain chain [*Herraiz et al*., 1996; *Stich et al*., 2006] and has also recorded significant uplift during the Neogene [*Stapel*, 1999]. Its southern margin is defined by a very sharp lineament (easily seen on satellite imagery and topography) that runs from the northern coast of the Gulf of Cadiz for over 200 km to the ENE (Figure 1b). This orientation crosscuts the Variscan structural trend (WNW-ESE in the Sierra Morena) and is perpendicular to the present-day maximum horizontal stress [*Cloetingh and Burov*, 1996], which supports the interpretation of the Sierra Morena range as an upper crust antiform associated to the presence of a south directed crustal-scale blind thrust [*De Vicente et al*., 2007].

5.7. Alternative Interpretations for Basement Deformation

Two alternatives have been contemplated for interpreting the source of basement deformation in the Algarve Basin. One is the possible origin of some of the basement structures (in particular the Guadalquivir Bank) as a westward propagating Subduction-Transform Edge Propagator (STEP) fault [*Govers and Wortel*, 2005]. The presence of a STEP fault along the northern limit of the Alborán block in an early stage of its evolution was proposed by *van Hinsbergen et al*. [2014]. Whereas the Guadalquivir Bank is indeed in a position that could be consistent for a STEP fault ahead of the propagating Gibraltar Arc subduction zone, such an interpretation would not account for the origin of the other basement structures observed in the basin. Furthermore, STEP faults are expected to lead dominantly to subsidence, not uplift as is observed in the Guadalquivir Bank. Neither could a STEP fault account for uplift as early as Oligocene (when the Gibraltar subduction zone was much further east [*Vergés and Fernàndez*, 2012]) nor is it compatible with the lack of evidence of slab tear along strike of the Guadalquivir Bank under the Betics [*Vergés and Fernàndez*, 2012].

The second alternative interpretation for basement deformation is strike-slip dominated deformation, in line with observations of strike-slip features in the area [*Zitellini et al*., 2009; *Carvalho et al*., 2012]. Once again, this possibility would be at odds with the dominant deformation mechanism observed for Cenozoic deformation in the Iberian plate. Furthermore, the main structures generating basement uplift in the Algarve Basin are mostly perpendicular to the maximum horizontal stress [*Olaiz et al*., 2009; *Muñoz-Martín et al*., 2012] and the recent convergence between Africa and Eurasia [*Rosenbaum et al*., 2002], making contractional structures the most likely elements driving deformation in the area. Extensional faulting of Cenozoic age in this area is limited to areas of mobile substrate (shale or evaporites [e.g., *Medialdea et al*., 2004; *Matias et al*., 2011]) and is therefore inferred to be related to shallow causes and not basement deformation.

5.8. Implications for Initial Stages of Passive Margin Inversion

Just as the inheritance of basement fabric appears to have had a strong control on inversion, crustal-scale structure may also have played a role in the localization of inversion structures. Some of the locations of major basement uplift documented in this margin coincide with the extensional faults with the largest throws (for instance T3 in Figure 11b or T2 in Figure 11d). Crustal-scale control on inversion is also observed in the western and northern Iberian margin. In the western Iberian margin *Peron-Pinvidic et al*. [2008] interpret that inversion locates only above continental mantle exhumed during extension. In northern Iberia, *Tugend et al*. [2014] suggest that inversion concentrates on thrusts that crosscut basinward dipping, crustal-scale faults in the domains of greatest extension of the margin. However, in both cases, inversion occurs in the most distal domain, similar to that documented by *Mohn et al*. [2012]. In the case of SW Iberia, however, crustal heterogeneities could be responsible for inversion across the necking domain of the rifted margin.

Finally, shortening is also observed in the shallowest units of the Algarve Basin. Contraction within the Mesozoic stratigraphy is driven by shortening at crustal scale, but its tectonic style and the wavelength of its structures are controlled by the Triassic evaporites acting as a detachment.

The result is a system in which deformation is partitioned and localized by the presence of heterogeneities within the rifted structure of the margin, the prerift basement, and the synrift stratigraphy.

6. Conclusions

The convergence of Africa and Eurasia during the Cenozoic has led to the formation of a system of roughly E-W to NE-SW regional-scale thrusts that extend from the Gorringe Bank in the west to the Betic orogen in the east (the Guadalquivir Basin and Sierra Morena). Four main, south verging thrusts, spaced at 20–50 km, have been identified in this system. Each thrust is associated to a southward dipping monocline, and they are interpreted to be deeply rooted in the basement and reactivate inherited Paleozoic northward dipping fabric (cleavage and thrusts). Extensional faults related to Mesozoic rifting are in most cases folded and steepened by these thick-skinned thrusts, leading to an inverted margin in which extensional faults have not been reactivated. Deformation in Mesozoic and Cenozoic strata is accommodated by buttressing, minor thrusting, and reactivation of diapirs.

At least four main stages of shortening have been documented for the thrusts and associated structures inverting the SW Iberian margin: Late Cretaceous to early Paleogene, late Paleogene to early Miocene, middle to late Miocene, and late Pliocene to present day. The present-day kinematics of these thrusts is compatible with the main compressive direction calculated from earthquake mechanisms and from GPS plate kinematics. These thrusts are considered to be responsible for the present-day seismic activity observed in SW Iberia.

Acknowledgments

This study was funded by Repsol Exploración (Madrid) and partially financially supported by the SALTECRES project (CGL2014-54118-C2-1-R MINECO/FEDER, UE). Adrià Ramos thanks Repsol Exploración for his Ph.D grant. The authors wish to thank Álvaro Arnaiz and Repsol Portugal Exploration Team for their support and enthusiasm. The authors also wish to thank S. Martínez-Loriente, M.A. Gutscher, and a third anonymous reviewer for their in-depth reviews and discussion that have greatly helped us to improve this paper. We also acknowledge Schlumberger and Midland Valley for the academic software licenses used for seismic interpretation and cross-section construction, respectively. Repsol and Partex-Oil&Gas provided us their proprietary vintage seismic surveys and a 3-D seismic cube, published with their permission. Seismic lines of the PDT00-PD00 survey have been provided by TGS and published with the permission of TGS (http://www.tgs.com). The seismic PDT00-PD00 survey is available for purchase from TGS and Entidade Nacional para o Mercado de Combustibles (http://www.enmc.pt).

References

Arsenikos, S., D. Frizon de Lamotte, N. Chamot-Rooke, G. Mohn, M.-C. Bonneau, and C. Blanpied (2013), Mechanism and timing of tectonic inversion in Cyrenaica (Libya): Integration in the geodynamics of the East Mediterranean, *Tectonophysics*, *608*, 319–329, doi:10.1016/j.tecto.2013.09.025.

Boldreel, L. O., and M. S. Andersen (1993), Late Paleocene to Miocene compression in the Faeroe-Rockall area, *Geol. Soc. London, Pet. Geol. Conf. Ser.*, *4*, 1025–1034, doi:10.1144/0041025.

Brune, S., C. Heine, P. D. Clift, and M. Pérez-Gussinyé (2016), Rifted margin architecture and crustal rheology: Reviewing Iberia-Newfoundland, central South Atlantic, and South China Sea, *Mar. Pet. Geol.*, doi:10.1016/j.marpetgeo.2016.10.018.

Carrera, N., and J. A. Muñoz (2013), Thick-skinned tectonic style resulting from the inversion of previous structures in the southern Cordillera Oriental (NW Argentine Andes), *Geol. Soc. London, Spec. Publ.*, *377*(1), 77–100, doi:10.1144/SP377.2.

Carrilho, F., P. Teves-Costa, I. Morais, J. Pagarete, and R. Dias (2004), GEOALGAR project: First results on seismicity and fault-plane solutions, *Pure Appl. Geophys.*, *161*(3), 589–606, doi:10.1007/s00024-003-02464-3.

Carvalho, J., H. Matias, T. Rabeh, P. T. L. Menezes, V. C. F. Barbosa, R. Dias, and F. Carrilho (2012), Connecting onshore structures in the Algarve with the southern Portuguese continental margin: The Carcavai fault zone, *Tectonophysics*, *570–571*, 151–162, doi:10.1016/j.tecto.2012.08.011.

Cloetingh, S., and E. B. Burov (1996), Thermomechanical structure of European continental lithosphere: Constraints from rheological profiles and EET estimates, *Geophys. J. Int.*, *124*(3), 695–723, doi:10.1111/j.1365-246X.1996.tb05633.x.

Cobbold, P. R., K. E. Meisling, and V. S. Mount (2001), Reactivation of an obliquely rifted margin, Campos and Santos Basins, southeastern Brazil, *AAPG Bull.*, *85*(11), 1925–1944.

Custódio, S., N. A. Dias, F. Carrilho, E. Góngora, I. Rio, C. Marreiros, I. Morais, P. Alves, and L. Matias (2015), Earthquakes in western Iberia: Improving the understanding of lithospheric deformation in a slowly deforming region, *Geophys. J. Int.*, *203*(1), 127–145, doi:10.1093/gji/ggv285.

Custódio, S., G. Silveira, L. Matias, I. Mata, C. Matos, J. M. Palma-Oliveira, F. Rocha, and F. C. Lopes (2016), Educating for earthquake science and risk in a tectonically slowly deforming region, *Seismol. Res. Lett.*, *87*(3), 773–782, doi:10.1785/0220150239.

De Vicente, G., and A. Muñoz-Martín (2013), The Madrid Basin and the Central System: A tectonostratigraphic analysis from 2D seismic lines, *Tectonophysics*, *602*, 259–285, doi:10.1016/j.tecto.2012.04.003.

De Vicente, G., and R. Vegas (2009), Large-scale distributed deformation controlled topography along the western Africa–Eurasia limit: Tectonic constraints, *Tectonophysics*, *474*(1–2), 124–143, doi:10.1016/j.tecto.2008.11.026.

De Vicente, G., et al. (2004), Evolución geodinámica y cenozoica de la placa ibérica y su registro en el antepaís, in *Geología de España*, edited by J. A. Vera, pp. 597–602, SGE-IGME, Madrid.

De Vicente, G., R. Vegas, A. Muñoz-Martín, P. Silva, P. Andriessen, S. Cloetingh, J. Gonzalezcasado, J. Vanwees, J. Alvarez, and A. Carbo (2007), Cenozoic thick-skinned deformation and topography evolution of the Spanish Central System, *Global Planet. Change*, *58*(1–4), 335–381, doi:10.1016/j.gloplacha.2006.11.042.

DeMets, C., R. G. Gordon, and D. F. Argus (2010), Geologically current plate motions, *Geophys. J. Int.*, *181*(1), 1–80, doi:10.1111/j.1365-246X.2009.04491.x.

Dercourt, J., et al. (1986), Geological evolution of the Tethys belt from the Atlantic to the Pamirs since the LIAS, *Tectonophysics*, *123*(1–4), 241–315, doi:10.1016/0040-1951(86)90199-X.

Dewey, J. F., W. C. Pitman, W. B. Ryan, and J. Bonnin (1973), Plate tectonics and the evolution of the Alpine system, *Geol. Soc. Am. Bull.*, *84*(10), 3137–3180.

Dewey, J. F., M. L. Helman, S. D. Knott, E. Turco, and D. H. W. Hutton (1989), Kinematics of the western Mediterranean, *Geol. Soc. London, Spec. Publ.*, *45*(1), 265–283, doi:10.1144/GSL.SP.1989.045.01.15.

Dias, R., and J. Cabral (1997), Neotectonic crustal vertical movements in Algarve (southern Portugal) 3a Conf. Anu. Grupo Geol. Estrutural E Tectónica Soc Geol Port. Livro Resumos.

Díaz Azpiazu, M., A. Castro, C. Fernández, S. López, J. C. Fernández Caliani, and I. Moreno-Ventas (2004), The contact between the Ossa Morena and the South Portuguese zones: Characteristics and significance of the Aracena metamorphic belt, in its central sector between Aroche and Aracena (Huelva), *J. Iber. Geol.*, *30*, 23–52.

Domènech, M. (2015), Rift opening and inversion in the Marrakech High Atlas: Integrated structural and thermochronologic study, PhD thesis, 157 pp., Universitat Autònoma de Barcelona.

Doré, A. G., E. R. Lundin, N. J. Kusznir, and C. Pascal (2008), Potential mechanisms for the genesis of Cenozoic domal structures on the NE Atlantic margin: Pros, cons and some new ideas, *Geol. Soc. London, Spec. Publ.*, *306*(1), 1–26, doi:10.1144/SP306.1.
Druet, M. (2016), Geodinámica del margen continental de Galicia: Estructura profunda y morfotectónica, PhD thesis, 251 pp., Universidad Complutense de Madrid, Madrid.
Duarte, J. C. (2011), Tectonics of the Gulf of Cadiz: The role of the Gibraltar Arc in the reactivation of the SW Iberia Margin, PhD thesis, 304 pp., Universidade de Lisboa.
Duarte, J. C., V. Valadares, P. Terrinha, F. Rosas, N. Zitellini, and E. Gràcia (2009), Anatomy and tectonic significance of WNW-ESE and NE-SW lineaments at a transpressive plate boundary (Nubia-Iberia), *Trab. Geol.*, *29*(29), 237–241.
Duarte, J. C., P. Terrinha, F. M. Rosas, V. Valadares, L. M. Pinheiro, L. Matias, V. Magalhães, and C. Roque (2010), Crescent-shaped morphotectonic features in the Gulf of Cadiz (offshore SW Iberia), *Mar. Geol.*, *271*(3–4), 236–249, doi:10.1016/j.margeo.2010.02.017.
Duarte, J. C., F. M. Rosas, P. Terrinha, W. P. Schellart, D. Boutelier, M.-A. Gutscher, and A. Ribeiro (2013), Are subduction zones invading the Atlantic? Evidence from the southwest Iberia margin, *Geology*, *41*(8), 839–842, doi:10.1130/G34100.1.
Faleide, J. I., F. Tsikalas, A. J. Breivik, R. Mjelde, O. Ritzmann, O. Engen, J. Wilson, and O. Eldholm (2008), Structure and evolution of the continental margin off Norway and the Barents Sea, *Episodes*, *31*(1), 82–91.
Feio, M. (1951), *A Evolução do Relevo do Baixo Alentejo a Algarve*, pp. 303–477, *Corn Serv Geol Port.*, *t.XXXII*, *2a parte*, Lisboa.
Fernández-Lozano, J. (2012), Cenozoic deformation of Iberia: A model for intraplate mountain building and basin development based on analogue modelling, PhD thesis, 173 pp., Utretcht Univ.
Flinch, J. F., and P. R. Vail (1998), Plio-Pleistocene sequence stratigraphy and tectonics of the Gibralter Arc, in *Mesozoic and Cenozoic Sequence Stratigraphy of European Basins*, vol. 60, edited by P. C. de Graciansky et al., pp. 199–208, SEPM Spec. Publ, Tulsa, Okla.
Galindo-Zaldívar, J. (2003), Active faulting in the internal zones of the central Betic Cordilleras (SE, Spain), *J. Geodyn.*, *36*(1–2), 239–250, doi:10.1016/S0264-3707(03)00049-8.
Gardosh, M. A., and Y. Druckman (2006), Seismic stratigraphy, structure and tectonic evolution of the Levantine Basin, offshore Israel, *Geol. Soc. London, Spec. Publ.*, *260*, 201–227, doi:10.1144/GSL.SP.2006.260.01.09.
Gomez, F., W. Beauchamp, and M. Barazangi (2000), Role of the Atlas Mountains (northwest Africa) within the African-Eurasian plate-boundary zone, *Geology*, *28*(9), 775–778, doi:10.1130/0091-7613(2000)28<775:ROTAMN>2.0.CO;2.
Govers, R., and M. J. R. Wortel (2005), Lithosphere tearing at STEP faults: Response to edges of subduction zones, *Earth Planet. Sci. Lett.*, *236*(1–2), 505–523, doi:10.1016/j.epsl.2005.03.022.
Gràcia, E., et al. (2003a), Mapping active faults offshore Portugal (36°N–38°N): Implications for seismic hazard assessment along the southwest Iberian margin, *Geology*, *31*(1), 83–86.
Gràcia, E., J. Dañobeitia, J. Vergés, R. Bartolomé, and D. Córdoba (2003b), Crustal architecture and tectonic evolution of the Gulf of Cadiz (SW Iberian margin) at the convergence of the Eurasian and African plates, *Tectonics*, *22*(4), 1033, doi:10.1029/2001TC901045.
Gutscher, M.-A., J. Malod, J.-P. Rehault, I. Contrucci, F. Klingelhoefer, L. Mendes-Victor, and W. Spakman (2002), Evidence for active subduction beneath Gibraltar, *Geology*, *30*(12), 1071, doi:10.1130/0091-7613(2002)030<1071:EFASBG>2.0.CO;2.
Gutscher, M.-A., S. Dominguez, G. K. Westbrook, and P. Leroy (2009), Deep structure, recent deformation and analog modeling of the Gulf of Cadiz accretionary wedge: Implications for the 1755 Lisbon earthquake, *Tectonophysics*, *475*(1), 85–97, doi:10.1016/j.tecto.2008.11.031.
Handy, M. R., S. M. Schmid, R. Bousquet, E. Kissling, and D. Bernoulli (2010), Reconciling plate-tectonic reconstructions of Alpine Tethys with the geological–geophysical record of spreading and subduction in the Alps, *Earth-Sci. Rev.*, *102*(3–4), 121–158, doi:10.1016/j.earscirev.2010.06.002.
Hernández-Molina, F. J., et al. (2014), Onset of Mediterranean outflow into the North Atlantic, *Science*, *344*(6189), 1244–1250, doi:10.1126/science.1251306.
Hernández-Molina, F. J., et al. (2016), Evolution of the gulf of Cadiz margin and southwest Portugal contourite depositional system: Tectonic, sedimentary and paleoceanographic implications from IODP expedition 339, *Mar. Geol.*, *377*, 7–39, doi:10.1016/j.margeo.2015.09.013.
Herraiz, M., G. de Vicente, R. Lindo, and J. G. Sánchez-Caba~nero (1996), Seismotectonics of the Sierra Albarrana area (southern Spain). Constraints for a regional model of the Sierra Morena-Guadalquivir Basin limit, *Tectonophysics*, *266*(1–4), 425–442, doi:10.1016/S0040-1951(96)00201-6.
Hill, K. A., G. T. Cooper, M. J. Richardson, C. J. Lavin, K. A. Hill, G. T. Cooper, M. J. Richardson, and C. J. Lavin (1994), Structural framework of the eastern Otway Basin: Inversion and interaction between two major structural provinces, structural framework of the eastern Otway Basin, *Explor. Geophys. Explor. Geophys.*, *25*(2), 79–87, doi:10.1071/EG994079.
Indrevær, K., R. H. Gabrielsen, and J. I. Faleide (2016), Early Cretaceous synrift uplift and tectonic inversion in the Loppa High area, southwestern Barents Sea, Norwegian shelf, *J. Geol. Soc.*, doi:10.1144/jgs2016-066.
IOC, IHO, and BODC (2003), *Centenary Edition of the GEBCO Digital Atlas, published on CDROM on behalf of the Intergovernmental Oceanographic Commission and the International Hydrographic Organization as part of the General Bathymetric Chart of the Oceans*, British Oceanographic Data Centre, Liverpool, U. K.
Iribarren, L., J. Vergés, F. Camurri, J. Fullea, and M. Fernàndez (2007), The structure of the Atlantic–Mediterranean transition zone from the Alboran Sea to the Horseshoe Abyssal Plain (Iberia–Africa plate boundary), *Mar. Geol.*, *243*(1–4), 97–119, doi:10.1016/j.margeo.2007.05.011.
Jiménez-Munt, I., M. Fernàndez, J. Vergés, J. C. Afonso, D. Garcia-Castellanos, and J. Fullea (2010), Lithospheric structure of the Gorringe Bank: Insights into its origin and tectonic evolution, *Tectonics*, *29*, TC5019, doi:10.1029/2009TC002458.
Johnson, H., J. D. Ritchie, K. Hitchen, D. B. Mcinroy, and G. S. Kimbell (2005), Aspects of the Cenozoic deformational history of the Northeast Faroe-Shetland Basin, Wyville-Thomson Ridge and Hatton Bank areas, *Geol. Soc. London, Pet. Geol. Conf. Ser.*, *6*, 993–1007, doi:10.1144/0060993.
Lundin, E., and A. G. Doré (2002), Mid-Cenozoic post-breakup deformation in the "passive" margins bordering the Norwegian-Greenland Sea, *Mar. Pet. Geol.*, *19*, 79–93, doi:10.1016/S0264-8172(01)00046-0.
Lanaja, J. M. (1987), *Contribución de la exploración petrolífera al conocimiento de la geología de España*, IGME, Madrid.
Ledesma, S. M. (2000), Astrobiocronología y estratigrafía de alta resolución del Neógeno de la Cuenca del Guadalquivir-Golfo de Cádiz, PhD thesis, 464 pp., Universidad de Salamanca.
Letouzey, J. (1990), Fault reactivation, inversion and fold-thrust belt, in *Petroleum and Tectonics in Mobile Belts*, edited by J. Letouzey, pp. 101–128, Technic, Paris.
Llave, E., H. Matias, F. J. Hernández-Molina, G. Ercilla, D. A. V. Stow, and T. Medialdea (2011), Pliocene–Quaternary contourites along the northern Gulf of Cadiz margin: Sedimentary stacking pattern and regional distribution, *Geo-Mar. Lett.*, *31*(5–6), 377–390, doi:10.1007/s00367-011-0241-3.

Lonergan, L., and N. White (1997), Origin of the Betic-Rif mountain belt, *Tectonics*, *16*(3), 504–522, doi:10.1029/96TC03937.
Maldonado, A., L. Somoza, and L. Pallarés (1999), The Betic orogen and the Iberian–African boundary in the Gulf of Cadiz: Geological evolution (central North Atlantic), *Mar. Geol.*, *155*(1–2), 9–43, doi:10.1016/S0025-3227(98)00139-X.
Malod, J. A., and D. Mougenot (1979), L'histoire geologique neogene du golfe de Cadix, *Bull. Soc. Geol. Fr.*, *S7–XXI*(5), 603–611, doi:10.2113/gssgfbull.S7-XXI.5.603.
Manuppella, G. (1992), *Carta geológica da região do Algarve*, Noticia explicativa da Carta Geologica da regiao do Algarve Serviços geológicos de Portugal.
Marques, F. O., J.-P. Burg, S. M. Lechmann, and S. M. Schmalholz (2010), Fluid-assisted particulate flow of turbidites at very low temperature: A key to tight folding in a submarine Variscan foreland basin of SW Europe, *Tectonics*, *29*, TC2005, doi:10.1029/2008TC002439.
Martínez del Olmo, W. (2002), Secuencias de depósito y estructuración diapírica en el Mesozoico y Neógeno del Prebético y Golfo de Valencia desde sondeos y líneas sísmicas, PhD thesis, 563 pp., Universidad Complutense de Madrid.
Martínez-Loriente, S., et al. (2013), Active deformation in old oceanic lithosphere and significance for earthquake hazard: Seismic imaging of the Coral Patch Ridge area and neighboring abyssal plains (SW Iberian Margin): Active Deformation Coral Patch Ridge, *Geochem. Geophys. Geosyst.*, *14*, 2206–2231, doi:10.1002/ggge.20173.
Martínez-Loriente, S., V. Sallarès, E. Gràcia, R. Bartolome, J. J. Dañobeitia, and N. Zitellini (2014), Seismic and gravity constraints on the nature of the basement in the Africa-Eurasia plate boundary: New insights for the geodynamic evolution of the SW Iberian margin: Thin oceanic crust at the CPR and SH, *J. Geophys. Res. Solid Earth*, *119*, 127–149, doi:10.1002/2013JB010476.
Martínez-Loriente, S., E. Grácia, R. Bartolome, H. Perea, D. Klaeschen, J. J. Dañobeitia, N. Zitellini, R. B. Wynn, and D. G. Masson (2016), Morphostructure, tectono-sedimentary evolution and seismic potential of the Horseshoe Fault, SW Iberian Margin, *Basin Res.*, doi:10.1111/bre.12225.
Martins, L. T., J. Madeira, N. Youbi, J. Munhá, J. Mata, and R. Kerrich (2008), Rift-related magmatism of the central Atlantic magmatic province in Algarve, southern Portugal, *Lithos*, *101*(1–2), 102–124, doi:10.1016/j.lithos.2007.07.010.
Matias, H. (2007), Hydrocarbon potential of the offshore Algarve Basin, PhD thesis, 324 pp., Faculdade de Ciências da Universidade Nova de Lisboa.
Matias, H., P. Kress, P. Terrinha, W. Mohriak, P. T. L. Menezes, L. Matias, F. Santos, and F. Sandnes (2011), Salt tectonics in the western Gulf of Cadiz, southwest Iberia, *AAPG Bull.*, *95*(10), 1667–1698, doi:10.1306/01271110032.
Medialdea, T., R. Vegas, L. Somoza, J. T. Vázquez, A. Maldonado, V. Díaz-del-Río, A. Maestro, D. Córdoba, and M. C. Fernández-Puga (2004), Structure and evolution of the "Olistostrome" complex of the Gibraltar Arc in the Gulf of Cádiz (eastern central Atlantic): Evidence from two long seismic cross sections, *Mar. Geol.*, *209*(1–4), 173–198, doi:10.1016/j.margeo.2004.05.029.
Michard, D., O. Frizon de Lamotte, O. Saddiqi, and A. Chalouan (2008), An Outline of the Geology of Morocco, in *Continental Evolution: The Geology of Morocco: Structure, Stratigraphy, and Tectonics of the Africa-Atlantic-Mediterranean Triple Junction*, edited by A. Michard, A. Chalouan, and O. Saddiqi, pp. 1–31, Lecture Notes in Earth Sciences, 116, Springer.
Medialdea, T., L. Somoza, L. M. Pinheiro, M. C. Fernández-Puga, J. T. Vázquez, R. León, M. K. Ivanov, V. Magalhaes, V. Díaz-del-Río, and R. Vegas (2009), Tectonics and mud volcano development in the Gulf of Cádiz, *Mar. Geol.*, *261*(1–4), 48–63, doi:10.1016/j.margeo.2008.10.007.
Mohn, G., G. Manatschal, M. Beltrando, E. Masini, and N. Kusznir (2012), Necking of continental crust in magma-poor rifted margins: Evidence from the fossil Alpine Tethys margins, *Tectonics*, *31*, TC1012, doi:10.1029/2011TC002961.
Mougenot, D. (1989), Geologia da margem portuguesa, PhD thesis, 259 pp., Univer. Pierre et Marie Curie, Paris VI.
Muñoz-Martín, A., et al. (2012), Mapa de esfuerzos activos en línea de la Península Ibérica a partir de Mecanismos Focales calculados desde el Tensor de Momento Sísmico, *Geotemas*, *13*, 1–4.
Olaiz, A. J., A. Muñoz-Martín, G. De Vicente, R. Vegas, and S. Cloetingh (2009), European continuous active tectonic strain–stress map, *Tectonophysics*, *474*(1–2), 33–40, doi:10.1016/j.tecto.2008.06.023.
Palano, M., P. J. González, and J. Fernández (2013), Strain and stress fields along the Gibraltar Orogenic Arc: Constraints on active geodynamics, *Gondwana Res.*, *23*(3), 1071–1088, doi:10.1016/j.gr.2012.05.021.
Palano, M., P. J. González, and J. Fernández (2016), Crustal deformation evidences for viscous coupling and fragmented lithosphere at the Nubia-Iberia plate boundary (Western Mediterranean), EGU General Assembly 2016, p. 12132, Vienna, Austria, 17–22 April.
Pedrera, A., et al. (2011), Is there an active subduction beneath the Gibraltar orogenic arc? Constraints from Pliocene to present-day stress field, *J. Geodyn.*, *52*(2), 83–96, doi:10.1016/j.jog.2010.12.003.
Pedrera, A., A. Ruiz-Constán, C. Marín-Lechado, J. Galindo-Zaldívar, A. González, and J. A. Peláez (2013), Seismic transpressive basement faults and monocline development in a foreland basin (eastern Guadalquivir, SE Spain), *Tectonics*, *32*(6), 1571–1586, doi:10.1002/2013TC003397.
Perconig, E. (1962), Sur la constitution géologique de l'Andalousie occidentale en particulier du bassin du Guadalquivir (Espagne méridionale), *Livre Mémoire du Professeur Paul Fallot*, *Mem. Hors-Ser. Soc. Geol. Fr.*, *1*, 229–256.
Pereira, M. F., M. Chichorro, J. B. Silva, B. Ordóñez-Casado, J. K. W. Lee, and I. S. Williams (2012), Early carboniferous wrenching, exhumation of high-grade metamorphic rocks and basin instability in SW Iberia: Constraints derived from structural geology and U–Pb and ^{40}Ar–^{39}Ar geochronology, *Tectonophysics*, *558–559*, 28–44, doi:10.1016/j.tecto.2012.06.020.
Pérez-Peña, A., J. Martín-Davila, J. Gárate, M. Berrocoso, and E. Buforn (2010), Velocity field and tectonic strain in southern Spain and surrounding areas derived from GPS episodic measurements, *J. Geodyn.*, *49*(3–4), 232–240, doi:10.1016/j.jog.2010.01.015.
Peron-Pinvidic, G., and G. Manatschal (2009), The final rifting evolution at deep magma-poor passive margins from Iberia-Newfoundland: A new point of view, *Int. J. Earth Sci.*, *98*(7), 1581–1597, doi:10.1007/s00531-008-0337-9.
Peron-Pinvidic, G., G. Manatschal, S. M. Dean, and T. A. Minshull (2008), Compressional structures on the West Iberia rifted margin: Controls on their distribution, *Geol. Soc. London, Spec. Publ.*, *306*(1), 169–183, doi:10.1144/SP306.8.
Ramos, A., L. Cascone, A. Olaiz, O. Fernández, A. Sánchez de la Muela, W. Hermoza, A. Arnaiz, and R. Rocca (2015), Crustal structure of the southern Portuguese Margin—Constraints from potential field methods, paper presented at 77th EAGE Conference and Exhibition 2015.
Ramos, A., O. Fernández, P. Terrinha, and J. A. Muñoz (2016), Extension and inversion structures in the Tethys–Atlantic linkage zone, Algarve Basin, Portugal, *Int. J. Earth Sci.*, *105*(5), 1663–1679, doi:10.1007/s00531-015-1280-1.
Ribeiro, A., M. T. Antunes, M. P. Ferreira, R. B. Rocha, A. F. Soares, G. Zbyszewski, F. M. de Almeida, D. de Carvalho, and J. H. Monteiro (1979), Introduction á la géologie générale du Portugal, 114 pp., Serviços Geológicos de Portugal, Lisboa.
Ribeiro, A., J. Cabral, R. Baptista, and L. Matias (1996), Stress pattern in Portugal mainland and the adjacent Atlantic region, West Iberia, *Tectonics*, *15*(3), 641–659, doi:10.1029/95TC03683.
Roca, E., J. A. Muñoz, O. Ferrer, and N. Ellouz (2011), The role of the Bay of Biscay Mesozoic extensional structure in the configuration of the Pyrenean orogen: Constraints from the MARCONI deep seismic reflection survey, *Tectonics*, *30*, TC2001, doi:10.1029/2010TC002735.
Roest, W. R., and S. P. Srivastava (1991), Kinematics of the plate boundaries between Eurasia, Iberia, and Africa in the North Atlantic from the Late Cretaceous to the present, *Geology*, *19*(6), 613, doi:10.1130/0091-7613(1991)019<0613:KOTPBB>2.3.CO;2.

Roque, C. (2007), Tectonostratigrafia do cenozóico das margens continentais sul e sudoeaste portuguesas: um modelo de correlação sismostratigráfica, PhD thesis, 310 pp., Universidade de Lisboa.
Rosenbaum, G., G. S. Lister, and C. Duboz (2002), Relative motions of Africa, Iberia and Europe during Alpine orogeny, *Tectonophysics*, *359*(1), 117–129.
Sallarès, V., A. Gailler, M.-A. Gutscher, D. Graindorge, R. Bartolomé, E. Gràcia, J. Díaz, J. J. Dañobeitia, and N. Zitellini (2011), Seismic evidence for the presence of Jurassic oceanic crust in the central Gulf of Cadiz (SW Iberian margin), *Earth Planet. Sci. Lett.*, *311*(1–2), 112–123, doi:10.1016/j.epsl.2011.09.003.
Sallarès, V., S. Martínez-Loriente, M. Prada, E. Grácia, C. Ranero, M.–A. Gutscher, R. Bartolome, A. Gailler, J. J. Dañobeitia, and N. Zitellini (2013), Seismic evidence of exhumed mantle rock basement at the Gorringe Bank and the adjacent Horseshoe and Tagus abyssal plains (SW Iberia), *Earth Planet. Sci. Lett.*, *365*, 120–131, doi:10.1016/j.epsl.2013.01.021.
Sartori, R., L. Torelli, N. Zitellini, D. Peis, and E. Lodolo (1994), Eastern segment of the Azores-Gibraltar line (central-eastern Atlantic): An oceanic plate boundary with diffuse compressional deformation, *Geology*, *22*(6), 555–558.
Schettino, A., and E. Turco (2011), Tectonic history of the western Tethys since the Late Triassic, *Geol. Soc. Am. Bull.*, *123*(1–2), 89–105.
Şengör, A. M. C. (1984), The Cimmeride orogenic system and the tectonics of Eurasia, *Geol. Soc. Am. Spec. Pap.*, *195*, 1–74, doi:10.1130/SPE195-p1.
Simancas, J. F., A. Tahiri, A. Azor, F. G. Lodeiro, D. J. Martínez Poyatos, and H. El Hadi (2005), The tectonic frame of the Variscan–Alleghanian orogen in southern Europe and northern Africa, *Tectonophysics*, *398*(3–4), 181–198, doi:10.1016/j.tecto.2005.02.006.
Soriano, C. (1996), Tectónica de cabalgamientos en la Faja Pirítica Ibérica (Zona Sur Portuguesa): el Antiforme de la Puebla de Guzmán, y la lámina de cabalgamiento de Sanlúcar de Guadiana, *Geogaceta*, *20*, 786–788.
Srivastava, S. P., H. Schouten, W. R. Roest, K. D. Klitgord, L. C. Kovacs, J. Verhoef, and R. Macnab (1990a), Iberian plate kinematics: A jumping plate boundary between Eurasia and Africa, *Nature*, *344*(6268), 756–759, doi:10.1038/344756a0.
Srivastava, S. P., W. R. Roest, L. C. Kovacs, G. Oakey, S. Levesque, J. Verhoef, and R. Macnab (1990b), Motion of Iberia since the Late Jurassic: Results from detailed aeromagnetic measurements in the Newfoundland Basin, *Tectonophysics*, *184*(3), 229–260.
Stapel, G. (1999), The nature of isostasy in West Iberia and its bearing on Mesozoic and Cenozoic regional tectonics, PhD thesis, 148 pp., Vrije Universiteit.
Stich, D., E. Serpelloni, F. de Lis Mancilla, and J. Morales (2006), Kinematics of the Iberia–Maghreb plate contact from seismic moment tensors and GPS observations, *Tectonophysics*, *426*(3–4), 295–317, doi:10.1016/j.tecto.2006.08.004.
Teixell, A., M.-L. Arboleya, M. Julivert, and M. Charroud (2003), Tectonic shortening and topography in the central High Atlas (Morocco), *Tectonics*, *22*(5), 1051, doi:10.1029/2002TC001460.
Terrinha, P. (1998), Structural geology and tectonic evolution of the Algarve Basin, South Portugal, PhD thesis, 430 pp., Imperial College, London.
Terrinha, P., M. Coward, and A. Ribeiro (1990), Salt tectonics in the Algarve Basin: The Loulé diapir, *Comun. Serviços Geológicos Port.*, *76*, 33–40.
Terrinha, P., C. Ribeiro, J. C. Kullberg, C. Lopes, R. Rocha, and A. Ribeiro (2002), Compressive episodes and faunal isolation during rifting, southwest Iberia, *J. Geol.*, *110*(1), 101–113.
Terrinha, P., et al. (2003), Tsunamigenic-seismogenic structures, neotectonics, sedimentary processes and slope instability on the southwest Portuguese Margin, *Mar. Geol.*, *195*(1–4), 55–73, doi:10.1016/S0025-3227(02)00682-5.
Terrinha, P., et al. (2009), Morphotectonics and strain partitioning at the Iberia–Africa plate boundary from multibeam and seismic reflection data, *Mar. Geol.*, *267*(3–4), 156–174, doi:10.1016/j.margeo.2009.09.012.
Terrinha, P., et al. (2013), A Bacia do Algarve: Estratigrafia, Paleogeografia e Tectónica, in *Geologia de Portugal, Vol. II, Geologia Meso-Cenozóica de Portugal*, edited by R. Dias et al., pp. 29–166, Cap III, Livraria Escolar Editora, Lisboa.
TGS (2005), PD00: Non-exclusive 2D survey, TGS online data zone. [Available at http://www.tgs.com/TGS/specsheets/PD-00_Spec.pdf.]
Thiebot, E., and M.-A. Gutscher (2006), The Gibraltar Arc seismogenic zone (part 1): Constraints on a shallow east dipping fault plane source for the 1755 Lisbon earthquake provided by seismic data, gravity and thermal modeling, *Tectonophysics*, *426*(1–2), 135–152, doi:10.1016/j.tecto.2006.02.024.
Torelli, L., R. Sartori, and N. Zitellini (1997), The giant chaotic body in the Atlantic Ocean off Gibraltar: New results from a deep seismic reflection survey, *Mar. Pet. Geol.*, *14*(2), 125–138, doi:10.1016/S0264-8172(96)00060-8.
Tortella, D., M. Torne, and A. Pérez-Estaún (1997), Geodynamic evolution of the eastern segment of the Azores-Gibraltar zone: The Gorringe Bank and the Gulf of Cadiz region, *Mar. Geophys. Res.*, *19*(3), 211–230.
Tugend, J., G. Manatschal, N. J. Kusznir, E. Masini, G. Mohn, and I. Thinon (2014), Formation and deformation of hyperextended rift systems: Insights from rift domain mapping in the Bay of Biscay-Pyrenees, *Tectonics*, *33*, 1239–1276, doi:10.1002/2014TC003529.
Vågnes, E., R. H. Gabrielsen, and P. Haremo (1998), Late Cretaceous-Cenozoic intraplate contractional deformation at the Norwegian continental shelf: Timing, magnitude and regional implications, *Tectonophysics*, *300*, 29–46, doi:10.1016/S0040-1951(98)00232-7.
van Hinsbergen, D. J. J., R. L. M. Vissers, and W. Spakman (2014), Origin and consequences of western Mediterranean subduction, rollback, and slab segmentation, *Tectonics*, *33*, 393–419, doi:10.1002/2013TC003349.
Vegas, R. (1980), Carboniferous subduction complex in the south Portuguese zone coeval with basement reactivation and uplift in the Iberian massif, Cuadernos do Laboratorio Xeolóxico de Laxe, vol. 1, pp. 187–200.
Vegas, R., T. Medialdea, M. Muñoz García, V. Díaz del Río, and L. Somoza (2004), Nature and tectonic setting of the Guadalquivier Bank (Gulf of Cadiz, SW Iberian Peninsula), *Rev. Soc. Geológica Esp.*, *17*(1–2), 49–60.
Vera, J. A. (1998), El Jurásico de la Cordillera Bética: Estado actual de conocimientos y problemas pendientes, *Cuad. Geol. Ibérica*, *24*, 17–42.
Vergés, J., and M. Fernàndez (2012), Tethys–Atlantic interaction along the Iberia–Africa plate boundary: The Betic–Rif orogenic system, *Tectonophysics*, *579*, 144–172, doi:10.1016/j.tecto.2012.08.032.
Ziegler, P. A. (1988), *Evolution of the Arctic-North Atlantic and the Western Tethys*, AAPG Memoir 43 ed., Amer Assn of Petroleum Geologists, Tulsa, Okla.
Zitellini, N., et al. (2001), Source of 1755 Lisbon earthquake and tsunami investigated, *Eos Trans. AGU*, *82*(26), 285–291, doi:10.1029/EO082i026p00285-01.
Zitellini, N., M. Rovere, P. Terrinha, F. Chierici, and L. Matias (2004), Neogene through Quaternary tectonic reactivation of SW Iberian passive margin, *Pure Appl. Geophys.*, *161*(3), 565–587, doi:10.1007/s00024-003-2463-4.
Zitellini, N., E. Gràcia, L. Matias, P. Terrinha, M. A. Abreu, G. DeAlteriis, J. P. Henriet, J. J. Dañobeitia, D. G. Masson, and T. Mulder (2009), The quest for the Africa–Eurasia plate boundary west of the Strait of Gibraltar, *Earth Planet. Sci. Lett.*, *280*(1–4), 13–50, doi:10.1016/j.epsl.2008.12.005.

APPENDIX 1.3

Impact of basin structure and evaporite distribution on salt tectonics in the Gulf of Cadiz, Southwest Iberian margin

Ramos, A., Fernández, O., Terrinha, P., Muñoz, J.A.
(submitted in Marine and Petroleum Geology).

Impact of basin structure and evaporite distribution on salt tectonics in the Algarve Basin, Southwest Iberian margin

Adrià Ramos[1], Oscar Fernández[2], Josep Anton Muñoz[1], Pedro Terrinha[3]

[1]Institut de Recerca Geomodels, Departament de Dinàmica de la Terra i de l'Oceà, Universitat de Barcelona, Barcelona, Spain

[2]Repsol Exploración, Dirección de Geología, Madrid, Spain

[3]Instituto Português do Mar e da Atmosfera, Divisão de Geologia e Georecursos Marinhos, Lisboa, Portugal

Email corresponding author adria_ramos@outlook.com

Abstract

The SW Iberian margin developed as a passive margin during Mesozoic times and was later inverted during the Cenozoic Alpine orogeny. The initial syn-rift deposits include a Lower Jurassic evaporite unit of variable thickness. In the onshore, this unit is observed to thicken basinward (i.e., southward), in fault-controlled depocenters, and salt-related structures are only present in areas of thick initial evaporites. In the offshore, multiple salt-structures cored by the Lower Jurassic evaporites are interpreted seismic reflection data and exploratory drilling. Offshore salt structures include the allochthonous Esperança Salt Nappe, which extends over an area roughly 40x60km. The abundance of salt-related structures and their geometry is observed to be controlled by the distribution of evaporite facies, which is in turn controlled by the structure of rift-related faulting. This paper presents a comprehensive study of salt tectonics over the entire onshore and offshore SW Iberian passive margin (south Portugal and southwest Spain), covering all aspects from initial evaporite composition and thickness to the evolution of salt-related structures through Mesozoic extension and Cenozoic basin inversion.

Keywords: salt diapir, salt canopy, passive margin, salt tectonics, Algarve Basin

1. Introduction

Many passive margin basins containing evaporite units and their related salt tectonics have been studied worldwide at local to basin scale during the past decades: Gulf of Mexico (e.g., Diegel et al.,

1995; Peel et al., 1995), offshore Morocco (e.g., Tari et al., 2000; Tari and Jabour, 2013), Kwanza Basin (e.g., Duval et al., 1992; Hudec and Jackson, 2002, 2004), Santos and Campos basins (e.g., Davison et al., 2012; Fiduk and Rowan, 2012; Mohriak et al., 1995) or Nova Scotia (e.g., Ings and Shimeld, 2006; Tari et al., 2012) to name a few. In most cases, post-depositional deformation of evaporite units coupled to the dimension of the systems makes it difficult to understand the initial configuration of the basin and the impact of factors such as evaporite distribution on structural evolution.

The Mesozoic evaporite basin of the Algarve Basin contains many of the elements observed in salt-related deformation in passive margins worldwide. Despite a relatively complex evolution, from extension in the Mesozoic to compression in the Cenozoic, the dimension of the basin and data availability make it a good basin to study the different factors that govern the evolution of a mid-size evaporite basin in a passive margin.

The Algarve Basin is located in the SW Iberian margin (Fig. 1) and developed as a passive margin during the Mesozoic, with evaporites being deposited during the early phase of rifting in the earliest Jurassic. This margin underwent compression during Cenozoic as the result of the Alpine orogeny (e.g., Dewey et al., 1989; Ziegler, 1988) and it is partially inverted at the present-day (Ramos et al., 2017a). The Cenozoic N-S convergence between the African and Eurasian plates led to the development of the Betic-Rif chain (Gibraltar Arc; e.g, Vergés and Fernàndez, 2012).

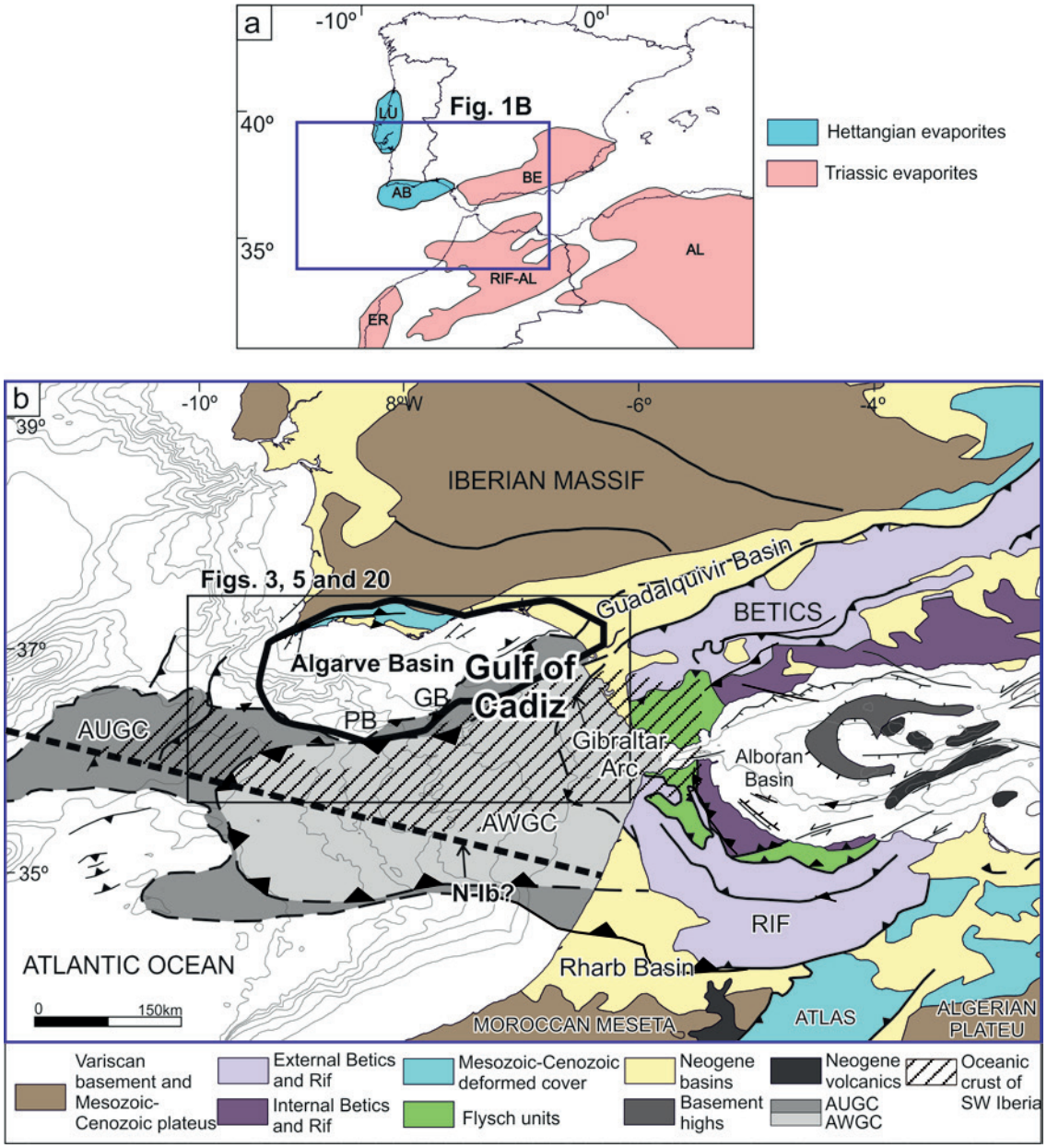

Figure 1. a) Map showing the distribution of basins containing salt structures (pink areas) in southern Iberia and NW Africa. Modified from Alves et al. (2006) and Hudec and Jackson (2007) RIF-AL: Atlas; BE: Betic; ER: Essaouira; GoC: Gulf of Cadiz; LU: Lusitania b) Map of the geological framework of the area comprised by the Gulf of Cadiz and the Gibraltar Arc (Betic-Rif orogen arc), showing the principal tectonic units and associated basins (modified from Iribarren et al., 2007). AB: Algarve Basin. AUGC: Allochthonous Unit of the Gulf of Cadiz; AWGC: Accretionary Wedge of the Gulf of Cadiz; GB: Guadalquivir Bank; N-Ib?: possible Nubia-Iberia plate boundary (Zitellini et al., 2009); PB: Portimão Bank.

The interest in salt tectonics in the Algarve Basin has increased in recent years in part due to the potential petroleum systems of the basin (Matias et al., 2011). Initially, in the onshore, a series of salt structures such as diapirs and salt walls were described (Afonso, 1983; Davison et al., 2016; Manuppella, 1992; Terrinha, 1998; Terrinha et al., 1990). The availability of seismic and gravity data led to the identification of more salt structures in the offshore portion of the SW Iberian margin (e.g., Fernández-Puga et al., 2007; Lopes et al., 2008; Maestro et al., 2003; Matias, 2007; Terrinha, 1998). One of the most interesting elements of the margin is the presence of an allochthonous salt nappe in the center of the northern Algarve Basin, the so-called Esperança salt structure (Matias, 2007; Matias et al., 2011; Terrinha, 1998). Most recently, Ramos et al. (2016) discussed the influence of the interaction of basement and salt structures on extension and contraction in the onshore part of the basin.

Matias et al. (2011) presented for the first time a description of salt-related structures, their distribution and the implications on petroleum systems in the western Algarve Basin based on the interpretation of a regional 2D multi-channel reflection seismic (MCS) survey. In this paper we present a more detailed description of salt-related structures that also extends to comprise the entire Algarve Basin. This study reveals significant variability in the structural style throughout the basin. The aim of this paper is to tie the origin of this variability to the structural evolution of the margin and to the initial configuration of the evaporite basin.

2. Geological Setting

The Algarve Basin is oriented roughly E-W (Fig. 1) and lies along the southwestern margin of Iberia, in the Gulf of Cadiz. The Algarve Basin has been historically used to refer to the Mesozoic basin cropping out along southern Portugal and its southward offshore extension. In this paper we will use the name Algarve Basin to refer to the sedimentary basin that developed along the northern Gulf of Cadiz and the immediate onshore in Portugal, and even present in some Mesozoic outcrops in the southwestern Spain, near the Portuguese borded. To the south and west the Algarve Basin opens to the Atlantic Ocean. The continuation of the southern Iberian margin east of the Gulf of Cadiz is at present overthrust by the Betic-Rif orogen (Crespo-Blanc, 2007; Fernández-Ibáñez and Soto, 2017; Flinch et al., 1996; Iribarren et al., 2009; Platt et al., 2013; Ramos et al., 2017b).

2.1. Tectono-stratigraphic evolution

The Algarve Basin started to develop in Late Triassic times, due to the break-up of Pangea (Schettino and Turco, 2009; Terrinha, 1998). Late Triassic red beds unconformably overlie a basement made up by Carboniferous flysch and older rocks. Rifting continued into Hettangian times. It is during this period that the key evaporitic units were deposited in the basin (e.g., Terrinha, 1998). Hettangian evaporites, as found onshore and in the offshore wells, consist of halite, anhydrite and gypsum and are interbedded with alluvial to lacustrine red shales, shallow water limestones and dolomites (e.g., Terrinha, 1998; Fig. 2). Dark grey siltstones are also interbedded with the salt, documented in the Loulé salt mine (Davison et al., 2016).

Late Triassic to Hettangian rifting was followed by tectonic quiescence during the Sinemurian, characterized by the development of a regional shallow water carbonate platform (Terrinha, 1998). From Pliensbachian to Callovian times the margin underwent renewed rifting (along ENE-WSW trending faults) due to the westward propagation of the Tethys (Ramos et al., 2017b; Ramos et al., 2016; Terrinha, 1998). Basement faulting and related thickness changes triggered initial salt tectonics in the area. Deposition during this time was dominated by carbonates.

Oceanization of the southern Iberian margin is interpreted to have occurred during the Middle to Late Jurassic (García-Hernández et al., 1989; Gutscher et al., 2002; Martínez-Loriente et al., 2014; Sallarès et al., 2011; Vera et al., 2004). The basin continued to be dominated by carbonates through the Late Jurassic. The Early Cretaceous, was characterized by a significant clastic input and limited subsidence (Terrinha, 1998). There was no further accommodation space generated during the Late Cretaceous, with only the development of very local depocenters related to salt tectonics (Lopes and Cunha, 2007).

During the Cenozoic, the convergence between Iberia and Africa led to the inversion of basins along the SW Iberian margin, causing uplift and local inversion of pre-existing Mesozoic faults and salt-related structures (Ramos et al., 2017a). Cenozoic sediments are clastic-dominated, and in general thicken southward (Ramos et al., 2017a). Within the Cenozoic, the transition from a condensed Paleogene section to the Miocene is marked by the BFU (Basal Foredeep Unconformity, Maldonado et al., 1999), an unconformity formed in response to the initial pulses of uplift in this area. After the Miocene, from Pliocene to Present, sedimentation was dominated by the Mediterranean Outflow Water (MOW) and the deposition of contourite drifts that control the present-day seafloor geometry (e.g., Hernández-Molina et al., 2016, 2014; Llave et al., 2011).

2.2. Age of Mesozoic evaporites

Vintage wells in the Spanish Algarve Basin reported the evaporites encountered below the Lower Jurassic carbonates as Keuper facies (Late Triassic) based on their stratigraphic position (Lanaja, 1987). However, more recently, a series of onshore paleontological dating of the evaporites in the onshore Algarve Basin, along with an oil well in the south Portuguese shelf (Ruivo-1), reported the evaporitic unit to be Hettangian in age (Doubinger et al., 1970; Palain, 1979; Terrinha, 1998). This dating is similar to that proposed for evaporites of the Lusitanian basin further north (Wilson, 1988). In this study we have therefore assumed that the Algarve Basin evaporites are Hettangian in age.

Nonetheless, to the east, in the Betics, recent studies confirm the age of the evaporite unit as Late Triassic (e.g., Pérez-Valera, 2005). To the west, in the Morocco-Nova Scotia margin and in the Grand Banks, evaporites are dated to be of Late Triassic to Hettangian in age (Tari et al., 2012; Welsink and Tankard, 2012), dating that is consistent with that for evaporites in the Atlas domain (Saura et al., 2014) and the Essaouiria Basin in Morocco (Hafid, 2000). A possible Late Triassic age or diachronicity of evaporite deposition across the Algarve Basin cannot be ruled out.

2.3. Structural configuration of the Gulf of Cadiz and Algarve Basin

The present-day configuration of the Gulf of Cadiz is the result of Mesozoic extensional structures overprinted by Cenozoic compression. The central and western parts of the Gulf of Cadiz are mostly floored by oceanic or transitional crust (Gutscher et al., 2002; Martínez-Loriente et al., 2014; Ramos et al., submitted grav; Sallarès et al., 2011) and are crossed by the Iberia-Africa plate boundary (Zitellini et al., 2009; Fig. 1a). The transition from the continental to the oceanic domain occurs south of the Portimão and Guadalquivir Banks (Fig. 1, Ramos et al., submitted grav). The Portimão Bank is an inverted Mesozoic graben, whereas the Guadalquivir Bank is a basement high that acted as an intra-basinal high during the Mesozoic that has been further uplifted since Miocene times (Ramos et al., 2017a; Terrinha, 1998). The Portimão and Guadalquivir Banks acted as a backstop to the propagation of the AWGC (the Accretionary Wedge of the Gulf of Cadiz, related to eastward-directed subduction under the Gibraltar Arc) and the AUGC (the Allochthonous Unit of the Gulf of Cadiz, an olistostromic mass reworking material from the AWGC) (Gutscher et al., 2002; Iribarren et al., 2007; Maldonado et al., 1999; Medialdea, 2005; Medialdea et al., 2004; Somoza et al., 1999; Torelli et al., 1997; Tortella et al., 1997; Fig. 1b). To the north of the Portimão and Guadalquivir Banks lies the Algarve Basin.

2.4. The Hettangian evaporite basin

Onshore, along the northern margin of the evaporite basin of the Algarve Basin, Hettangian sediments are in the order of 100m thick and locally up to 200m. In the west, the Hettangian is dominated by shales, dolomites and anhydrites, with locally interbedded volcanic rocks (Rocha, 1976) whereas further east it becomes dominated by shales (e.g., Almonte-1 well in Lanaja, 1987; Fig. 2). Basinward (to the south), the Hettangian sediments become thicker in fault-controlled depocenters and richer in evaporites which led to the development of salt structures during the Middle to Late Jurassic (Matias et al., 2011; Ramos et al., 2016). Onshore, the increase of halite basinward is observed from the Albufeira diapir to the Loulé diapir (Terrinha, 1998; Terrinha et al., 1990). Offshore, in distal areas of the basin, the Hettangian succession is dominated by halite (GC C-1, Orion 2-1; Fig. 2). From these areas, halite grades laterally into anhydrite and shale interlayered with carbonates, both eastwards (Asperillo-1 and Almonte-1 wells, Lanaja, 1987) and southwards to the Guadalquivir Bank (GC 6Y-BIS well, Lanaja, 1987; Fig. 2). This latter trend indicates that the Guadalquivir Bank was a relative high during the deposition of Hettangian sediments.

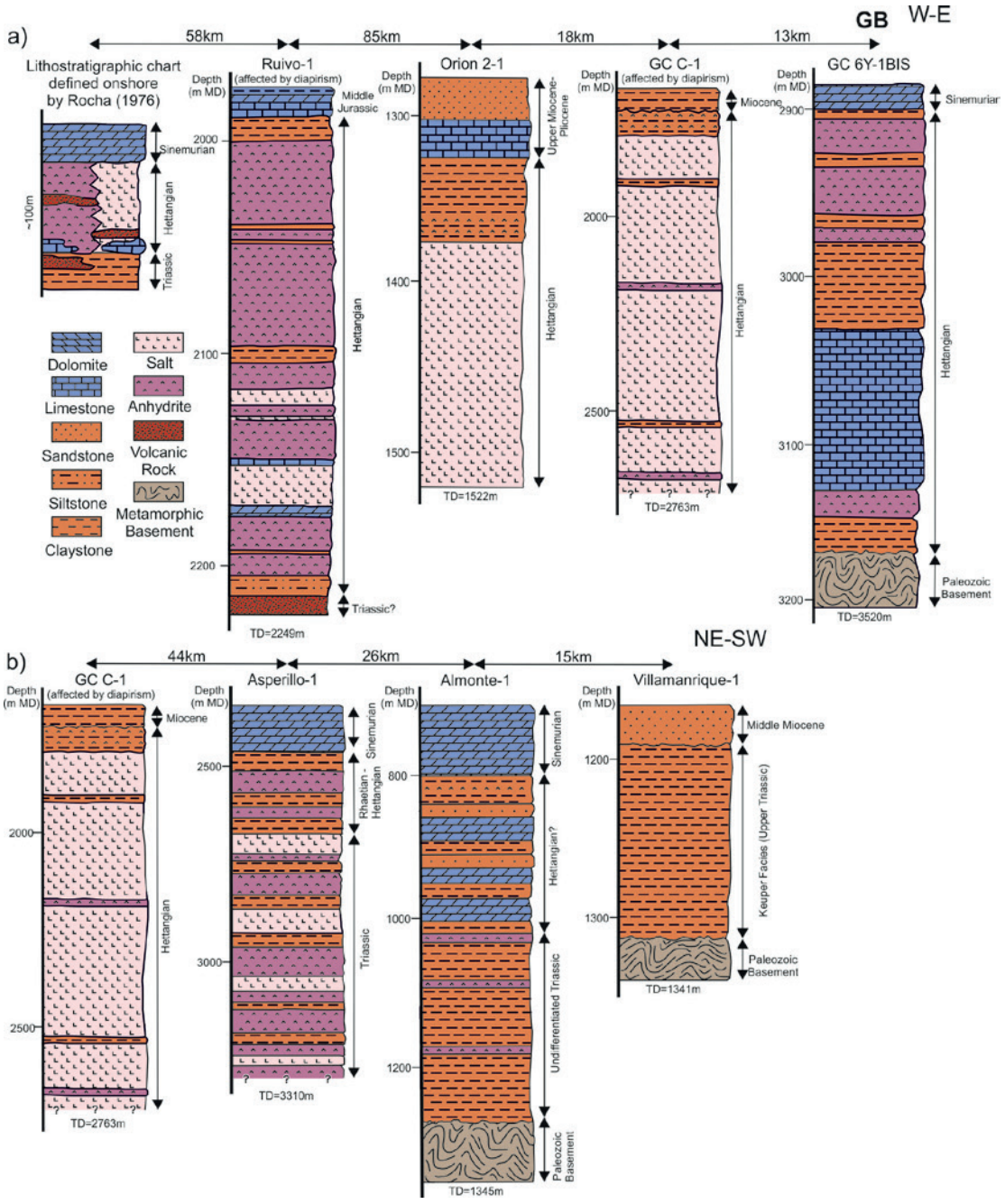

Figure 2. Correlation panels showing variability of the Hettangian and Upper Triassic evaporite unit across the Algarve Basin. a) Panel oriented roughly NW to SE crossing the Algarve Basin from the onshore in the north (left) to the Guadalquivir Bank in the south (right). b) Panel running roughly SW to NE along the basin axis from the center of the basin (left) to its eastern margin (right). See Figure 3 for location. Stratigraphy for the wells has been obtained from Lanaja (1987), Matias et al. (2011), Rocha (1976) and Roque (2007).GB: Guadalquivir Bank.

3. Data-set

The observations and interpretations presented in this paper are based on geological mapping of the northern margin of the Algarve Basin (Manuppella, 1992; Ramos et al., 2016), interpretation of reflection seismic data over the entire Algarve Basin, and data from hydrocarbon exploration wells Lanaja (1987), Matias (2007), Rocha (1976) and Roque (2007).

Seismic data consist of several publically available vintage 2D MCS surveys covering the entire Algarve Basin (www.info.igme.es/visorweb/), a regional 2D seismic survey (PDT00-PD00) covering the offshore western Algarve Basin and a 1500 km^2 3D seismic survey (Fig. 3), shot by Repsol in 2012. The PDT00-PD00 survey was acquired by TGS-NOPEC in 2001. This seismic survey consists on a set of 58 lines of 2D MCS profiles, oriented NNW-SSE and ENE-WSW and migrated in time (TGS, 2005).

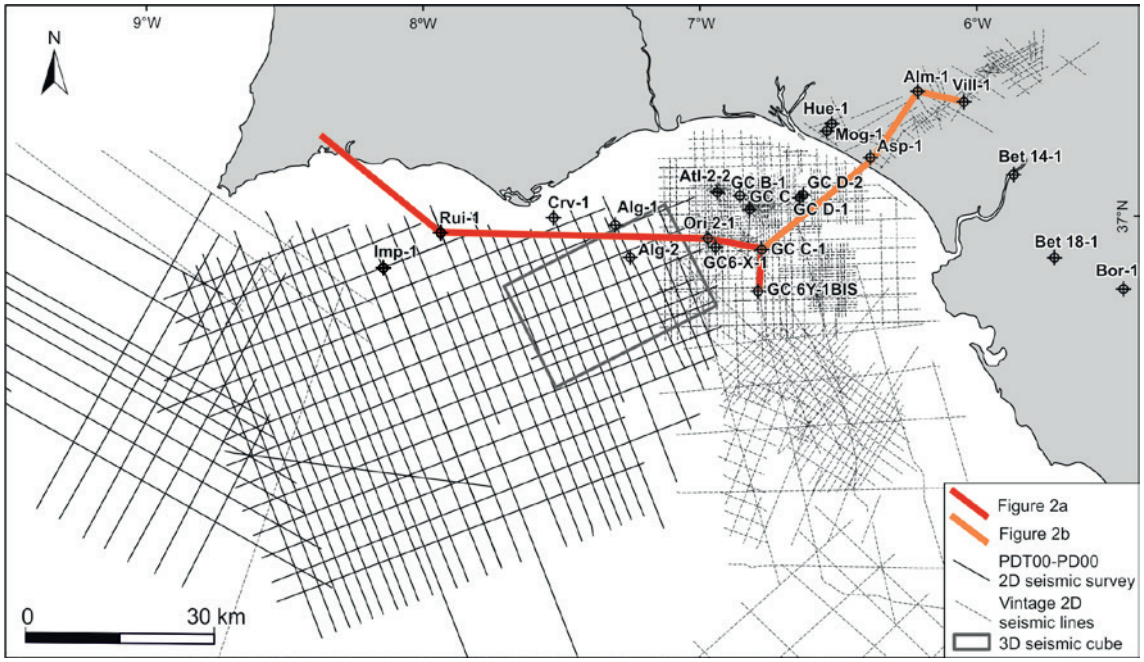

Figure 3. Available data in the Algarve Basin used in this study. Wells: Alg-1: Algarve-1; Alg-2; Algarve-2; Alm-1: Almonte-1; Asp-1: Asperillo-1; Atl-2-2: Atlantida-2-2; Bet 14-1: Betica 14-1; Bet 18-1: Betica 18-1; Bor-1: Bornos-1; Crv-1: Corvina-1; GC B-1: Gulf of Cadiz B-1; GC B-6: Gulf of Cadiz B-6; GB D-1: Gulf of Cadiz D-2; GB D-2: Gulf of Cadiz D-2; GB C-3: Gulf of Cadiz C-3; GB 6Y-1bis: Gulf of Cadiz 6Y-1bis; Hue-1: Huelva-1; Imp-1: Imperador-1; Mog-1: Moguer-1; Ori 2-1: Orion 2-1; Rui-1: Ruivo-1. See Fig. 1b for location.

The 3D seismic cube recorded up to 12 seconds TWT and was pre-stack migrated in time and in depth (migration up to 6000m depth). Ship-borne gravity data was acquired with the 3D seismic survey, and the corrected free-air gravity data has also been used to further qualitatively constrain seismic interpretation.

Seismic interpretation was calibrated taking into account 5 wells in offshore Portugal (e.g., Roque, 2007), along with 14 wells in the Spanish Gulf of Cadiz and Betics (Lanaja, 1987), using Petrel (software by Schlumberger).

4. Seismo-stratigraphy

Interpretation of seismic data throughout the Algarve Basin has been guided by the tie with the available wells and propagated based on seismic character and geometric relationships of the interpreted intervals. Examples of seismic facies and geometries are shown in Figure 4 and described here from bottom to top.

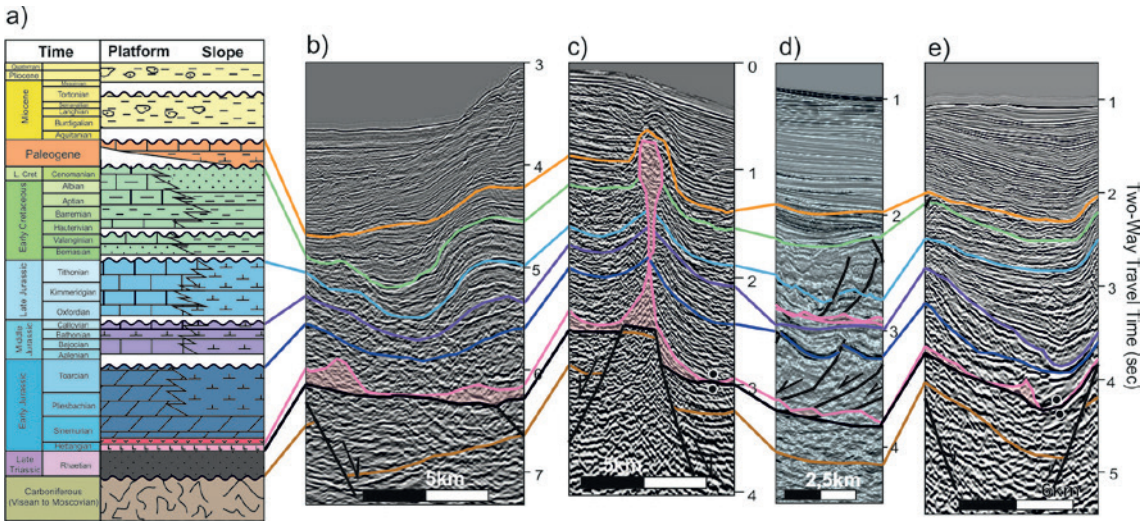

Figure 4. a) Synthetic stratigraphy of the Algarve Basin. b-e) Illustration of seismic facies for each of the intervals at different locations within the basin. See Figure 5 for the location of individual images. Data courtesy of TGS (b, c, e) and Repsol (d).

The deepest unit interpreted on seismic is the pre-rift Paleozoic basement, imaged as chaotic or occasionally transparent facies. The top of this unit is locally marked by a bright reflector. Where a bright top of basement reflector is absent, the top of basement has been placed where the seismic facies change

from chaotic below to layered seismic facies above. Layered seismic facies with high amplitudes above the Paleozoic correspond to Triassic red beds, deposited in grabens and half-grabens identified by the lack of lateral continuity of Triassic reflectors. Locally, Triassic units are also characterized by chaotic facies. Although the correlation of this unit is difficult, Triassic has been identified by intersecting seismic profiles.

Above the Triassic clastics, the Hettangian evaporitic unit is characterized by a high-amplitude reflector at its top, with highly irregular geometry (e.g., Fig. 4). The base of the Hettangian evaporites is also seen as a strong reflector that is clearly visible away from the salt structures but often masked under salt structures. Internally, the autochthonous evaporites display transparent or chaotic seismic facies. Allochthonous salt bodies have a similar seismic response: a bright top and base and internally transparent or chaotic facies, or even stratified facies in some local areas.

In the basins developed above the Hettangian evaporites, the first unit identified is the Lower Jurassic carbonate sequence, characterized by low frequency, high amplitude reflectors of limited lateral continuity. In some areas, the Lower Jurassic succession presents transparent facies. Above this unit, the Middle and Upper Jurassic sediments show a similar seismic response but with greater lateral continuity of reflectors. Locally, the Middle Jurassic succession presents internal unconformities which are interpreted to correspond to those described by Terrinha (1998), with the Bajocian-Bathonian unconformity as the most easily identifiable discontinuity. The contact between the Middle and Upper Jurassic rocks is also usually represented by an angular unconformity (Callovian-Oxfordian contact; Terrinha et al., 2002), characterized by the onlap of the Upper Jurassic reflectors. The top of the Upper Jurassic succession is a high amplitude reflector, normally affected by gentle folding. The Jurassic carbonates (mostly limestones, dolomites and marls) are covered by the Lower Cretaceous sediments, which display mid to high frequency and medium amplitude reflectors of good lateral continuity. Locally, the Lower Cretaceous sediments are represented by nearly transparent facies.

Upper Cretaceous and Paleogene and sediments are absent or highly condensed over most of the area. Where present, Upper Cretaceous and Paleogene are represented by strong low amplitude and low frequency laterally continuous reflectors and tend to onlap the top of the Lower Cretaceous. Finally, the shallowest layered package corresponds to the Neogene-Quaternary succession. This unit is characterized by high frequency and low amplitude continuous reflectors. The unit is bounded at the top by the seafloor,

while its base is represented by an erosional surface corresponding to the BFU (Basal Foredeep Unconformity). The units immediately beneath the BFU (Paleogene, Lower Cretaceous and Upper Jurassic) are truncated by this surface. The lowermost Miocene sediments onlap onto the relief defined by the BFU. Internally, the Neogene-Quaternary unit shows several unconformities that suggest continuous syn-depositional uplift (Hernández-Molina et al., 2016; Adrià Ramos et al., 2017). To the south, at a depth similar to the Neogene-Quaternary unit, the AUGC/AWGC (Allochthonous Unit of the Gulf of Cadiz/Accretionary Wedge of the Gulf of Cadiz, Late Miocene in time) are identified as a body with a relatively flat or gently folded base that truncates underlying sediments and an irregular top with chaotic to transparent internal facies. Its top is onlapped by Miocene to Recent sediments.

5. Salt structures and tectonic styles

Integration of field mapping, well data and seismic interpretation has made it possible to map the salt structures of the Algarve Basin (Fig. 5). The basin is characterized by a variety of types of salt structures, of which diapirs, salt walls and allochthonous salt bodies are the most relevant. Structural style of the salt structures in the Algarve Basin depends on the variation in the lithological characteristics and thickness variations of the Hettangian evaporitic layer, from the proximal areas to the distal parts of the basin, as well as on the location of structures with respect the extensional fault system that resulted from crustal thinning of the SW Iberian margin. This section describes the different type of salt-related features, their origin and evolution, and their distribution.

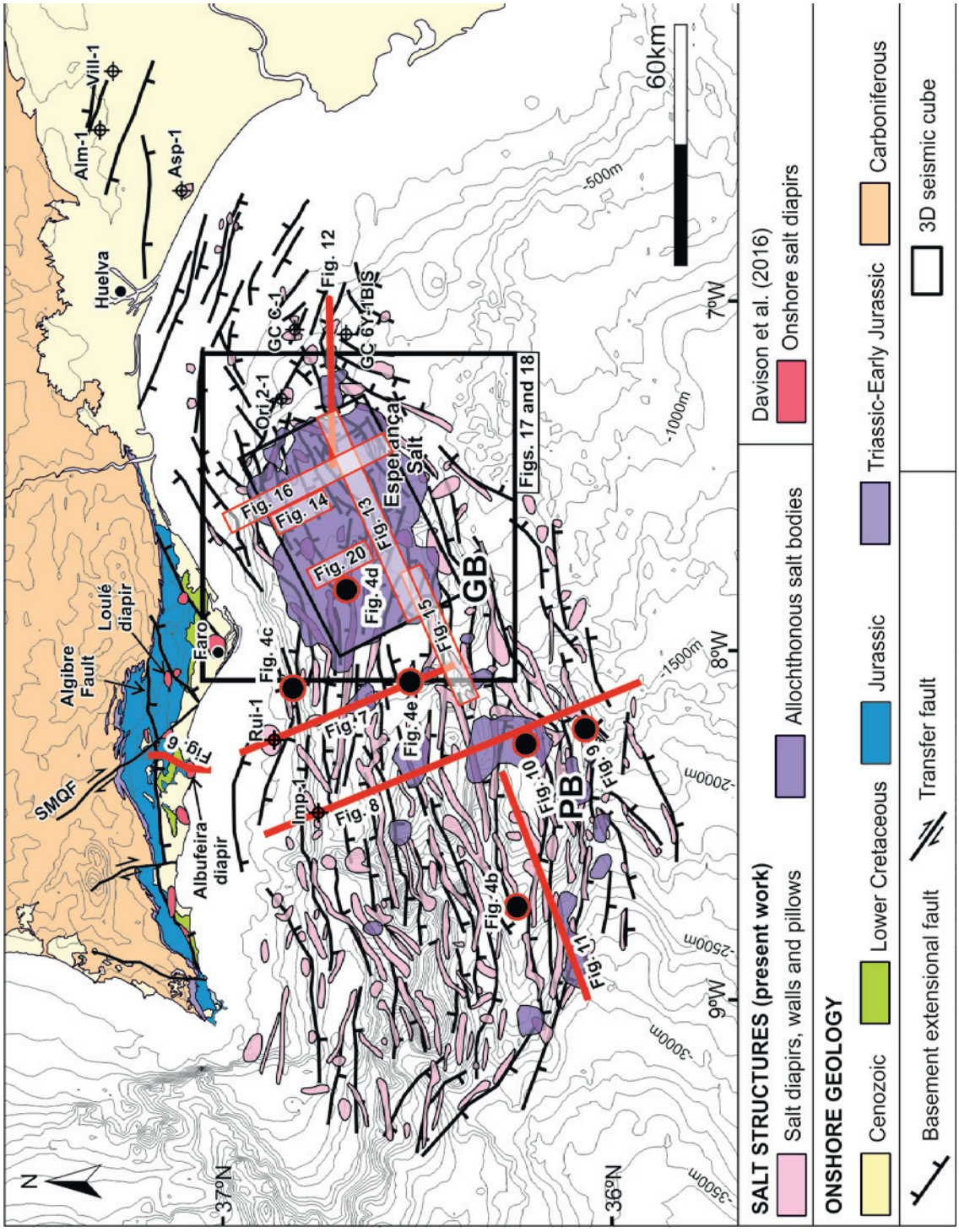

249

250 **Figure 5.** Map of salt structures and the basement extensional fault system in the Algarve Basin on the
251 SW Iberian margin. Autochthonous and parautochthonous salt structures mapped in this paper are
252 depicted by pink polygons, their area defined by the cut-off of the top of the Lower Jurassic.
253 Allochthonous units are shown by lilac polygons, mapped according to their greatest lateral extent.
254 Onshore diapirs are taken from Davison et al. (2016).GB: Guadalquivir Bank; PB: Portimão Bank. Notice
255 the same orientation and location between the basement extensional faults and the salt structures through

256 the margin, from onshore to offshore. The precise location of Figures 13 through 16 and 19, that cross the
257 3D seismic survey, are not shown due to confidentiality issues; the outline of the 3D seismic cube is
258 shown nonetheless.

259 *5.1. Onshore and proximal-offshore e salt structures (marginal Algarve Basin)*

260 Along the northern and eastern, onshore margin of the Algarve Basin, Hettangian evaporites are thin,
261 dominated by anhydrite interbedded with abundant shales and they do not develop any significant diapiric
262 deformation. Major structures in the evaporites onshore only appear in the basin south of the Algibre
263 Fault (Ramos et al., 2016) (Fig. 5). South of this fault evaporite thickness increases significantly and so
264 does halite content (in excess of 90% halite in the Loulé diapir, for instance Lopes et al., 1998).

265 Along the Algibre Fault and to the south, numerous salt diapirs have been documented in the area
266 (Davison et al., 2015; Ramos et al., 2016; Terrinha, 1998; Figs. 5 and 6). Diapirs are mostly located in the
267 hanging-wall of the regional Algibre Fault (Fig. 5). To the east, diapirs lie in the footwall of NE-SW
268 trending extensional faults (Fig. 5). Diapirs developed during the Jurassic and Early Cretaceous and were
269 subsequently reactivated and squeezed during the Paleogene-Miocene contractional deformation (Davison
270 et al., 2016).

271 Thick evaporites south of the Algibre Fault also act as a major décollement level between the Triassic
272 red beds and the overlying Mesozoic. For instance, the roll-over geometry of the Jurassic syn-rift
273 sediments in the hangingwall of the Algibre extensional fault and the subsequent tightening of the roll-
274 over anticline during the Cenozoic inversion suggest decoupling of the Mesozoic succession from the
275 basement and Triassic sediments along the Hettangian evaporites (Fig. 6; Ramos et al., 2016). This
276 decoupling also accounts for the development of a minor Jurassic extensional roll-over structure in the
277 footwall of the Algibre Fault that was thrust over Cretaceous sediments during Cenozoic inversion by the
278 Algibre Thrust (Fig. 6).

279 South of the Algibre structures the Hettangian evaporites also fed the Albufeira diapir (Fig. 6). This
280 diapir developed in the footwall of a non-outcropping basement-involved extensional fault that controlled
281 the deposition of the Jurassic succession. The relatively constant thickness of Upper Jurassic sediments
282 overlying the diapir suggest that the salt layer was welded in the hangingwall of the Algibre Fault at that
283 time, as the extensional roll-over continued to develop. The diapir subsequently collapsed during

continuous extensional deformation until Early Cretaceous times. Finally, the diapir was reactivated during the Cenozoic in contraction to form the observed thrusts, some of them inverting the previous extensional faults (Fig. 6).

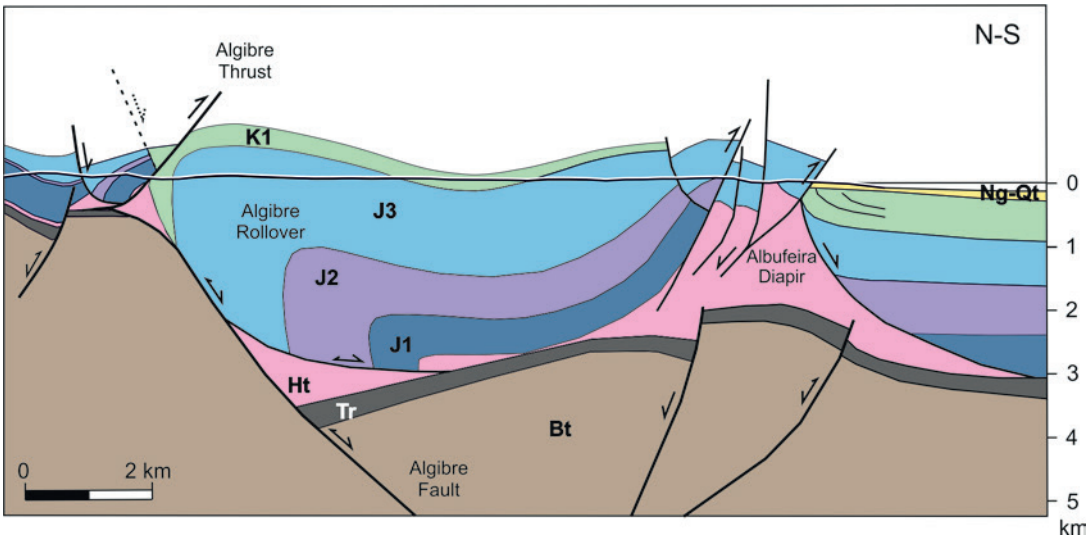

Figure 6. Cross section of two onshore salt related structures: the Algibre rollover, the Algibre Thrust and the Albufeira diapir. Evaporite thickness is controlled by the extensional Algibre Fault. See Figure 5 for location and Figure 7 for legend. Modified from Ramos et al. (2016).

Offshore, in the present-day shelf area, salt rollers developed related to listric extensional faults detached on the Hettangian evaporites. Locally, these rollers evolved to diapirs similar to the onshore salt structures, with their source layers possibly welding at the end of the Middle Jurassic (for instance, the diapir under the Ruivo-1 well on Fig. 7).

The present-day shelf-break area is marked by the presence of diapirs that grew at least until the Late Jurassic and possibly the Early Cretaceous, inferred to be sourced by a thicker initial salt layer. This is the case of the diapir/salt wall under the Imperador-1 well (although later squeezed by Cenozoic compression, Fig. 8). Despite the lack of good quality seismic profiles in the area, it is interpreted that the diapirs pierced by the wells Gulf of Cadiz C1 and Orion 2-1 (Figs. 3 and 5) are analogous to the Imperador-1 structure. In the case of the Orion 2-1 diapir, the draping of Upper Miocene sediments on the diapir's caprock (Fig. 2) indicates diapirism, most probably driven by compression, lasted well into the Miocene in this area.

5.2. Salt structures in the deep offshore (distal Algarve Basin)

Most of the salt structures have developed in the distal parts of the Algarve Basin (Fig. 5). They are mainly evidenced by antiforms involving the BFU and part of the Neogene succession and in general by areas where the bottom of the Miocene sediments is structurally above the regional elevation (e.g., Figs. 7, 8 and 11). Thick packages of reflectors are adjacent to or in between these antiforms and they correspond to extensional basins or minibasins filled by Jurassic-Early Cretaceous sediments. Geometry of the depocenters and the adjacent antiforms cored by transparent seismic facies suggest that minibasins were formed by diapirism (Figs. 7 and 8). These structures and some of the faults were reactivated during the Late Cretaceous to Present contractional deformation.

In the deeper part of the basin short wavelength folds involving mostly the Upper Jurassic and Lower Cretaceous sediments, but also the Paleogene and Lower Miocene packages, have been interpreted as minibasins developed between salt diapirs. Some of these minibasins developed above thin sheets of allochthonous salt (Fig. 7). These allochthonous salt bodies developed from the diapirs in the footwall of the basement-involved extensional faults and, in general, extend less than 10km away from the main salt stock (Fig. 7).

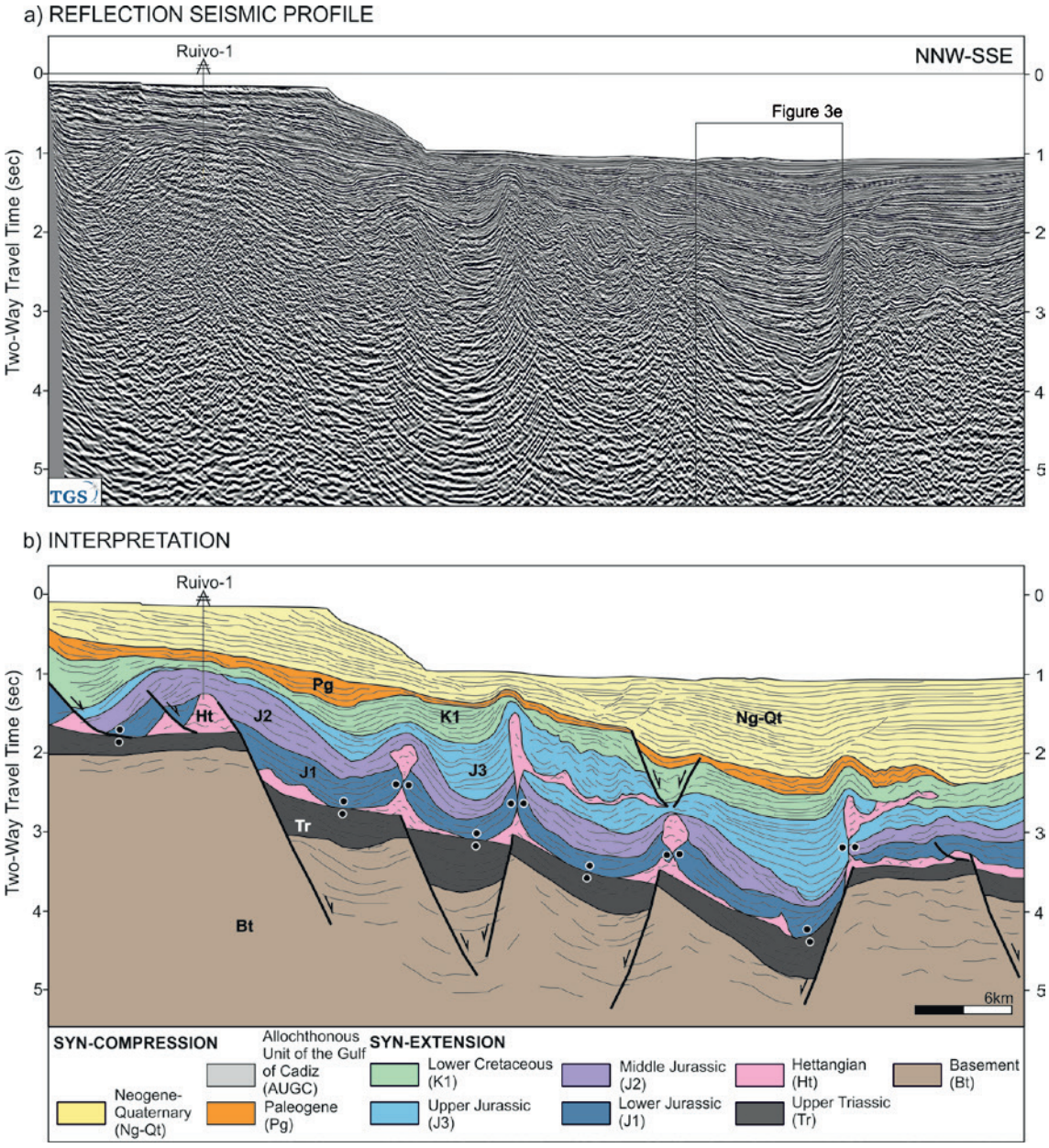

Figure 7. a) Seismic section in time. b) Interpreted section illustrating various salt-related structures and their link to underlying basement structures. See Figure 5 for location. Data courtesy of TGS.

The persistence along strike of salt structures above some of basement-involved faults on multiple seismic profiles has been interpreted to mean that some of these salt structures are in fact salt walls, as opposed to merely isolated diapirs (Fig. 9). As a general trend, the interpretation of the 2D seismic lines show that salt walls possibly become more dominant in the southern and western part of the Algarve Basin (Fig. 5). The western portion of this basin also has a greater presence of allochthonous bodies (mainly salt tongues, Fig. 10) and tear-drop diapirs with broader bulbs (Figs. 5 and 8).

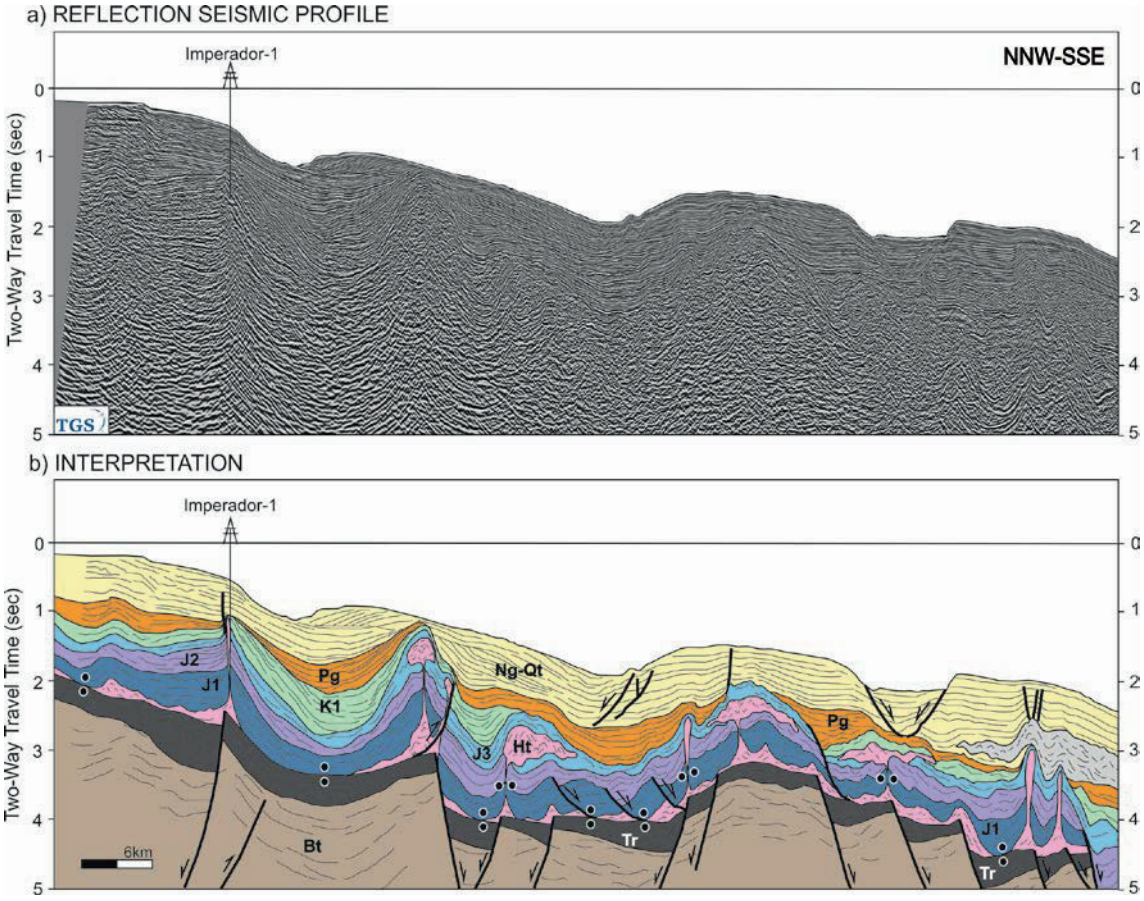

329

330 **Figure. 8** a) Seismic section in time across the Imperador-1 well in the western Algarve Basin. b)
331 Interpretation of the seismic line showing numerous salt pillows, diapirs and allochthonous salt bodies.
332 Note locally the presence of extensional and reverse faulting detaching on the Hettangian autochthonous
333 salt unit, and the location of many salt structures above the footwall of basement extensional faults. See
334 Figure 5 for location and Figure 7 for legend. Data courtesy of TGS.

335

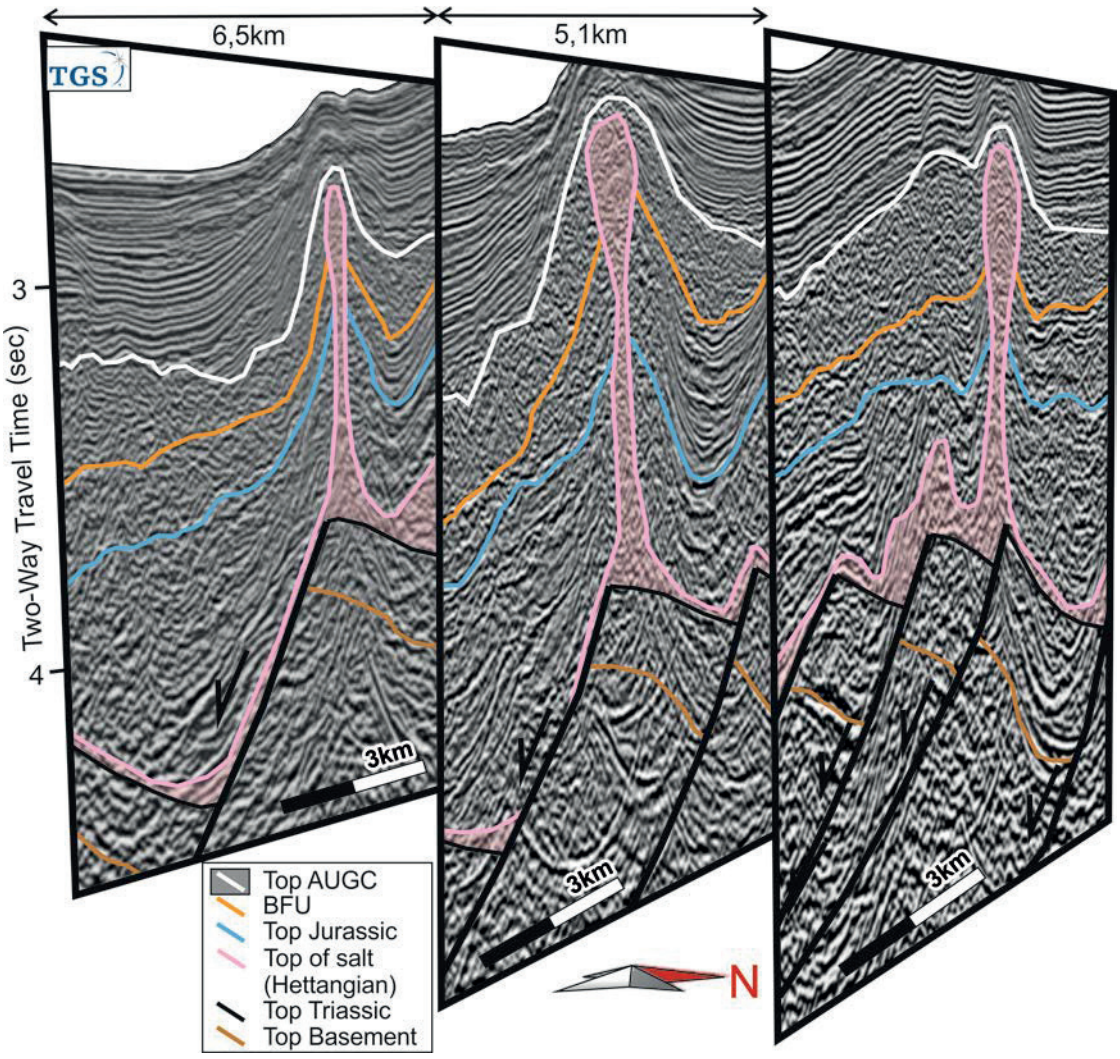

Figure 9. Oblique 3D view of 3 parallel seismic sections across a salt wall formed above the footwall of a Mesozoic-age extensional fault. BFU: Basal Foredeep Unconformity. See Figure 5 for location. Data courtesy of TGS.

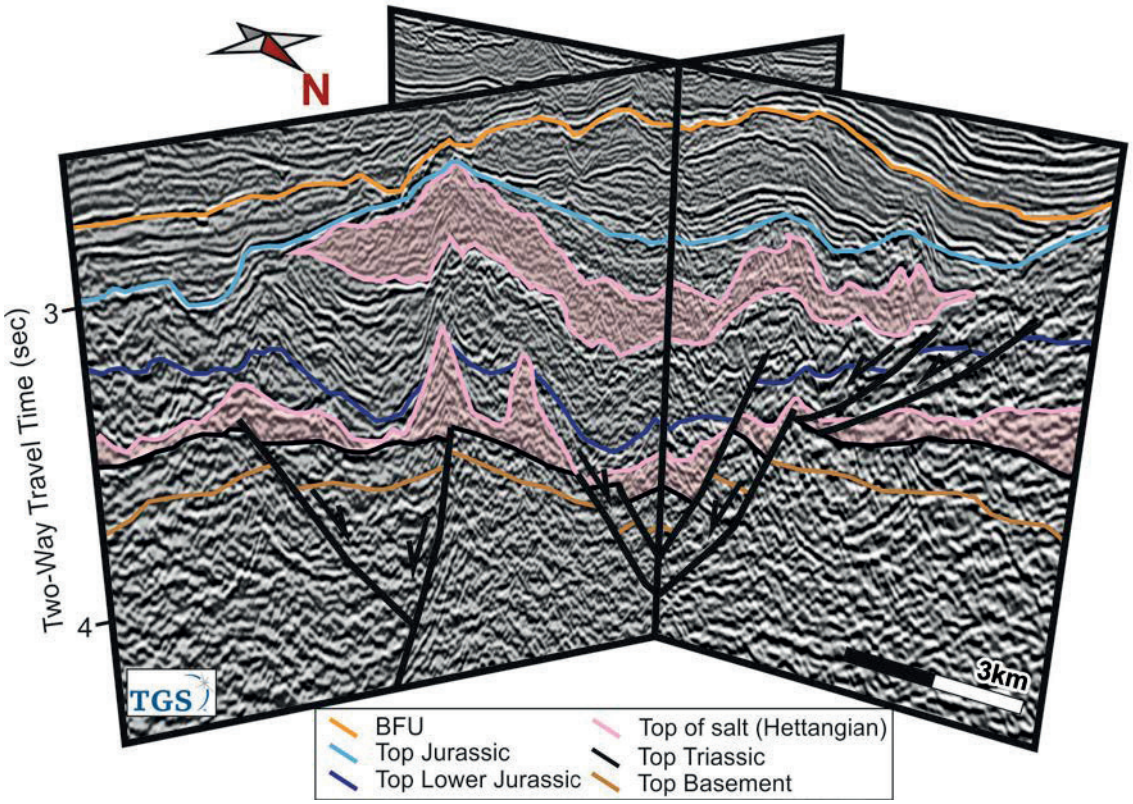

341

342

343 **Figure 10**. Oblique 3D view of two intersecting seismic sections across an allochthonous salt wing. See
344 Figure 5 for location and Figure 9 for legend. Data courtesy of TGS.

345 In this western part of the Algarve Basin, salt structures grow by downbuilding of the Mesozoic
346 layers from Early Jurassic to Early Cretaceous (Figs. 7 and 8). Paleogene sediments locally thicken into
347 minibasins (e.g., south of well Ruivo-1 on Fig. 7) or expulsion features (e.g. Paleogene fault and
348 depocenter on the southern part of Fig. 8).

349 Growth of salt structures by downbuilding is interpreted to have ended mostly by Paleogene times in
350 agreement with the distribution and thickness of the Paleogene sediments. Generalized downbuilding and
351 passive growth of diapirs is only seen to continue past the Paleogene in the westernmost part of the study
352 area (Fig. 11, and Dom Carlos diapir on the Portimão Bank; refer to Fig. 9 of Ramos et al., submitted).
353 Thickening of Miocene units towards these diapirs and the position of the salt bulbs within Miocene
354 sediments indicate that downbuilding activity lasted at least into the Early or Middle Miocene. Such
355 prolonged activity with similar overburden thickness possibly indicates a greater initial salt layer

thickness in the westernmost Algarve Basin than further east and north. Bathymetric relief above these diapirs (< 100 m) reflects reactivation due to squeezing of the salt stems.

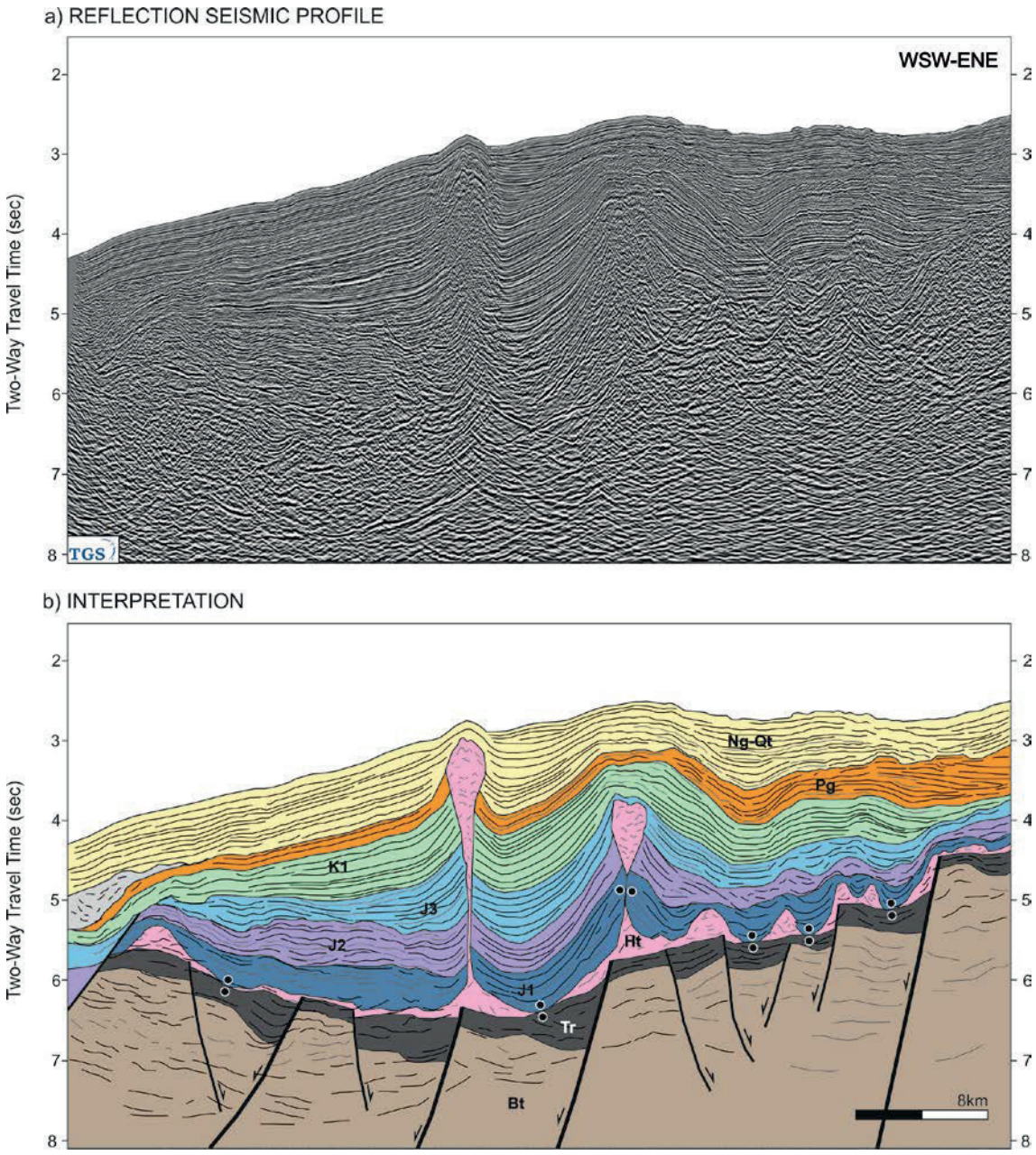

Figure 11. a) Seismic section in time across the westernmost Algarve Basin. b) Interpretation of the seismic line. Diapirs on this section have been active since Early Jurassic times to present. See Figure 5 for location and Figure 7 for legend. Data courtesy of TGS.

The easternmost part of the Algarve Basin is characterized by the presence of isolated diapirs (Fig. 5). The diapirs in this area mobilize large amounts of salt, generating large bulbs or associated allochthonous sheets (Fig. 12). However, spacing between salt structures is in general more similar to that

of the onshore and near-offshore part of the basin. In this eastern part of the basin, the control of basement-involved faults on the location of salt structures is more difficult to ascertain due to the poor quality of reflection seismic profiles, but it is assumed to be similar to that observed over the rest of the basin.

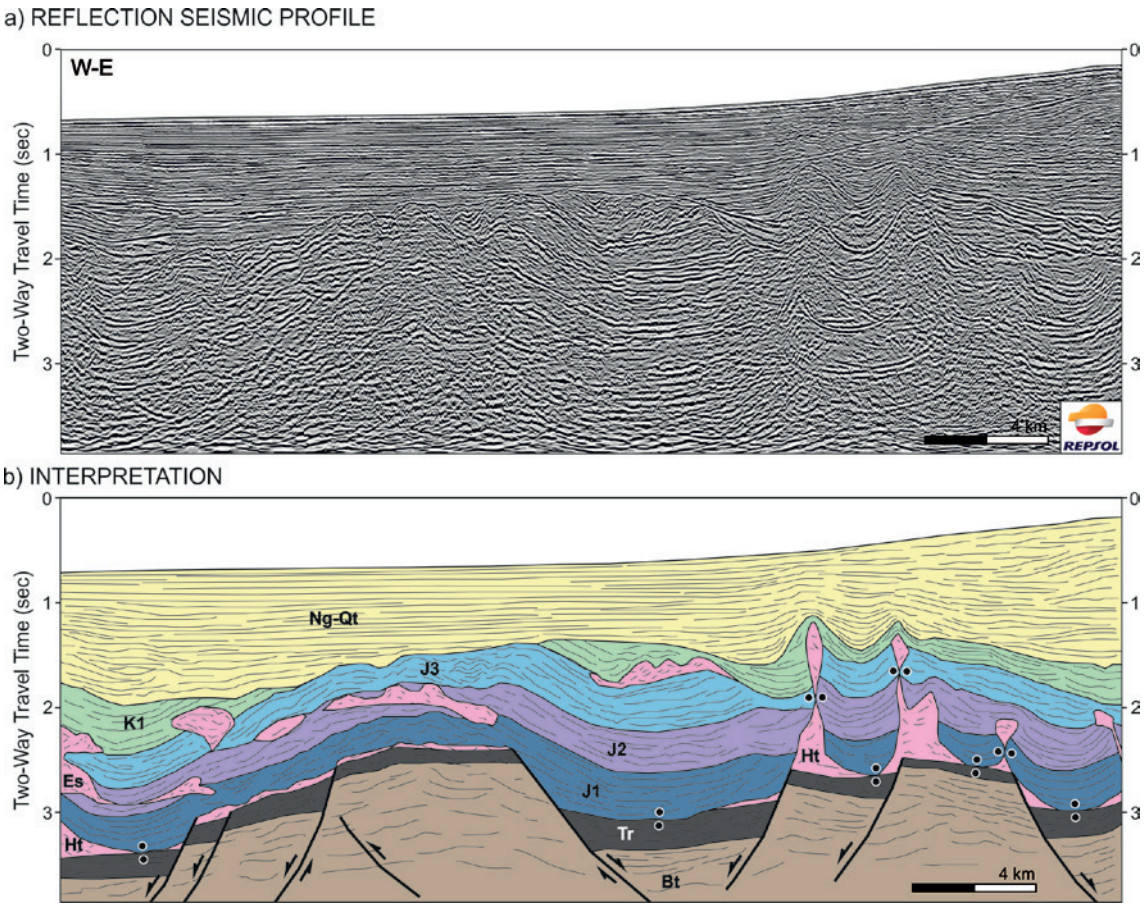

Figure 12. a) Seismic section in time across the eastern Algarve Basin. b) Interpretation of the seismic section. Es: Esperança salt structure. See Figure 5 for location and Figure 7 for legend. Data courtesy of Repsol.

In this sector, the BFU, which truncates the Upper Jurassic and Lower Cretaceous, is folded above diapirs, while the Upper Cretaceous and Paleogene is absent over large areas (Fig. 12). Miocene sediments onlap the deformed BFU over the diapir crests, in a manner similar to that observed in the western part of the basin. This is assumed to record Early Miocene compression and squeezing of diapir stems. The lack of Upper Cretaceous and Paleogene over parts of the eastern Algarve Basin is in part interpreted as a result of the shallower position of this part of the basin (less tectonic and thermal

subsidence during the Mesozoic) and also due to Late Cretaceous to Late Paleogene uplift of the basement (as recorded by the truncation of Lower Cretaceous strata below the BFU on Fig. 12).

5.3. The Esperança Salt Nappe

Perhaps the most striking feature of the Hettangian evaporite basin of the Algarve Basin is the Esperança Salt Nappe (Matias, 2007; Matias et al., 2011; Terrinha, 1998). This is the largest allochthonous salt body of the margin and is located in the transition between the western Algarve Basin, dominated by salt walls, diapirs and minor allochthonous bodies, and the eastern part of the basin isolated diapirs (Fig. 5). It extends over an area of approximately 1800 km^2, from the offshore Portugal-Spain border, in the east, to south of Faro in the west. To the north it is limited by the present-day shelf-break, whereas to the south it is limited by the Guadalquivir Bank.

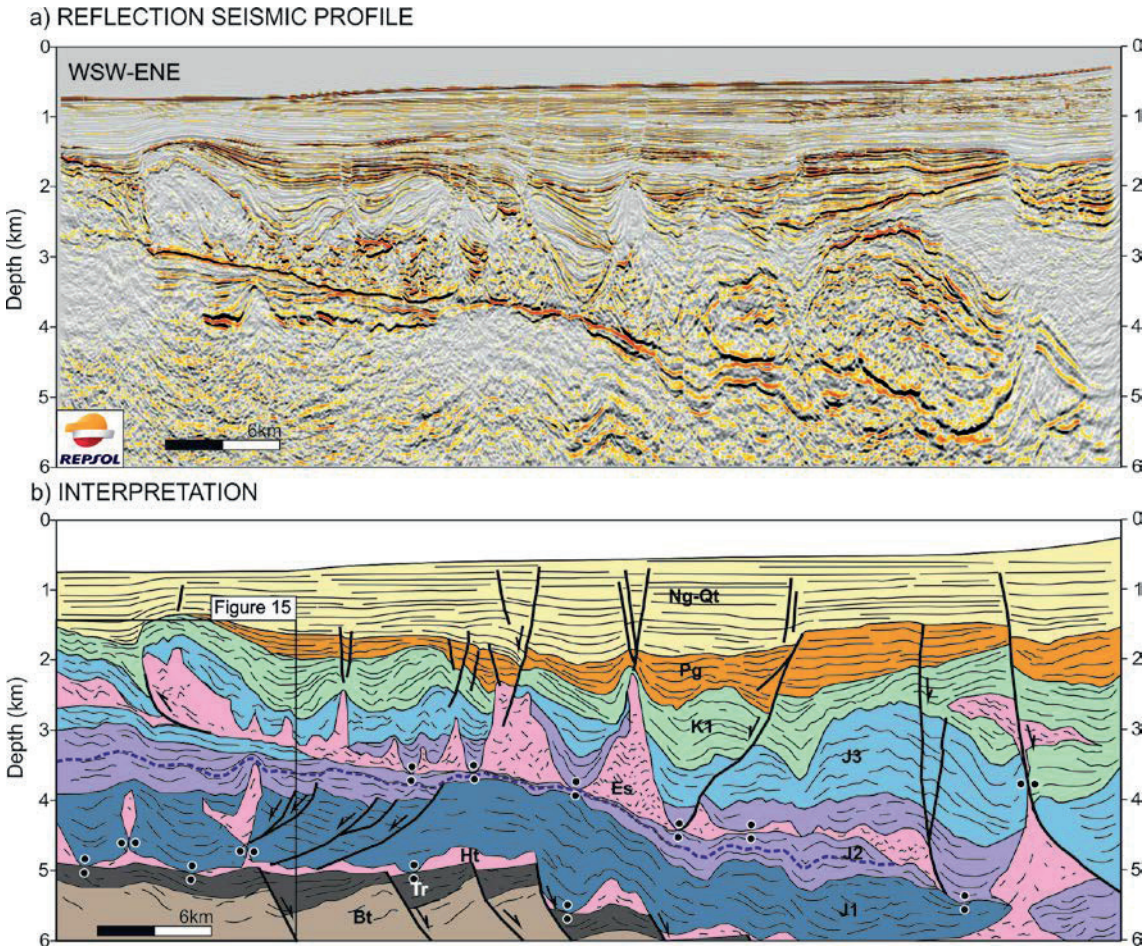

Figure 13. a) Seismic section in depth across the Esperança salt structure. b) Interpretation of the seismic section. The section shows how the base of the Esperança salt structure truncates progressively younger sediments towards the west. It also illustrates the contrast between the strong control of

394 halokinetics on sediments above the allochthonous Esperança salt structure, and the limited amount of
395 salt-related deformation observed below the salt structure, except for the eastern part of the section. The
396 dashed line within the Middle Jurassic is the unconformity mapped to generate the map in Fig. 17. See
397 Figure 5 for location and Figure 7 for legend. Es: Esperança Salt. Data courtesy of Repsol.

398 The Esperança salt body imaged on 2D seismic (Matias et al., 2011) but it is now better characterized
399 by combining regional 2D seismic with 3D seismic. The Esperança salt structure is characterized by a
400 continuous strong reflector at its base and a highly irregular top above which multiple minibasins have
401 developed (Fig. 13). The base of the Esperança salt structure is a very smooth surface and is observed to
402 truncate underlying Jurassic sediments (Figs. 13, 14 and 16) indicating the salt body climbed up
403 stratigraphy from east to west (Fig. 13) and from north to south (Figs. 14 and 16). The base of the
404 allochthonous salt is highly continuous and smooth and is not affected by Jurassic age faulting, unlike the
405 autochthonous Hettangian evaporite unit. The age of the sediments underlying the Esperança salt
406 structure is correlated from wells Ruivo-1 and Imperador-1 in the Portuguese offshore, given the good
407 image quality of the 2D seismic profiles. Despite the uncertainties in the interpretation, it is believed that
408 the westernmost tip of the Esperança Salt is emplaced on top of Upper Jurassic or even Lower Cretaceous
409 sediments (Fig. 15). Below the Esperança Salt, the thickness of Jurassic sediments varies, but overall
410 thickness of the entire Mesozoic above and below the allochthonous salt remains mostly constant across
411 the area (Figs. 13 and 16)., Jurassic sediments thin and young towards the west above the allochthonous
412 salt layer, with only some Upper Jurassic capping the Esperança Salt at its leading edge (Fig. 13).

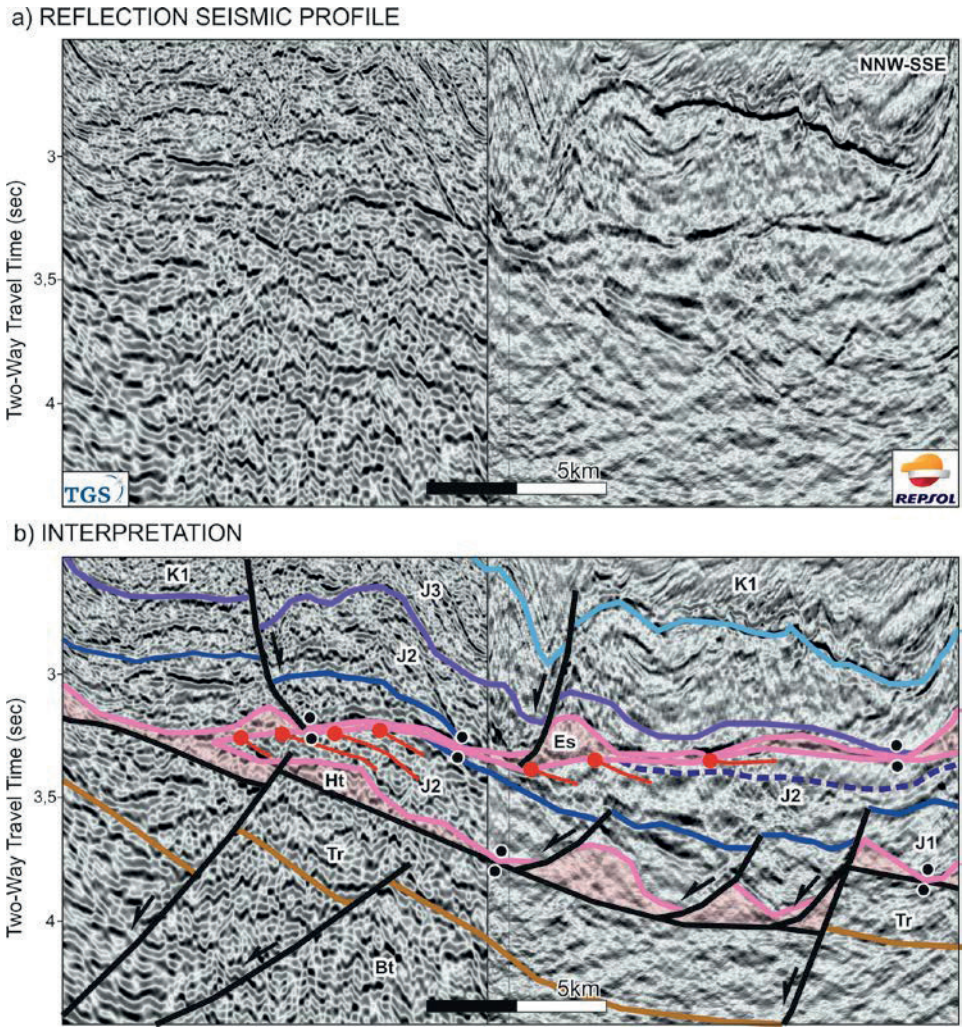

413

414 **Figure 14**. a) Composite seismic section in time across the central Algarve Basin. b) Interpretation of the
415 composite seismic section in time showing a detail of the truncations of Lower and Middle Jurassic
416 horizons under the Esperança Salt. The right panel of the seismic composite is from the PSTM version of
417 the 3D volume, the left panel is from the PDT00-PD00 survey. The dashed line within the Middle
418 Jurassic is the unconformity mapped to generate the map in Figure 17. See Figure 5 for location and
419 Figure 7 for legend. Data courtesy of TGS and Repsol.

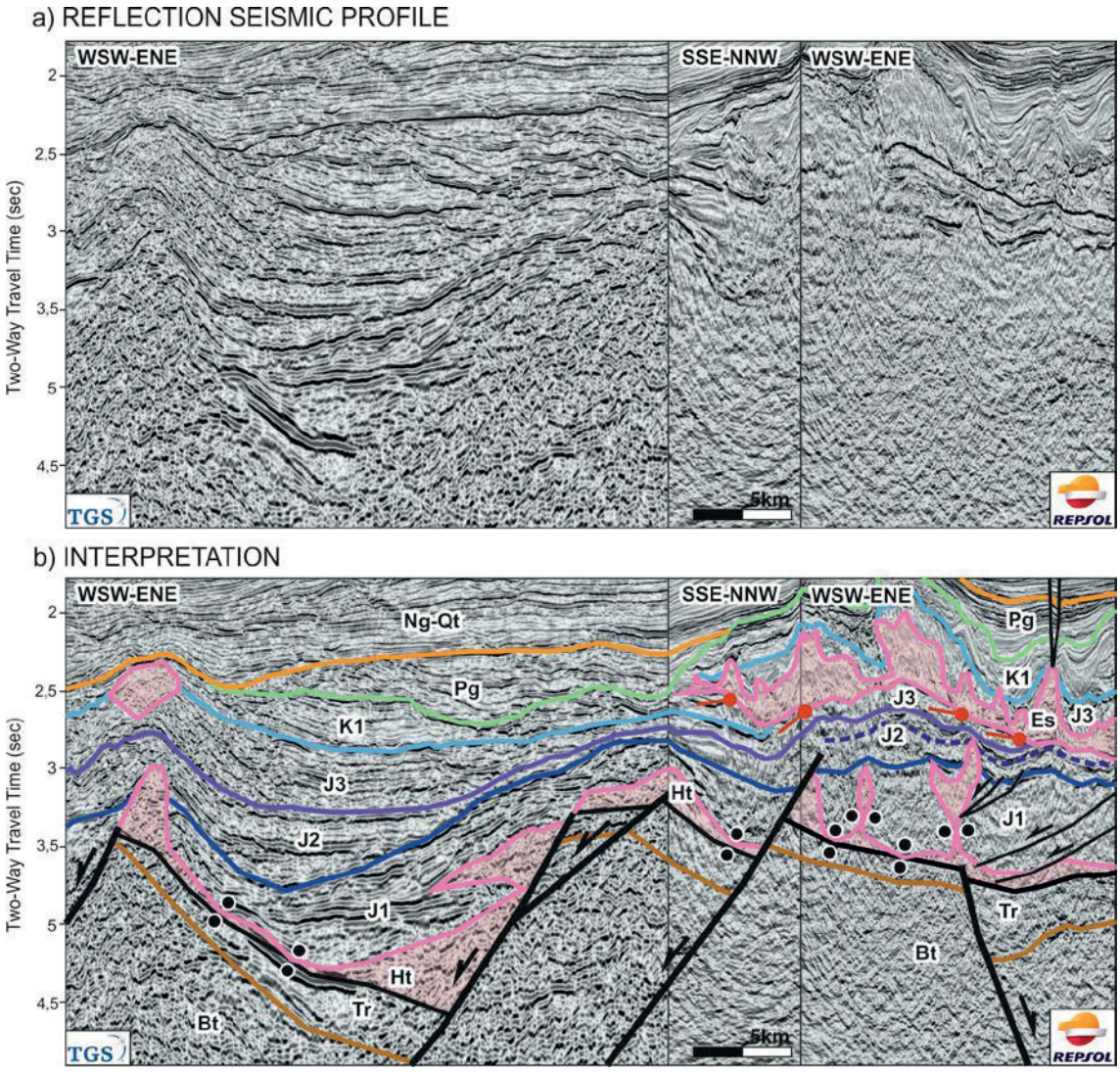

420

421 **Figure 15**. a) Composite seismic section in time across the central Algarve Basin. b) Interpretation of the
422 composite seismic section across the western termination of the Esperança salt structure (Es) showing the
423 correlation of sub-salt horizons. The two panels on the right are from the 3D seismic PSTM volume (in
424 contrast to the PSDM version on Figure 13) and the left panel is from the PDT00-PD00 survey. See
425 Figure 5 for location and Figure 7for legend. Data courtesy of TGS and Repsol.

426

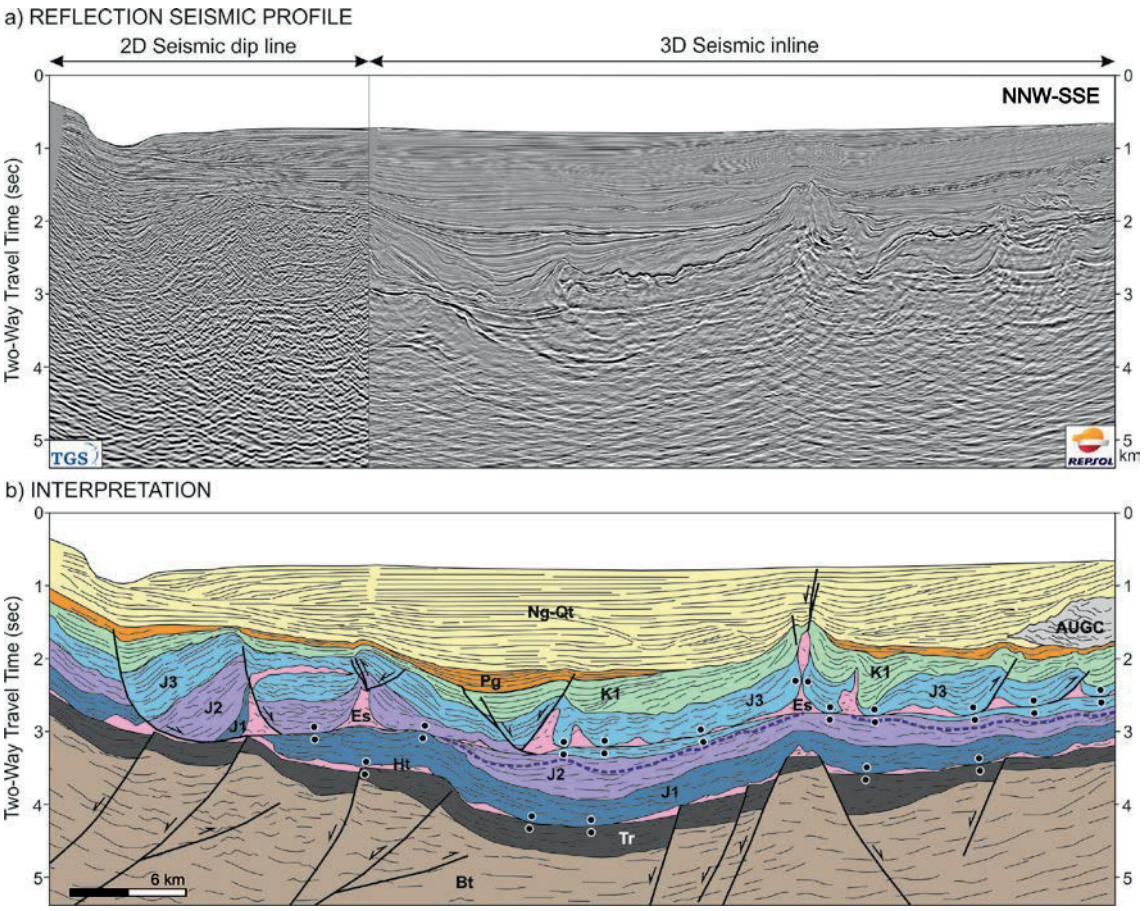

427

428 **Figure 16.** a) Composite section in time between a 2D seismic line and an inline from the 3D seismic
429 cube across the Esperança salt structure and the area that connect both autochthonous and allochthonous
430 salt unit to the north b) Interpretation of the seismic section. The base of the Esperança Salt ramps up to
431 the south, truncating Jurassic units below. Note that the southward tilt of the basement and Mesozoic
432 units along the northern end of the section is related to Cenozoic inversion. The dashed line within the
433 Middle Jurassic is the unconformity mapped to generate the map in Fig. 17. See Figure 5 for location and
434 Figure 7 for legend. Data courtesy of TGS and Repsol.

435 The source of the allochthonous salt of the Esperança salt structure has been mapped by picking the
436 intersection between the base of the Esperança Salt and three Jurassic markers: the base of the Sinemurian
437 (the top of the autochthonous evaporite unit), a Middle Jurassic unconformity (unconformity shown on
438 Figs. 13, 14 and 16), and the top of the Middle Jurassic. The trace of the two deeper intersections (the
439 base of Sinemurian and the Middle Jurassic unconformity) indicates the source for the allochthonous salt
440 is elongate and over 80km long (Fig. 17). Both intersections define a roughly L-shaped trace in map view:
441 trending WSW-ENE along the north and NNW-SSE along the east of the Esperança Salt (Fig. 17). The

relative position of the intersections indicates that salt was emplaced over a feeder ramp that climbs up to the south and west. This pattern is consistent with the trace of the intersection of the top of the Middle Jurassic and the base of the Esperança Salt (Fig. 17).

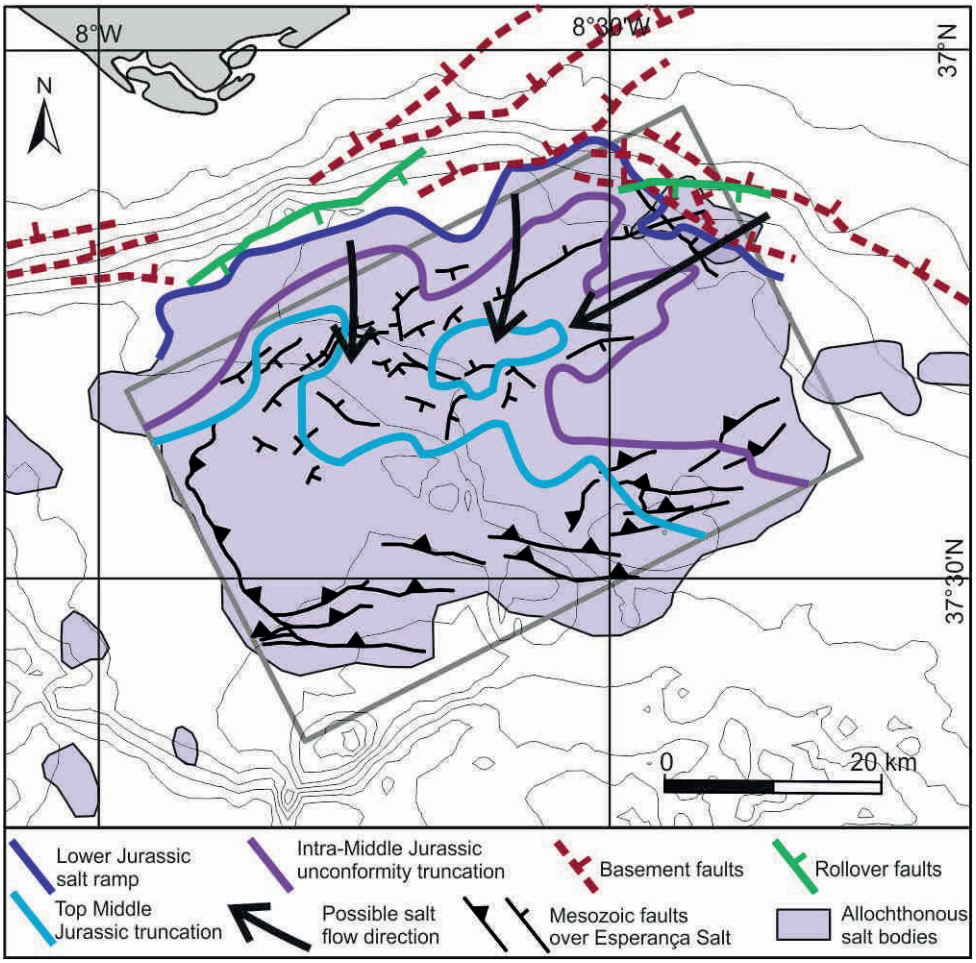

Figure 17. Map of features associated with the emplacement of the Esperança Salt. The Lower Jurassic salt ramp refers to the intersection between the top Lower Jurassic and the base of the Esperança Salt structure. Grey thin lines: bathymetry contour lines separated each 100m. The intersection of the base of the Esperança Salt with 3 underlying Jurassic horizons indicates south and west directed emplacement, consistent with supra-salt deformation features indicating extension in the north and contraction along the southern and western edge of the allochthonous salt. The L-shaped trace of the feeder ramp for the Esperança Salt is related to the configuration of basement faults that controlled evaporite deposition. In this map only a selection of basement faults is shown; a more complete map can be seen in Figure 19.

The extensional collapse of the overburden by south-dipping extensional supra-salt faults in the northern portion of the Esperança body, suggest that the overall transport of the allochthonous salt is

south and west directed. This extension is reflected in WSW-ENE and NW-SE extensional faults of variable throw and dimension, and their associated Mesozoic depocenters (Figs. 13 and 16). South and west directed progression of the allochthonous salt also led to the formation of thrusts and shortening features along the southern and western edges of the Esperança Salt (Figs. 13 and 16). The strike of these contractional features is consistently NW-SE WSW-ENE (perpendicular to salt emplacement). When these features are mapped out, a clear pattern emerges (Fig. 17) in which the northern and northeastern portions of the Esperança salt structure are bordered by the feeder ramp and dominated by supra-salt extensional collapse features, whereas the southern and western edges are dominated by supra-salt thrusts and folds.

The origin of the L shape in the feeder ramp is interpreted to relate to the geometry of the basins from which the Esperança Salt is sourced. Regional mapping and seismic interpretation reveal the presence of both WSW-ENE and NW-SE trending basement faults (as already indicated by Matias et al., 2011, and Ramos et al., 2016). The inflection in the feeder ramp coincides with the intersection of two trends of basement faults striking WSW-ENE and NW-SE (Fig. 17). These landward-dipping faults are interpreted to have led to thicker evaporite deposition immediately to the north and east of the Esperança Salt (Fig. 18). After an early stage of limited basement faulting and sedimentation during the Early Jurassic, an increase in basement faulting and sediment accumulation during the Middle Jurassic led to salt inflation in the footwall of the basement faults leading to the development of diapirs and salt rollers (Fig. 18). Sediments above these diapirs and salt rollers collapsed above basinward-dipping listric extensional faults driving initial expulsion of salt (Fig. 18). Where seismic quality permits rollover anticlines related to the process of expulsion can be mapped to strike parallel to the basement-involved faults and the feeder ramp (Fig. 17). Once the initial canopy was emplaced, it was remobilized by roof sedimentation leading to its allochthony (e.g., Diegel et al., 1995; Peel et al., 1995; Schuster, 1995; Fig. 18). The result of this process is that the basal ramp of the salt sheet gradually truncates the underlying stratigraphy during emplacement. This mechanism of emplacement can be accounted for with a limited amount of salt. The final configuration observed for the northern margin of the Esperança Salt is conditioned by the inversion of Mesozoic extensional faults which imposes a southward tilt on this part of the basin (Fig. 16).

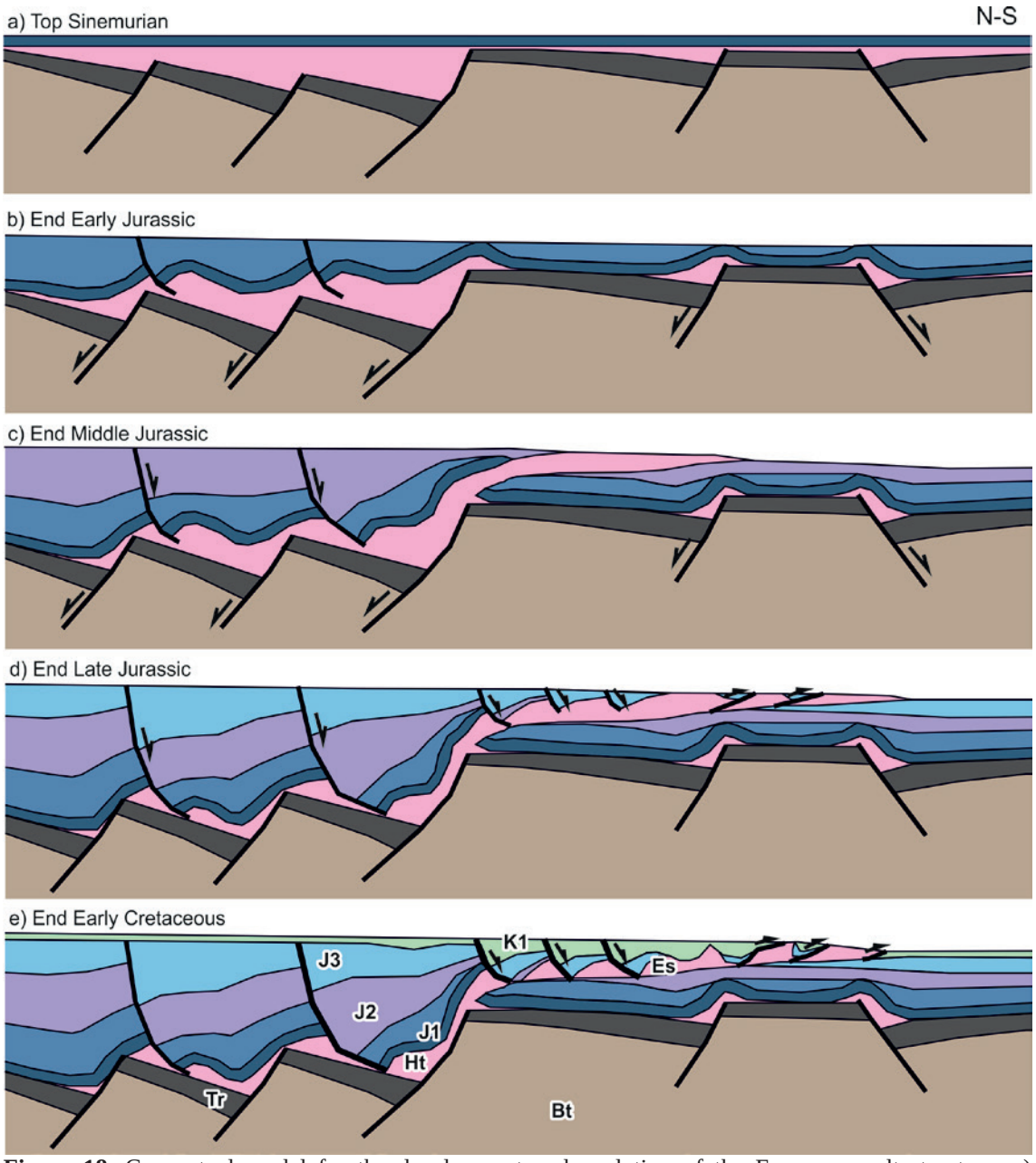

Figure 18. Conceptual model for the development and evolution of the Esperança salt structure. a) Evaporite depocenters formed during the Hettangian in fault-bounded half-grabens are capped by Sinemurian units during a period of tectonic quiescence. b) Reactivation of basement faulting during the latter part of the Early Jurassic causes initial development of salt rollers due to extension of the overburden. c) Continued extensional faulting of the basement during the Middle Jurassic caused basement fault blocks to tilt further basinward, facilitating the development of listric extensional faults and salt evacuation basinward above a relative basement high. d) Welding in the feeder area coincides with the final stages of extension in the Late Jurassic. A roho system developed above the salt sheet with a linked contractional system at the toe. e) During the Early Cretaceous, basement faulting had ceased and evolution of the Esperança salt structure was controlled by sediment-driven salt evacuation. The

Continent-Ocean Boundary is located south of the sketch. This sketch do not incorporate horizontal nor vertical scale. Horizontal scale is approximate to the Figure 16, and vertically exaggerated. See Figure 7 for legend.

The structure of the basement under the Esperança Salt (and the overlying sub-salt Jurassic sediments) has been interpreted based on the integration of seismic interpretation with gravity data (Fig. 19, Ramos et al., submitted grav). As discussed for the geometry of the feeders, basement-involved faults under the Esperança Salt trend both WSW-ENE (parallel to the SW Iberia passive margin) and NW-SE (a trend interpreted to represent transfer faults in the Mesozoic extensional system, Matias et al., 2011; Ramos et al., 2016). The western edge of the Esperança Salt coincides with a basement high (Figs. 13 and 15) defined by a series of NW-SE faults (Fig. 19a). Likewise, towards the south the Esperança Salt is bounded by the Guadalquivir Bank (Fig. 19a), which was an intra-basinal high throughout the Mesozoic (Ramos et al., 2017a), and acted as a backstop for the salt advance to the south.

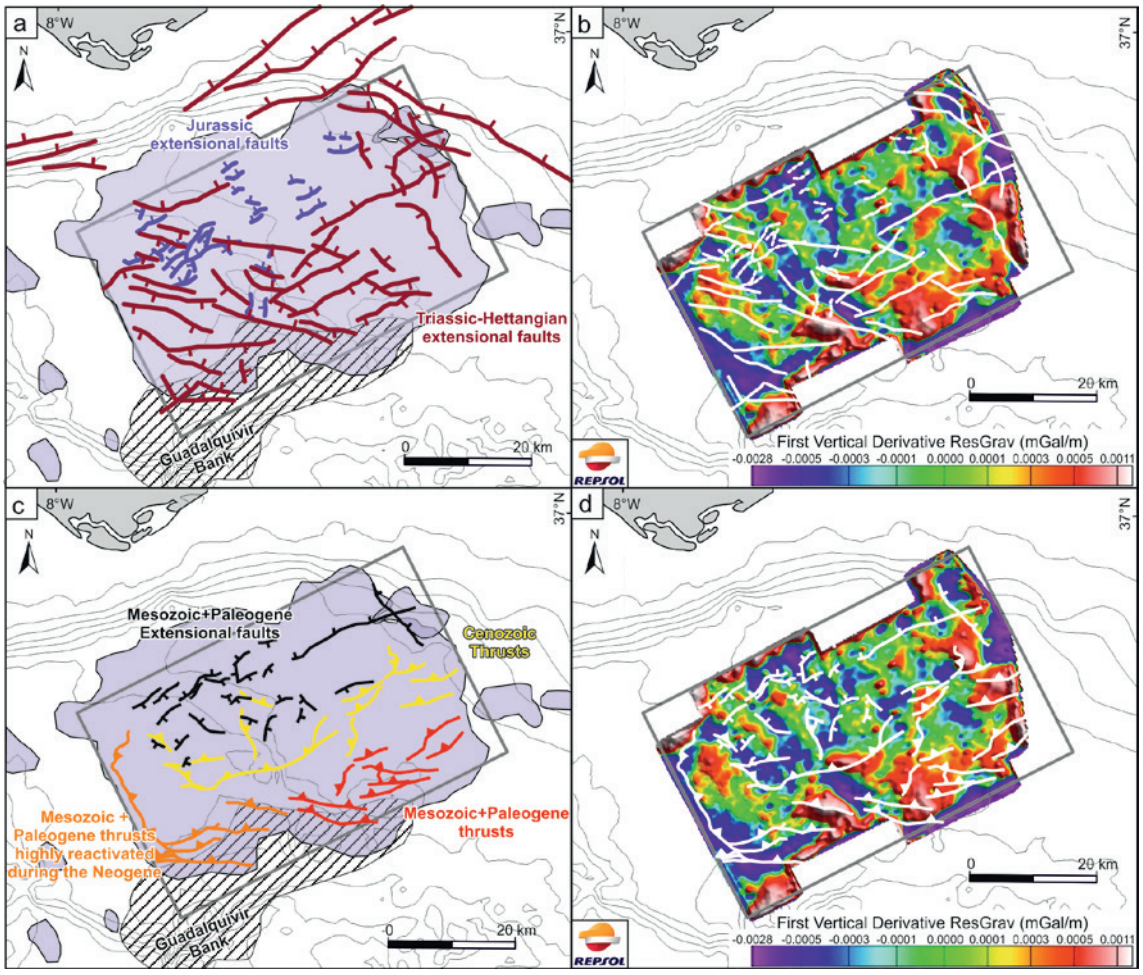

Figure 19. Maps of sub- and supra-Esperança structures and their gravimetric signal. a) Sub-Esperança structures: Mesozoic-age extensional faults affecting the basement (brown) and shallow detachment faults causing tilting of Jurassic fault blocks (purple). b) Overlay of the structures in (a) on a map of the first vertical derivative of the second-order residual Bouguer anomaly. c) Supra-Esperança structures: Extensional faults (black) and thrusts (red and orange) related to the emplacement of the Esperança Salt in the Mesozoic, and Cenozoic-age thrusts detached in the Esperança Salt formed during contraction (yellow). d) Overlay of the structures in (c) on a map of the first vertical derivative of the second-order residual Bouguer anomaly. See Fig. 5 for location. Data courtesy of Repsol

Above the basement, and under the Esperança Salt, Early and Middle Jurassic sediments are observed to thin and thicken in response to ongoing basement faulting and halokinesis of the autochthonous evaporite layer, but without major salt-related structures (e.g. salt diapirs or salt walls). These sub-Esperança Jurassic units are faulted into tilted blocks, with some faults detaching within the autochthonous evaporite (Figs. 13, 14 and 20). Faults detached within the autochthonous evaporite layer appear to be distributed over most of the area, but due to limited sub-salt imaging, they are only seen unambiguously in some sectors. Where these faults can be mapped (Fig. 19a) they have reduced throw (hundreds of meters), are only a few kilometres long, and do not have a measurable gravimetric response (Fig. 19a,b) which differentiates them from basement-involved faults.

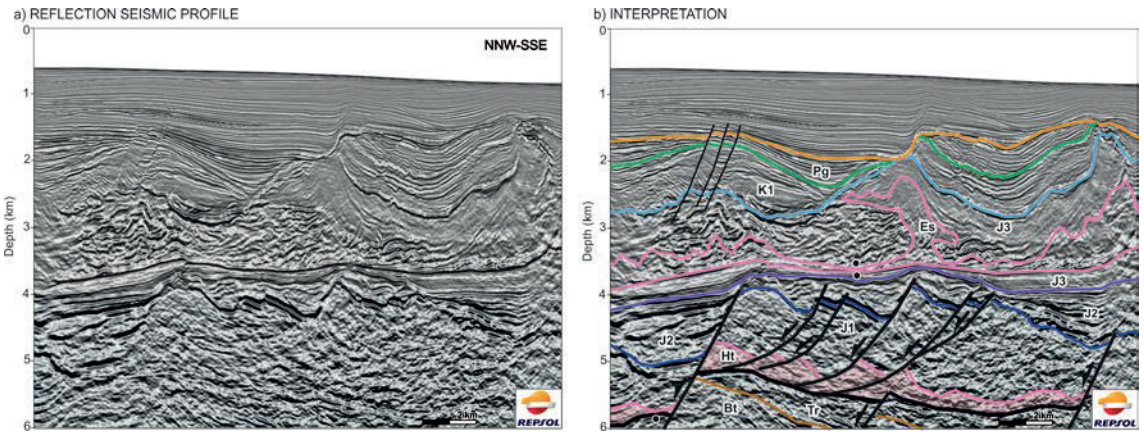

Figure 20. Seismic section in depth across the Esperança Salt showing a detail of sub-salt deformation. Transparent facies below the Middle Jurassic (J2) are interpreted to correspond to the Lower Jurassic (J1) in line with similar facies on other sections in the area. An alternative interpretation with a thinner Lower Jurassic and thicker autochthonous Hettangian evaporite layer cannot be completely ruled out. This

section is taken from the PSDM version of the 3D seismic cube (limited to 6km depth). The PSTM version of the 3D seismic does not provide adequate imaging of the subsalt section. See Figure 5 for location and Figure 7 for legend. Data courtesy of Repsol.

The style of deformation of the subsalt Jurassic contrasts with that observed above the Esperança Salt and the areas surrounding the Esperança Salt. The sediments above the Esperança Salt are influenced by the intense diapirism (Figs. 13 and 16) and the development of a linked extensional-contractional system (as discussed above). The structure above the Esperança Salt is further complicated by the presence of post-Mesozoic shortening (Ramos et al., 2017a) that causes reactivation of some salt structures in compression (e.g., uplifted tip of the allochthon and deformation of Cenozoic and Mesozoic sediments in Fig. 13, or tightening of the diapir in the south-central portion of Fig. 16, and thrusts in Fig. 5 in (Ramos et al., 2017a). Contractional structures dominantly reactivate pre-existing salt structures trending WSW-ENE and they cause folding of Mesozoic, Paleogene and Neogene strata. In contrast, some of the older thrusts and folds associated with the Jurassic emplacement of the allochthonous salt do not affect Neogene strata (southern end of Fig. 16). The gravimetric response of this complex system of Mesozoic and Cenozoic supra-salt extensional and contractional faults is also observed on gravity anomaly maps (Fig. 19c,d). Despite deformation on the allochthonous salt body being mostly fossilized, local collapse and reactivation of some salt structures have continued throughout the Cenozoic(e.g., Fig. 13).

6. Discussion

The interpretation and mapping of salt-related structures in the Algarve Basin makes it possible to characterize the Hettangian evaporite basin and its evolution. This has been done by firstly defining domains within the basin that show different styles of deformation. The extent of these domains can be correlated with the evaporite facies and their initial thickness. The relationship between individual salt structures and their surrounding sediments then makes it possible to define how salt-related structures evolved in the basin.

6.1. Domains of salt tectonics and their relation to the Hettangian evaporite basin

The Algarve Basin can be subdivided into three main domains based on the deformation style observed for salt-related structures (Fig. 21a). The northern and eastern onshore margin of the basin is mostly devoid of salt-related structures due to the reduced thickness of the Hettangian evaporites (mostly

561 <100m). In this sector the Hettangian succession is mostly dominated by claystone and anhydrite
562 (onshore column by Rocha, 1976, wells Almonte-1 and Villamanrique-1 in Fig. 2). This domain devoid
563 of any major salt-related structures defines a roughly 30km wide strip running along the northern and
564 eastern onshore basin margin.

565 To the south and west, as the evaporite units thicken, a domain of isolated diapirs, salt rollers salt
566 pillows developed (Fig. 6, northern end of Figs. 7 and 8 and the eastern end of Fig. 12). In this domain
567 halite is predominant and shales and dolomite tend to be reduced or absent (wells Ruivo-1, Asperillo-1,
568 GC C-1 in Fig. 2). This domain covers the onshore closest to the present-day coast and a swathe 30-60km
569 wide of the shallowest offshore (Fig. 21). Its northern boundary is locally marked by major basin-
570 bounding faults (e.g., the Algibre Fault, Figs. 4 and 6). In the central part of the basin, a extension of this
571 domain is seen along the Guadalquivir Bank and in the area now covered by the Esperança Salt (Fig.
572 21a): under the Esperança Salt, autochthonous salt-related structures are mostly limited to salt rollers
573 (Figs. 14 and 20), although some pillows and diapirs also exist (Figs. 13 and 15).

574 Finally, the central and southwest portion of the Algarve Basin is dominated by intense salt
575 tectonism. In this area diapirs are ubiquitous, with well-developed bulbs in most cases and locally
576 developing allochthonous salt wings. Most diapiric structures in this domain are controlled by underlying
577 basement-involved faults. Salt walls developed above the footwall of Mesozoic extensional faults (Fig. 9,
578 southern portion of Figs. 7 and 8). Despite the lack of well control in this domain, it is interpreted to be a
579 halite rich domain (in line with observations from wells Orion 2-1and GC C-1, Fig. 2).

580 The map of salt-related structures in the Algarve Basin (Fig. 5) has been used in conjunction with the
581 available well and outcrop data to infer the distribution of the dominant evaporitic facies of the
582 Hettangian basin (Fig. 21a), assuming that mineralogy of evaporites plays a major role in the mobility of
583 evaporites and hence in the style of deformation (e.g., Stewart, 2007; van Keken et al., 1993; Wagner and
584 Jackson, 2011; Zulauf et al., 2009). This map reveals a northern and eastern margin of the basin
585 dominated by claystone and dolomite, fringed to the south by a domain rich in anhydrite. Towards the
586 south and west evaporitic facies are interpreted to transition to a halite-rich environment. The result is a
587 bulls-eye pattern with the most soluble salts in the basin center (consistent with the observations of
588 Nichols, 2009, and the example of the North Sea Zechstein basin in Stewart, 2007) . This trend is only
589 locally disrupted along the Guadalquivir Bank (Fig. 21a), that acted as an intra-basinal high during the

590 Mesozoic and is assumed to present a facies equivalent to shallower parts of the basin (as documented by
591 well GC 6Y-1BIS).

592 The map of evaporite facies has been complemented with an estimate of the original stratigraphic
593 thickness of the Hettangian (Fig. 21a). Thickness has been calculated from outcrop data, seismic sections,
594 or well observations where deformation of the Hettangian is limited (e.g., GC 6Y-1BIS, Asperillo-1,
595 Almonte-1). Where deformation of the Hettangian unit is significant, particularly in the distal Algarve
596 Basin, the initial thickness has been estimated based on the total cross-sectional area of the Hettangian
597 interpreted at present-day, assuming the preservation of area on each section and no loss of evaporite
598 through time. These estimates provide a conservative estimate of initial evaporite thickness: the
599 magnitude of initial thickness may be incorrect, but the relative values and trends observed are assumed
600 to be representative. The result is a map that indicates progressive thickening to the south and west. The
601 transition in thickness from 400 to 600m appears to be particularly relevant as it marks the transition from
602 anhydrite to halite dominated facies as well as from the domain of isolated diapirism to the domain of
603 pervasive salt tectonism (Fig. 21a).

604 The map of evaporite facies and of deformation styles also reveals the relevance of Triassic to
605 Jurassic basement structures on basin evolution. The main trend observed in the map in Figure 21 is an E-
606 W trend dominated by the WSW-ENE trend of basement-involved extensional faults. The extent of
607 evaporites and salt structures along the northern margin of the basin is controlled by faults such as the
608 Espiche-Algibre and Faro-Tavira faults (Fig. 21b). Southward and offshore salt structures are controlled
609 by the progressive thickening of evaporites and the increase of the proportion of halite, as well as the
610 structure of the passive margin. The greatest, concentration of allochthonous bodies (aside from the
611 Esperança Salt) in the basin coincides with the western part of basin where the margin's necking domain
612 is broadest (as defined by Ramos et al., 2017b; Fig. 21b). Further to the east, in the area of the
613 Guadalquivir Bank and well GC 6Y-1BIS, the necking domain is narrower. There, the relative uplift of
614 the shoulder of the necking fault resulted in a thinner evaporitic succession with prevalence of anhydrite
615 that limited salt tectonism. To the south and southeast the transition to the oceanic crust underneath the
616 AWGC (ocean-continent transition, as defined by Ramos et al., 2017b) marks the present-day southern
617 limit of the evaporite basin.

618 The general E-W trend discussed above is interrupted by NW-SE trending transfer faults oblique to the
619 general trend of the WSW-ENE extensional faults (Ramos et al., 2016). One of these transfer faults, the
620 São Marcos-Quarteira Fault (SMQF; Figs. 5 and 21), marks a boundary between evaporite facies
621 observed in onshore and offshore diapirs (Fig. 21b). Its offshore continuation is not evident, but it is
622 probably relayed by a set of faults with equivalent trend that lie further to the east (Fig. 21b). This set of
623 faults controlled the evaporite depocenter from which the Esperança Salt was sourced (Fig. 19a and
624 discussion in Section 5.3) and accounts for the presence of pervasive diapirism in the central part of the
625 Algarve Basin (Fig. 21b). Finally, another major lineament of NW-SE trend (Gulf of Cadiz-Betics
626 transfer zone, Fig. 21b) limits the evaporite basin to the east. The Gulf of Cadiz-Betics transfer zone is
627 interpreted to represent a major step in the paleogeography of the southern Iberian passive margin,
628 causing a major southward shift in the northern limit of the Mesozoic passive margin from the Gulf of
629 Cadiz to the Betic basin (Fig. 21b, Fig. 1a; Ramos et al., 2017b). To the west, the evaporite basin is
630 limited by the also NW-SE trending Gorringe-Gulf of Cadiz transfer zone (Fig. 21; Ramos et al., 2017b).

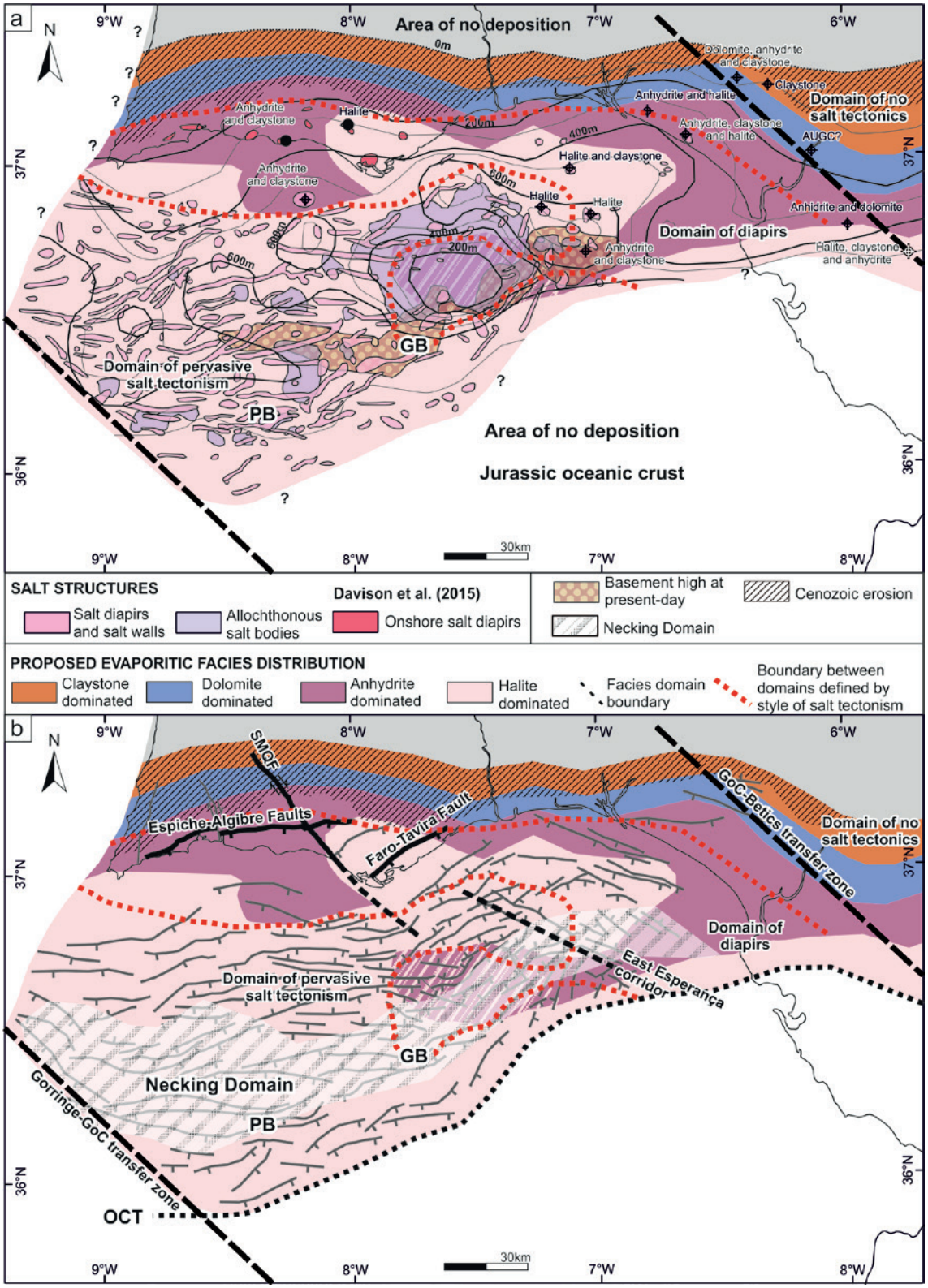

Figure 21. a) Map of Hettangian evaporite facies (in color) and thickness (isopach contours) across the Algarve Basin. The map is based on well and outcrop data, interpreted seismic sections, and the salt tectonic style. Overlain are the map of salt-related structures (as in Fig. 5) and the boundaries between domains defined based on style of salt tectonism. GB: Guadalquivir Bank; PB: Portimão Bank; SMQF:

São Marcos Quarteira Fault. b) Basement extensional faults (as in Fig. 5), necking domain and Ocean-Continent Transition (OCT; from Ramos et al., 2017b) overlain on the Hettangian evaporite facies distribution. Note the coincidence between basement trends and evaporite facies limits and domains of salt tectonism.

6.2. Development of the allochthonous Esperança Salt

As has been discussed, the allochthonous Esperança salt structure is sourced from the Hettangian evaporites that deposited in fault bound depocenters to the north and east of the present-day allochthonous body (Fig. 17). The source area for the allochthonous salt is interpreted to be a halite rich domain in which the Hettangian was at least 600m thick (Fig. 21a). The Esperança Salt was emplaced over a domain of reduced evaporite thickness and possibly more rich in anhydrite (Fig. 21), interpreted to be a relative basement high during the Mesozoic (Fig. 22). The Esperança salt structure lies along the offshore prolongation of the SMQF (Fig. 5) which is known to have acted as a significant paleogeographic limit during Mesozoic rifting, with deepening od Mesozoic deposition in the eastern block (Ramos et al., 2016; Terrinha, 1998). The SMQF defines the western limit of the depocenters sorcing the Esperança Salt.

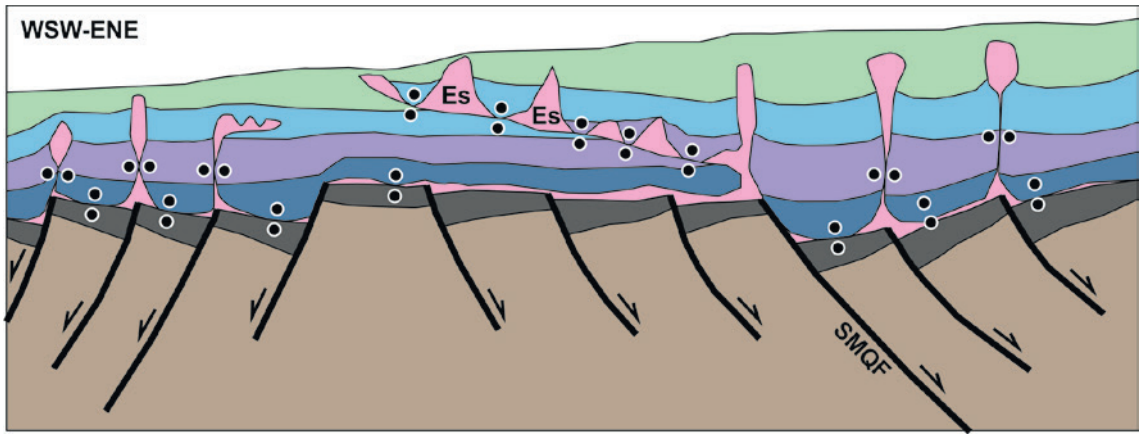

Figure 22. Synthetic illustration of an along strike (WSW-ENE) cross-section of the Algarve Basin in Early Cretaceous times. Es: Esperança Salt structure; SMQF: São Marcos Quarteira Fault. Salt structures are nucleated by the basement-involved extensional fault system. The Esperança salt structure progressed basinward over a relatively uplifted area, where the autochthonous evaporitic unit is thinner than in other parts of the margin and few salt structures have been identified. See Figure 7 for legend.

The result of the interference of NW-SE and WSW-ENE trending basement faults is the L-shaped feeder documented for the Esperança Salt (Fig. 17). Basement faulting was also directly responsible for

659 the process of initial salt expulsion. After a period of tectonic quiescence during the middle Early Jurassic
660 (Ramos et al., 2016), renewed extension along basement faults in the late Early Jurassic and Middle
661 Jurassic led to the development of the system of salt structures and tilting that drove salt expulsion (Fig.
662 18).

663 The velocity of Esperança salt structure frontal advance is not straightforward to calculate due to the
664 converging geometry of flow expected based on the feeder ramp geometry (Fig. 17). However, an
665 estimate of a progression of approximately 20-30km in a time span of 35Ma (during the Early Jurassic up
666 to the end of the Middle Jurassic) yields a global rate of less than 1mm/yr. This rate is lower than rates
667 quoted in Hudec and Jackson (2006)Hudec & Jackson (2006) and comparable to rates that can be
668 extracted for the Sigsbee Salt in the Gulf of Mexico (e.g., Peel et al., 1995). Nonetheless, the irregularity
669 of the intersection of both the Middle Jurassic unconformity and the top of the Middle Jurassic (Fig. 17)
670 is indicative of the variability in the direction and velocity of salt emplacement. Therefore, locally higher
671 and lower velocities than those estimated are to be expected.

672 *6.3. Timing and evolution of diapiric structures*

673 As has been widely discussed above, salt structures are related to the location of basement faults.
674 During the main extensional phase of evolution of the margin (Early to Late Jurassic), most diapiric
675 structures developed in the footwall of extensional faults (Fig. 23a-e). Diapirism continued to develop
676 passively during the thermal subsidence stage of the SW Iberian passive margin in the Early Cretaceous
677 (Fig. 23f).

678 Shortening and inversion of the margin during the Late Paleogene and Neogene (Adrià Ramos et al.,
679 2017) caused the reactivation of diapirs and the squeezing of their stems (generating secondary welds,
680 Fig. 23g,h). The deformation seems to be fossilized by the most recent sediments (Pliocene to present-
681 day; Figs. 7 and 8), as documented by Ramos et al. (2017a). In some instances, the Hettangian evaporite
682 layer acts as a detachment for south-directed thrusting (Algibre Thrust on Fig. 6, thrust south of the
683 Imperador-1 well on Fig. 8, and thrusting in Fig. 5 of Ramos et al. (2017a). This late folding and thrusting
684 causes folding of the BFU, which is onlapped by Neogene to Recent sediments (Adrià Ramos et al.,
685 2017), and of the AUGC/AWGC (Fernández-Puga et al., 2007). In the westernmost sectors of the Algarve
686 Basin, some diapirs continue to have a bathymetric (e.g., Fig. 11), indicating a growth until Recent. Late

stages of growth have been recorded in the diapirs that have not been pinched-off during the contractional deformation. Over the rest of the basin, most diapirism ceased by Late Cretaceous or Paleogene times.

Onshore, the Hettangian evaporite level played a major role in localizing deformation during the Cenozoic inversion of the margin (Ramos et al., 2016). In the central and eastern Algarve Basin, the most recent activity recorded on most salt structures can be correlated to this Cenozoic phase of deformation.

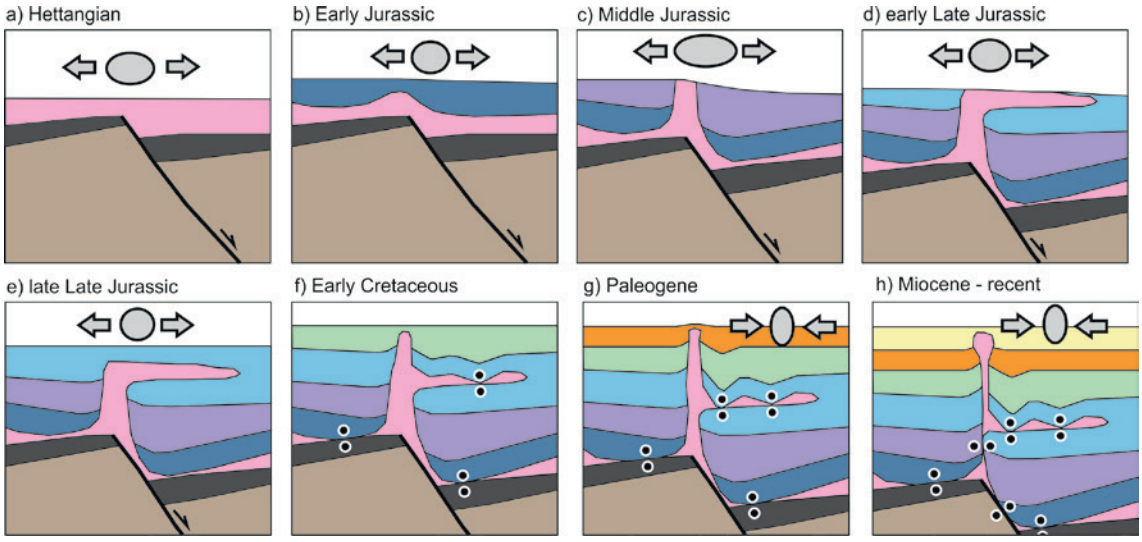

Figure 23. Schematic evolution of a diapir in the SW Iberian margin. Note the nucleation of the diapir above the footwall of a basement fault. The evolution of diapirism can be summarized by 3 phases: 1a-e) reactive to active diapirism (Early Jurassic - Late Jurassic) with the possible development of allochthonous salt bodies; f) passive diapirism (Early Cretaceous); g-h) diapir reactivation during contractional deformation (Paleogene - Present-day). Grey arrows: direction of strain; grey circles; tentative strain ellipses. See Figure 7 for legend.

8. Conclusions

The Mesozoic basement structure of the Algarve Basin controlled the distribution of facies and thickness of the Hettangian evaporite unit. This played a critical role in controlling the distribution of salt tectonic styles and evolution of individual salt structures though time. Salt structures in the Algarve Basin started to develop in the Early Jurassic and ceased growing in the Early Cretaceous, being mostly fossilized by Late Cretaceous to Paleogene times. In the western Algarve Basin passive downbuilding has continued to Neogene times, whereas in the central and eastern Algarve Basin Neogene activity of salt structures has been limited to shortening related to Cenozoic inversion.

The facies distribution of the evaporite basin follows a concentric pattern, with the most proximal facies towards the north and north-east. To the south, the absence of evaporates is due to the ~500 km eastward drifting of the NW African conjugate margin (e.g., Schettino and Turco 2011). The NW African margin would present a symmetric evaporitic facies distribution interpreted in the SW Iberian margin (swallowing of evaporites to the south), completing and closing the concentric facies pattern to the south. In the center of the basin, where the facies were supposedly dominated by halite and the thickness of the initial evaporite unit was greatest, salt tectonics was more intense. The general concentric pattern of facies and thickness distribution is broken in the distal domain of the passive margin due to rift-related uplift of this area.

Within the domain of most intense salt tectonics in the central and eastern Algarve Basin, the Esperança salt structure is a large salt canopy emplaced from Middle Jurassic to Early Cretaceous times within Mesozoic strata. It is sourced from an L-shape linear feeder along its northern margin. Above the allochthonous salt, deformation of the overburden is accommodated through extensional faults to the north and contractional faults to the south.

Acknowledgments

This study was funded by Repsol Exploración (Madrid) and partially financially supported by the SALTECRES project (CGL2014-54118-C2-1-R). Adrià Ramos thanks Repsol Exploración for his Ph.D grant. The authors wish to thank Repsol Exploración and Partex-Oil&Gas for permission to present this work, and Álvaro Arnaiz and Portugal Exploration Team for his support and enthusiasm. We also acknowledge Schlumberger and Midland Valley for the academic software licenses used for seismic interpretation and cross-section construction respectively. Repsol and Partex-Oil&Gas provided us their proprietary vintage seismic surveys and a 3D seismic cube, published with their permission. Seismic lines of the PDT00-PD00 survey have been provided by TGS and published with the permission of TGS. The seismic PDT00-PD00 survey is available for purchase from TGS and ENMC (Entidade Nacional para o Mercado de Combustibles).

References

Afonso, A.R.A., 1983. O problema inverso linear em prospecção gravimétrica. Algumas considerações sobre os jazigos de sal-gema di Algarve. Dep Física Fac Ciênc. Univ Lisb. 59.

Alves, T.M., Moita, C., Sandnes, F., Cunha, T., Monteiro, J.H., Pinheiro, L.M., 2006. Mesozoic-Cenozoic evolution of North Atlantic continental-slope basins: The Peniche basin, western Iberian margin. AAPG Bull. 90, 31–60. doi:10.1306/08110504138

738 Crespo-Blanc, A., 2007. Superimposed folding and oblique structures in the palaeomargin-derived units
739 of the Central Betics (SW Spain). J. Geol. Soc. 164, 621–636. doi:10.1144/0016-76492006-084
740 Davison, I., Anderson, L., Nuttall, P., 2012. Salt deposition, loading and gravity drainage in the Campos
741 and Santos salt basins. Geol. Soc. Lond. Spec. Publ. 363, 159–174. doi:10.1144/SP363.8
742 Davison, I., Barreto, P., Andrade, A., Terrinha, P., 2015. Loulé: a shunted diapir affected by Late
743 Cretaceous dyke intrusions and Alpine inversion, Algarve Basin, Portugal. AAPG European
744 Regional Conference and Exhibition, Lisbon, 18–19th May 2015.
745 Davison, I., Barreto, P., Andrade, A.J.M., 2016. Loulé: the anatomy of a squeezed diapir, Algarve Basin,
746 southern Portugal. J. Geol. Soc. jgs2016-035. doi:10.1144/jgs2016-035
747 Dewey, J.F., Helman, M.L., Knott, S.D., Turco, E., Hutton, D.H.W., 1989. Kinematics of the western
748 Mediterranean. Geol. Soc. Lond. Spec. Publ. 45, 265–283. doi:10.1144/GSL.SP.1989.045.01.15
749 Diegel, F.A., Karlo, J.F., Schuster, D.C., Shoup, R.C., Tauvers, and P.R., 1995. Cenozoic Structural
750 Evolution and Tectono-Stratigraphic Framework of the Northern Gulf Coast Continental Margin,
751 in: M. P. A. Jackson, D. G. Roberts, and S. Snelson, Eds., Salt Tectonics: A Global Perspective:
752 AAPG Memoir 65. pp. 109–151.
753 Doubinger, J., Adloff, M.-C., Palain, C., 1970. Nouvelles precisions stratigraphiques sur la série de base
754 du Mesozoique portugais. Comptes Rendus L'Academie Sci. 270, 1700–1772.
755 Duval, B., Cramez, C., Jackson, M.P.A., 1992. Raft tectonics in the Kwanza Basin, Angola. Mar. Pet.
756 Geol. 9, 389–404. doi:10.1016/0264-8172(92)90050-O
757 Fernández-Ibáñez, F., Soto, J.I., 2017. Pore pressure and stress regime in a thick extensional basin with
758 active shale diapirism (western Mediterranean). AAPG Bull. 101, 233–264.
759 doi:10.1306/07131615228
760 Fernández-Puga, M.C., Vázquez, J.T., Somoza, L., Rio, V.D. del, Medialdea, T., Mata, M.P., León, R.,
761 2007. Gas-related morphologies and diapirism in the Gulf of Cádiz. Geo-Mar. Lett. 27, 213–221.
762 doi:10.1007/s00367-007-0076-0
763 Fiduk, J.C., Rowan, M.G., 2012. Analysis of folding and deformation within layered evaporites in Blocks
764 BM-S-8 & -9, Santos Basin, Brazil. Geol. Soc. Lond. Spec. Publ. 363, 471–487.
765 doi:10.1144/SP363.22
766 Flinch, J.F., Bally, A.W., Wu, S., 1996. Emplacement of a passive-margin evaporitic allochthon in the
767 Betic Cordillera of Spain. Geology 24, 67–70.
768 García-Hernández, M., López-Garrido, Á.C., Martín-Algarra, A., Cámara, J.M., Ruiz-Ortiz, P.A., Vera,
769 J.A., 1989. Las discontinuidades mayores del Jurásico de las Zonas Externas de las Cordilleras
770 Béticas: análisis e interpretación de los ciclos sedimentarios. J. Iber. Geol. 35–52.
771 Gutscher, M.-A., Malod, J., Rehault, J.-P., Contrucci, I., Klingelhoefer, F., Mendes-Victor, L., Spakman,
772 W., 2002. Evidence for active subduction beneath Gibraltar. Geology 30, 1071.
773 doi:10.1130/0091-7613(2002)030<1071:EFASBG>2.0.CO;2
774 Hafid, M., 2000. Triassic–early Liassic extensional systems and their Tertiary inversion, Essaouira Basin
775 (Morocco). Mar. Pet. Geol. 17, 409–429. doi:10.1016/S0264-8172(98)00081-6
776 Hernández-Molina, F.J., Sierro, F.J., Llave, E., Roque, C., Stow, D.A.V., Williams, T., Lofi, J., Van der
777 Schee, M., Arnáiz, A., Ledesma, S., Rosales, C., Rodríguez-Tovar, F.J., Pardo-Igúzquiza, E.,
778 Brackenridge, R.E., 2016. Evolution of the gulf of Cadiz margin and southwest Portugal
779 contourite depositional system: Tectonic, sedimentary and paleoceanographic implications from
780 IODP expedition 339. Mar. Geol. 377, 7–39. doi:10.1016/j.margeo.2015.09.013
781 Hernández-Molina, F.J., Stow, D.A.V., Alvarez-Zarikian, C.A., Acton, G., Bahr, A., Balestra, B.,
782 Ducassou, E., Flood, R., Flores, J.-A., Furota, S., Grunert, P., Hodell, D., Jimenez-Espejo, F.,
783 Kim, J.K., Krissek, L., Kuroda, J., Li, B., Llave, E., Lofi, J., Lourens, L., Miller, M., Nanayama,
784 F., Nishida, N., Richter, C., Roque, C., Pereira, H., Sanchez Goni, M.F., Sierro, F.J., Singh,
785 A.D., Sloss, C., Takashimizu, Y., Tzanova, A., Voelker, A., Williams, T., Xuan, C., 2014. Onset
786 of Mediterranean outflow into the North Atlantic. Science 344, 1244–1250.
787 doi:10.1126/science.1251306
788 Hudec, M.R., Jackson, M.P., 2002. Structural segmentation, inversion, and salt tectonics on a passive
789 margin: Evolution of the Inner Kwanza Basin, Angola. Geol. Soc. Am. Bull. 114, 1222–1244.
790 Hudec, M.R., Jackson, M.P.A., 2007. Terra infirma: Understanding salt tectonics. Earth-Sci. Rev. 82, 1–
791 28. doi:10.1016/j.earscirev.2007.01.001
792 Hudec, M.R., Jackson, M.P.A., 2006. Advance of allochthonous salt sheets in passive margins and
793 orogens. AAPG Bull. 90, 1535–1564. doi:10.1306/05080605143
794 Hudec, M.R., Jackson, M.P.A., 2004. Regional restoration across the Kwanza Basin, Angola: Salt
795 tectonics triggered by repeated uplift of a metastable passive margin. AAPG Bull. 88, 971–990.
796 doi:10.1306/02050403061

Ings, S.J., Shimeld, J.W., 2006. A new conceptual model for the structural evolution of a regional salt detachment on the northeast Scotian margin, offshore eastern Canada. AAPG Bull. 90, 1407–1423. doi:10.1306/04050605159

Iribarren, L., Vergés, J., Camurri, F., Fullea, J., Fernàndez, M., 2007. The structure of the Atlantic–Mediterranean transition zone from the Alboran Sea to the Horseshoe Abyssal Plain (Iberia–Africa plate boundary). Mar. Geol. 243, 97–119. doi:10.1016/j.margeo.2007.05.011

Iribarren, L., Vergés, J., Fernàndez, M., 2009. Sediment supply from the Betic–Rif orogen to basins through Neogene. Tectonophysics 475, 68–84. doi:10.1016/j.tecto.2008.11.029

Lanaja, J.M., 1987. Contribución de la exploración petrolífera al conocimiento de la geología de España. IGME, Madrid.

Llave, E., Matias, H., Hernández-Molina, F.J., Ercilla, G., Stow, D.A.V., Medialdea, T., 2011. Pliocene–Quaternary contourites along the northern Gulf of Cadiz margin: sedimentary stacking pattern and regional distribution. Geo-Mar. Lett. 31, 377–390. doi:10.1007/s00367-011-0241-3

Lopes, A., Matos, S., Luís, T., 1998. Prospecto da mina campina de cima Loulé. Em colaboração com a Agência Nacional para a Cultura Científica e Tecnológica – Ciência Viva. http://www.cienciaviva.pt/veraocv/2014/downloads/Mina_de_Sal-gema_Campina_de_Cima.pdf (accessed 06.01.2017).

Lopes, F.C., Cunha, P.P. (Eds.), 2007. Tectono-sedimentary phases of the latest Cretaceous and Cenozoic compressive evolution of the Algarve margin (southern Portugal), in: Sedimentary Processes, Environments and Basins: A Tribute to Peter Friend (Eds G. Nichols, E. Williams and C. Paola), Blackwell Publishing Ltd., Oxford, UK.

Lopes, F.C., Cunha, P.P., Le Gall, B., Mendes-Victor, L.A., 2008. Tectónica salífera cenozóica na Margem Algarvia. Terra Conflitos E Ordem Uma Homenagem António Ferreira Soares MMGUC Publ. Coimbra 231–242.

Maestro, A., Somoza, L., Medialdea, T., Talbot, C.J., Lowrie, A., Vazquez, J.T., Diaz-del-Rio, V., 2003. Large-scale slope failure involving Triassic and Middle Miocene salt and shale in the Gulf of Cadiz (Atlantic Iberian Margin). Terra Nova 15, 380–391. doi:10.1046/j.1365-3121.2003.00513.x

Maldonado, A., Somoza, L., Pallarés, L., 1999. The Betic orogen and the Iberian–African boundary in the Gulf of Cadiz: geological evolution (central North Atlantic). Mar. Geol. 155, 9–43. doi:10.1016/S0025-3227(98)00139-X

Manuppella, G., 1992. Carta geológica da região do Algarve. Noticia explicativa da Carta Geologica da regiao do Algarve. Serviços geológicos de Portugal.

Martínez-Loriente, S., Sallarès, V., Gràcia, E., Bartolome, R., Dañobeitia, J.J., Zitellini, N., 2014. Seismic and gravity constraints on the nature of the basement in the Africa-Eurasia plate boundary: New insights for the geodynamic evolution of the SW Iberian margin: Thin oceanic crust at the CPR and SH. J. Geophys. Res. Solid Earth 119, 127–149. doi:10.1002/2013JB010476

Matias, H., 2007. Hydrocarbon potential of the offshore Algarve Basin. PhD Thesis, Faculdade de Ciências da Universidade Nova de Lisboa (324 pp).

Matias, H., Kress, P., Terrinha, P., Mohriak, W., Menezes, P.T.L., Matias, L., Santos, F., Sandnes, F., 2011. Salt tectonics in the western Gulf of Cadiz, southwest Iberia. AAPG Bull. 95, 1667–1698. doi:10.1306/01271110032

Medialdea, T., 2005. Estructura y evolución tectónica del Golfo de Cádiz. PhD Thesis, Universidad Complutense (318 pp).

Medialdea, T., Vegas, R., Somoza, L., Vázquez, J.T., Maldonado, A., Díaz-del-Río, V., Maestro, A., Córdoba, D., Fernández-Puga, M.C., 2004. Structure and evolution of the "Olistostrome" complex of the Gibraltar Arc in the Gulf of Cádiz (eastern Central Atlantic): evidence from two long seismic cross-sections. Mar. Geol. 209, 173–198. doi:10.1016/j.margeo.2004.05.029

Mohriak, W.U., Macedo, J.M., Castellani, R.T., Rangel, H.D., Barros, A.Z.N., Latge, M. a. L., Mizusaki, A.M.P., Szatmari, P., Demercian, L.S., Rizzo, J.G., Aires, J.R., 1995. Salt Tectonics and Structural Styles in the Deep-Water Province of the Cabo Frio Region, Rio de Janeiro, Brazil, in: M. P. A. Jackson, D. G. Roberts, and S. Snelson, Eds., Salt Tectonics: A Global Perspective: AAPG Memoir 65. pp. 273–304.

Nichols, G., 2009. Sedimentology and stratigraphy, 2nd ed. ed. Wiley-Blackwell, Chichester, UK ; Hoboken, NJ.

Palain, C., 1979. Connaissances stratigraphiques sur la base du Mesozoique portugais. Ciênc. Terra 5, 11–28.

Peel, F.J., Travis, C.J., Hossack, J.R., 1995. Genetic structural provinces and salt tectonics of the Cenozoic offshore US Gulf of Mexico: a preliminary analysis, in: M. P. A. Jackson, D. G.

Roberts, and S. Snelson, Eds., Salt Tectonics: A Global Perspective: AAPG Memoir 65. pp. 153–175.
Pérez-Valera, F., 2005. Estratigrafía y tectónica del Triásico Sudibérico en el sector oriental de la Cordillera Bética. PhD Thesis, Universidad de Granada (220 pp).
Platt, J.P., Behr, W.M., Johanesen, K., Williams, J.R., 2013. The Betic-Rif Arc and Its Orogenic Hinterland: A Review. Annu. Rev. Earth Planet. Sci. 41, 313–357. doi:10.1146/annurev-earth-050212-123951
Ramos, A., Fernández, O., Terrinha, P., Muñoz, J.A., 2017. Neogene to recent contraction and basin inversion along the Nubia-Iberia boundary in SW Iberia. Tectonics 36, 2016TC004262. doi:10.1002/2016TC004262
Ramos, A., Fernández, O., Terrinha, P., Muñoz, J.A., 2016. Extension and inversion structures in the Tethys–Atlantic linkage zone, Algarve Basin, Portugal. Int. J. Earth Sci. 105, 1663–1679. doi:10.1007/s00531-015-1280-1
Ramos, A., Fernández, O., Terrinha, P., Muñoz, J.A., submitted tectonics. Neogene to recent contraction and basin inversion along the Africa-Iberia boundary in SW Iberia. Tectonics.
Ramos, A., Fernández, O., Torne, M., Sánchez de la Muela, A., Muñoz, J.A., Terrinha, P., Manatschal, G., Salas, M.C., 2017. Crustal structure of the SW Iberian passive margin: The westernmost remnant of the Ligurian Tethys? Tectonophysics (in press). doi:10.1016/j.tecto.2017.03.012
Ramos, A., Torne, M., Fernández, O., Manatschal, G., Sánchez de la Muela, A., Muñoz, J.A., Terrinha, P., Salas, M.C., submitted grav. Crustal structure of the SW Iberian passive margin: The westernmost remnant of the Ligurian Tethys? Tectonophysics.
Rocha, R.B., 1976. Estudo estratigráfico e paleontológico do jurássico do Algarve Ocidental. PhD Thesis, Universidade Nova de Lisboa, Lisboa (178 pp).
Roque, C., 2007. Tectonostratigrafia do cenozóico das margens continentais sul e sudoeaste portuguesas: um modelo de correlação sismostratigráfica. PhD Thesis, Universidade de Lisboa (310 pp).
Sallarès, V., Gailler, A., Gutscher, M.-A., Graindorge, D., Bartolomé, R., Gràcia, E., Díaz, J., Dañobeitia, J.J., Zitellini, N., 2011. Seismic evidence for the presence of Jurassic oceanic crust in the central Gulf of Cadiz (SW Iberian margin). Earth Planet. Sci. Lett. 311, 112–123. doi:10.1016/j.epsl.2011.09.003
Saura, E., Vergés, J., Martín-Martín, J.D., Messager, G., Moragas, M., Razin, P., Grélaud, C., Joussiaume, R., Malaval, M., Homke, S., others, 2014. Syn-to post-rift diapirism and minibasins of the Central High Atlas (Morocco): the changing face of a mountain belt. J. Geol. Soc. 171, 97–105.
Schettino, A., Turco, E., 2009. Breakup of Pangaea and plate kinematics of the central Atlantic and Atlas regions. Geophys. J. Int. 178, 1078–1097. doi:10.1111/j.1365-246X.2009.04186.x
Schuster, D.C., 1995. Deformation of allochthonous salt and evolution of related salt-structural systems, eastern Louisiana Gulf Coast, in: M. P. A. Jackson, D. G. Roberts, and S. Snelson, Eds., Salt Tectonics: A Global Perspective: AAPG Memoir 65. pp. 177–198.
Somoza, L., Maestro, A., Lowrie, A., 1999. Allochthonous Blocks as Hydrocarbon Traps in the Gulf of Cadiz. Offshore Technology Conference, 3-6 May, Houston, Texas. doi:10.4043/10889-MS
Stewart, S.A., 2007. Salt tectonics in the North Sea Basin: a structural style template for seismic interpreters. Geol. Soc. Lond. Spec. Publ. 272, 361.
Tari, G., Brown, D., Jabour, H., Hafid, M., Louden, K., Zizi, M., 2012. The conjugate margins of Morocco and Nova Scotia, in: Regional Geology and Tectonics: Principles of Geologic Analysis – Volume 1C, Edition: 1st, Chapter: 7.1, Publisher: Elsevier, Editors: David G. Roberts & Albert W. Bally, pp.265-300. pp. 284–323.
Tari, G., Jabour, H., 2013. Salt tectonics along the Atlantic margin of Morocco. Geol. Soc. Lond. Spec. Publ. 369, 337–353. doi:10.1144/SP369.23
Tari, G., Molnar, J., Ashton, P., Hedley, R., 2000. Salt tectonics in the Atlantic margin of Morocco. Lead. Edge 19, 1074–1078.
Terrinha, P., 1998. Structural geology and tectonic evolution of the Algarve Basin, South Portugal. PhD Thesis, Imperial College, London (430 pp).
Terrinha, P., Coward, M., Ribeiro, A., 1990. Salt tectonics in the Algarve Basin: The Loulé diapir. Comun. Serviços Geológicos Port. 76, 33–40.
Terrinha, P., Ribeiro, C., Kullberg, J.C., Lopes, C., Rocha, R., Ribeiro, A., 2002. Compressive episodes and faunal isolation during rifting, Southwest Iberia. J. Geol. 110, 101–113.
TGS, 2005. PD00: non-exclusive 2D Survey, TGS online data zone. (http://www.tgs.com/TGS/specsheets/PD-00_Spec.pdf).

914 Torelli, L., Sartori, R., Zitellini, N., 1997. The giant chaotic body in the Atlantic Ocean off Gibraltar: new
915 results from a deep seismic reflection survey. Mar. Pet. Geol. 14, 125–138. doi:10.1016/S0264-
916 8172(96)00060-8
917 Tortella, D., Torne, M., Pérez-Estaún, A., 1997. Geodynamic evolution of the eastern segment of the
918 Azores-Gibraltar zone: the Gorringe Bank and the Gulf of Cadiz region. Mar. Geophys. Res. 19,
919 211–230.
920 van Keken, P.E., Spiers, C.J., van den Berg, A.P., Muyzert, E.J., 1993. The effective viscosity of rocksalt:
921 implementation of steady-state creep laws in numerical models of salt diapirism. Tectonophysics
922 225, 457–476. doi:10.1016/0040-1951(93)90310-G
923 Vera, J.A., Molina, J.M., Aguado, R., 2004. Calcarenitas de Microcodium (Formación Majalcorón,
924 Paleoceno, Subbético): descripción, bioestratigrafía y significado en el Terciario de la Cordillera
925 Bética. Bol. Geológico Min. Esp. 115, 453–468.
926 Vergés, J., Fernàndez, M., 2012. Tethys–Atlantic interaction along the Iberia–Africa plate boundary: The
927 Betic–Rif orogenic system. Tectonophysics 579, 144–172. doi:10.1016/j.tecto.2012.08.032
928 Wagner, B.H., Jackson, M.P.A., 2011. Viscous flow during salt welding. Tectonophysics 510, 309–326.
929 doi:10.1016/j.tecto.2011.07.012
930 Welsink, H., Tankard, A., 2012. Extensional tectonics and stratigraphy of the Mesozoic Jeanne d'Arc
931 basin, Grand Banks of Newfoundland A2 - Roberts, D.G., in: Bally, A.W. (Ed.), Regional
932 Geology and Tectonics: Phanerozoic Rift Systems and Sedimentary Basins. Elsevier, Boston, pp.
933 336–381.
934 Wilson, R.C.L., 1988. Mesozoic development of the Lusitanian basin, Portugal. Rev. Soc. Geológica Esp.
935 1, 393–407.
936 Ziegler, P.A., 1988. Evolution of the Arctic-North Atlantic and the Western Tethys, AAPG Memoir 43
937 edition. ed. Amer Assn of Petroleum Geologists, Tulsa, Okla., U.S.A.
938 Zitellini, N., Gràcia, E., Matias, L., Terrinha, P., Abreu, M.A., DeAlteriis, G., Henriet, J.P., Dañobeitia,
939 J.J., Masson, D.G., Mulder, T., 2009. The quest for the Africa–Eurasia plate boundary west of
940 the Strait of Gibraltar. Earth Planet. Sci. Lett. 280, 13–50. doi:10.1016/j.epsl.2008.12.005
941 Zulauf, G., Zulauf, J., Bornemann, O., Kihm, N., Peinl, M., Zanella, F., 2009. Experimental deformation
942 of a single-layer anhydrite in halite matrix under bulk constriction. Part 1: Geometric and
943 kinematic aspects. J. Struct. Geol. 31, 460–474. doi:10.1016/j.jsg.2009.01.013
944

APPENDIX 1.4

Crustal structure of the SW Iberian passive margin: The westernmost remnant of the Ligurian Tethys?

Ramos, A., Fernández, O., Torne, M., Sánchez de la Muela, A., Muñoz, J.A., Terrinha, P., Manatschal, G., Salas, M.C. Tectonophysics 705, 42-62. doi:10.1016/j.tecto.2017.03.012.

Tectonophysics 705 (2017) 42–62

Contents lists available at ScienceDirect

Tectonophysics

journal homepage: www.elsevier.com/locate/tecto

Review Article

Crustal structure of the SW Iberian passive margin: The westernmost remnant of the Ligurian Tethys?

A. Ramos [a,*], O. Fernández [b], M. Torne [c], A. Sánchez de la Muela [d], J.A. Muñoz [a], P. Terrinha [e], G. Manatschal [f], M.C. Salas [b]

[a] Institut de Recerca Geomodels, Departament de Dinàmica de la Terra i de l'Oceà, Universitat de Barcelona, Barcelona, Spain
[b] Repsol Exploración, Dirección de Geociencias, Madrid, Spain
[c] Institute of Earth Sciences Jaume Almera, ICTJA-CSIC, Spain
[d] Department of Geography, University College of London, London, UK
[e] Instituto Português do Mar e da Atmosfera, Divisão de Geologia e Georecursos Marinhos, Lisboa, Portugal
[f] Institut Physique du Globe de Strasbourg, Université de Strasbourg - CNRS, Strasbourg, France

ARTICLE INFO

Article history:
Received 11 August 2016
Received in revised form 16 March 2017
Accepted 20 March 2017
Available online 28 March 2017

Keywords:
SW Iberian margin
Transform margin
Margin inversion
Crustal structure
Gravity
Seismic interpretation

ABSTRACT

At present, the SW Iberian margin is located along the convergent Iberia-Nubia plate boundary. In Mesozoic times, the margin was located at the triple junction of the Ligurian Tethys, Central Atlantic and Northern Atlantic. The characterization of its crustal structure has allowed us to propose a configuration for this triple junction and to determine the role that this transform margin played within the plate kinematic system. In this paper we present an integrated study based on the interpretation of a 2D regional multichannel seismic survey consisting of 58 profiles, tied with onshore geology and exploratory wells, and on gravimetric modeling performed over four NW-SE trending profiles.

Integrated interpretation of MCS data combined with 2D gravity modeling reveals a complex pattern in the southward crustal thinning of SW Iberia and supports the possible presence of oceanic crust under the Gulf of Cadiz. The tapering of Iberian crust is characterized by steps with rapid changes in the thickness of the crust, and thinning to <10 km under the outer portions of the margin. Based on gravimetric modeling results and the structures interpreted on reflection seismic profiles, 3 crustal domains reflecting progressive thinning have been defined for the SW Iberian margin. These domains trend roughly WSW-ENE, parallel to the main extensional fabric of the margin. Gravimetric modeling results are compatible with the presence of exhumed sub-continental mantle in the distal part of the margin. Integrated modeling also supports the fact that Cenozoic contraction is responsible for major uplift along the Guadalquivir Bank. Margin inversion and the pre-existing extensional crustal structure are responsible for the areal distribution and amplitude of the prominent positive gravity anomaly observed in the Gulf of Cadiz.

Contents

* Corresponding author.
E-mail address: adria_ramos@outlook.com (A. Ramos).

http://dx.doi.org/10.1016/j.tecto.2017.03.012
0040-1951/

1. Introduction

The SW Iberian margin is part of the transform to oblique margin that connected the Ligurian Tethys with the Atlantic (Fig. 1). Left-lateral translation of the Iberian plate during the opening of the Central Atlantic in the Early to Middle Jurassic led to the development of transform margins along southern Iberia and northwestern Nubia. Oceanic crust accreted between Iberia and Nubia during the Mesozoic (Bortolotti and Principi, 2005; Schettino and Turco, 2011) and was later mostly subducted during the emplacement of the Betic-Rif orogen (Gutscher et al., 2012; Schettino and Turco, 2011; Spakman and Wortel, 2004; van Hinsbergen et al., 2014; Vergés and Fernàndez, 2012). This orogen also largely overprinted the former passive margin structure, which is either inverted within the orogen or buried under its thrust system. The only segment of the Iberia-NW Nubia transform margin that has been preserved almost intact to present day is the SW margin of Iberia, running along the northern border of the Gulf of Cadiz (Fig. 1).

The existence of highly thinned crust in SW Iberia was initially documented in 1990s along a transect extending from onshore Iberia to the eastern end of the Horseshoe Abyssal Plain (González et al., 1996) (Fig. 1). Based on wide-angle seismic reflection data and gravity modeling, these authors concluded that the crust underwent a strong but continuous thinning from 31 km onshore Iberia to <15 km in the Horseshoe Abyssal Plain. Subsequently, a number of geophysical studies have been conducted to investigate the deep structure of the Gulf of Cadiz (Dañobeitia et al., 1999; Gràcia et al., 2003; Gutscher et al., 2002, 2009; Zeyen et al., 2005). The results of these studies show that the crust gently thins from 30 to 32 km under the Iberian mainland to 25 km in the central part of the Gulf of Cadiz and to 15 km in its most western parts. More recently, Sallarès et al. (2011) have published a refraction seismic profile running from the southern Portuguese coast to the deeper western end of the Gulf of Cadiz, which records an abrupt thinning of the continental crust and the transition to oceanic crust occurring in the western Gulf of Cadiz (Fig. 1). Gutscher et al. (2009) and Martínez-Loriente et al. (2014) proposed the prolongation of this oceanic crust to the east under the Gibraltar arc (Fig. 1) (Spakman and Wortel, 2004; van Hinsbergen et al., 2014; Vergés and Fernàndez, 2012).

The nature and origin of the crust under the Gulf of Cadiz is still under dispute. Some authors postulate that the Gulf is floored by Avalonian continental crust north of the Guadalquivir and Portimão Banks (Gràcia et al., 2003; Tortella et al., 1997; Zeyen et al., 2005). According to these authors, the transition to the Atlantic oceanic domain is located to the west and no oceanic crust is interpreted south of the Banks. Alternative interpretations suggest that south of Guadalquivir and Portimão Banks (Fig. 1), there is a corridor of oceanic crust identified on seismic refraction profiles and seismic tomography interpreted as a remnant of the Ligurian Tethys (Gutscher et al., 2002; Martínez-Loriente et al., 2014; Sallarès et al., 2011). Plate kinematic reconstructions that are based on magnetic lineations in the Atlantic (Roeser et al., 2002; Schettino and Turco, 2011; Stampfli and Borel, 2002) suggest a Middle to Late Jurassic age for the first oceanic crust formed along southern Iberia. Nevertheless, the absence of well-defined magnetic anomalies in the area has not permitted the dating of this possible oceanic crust or assigning it unambiguously to the Atlantic or Tethyan domains.

Gràcia et al. (2003) and Zeyen et al. (2005) identified the Guadalquivir-Portimão Bank as a feature across which dramatic crustal thinning occurred. This thinning coincides with an ENE-WSW striking gravity anomaly high that extends along the Guadalquivir and Portimão Banks (Fig. 2).The gravity anomaly shows three local highs reaching maximum values above 100 mGal over the Guadalquivir Bank (Fig. 2). This gravity anomaly has been poorly sampled by deep seismic sounding. Reflection profile GC1 (Dañobeitia et al., 1999) was acquired crossing the western part of the anomaly, and refraction profile of Sallarès et al. (2011) was acquired west of the anomaly. As a result, the precise nature of the Gulf of Cadiz gravity anomaly is still under debate.

The aim of this paper is to provide a geological framework that accounts for the diverse observations made on the crustal structure of the Gulf of Cadiz. The ultimate objective is to understand the crustal structure of the SW Iberian margin and to determine the: 1) the role it played during the Middle to Late Jurassic rifting-drifting stages through to the present-day collisional stage, and 2) its relation to the Nubia-Iberia diffuse plate boundary. In order to achieve these goals we use commercial multichannel seismic reflection (MCS) profiles and published gravity data to construct four profiles that represent the structure of the Gulf of Cadiz.

2. Evolution of the Gulf of Cadiz - Algarve Basin

The Algarve Basin is located along the southern margin of Portugal and extends both onshore and offshore in the Gulf of Cadiz. The evolution of the basin has been documented by many authors; the description contained here is derived from the work of Ramos et al. (2016) and Terrinha (1998) and authors therein, and summarized in Fig. 3.

Rifting in the Algarve Basin initiated in the Triassic, with the generation of isolated half-grabens trending roughly E-W. Triassic siliciclastic continental sediments unconformably overlie Carboniferous flysch deposits belonging to the foreland of the Variscan orogen. Triassic sediments are overlain by earliest Jurassic sediments: Hettangian evaporites and coeval terrigenous clastics, whose distribution is strongly controlled by E-W trending extensional faults. The initial clastic-evaporitic series are capped by a volcanic-sedimentary complex Hettangian-Sinemurian in age that is associated with the Central Atlantic Magmatic Province (CAMP; e.g., Martins et al., 2008). Sinemurian to Toarcian sediments blanket the isolated basins of the first phase of extension and record progressive deepening of the basin. This Early Jurassic subsidence phase ended at the transition to the Middle Jurassic (Terrinha et al., 2002).

Middle Jurassic reactivation of older extensional basins triggered an initial phase of salt tectonism (involving Hettangian evaporites). Extension at this time was dominated by E-W to ENE-WSW trending extensional faults and a NW-SE to NNW-SSE trending relay or transfer zones. Extension and salt tectonism continued through the Middle and Late Jurassic. Middle to Late Jurassic sediments are dominated by carbonates and have highly variable thickness on account of both salt tectonism and extensional faulting. Lower Cretaceous siliciclastics mostly draped over the entire basin and they only locally exhibited variations in thickness related to ongoing salt tectonism or extensional faulting. During the Late Cretaceous sedimentation was very localized and Upper Cretaceous sediments are mostly absent in the basin. The Paleogene is restricted to the offshore as

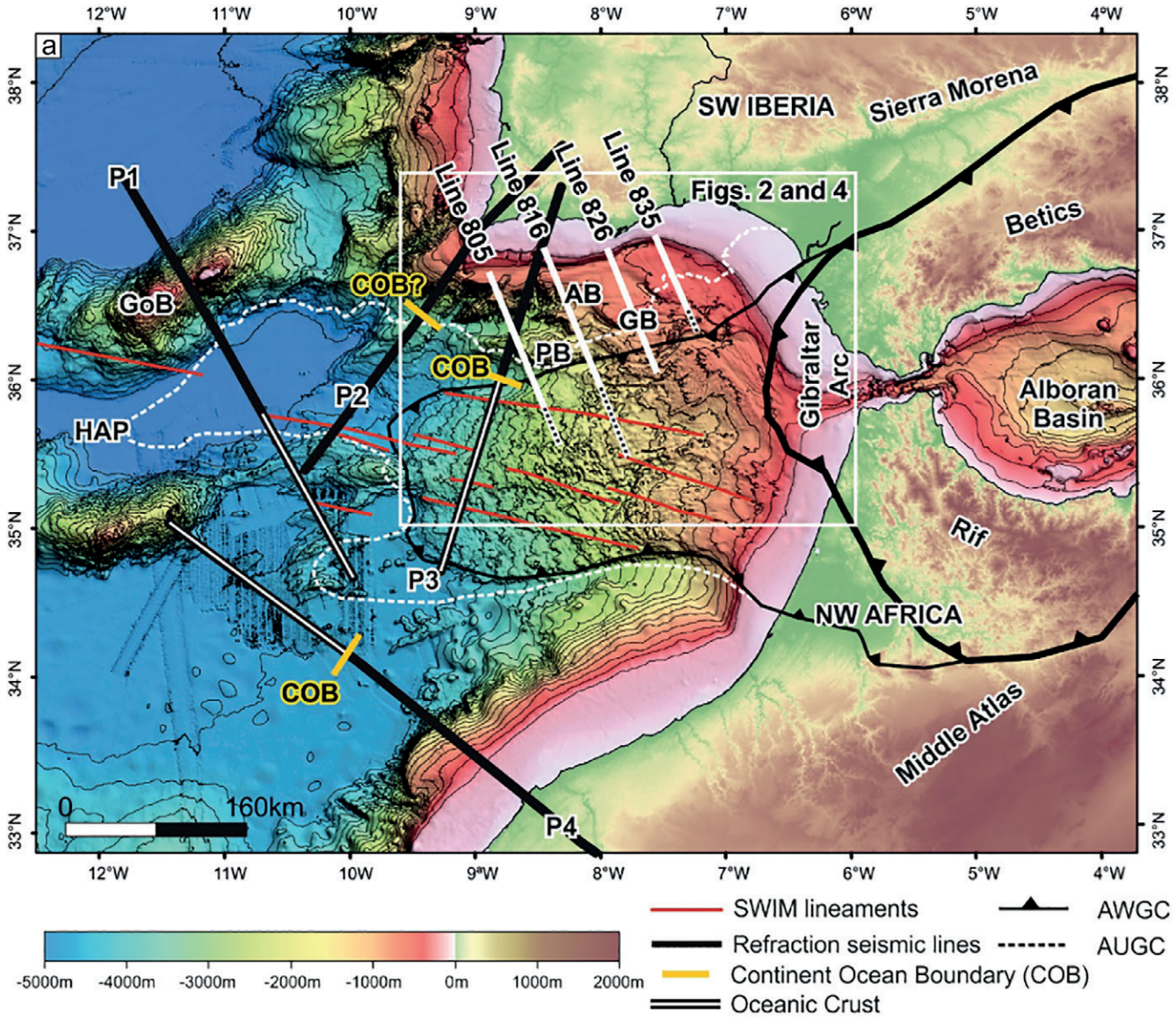
a
12°W
11°W
10°W
9°W
8°W
7°W
6°W
5°W
4°W
38°N
37°N
36°N
35°N
34°N
33°N
SW IBERIA
Sierra Morena
Betics
Alboran Basin
Gibraltar Arc
Rif
NW AFRICA
Middle Atlas
Figs. 2 and 4
Line 805
Line 816
Line 826
Line 835
P1
P2
P3
P4
GoB
HAP
COB?
COB
COB
AB
GB
PB
0
160km
-5000m
-4000m
-3000m
-2000m
-1000m
0m
1000m
2000m
SWIM lineaments
Refraction seismic lines
Continent Ocean Boundary (COB)
Oceanic Crust
AWGC
AUGC

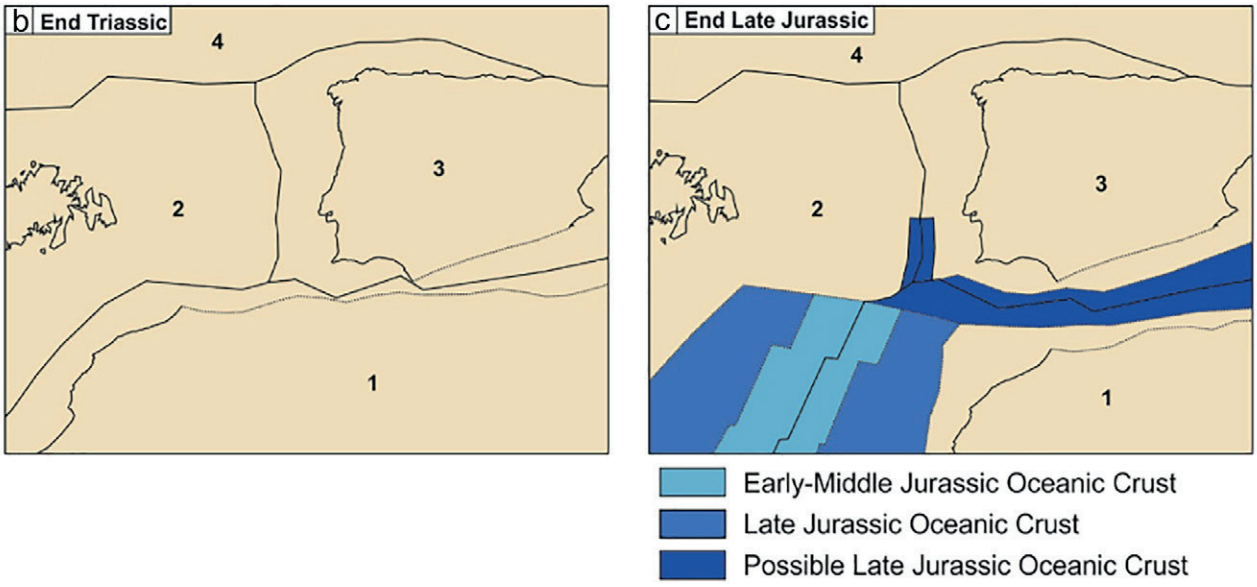
b End Triassic
c End Late Jurassic
1
2
3
4
Early-Middle Jurassic Oceanic Crust
Late Jurassic Oceanic Crust
Possible Late Jurassic Oceanic Crust

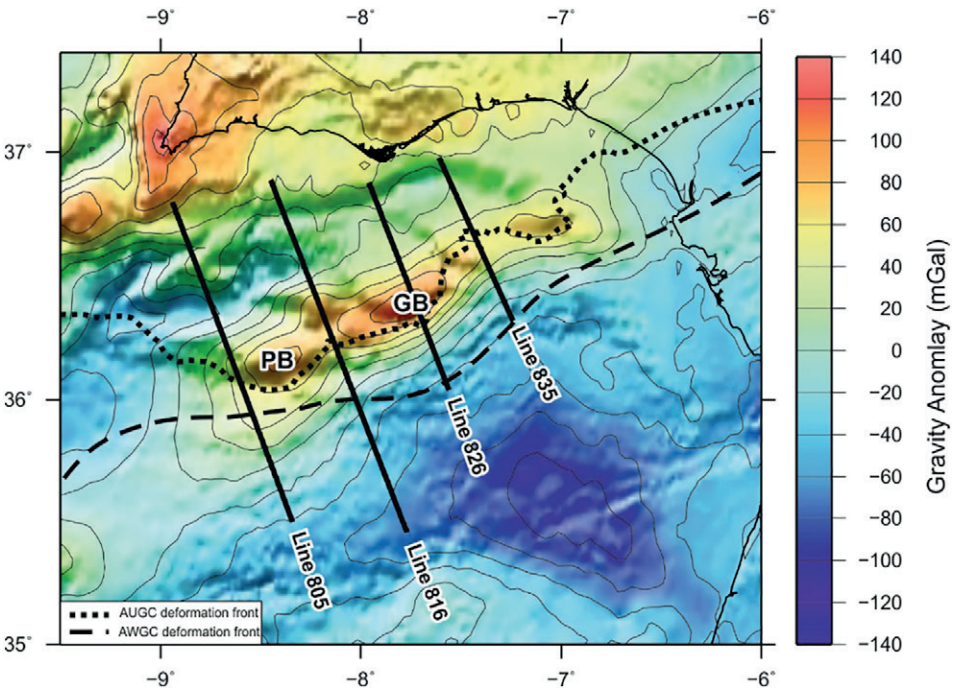

Fig. 2. Map of free-air gravity anomaly offshore and Bouguer anomaly onshore. Black lines show the location of the 2D gravimetric profiles presented in this study. Note the ENE-WSW trending positive gravity anomaly located offshore (>40 mGal), and the negative gravity anomaly (<−60 mGal) to the SE. GB: Guadalquivir Bank; PB: Portimão Bank.

shallow water carbonates. A hiatus at Late Cretaceous-Paleogene times together with an angular unconformity between the Upper Cretaceous and Lower Paleogene successions are evidence of incipient regional uplift during this time.

Sedimentation resumed in the Oligocene with the early pulses of compression between Iberia and Nubia. The base of the Miocene is represented in the Gulf of Cadiz by a regional unconformity (BFU: base foredeep unconformity; Ledesma, 2000). N-S to NW-SE directed shortening during the Neogene led to the partial inversion of the passive margin, with the development of southward directed thrusts that have resulted in a stair-stepped topography and bathymetry (Ramos et al., 2017). During compression, most likely during the Tortonian, the Accretionary Wedge of the Gulf of Cadiz (AWGC; chaotic and mélange-like assemblage of Mesozoic to Cenozoic sediments, Fig. 1) was tectonically emplaced along the entire front of the Betic and Rif into the Atlantic, due to the westward emplacement of the Betic-Rif orogen (Iribarren et al., 2007; Torelli et al., 1997; Gutscher et al., 2002, 2012). The AWGC is partially reworked in the Allochthonous Unit of the Gulf of Cadiz (AUGC; Fig. 1), a gravitationally emplaced submarine debris flows sourced from the AWGC (Iribarren et al., 2007).

3. Data

3.1. Reflection seismic and hydrocarbon exploratory wells

Interpretation of the offshore structure of the Algarve Basin and Gulf of Cadiz is based on a 2D regional seismic survey acquired by TGS in 2001 (PDT00-PD00) and 2D vintage seismic lines property of Repsol covering the proximal Gulf of Cadiz (Fig. 4). The PDT00-PD00 survey consists of 58 lines of 2D multichannel reflection profiles (MCS), striking both NNW-SSW and ENE-WSW. These lines, record down to 12 s TWT (two-way time) and were acquired with an streamer length of 6 km, and migrated in time (TGS, 2005).

The seismic interpretation is tied to onshore geology (Ramos et al., 2016), to 5 wells in the Portuguese offshore (Roque, 2007) and up to 39 wells in the Spanish Gulf of Cadiz area (Lanaja, 1987) (Fig. 4).

Interpretation was performed in Petrel (Schlumberger) taking into account the unconformity bounded sequences defined by Roque (2007) and Terrinha (1998), which were useful to correlate the MCS seismic reflectors through the margin. Seismic sections and their interpretation were converted to depth using Move 2015.1 (by Midland Valley Exploration). Average velocities for three stratigraphic intervals (Neogene-Quaternary, top Paleogene to top Middle Jurassic and top Middle Jurassic to Basement) were derived from the check-shot data from wells Algarve-1, Algarve-2, Corvina-1, Imperador-1 and Ruivo-1 (Fig. 5).

Besides formation picks, density values for each stratigraphic unit were derived from the logs available for these 5 wells. Vintage well logs of the Spanish Gulf of Cadiz did not fulfil the quality criteria to be used to obtain density values.

3.2. Gravity

Onshore Bouguer gravity anomalies have been taken from a recent compilation of gravity data on Iberia (Ayala et al., 2016). Offshore, free-air gravity anomalies come from the global satellite altimetry data model V16.1 (Smith and Sandwell, 1997, updated 2007) (Fig. 2). The gravity anomaly in the Gulf of Cadiz is characterized by the presence of an elongated NE-SW gravity high composed by three local highs with values ranging from 40 to 110 mGal. The highest values, above 100 and 80 mGal, coincide with the Guadalquivir and Portimão Banks,

Fig. 1. a) Location of the study area. Traces of refraction seismic profiles acquired between SW Iberia and NW Africa are from Martínez-Loriente et al. (2014) (P1); González et al. (1996) (P2); Sallarès et al. (2011) (P3); and Contrucci et al. (2004) (P4). The location of the continent-ocean boundary (COB) defined on these lines is shown. The reflection seismic lines interpreted in this work are represented by white lines, while their prolongation to the SE for gravimetric modeling is marked with black dotted lines. AB: Algarve Basin; AUGC: Allochthonous Unit of Gulf of Cadiz; AWGC: Accretionary Wedge of Gulf of Cadiz; GB: Guadalquivir Bank; GoB: Gorringe Bank; HAP: Horseshoe Abyssal Plain; PB: Portimão Bank. SWIM faults come from Zitellini et al. (2009). Bathymetry is taken from the General Bathymetric Chart of Oceans (GEBCO) digital atlas (IOC et al., 2003) and topography from European Environment Agency (EEA). (b) Plate reconstruction at end of Triassic (203 Ma) and (c) at end of Jurassic times (151 Ma) modified after Schettino and Turco (2011), Seton et al. (2012), and Sibuet et al. (2012). 1: NW Nubia, 2: North America, 3: Iberia, 4: Armorica-Greenland.

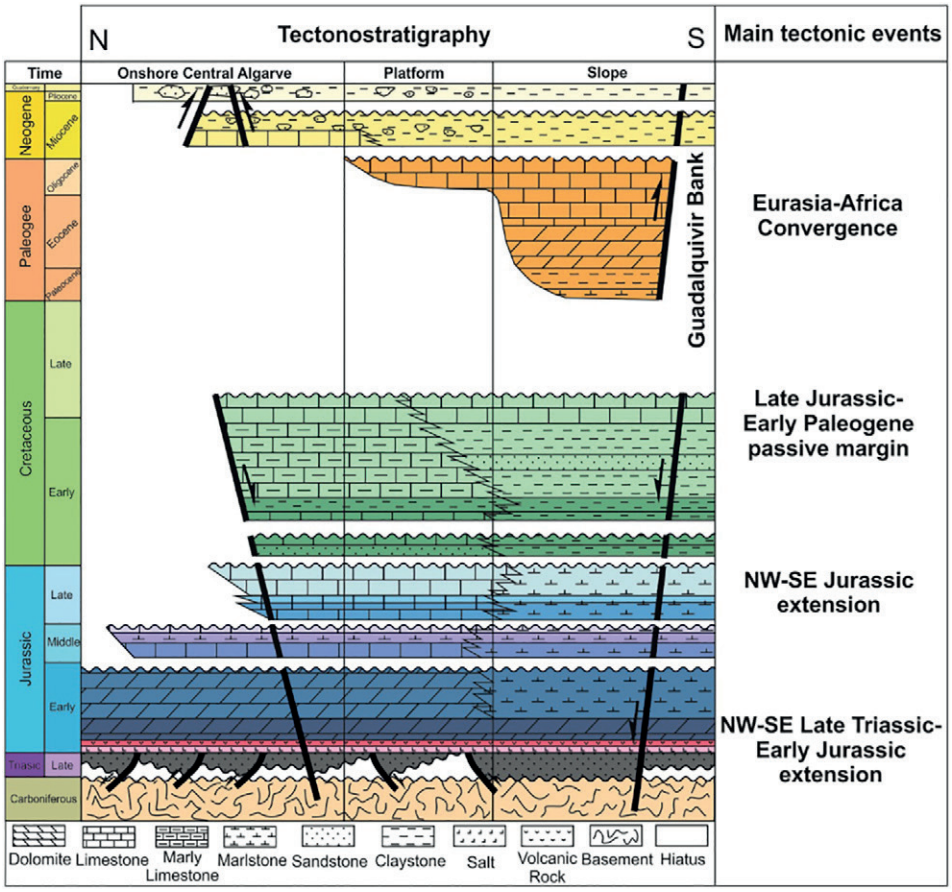

Fig. 3. Tectono-sedimentary diagram of the Algarve Basin showing the main stratigraphic units and tectonic events. (Modified from Ramos et al. (2016).)

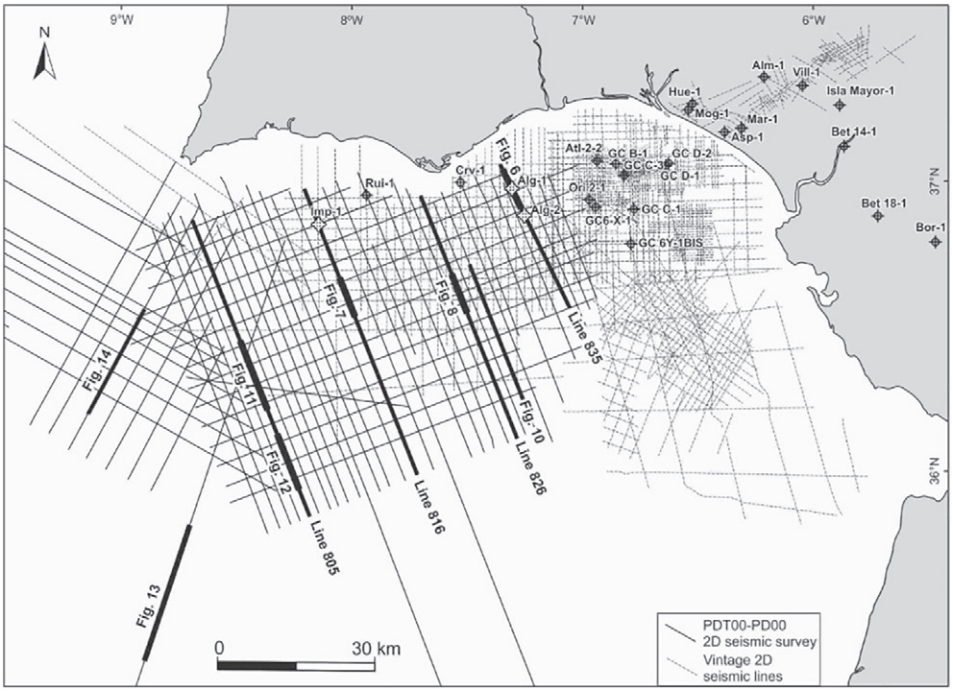

Fig. 4. Data in the Gulf of Cadiz used in this study. The most representative and complete wells shown in this figure are: Alg-1: Algarve-1; Alg-2; Algarve-2; Alm-1: Almonte-1; Asp-1: Asperillo-1; Atl-2-2: Atlantida-2-2; Bet 14-1: Betica 14-1; Bet 18-1: Betica 18-1; Bor-1: Bornos-1; Crv-1: Corvina-1; GC6-X-1; Gulf of Cadiz 6-X-1; GC B-1: Gulf of Cadiz B-1; GC B-2: Gulf of Cadiz B-2; GB D-1: Gulf of Cadiz D-2; GB D-2: Gulf of Cadiz D-2; GB 6Y-1Bis: Gulf of Cadiz 6Y-1Bis; Hue-1: Huelva-1; Imp-1: Imperador-1; Mar-1: Marismas-1; Mog-1: Moguer-1; Ori 2-1: Orion 2-1; Rui-1: Ruivo-1.

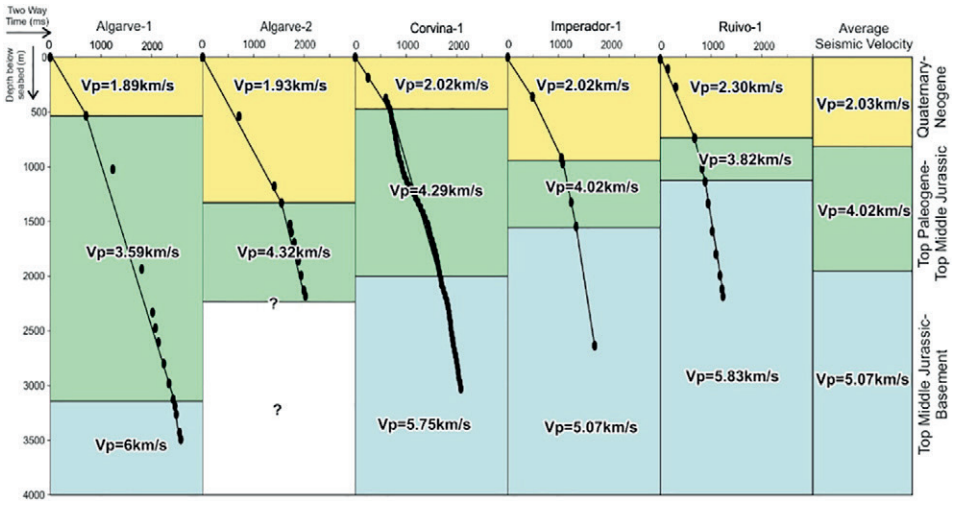

Fig. 5. Checkshot data from the 5 wells in the Portuguese Algarve Basin. See Fig. 4 for location. The time-depth relationships from the 5 wells have been used to define 3 velocity intervals: Neogene-Quaternary (yellow), top Paleogene to top Middle Jurassic (green) and top Middle Jurassic to top of Basement (blue). (For interpretation of the references to colour in this figure legend, the reader is referred to the web version of this article.)
(Data courtesy of Repsol.)

respectively (see Fig. 1a). The Guadalquivir Bank is a basement high along which the metamorphosed slates and greywackes of Carboniferous age of the South Portuguese Zone locally crop out at the seafloor (Vegas et al., 2004). The Portimão Bank is a bathymetric high related to an inverted Mesozoic basin (Terrinha et al., 2009). To the north of these Banks, a NE-SW gravity low, with values in a range of −20 to −40 mGal delineates the presence of a large submarine valley that incises the continental slope (Terrinha et al., 2009).The Iberian margin is characterized by positive gravity values (above 20 mGal) that extend from SW Iberia mainland (Fig. 2). As pointed out by Torne et al. (2015), the regional gravity high that delineates the southwestern Variscan terranes of the Ossa Morena and South Portuguese zones is related to the combination of a slight thinning of the crust towards the shoreline and to the presence of a somewhat denser crust relative to the average of the Alpine Iberia (15 to 20 kg/m^3 denser). These results agree with previous seismic studies which found that the mid/lower crust was intruded by a regional high velocity/reflective body and that the base of the crust is located at about 31–32 km (e.g., Carbonell et al., 2004; Palomeras et al., 2009).

By contrast, the central region of the Gulf is characterized by a gravity low (below −100 mGal) that roughly delineates the presence of the low density rocks forming the accretionary wedge (AWGC in Figs. 1a and 2). The wedge thickens towards the east where it reaches thicknesses between 10 km (Thiebot and Gutscher, 2006) and 11.5 km (Iribarren et al., 2007). It consists of a low-density pile of sediments deformed by westward verging imbricate thrust system. Thus the Gulf of Cadiz shows a contrasting duality, the northern segment with predominance of positive free-air gravity anomalies which contrasts with the negative character of its southern areas (Fig. 2). As expected for the offshore free-air gravity anomaly map, short wavelength anomalies correlate to local bathymetry features, but this correlation is not observed for its medium to long-wave length component as this is associated to deeper density lateral variations (see Figs. 1a and 2).

4. Seismic interpretation and gravity modeling

4.1. Seismic interpretation strategy

The interpretation of the offshore structure has been an iterative process involving well-seismic correlation, seismic interpretation and gravity modeling. Interpretation was started from the well locations with wells tied to the time seismic (using the time-depth functions in

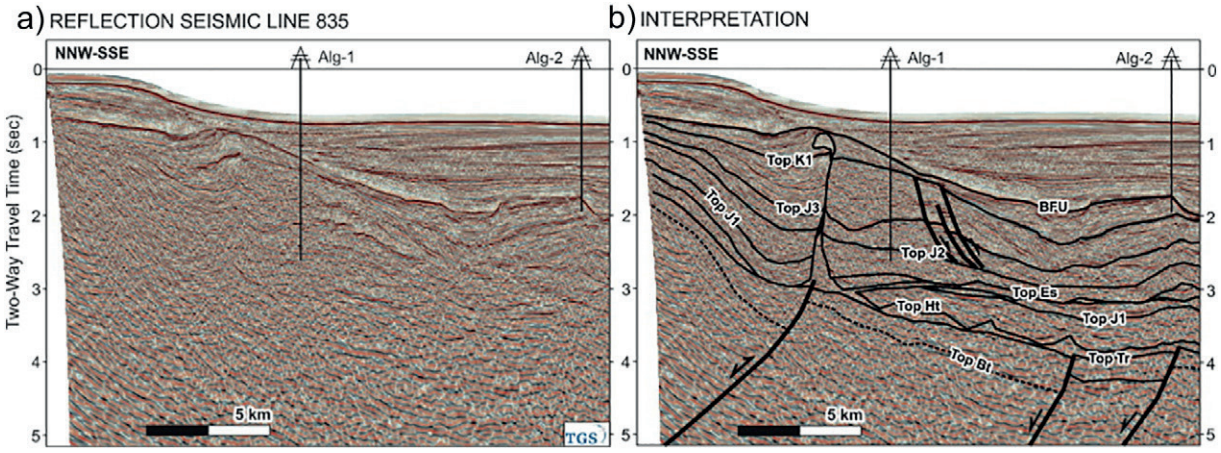

Fig. 6. Portion of seismic line 835 across wells Algarve-1 and Algarve-2 in time (a), and seismic interpretation (b). BFU: base foredeep unconformity; K1: Lower Cretaceous; J3: Upper Jurassic; J2: Middle Jurassic; J1: Upper Jurassic; Tr: Triassic; Ht: Hettangian. The allochthonous Esperança salt unit (Matias et al., 2011) is also identified (Es). See Fig. 4 for location.

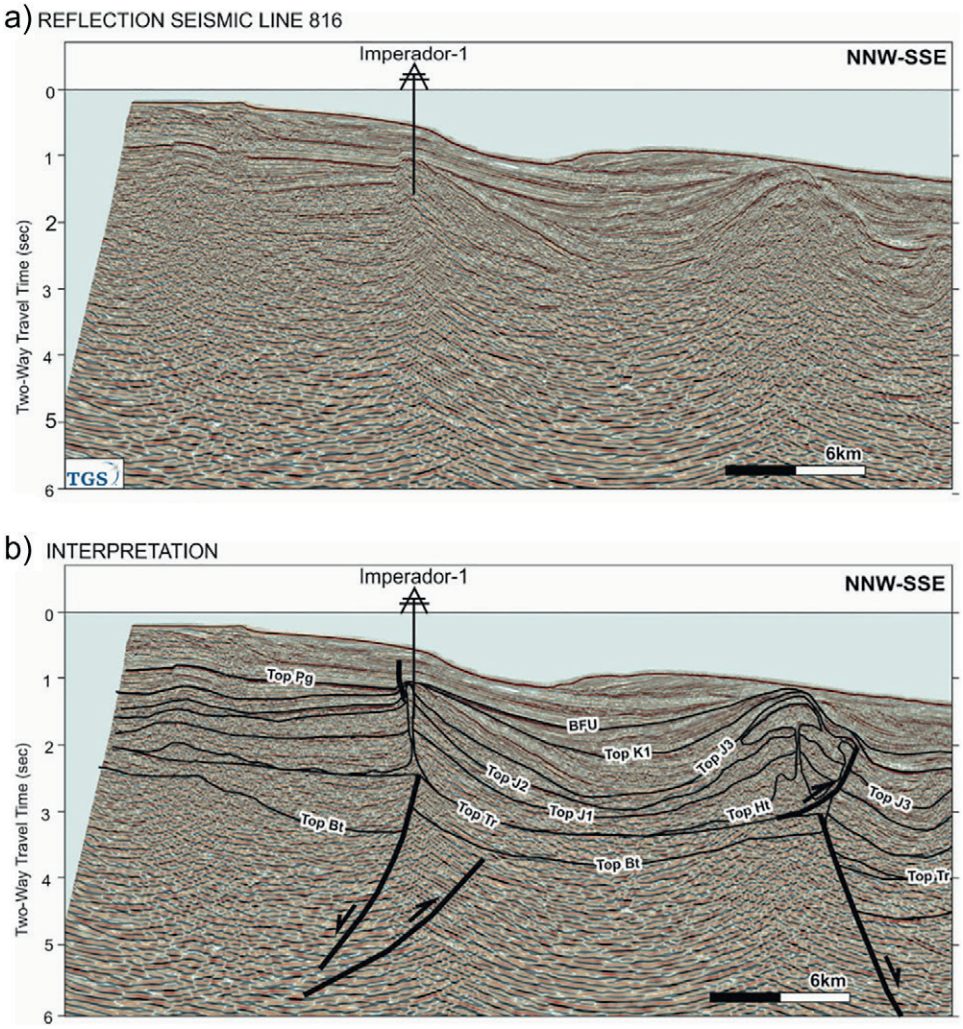

Fig. 7. Portion of seismic line 816 across the well Imperador-1, in time (a) and seismic interpretation (b). See Fig. 4 for location and Fig. 6 for acronyms. (Data courtesy of TGS.)

Fig. 5). Wells offshore Portugal make it possible to constrain horizons down to Middle Jurassic age (Figs. 6 and 7).

Interpretation of seismic profiles has been performed to map the main stratigraphic units defined by Terrinha (1998) (Triassic, Jurassic, Cretaceous and Cenozoic) (Figs. 6, 7 and 8) as well as the main faults, salt diapirs and allochthonous salt bodies (Matias et al., 2011). Each unit has characteristic seismic facies that make it possible to correlate them across faults and salt structures. The Cenozoic is dominated by continuous bright reflectors with multiple wedge and onlap geometries. It can be subdivided internally into the Neogene and Paleogene that are separated by a regional unconformity interpreted to be the base of the Betic foredeep (BFU; Ledesma, 2000). This unconformity, which is easily identified on seismic, corresponds with a strong reflector that truncates underlying units where they are folded or tilted (for instance, in Fig. 6 over the diapir north of well Algrave-1, or south of well Algarve-2).

Along the southern end of some seismic sections (e.g., Figs. 10, 12), the AWGC/AUGC complex is at the same structural position that the Paleogene and Neogene successions. These bodies display internally chaotic or transparent seismic facies. Their top and base are not defined by any characteristic reflectivity but rather by a sharp transition to layered seismic facies above and below (e.g., Fig. 10). Cenozoic sediments deposited above the AWGC/AUGC form mini-basins bounded by shale structures sourced from the allochthonous bodies (e.g., Hernández-Molina et al., 2016; Medialdea et al., 2009). At their base, the AWGC/AUGC can be observed to truncate or be parallel to the underlying Neogene and Paleogene beds (Figs. 12, 13).

The base of the Cenozoic is defined by another, less prominent unconformity. The base Cenozoic unconformity only locally truncates the units below (e.g., south of well Imperador-1 on Fig. 7). Below this unconformity the Cretaceous is characterized by bright and continuous reflectors of lower frequency than the Cenozoic. The Upper Cretaceous is absent in most of the offshore Gulf of Cadiz and the Cenozoic is underlain directly by the Lower Cretaceous. Thickness changes and internal angularities in the Lower Cretaceous related to halokinesis are frequent throughout the area (as in the onshore, Ramos et al., 2016).

The Upper Jurassic lies mostly conformably under the Cretaceous and is dominated by mostly bright but short reflectors of low frequency. The Middle and Lower Jurassic below have a similar seismic facies. Angularities observed within the Jurassic package could correspond to regional unconformities that punctuate rifting of the margin (such as those defined by Terrinha, 1998)and were used to interpret the boundaries between the Lower, Middle and Upper Jurassic. In the proximity of salt diapirs and in some mini-basins, unconformities within the Jurassic are controlled by halokinetic processes. However, major changes in thickness of the Jurassic across basement faults are interpreted to be controlled by extensional faults (for instance, change in thickness across

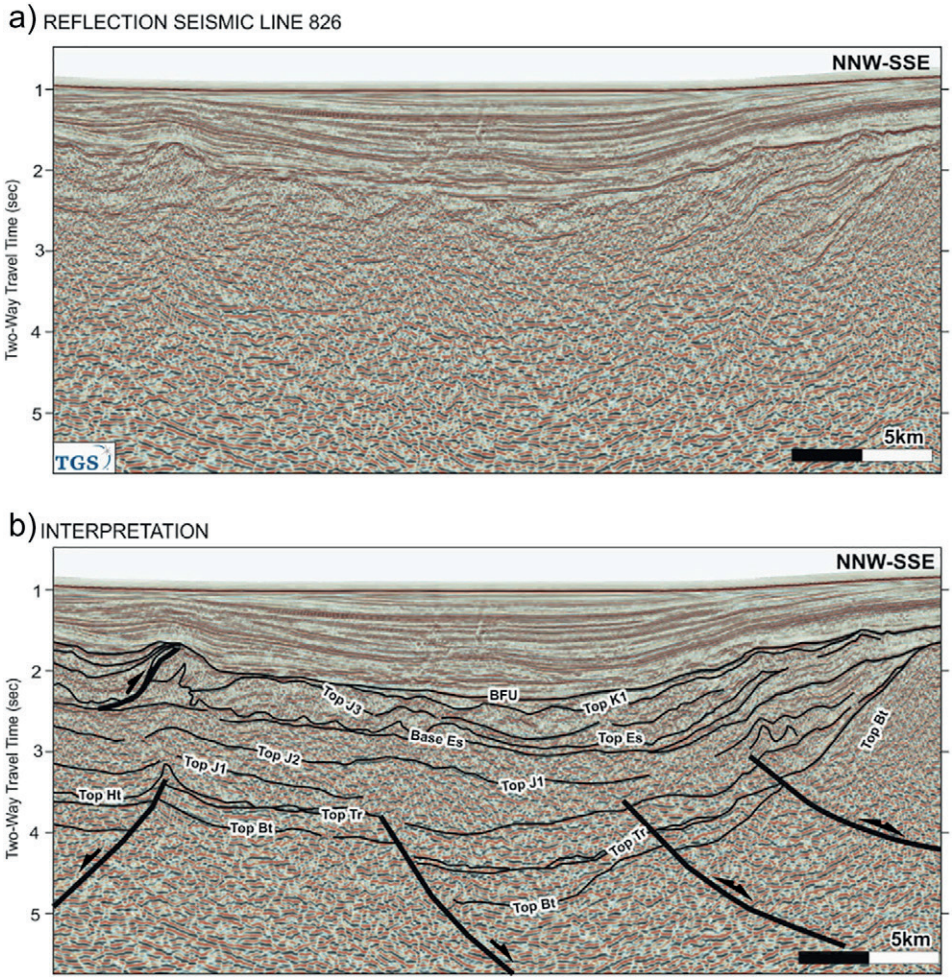

Fig. 8. Portion of seismic line 826 in the central part of the Algarve Basin, in time (a) and seismic interpretation (b) in the central part of the basin, north of Guadalquivir Bank. Es: Esperança Salt. See Fig. 4 for location and Fig. 8 for acronyms.
(Data courtesy of TGS.)

the basement fault on the southern end of Fig. 7, or thickness changes on Figs. 8 and 11).

The Hettangian evaporite interval, which is deformed into diapirs and salt walls, is the base of the Jurassic succession in the basin. The top and base of the Hettangian evaporites are frequently bright reflectors, and the unit is internally chaotic to transparent. This unit is the deepest unit that is easiest to pick as it is at the base of diapir-related folding and marks the base of halokinetic growth strata. Locally, Hettangian salt is extruded and forms parautochthonous and allochthonous salt bodies (e.g., Matias et al., 2011). Figs. 6 and 8 show one such instance where salt is extruded to form a broad allochthonous salt body (the Esperança Salt) that is emplaced mostly within the Jurassic. Image below this salt body is poor but control on the sub-salt structure is supported by the image in surrounding areas (for instance on Fig. 8). Above the Esperança Salt, mini-basins of Middle Jurassic to Lower Cretaceous developed, with fanning geometries, strong tilting and folding.

Below the Jurassic, the presence of Triassic clastics and volcanics deposited in fault-bounded grabens or half-grabens has been interpreted, by analogy with the onshore (Manuppella, 1992; Ramos et al., 2016; Terrinha, 1998) (for instance, see the half-grabens on the southern end of Fig. 8). The irregular distribution of the Triassic is confirmed by the fact that the only well in the offshore that drilled through the Hettangian evaporites (GC6Y-1BIS, Fig. 4) did not encounter Triassic deposits above the basement. The top of the Triassic unit was mapped on seismic by picking the base of the Hettangian evaporites.

The base of the Triassic has been defined by picking the top of the basement. The position of the top of the basement in the offshore is constrained by well GC6Y-1BIS (Fig. 4) and by its outcrop at the seabed along the Guadalquivir Bank (Vegas et al., 2004). The top of the basement has been interpreted as a bright reflector at the base of fault-bounded growth packages (southern end of Fig. 8). This reflector is sometimes ambiguous on seismic data as the basement is often characterized by reflective facies: its shallower units are Variscan foreland flysch deposits which have limited impedance contrast with the overlying Triassic clastics. The final interpretation of the top of basement has therefore been constrained based on geometric relationships (it is expected to be offset by the same faults as the overlying Mesozoic units).

4.2. Main features of the Algarve Basin

Seismic interpretation of the available 2D surveys has made it possible to achieve two key targets. The first one has been to map the basement faults that control the structure of the basin. The most evident faults are the extensional faults that developed during Mesozoic rifting (Figs. 6, 7, 8 and 9a). These faults are observed to trend mostly in a WSW-ENE direction (similar to those on the onshore, Ramos et al., 2016) (Fig. 9a). At the western and eastern ends of the basin, some

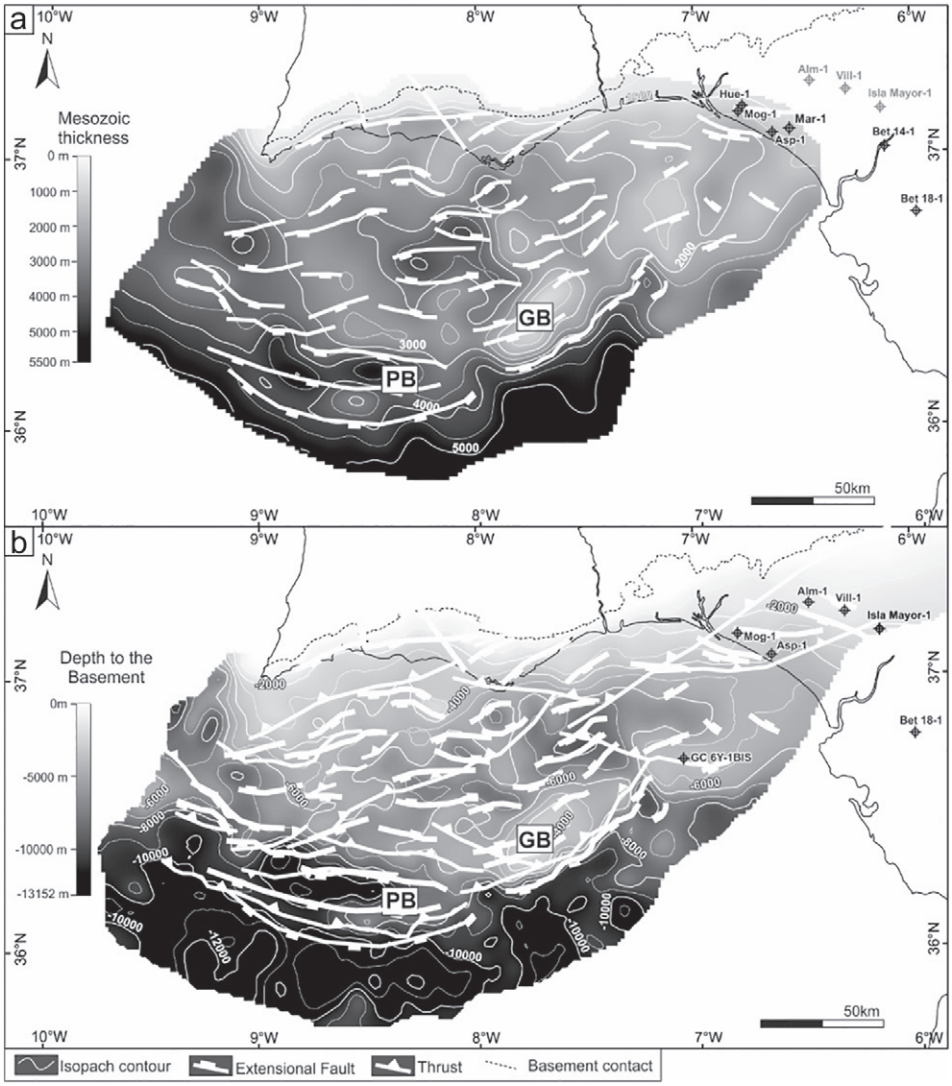

Fig. 9. (a) Vertical thickness of Mesozoic (Triassic to Lower Cretaceous) in the SW Iberian margin, with the main Mesozoic extensional faults overlain. Wells on the onshore that encounter Mesozoic sediments are shown in black. Wells that encountered no autochthonous Mesozoic are shown in grey. The Betica 14-1 was finalized upon reaching the top of the autochthonous Mesozoic (Upper Jurassic) and no reliable thickness value can be derived. The Betica 18-1 well drilled 2700 m of Mesozoic (Upper and Lower Cretaceous, Jurassic and Triassic). (b) Structural map of the top of basement, affected by Mesozoic extensional faults and Cenozoic thrusts (thrusts from Ramos et al., 2017). Wells reaching the basement are represented in the figure. The Betica 18-1 well encountered the basement at 4280 m bsl, but has not been incorporated in the map due to lack of constraint from MCS profiles. See Fig. 4 for complete well names and location of MCS profiles.

NW-SE trending faults are observed. Thickness of the Mesozoic is controlled by these faults (Fig. 9a).

Roughly N-S directed compression during the Mesozoic caused the partial inversion of the basin (Ramos et al., 2017) resulting in the present-day configuration of the basement of the basin (Fig. 9b). The faults responsible for inversion are not evident on seismic and have been inferred from multiple criteria, mainly from the tilting and truncation of Mesozoic and Cenozoic units and the geometry of the BFU unconformity (Ramos et al., 2017) (Fig. 10). Despite the inversion of the basin, an overall deepening of the basement towards the south and west is still observed (Fig. 9b), consistent with rifting that generated greater accommodation space in that same direction (Fig. 9a).

The second key target achieved through seismic interpretation was to define the offshore extent of the Algarve Basin. Previous authors have considered the Guadalquivir and Portimão Banks as the southern limit of the Algarve Basin (e.g., Gràcia et al., 2003; Matias et al., 2011; Terrinha et al., 2002). This interpretation was mostly driven by the observed thinning of Mesozoic units onto the Guadalquivir Bank (Figs. 8, 10). Both Banks were interpreted to respond to the same structure. This interpretation has been revised in favor of a combined origin. The Guadalquivir Bank is interpreted as a Mesozoic extensional horst now being carried on top of a southward vergent thrust (Ramos et al., 2017 and Fig. 10). The basement in the Guadalquivir Bank is interpreted to be relatively shallow (<2 km under the seabed, and locally outcropping) (Malod and Mougenot, 1979; Vegas et al., 2004) and uplifted in the order of 5 km in Neogene times due to a major south-directed thrust (Fig. 10). On the other hand, the bathymetric relief of the Portimão Bank is due to the inversion of a Mesozoic extensional half-graben (Ramos et al., 2017; Terrinha et al., 2009 and Fig. 11). As opposed to the Guadalquivir Bank, it is not a basement high, and hence basement depth does not change as dramatically across this feature (Fig. 9b). Thus, the Guadalquivir and Portimão Banks are not considered to be the southern limit of the Algarve Basin.

The southern extent of the basin cannot be mapped precisely. However, Mesozoic units are observed to extend south of the Portimão Bank, under the AWGC, possibly over continental basement (Fig. 12). It is further south that oceanic crust can be easily picked on seismic (Fig. 13). The oceanic crust is characterized by a top bright, continuous reflector seen clearly even below the AWGC at roughly 8 s TWT (two-way time). The continent-ocean boundary seen on Fig. 13 is at a location

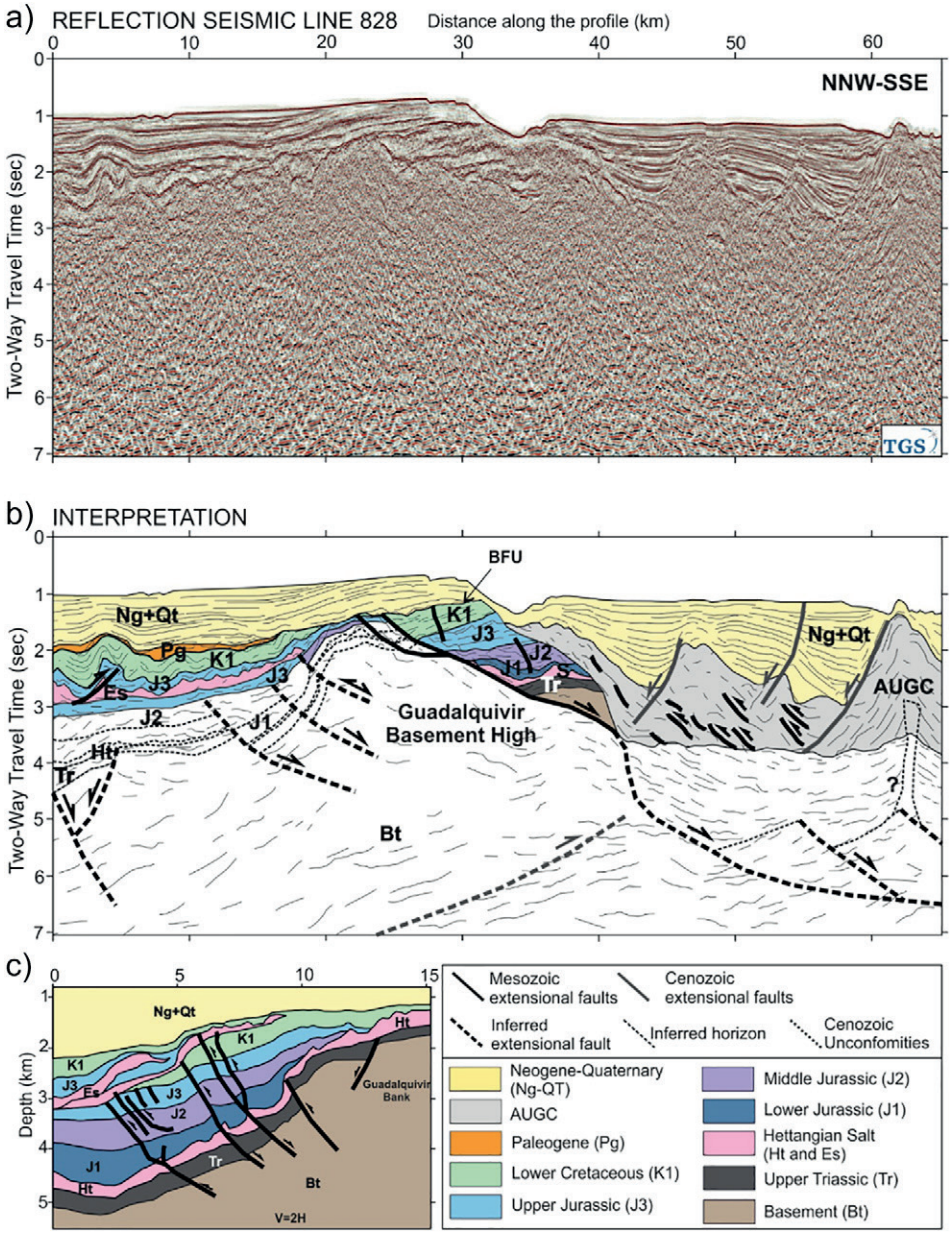

Fig. 10. Portion of seismic line 828 across the Guadalquivir Bank in time (a) and seismic interpretation (b). The interpretation below 3–4 s of TWT is inferred due to the poor deep seismic quality. Interpretation of the northern flank of the Guadalquivir Bank is based on the interpretation performed on 3D seismic (c) of the same structure slightly along strike by (Ramos et al., 2017). See Fig. 4 for location.
(Data courtesy of TGS.)

consistent with the continent-ocean boundary documented by Sallarès et al. (2011). Despite the lack of reliable seismic image further to the east, it is interpreted that the southern limit of the Algarve Basin in that direction also lies at the transition to the oceanic crust proposed to be present by Gutscher et al. (2002), Martínez-Loriente et al. (2014), and Sallarès et al. (2011).

To the east, the Algarve Basin is known to terminate roughly along the present-day coast of SW Spain, where the basement rises (Fig. 9b). Control on the depth of the basement in this area is provided mainly by onshore wells (Fig. 4). Seismic profiles in this area are of limited quality, but some extensional faults have tentatively been mapped to strike NW-SE (Fig. 9a).

The western termination of the Algarve Basin is the only one that has been observed on seismic (Fig. 14). This limit of the basin is characterized by mostly southwestward dipping extensional faults that cause a drastic drop of the basement towards the southwest. The bathymetry in this area is strongly controlled by contouritic currents of the Mediterranean Outflow Water and submarine canyons, but the overall NW-SE trend in the sea bottom runs parallel to the interpreted basement faults. The transition into the oceanic domain on this side of the basin has not been identified on seismic. However, the basement on seismic profiles in this area is interpreted to drop down to 8 s TWT, which is similar to the depth of the top of oceanic crust in Fig. 13 with a similar water column. It is therefore inferred that the continent-ocean boundary does not lie far to the west (or even within the profile).

4.3. Interpreted structure

To represent the structure of the Gulf of Cadiz, four cross-sections have been interpreted following key seismic profiles (Fig. 15). These sections strike NNW-SSE, with the objective of intersecting the southern limit of the Algarve Basin and the prominent positive gravity anomaly

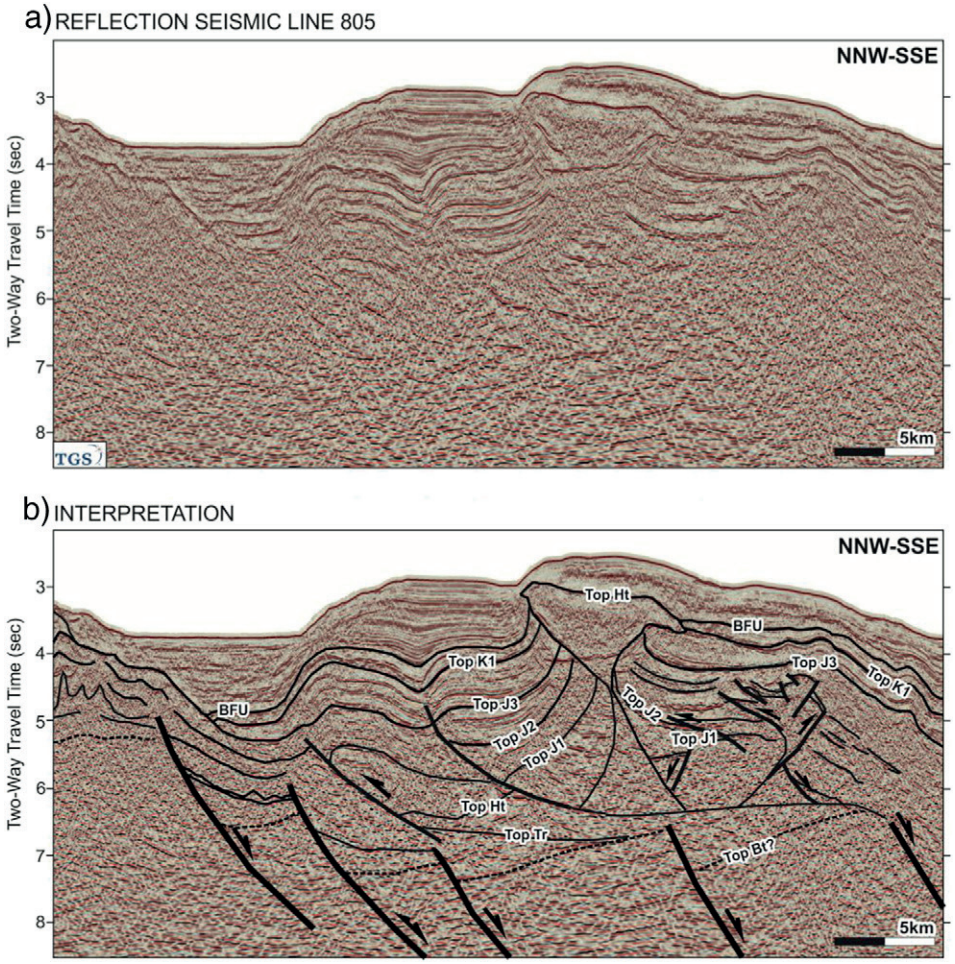

Fig. 11. Portion of seismic line 805 across the Portimão Bank in time (a) and seismic interpretation (b). The Portimão Bank is imaged as an inverted Mesozoic graben. See Fig. 4 for location and Fig. 8 for acronyms.
(Data courtesy of TGS.)

that runs along the Guadalquivir and Portimão Banks (Fig. 2). Interpretation on these sections was driven by seismic (e.g., Figs. 6 through 11) for the shallower Algarve Basin (the area north of the Guadalquivir and Portimão Banks).

The structure of the shallow Algarve Basin is characterized by both south and north dipping extensional faults, with growth from Triassic to Middle Jurassic (Fig. 15). Throw on the faults and thickness of Jurassic depocenters increases progressively southwards (Figs. 9a and 15). Thickness changes in the Jurassic are partly controlled by salt tectonics (e.g., mini-basin south of Imperador-1 in Fig. 7) and partly fault-driven (e.g., Mesozoic half-graben in Fig. 11). In the case of the Lower Cretaceous and Paleogene, thickness changes are largely controlled by salt

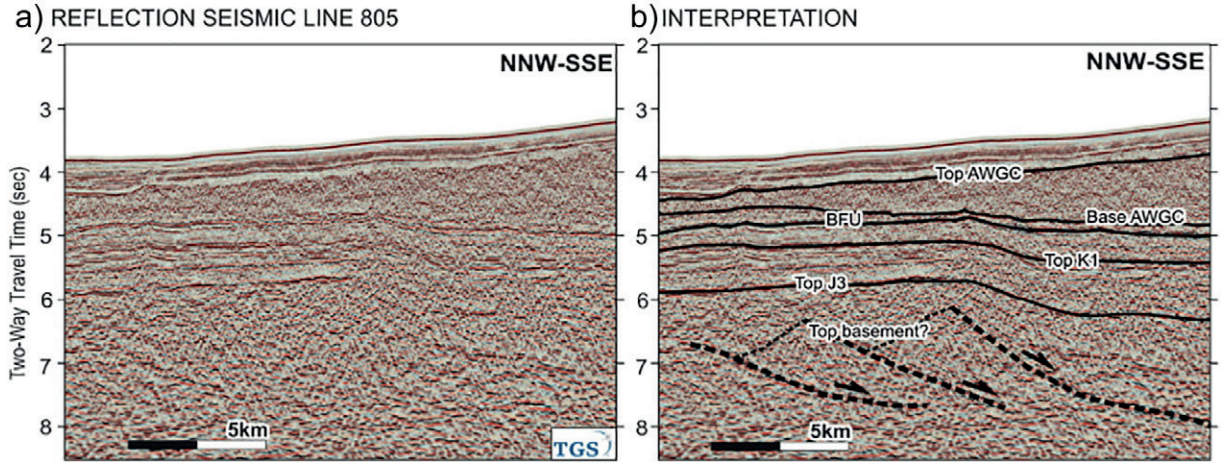

Fig. 12. Portion of seismic line 805 south of the Portimão Bank, across a distal portion of the AWGC, in time (a) and seismic interpretation (b). Note that Mesozoic units are visible under the AWGC and the top of the basement is imaged around 7 s of TWT. See Fig. 4 for location and Fig. 8 for acronyms.
(Data courtesy of TGS.)

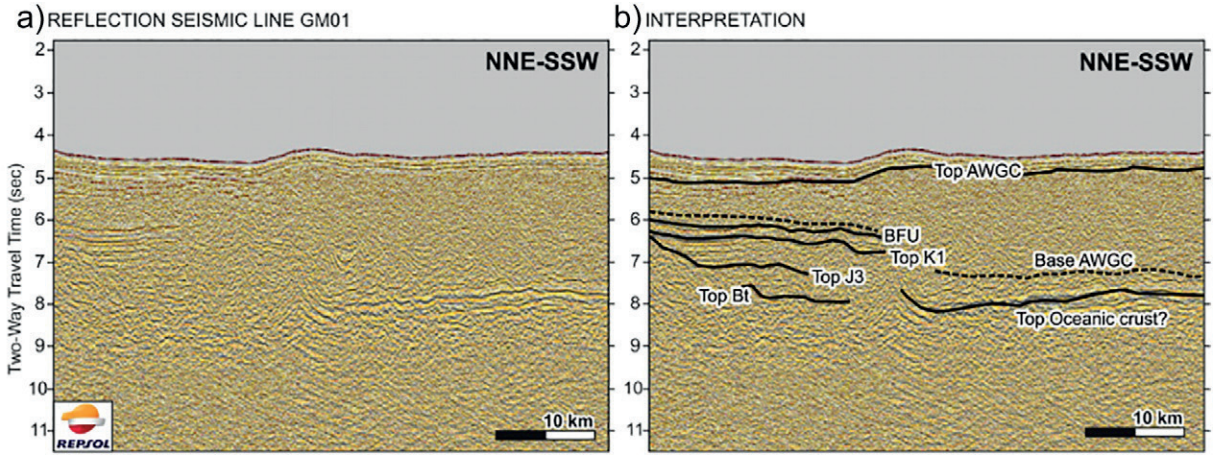

Fig. 13. Portion of a seismic profile GM01 across the outer Gulf of Cadiz in time (a) and seismic interpretation (b). Note the bright continuous reflectors under the AWGC interpreted to be the top of oceanic crust. See Fig. 4 for location.
(Data courtesy of Repsol.)

withdrawal in mini-basins (e.g., depocenters flanking the structure near well Algarve-1 on Fig. 6) and by erosion during uplift (e.g., over diapir south of well Imperador-1 on Fig. 7).

To the south of these Banks, image quality makes it difficult to define the structure unambiguously. Initial gravity modeling of key sections in the area (Giraldo et al., 2014; Ramos et al., 2015) demonstrated that the basement on the southern side of the Guadalquivir-Portimão Bank lies 5–7 km deeper than under the Algarve Basin, indicating that the crust needs to be significantly thinner. Thinning of the crust is consistent with the interpreted drop in the top of the basement and southward increase in Mesozoic accommodation space (Fig. 9). However, greater thickness of Miocene-Present sediments and the presence of the AWGC and AUGC south of the Guadalquivir-Portimão Bank pose major challenges to correlate Mesozoic horizons from the Algarve Basin into deeper water areas. Interpretation to the south of the Guadalquivir and Portimão Banks was therefore focused on identifying the base of the AWGC/AUGC and the most likely top of basement (e.g., Figs. 10 and 12).

4.4. Gravity modeling

The four representative cross-sections presented in Fig. 15 were modeled for their gravimetric response with three objectives: 1) to validate the interpreted depth to basement, particularly relevant in areas of poor seismic imaging; 2) to constrain the structure to the south of the Guadalquivir-Portimão Bank, where the AUGC/AWGC obscures the deep structure; and 3) to characterize the crustal structure of the passive margin by combining gravity with available well log data to constraint densities at upper crustal levels and available seismic wide angle and refraction data to constraint the depth to the base of the crust and the densities at mid-lower crustal and uppermost lithospheric mantle levels. For the sedimentary cover and geometry of top of basement, the gravity models shown in Fig. 16 were built using the geometry derived from the seismic interpretation discussed above (Fig. 15) and well log data. For the deeper part of the profiles, from top basement to the base of the crust we have used information from all available wide-angle and refraction seismic data, and previous 2D crustal and lithosphere geophysical modeling (Fernàndez et al., 2004; González et al., 1998; Gutscher et al., 2002; Zeyen et al., 2005). Along the Iberia continental margin, Moho depths were taken from the compilation of Diaz et al. (2016) and the profiles of Palomeras et al. (2009). For the distal parts of the profiles we have taken the data from Gutscher et al. (2012). For the continental domain of the westernmost profiles Moho depths were taken from Sallarès et al. (2011). Well logs were mainly used to constrain the density of the main sedimentary units while the density of the crystalline crust were converted from P-wave velocities to densities by using the Brocher (2005) empirical relationship. The crust is modeled as: sedimentary layers with densities that range from 2200 to 2600 kg/m^3, an underlying upper/middle crust with an average density of 2750 kg/m^3, while for the lower crust and uppermost lithospheric mantle we have used 2900 and 3300 kg/m^3, respectively. The forward modeling has been performed using GM-SYS (modeling

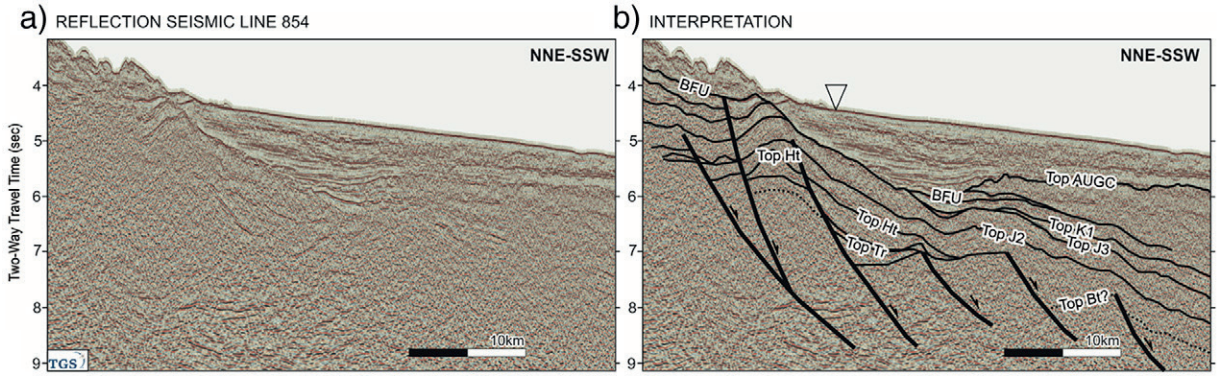

Fig. 14. Portion of reflection seismic profile 854 across the western portion of the margin (a) and the corresponding interpretation (b). The triangle on the seabed marks the location of the transfer discussed in Fig. 18. See Fig. 4 for location.
(Data courtesy of TGS.)

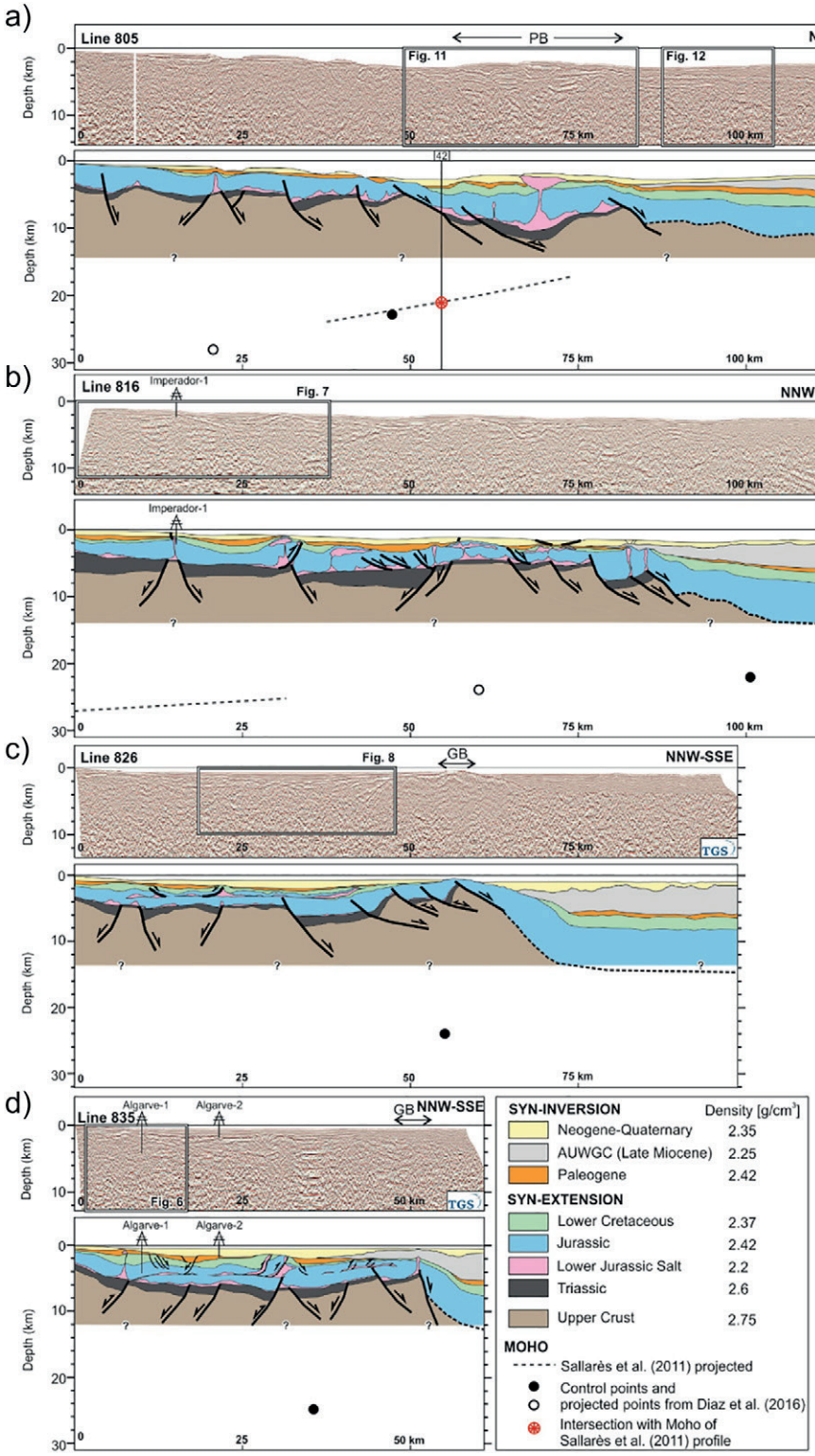

Fig. 15. Interpretation of depth converted seismic profiles through the Algarve Basin, shown from west (top) to east (bottom): a) Line 805; b) Line 816; c) Line 826; and d) Line 835. The control points on the depth of Moho from the compilation of Diaz et al. (2016) and the profile of Sallarès et al. (2011) are shown. Average interval densities are shown in the legend. GB: Guadalquivir Bank; PB: Portimão Bank. See Figs. 1a and 4 for location.
(Data courtesy of TGS.)

application of Oasis Montaj, Geosoft software), which calculates the gravity response of the density models built using the methods of (Talwani, 1965; Talwani et al., 1959). For all transects (Figs. 16 and 17) the calculated gravity values lie very close to measurements.

5. Results: crustal structure of the SW Iberian margin

The results of the modeling process are 4 profiles (Figs. 16 and 17) that capture the key aspects of the SW Iberian passive margin. These

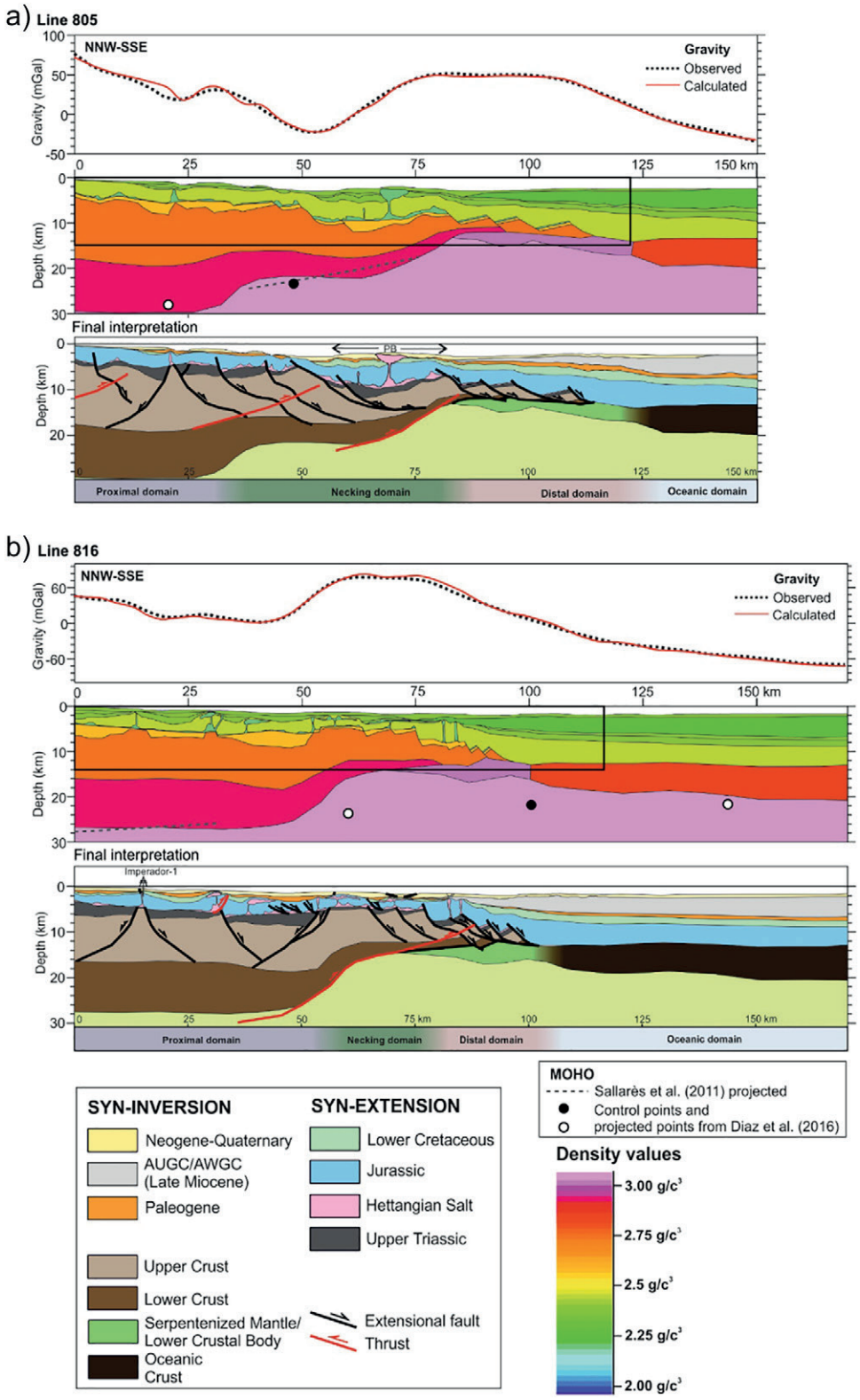

Fig. 16. Composition of observed and forward modeled gravity, density model and final interpretation for profiles along lines 805 (a) and 816 (b). The geometry of the sedimentary layers, from Triassic to Quaternary, has been derived from the interpretation of MCS data (Fig. 15). Extent of the seismic profiles is represented by a black box on the density model. Densities used are also shown in the table on Fig. 15. The Moho from the profile of Sallarès et al. (2011) has been projected onto the density models over the pertinent segments. Points from the compilation by Diaz et al. (2016) lying on the modeled profiles (black) and projected from nearby locations (white) are also shown on the density model. On the final interpretation note the combination of Mesozoic extensional and Cenozoic contractional features (from Ramos et al., 2017). See text for a discussion of the defined crustal domains. PB: Portimão Bank. See Fig. 2 for location.

profiles follow the seismic lines shown in Fig. 15, and are extended towards the south, into the region of the negative free-air gravity anomaly (Fig. 2).

Modeling results demonstrate that the originally interpreted top of basement is regionally valid. Locally, however, gravimetric modeling reveals that depocenters under the Hettangian evaporites are thicker than initially interpreted. Results have therefore been used to fine tune the interpretation in these sectors (revised interpretation shown in Figs. 16 and 17). The final interpreted thickness of some of these Triassic depocenters is much greater than that observed onshore (few hundreds of meters, Ramos et al., 2016) but in line with thicknesses observed in basins such as the High Atlas or Essaouira (Domènech et al., 2015; Ellouz et al., 2003; Le Roy and Piqué, 2001).

At the crustal scale, gravimetric modeling supports the interpretation of thinning of the crust towards the axial parts of the Gulf of Cadiz. The transition from the thick crust along the northern end of the profiles to the thin crust along the southern end of the profiles is interpreted as defining four key domains. The northernmost domain (proximal domain, Figs. 16 and 17) is characterized by a limited amount of thinning (the pre-rifting crust is 20–26 km thick, equivalent to β between 1.25 and 1.6). This proximal domain has approximately constant crustal thickness, water depth and depth to basement. From this domain to the south the first increase in the gravity signal occurs above the point where the crust starts to thin significantly along with an increase in water depth. Thinning is gradual in the eastern profiles (lines 826, 835, Fig. 17). In the west, crustal thinning concentrates across one or two relatively narrow steps, 10 to 15 km wide (lines 805, 816, Fig. 16). The domain of thinning (necking domain) is wider in the west (in the order of 75 km, line 805, Fig. 16) and becomes narrower towards the east (<50 km wide, line 835, Fig. 17).

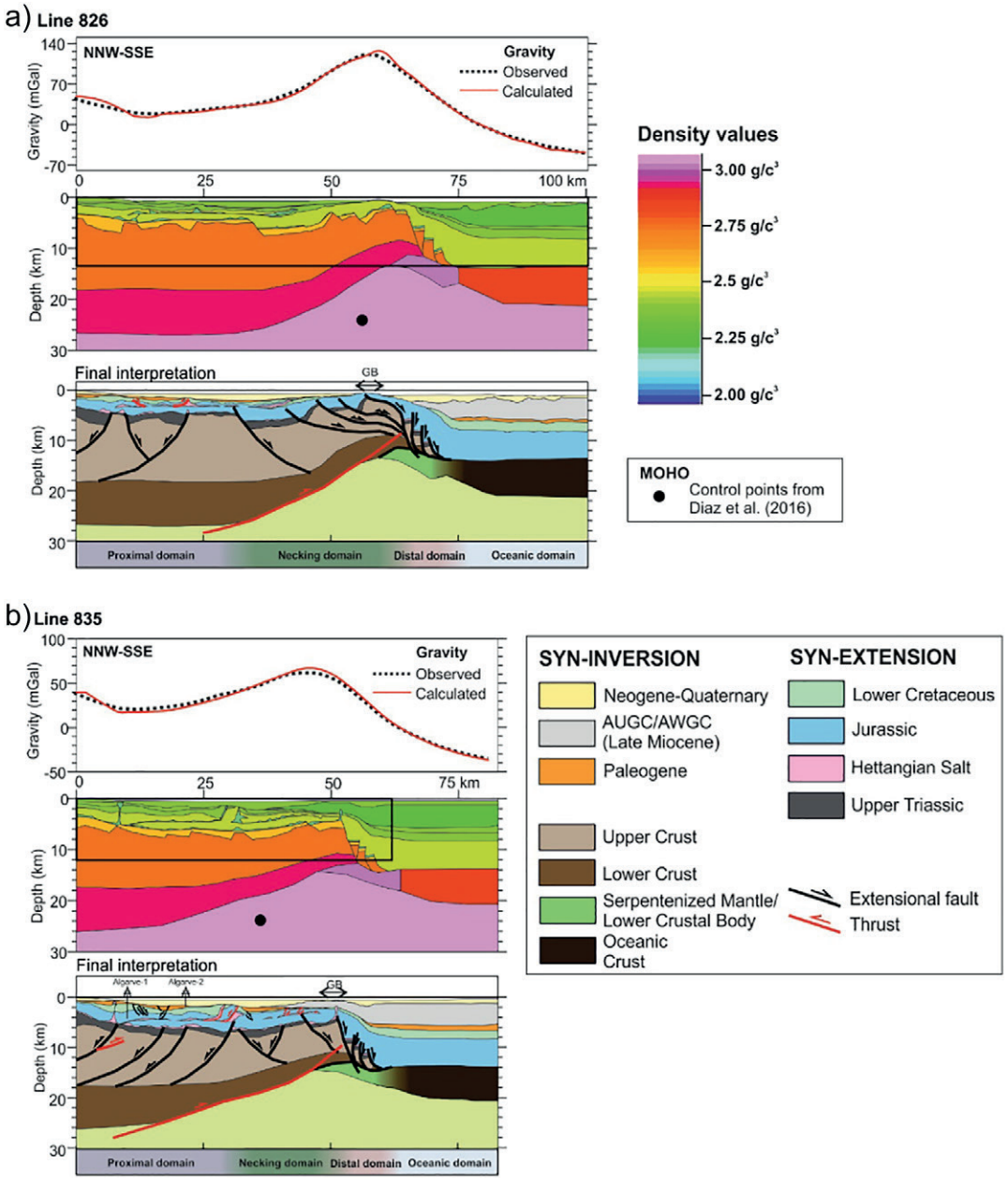

Fig. 17. Composition of observed and forward modeled gravity, density model and final interpretation for profiles along lines 826 (a) and 835 (b). The geometry of the sedimentary layers, from Triassic to Quaternary, has been derived from the interpretation of MCS data (Fig. 15). Extent of the seismic profiles is represented by a black box on the density model. Densities used are also shown in the table on Fig. 15. The Moho control points from Diaz et al. (2016) are shown on the density model. On the final interpretation note the combination of Mesozoic extensional and Cenozoic contractional features (from Ramos et al., 2017). The geometry on the southern end of the profiles is partly inferred from that seen on the western profiles (Fig. 16). See text for a discussion of the defined crustal domains. GB: Guadalquivir Bank. See Fig. 2 for location.

Gravimetric modeling also suggests that the most pronounced thinning of the continental crust occurs at the southern end of the necking domain, just underneath the gravity high. At this location, the Moho is modeled to be only 15 km deep and the crust 10 km thick or less (Figs. 16, 17). The crust in this area is known to be continental. Carboniferous basement rocks have been dredged from the Guadalquivir Bank (Vegas et al., 2004) and the Portimão Bank is a Mesozoic graben that must have developed over continental crust.

South of the necking domain we have interpreted the presence of a domain of highly attenuated continental crust (distal domain). Continental crust in the distal domain has been interpreted to be faulted and rotated by low-angle extensional faults (Figs. 16, 17). This interpretation is partly based on observations made on seismic data, such as the folded geometry of Mesozoic strata south of the Portimão Bank (Fig. 12) or the local presence of diapirs rising from the deep Mesozoic strata south of the Guadalquivir Bank (our interpretation in Fig. 10 and Medialdea et al., 2004).

We have assumed that serpentinized mantle could be present in the distal domain by exhumation of the uppermost lithospheric mantle during Jurassic extension. The gravity contribution of serpentinized mantle bodies is in the range of 20 to 30 mGal. Although we do not have any direct evidence for the presence of Jurassic exhumed mantle in the study region, we have assumed its presence by affinity with what is observed in the West Iberian Atlantic Margin (e.g., Peron-Pinvidic and Manatschal, 2009). Serpentinized sub-continental mantle exhumed in the Late Jurassic to Early Cretaceous has also been documented in neighboring areas such as the Gorringe Bank (Cornen et al., 1999; Jiménez-Munt et al., 2010) or the Rif (Michard et al., 2007).

In the longer profiles (Fig. 16), a thin high density crust has been interpreted in the southernmost part. This crust has been interpreted as a possible oceanic crust (density of 2900 kg/m^3), driven by the observations on reflection seismic in this area (Fig. 13) and by the work of previous authors (e.g., Gutscher et al., 2009; Martínez-Loriente et al., 2014; Sallarès et al., 2011).

The effect of Cenozoic inversion of the SW Iberian margin is also observed on the modeled profiles. Inversion in this margin has localized mainly in the necking and distal domains. In the west the necking domain is broad and the transition to the distal domain is gradual and located south of the Portimão Bank (Fig. 16a). In this sector, Cenozoic contraction caused the inversion of pre-existing rift structures, but did not cause major uplift of the basement. Towards the east the necking domain becomes narrower and the transition to the distal and oceanic domains becomes very sharp (Fig. 17b). This transition is located immediately south of the Guadalquivir Bank. To account for this geometry, we interpret that the extensional structure of the southern flank of the Guadalquivir Bank was originally similar to that south of the Portimão Bank. Cenozoic inversion in the Guadalquivir Bank subsequently occurred along crustal-scale thrusts that caused major uplift along the Bank and folded and tilted the pre-existing extensional structure into its present-day geometry.

According to our preferred interpretation, the width of the necking and distal domains accounts for the varying wavelength of the positive gravity anomaly of the Gulf of Cadiz. In the case of Portimão Bank (Fig. 16a) the anomaly is broad due to the greater width of the necking domain and is not related to a basement high (the top of the basement is in the order of 8 km deep; Figs. 11 and 15a). On the other hand, crustal thinning further east (Fig. 17b) is more abrupt on account of the superposition of the initial extensional geometry and subsequent basement uplift (Guadalquivir Bank: Ramos et al., 2017; Vegas et al., 2004). This explains the narrower and stronger positive anomaly.

6. Discussion

The present-day crustal structure of the SW Iberian margin is the result of the superposition of Mesozoic extension and Cenozoic to Present shortening. The discussion below will first describe the more recent contractional overprint before discussing the original crustal structure related to extension.

6.1. Inversion of the SW Iberian margin

The effects of Cenozoic shortening are most evident in the eastern part of the Algarve Basin, in particular along the Guadalquivir Bank (Figs. 10 and 17). In this eastern part of the basin, the Guadalquivir Bank is uplifted by at least 2 km due to Cenozoic basement-involving thrusting (Ramos et al., 2017). To the west, the Portimão Bank is observed to be mildly inverted with no evidence of significant thrusting in the basement (Fig. 11; Ramos et al., 2017). This difference in the magnitude of Cenozoic shortening accounts for the differences in the geometry of the transition from the necking to the distal domains. In the west, the necking domain is broad and it transitions gradually into the distal domain. The result is a broad high in the Moho (Figs. 16 and 18a). In the east, this structure has been strongly overprinted by contraction and uplift, resulting in what appears as a narrow antiformal geometry of the Moho (Fig. 17). The geometry of the distal domain is also interpreted to be highly affected by uplift and tilting due to contraction (Figs. 17). The contractional overprint leads to the shallow in the base of the crust becoming much narrower and offset further southeast in the eastern sections (Fig. 18a). The offset observed in the base of the crust coincides with the trace of a NW-SE trending thrust identified by Ramos et al. (2017)that also causes a major step in the map trace of the necking zone (Fig. 18b), supporting the crustal nature of these thrusts.

The main inversion structure in the Gulf of Cadiz coincides in location and strike with the necking zone along the Guadalquivir Bank (Figs. 17, 18b). This raises the possibility that the thrust under the Guadalquivir Bank takes advantage of the tilting of the lower crust and Moho induced initially during extensional necking (Fig. 17). The localization of inversion along the necking zone contrasts with the inversion documented by Tugend et al. (2014) along northern Iberia and Druet (2016) along northwest Iberia, where thrusting is located in the distal domain or the continent-ocean transition. The possibility of similar structures in the deep part of the modeled profiles cannot be ruled out but they cannot be identified due to the masking by the AWGC/AUGC.

Inversion of the Guadalquivir Bank can help explain the apparent lack of isostatic equilibrium of the structure based on the interpreted crustal structure. Based on the water column (<1 km) and relatively shallow depth to basement (<1 km below seabed) in the Guadalquivir Bank on line 826 (Fig. 15c), the Moho would be expected to be in the order of 28 km deep (by comparison with the onshore Iberian Moho at 32 km depth and assuming a 2800 kg/m^3 average crustal density and Airy isostasy). This value is significantly deeper than estimates from DSS (Diaz et al., 2016) and our model (Fig. 17a) that place it at 24 or 15 km depth respectively. This contrasts with the Portimão Bank where under roughly 2 km of water and 8 km of sediments, the Moho is expected at 18 km depth, in line with our model (Fig. 16a). The relevance of flexure in supporting isostatic disequilibrium cannot be ignored. Flexure of the lithosphere west of the Gibraltar Arc subduction could be responsible for the broad negative anomaly observed south of the lines 826 and 835 (Fig. 2).

6.2. Extensional crustal structure of SW Iberia

What remains at crustal level after discounting the effects of Cenozoic contraction is a gross southeastward directed thinning of the SW Iberian margin (Fig. 18b). Southeastward thinning is the result of extension in the Mesozoic, which was dominated by WSW-ENE to E-W faulting, with NW-SE trending transfer faults (Fig. 9b; trends also in the onshore: Ramos et al., 2016).

The orientation of the crustal domains resulting from thinning in the westernmost Algarve Basin rotates to a southwestward direction (Fig. 18b). This western margin of the basin coincides with a sharp rise in

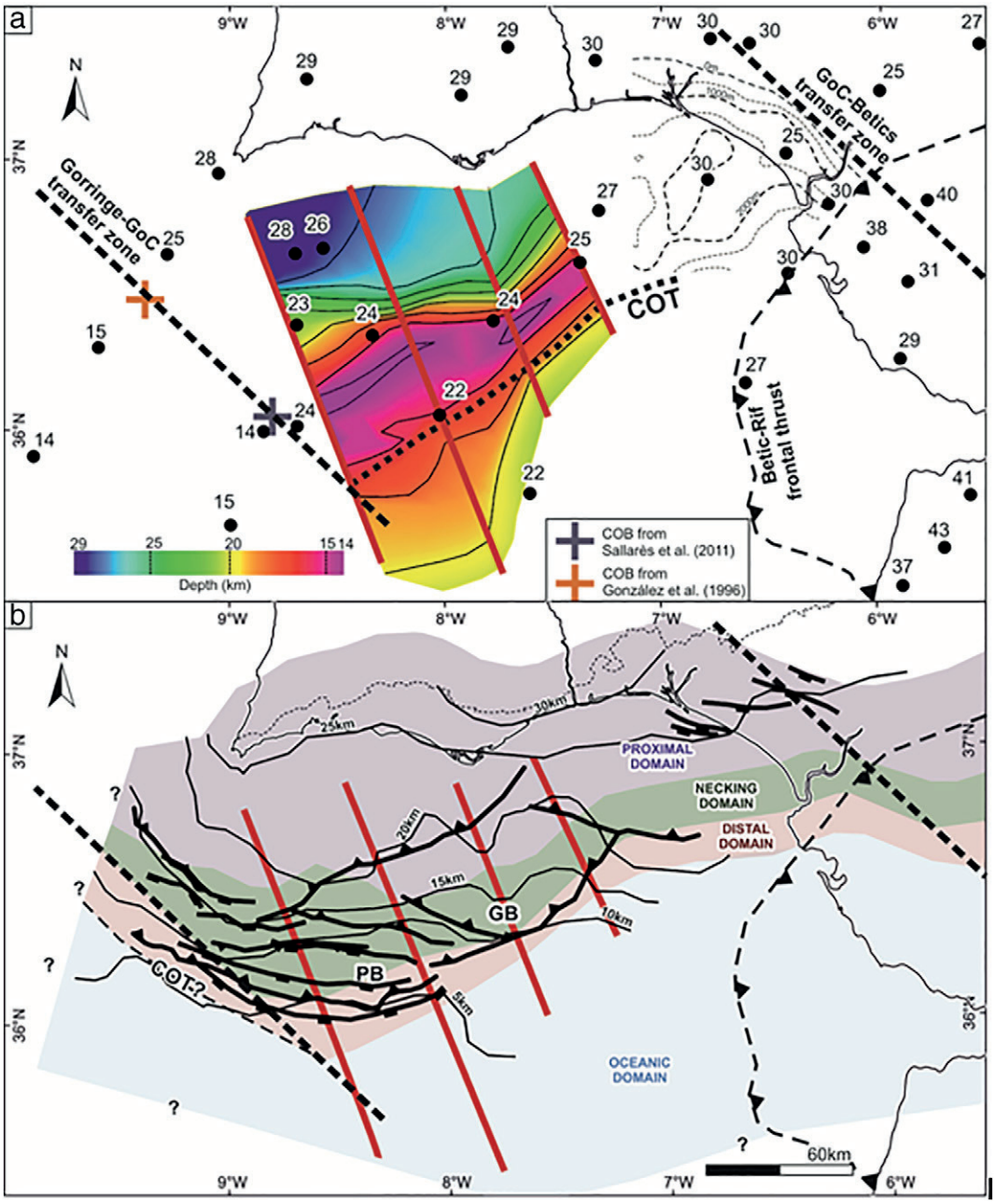

Fig. 18. a) Map of the base of the crust derived from seismic interpretation and gravimetric modeling. The COT (continent-ocean transition) derived from gravimetric modeling is shown by the bold dashed line. Points with numbers indicate the depth to the base of the crust from the compilation of Diaz et al. (2016). The western limit of the Gulf of Cadiz (GoC) segment of the margin is marked by the Gorringe-GoC transfer zone along the transition from continental to ocean domains defined by González et al. (1996) and Sallarès et al. (2011). The eastern limit of the margin segment is located along the GoC-Betic transfer zone, across which Mesozoic thickness drops (dashed contours indicate Mesozoic thickness in this area from the map in Fig. 9a). b) Map of crustal thickness of SW Iberia with crustal domains (proximal, necking, and distal) defined through gravimetric modeling and from crustal thickness. Thrusts relevant to the discussion, mapped by Ramos et al. (2017), and relevant extensional faults from Fig. 9a are superimposed.

the Moho that trends NW-SE (Fig. 18a), parallel to the transfer faults of the extensional system. It is therefore proposed that southeastward thinning is due to margin-perpendicular extension, whereas crustal thinning across the western end of the margin occurs across transfer faults (e.g., Fig. 14).

This proposed orientation of the margin accounts for the main difference between our models and the interpretation of Sallarès et al. (2011). These authors interpret continental crust to transition directly to oceanic crust at the point where crust thins to <10 km immediately south of the Portimão Bank. This rapid transition contrasts with the more gradual transition suggested by our modeling (Fig. 16). The difference arises because the continent-ocean transition in the profile of Sallarès et al. (2011) occurs across the transform system bounding the Algarve Basin to the west (Fig. 18a). On the other hand, the transects presented in this paper are drawn perpendicular to the dominant extensional faults and therefore provide an image of the transition from continental to oceanic crust in the direction of extension.

The orientation of this margin is consistent with that expected from the relative motion between Iberia and NW Nubia during the Jurassic (Fig. 1b and c; Schettino and Turco, 2011). This trend is noticeably different to the N-S to NE-SW trend of the Atlantic margins (Fig. 1) and makes the SW Iberian passive margin the likely westward continuation of the southern Iberian passive margin (currently inverted in the Betics) and possibly the Ligurian Tethys.

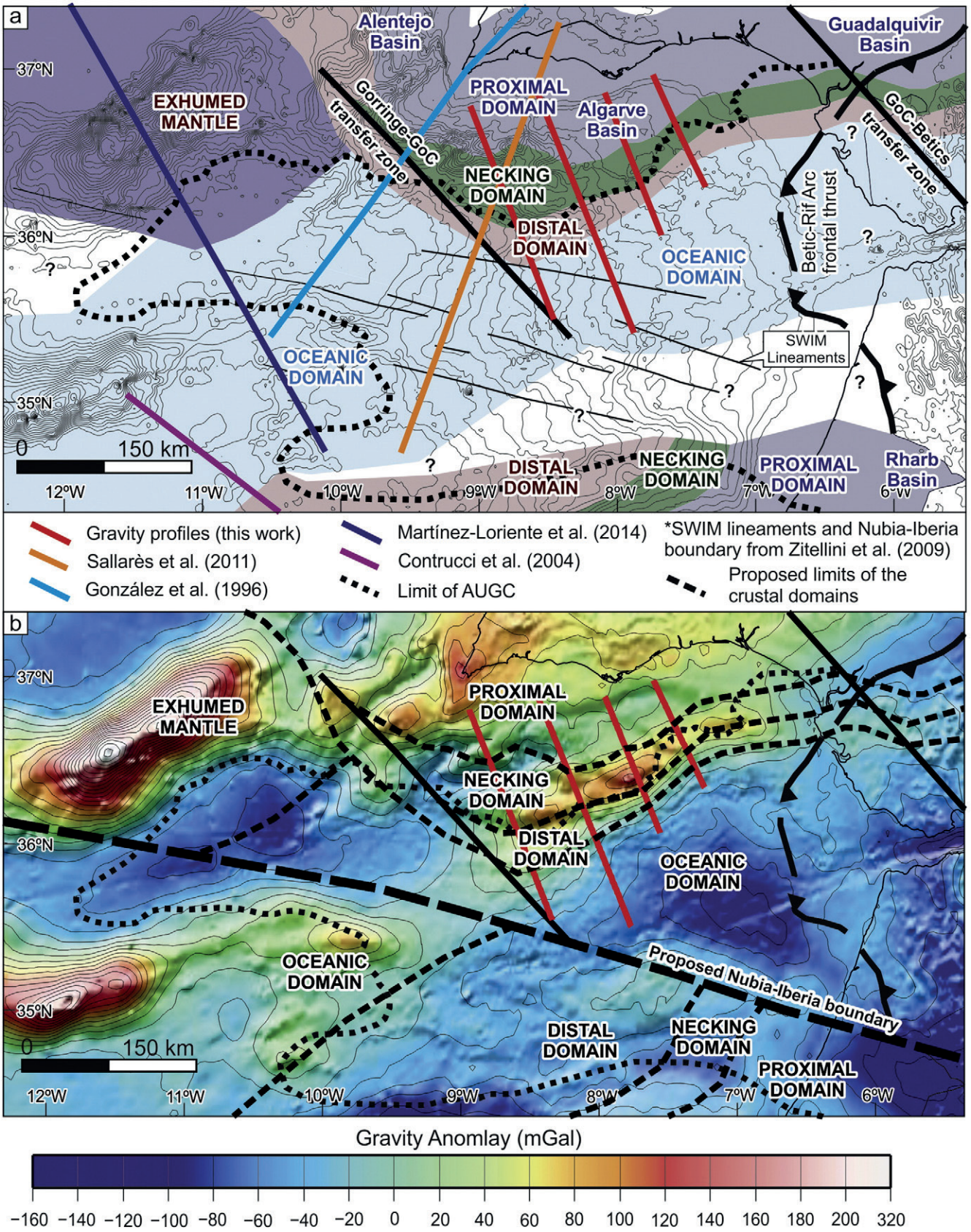

Fig. 19. a) Map of the main crustal domains of the Gulf of Cadiz and surrounding areas. Bathymetry is shown in the background (contours every 200 m). The location of bibliographic profiles is shown. The domains defined for the Morocco margin are derived by projecting the domains defined by Contrucci et al. (2004). b) Map of the free-air gravity anomaly map (offshore) and Bouguer gravity anomaly (onshore) of the SW Iberian margin with the crustal domain distribution based on integrated regional 2D seismic data and gravimetric modeling. Thin dashed black lines: crustal domain boundaries.

Oceanization in southern Iberia is understood to have occurred during the Late Jurassic (García-Hernández et al., 1989; Vera et al., 2004), an age similar to the age of ophiolites of the Ligurian Tethys (Bortolotti and Principi, 2005). In this context, it is possible that the thin, relatively high density crust interpreted at the southern end of the 4 profiles (Figs. 16 and 17) is actually Late Jurassic oceanic crust.

The prominent ENE-WSW trending positive gravity anomaly of the Gulf of Cadiz is therefore interpreted to represent the locus of extreme crustal thinning and the presence of high density bodies (serpentinized mantle) in the transition from continental to oceanic crust, as observed further north in the Iberian Atlantic and Cantabrian margins (Peron-Pinvidic and Manatschal, 2009; Tugend et al., 2014). It is interpreted that the rise in the mantle is locally driven by thinning of the lower crust (Figs. 17a,b), indicating heterogeneous thinning of the crust during rifting. The width of the necking domain and the Cenozoic inversion are the factors that control the width and amplitude of the positive anomaly.

6.3. Regional context

The continent-ocean transition proposed from gravimetric modeling (Fig. 17) trends roughly WSW-ENE (Fig. 18b), consistent with the regional trend of the margin. It provides a better estimate of the northern limit of oceanic crust in the Gulf of Cadiz than those proposed to date (e.g., Gutscher et al., 2009; Martínez-Loriente et al., 2014).

The lateral continuity of the passive margin as mapped in Fig. 18b is limited to both east and west. To the east, interpretation of vintage seismic and well data that shows a rapid eastward rise in the basement and decrease in Mesozoic thickness just east of the present-day coastline (Fig. 9). The basement remains relatively shallow and the Mesozoic is absent under the foreland Guadalquivir Basin (Lanaja, 1987). This transition is interpreted to occur across a NW-SE zone of transfer (already proposed by Lanaja, 1987) dominated by NW-SE striking extensional or transtensional faults, labelled Gulf of Cadiz-Betics transfer zone in Fig. 18a.

To the west, a similar transition is inferred where the Moho becomes shallow, west of the Portimão Bank (Fig. 18a). This transition is observed to be controlled by westward dipping extensional faults (Figs. 9, 14) that drop the top of basement to depths similar (10-12 km) with that of the oceanic crust interpreted in the Horseshoe Abyssal Plain by Martínez-Loriente et al. (2014). The faults identified along the western Algarve Basin coincide in location (see triangle on the seabed in Fig. 14) with a sudden rise in the Moho that trends NW-SE (based on the profiles of González et al., 1996 and Sallarès et al., 2011; Fig. 18a). This is interpreted to represent another NW-SE trending transfer zone that in this case may link the site of Mesozoic mantle exhumation of the Gorringe Bank with the proposed exhumed mantle of the Portimão Bank (Gorringe-Gulf of Cadiz transfer, Fig. 19).

The SW Iberian passive margin in the Gulf of Cadiz is therefore interpreted to correspond to a segment of the transform margin that connected the Central Atlantic and the Ligurian Tethys during the Jurassic and Cretaceous. Assuming oceanization of this margin occurred in the Late Jurassic (Bortolotti and Principi, 2005; García-Hernández et al., 1989; Vera et al., 2004), oceanic crust would have formed as part of the Iberia-Africa conjugate (Fig. 1c), at the westernmost end of the Ligurian Tethys.

To the south, the contact with the Nubia plate is not identifiable in our models due to their limited length. Nonetheless, the SWIM lineaments (Zitellini et al., 2009) continue to be a good candidate for the location for this boundary. The SWIM lineaments coincide with the location of a roughly E-W trending boundary in the free-air gravity anomaly (Fig. 19) which may reflect the boundary between both plates. In the eastern portion this boundary is between Nubia continental crust and possibly Tethyan oceanic crust. In the center and to the west, the boundary juxtaposes oceanic crust on both sides (Fig. 19). The nature of the crust south of the Gorringe Bank is not certain but has been proposed by Martínez-Loriente et al. (2014) to be Tethyan.

7. Conclusions

Integrated seismic interpretation and gravimetric modeling have made it possible to propose a crustal structure in a regional context for the SW Iberian margin. The crustal structure of the SW Iberian margin is observed to result from the superposition of Mesozoic extension and Cenozoic inversion of the margin. The result of Mesozoic extension was a southward thinning of the SW Iberian margin. This structure is best preserved in the western Gulf of Cadiz where the effects of Cenozoic inversion are less strong, and indicates that crustal thinning occurs in a stepped manner across a zone nearly 100 km wide.

The SW Iberian margin is interpreted to correspond to the westernmost segment of the Ligurian Tethys. In this context, the Gulf of Cadiz represents a segment of the margin comprised between the Betic margin in the east and a possibly Atlantic domain to the west.

The large positive gravity anomaly of the Gulf of Cadiz corresponds to the zone of greatest crustal attenuation, where the continental crust is interpreted to be as thin as 10 km or less. Cenozoic inversion in the eastern Gulf of Cadiz concentrated in this domain of thin continental crust, causing folding at crustal level. The result is a larger amplitude and narrower gravity anomaly.

Acknowledgements

This study was funded by Repsol Exploración (Madrid) and partially supported by the SALTECRES project (CGL2014-54118-C2-1-R MINECO/FERDER, UE). A. Ramos' PhD research is funded by Repsol Exploración. The authors wish to thank L. Cascone, A. Olaiz, W. Hermoza, R. Rocca and C. Giraldo preceded our work on the structure of the south Portuguese margin and set us on the right track. We also are grateful to A. Arnaiz and the Iberia Exploration Team at Repsol for continued support and enriching discussions. The authors also wish to thank four anonymous reviewers for the discussion that have greatly helped us improve this paper. We also acknowledge Schlumberger, Midland Valley and Oasis Montaj for the academic software licenses used for seismic interpretation, cross-section construction and gravity modeling respectively. Fig. 2 and the background maps of Fig. 19 have been made using GMT academic software (Wessel and Smith, 1998). Repsol and Partex-Oil&Gas provided us their proprietary vintage seismic surveys and a 3D seismic cube, published with their permission. Seismic lines of the PDT00-PD00 survey have been provided by TGS and published with the permission of TGS. The seismic PDT00-PD00 survey is available for purchase from TGS and ENMC (Entidade Nacional para o Mercado de Combustibles).

References

Ayala, C., Bohoyo, F., Maestro, A., Reguera, M.I., Torne, M., Rubio, F., Fernàndez, M., García-Lobón, J.L., 2016. Updated Bouguer anomalies of the Iberian Peninsula: a new perspective to interpret the regional geology. J. Maps:1–4 http://dx.doi.org/10.1080/17445647.2015.1126538.

Bortolotti, V., Principi, G., 2005. Tethyan ophiolites and Pangea break-up. Island Arc 14: 442–470. http://dx.doi.org/10.1111/j.1440-1738.2005.00478.x.

Brocher, T.M., 2005. Empirical relations between elastic wavespeeds and density in the Earth's crust. Bull. Seismol. Soc. Am. 95:2081–2092. http://dx.doi.org/10.1785/0120050077.

Carbonell, R., Simancas, F., Juhlin, C., Pous, J., Pérez-Estaún, A., Gonzalez-Lodeiro, F., Muñoz, G., Heise, W., Ayarza, P., 2004. Geophysical evidence of a mantle derived intrusion in SW Iberia. Geophys. Res. Lett. 31. http://dx.doi.org/10.1029/2004GL019684 (n/a–n/a).

Contrucci, I., Klingelhöfer, F., Perrot, J., Bartolome, R., Gutscher, M.-A., Sahabi, M., Malod, J., Rehault, J.-P., 2004. The crustal structure of the NW Moroccan continental margin from wide-angle and reflection seismic data. Geophys. J. Int. 159:117–128. http://dx.doi.org/10.1111/j.1365-246X.2004.02391.x.

Cornen, G., Girardeau, J., Monnier, C., 1999. Basalts, underplated gabbros and pyroxenites record the rifting process of the West Iberian margin. Mineral. Petrol. 67:111–142. http://dx.doi.org/10.1007/BF01161518.

Dañobeitia, J.J., Bartolomé, R., Checa, A., Maldonado, A., Slootweg, A.P., 1999. An interpretation of a prominent magnetic anomaly near the boundary between the Eurasian and African plates (Gulf of Cadiz, SW margin of Iberia). Mar. Geol. 155:45–62. http://dx.doi.org/10.1016/S0025-3227(98)00140-6.

Diaz, J., Gallart, J., Carbonell, R., 2016. Moho topography beneath the Iberian-Western Mediterranean region mapped from controlled-source and natural seismicity surveys. Tectonophysics http://dx.doi.org/10.1016/j.tecto.2016.08.023.

Domènech, M., Teixell, A., Babault, J., Arboleya, M.-L., 2015. The inverted Triassic rift of the Marrakech High Atlas: a reappraisal of basin geometries and faulting histories. Tectonophysics 663:177–191. http://dx.doi.org/10.1016/j.tecto.2015.03.017.

Druet, M., 2016. Geodinámica del margen continental de Galicia: estructura profunda y morfotectónica. PhD Thesis. Universidad Complutense de Madrid, Madrid (251 pp).

Ellouz, N., Patriat, M., Gaulier, J.-M., Bouatmani, R., Sabounji, S., 2003. From rifting to Alpine inversion: Mesozoic and Cenozoic subsidence history of some Moroccan basins. Sediment. Geol. 156:185–212. http://dx.doi.org/10.1016/S0037-0738(02)00288-9.

Fernàndez, M., Marzán, I., Torne, M., 2004. Lithospheric transition from the Variscan Iberian Massif to the Jurassic oceanic crust of the Central Atlantic. Tectonophysics 386: 97–115. http://dx.doi.org/10.1016/j.tecto.2004.05.005.

García-Hernández, M., López-Garrido, Á.C., Martín-Algarra, A., Cámara, J.M., Ruiz-Ortiz, P.A., Vera, J.A., 1989. Las discontinuidades mayores del Jurásico de las Zonas Externas de las Cordilleras Béticas: análisis e interpretación de los ciclos sedimentarios. J. Iber. Geol. 35–52.

Giraldo, C., Hermoza, W., Amigo, B., Rocca, R., Martínez, C., Malmcrona, Y., Rosales, C., Baudino, R., Martín-Monge, A., Fernández, O., Welsink, H., Cascone, L., Olaiz, A., García-Mojonero, C., Arnaiz, A., 2014. Evidences of Salt Tectonics around the Guadalquivir bank, Gulf of Cádiz (SW Iberia). Presented at the AAPG 2014 European Regional Conference & Exhibition, Barcelona, Spain, May 13–15, 2014. Search and Discovery Article #50980.

González, A., Torne, M., Córdoba, D., Vidal, N., Matias, L.M., Díaz, J., 1996. Crustal thinning in the southwestern Iberia margin. Geophys. Res. Lett. 23:2477–2480. http://dx.doi.org/10.1029/96GL02299.

González, A., Córdoba Barba, D., Vegas, R., Matías, L.M., González Fernández, A., Córdoba Barba, D., Vegas, R., Matías, L.M., 1998. Seismic crustal structure in the southwest of the Iberian Peninsula and the Gulf of Cadiz. Tectonophysics 296, 317–331.

Gràcia, E., Dañobeitia, J., Vergés, J., Bartolomé, R., Córdoba, D., 2003. Crustal architecture and tectonic evolution of the Gulf of Cadiz (SW Iberian margin) at the convergence of the Eurasian and African plates. Tectonics 22:1033. http://dx.doi.org/10.1029/2001TC901045.

Gutscher, M.-A., Malod, J., Rehault, J.-P., Contrucci, I., Klingelhoefer, F., Mendes-Victor, L., Spakman, W., 2002. Evidence for active subduction beneath Gibraltar. Geology 30:1071. http://dx.doi.org/10.1130/0091-7613(2002)030<1071:EFASBG>2.0.CO;2.

Gutscher, M.-A., Dominguez, S., Westbrook, G.K., Leroy, P., 2009. Deep structure, recent deformation and analog modeling of the Gulf of Cadiz accretionary wedge: implications for the 1755 Lisbon earthquake. Tectonophysics 475:85–97. http://dx.doi.org/10.1016/j.tecto.2008.11.031.

Gutscher, M.-A., Dominguez, S., Westbrook, G.K., Le Roy, P., Rosas, F., Duarte, J.C., Terrinha, P., Miranda, J.M., Graindorge, D., Gailler, A., Sallares, V., Bartolome, R., 2012. The Gibraltar subduction: a decade of new geophysical data. Tectonophysics 574–575: 72–91. http://dx.doi.org/10.1016/j.tecto.2012.08.038.

Hernández-Molina, F.J., Sierro, F.J., Llave, E., Roque, C., Stow, D.A.V., Williams, T., Lofi, J., Van der Schee, M., Arnáiz, A., Ledesma, S., Rosales, C., Rodríguez-Tovar, F.J., Pardo-Igúzquiza, E., Brackenridge, R.E., 2016. Evolution of the gulf of Cadiz margin and southwest Portugal contourite depositional system: tectonic, sedimentary and paleoceanographic implications from IODP expedition 339. Mar. Geol. 377:7–39. http://dx.doi.org/10.1016/j.margeo.2015.09.013.

van Hinsbergen, D.J.J., Vissers, R.L.M., Spakman, W., 2014. Origin and consequences of western Mediterranean subduction, rollback, and slab segmentation. Tectonics 33: 393–419. http://dx.doi.org/10.1002/2013TC003349.

IOC, IHO, BODC, 2003. Centenary Edition of the GEBCO Digital Atlas, Published on CDROM on Behalf of the Intergovernmental Oceanographic Commission and the International Hydrographic Organization as Part of the General Bathymetric Chart of the Oceans. British Oceanographic Data Centre, Liverpool, UK.

Iribarren, L., Vergés, J., Camurri, F., Fullea, J., Fernàndez, M., 2007. The structure of the Atlantic–Mediterranean transition zone from the Alboran Sea to the Horseshoe Abyssal Plain (Iberia–Africa plate boundary). Mar. Geol. 243:97–119. http://dx.doi.org/10.1016/j.margeo.2007.05.011.

Jiménez-Munt, I., Fernàndez, M., Vergés, J., Afonso, J.C., Garcia-Castellanos, D., Fullea, J., 2010. Lithospheric structure of the Gorringe Bank: Insights into its origin and tectonic evolution. Tectonics 29. http://dx.doi.org/10.1029/2009TC002458 (n/a-n/a).

Lanaja, J.M., 1987. Contribución de la exploración petrolífera al conocimiento de la geología de España. IGME, Madrid.

Le Roy, P., Piqué, A., 2001. Triassic–Liassic Western Moroccan synrift basins in relation to the Central Atlantic opening. Mar. Geol. 172:359–381. http://dx.doi.org/10.1016/S0025-3227(00)00130-4.

Ledesma, S.M., 2000. Astrobiocronología y estratigrafía de alta resolución del Neógeno de la Cuenca del Guadalquivir-Golfo de Cádiz. PhD Thesis. Universidad de Salamanca (464 pp).

Malod, J.A., Mougenot, D., 1979. L'histoire geologique neogene du golfe de Cadix. Bull. Soc. Geol. Fr. S7–XXI:603–611. http://dx.doi.org/10.2113/gssgfbull.S7-XXI.5.603.

Manuppella, G., 1992. Carta geológica da região do Algarve. Noticia explicativa da Carta Geologica da regiao do Algarve. Serviços geológicos de Portugal.

Martínez-Loriente, S., Sallarès, V., Gràcia, E., Bartolome, R., Dañobeitia, J.J., Zitellini, N., 2014. Seismic and gravity constraints on the nature of the basement in the Africa-Eurasia plate boundary: new insights for the geodynamic evolution of the SW Iberian margin: thin oceanic crust at the CPR and SH. J. Geophys. Res. Solid Earth 119: 127–149. http://dx.doi.org/10.1002/2013JB010476.

Martins, L.T., Madeira, J., Youbi, N., Munhá, J., Mata, J., Kerrich, R., 2008. Rift-related magmatism of the Central Atlantic magmatic province in Algarve, Southern Portugal. Lithos 101:102–124. http://dx.doi.org/10.1016/j.lithos.2007.07.010.

Matias, H., Kress, P., Terrinha, P., Mohriak, W., Menezes, P.T.L., Matias, L., Santos, F., Sandnes, F., 2011. Salt tectonics in the western Gulf of Cadiz, southwest Iberia. AAPG Bull. 95:1667–1698. http://dx.doi.org/10.1306/01271110032.

Medialdea, T., Vegas, R., Somoza, L., Vázquez, J.T., Maldonado, A., Diaz-del-Rio, V., Maestro, A., Córdoba, D., Fernández-Puga, M.C., 2004. Structure and evolution of the "Olistostrome" complex of the Gibraltar Arc in the Gulf of Cádiz (eastern Central Atlantic): evidence from two long seismic cross-sections. Mar. Geol. 209:173–198. http://dx.doi.org/10.1016/j.margeo.2004.05.029.

Medialdea, T., Somoza, L., Pinheiro, L.M., Fernández-Puga, M.C., Vázquez, J.T., León, R., Ivanov, M.K., Magalhaes, V., Díaz-del-Río, V., Vegas, R., 2009. Tectonics and mud volcano development in the Gulf of Cádiz. Mar. Geol. 261:48–63. http://dx.doi.org/10.1016/j.margeo.2008.10.007.

Michard, A., Negro, F., Frizon de Lamotte, D., Saddiqi, O., 2007. Serpentinite slivers and metamorphism in the external Maghrebides: arguments for an intracontinental suture in the African paleomargin (Morocco, Algeria). Rev. Soc. Geol. Esp. 20, 173–185.

Palomeras, I., Carbonell, R., Flecha, I., Simancas, F., Ayarza, P., Matas, J., Martínez Poyatos, D., Azor, A., González Lodeiro, F., Pérez-Estaún, A., 2009. Nature of the lithosphere across the Variscan orogen of SW Iberia: dense wide-angle seismic reflection data. J. Geophys. Res. 114. http://dx.doi.org/10.1029/2007JB005050.

Peron-Pinvidic, G., Manatschal, G., 2009. The final rifting evolution at deep magma-poor passive margins from Iberia-Newfoundland: a new point of view. Int. J. Earth Sci. 98:1581–1597. http://dx.doi.org/10.1007/s00531-008-0337-9.

Ramos, A., Cascone, L., Olaiz, A., Fernández, O., Sánchez de la Muela, A., Hermoza, W., Arnaiz, A., Rocca, R., 2015. Crustal Structure of the Southern Portuguese Margin - Constraints from Potential Field Methods, paper presented at 77th EAGE Conference and Exhibition 2015. Presented at the 77th EAGE Conference and Exhibition 2015. http://dx.doi.org/10.3997/2214-4609.201412974.

Ramos, A., Fernández, O., Terrinha, P., Muñoz, J.A., 2016. Extension and inversion structures in the Tethys–Atlantic linkage zone, Algarve Basin, Portugal. Int. J. Earth Sci. 105:1663–1679. http://dx.doi.org/10.1007/s00531-015-1280-1.

Ramos, A., Fernández, O., Terrinha, P., Muñoz, J.A., 2017. Neogene to recent contraction and basin inversion along the Nubia-Iberia boundary in SW Iberia. Tectonics 36, 2016TC004262. http://dx.doi.org/10.1002/2016TC004262.

Roeser, H.A., Steiner, C., Schreckenberger, B., Block, M., 2002. Structural development of the Jurassic Magnetic Quiet Zone off Morocco and identification of Middle Jurassic magnetic lineations. J. Geophys. Res. Solid Earth 107:1–23, EPM 1-1-EPM. http://dx.doi.org/10.1029/2000JB000094.

Roque, C., 2007. Tectonostratigrafia do cenozóico das margens continentais sul e sudoeaste portuguesas: um modelo de correlação sismostratigráfica. PhD Thesis. Universidade de Lisboa (310 pp).

Sallarès, V., Gailler, A., Gutscher, M.-A., Graindorge, D., Bartolomé, R., Gràcia, E., Díaz, J., Dañobeitia, J.J., Zitellini, N., 2011. Seismic evidence for the presence of Jurassic oceanic crust in the central Gulf of Cadiz (SW Iberian margin). Earth Planet. Sci. Lett. 311: 112–123. http://dx.doi.org/10.1016/j.epsl.2011.09.003.

Schettino, A., Turco, E., 2011. Tectonic history of the western Tethys since the Late Triassic. Geol. Soc. Am. Bull. 123, 89–105.

Seton, M., Müller, R.D., Zahirovic, S., Gaina, C., Torsvik, T., Shephard, G., Talsma, A., Gurnis, M., Turner, M., Maus, S., Chandler, M., 2012. Global continental and ocean basin reconstructions since 200 Ma. Earth-Sci. Rev. 113:212–270. http://dx.doi.org/10.1016/j.earscirev.2012.03.002.

Sibuet, J.-C., Rouzo, S., Srivastava, S., 2012. Plate tectonic reconstructions and paleogeographic maps of the central and North Atlantic oceans. Can. J. Earth Sci. 49: 1395–1415. http://dx.doi.org/10.1139/e2012-071.

Smith, W.H., Sandwell, D.T., 1997. Global sea floor topography from satellite altimetry and ship depth soundings. Science 277, 1956–1962.

Spakman, W., Wortel, R., 2004. A tomographic view on western mediterranean geodynamics. In: Cavazza, P.D.W., Roure, D.F., Spakman, P.W., Stampfli, P.G.M., Ziegler, P.P.A. (Eds.), The TRANSMED Atlas. The Mediterranean Region from Crust to Mantle. Springer, Berlin Heidelberg, pp. 31–52.

Stampfli, G.M., Borel, G.D., 2002. A plate tectonic model for the Paleozoic and Mesozoic constrained by dynamic plate boundaries and restored synthetic oceanic isochrons. Earth Planet. Sci. Lett. 196, 17–33.

Talwani, M., 1965. Computation with the help of a digital computer of magnetic anomalies caused by bodies of arbitrary shape. Geophysics 30:797–817. http://dx.doi.org/10.1190/1.1439654.

Talwani, M., Worzel, J.L., Landisman, M., 1959. Rapid gravity computations for two-dimensional bodies with application to the Mendocino submarine fracture zone. J. Geophys. Res. 64:49–59. http://dx.doi.org/10.1029/JZ064i001p00049.

Terrinha, P., 1998. Structural Geology and Tectonic Evolution of the Algarve Basin, South Portugal. PhD Thesis. Imperial College, London (430 pp).

Terrinha, P., Ribeiro, C., Kullberg, J.C., Lopes, C., Rocha, R., Ribeiro, A., 2002. Compressive episodes and faunal isolation during rifting, Southwest Iberia. J. Geol. 110, 101–113.

Terrinha, P., Matias, L., Vicente, J., Duarte, J., Luís, J., Pinheiro, L., Lourenço, N., Diez, S., Rosas, F., Magalhães, V., Valadares, V., Zitellini, N., Roque, C., Víctor, L.M., 2009. Morphotectonics and strain partitioning at the Iberia–Africa plate boundary from multibeam and seismic reflection data. Mar. Geol. 267:156–174. http://dx.doi.org/10.1016/j.margeo.2009.09.012.

TGS, 2005. PD00: Non-exclusive 2D Survey. TGS online data zone. http://www.tgs.com/TGS/specsheets/PD-00_Spec.pdf.

Thiebot, E., Gutscher, M.-A., 2006. The Gibraltar Arc seismogenic zone (part 1): constraints on a shallow east dipping fault plane source for the 1755 Lisbon earthquake

provided by seismic data, gravity and thermal modeling. Tectonophysics 426: 135–152. http://dx.doi.org/10.1016/j.tecto.2006.02.024.
Torelli, L., Sartori, R., Zitellini, N., 1997. The giant chaotic body in the Atlantic Ocean off Gibraltar: new results from a deep seismic reflection survey. Mar. Pet. Geol. 14: 125–138. http://dx.doi.org/10.1016/S0264-8172(96)00060-8.
Torne, M., Fernàndez, M., Vergés, J., Ayala, C., Salas, M.C., Jimenez-Munt, I., Buffett, G.G., Díaz, J., 2015. Crust and mantle lithospheric structure of the Iberian Peninsula deduced from potential field modeling and thermal analysis. Tectonophysics 663: 419–433. http://dx.doi.org/10.1016/j.tecto.2015.06.003.
Tortella, D., Torne, M., Pérez-Estaún, A., 1997. Geodynamic evolution of the eastern segment of the Azores-Gibraltar zone: the Gorringe Bank and the Gulf of Cadiz region. Mar. Geophys. Res. 19, 211–230.
Tugend, J., Manatschal, G., Kusznir, N.J., Masini, E., Mohn, G., Thinon, I., 2014. Formation and deformation of hyperextended rift systems: insights from rift domain mapping in the Bay of Biscay-Pyrenees. Tectonics 33:1239–1276. http://dx.doi.org/10.1002/2014TC003529.
Vegas, R., Medialdea, T., Muñoz García, M., Díaz del Río, V., Somoza, L., 2004. Nature and tectonic setting of the Guadalquivier Bank (Gulf of Cadiz, SW Iberian Peninsula). Rev. Soc. Geol. Esp. 17, 49–60.
Vera, J.A., Molina, J.M., Aguado, R., 2004. Calcarenitas de Microcodium (Formación Majalcorón, Paleoceno, Subbético): descripción, bioestratigrafía y significado en el Terciario de la Cordillera Bética. Bol. Geológico Min. Esp. 115, 453–468.
Vergés, J., Fernàndez, M., 2012. Tethys–Atlantic interaction along the Iberia–Africa plate boundary: the Betic–Rif orogenic system. Tectonophysics 579:144–172. http://dx.doi.org/10.1016/j.tecto.2012.08.032.
Wessel, P., Smith, W.H.F., 1998. New, improved version of generic mapping tools released. EOS Trans. Am. Geophys. Union 79:579. http://dx.doi.org/10.1029/98EO00426.
Zeyen, H., Ayarza, P., Fernàndez, M., Rimi, A., 2005. Lithospheric structure under the western African-European plate boundary: a transect across the Atlas Mountains and the Gulf of Cadiz. Tectonics 24, TC2001. http://dx.doi.org/10.1029/2004TC001639.
Zitellini, N., Gràcia, E., Matias, L., Terrinha, P., Abreu, M.A., DeAlteriis, G., Henriet, J.P., Dañobeitia, J.J., Masson, D.G., Mulder, T., 2009. The quest for the Africa–Eurasia plate boundary west of the Strait of Gibraltar. Earth Planet. Sci. Lett. 280:13–50. http://dx.doi.org/10.1016/j.epsl.2008.12.005.

APPENDIX 1.5

Paleogeographic evolution of a segmented oblique passive margin: the case of the SW Iberian margin

Ramos, A., Fernández, O., Terrinha, P., Muñoz, J.A., Arnaiz, A.
(in preparation)

Paleogeographic evolution of a segmented oblique passive margin: the case of the SW Iberian margin

Ramos, A. (1), Fernández, O. (2), Terrinha, P. (3), Muñoz, J.A. (1), Arnaiz, Á (2)

[1]Institut de Recerca Geomodels, Departament de Dinàmica de la Terra i de l'Oceà, Universitat de Barcelona, Barcelona, Spain

[2]Repsol Exploración, Madrid, Spain.

[3]Instituto Português do Mar e da Atmosfera, Divisão de Geologia e Georecursos Marinhos, Lisboa, Portugal

Abstract

The SW Iberian margin is an oblique passive margin developed during the Mesozoic, as part of the opening of the westernmost Ligurian Tethys. The Algarve Basin developed on the SW Iberian margin and its sedimentary record was strongly conditioned by the tectonic evolution of the margin. The Algarve Basin was dominated during the Mesozoic by ENE-WSW trending extensional faults, and their associated depocenters. These extensional structures were segmented by oblique NW-SE transfer zones. Two major NW-SE transfer zones connected the Algarve Basin to the Gorringe Bank in the west and to the Betic Basin in the east. The SW Iberian margin was later partially inverted during Late Cretaceous to Cenozoic times, due to convergence between Africa and Iberia. Inversion of the Algarve Basin and the SW Iberian margin was controlled by both the ENE-WSW and NW-SE structures formed during the passive margin phase. The passive margin evolution of the Algarve Basin during the Mesozoic and up to the Paleogene (prior to the main phase of margin inversion) is documented in this paper through paleogeographic reconstructions based on field geology in the onshore, and seismic interpretation and well data in the offshore.

Keywords: oblique passive margin, SW Iberian margin, depositional environment, Tethys-Atlantic link, margin inversion

Introduction

The structural framework of oblique rift systems is known to control deposition of syn-rift sediments (e.g., Gawthorpe and Hurst, 1993; Gawthorpe and Leeder, 2000). As a rift system progresses into a passive margin, the impact of the early segmentation can persist under the blanketing effect of post-rift sedimentation and can condition the subsequent evolution of petroleum systems (e.g., Meisling et al., 2001). The south Iberian margin is one such segmented oblique passive margin, developed in the Jurassic as part of the linkage between the Central Atlantic and the Ligurian Tethys. The Mesozoic Betic and Algarve Basins developed on this margin (Fig. 1), compartmentalized by roughly NW-SE trending transfer zones (Ramos et al., 2017b). Whereas the Betic Basin has been mostly overthrust by the Betic orogen and covered by the Cenozoic Guadalquivir foreland basin, the Algarve Basin in the Gulf of Cadiz, remains preserved and is only partially inverted by Cenozoic compression (Ramos et al., 2017a). This makes the Algarve Basin an ideal candidate to explore the Mesozoic development of the SW Iberian oblique rifted margin.

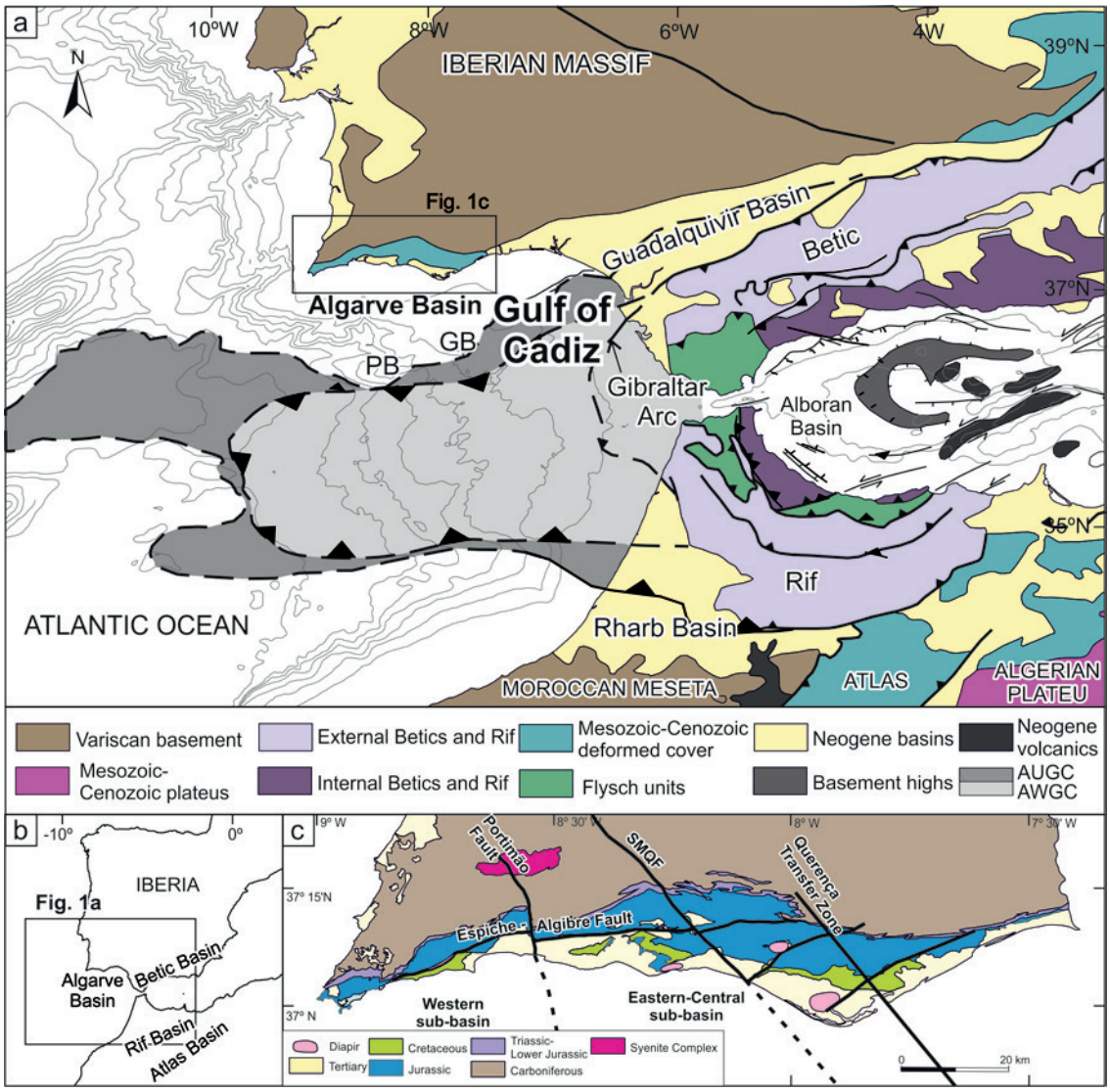

Fig. 1. (a) Tectonic map of southwest Iberia, showing the main tectonic units and their associated basins (modified from Iribarren et al., 2007). AUGC: Allochthonous Unit of the Gulf of Cadiz; AWGC: Accretionary Wedge of the Gulf of Cadiz; GB: Guadalquivir Bank; PB: Portimão Bank; GoC: Gulf of Cadiz; SMQF: São Marcos Quarteira Fault. (b) Location of the southwest Iberian margin. (c) Simplified geological map of the onshore Algarve Basin showing major tectonic features. Modified after (Ramos et al., 2016).

Several authors have worked on the evolution of the Algarve Basin and the broader SW Iberian margin (Lopes et al., 2006; Matias, 2007; Roque, 2007; Terrinha, 1998). The control of oblique transfer faults on the distribution and thickness of Mesozoic sediments has been addressed by multiple authors (Correia, 1989; Manuppella et al., 1988; Palain, 1976; Ramos et al., 2016; Terrinha, 1998; Terrinha et al., 2013). These studies have been limited to the onshore outcrop of the Algarve Basin and do not address

the role of the oblique transfer zones in the more extensive offshore Algarve Basin. Furthermore, previous studies have not addressed the role of the Algarve Basin in the broader regional context of the southern Iberian passive margin that developed during the Mesozoic.

This paper tries to document the regional geologic and paleogeographic evolution of the Algarve Basin from Mesozoic extension to Cenozoic inversion, as a segment of the broader southern Iberian margin. This analysis is based on field geology, interpretation of 2D and 3D reflection seismic data along with well data and the integration of knowledge of the southern Iberian passive margin. A sequentially restored section of the margin and isopach maps of syn- to post-rift units have been used to describe the evolution of the margin and depositional environments.

Geological setting

The Algarve Basin is the westernmost segment of the SW Iberian margin and at present-day extends from the onshore of southern Portugal into the Gulf of Cadiz. It lies north of the present-day transform plate boundary between Africa (Nubia) and Iberia. To the west, the SW Iberian passive margin transitions to the Central/North Atlantic oceanic domain across the Gorringe-Gulf of Cadiz transfer zone (Ramos et al., 2017b) (Fig. 1a). To the east, the Algarve Basin is bounded by the Gulf of Cadiz-Betic transfer zone (Ramos et al., 2017b; Fig. 1a) which separates it from the Mesozoic Betic Basin.

Tectonic evolution

The Algarve Basin, started to develop in Triassic times, during the break-up of Pangea (Terrinha, 1998). Rifting intensified in Jurassic times, influenced by rifting and opening of the Central Atlantic and the westernmost Ligurian Tethys (Terrinha, 1998; Fig. 2). Rifting culminated in break-up and oceanization of the margin in Late Jurassic times (e.g., Vera et al., 1997; Fig. 2). During the Cenozoic the margin was partially inverted as the result of the convergence between Africa (Nubia) and Eurasia (Ramos et al., 2017a).

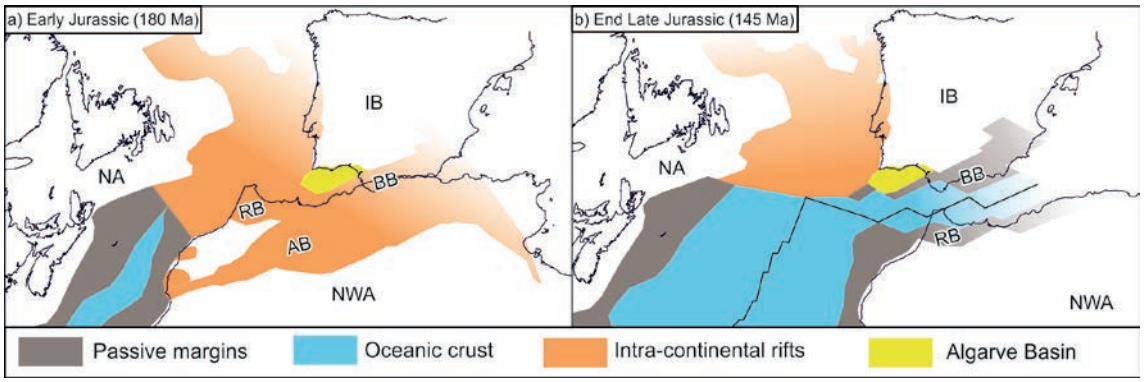

Fig. 2 Palinspastic reconstruction of the SW Iberian margin at the Early Jurassic (a) and Late Jurassic (b). AB: Atlas Basin; BB: Betic Basin; IB: Iberia; NA: North America; NWA: Northwest Africa; RF: Rif Basin.

The structure of the SW Iberian margin is dominated by the thinning of continental crust towards the south (Ramos et al., 2017b), controlled by roughly WSW-ENE trending extensional faults active throughout the Jurassic (Matias, 2007; Ramos et al., 2016; Terrinha, 1998). To the south and southwest, the presence of oceanic crust has been proposed by gravity modelling and refraction seismic data (Gutscher et al., 2002; Martínez-Loriente et al., 2014; Ramos et al., 2017b; Sallarès et al., 2011). Mesozoic depocenters were mainly controlled by basement faulting during the Triassic and Jurassic. Salt tectonism, which was triggered and controlled by basement faulting, was active from Jurassic to Cretaceous times, and was the main control on the development of Cretaceous depocenters (Matias et al., 2011).

The Mesozoic extensional system was compartmentalized by several transfer faults and diffuse transfer zones in the onshore Algarve Basin (Arthaud and Matte, 1977; Barreto et al., 2015; Manuppella, 1992; Ramos et al., 2016; Terrinha, 1998). These faults are oriented from N-S (Portimão Fault) to NW-SE (São Marcos - Quarteira Fault and Querença transfer zone; Fig. 1b) and are parallel to Late Variscan thrusts documented in the Carboniferous basement in SW Iberia (Arthaud and Matte, 1977; Manuppella, 1992; Ramos et al., 2016; Terrinha, 1998). In the onshore, Terrinha (1998) documented the control these faults exerted on the deposition of the Mesozoic. In general, the eastern blocks of these faults recorded shallower bathymetry but greater accommodation space during the Mesozoic. The Portimão Fault has been used previously to sub-divide the onshore Algarve Basin into a western and central-eastern sub-basins (Ramos et al., 2016), These sub-basins recorded different depositional environments and

100 subsidence history mainly through the Jurassic and Early Cretaceous (Manuppella, 1988; Manuppella et
101 al., 1988; Ramos et al., 2016; Terrinha, 1998) .

102 Rifting of the SW Iberian margin is interpreted to finalize with continental break-up during the late
103 Middle Jurassic to earliest Late Jurassic (García-Hernández et al., 1989; Vera, 1988). This is the age of
104 Ligurian Tethys ophiolites (Bortolotti and Principi, 2005) and is synchronous with volcanism in
105 neighbouring Mesozoic basins, such as the Betics (Vera et al., 1997) and the Atlas (Frizon de Lamotte et
106 al., 2008).

107 Cenozoic compression led to the inversion of some extensional faults and salt structures, and the
108 development of E-W to NE-SW striking, south-directed basement thrusts that tilted pre-existing
109 extensional structures (Ramos et al., 2017a; Terrinha et al., 2009). Most of the oblique transfer faults were
110 also inverted in transpression (Barreto et al., 2015; Ramos et al., 2016; Terrinha, 1998). Within the
111 Mesozoic and Cenozoic sedimentary cover, shortening was accommodated by minor thrusts detaching on
112 evaporites, reactivation of diapirs and buttressing against extensional faults (Ramos et al., 2016; 2017a).

113 ***Stratigraphy***

114 The stratigraphy of the Algarve Basin (and the broader Gulf of Cádiz) has been described by several
115 authors in the onshore and the shallow offshore (Lopes, 2002; Manuppella et al., 1988; Matias, 2007;
116 Roque, 2007; Terrinha, 1998). The stratigraphy of the basin is summarized in Figures 3 and 4.

117 Mesozoic and Cenozoic sediments lay unconformably over Paleozoic flysch basement
118 (Carboniferous and older) deformed in the foreland of the Variscan orogen. The earliest sediments of the
119 basin are Upper Triassic red continental alluvial clastics filling half-grabens and grabens trending
120 roughly E-W. Paleocurrent directions and provenance studies indicate drainage of the SW Iberian margin
121 towards the W and SW as well as sediment sourcing from the North American continent in the SW
122 (Palain, 1976; Pereira et al., 2016).

123 According to Palain (1976), the greatest thickness of Triassic in the onshore (250 m; Terrinha, 1998)
124 occurs in the central part of the onshore Algarve Basin, probably related to the extensional to
125 transtensional character of the São Marcos Quarteira Fault (SMQF; Terrinha, 1998). Triassic sediments
126 have not been described in the offshore as they have not been encountered by any of the exploratory wells
127 drilled in the area (Fig. 4). Only well GC6Y-1BIS drilled deep enough but encountered Carboniferous

rocks directly underlying Hettangian evaporites, which is interpreted to mean that this well drilled the uplifted footwall of a Triassic extensional fault.

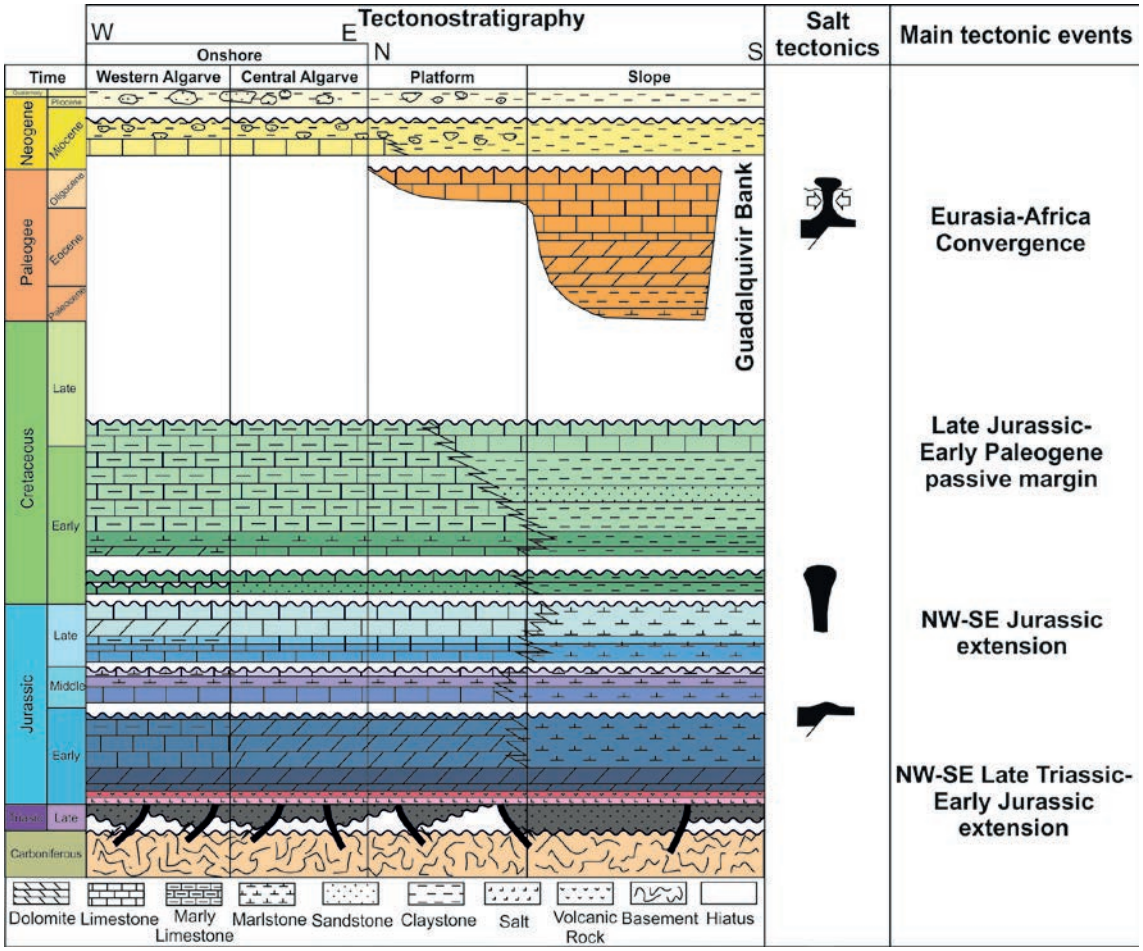

Fig. 3. Tectono-sedimentary diagram of the Algarve Basin showing the main stratigraphic units, from west to east, and from the onshore to the continental slope. Modified after Ramos et al. (2016).

Triassic sediments are overlain by Hettangian evaporites and coeval terrigenous clastics and carbonates. The Hettangian evaporite unit crops out along the northern margin of the basin where it is normally less than 200 m thick. Southward, but still onshore, Hettangian evaporites are responsible for diapirism south of the Espiche-Algibre Fault (a major Mesozoic extensional fault; Terrinha, 1998; Ramos et al, 2016; Fig. 1c). Hettangian evaporites are also encountered by wells in the onshore and offshore (e.g., Almonte-1; Asperillo-1; Gulf of Cadiz B-1; Ruivo-1, Orion 2-1, GC6Y-1BIS, Moguer-1). The Hettangian unit drilled by these wells is less than 500 m thick when not affected by diapirism (GC6Y-1BIS, Moguer-1). In these wells this unit is dominated by anhydrite and shales, similar to the northern outcrop, in contrast to the halite-dominated diapirs in the onshore and offshore.

142 Hettangian evaporite unit is locally overlain by a Hettangian-Sinemurian volcanic-sedimentary
143 complex associated with the Central Atlantic Magmatic Province (Martins et al., 2008; Verati et al.,
144 2007). This unit is composed of basaltic lavas and pyroclastic rocks interlayered with dolomites and red
145 shales, and is less than 160 m thick where present.

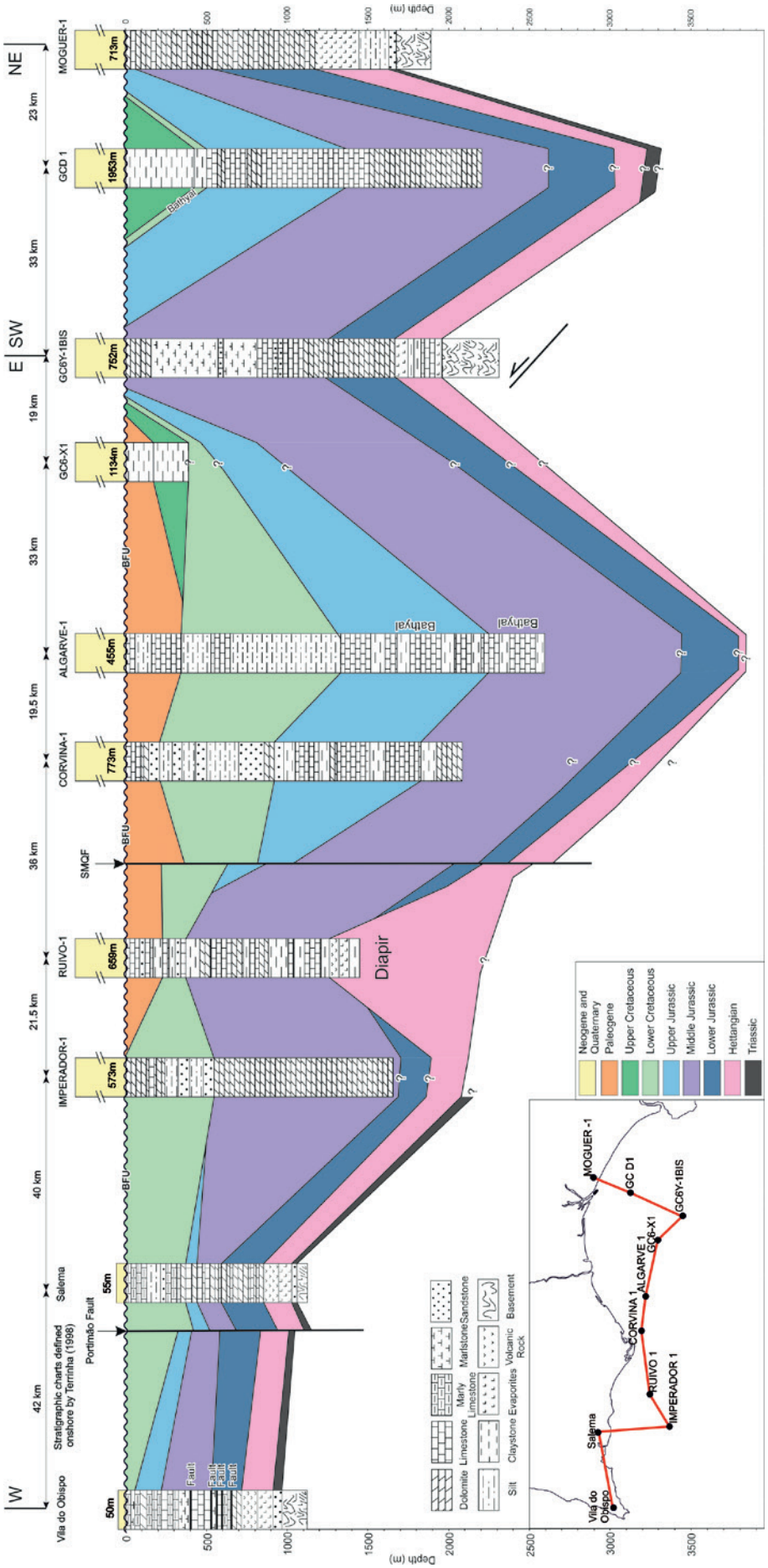
W
E
SW
NE
Vila do Obispo
Stratigraphic charts defined onshore by Terrinha (1998)
Portimão Fault
Salema
IMPERADOR-1
RUIVO-1
SMQF
CORVINA-1
ALGARVE-1
GC6-X1
GC6Y-1BIS
GCD 1
MOGUER-1
42 km
40 km
21.5 km
36 km
19.5 km
33 km
19 km
23 km
33 km
50m
55m
573m
659m
773m
455m
1134m
752m
1953m
713m
BFU
Fault
Bathyal
Diapir
Depth (m)
Dolomite
Limestone
Marly Limestone
Marlstone
Sandstone
Basement
Silt
Claystone
Evaporites
Volcanic Rock
Neogene and Quaternary
Paleogene
Upper Cretaceous
Lower Cretaceous
Upper Jurassic
Middle Jurassic
Lower Jurassic
Hettangian
Triassic
MOGUER -1
GC D1
GC6Y-1BIS
GC6-X1
ALGARVE 1
CORVINA 1
RUIVO 1
IMPERADOR 1
Salema
Vila do Obispo

147 **Fig. 4.** Stratigraphic correlation of Mesozoic and Paleocene along the northern portion of the margin. The
148 correlation panel is flattened to the BFU. Note that the Neogene to Quaternary thickness is not drawn to
149 scale. Both Mesozoic and Cenozoic strata thicken towards the Algarve-1 well, located in the central part
150 of the shelf of the Gulf of Cadiz. Depositional environment for all Mesozoic and Paleogene units is
151 neritic, excepting for well Algarve-1 where the Middle and Upper Jurassic were deposited in a bathyal
152 environment. The deposition of Mesozoic sediments is affected by the Portimão and the São Marcos
153 Quarteira (SMQF) faults, Jurassic-Lower Cretaceous diapiric activity (Ruivo-1 well) and Paleogene
154 thrusts (GC6Y-1BIS well). Well stratigraphic composites of the Gulf of Cadiz were taken from Lanaja
155 (1987), and those located in the Algarve Basin are taken from Terrinha (1998). Stratigraphic chart from
156 Terrinha (1998) and depositional environments were interpreted by Roque (2007) and well reports. Map
157 location in the bottom left of the figure.

158 The remaining Lower Jurassic is dominated by carbonates. It is less than 1000 m thick in the onshore
159 and up to 500 m in some wells. It is locally absent above salt diapirs (e.g., Ruivo-1 well). The Lower
160 Jurassic can be internally subdivided into two sub-units: the Sinemurian and the Pliensbachian-Toarcian.
161 Sinemurian shallow water limestones and dolomites are roughly 100-200 m thick in the west to 500 m
162 thick in the east, and are considered to record a phase of tectonic quiescence (Terrinha, 1998). Above the
163 Sinemurian, the Pliensbachian to Toarcian is represented by hemipelagic dolomites, limestones and marls
164 deposited in a shallow water environment. The Pliensbachian-Toarcian is up to 200 m thick in the
165 Western sub-basin (west of the Portimão Fault), whereas it locally reaches 600 m thickness in the east
166 (Terrinha, 1998). Thickness changes of this unit are interpreted to be controlled by renewed extensional
167 faulting (Ramos et al., 2016; Terrinha, 1998) and salt diapirism. Profuse ammonoids record the
168 progressive deepening of the basin, a subsiding phase that ended at the transition to the Middle Jurassic
169 (Terrinha et al., 2002).

170 Sedimentation of the Middle Jurassic was mainly hemipelagic in the Western sub-basin (up to 250 m
171 thick) as well as in in the Central-Eastern sub-basin (up to 500 m thick). The Middle Jurassic expands
172 significantly in the offshore wells (up to 1200 m) and is still interpreted to have deposited in a shallow
173 water setting (except for slope to deep water conditions interpreted for well Algarve-1; Roque, 2007). The
174 Middle Jurassic shows numerous internal unconformities which have been interpreted to represent mild
175 pulses of inversion during rifting (Terrinha, 1998; Terrinha et al., 2002). At the top, the Middle Jurassic is
176 truncated by the Callovian-Oxfordian erosional unconformity (Terrinha et al., 2002). This unconformity

177 is equivalent to the regional “Callovian regression or crisis” (Manuppella et al., 1988; Mouterde, 1971;
178 Rocha, 1976), which also affected the neighbouring Lusitanian and Betic basins (Alves et al., 2009;
179 García-Hernández et al., 1989; Montenat et al., 1988; Pereira and Alves, 2012; Vera, 1988; Wilson,
180 1988), other Iberian basins (Hiscott et al., 1990; Stapel et al., 1996), and the Atlas and External Rif basins
181 of northwest Africa (Aïfa and Zaagane, 2014; Flinch, 1994; Zizi, 1996). This unconformity in SW Iberia
182 possibly indicates the age of continental break-up.

183 Above the Callovian-Oxfordian unconformity, the Upper Jurassic succession is also strongly
184 differentiated in the two sub-basins. The Upper Jurassic is up to 200 m thick in the west and dominated
185 by limestones and marls deposited in an internal platform setting. It is over 1600 m thick in the east and
186 dominated by limestones and marls deposited between internal and external platform settings. Frequent
187 lateral facies changes within the Oxfordian to Lower Kimmeridgian are interpreted to indicate internal
188 fault-related compartmentalization of the Central-Eastern sub-basin (Terrinha, 1998), whereas the Upper
189 Kimmeridgian to Tithonian are uniform throughout the sub-basin (Terrinha, 1998). Wells in the offshore
190 encounter a variable thickness of Upper Jurassic due to syn-sedimentary extensional faulting, salt
191 tectonism (e.g., Imperador-1, Ruivo-1) and erosion and truncation during the Cenozoic (e.g., GC6Y-
192 1BIS). Thickness in the offshore is less than 1100 m and most wells encounter carbonates deposited in
193 shallow water settings (other than the Algarve-1 well in which bathyal conditions are recorded; Roque,
194 2007).

195 The Lower Cretaceous often overlies a major unconformity. This unit is represented onshore by
196 shallow marine limestones and marls, alternating with detrital lithologies (Terrinha, 1998). This unit is
197 thicker in the Central-Eastern sub-basin (roughly 1500 m thick) than in the Western sub-basin (500 m).
198 To the east the facies are marine-dominated, while to the west the facies are continental and littoral
199 (Correia, 1989; Terrinha, 1998). Variations in the thickness of the Lower Cretaceous unit in offshore
200 wells, up to 1000 m and dominated by shallow water settings, are due to ongoing salt tectonism (Ramos
201 et al., under review).

202 Upper Cretaceous sediments are mostly absent in the onshore portion of the Algarve Basin due to
203 Cenozoic inversion and uplift (Ramos et al., 2016; Terrinha, 1998). Offshore, this unit is not well
204 preserved, and is only drilled by a few isolated wells in the Gulf of Cadiz (e.g., GC6-X1).

205 As with the Upper Cretaceous, the Paleogene is also absent in the onshore. In the offshore this unit is
206 of limited variable extent and is represented by shallow water carbonates. The Paleogene represents the
207 final unit deposited in a passive margin setting prior to Cenozoic inversion.

208 Mesozoic to Paleogene rocks are bounded at the top by a regional erosional unconformity related to
209 the initiation of contractional deformation and subsidence in the area (Basal Foredeep Unconformity,
210 BFU; Ledesma, 2000; Maldonado et al., 1999). The BFU is covered and onlapped by Miocene shallow
211 marine limestones that grade upwards into siltstones and fine sandstones. In the onshore, this unit was
212 later karstified and covered by Pliocene to Pleistocene fluvial and marine clastic sediments. In the deeper
213 offshore, Pliocene to Present sediments are controlled by the Mediterranean Outflow Water (MOW),
214 resulting in the deposition of fine-grained contourite drifts due to deep sea currents (Hernández-Molina et
215 al., 2014). Lithified Holocene beach sand and dunes are the youngest sediments in the Algarve Basin.

216 Along the southern Algarve Basin, and overlying the BFU and Lower Miocene sediments, a mélange
217 unit was emplaced synchronously with the development of the Betic-Rif orogen (Gutscher et al., 2002).
218 This unit is divided in two sub-units of different origin: the Accretionary Wedge of the Gulf of Cadiz
219 (AWGC) and the Allochthonous Unit of the Gulf of Cadiz (AUGC). The AWGC consists of an east-
220 thickening mélange of Mesozoic to Cenozoic sediments affected by west-directed imbricate thrusts. The
221 AUGC is an olistostrome, gravitationally emplaced as a submarine debris flows sourced from the AWGC
222 (Iribarren et al., 2007; Torelli et al., 1997).

223

224 **Available Data**

225 Observations, interpretation and results presented here are based on the integration of multiple data
226 sources: 2D and 3D reflection seismic data, well data, and geological mapping of the onshore Algarve
227 Basin.

228 The 2D seismic data used in this work consists of two different sets of seismic reflection surveys: a
229 set of vintage 2D seismic surveys covering the Spanish Gulf of Cadiz (www.info.igme.es/visorweb/), and
230 a more recent 2D seismic survey acquired by TGS in 2001 during the PDT00 and PD00 cruises (TGS,
231 2005; Fig. 5). The PDT00-PD00 regional survey comprises a set of 58 lines of 2D multichannel reflection
232 seismic data (Fig. 5). The survey has a shotpoint interval of 12.5, and consists of a two perpendicular sets

of lines: one oriented NNW-SSE spaced every 4km and other oriented ENE-WSW spaced every 8km (Fig. 5). Recording length was 12 seconds of two-way travel time (TWTT). The interpretation on this survey was performed on the pre-stack time migration.

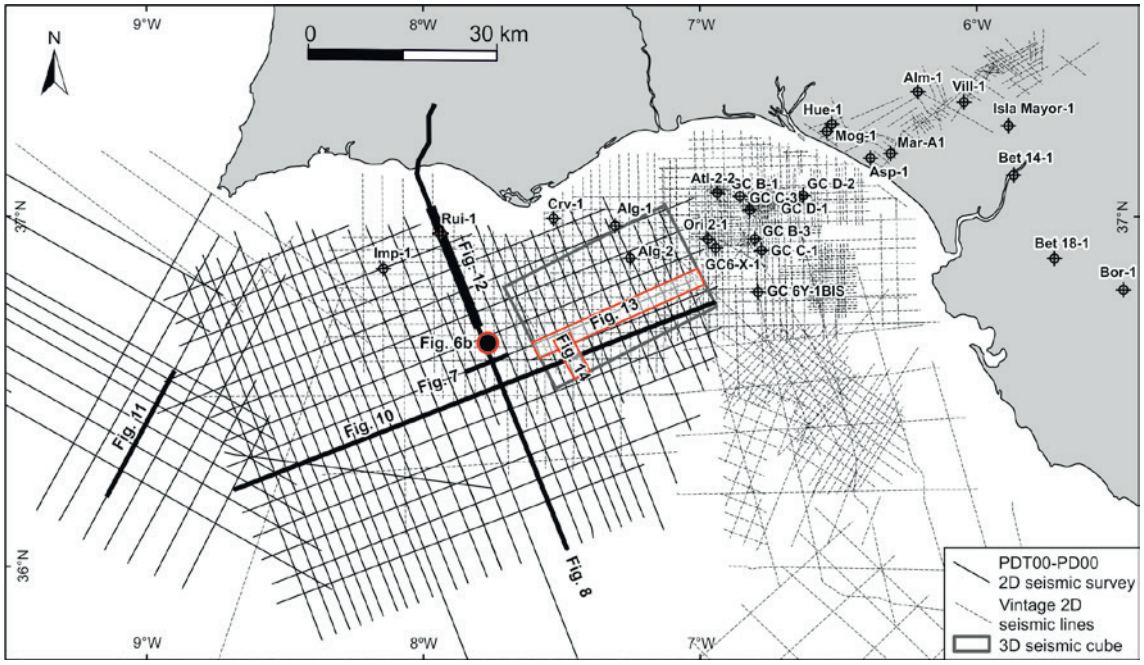

Fig. 5. Data available in the Gulf of Cadiz used in this study. Alg-1: Algarve-1; Alg-2; Algarve-2; Alm-1: Almonte-1; Asp-1: Asperillo-1; Atl-2-2: Atlantida-2-2; Bet 14-1: Betica 14-1; Bet 18-1: Betica 18-1; Bor-1: Bornos-1; Crv-1: Corvina-1; GC6-X-1: Gulf of Cadiz 6-X-1; GC B-1: Gulf of Cadiz B-1; GC B-2: Gulf of Cadiz B-2; GC D-1: Gulf of Cadiz D-2; GC D-2: Gulf of Cadiz D-2; GC 6Y-1Bis: Gulf of Cadiz 6Y-1Bis; Hue-1: Huelva-1; Imp-1: Imperador-1; Mog-1: Moguer-1; Ori 2-1: Orion 2-1; Rui-1: Ruivo-1.

2D seismic profiles are complemented by a 3D seismic volume acquired by Repsol in 2012 in the central part of the Gulf of Cadiz (Fig. 5). The seismic cube covers an area of 1500 km^2 acquired in 151 shot lines oriented NNW-SSE, with a shotpoint spacing of 18.5m and shotlines spaced every 375 m. The recording length is 7.2 seconds of TWTT. This 3D cube has been interpreted in the pre-stack time and depth migrated versions.

Seismic interpretation of 2D and 3D seismic surveys was constrained by the calibration with five wells in offshore Portugal (Roque, 2007; Terrinha, 1998) and a further 67 wells in the Gulf of Cadiz and Guadalquivir Basin (Lanaja, 1987; the most relevant are illustrated in Figure 3).

Seismic profiles were interpreted in time and converted to depth using seismic velocities derived from checkshots from the 5 Portuguese wells. Three stratigraphic intervals were defined based on their average velocities: Neogene-Quaternary, top Paleogene to top Middle Jurassic and top Middle Jurassic to Basement. The depth image of the depth migrated 3D seismic cube was also used to calibrate the interval velocities, and therefore gain confidence in the depth conversion of 2D lines in the deeper portions of the basin.

The interpretation converted to depth was interpolated to obtain a grid for interpreted horizons. These surfaces were used to calculate the vertical thickness for each stratigraphic unit. In this manner, isopach maps were constructed honouring the seismic interpretation, the well data and the field data.

Seismic interpretation

Seismic interpretation was carried out based on the unconformity bounded sequences defined by (Terrinha, 1998) and (Roque, 2007). These units have been correlated on seismic throughout the basin. The published data from the onshore Algarve Basin (Manuppella, 1992; Ramos et al., 2016; Terrinha, 1998) was also integrated with the seismic interpretation. This section includes a description of the seismic-stratigraphic units from the bottom to the top.

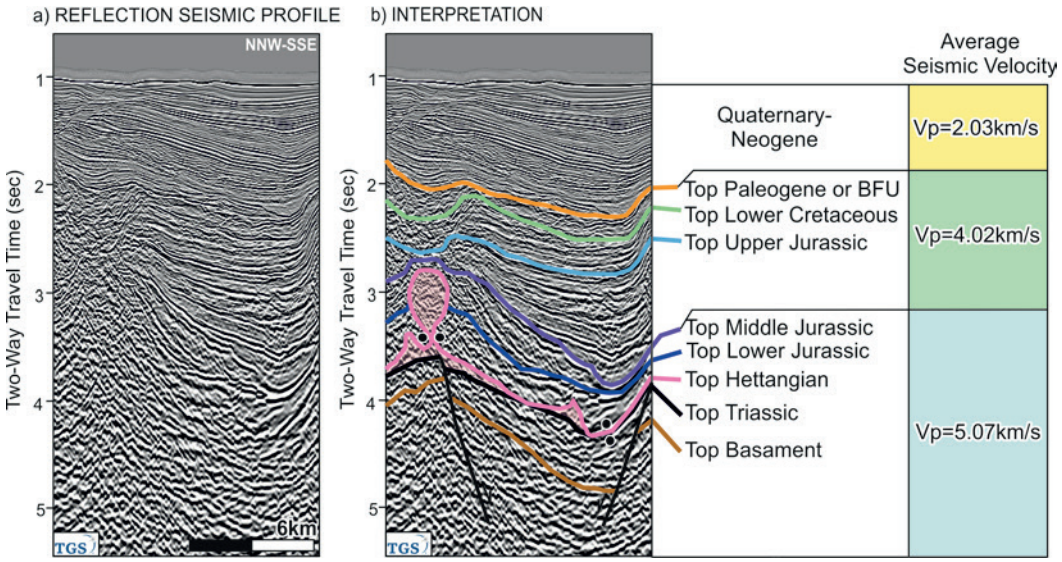

Fig. 6. Illustration of seismic facies for each interpreted interval. (a) Reflection seismic profile and (b) interpretation of the profile. Velocities used for depth conversion are shown on the right. See Fig. 5 and 8 for location of the seismic image. Data courtesy of TGS.

The deepest unit interpreted corresponds to the Paleozoic basement. It is characterized by chaotic seismic facies. The basement occasionally presents stratified seismic facies. The basement has been interpreted by picking its top, which is a bright reflector that is locally discontinuous and frequently offset by extensional faulting (Fig. 6). Recent understanding of inversion of the margin (Ramos et al., 2017a) and gravity modelling (Ramos et al., 2017b) helped to constrain the picking of the top of basement in areas where this pick is uncertain.

The following unit is the Triassic, represented by a package of mid-high frequency and high amplitude reflectors (Fig. 6). The Triassic depocenters are bounded by high angle basement-involved extensional faults. Triassic depocenters are larger offshore than those observed in the onshore (e.g., Ramos et al., 2016), indicating that extensional faults are possibly more spaced offshore. Smaller depocenters such as those observed in the onshore may also present offshore but it has not been possible to interpret them on the available seismic.

Above, the Hettangian evaporites are imaged on seismic by transparent to chaotic seismic facies. This unit is bounded at the top by an irregular high-amplitude reflector and at its base by a smooth but faulted mid-amplitude reflector that can be occasionally obscured by diapirism (Fig. 6). Allochthonous salt bodies sourced from the Hettangian evaporite unit have a similar seismic response (Fig. 6). Due to their deposition during extension, Hettangian evaporites were originally thicker in the grabens and in the centre of the basin, while they thinned towards the basin margin.

The Lower Jurassic shows low frequency and high amplitude reflectors (Figs. 6 and 7). Sinemurian is represented by a roughly constant thickness package at the base and a variable thickness Pliensbachian–Toarcian package. Thickness changes in the upper Lower Jurassic relate to extensional tectonics and salt tectonics. The uppermost part of the Lower Jurassic is truncated by an erosional unconformity and is unconformably overlain by the Middle Jurassic (Fig. 7). This unconformity is more accused in the areas affected by salt tectonism (Figs. 6 and 7).

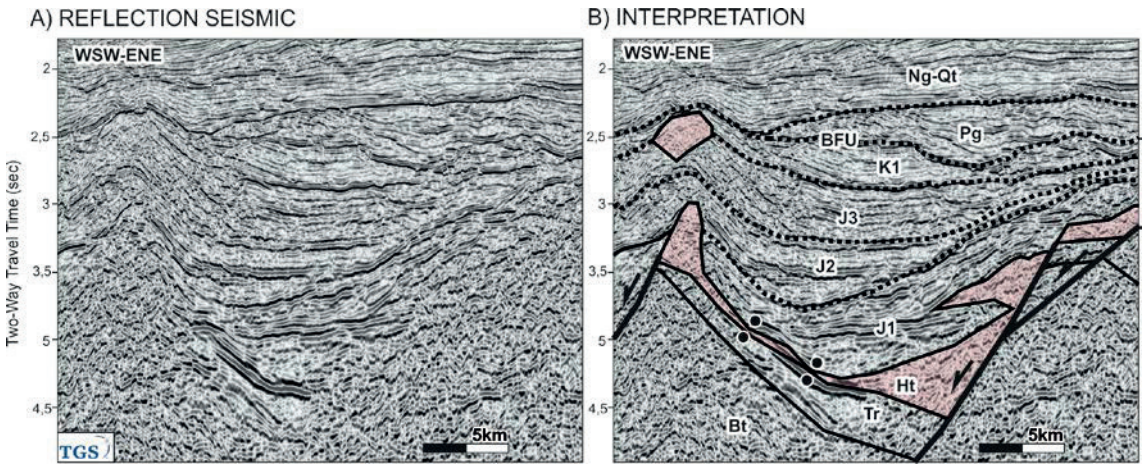

Fig. 7. Illustration of the main unconformities correlated throughout the Algarve Basin. (a) Reflection seismic profile and (b) the corresponding interpretation. The sedimentary units in this illustration are affected by salt tectonism and motion on basement faults. Black dotted line: unconformity. From top to bottom: Ng-Qt: Neogene-Quaternary; Pg: Paleogene; BFU: Basal Foredeep Unconformity; K1: Lower Cretaceous; J3: Upper Jurassic; J2: Middle Jurassic; J1: Lower Jurassic; Ht: Hettangian; Tr: Triassic; Bt: Basement. The other unconformities do not have a name. See Fig. 5 for location. Data courtesy of TGS.

The Middle and Upper Jurassic successions show similar seismic response, with reflectors with greater lateral continuity than in the Lower Jurassic unit. The Upper Jurassic lays unconformably over the Middle Jurassic, with more pronounced angularities in the flanks of salt withdrawal minibasins (Fig. 7). The top of the Upper Jurassic is an unconformity marked by a gently folded high amplitude reflector. This unconformity is onlapped by the Lower Cretaceous, which is characterized by mid to high frequency and medium amplitude reflectors of good lateral continuity (Figs. 6 and 7). The Lower Cretaceous is represented locally by nearly transparent facies. Towards its roof, the Lower Cretaceous is truncated in some areas by the base of the Upper Cretaceous or Paleogene (Figs. 6 and 7). Where present, these units are highly condensed and are represented by strong mid-amplitude and mid-frequency continuous reflectors. These units onlap the top of the Lower Cretaceous (Figs. 6 and 7).

The Mesozoic is capped by the regional BFU, a bright reflector that truncates underlying tilted strata and is very continuous throughout the entire study area (Fig. 6). Neogene-Quaternary units onlap the BFU and are represented in seismic by high frequency and variable amplitude continuous reflectors (Figs. 6 and 7). The top of this unit is the seafloor (Figs. 6 and 7).

318 Finally, the AWGC and the AUGC are seismically identified in this paper as a single unit, bounded
319 at its top by a highly irregular reflector, which is in turn onlapped by Miocene to Recent sediments (e.g.,
320 Fig. 11). Their base describes a relative smooth geometry, truncating the underlying sediments. Internally,
321 these units have chaotic to transparent facies. To the south, the AUGC/AWGC obscures the imaging of
322 deeper reflectors.

323

324 **Structure of the Algarve Basin**

325 The structure of the Algarve Basin is dominated by extensional tectonics and can be illustrated by the
326 geometry of the top of the basement (Fig. 8). Extensional faults that involve the basement trend mainly
327 WSW-ENE (Fig. 8).

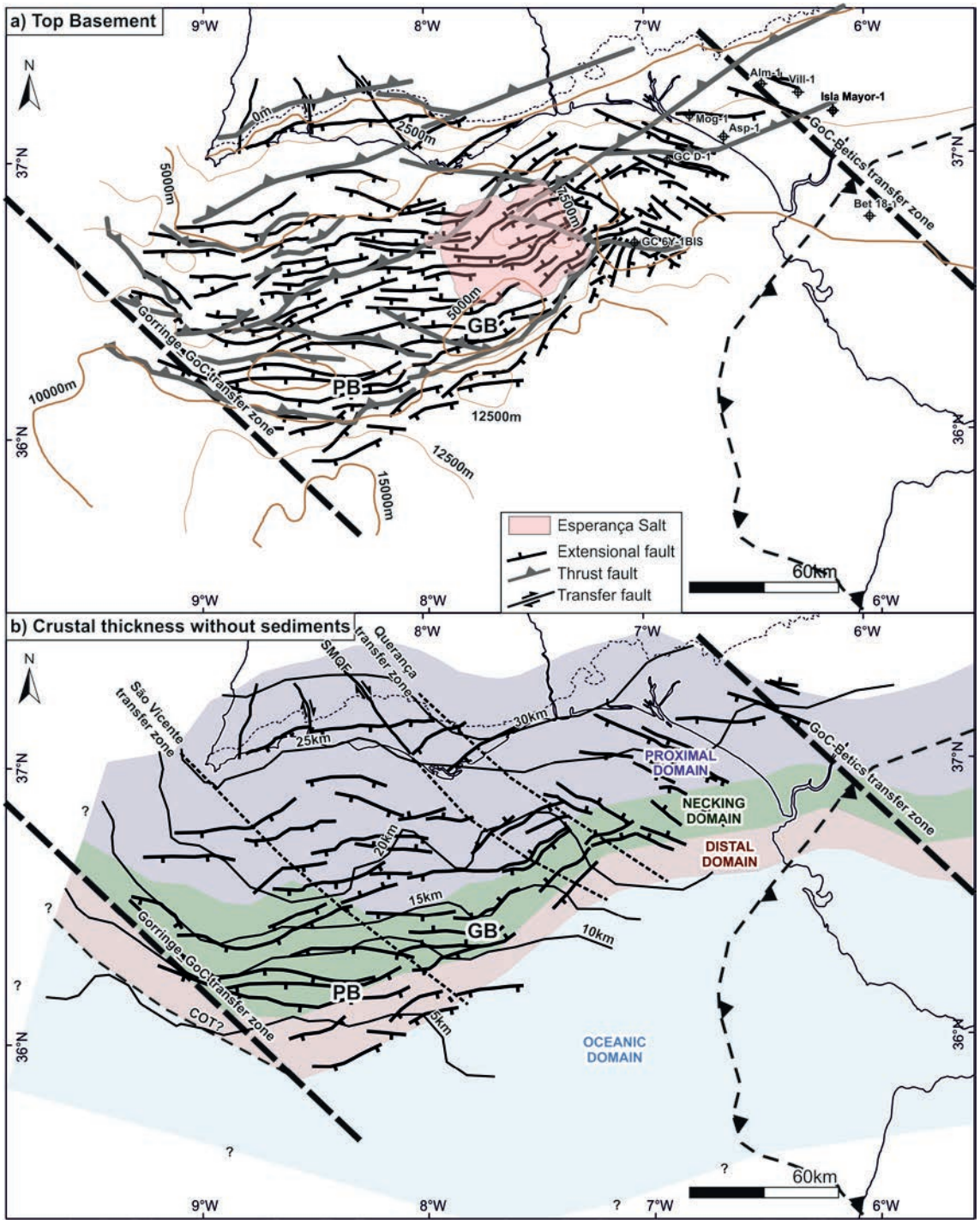

328

329 **Fig. 8.** (a) Isobath map of the top of basement with the main structures overlain. The wells reaching the
330 basement are shown. (b) Map of thickness between the top of basement and the Moho with and overlay of
331 the main extensional faults and crustal domains (depth to Moho and crustal domains according to Ramos
332 et al. (2017b).

333 The extensional faults and their impact on basement structure can also be seen on the regional section
334 in Figure 9. On this section, the basement and the bathymetry are observed to drop from north to south,.

This trend is locally interrupted by structures uplifted during Cenozoic inversion (namely, the Guadalquivir Bank). Offshore, seismic interpretation along with gravity modelling (Ramos et al., 2017b) indicate that fault-bounded basement grabens are filled with major Triassic depocenters, thicker than those onshore. Extensional faults also control the location of the greater depocenters of Lower and Middle Jurassic in the offshore portion of the basin. Extensional faults are also observed to control the location of salt structures. The geometry and structure of the domain south of the Guadalquivir Bank below the AUGC/AWGC, is inferred based on gravity modelling, peak rifting time (inferred to occur during the Middle Jurassic, prior to continental breakup; Ramos et al., 2017b).

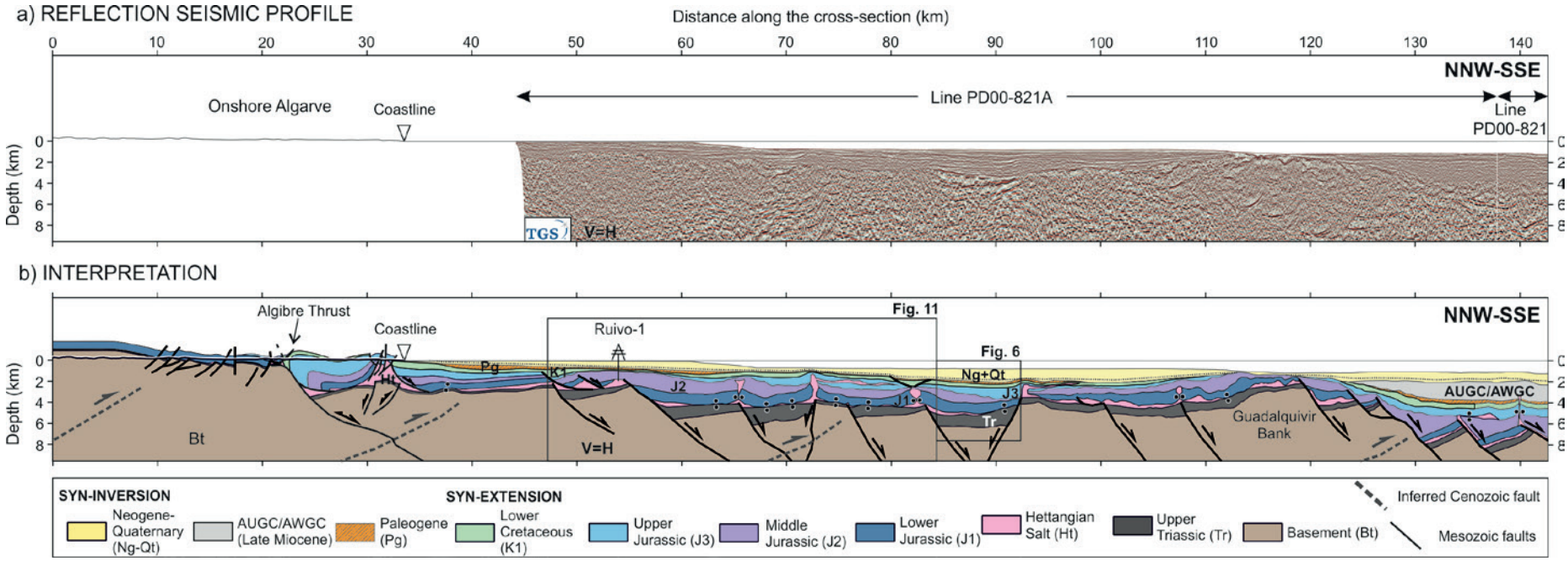
a) REFLECTION SEISMIC PROFILE
Distance along the cross-section (km)
0 10 20 30 40 50 60 70 80 90 100 110 120 130 140
NNW-SSE
Onshore Algarve
Coastline
Line PD00-821A
Line PD00-821
Depth (km)
0 2 4 6 8
TGS
V=H
b) INTERPRETATION
NNW-SSE
Algibre Thrust
Coastline
Ruivo-1
Fig. 11
Fig. 6
Ht
Pg
K1
J2
J1
J3
Tr
Ng+Qt
AUGC/AWGC
Guadalquivir Bank
Bt
V=H
SYN-INVERSION
SYN-EXTENSION
Neogene-Quaternary (Ng-Qt)
AUGC/AWGC (Late Miocene)
Paleogene (Pg)
Lower Cretaceous (K1)
Upper Jurassic (J3)
Middle Jurassic (J2)
Lower Jurassic (J1)
Hettangian Salt (Ht)
Upper Triassic (Tr)
Basement (Bt)
Inferred Cenozoic fault
Mesozoic faults

Fig. 9. Cross-section through the central Algarve Basin showing the major structures identified in offshore and onshore. See text for a detailed description. Black dots represent salt welds. See Fig. 5 for location. Seismic data courtesy of TGS.

Oblique transfer zones

Besides the margin-parallel extensional faults, the offshore prolongation of the oblique structures defined in the onshore has also been interpreted. The SMQF and the Querença transfer zone (QTZ) cannot be identified on seismic data as discrete faults. However, the offshore prolongation of the QTZ coincides with the presence of NW-SE trending extensional faults that define the northeastern boundary of the Esperança salt sheet and a domain of dominantly NW-SE trending faulting to the east (Fig. 8a). The SMQF in turn coincides with lateral ramps of the Cenozoic south-directed thrusts defined by Ramos et al. (2017a) (Fig. 8a). The offshore prolongation of the Portimão Fault, however, appears to have no impact on the extensional or inversion structure of the Algarve basin, although it does have recent activity, as shown by its coincidence with a submarine canyon with its same N-S trend (Terrinha et al., 1999).

In the western part of the Algarve Basin, a set of features are observed to align along a NW-SE trend: a decrease in the crustal thickness (Fig. 8b) and southwestward drop in the basement (Figs. 8a and 10); a southwestward thickening of Mesozoic depocenters and increased diapirism (Fig. 10); an drop in the bathymetry in a SW direction (Fig. 10); a change in tectonic style between the Portimão Bank (inverted half-graben) and the Guadalquivir Bank (inverted basinward dipping extensional fault; Ramos et al., 2017a); the presence of lateral ramps in the inversion thrust system (Ramos et al., 2017a; Fig. 8a); and a change in the character of the crustal necking domain (Ramos et al., 2017b; Fig. 8a). The coincidence of these features along a NW-SE trend is inferred to indicate the possible presence of a previously unidentified NW-SE transfer zone akin to the SMQF and QTZ. This zone of alignment has been called the São Vicente transfer zone (SVTZ; Fig. 8a).

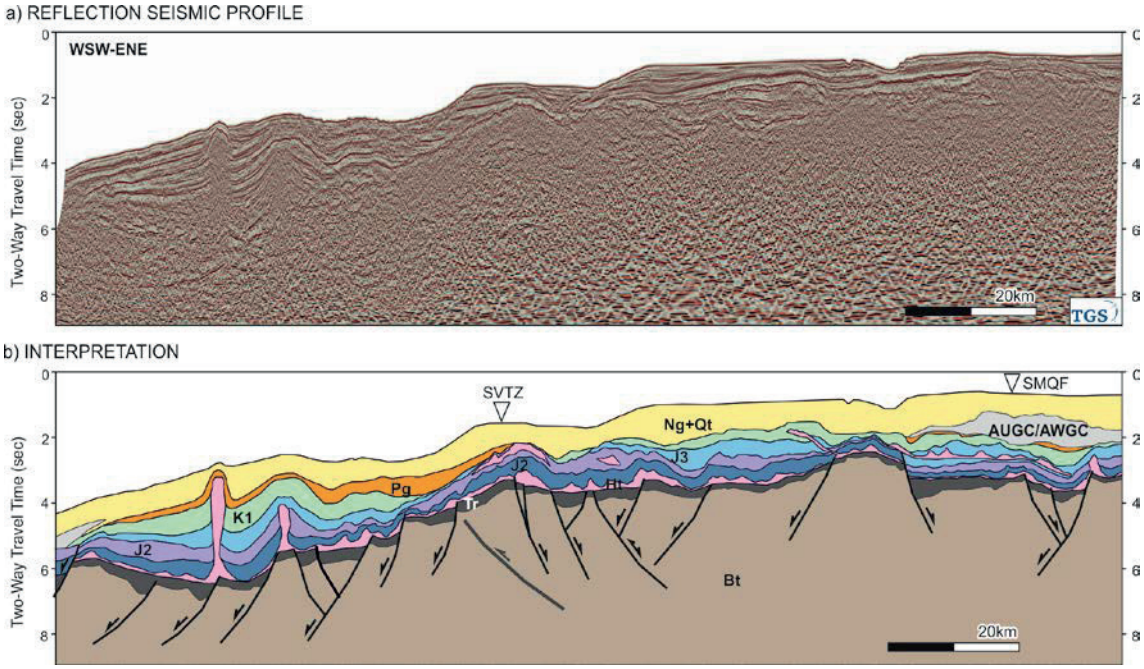

368

369 **Fig. 10.** (a) Seismic section along the axis of the Algarve Basin, trending roughly from west to east. (b)
370 Interpretation of the seismic profile showing a deepening of the basement and thickening of Mesozoic
371 towards the west. The triangles on the seabed marks the location of the São Vicente transfer zone and the
372 SMQF. See Fig. 5 for location and Fig. 9 for legend. Data courtesy of TGS.

373 To the west, the Algarve Basin is limited by a set of southwest dipping extensional faults that cause a
374 sudden drop of the basement towards the southwest (Fig. 11). This drop in the basement is coincident
375 with a similar southwestward drop in the bathymetry. This set of faults is interpreted to represent the
376 Gorringe-GoC transfer zone (Ramos et al., 2017b), which offsets this passive margin from the Algarve
377 Basin to a position equivalent to that occupied at present by the Gorringe Bank. West of this system of
378 transfer faults, the crust is much thinner and interpreted to be oceanic in nature (Sallarès et al., 2011).

379 To the east, we interpret the Algarve Basin is bound by a similar system of faults. Some of these have
380 been identified on seismic east of the QTZ (Fig. 8a). The main zone of transfer is however interpreted to
381 occur in the onshore. This NW-SE transfer, the Gulf of Cadiz-Betics transfer zone (Ramos et al., 2017b)
382 (Fig. 8), connects the Algarve Basin with the Betic domain (Ramos et al., 2017b).

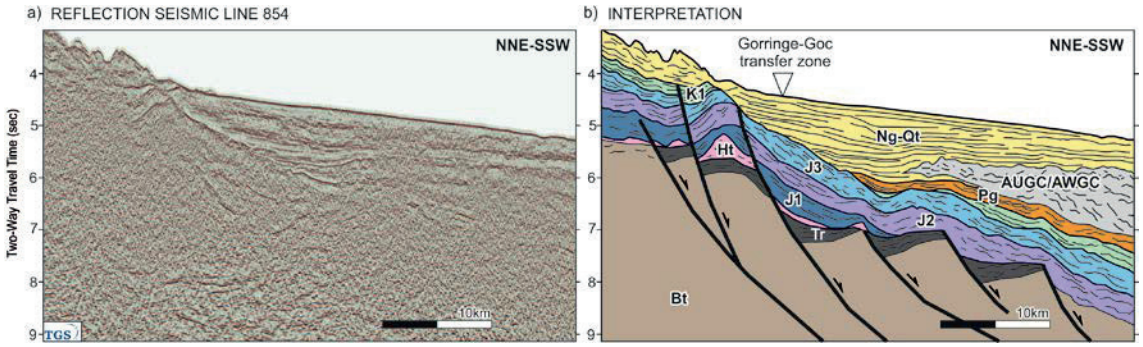

Fig. 11. Reflection seismic profile across the western portion of the Algarve Basin (a) and the corresponding interpretation (b). The triangle on the seabed marks the location of the Gorringe-GoC transfer zone. See Fig. 5 for location and Fig. 9 for legend. Data courtesy of TGS.

Salt tectonics

The basement structure of the Algarve Basin is locally masked by salt tectonics. Diapirs are prominent throughout the Basin, with intervening salt withdrawal mini-basins filled mainly with Jurassic and Lower Cretaceous sediments (Fig. 12). Some diapirs developed allochthonous salt units that were emplaced within the Jurassic successions and extended up to 10 km away from their source (Fig. 12). The most prominent allochthonous salt body in the Algarve Basin is the Esperança salt sheet (Matias et al., 2011), located in the central part of the offshore basin, north of the Guadalquivir Bank (Fig. 8a).

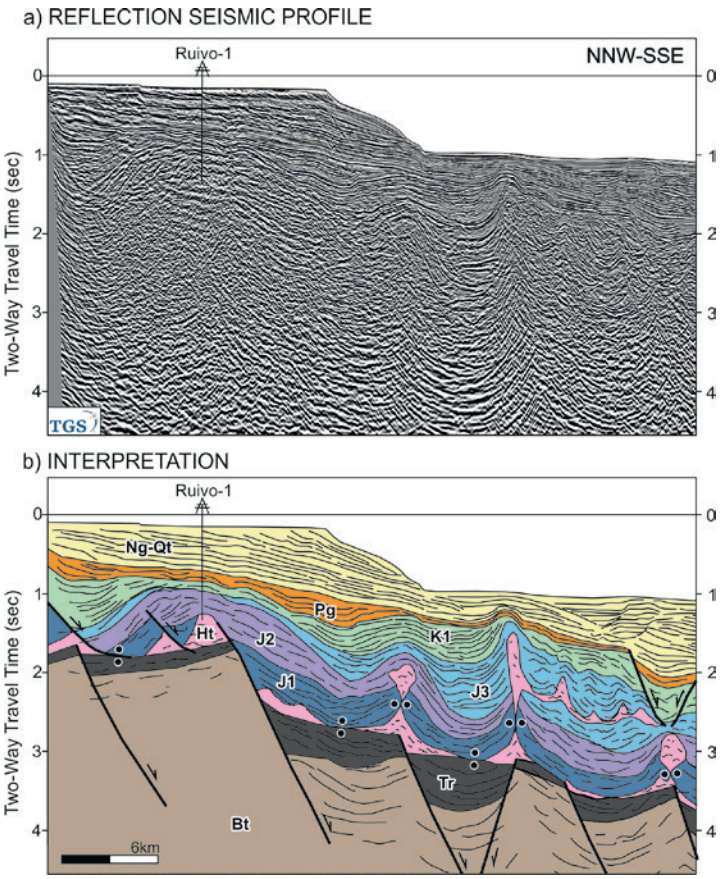

394

395 **Fig. 12.** (a) Seismic section in time across the Ruivo-1 well. (b) Interpreted section illustrating various
396 salt-related structures. See Figs. 5 and 8 for location and Fig. 9 for legend. Data courtesy of TGS.

397 The Esperança salt sheet is characterized by a strong, continuous reflector at its base, which is not
398 affected by Jurassic age faulting. Its roof is imaged as a bright reflector with a highly irregular geometry
399 (Fig. 13). Above the Esperança salt sheet, Jurassic sediments young and thin towards the west and south.
400 This unit is interpreted to have been emplaced progressively from Early Jurassic to Early Cretaceous,
401 truncating successively younger sediments westwards and southwards (Fig. 13).

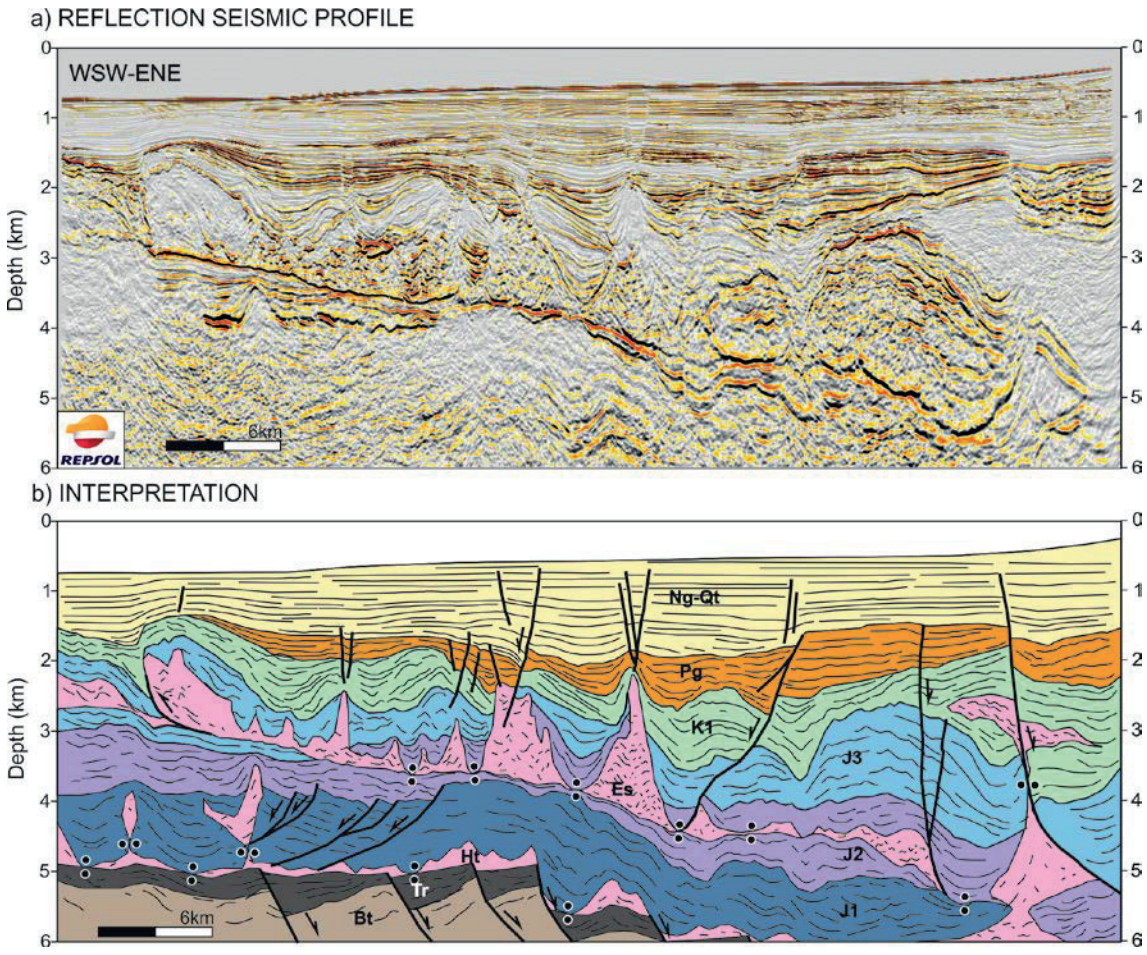

Fig. 13. (a) Seismic section in depth across the Esperança salt sheet. (b) Interpretation of the seismic section. The section is a WSW-ENE trending section through the 3D seismic survey shown in Figure 5 (the precise location is not shown due to confidentiality). Note that despite intense salt-related deformation above the Esperança salt sheet layer, diapirism sourced from the autochthonous layer is minimal. See Fig. 9 for legend. Data courtesy of Repsol. Modified after Ramos et al. (under review).

Cenozoic inversion

The extensional structures of the Algarve Basin are partially overprinted by Cenozoic inversion. Inversion led to the development of thin-skinned structures (thrusts detaching within the Mesozoic layers, Figs. 9 and 12) and basement-involving structures (mainly south-directed blind thrusts; (Ramos et al., 2017a). One of these south-directed thrusts is responsible for the uplift of the Guadalquivir Bank (Fig. 14). The mainly WSW-ENE trending basement thrusts are linked by numerous NW-SE trending lateral ramps that coincide with the key oblique transfer zones of the extensional system (Fig. 8).

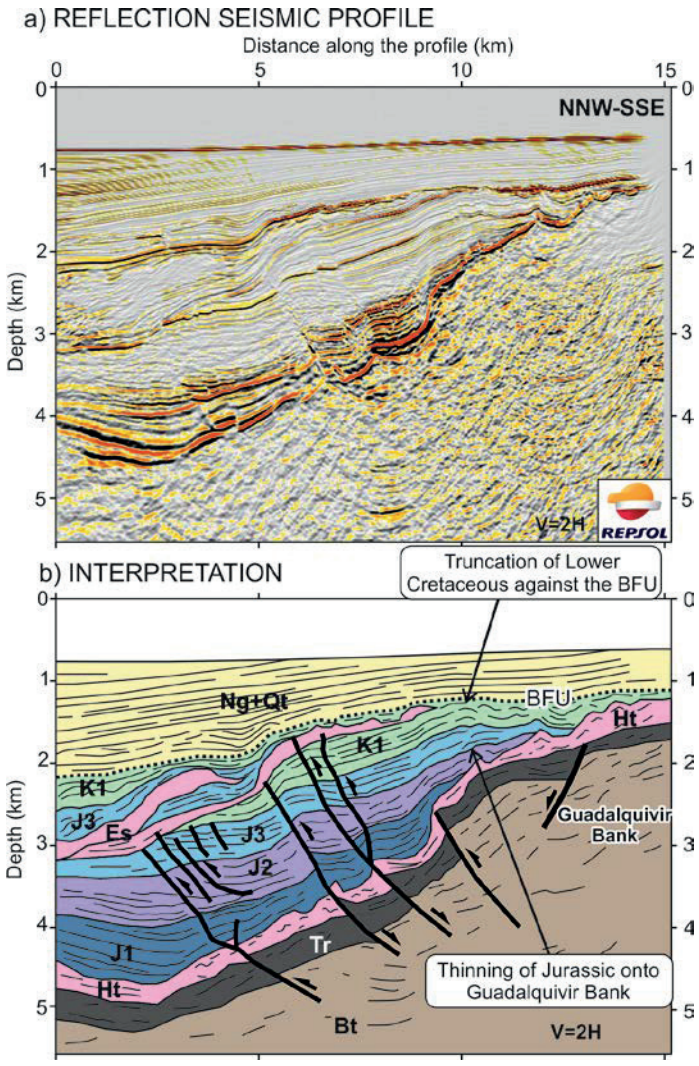

415

416 **Fig. 14.** (a) Portion of a 3D seismic line across the northern flank of the Guadalquivir bank in depth and
417 (b) its interpretation. Note that the Guadalquivir Bank acted as an intra-basinal high during the Mesozoic
418 (Jurassic sediments thin onto the northern flank of the basement high). The Guadalquivir Bank was
419 subsequently uplifted in the Neogene, causing the erosive truncation of Paleogene and older sediments.
420 Locally, the entire Mesozoic is eroded. Modified after Ramos et al., 2017a). See Fig. 5 for location and
421 Fig. 9 for legend. Data courtesy of TGS.

422 *Structure of the Mesozoic to Paleogene sedimentary cover*

423 The description of the 3D structure of the Algarve Basin is completed with isobath maps for the main
424 stratigraphic horizons from Triassic to the BFU (Fig. 15).

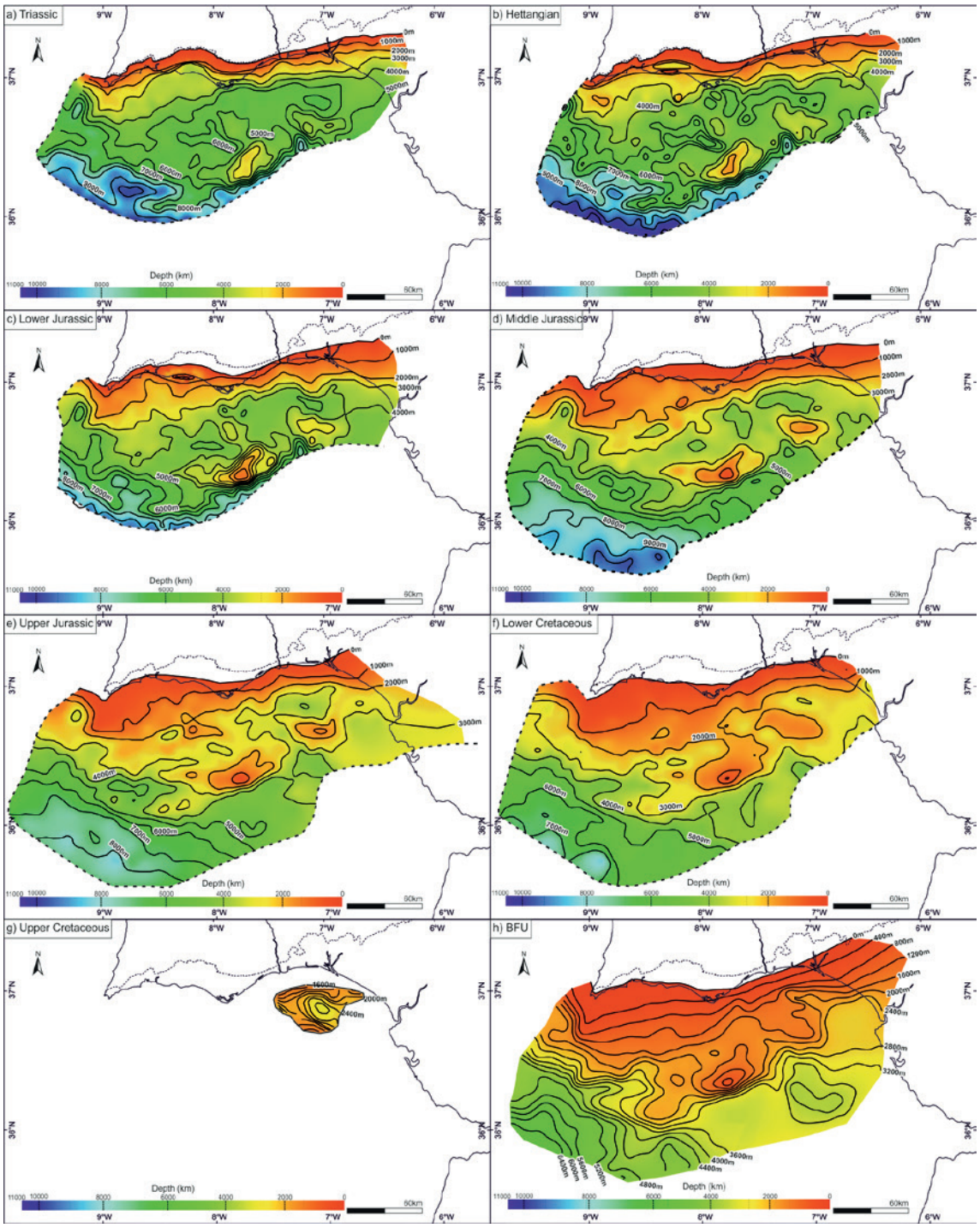

425

426 **Fig. 15.** Isobath maps in meters of the following units: a) Triassic; b) Hettangian; c) Lower Jurassic; d)
427 Middle Jurassic; e) Upper Jurassic; f) Lower Cretaceous; g) Upper Cretaceous; h) BFU. See text for a
428 detailed description.

429 The maps of these units show a general pattern of southward deepening in the central and eastern
430 parts of the basin. In the western part of the basin the horizons tend to deepen towards the southwest and
431 west (Fig. 15). Another general feature common in all maps, with the exception of the Upper Cretaceous,

is the presence of an intra-basinal high that becomes wider in the most recent maps, corresponding to the Guadalquivir Bank (Fig. 15).

The deepest units (Triassic to Middle Jurassic) show shorter wavelength highs and lows due to the control exerted by basement extensional faults (Figs. 8 and 11). The geometry of the Lower Jurassic to Early Cretaceous is also controlled by syn-sedimentary salt tectonic structures. Younger units present smoother geometries as they post-date extensional faulting and most salt movement, and are only affected by broad inversion structures (e.g., Figs. 8 and 9).

Tectonic evolution of the SW Iberian margin

The evolution of the SW Iberian margin can be illustrated with the restoration of the regional 2D section presented in Fig. 8 (Fig. 16)., This section is oriented NNW-SSE, perpendicular to the main extensional and contractional structures. For this restoration we assumed plane-strain deformation. The process of backstripping involved removing fault displacement for each stratigraphic interval, and decompacting sediments sequentially using compaction curves based on Sclater and Christie (1980). For the purpose of compensating for thermal subsidence, we have assumed, based on fault throw and thickness in depocenters, that the peak in rifting took place in the Middle Jurassic. The stretching factor used for thermal subsidence estimates (modelled according to McKenzie; 1978) was computed from the crustal thickness relative to unstretched crust (from Palomeras et al., 2009; Ramos et al., 2017b). At each step, the section was compensated for Airy isostasy and for thermal subsidence. Throughout, salt was restored according to the methodology of Rowan (1993).

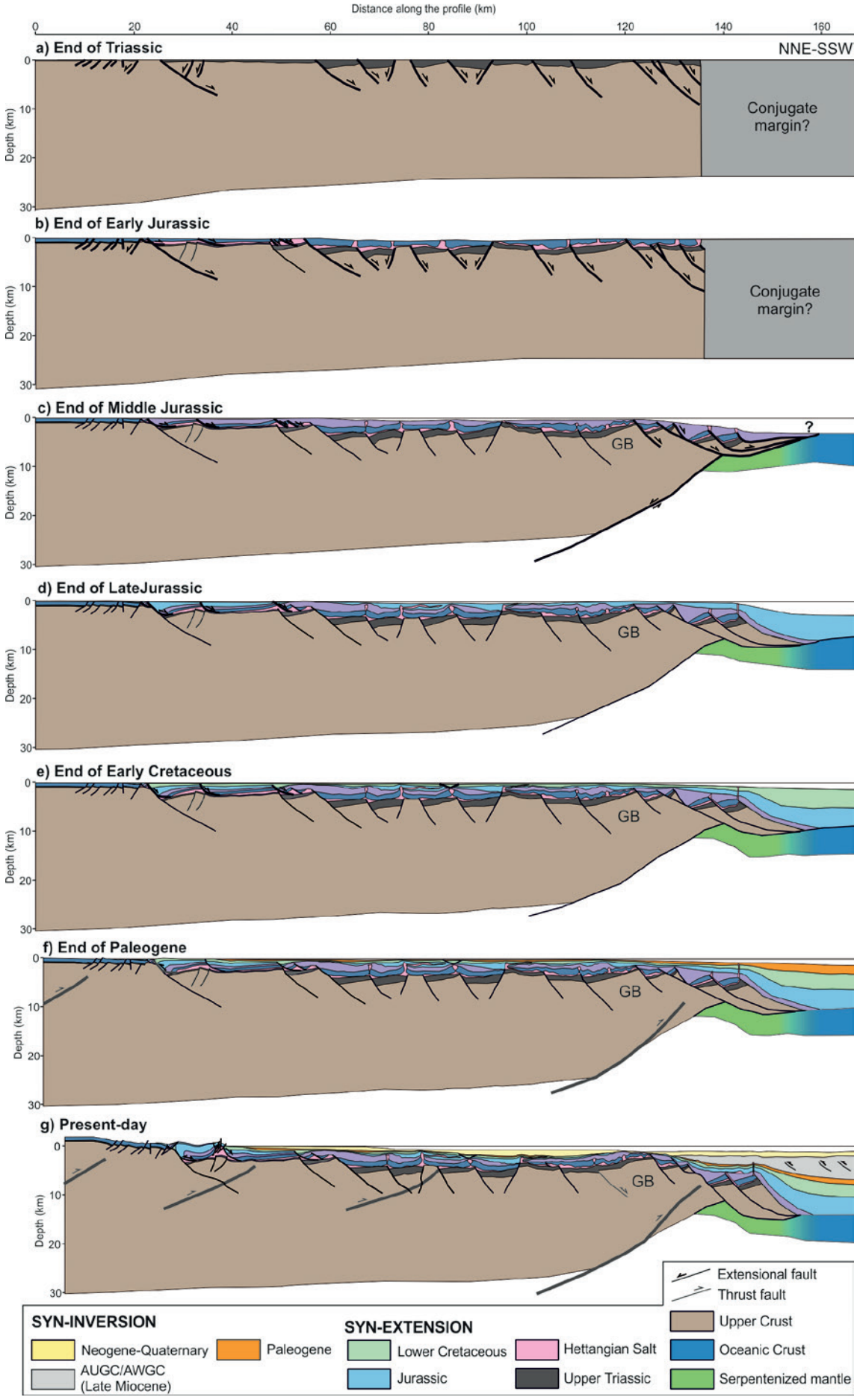
Distance along the profile (km)
0
20
40
60
80
100
120
140
160
a) End of Triassic
NNE-SSW
Conjugate margin?
b) End of Early Jurassic
Conjugate margin?
c) End of Middle Jurassic
GB
?
d) End of LateJurassic
GB
e) End of Early Cretaceous
GB
f) End of Paleogene
GB
g) Present-day
GB
Depth (km)
0
10
20
30
SYN-INVERSION
Neogene-Quaternary
Paleogene
AUGC/AWGC (Late Miocene)
SYN-EXTENSION
Lower Cretaceous
Hettangian Salt
Jurassic
Upper Triassic
Extensional fault
Thrust fault
Upper Crust
Oceanic Crust
Serpentenized mantle

452

Fig. 16. Restoration of a WNW-ESE regional cross-section during its evolution from the Triassic to present-day (a-g). Thicker lines with arrows represent active faults for each period. GB: Guadalquivir Bank. (a) Triassic clastics were deposited during the initial rifting phase in fault-bound grabens and half-grabens. (b) The Hettangian evaporites deposited during ongoing rifting, with greater thickness basinward. The remaining Lower Jurassic deposited in salt withdrawal minibasins, marking the onset of salt tectonics. (c) The Middle Jurassic marks the rift climax, with the Guadalquivir Bank acting as an intra-basinal high and the development of a highly-extended domain in the distal part of the margin (right end of the section). Initial oceanic crust may have formed at the latest Middle or the early Late Jurassic. (d) and (e) represent the stages of post-rift (Late Jurassic and Early Cretaceous), with major thickening only in the distal part of the margin. Diapirism continued to be active. (f) During the Paleogene, initial inversion occurred mainly along the northern margin of the basin and in the Guadalquivir Bank. (g) During the Neogene-Quaternary, inversion extended through the entire margin. The AUGC/AWGC was emplaced over the distal domain in Miocene times. During the Cenozoic, salt structures were reactivated in compression.

Extension initiates over the entire section at Triassic times. Extension is greater towards the south of the section. At this time, it is assumed that the SW Iberian margin formed a continuous rift with NW Africa, its future conjugate margin. During the Early Jurassic and then the Middle Jurassic, extensional faulting concentrated gradually in the southern half of the section. We interpret that continental break-up occurs at Middle Jurassic times, with the exhumation of deeper crustal units or even sub-continental mantle in the most distal domain (southern end of the section; Ramos et al., 2017b).

During the Late Jurassic most extensional fault activity has ceased. In most of the basin, sediments of this age thicken mainly due to ongoing salt tectonism. In the more distal parts, sediments infill the accommodation space generated by break-up and thermal subsidence. The Lower Cretaceous sediments are even more restricted in extent to salt withdrawal basins. During this stage, thermal subsidence is most relevant in the most distal part of the margin.

The Paleogene marks the onset of inversion. The development of the first shortening structures is coeval with the generation of accommodation space in the offshore. Finally, subsidence increases during Neogene inversion due to flexure in the foreland of the Betic-Rif orogen, causing a significant deepening of the most distal part of the section.

482

483 **Accommodation space and depositional environments**

484 The depositional environments and sediment thickness in the onshore of the Algarve Basin have been
485 described by several authors (Manuppella et al., 1988; Terrinha, 1998; Terrinha et al., 2002). In an
486 attempt to extend this analysis into the offshore, isopach thickness maps for each unit from Triassic to
487 Paleogene (generated from the maps in Figure 15) have been used to infer the magnitude of subsidence
488 and the possible depositional environments. For each time interval, we have generated an isopach map
489 with an overlay of the interpreted depositional environments (in terms of water depths; Figs.17 and 18).
490 Beyond the points of well and outcrop control, the definition of depositional environments is based on the
491 assumption that greater thickness equates to greater tectonic subsidence and possibly deeper water setting.
492 This general assumption is modulated locally to account for the interpreted geodynamic evolution of the
493 margin (e.g., progressive deepening to the south during the Jurassic, the role of the Guadalquivir High as
494 an intra-basinal high, ...) and to account for salt tectonics where relevant. Furthermore, the offshore
495 environments are interpreted to be possibly controlled by the same transfer features as documented
496 onshore (SMQF, Portimão Fault, Querença transfer, SVTZ) or their lateral equivalents.

497 For all maps, the northern limit of deposition cannot be established firmly. In the case of the Lower
498 Cretaceous and Paleogene, there is no evidence of deposition north of the present-day outcrop limit of the
499 basin. However, for Triassic and Jurassic intervals there is the possibility that sediments once extended
500 beyond the present-day outcrop limit but they have been eroded after Neogene uplift. Hence, the northern
501 limit of deposition shown on Triassic and Jurassic maps is inferred.

502 *Triassic*

503 Triassic is represented by limited thickness (up to 200 m thick) along the northern and eastern basin
504 margins. The presence of isolated Triassic outcrops north of the present-day outcrop limit of the basin, in
505 areas uplifted by Cenozoic inversion, indicates that the northern margin of the Triassic basin possibly
506 extended north of the preserved outcrops. Moguer-1, located in the onshore Guadalquivir Basin, is the
507 only well that drilled Triassic (46 m of proximal continental sediments). Outcrops and wells record
508 alluvial to fluvial facies throughout the entire basin margin.

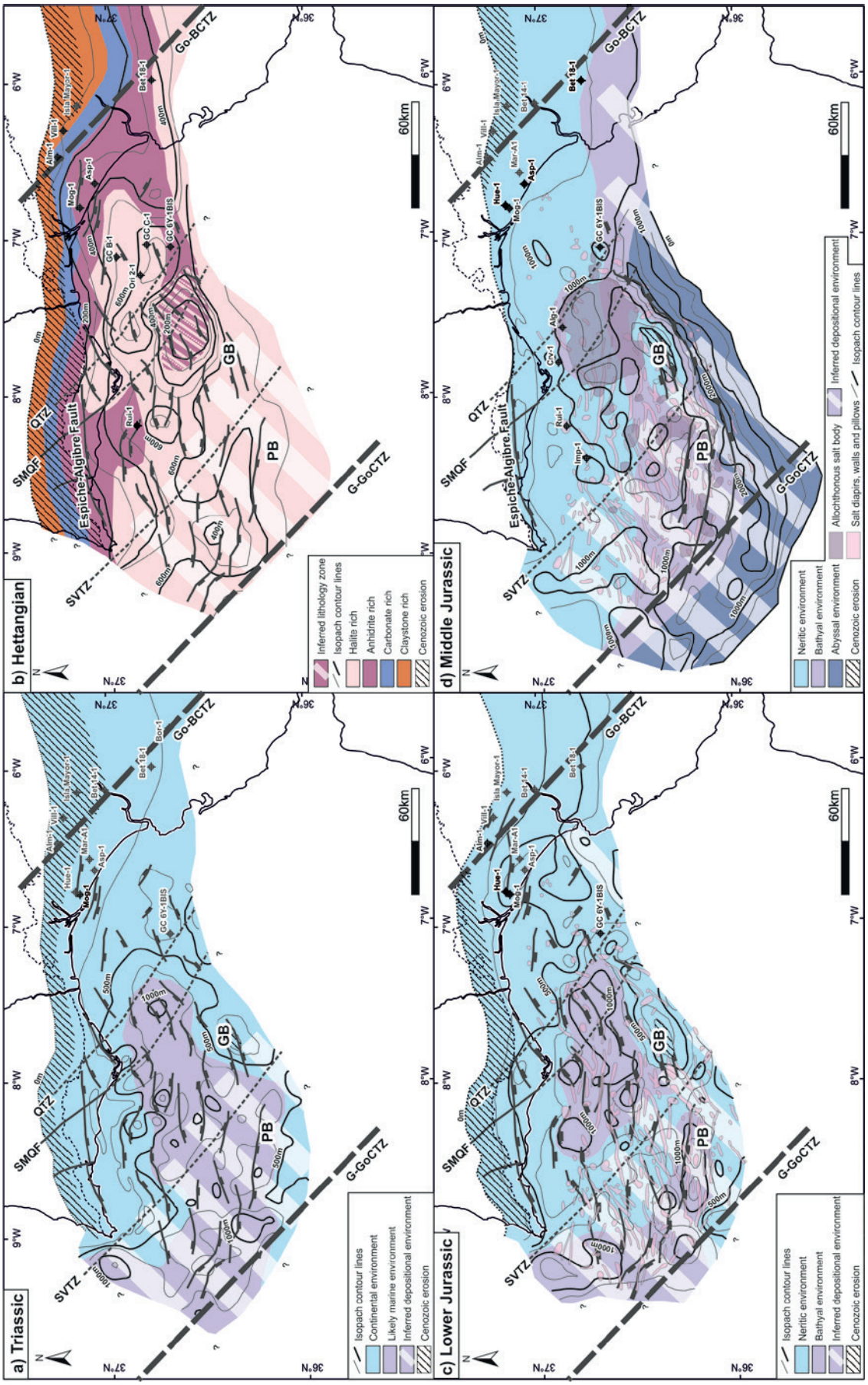
a) Triassic
b) Hettangian
c) Lower Jurassic
d) Middle Jurassic
SMQF
QTZ
SVTZ
Espiche-Algibre Fault
GB
PB
Go-BCTZ
G-GoCTZ
Alm-1
Vib-1
Isla Mayor-1
Bet-14-1
Bet-16-1
Bor-1
Mar-A1
Asp-1
Hue-1
Mog-1
GC 6Y-1BIS
GC B-1
GC C-1
Ori 2-1
Rui-1
Alg-1
Cry-1
Imp-1
60km
Isopach contour lines
Continental environment
Likely marine environment
Inferred depositional environment
Cenozoic erosion
Inferred lithology zone
Halite rich
Anhidrite rich
Carbonate rich
Claystone rich
Neritic environment
Bathyal environment
Abyssal environment
Allochthonous salt body
Salt diapirs, walls and pillows

509

Fig. 17. Isopach maps of Triassic to Middle Jurassic units of the SW Iberian margin with interpreted paleogeographic water depths. (a) Triassic. (b) Hettangian map, with the distribution of evaporitic facies (Ramos et al., under review). (c) Early Jurassic. (d) Middle Jurassic. See text for a full description of each map. GB: Guadalquivir Bank. G-GoCTZ: Gorringe-Gulf of Cadiz transfer zone; GoC-BTZ: Gulf of Cadiz-Betics transfer zone; PB: Portimão Bank; QTZ: Querença transfer zone; SMQF: São Marcos Quarteira Fault; SVTZ: São Vicente transfer zone.

To the south and west, seismic interpretation and gravimetric modelling (Ramos et al., 2017b) reveal broader depocenters, up to 1000 m thick (Fig. 17a), running in a WSW-ENE direction north of the Guadalquivir Bank. The Triassic thins again over the Guadalquivir Bank, which acted as an intra-basinal high during the Mesozoic extension. The Triassic is even locally absent in well GC 6Y-1BIS, which is interpreted to drill a tilted basement block in the footwall of a minor extensional fault. Neogene inversion caused local erosion of the Triassic above the Guadalquivir Bank (Fig. 14.

Two main depocenters are interpreted to have developed during the Triassic. A NW-SE trending depocenter formed along the western margin of the Algarve Basin, west of the SVTZ. An ENE-WSW trending depocenter developed east of the SVTZ and west of the Querença transfer zone (Fig. 17a). In both of these depocenters, sediments may be dominated by finer grained deposits.

Beyond the SW Iberian margin, Triassic sediments are known to extend eastward into the Betic Basin, based on numerous outcrops of Triassic in the Betic orogen (Pérez-Valera, 2005) and its presence under the Betic foredeep documented by wells (Lanaja, 1987). Towards the west, the Gorringe-GoC transfer zone marks the transition into an oceanic domain (Sallarès et al., 2011) younger than Triassic. The southern limit of the margin at this time is interpreted to be in continuity with the NW African conjugate.

Hettangian

The Hettangian evaporite unit is observed to be thin (<200 m) along the northern outcrop limit of the basin and in the wells in the eastern Algarve Basin (e.g., Moguer-1, Almonte-1 and Villamanrique-1 in Fig. 16b). Basinward, this unit is strongly involved in diapiric structures. Therefore, thickness encountered by wells Orion 2-1 or Ruivo-1 is not considered representative of true initial stratigraphic thickness. To represent the initial, pre-diapiric deposition of this unit, the total cross-sectional area of the

Hettangian at present-day on dip sections (NW-SE) was used to estimate initial thickness assuming the preservation of area and no loss of evaporite through time. For most allochthonous salt bodies, the distance from the source area is negligible at the basin scale. However, for the allochthonous Esperança salt sheet, the corresponding volume has been assumed to be sourced to the N and E of the allochthonous nappe (Ramos et al., under review).

The isopach thickness map obtained in this way is a conservative estimate of initial thickness and can be considered to honour adequately lateral variations in initial evaporite thickness. The isopach map shows that the Hettangian evaporite unit mainly thickens towards the south and west, up to roughly 600 m (Fig. 17b). The thickening took place from the Algibre-Espiche extensional fault, which differentiates the evaporite basin between halite to the north and anhydrite to the south (Fig. 17b). This south- and westward thickening trend is interrupted by an area of limited initial thickness along the Guadalquivir Bank and under the present-day location of the Esperança salt sheet (Fig. 17b). The source of the Esperança salt sheet is interpreted to be in the depocenter that formed to the east of the QTZ (Fig. 17b).

The trends in the initial thickness of the evaporite unit coincide with the variations in the dominant evaporite facies encountered in outcrop and wells. Along the basin margins, where original thickness was smaller, facies are dominated by shales and anhydrite (Fig. 17b). Central parts of the basin with thicker original evaporites are dominated by halite (Fig. 17b). The distribution follows the model of a bulls-eye pattern, with the most soluble salts in the basin centre (Nichols, 2009). This trend is disrupted by the presence of the Guadalquivir Bank as a structural high during the Hettangian (Fig. 17b) on which anhydrite-dominated facies are present (documented by well Gulf of Cadiz 6Y-1BIS).

As with the Triassic, the Hettangian basin is limited to the west by the Gorringe-Gulf of Cadiz transfer zone at present day. To the south it connected with the conjugate NW African margin. And to the east it extends into the Betic Basin across the Gulf of Cadiz- Betic transfer. In the Betic Basin, the evaporite basin is not merely Hettangian but is also known to have started developing in the Late Triassic (e.g., De Torres and Sánchez, 1990; Vera, 1983).

Lower Jurassic

The Lower Jurassic (excluding Hettangian evaporites) is less than 500 m thick along the northern outcrop of the basin (Fig. 17c). Its thickness distribution is irregular, but increases basinward (to south

566 and west), with major depocenters in the central part of the basin up to 1000 m thick (Fig. 17c). This
567 southward thickening is interpreted to respond mainly to ongoing extensional faulting and subsidiarily to
568 salt evacuation. As with underlying units, the Lower Jurassic thins onto the Guadalquivir Bank.

569 Two main depocenters can be identified. One is in the central part of the basin with a roughly E-W
570 trend, controlled by extensional faults with the same orientation. The second depocenter lies to the west,
571 with a NNW-SSE orientation that is roughly parallel to the Gorringe-GoC transfer zone and associated
572 faults (Fig. 17c). The SVTZ separates the two main depocenters and the QTZ coincides with the eastern
573 limit of the eastern depocenter (Fig. 17c).

574 Onshore exposures of Lower Jurassic carbonates and wells in the Guadalquivir Basin show shallow
575 marine carbonates, likely deposited in neritic conditions. Offshore, the only well reaching the Lower
576 Jurassic is the GC 6Y-1BIS which also documents a neritic environment. It is therefore interpreted that
577 the Lower Jurassic was deposited throughout the margin as a shallow platform. Bathyal conditions are
578 interpreted to have been possible in the high subsidence areas, possibly resulting in the deposition of finer
579 grained carbonates (e.g., marls). Local disruptions of these trends are to be expected around salt
580 structures.

581 We interpret that to the south and west of the Algarve Basin there is no Lower Jurassic as the basin
582 transitions to a post-Early Jurassic oceanic domain towards the south and across the Gorringe-Gulf of
583 Cadiz transfer. To the east, the Early Jurassic basin is continuous but offset to the south across the Gulf of
584 Cadiz-Betic transfer.

585 *Middle Jurassic*

586 The northern limit of Middle Jurassic deposition is mainly controlled onshore by the E-W Algibre
587 and ESE-WNE Espiche extensional faults (Ramos et al., 2016; Fig. 17d). In the hangingwall of these
588 faults, the Middle Jurassic is a few hundreds of meters thick. From there, this unit progressively thickens
589 towards the south. A local L-shaped depocenter developed above the source area of the Esperança salt
590 sheet (Fig. 17c) which is interpreted to relate to evacuation of salt during the emplacement of the
591 Esperança salt sheet.

From the Guadalquivir and Portimão Banks to the south, thickness of the Middle Jurassic is interpreted to increase up to 2000 m. This is assumed to represent the climax in the generation of rifting-related accommodation space.

WNW-ESE transfer zones controlled the deposition of Middle Jurassic. A NW-SE orientation of depocenters can be observed in the vicinity of these transfer zones, particularly along the QTZ and SMQF and west of the SVTZ.

Middle Jurassic carbonates in the present-day onshore and the near offshore were deposited in a neritic environment (Roque, 2007; Terrinha, 1998). To the south, the basin is known to deepen at least in the Algarve-1 well in which a bathyal environment has been identified (Roque, 2007). This is a possible reflection of the influence of salt tectonics on depositional environments in the basin, as the Algarve-1 well sits in the depocenter associated with the expulsion of the salt that fed the Esperança salt sheet. As with the Lower Jurassic, it is expected that smaller salt structures also controlled facies and thickness distribution locally.

Upper Jurassic

The Upper Jurassic follows roughly the same pattern as the Middle Jurassic: its northern limit is controlled by the Espiche-Algibre extensional faults, and thickness increases to the south, with the greatest thickness (2500 m) south of the Portimão and Guadalquivir Banks (Fig. 18a). The southward thickening trend is only interrupted locally by thinning onto the Guadalquivir Bank. Other local thickness variations in the Upper Jurassic are interpreted to be due to salt motion (e.g., thinning and thickening of the Upper Jurassic seen on Figs. 10 and 12).

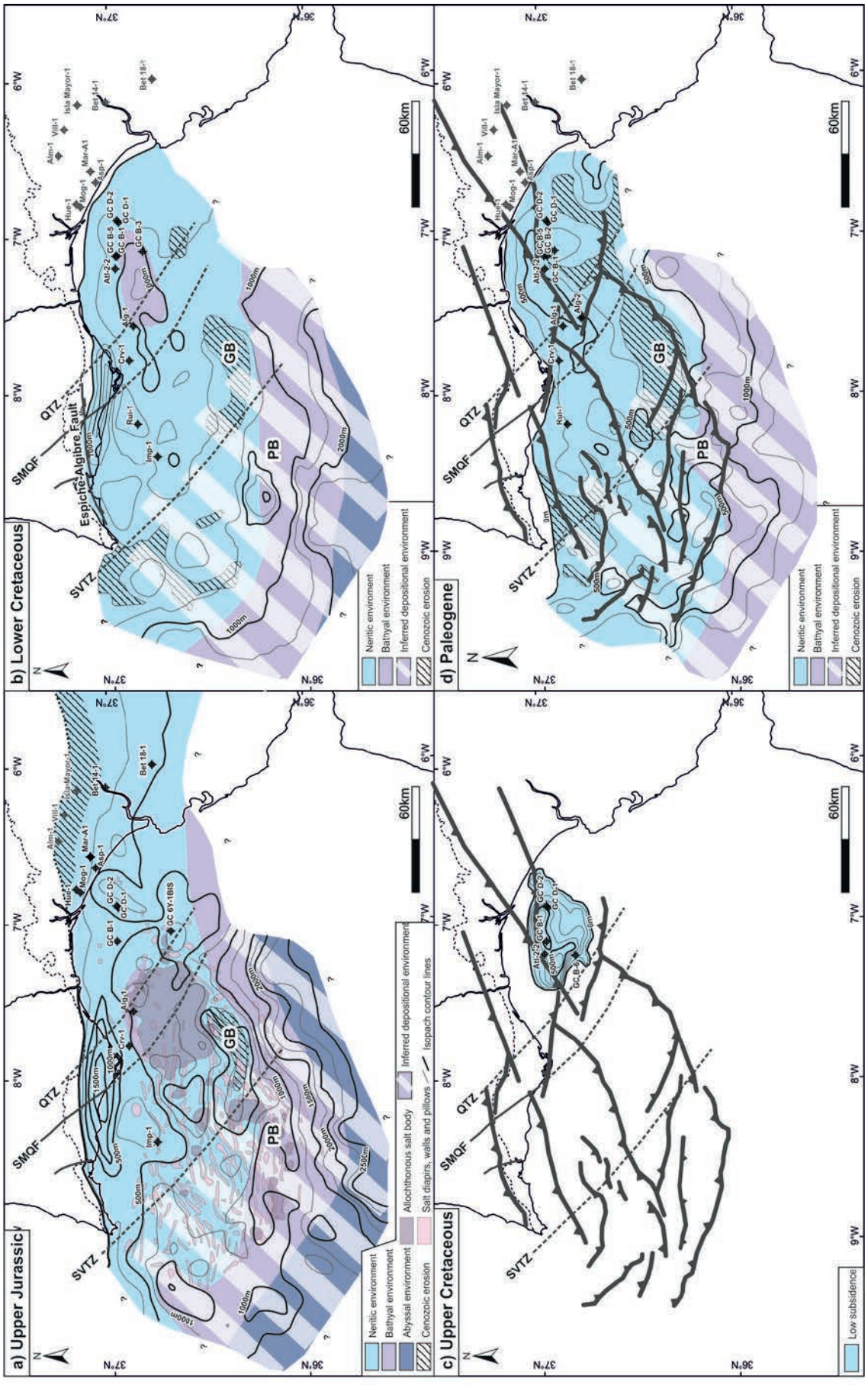
a) Upper Jurassic
b) Lower Cretaceous
c) Upper Cretaceous
d) Paleogene
SMQF
QTZ
SVTZ
Espichel-Algibre Fault
PB
GB
Neritic environment
Bathyal environment
Abyssal environment
Allochthonous salt body
Inferred depositional environment
Cenozoic erosion
Salt diapirs, walls and pillows
Isopach contour lines
Low subsidence
60km

612

Fig. 18. Isopach maps of Late Jurassic to Paleogene units of the SW Iberian margin with interpreted paleogeographic water depths. (a) Late Jurassic. (b) Early Cretaceous. Note an increase in the number of the eroded areas, mostly towards the west. c) Late Cretaceous. (d) Paleogene map. See text for a full description of each map. GB: Guadalquivir Bank; PB: Portimão Bank; QTZ: Querença transfer zone; SMQF: São Marcos Quarteira Fault; SVTZ: São Vicente transfer zone.

Neritic conditions were stablished near the shore during the Late Jurassic, attested by well data (Roque, 2007; Fig. 18a). South of the Guadalquivir-Portimão Bank, the margin deepen to bathyal and abyssal environments (Fig. 18a), as the case of the Middle Jurassic (Fig. 17d).

Lower Cretaceous

The extent of Lower Cretaceous is limited to the north by the onshore Espiche-Algibre extensional fault (Fig. 18b). The presence of this unit is confirmed in the offshore by wells in the inner part of the Gulf of Cadiz and in the Portuguese platform (Fig. 18b).

The Lower Cretaceous presents thicknesses between 500 and 1000 m through the proximal part of the margin, except for a restricted area south of the present-day shelf-break, where this unit reaches thickness values of more than 1000 m.. To the south of the Guadalquivir Bank the thickness increases up to more than 2000 m and we interpret the deepening of the environmental conditions in the same direction (Fig. 18b). The Lower Cretaceous is interpreted to be a distinctly post-rift unit, with local thickness changes driven only by salt tectonics.

This unit is also subject to significant erosion during Cenozoic inversion. The Guadalquivir Bank is the site of a broad eroded area that also truncates into underlying units (Fig. 14. To the west and east there are other eroded areas that are the result of Cenozoic inversion. The roughly NNW-SSE trend of the eroded areas in the western Algarve basin are interpreted to be due to the inversion of oblique structures, associated to NW-SE trending transfer features.

Upper Cretaceous

The Upper Cretaceous succession has been only found in offshore wells in the northeastern part of the Gulf of Cadiz (Fig. 18c). This unit is restricted to an area of roughly 70x40km, possibly controlled by

639 the contractional structures documented by Ramos et al. (2017a) and by ongoing salt tectonism,. This unit
640 presents thickness up to 600 m and was deposited in a neritic environment.

641 *Paleogene*

642 The Paleogene has been recognized in some wells in the offshore, which document neritic conditions
643 (Fig. 18d). It covers almost the entire offshore margin, as most of the Mesozoic units and represents the
644 final unit deposited prior to generalized inversion of the margin. Its thickness reaches over 1000 m in the
645 distal parts of the basin (Fig. 18d). In this area, the depositional environment is also interpreted to deepen.
646 The locally irregular thickness pattern of the Paleogene possibly indicates the initial development of
647 contractional structures as well as ongoing salt tectonism in the westernmost Algarve Basin. Erosion of
648 the Paleogene is more generalized than for previous units and controlled by Neogene inversion.

649

650 **Discussion**

651 *Mesozoic and Cenozoic paleogeography of the SW Iberian margin*

652 Margin evolution has strong impact on deposition in the SW Iberian margin. Three main stages were
653 identified: early rift, rift climax to post-rift, and inversion. The early-rift phase (Triassic to Early Jurassic)
654 was responsible for the formation of a WSW-ENE trough, between the basin margin to the north and the
655 Guadalquivir Bank to the south. To the west, a NW-SE depocenter developed, controlled by the
656 Gorringe-Gulf of Cadiz transfer zone (Fig. 17). To the south, beyond the Guadalquivir Bank, another
657 depocenter is interpreted to have developed. The paleobathymetry in this depocenter increases south of
658 the Guadalquivir Bank, and it possibly extended onto the conjugate NW African margin. The depocenters
659 generated during this phase of early rifting, and the intra-basinal high of the Guadalquivir Bank were
660 strongly controlled by basement extensional faults.

661 As in the case of the Algarve Basin, the Betic Basin was dominated by the presence of fault-
662 controlled depocenters (highly subsiding settings) and intra-basinal highs (shallow settings) during this
663 early rift stage (Vera, 1988; Fig. 19). The sediments deposited in the Betic Basin during the initial rifting
664 phase are similar to those in the Algarve Basin: Triassic continental deposits, Upper Triassic evaporites
665 and shallow carbonated from the Lower Jurassic (Vera, 1988).

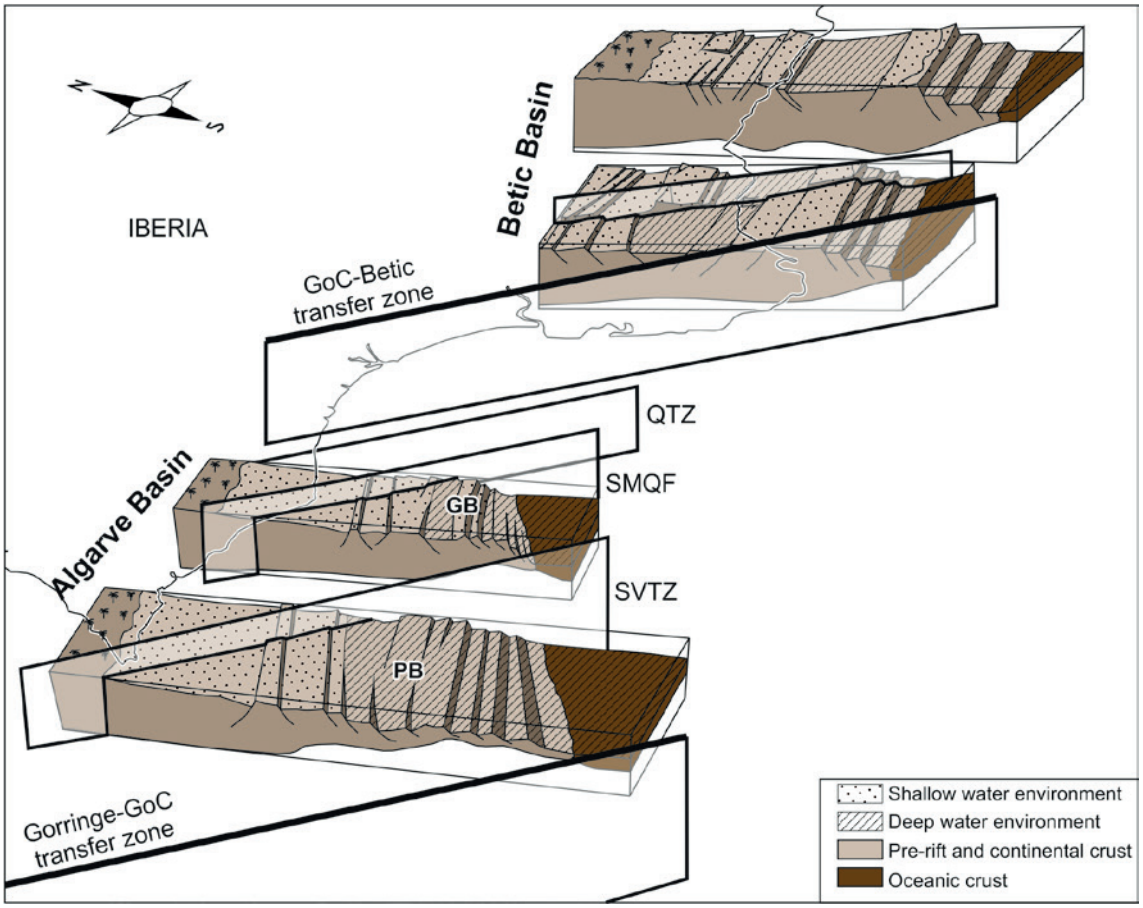

666

667 **Fig. 19.** Three-dimensional sketch of the South Iberian margin comprising the Algarve Basin to the west
668 and the Betic Basin to the east at the moment of oceanization, at the beginning of the Late Jurassic.
669 Notice the swells and troughs formed by extensional faulting and the presence of transfer faults that
670 differentiate the PB and the GB (SVTZ), and the Gulf of Cadiz from the Betic Basin (GoC-Betic transfer
671 zone). Sketches from the Betic Basin are modified from Vera (1988), while those of the Algarve Basin
672 were constructed from the sections from Ramos et al. (2017b).

673 The rift climax (Middle Jurassic) led to the southward migration of the fault activity, increasing the
674 thickness and the deepening for the depositional environments in the distal domain, mostly south of the
675 Guadalquivir and Portimão Banks. The Gorringe-Gulf of Cadiz transfer zone controls the geometry of the
676 western domain of the margin during this period. The following post-rift sequences (Upper Jurassic and
677 Lower Cretaceous) post-date any extensional basement fault activity and follow the same pattern as the
678 Middle Jurassic, with major thickness in the southernmost domains. The units deposited during rift
679 climax to post-rift have ENE-WSW trending depocenters located mainly beyond the Guadalquivir Bank
680 (Fig. 18a,b).

The Upper Cretaceous records the initial inversion of the margin. The location of the Upper Cretaceous depocenter indicates that the input of clastics possibly occurred from the eastern margin of the basin, across the GoC-Betic transfer zone (Fig. 18c). Paleogene sediments are more widespread than the Upper Cretaceous (Fig. 18d), and record a period of relative quiescence prior to the more pronounced inversion that took place during Neogene times.

Oblique structures

The oblique faults and transfer zones of the Algarve Basin played a key role in the margin evolution during the Mesozoic and Cenozoic. The presence of a NW-SE trending depocenter in the western portion of the basin is controlled by the Gorringe-GoC transfer zone and SVTZ (see the maps of the Figs. 17 and 18).

At a smaller scale, the SVTZ separates the Portimão Bank and Guadalquivir Bank, allowing for the major difference in tectonic style between both (basin vs intra-basinal high). The impact of the SVTZ can also be seen at crustal level, where it is possible that this transfer zone defines the boundary between the narrower necking zone of the eastern Algarve Basin and the broader necking zone observed in the westernmost Algarve Basin (Fig. 8b).

To the east, the QTZ defines the eastern limit and source area of the Esperança salt sheet and a domain of pervasive salt structures (e.g., Fig. 17). The SVTZ, SMQF, and QTZ also control the location and trend of smaller magnitude depocenters north of the Guadalquivir Bank during the rift to post-rift stages (Figs. 17 and 18). The SMQF is also described onshore and offshore as a transfer fault controlling the deposition of Mesozoic sediments (Barreto et al., 2015; Ramos et al., 2016; Terrinha, 1998).

This relevant role of oblique structures during extension observed in the Algarve Basin has also been observed in the Betic Basin (Vera, 1988, Fig. 19).

The role of Mesozoic extensional transfer zones in controlling basin architecture continued into the Cenozoic as they were inverted/reactivated during the margin inversion. The main thrusts of the contractional fault system are relayed by WNW-ESE lateral ramps, which are parallel to and coincide in location with the SVTZ, SMQF and QTZ (Figs. 18c,d). We interpret that the lateral ramps are inverted extensional features from previous transfer zones.

The control of oblique structures on the contractional deformation can also be seen throughout the broader SW Iberian margin. To the west, the shortening in the Gorringe Bank is estimated to be 20km (Galindo-Zaldívar, 2003; Jiménez-Munt et al., 2010), in contrast of the 5-10 km of shortening calculated in the Algarve Basin (Ramos et al., 2017a). This difference in shortening is assumed to indicate compartmentalization of shortening along the SW Iberian margin across the NW-SE Gorringe-GoC transfer zone.

To the east, NW-SE transfer zones may also be controlling the process of subduction of the oceanic crust of the Gulf of Cadiz under the Gibraltar Arc. The subducting lithospheric slab is interpreted to tear under the Betics (Vergés and Fernàndez, 2012) and further east three segments can be identified under the Algerian Sea, according to Fichtner and Villaseñor (2015; Fig. 20). The potential tear described by Vergés and Fernández (2012) coincides in location with the Gulf of Cadiz-Betic transfer zone, which might have acted as the locus of initiation for the tearing event. Likewise, the segments of the subducting oceanic slab identified by Fichtner and Villaseñor (2015) are offset in the same NW-SE trend as the transfer zones described in this paper (Fig. 20). This raises the possibility that the passive margin transfer zones may have played a role in the configuration of the subduction process.

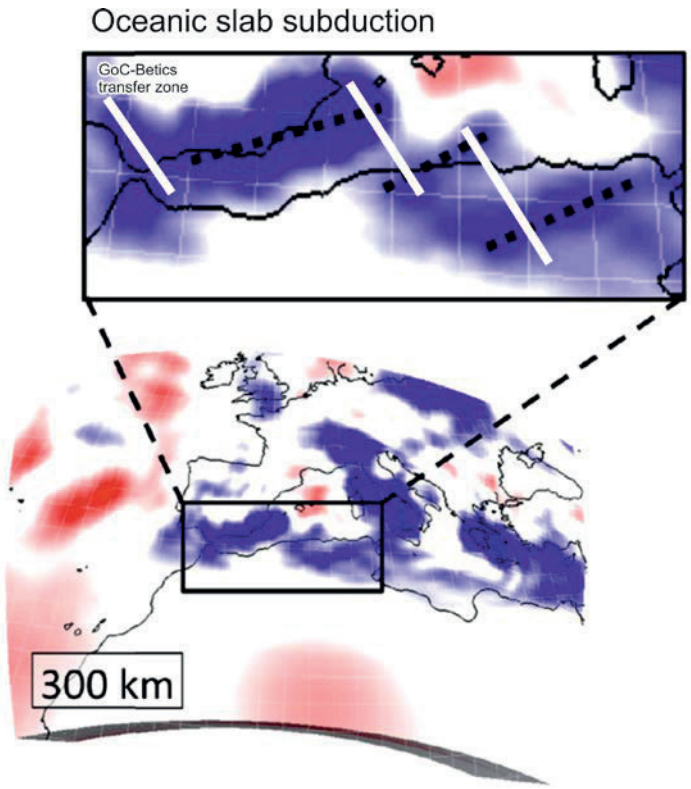

Fig. 20. Illustration of the possible impact of NW-SE transfer zones in the present-day subduction geometry under the Alboran Sea. A horizontal slice at 300km depth coloured for the absolute variations of isotropic S velocity (modified from Fichtner and Villaseñor, 2015) reveals a possible segmentation in the subducting oceanic slab. Features drawn in the enlarged panel are described as follows: dotted black line: possible segments of the Tethyan oceanic slab; white lines: possible transfer faults.

Conclusions

The SW Iberian margin is a segmented oblique passive margin formed during the Mesozoic as part of the opening of the westernmost Ligurian Tethys. The margin was subsequently partially inverted during the Late Cretaceous to present-day due to convergence between Africa and Iberia.

The evolution of the SW Iberian margin and the Algarve Basin was dominated by ENE-WSW extensional faults that controlled the development of the main depocenters. Mesozoic rifting was compartmentalized at different scales by oblique NW-SE trending transfer zones. At a more local scale, within the SW Iberian margin, transfer faults also partially controlled the deposition of the syn-rift Mesozoic sediments and the tectonic style during extension and inversion. Differences in the development of salt tectonics within the Algarve Basin can also be accounted for by the presence of NW-SE trending transfer zones. At the more regional scale, the SW Iberian margin was separated from rifting in the Betic Basin and the present-day Gorringe Bank by two major NW-SE transfer zones. It is also proposed here that NW-SE trending transfers may have also had an impact on the development of the subduction of Gulf of Cadiz oceanic crust under the Betics and Alboran Sea.

Acknowledgments

This study was funded by Repsol Exploración (Madrid) and partially financially supported by the SALTECRES project (CGL2014-54118-C2-1-R MINECO/FERDER, UE). Adrià Ramos thanks Repsol Exploración for his Ph.D grant. The authors wish to thank Repsol Exploración and Partex-Oil&Gas for permission to present this work, and Portugal Exploration Team for his support and enthusiasm. We also acknowledge Schlumberger and Midland Valley for the academic software licenses used for seismic

interpretation (Petrel TM) and depth conversion and cross-section construction (Move) respectively. Repsol and Partex-Oil&Gas provided us their proprietary vintage seismic surveys and a 3D seismic cube, published with their permission. Seismic lines of the PDT00-PD00 survey have been provided by TGS and published with the permission of TGS (http://www.tgs.com). The seismic PDT00-PD00 survey is available for purchase from TGS and ENMC (Entidade Nacional para o Mercado de Combustibles; http://www.enmc.pt).

References

Aïfa, T., Zaagane, M., 2014. Brittle tectonics within the Jurassic formations of the Ouarsenis culminating area, northwestern Algeria. J. Afr. Earth Sci. 96, 39–50. doi:10.1016/j.jafrearsci.2014.03.020

Alves, T.M., Moita, C., Cunha, T., Ullnaess, M., Myklebust, R., Monteiro, J.H., Manuppella, G., 2009. Diachronous evolution of Late Jurassic-Cretaceous continental rifting in the northeast Atlantic (west Iberian margin). Tectonics 28, n/a-n/a. doi:10.1029/2008TC002337

Arthaud, F., Matte, P., 1977. Late Paleozoic strike-slip faulting in southern Europe and northern Africa: Result of a right-lateral shear zone between the Appalachians and the Urals. Geol. Soc. Am. Bull. 88, 1305–1320. doi:10.1130/0016-7606(1977)88<1305:LPSFIS>2.0.CO;2

Barreto, P., Silva, C., Leonardo, P., Sousa, J., Caeiro, M.H., Maciel, C., Guerreiro, L., 2015. The relationship between the onshore and offshore structure of São Marcos-Quarteira Fault System, Algarve Basin, Portugal. Presented at the AAPG European Regional Conference and Exhibition, Lisbon.

Bortolotti, V., Principi, G., 2005. Tethyan ophiolites and Pangea break-up. Isl. Arc 14, 442–470. doi:10.1111/j.1440-1738.2005.00478.x

Correia, F., 1989. Estudo biostratigráfico e microfácies do Cretácico carbonatado da bacia sedimentar meridional portuguesa (Algarve). Faculdade de Ciências da Universidade Nova de Lisboa.

De Torres, T., Sánchez, A., 1990. Espesores de la Facies Keuper en la Rama Castellana de la Cordillera Ibérica, Prebético y Subbético frontal. Ortí F Salvany JM Eds Form. Evaporíticas Cuenca Ebro Cadenas Periféricas Zona Levante Nuevas Aportaciones Guía Superf. ENRESA E Univ. Barc. Barc. Pp 212–218.

Duarte, J.C., Rosas, F.M., Terrinha, P., Schellart, W.P., Boutelier, D., Gutscher, M.-A., Ribeiro, A., 2013. Are subduction zones invading the Atlantic? Evidence from the southwest Iberia margin. Geology 41, 839–842. doi:10.1130/G34100.1

Fichtner, A., Villaseñor, A., 2015. Crust and upper mantle of the western Mediterranean – Constraints from full-waveform inversion. Earth Planet. Sci. Lett. 428, 52–62. doi:10.1016/j.epsl.2015.07.038

Flinch, J.F., 1994. Tectonic evolution of the Gibraltar Arc. PhD Thesis. Rice University (811 pp).

Frizon de Lamotte, D., Zizi, M., Missenard, Y., Hafid, M., Azzouzi, M.E., Maury, R.C., Charrière, A., Taki, Z., Benammi, M., Michard, A., 2008. The Atlas System, in: Michard, A., Saddiqi, O., Chalouan, A., Lamotte, D.F. de (Eds.), Continental Evolution: The Geology of Morocco, Lecture Notes in Earth Sciences. Springer Berlin Heidelberg, pp. 133–202.

Galindo-Zaldívar, J., 2003. Active faulting in the internal zones of the central Betic Cordilleras (SE, Spain). J. Geodyn. 36, 239–250. doi:10.1016/S0264-3707(03)00049-8

García-Hernández, M., López-Garrido, Á.C., Martín-Algarra, A., Cámara, J.M., Ruiz-Ortiz, P.A., Vera, J.A., 1989. Las discontinuidades mayores del Jurásico de las Zonas Externas de las Cordilleras Béticas: análisis e interpretación de los ciclos sedimentarios. J. Iber. Geol. 35–52.

Gawthorpe, R.L., Hurst, J.M., 1993. Transfer zones in extensional basins: their structural style and influence on drainage development and stratigraphy. J. Geol. Soc. 150, 1137–1152. doi:10.1144/gsjgs.150.6.1137

Gawthorpe, R.L., Leeder, M.R., 2000. Tectono-sedimentary evolution of active extensional basins. Basin Res. 12, 195–218. doi:10.1111/j.1365-2117.2000.00121.x

Gutscher, M.-A., Malod, J., Rehault, J.-P., Contrucci, I., Klingelhoefer, F., Mendes-Victor, L., Spakman, W., 2002. Evidence for active subduction beneath Gibraltar. Geology 30, 1071. doi:10.1130/0091-7613(2002)030<1071:EFASBG>2.0.CO;2

Hernández-Molina, F.J., Stow, D.A.V., Alvarez-Zarikian, C.A., Acton, G., Bahr, A., Balestra, B., Ducassou, E., Flood, R., Flores, J.-A., Furota, S., Grunert, P., Hodell, D., Jimenez-Espejo, F., Kim, J.K., Krissek, L., Kuroda, J., Li, B., Llave, E., Lofi, J., Lourens, L., Miller, M., Nanayama, F., Nishida, N., Richter, C., Roque, C., Pereira, H., Sanchez Goni, M.F., Sierro, F.J., Singh, A.D., Sloss, C., Takashimizu, Y., Tzanova, A., Voelker, A., Williams, T., Xuan, C., 2014. Onset of Mediterranean outflow into the North Atlantic. Science 344, 1244–1250. doi:10.1126/science.1251306

Hiscott, R.N., Wilson, R.C.L., Gradstein, F.M., (5), V.P., (5), J.G.-M., (6), R.R.B., (6), H. a. W., 1990. Comparative Stratigraphy and Subsidence History of Mesozoic Rift Basins of North Atlantic (1). AAPG Bull. 74, 60–76.

Iribarren, L., Vergés, J., Camurri, F., Fullea, J., Fernàndez, M., 2007. The structure of the Atlantic–Mediterranean transition zone from the Alboran Sea to the Horseshoe Abyssal Plain (Iberia–Africa plate boundary). Mar. Geol. 243, 97–119. doi:10.1016/j.margeo.2007.05.011

Jiménez-Munt, I., Fernàndez, M., Vergés, J., Afonso, J.C., Garcia-Castellanos, D., Fullea, J., 2010. Lithospheric structure of the Gorringe Bank: Insights into its origin and tectonic evolution. Tectonics 29, n/a-n/a. doi:10.1029/2009TC002458

Lanaja, J.M., 1987. Contribución de la exploración petrolífera al conocimiento de la geología de España. IGME, Madrid.

Ledesma, S.M., 2000. Astrobiocronología y estratigrafía de alta resolución del Neógeno de la Cuenca del Guadalquivir-Golfo de Cádiz. PhD Thesis. Universidad de Salamanca (464 pp).

Lopes, C.M., 2002. Análise e modelação da bacia do Algarve. PhD Thesis, Faculdade de Ciências da Universidade Nova de Lisboa (173 pp).

Lopes, F.C., Cunha, P.P., Le Gall, B., 2006. Cenozoic seismic stratigraphy and tectonic evolution of the Algarve margin (offshore Portugal, southwestern Iberian Peninsula). Mar. Geol. 231, 1–36. doi:10.1016/j.margeo.2006.05.007

Maldonado, A., Somoza, L., Pallarés, L., 1999. The Betic orogen and the Iberian–African boundary in the Gulf of Cadiz: geological evolution (central North Atlantic). Mar. Geol. 155, 9–43. doi:10.1016/S0025-3227(98)00139-X

Manuppella, G., 1992. Carta geológica da região do Algarve. Noticia explicativa da Carta Geologica da regiao do Algarve. Serviços geológicos de Portugal.

Manuppella, G., 1988. Litoestratigrafia e tectónica da Bacia Algarvia. Geonovas 10, 67–71.

Manuppella, G., Marques, B., Rocha, R.B., 1988. Évolution tectono-sédimentaire du bassin de l'Algarve pendant le Jurassique, in: 2nd International Symposium on Jurassic Stratigraphy, Lisboa. pp. 1031–1046.

Martínez-Loriente, S., Sallarès, V., Gràcia, E., Bartolome, R., Dañobeitia, J.J., Zitellini, N., 2014. Seismic and gravity constraints on the nature of the basement in the Africa-Eurasia plate boundary: New insights for the geodynamic evolution of the SW Iberian margin: Thin oceanic crust at the CPR and SH. J. Geophys. Res. Solid Earth 119, 127–149. doi:10.1002/2013JB010476

Martins, L.T., Madeira, J., Youbi, N., Munhá, J., Mata, J., Kerrich, R., 2008. Rift-related magmatism of the Central Atlantic magmatic province in Algarve, Southern Portugal. Lithos 101, 102–124. doi:10.1016/j.lithos.2007.07.010

Matias, H., 2007. Hydrocarbon potential of the offshore Algarve Basin. PhD Thesis, Faculdade de Ciências da Universidade Nova de Lisboa (324 pp).

Matias, H., Kress, P., Terrinha, P., Mohriak, W., Menezes, P.T.L., Matias, L., Santos, F., Sandnes, F., 2011. Salt tectonics in the western Gulf of Cadiz, southwest Iberia. AAPG Bull. 95, 1667–1698. doi:10.1306/01271110032

McKenzie, D., 1978. Some remarks on the development of sedimentary basins. Earth Planet. Sci. Lett. 40, 25–32.

Meisling, K.E., Cobbold, P.R., Mount, V.S., 2001. Segmentation of an obliquely rifted margin, Campos and Santos basins, southeastern Brazil. AAPG Bull. 85, 1903–1924.

Montenat, C.H., Guery, F., Jamet, M., Berthou, P.Y., 1988. Mesozoic evolution of the Lusitanian Basin: comparison with the adjacent margin, in: Proceedings of the Ocean Drilling Program, Scientific Results. pp. 757–775.

Mouterde, R., 1971. Esquisse de l'e´volution biostratigraphique de la Pe´ninsule Ibe´rique au Jurassique. Cuad. Geol. Ibérica 2, 21–31.

Nichols, G., 2009. Sedimentology and stratigraphy, 2nd ed. ed. Wiley-Blackwell, Chichester, UK ; Hoboken, NJ.

Palain, C., 1976. Una serie detritique terrigene, les “Gras de Silves”: Trias et Uas lnferieur du Portugal. Sar Geol Port. Mem. N^{o} 25 Lisb. 377.
Palomeras, I., Carbonell, R., Flecha, I., Simancas, F., Ayarza, P., Matas, J., Martínez Poyatos, D., Azor, A., González Lodeiro, F., Pérez-Estaún, A., 2009. Nature of the lithosphere across the Variscan orogen of SW Iberia: Dense wide-angle seismic reflection data. J. Geophys. Res. 114. doi:10.1029/2007JB005050
Pereira, M.F., Ribeiro, C., Gama, C., Drost, K., Chichorro, M., Vilallonga, F., Hofmann, M., Linnemann, U., 2016. Provenance of upper Triassic sandstone, southwest Iberia (Alentejo and Algarve basins): tracing variability in the sources. Int. J. Earth Sci. doi:10.1007/s00531-016-1295-2
Pereira, R., Alves, T.M., 2012. Tectono-stratigraphic signature of multiphased rifting on divergent margins (deep-offshore southwest Iberia, North Atlantic): TECTONIC SIGNATURE OF MULTIPHASED RIFTS. Tectonics 31, n/a-n/a. doi:10.1029/2011TC003001
Pérez-Valera, F., 2005. Estratigrafía y tectónica del Triásico Sudibérico en el sector oriental de la Cordillera Bética. PhD Thesis, Universidad de Granada (220 pp).
Ramos, A., Fernández, O., Terrinha, P., Muñoz, J.A., 2017a. Neogene to recent contraction and basin inversion along the Nubia-Iberia boundary in SW Iberia. Tectonics In press, 2016TC004262. doi:10.1002/2016TC004262
Ramos, A., Fernández, O., Terrinha, P., Muñoz, J.A., 2017b. Neogene to recent contraction and basin inversion along the Nubia-Iberia boundary in SW Iberia. Tectonics 36, 2016TC004262. doi:10.1002/2016TC004262
Ramos, A., Fernández, O., Terrinha, P., Muñoz, J.A., 2016. Extension and inversion structures in the Tethys–Atlantic linkage zone, Algarve Basin, Portugal. Int. J. Earth Sci. 105, 1663–1679. doi:10.1007/s00531-015-1280-1
Ramos, A., Fernández, O., Terrinha, P., Muñoz, J.A., under review. Impact of basin structure and evaporite distribution on salt tectonics in the Gulf of Cadiz, Southwest Iberian margin. Mar. Pet. Geol.
Ramos, A., Fernández, O., Torne, M., Sánchez de la Muela, A., Muñoz, J.A., Terrinha, P., Manatschal, G., Salas, M.C., 2017b. Crustal structure of the SW Iberian passive margin: The westernmost remnant of the Ligurian Tethys? Tectonophysics (in press). doi:10.1016/j.tecto.2017.03.012
Rocha, R.B., 1976. Estudo estratigráfico e paleontológico do jurássico do Algarve Ocidental. PhD Thesis, Universidade Nova de Lisboa, Lisboa (178 pp).
Roque, C., 2007. Tectonostratigrafia do cenozóico das margens continentais sul e sudoeaste portuguesas: um modelo de correlação sismostratigráfica. PhD Thesis, Universidade de Lisboa (310 pp).
Rowan, M.G., 1993. A systematic technique for the sequential restoration of salt structures. Tectonophysics 228, 331–348.
Sallarès, V., Gailler, A., Gutscher, M.-A., Graindorge, D., Bartolomé, R., Gràcia, E., Díaz, J., Dañobeitia, J.J., Zitellini, N., 2011. Seismic evidence for the presence of Jurassic oceanic crust in the central Gulf of Cadiz (SW Iberian margin). Earth Planet. Sci. Lett. 311, 112–123. doi:10.1016/j.epsl.2011.09.003
Sclater, J.G., Christie, P.A.F., 1980. Continental stretching; an explanation of the post-Mid-Cretaceous subsidence of the central North Sea basin. J. Geophys. Res. 85, 3711–3739.
Stapel, G., Cloetingh, S., Pronk, B., 1996. Quantitative subsidence analysis of the Mesozoic evolution of the Lusitanian basin (western Iberian margin). Tectonophysics, Dynamics of Extensional Basins and Inversion Tectonics 266, 493–507. doi:10.1016/S0040-1951(96)00203-X
Terrinha, P., 1998. Structural geology and tectonic evolution of the Algarve Basin, South Portugal. PhD Thesis, Imperial College, London (430 pp).
Terrinha, P., Dias, R.P., Ribeiro, A., Cabral, J., 1999. The Portimão Fault, Algarve Basin, South Portugal. Comun Inst Geol Min. 86, 107–120.
Terrinha, P., Matias, L., Vicente, J., Duarte, J., Luís, J., Pinheiro, L., Lourenço, N., Diez, S., Rosas, F., Magalhães, V., Valadares, V., Zitellini, N., Roque, C., Víctor, L.M., 2009. Morphotectonics and strain partitioning at the Iberia–Africa plate boundary from multibeam and seismic reflection data. Mar. Geol. 267, 156–174. doi:10.1016/j.margeo.2009.09.012
Terrinha, P., Ribeiro, C., Kullberg, J.C., Lopes, C., Rocha, R., Ribeiro, A., 2002. Compressive episodes and faunal isolation during rifting, Southwest Iberia. J. Geol. 110, 101–113.
Terrinha, P., Rocha, R.B., Rey, J., Cachão, M., Moura, D., Roque, C., Martins, L., Valadares, V., Cabral, J., Azevedo, M.R., Barbero, L., Clavijo, E., Dias, R.P., Gafeira, J., Matias, H., Matias, L., Madeira, C.M.S., Munhã, J., Rebêlo, L.P., Ribeiro, C., Vicente, J., Noiva, J., Youbi, N., Bensalah, M.K., 2013. A Bacia do Algarve: Estratigrafia, Paleogeografia e Tectónica. In: Geologia de Portugal, Vol. II: Geologia Meso-cenozóica de Portugal. Eds. Rui Dias, Alexandre

Araújo, Pedro Terrinha, José Carlos Kullberg. Lisboa : Livraria Escolar Editora, Cap III: p. 29-166.
TGS, 2005. PD00: non-exclusive 2D Survey, TGS online data zone. (http://www.tgs.com/TGS/specsheets/PD-00_Spec.pdf).
Torelli, L., Sartori, R., Zitellini, N., 1997. The giant chaotic body in the Atlantic Ocean off Gibraltar: new results from a deep seismic reflection survey. Mar. Pet. Geol. 14, 125–138. doi:10.1016/S0264-8172(96)00060-8
Vera, J.A., 1988. Evolución de los sistemas de depósito en el margen ibérico de la Cordillera Bética. Rev. Soc. Geológica Esp. 1, 373–391.
Vera, J.A., 1983. Las zonas externas de las cordilleras Béticas. Comba JA Ed Geol. Esp. 2 Libro Jubil. J M Rios IGME Madr. Pp 218-251.
Vera, J.A., Molina, J.M., Montero, P., Bea, F., 1997. Jurassic guyots on the Southern Iberian Continental Margin: a model of isolated carbonate platforms on volcanic submarine edifices. Terra Nova 9, 163–166. doi:10.1046/j.1365-3121.1997.d01-22.x
Verati, C., Rapaille, C., Féraud, G., Marzoli, A., Bertrand, H., Youbi, N., 2007. 40Ar/39Ar ages and duration of the Central Atlantic Magmatic Province volcanism in Morocco and Portugal and its relation to the Triassic–Jurassic boundary. Palaeogeogr. Palaeoclimatol. Palaeoecol. 244, 308–325. doi:10.1016/j.palaeo.2006.06.033
Vergés, J., Fernàndez, M., 2012. Tethys–Atlantic interaction along the Iberia–Africa plate boundary: The Betic–Rif orogenic system. Tectonophysics 579, 144–172. doi:10.1016/j.tecto.2012.08.032
Wilson, R.C.L., 1988. Mesozoic development of the Lusitanian basin, Portugal. Rev. Soc. Geológica Esp. 1, 393–407.
Zizi, M., 1996. Triassic-Jurassic extensional systems and their Neogene reactivation in northern Morocco (the Rides Prerifaines and Guercif Basin). PhD thesis, Rice University (574 pp).

APPENDIX 2

Dip data

Outcrop Nº	Latitude	Longitude	Elevation (m)	Stratigraphy	Dip Direction	Dip
1	37,15866404	-8,306972	104	Lower Cretaceous	352	20
2	37,19873901	-8,297421	94	Lower Jurassic	342	24
3	37,19906799	-8,297355	96	Lower Jurassic	316	16
4	37,23725997	-8,279315	126	Lower Jurassic	326	12
5	37,15937901	-8,303943	90	Lower Cretaceous	353	20
6	37,250137	-8,283293	164	CVS	159	12
7	37,25002502	-8,283694	163	CVS	221	52
8	37,25008001	-8,283937	161	CVS	224	45
9	37,17303196	-8,208851	53	Oxfordian	358	36
10	37,16941299	-8,208455	44	Oxfordian	241	21
11	37,16985698	-8,208564	43	Kimmeridgian-Tithonian	351	20
12	37,16578899	-8,203435	64	Quaternary	204	18
13	37,18362702	-8,211252	47	Upper Jurassic	31	20
14	37,21632499	-8,233972	95	Upper Jurassic	194	28
15	37,23163202	-8,206286	105	Lower Jurassic	77	26
16	37,23186596	-8,204005	109	Lower Jurassic	178	23
17	37,24135403	-8,187589	245	Triassic	228	23
18	37,25197096	-8,184177	238	Triassic	176	16
19	37,13605402	-8,255464	97	Oxfordian	209	12
20	37,13630799	-8,247068	108	Oxfordian	232	23
21	37,14182303	-8,251681	101	Oxfordian	187	19
22	37,14191004	-8,251105	102	Oxfordian	196	21
23	37,14804802	-8,217438	126	Lower Jurassic	282	22
24	37,193662	-8,01192	92	Carboniferous	83	55
25	37,23984101	-8,020584	151	Contact Carboniferous-Triassic	140	16
26	37,26569499	-8,291037	76	Carboniferous	33	62
27	37,25284796	-8,287265	155	CVS	218	30
28	37,21025599	-7,991277	182	Carboniferous	50	50
29	37,21025599	-7,991277	182	Triassic	208	23
30	37,19877203	-8,004377	141	Triassic	340	20
31	37,20110597	-7,997323	172	Lower Jurassic	360	33
32	37,19638101	-7,979835	174	Carboniferous	336	35
33	37,19638101	-7,979835	174	Triassic	306	47
34	37,19392603	-7,98146	163	Carboniferous	50	55
35	37,19368103	-7,981976	161	Carboniferous	10	16
36	37,19423398	-7,982774	159	Carboniferous	14	12
37	37,19452098	-7,983532	158	Carboniferous	28	23
38	37,19331902	-7,986147	169	Carboniferous	23	11
39	37,19187104	-7,988042	166	Carboniferous	6	19
40	37,19113	-7,989223	165	Carboniferous	52	35
41	37,18937399	-7,989118	178	Carboniferous	70	28
42	37,18937399	-7,989118	178	Triassic	255	38
43	37,23649797	-8,004419	208	Triassic	117	10

44	37,24142603	-8,097738	299	Lower Jurassic	149	18
45	37,22979798	-8,118037	268	Lower Jurassic	2	19
46	37,22837197	-8,11643	262	Lower Jurassic	130	29
47	37,22253196	-8,106715	215	Lower Jurassic	322	15
48	37,21750701	-8,100242	259	Lower Jurassic	151	20
49	37,19953998	-8,08573	184	Lower Jurassic	173	34
50	37,150144	-8,109844	192	Contact Kimmeridgian-Tithonian	338	21
51	37,14830702	-8,122231	170	Upper Jurassic	151	14
52	37,14920699	-8,124373	154	Upper Jurassic	20	18
53	37,16126201	-8,251196	86	Upper Jurassic	348	70
54	37,16195896	-8,251348	84	Upper Jurassic	358	85
55	37,16523201	-8,248752	77	Lower Cretaceous	13	58
56	37,16276698	-8,247386	78	Upper Jurassic	179	81
57	37,16670203	-8,248476	95	Lower Cretaceous	10	59
58	37,16748498	-8,248511	119	Upper Jurassic	331	48
59	37,16784398	-8,247957	126	Upper Jurassic	215	40
60	37,16803199	-8,248406	130	Upper Jurassic	350	49
61	37,16666004	-8,246886	108	Lower Cretaceous	6	53
62	37,16698299	-8,24605	115	Upper Jurassic	358	31
63	37,164108	-8,236795	92	Lower Cretaceous	351	63
64	37,16837397	-8,23353	132	Lower Jurassic	24	29
65	37,22751098	-8,240673	126	Lower Jurassic	332	28
66	37,25208596	-8,247706	153	Triassic	146	21
67	37,24624202	-8,244851	193	Lower Jurassic	192	22
68	37,24750701	-8,246137	190	Contact Triassic-Lower Jurassic	160	27
69	37,19710998	-8,308561	96	Lower Jurassic	351	24
70	37,25508903	-8,243802	126	Triassic	193	22
71	37,26022798	-8,233355	230	Carboniferous	84	17
72	37,26022798	-8,233355	230	Hettangian	339	35
73	37,26061002	-8,227828	260	Lower Jurassic	109	55
74	37,18320902	-7,965625	162	Lower Jurassic	188	40
75	37,13391102	-8,140772	88	Hettangian	218	28
76	37,13391102	-8,140772	88	CVS	218	14
77	37,133922	-8,14078	87	Kimmeridgian	122	13
78	37,17435203	-7,997558	315	Upper Jurassic	28	25
79	37,17935602	-7,998114	314	Upper Jurassic	208	28
80	37,17391399	-8,000777	329	Oxfordian	321	20
81	37,17552097	-8,002564	356	Upper Jurassic	303	36
82	37,18234601	-7,999406	296	Upper Jurassic	324	21
83	37,18465699	-7,99223	215	Upper Jurassic	251	42
84	37,243377	-8,089803	276	Hettangian	185	34
85	37,24462104	-8,08907	256	Contact Hettangian-CVS	201	30
86	37,246096	-8,087919	249	Triassic	182	30
87	37,24756502	-8,089424	269	Triassic	190	21

88	37,25022501	-8,107833	340	Hettangian	148	22
89	37,25233901	-8,088449	372	Carboniferous	29	38
90	37,25641496	-8,091891	423	Lower Jurassic	330	40
91	37,25275601	-8,086606	377	Carboniferous	28	52
92	37,25263699	-8,08406	364	Carboniferous	52	28
93	37,25194003	-8,082444	352	Carboniferous	26	22
94	37,24877997	-8,083467	283	Carboniferous	10	12
95	37,24655299	-8,081528	247	Triassic	168	34
96	37,15191199	-8,108254	180	Oxfordian	171	28
97	37,17583797	-8,091238	139	Oxfordian	219	17
98	37,176467	8,093839	182	Oxfordian	183	6
99	37,173988	-8,098514	227	Oxfordian	313	28
100	37,17329901	-8,106642	279	Oxfordian	168	27
101	37,18181804	-8,093734	165	Oxfordian	6	61
102	37,186457	-8,100893	127	Oxfordian	209	20
103	37,18583096	-8,100868	138	Oxfordian	245	25
104	37,18318596	-8,101332	157	Oxfordian	58	27
105	37,18742704	-8,110111	119	Lower Jurassic	192	32
106	37,18550599	-8,116316	109	Oxfordian	186	32
107	37,19454696	-8,103299	123	Lower Jurassic	171	34
108	37,25073497	-8,048265	242	Triassic	201	34
109	37,25127501	-8,042379	235	Carboniferous	319	28
110	37,248252	-8,034816	243	Triassic	201	54
111	37,248567	-8,032053	254	Carboniferous	66	40
112	37,23996598	-8,10774	262	Lower Jurassic	358	23
113	37,22955901	-8,166081	198	Lower Jurassic	218	19
114	37,12313198	-8,215742	51	Upper Jurassic	322	9
115	37,12363003	-8,195383	39	Upper Jurassic	257	22
116	37,17632898	-8,079331	114	Kimmeridgian	11	42
117	37,17537696	-8,079183	92	Kimmeridgian	2	37
118	37,16819602	-8,086809	138	Upper Jurassic	208	10
119	37,16768397	-8,086611	140	Upper Jurassic	185	22
120	37,16617296	-8,084941	158	Upper Jurassic	195	23
121	37,16279799	-8,081027	185	Upper Jurassic	192	19
122	37,15982703	-8,073259	160	Upper Jurassic	143	48
123	37,15784504	-8,069982	143	Upper Jurassic	329	52
124	37,170609	-8,058312	147	Upper Jurassic	26	41
125	37,17231003	-8,056715	135	Upper Jurassic	284	70
126	37,19298198	-8,083393	138	Lower Jurassic	134	38
127	37,20576103	-8,124066	282	Lower Jurassic	159	12
128	37,19586996	-8,134843	170	Lower Jurassic	165	35
129	37,16650799	-8,134516	210	Oxfordian?	198	4
130	37,13496102	-8,15151	83	Upper Jurassic	144	25
131	37,23196403	-8,203607	128	Lower Jurassic	92	9
132	37,18710702	-7,97902	213	Hettangian-Lower Jurassic	184	20

133	37,14986597	-8,023524	219	Oxfordian	236	12
134	37,15425901	-8,022483	257	Oxfordian	267	28
135	37,15734699	-8,021138	267	Oxfordian	187	17
136	37,16542999	-8,025536	240	Oxfordian	59	12
137	37,17837903	-8,02213	175	Kimmeridgian	359	33
138	37,19552999	-8,0227	182	Hettangian	210	39
139	37,20792901	-8,028415	258	Lower Jurassic	210	47
140	37,21161	-8,031938	265	Hettangian	194	20
141	37,22917504	-8,039898	191	Lower Jurassic	258	50
142	37,22828798	-8,037312	193	Lower Jurassic	163	23
143	37,22960302	-8,035509	176	Lower Jurassic	164	16
144	37,23210401	-8,023879	208	CVS	278	28
145	37,23337999	-8,018045	186	Hettangian	167	55
146	37,23545501	-8,017572	189	Triassic	210	24
147	37,23641499	-8,017448	200	Carboniferous	72	77
148	37,23641499	-8,017448	200	Hettangian	233	24
149	37,23790504	-8,013837	188	Carboniferous	28	22
150	37,23599598	-8,00891	189	Triassic	206	36
151	37,22829703	-8,004877	218	Triassic	208	37
152	37,22357299	-8,00578	243	Hettangian	194	18
153	37,206144	-7,992396	231	Hettangian	278	21
154	37,19429601	-8,213826	71	Lower Jurassic	208	3
155	37,17628598	-8,197181	101	Oxfordian	226	10
156	37,17395204	-8,191293	123	Oxfordian	316	20
157	37,17403603	-8,189106	131	Oxfordian	119	10
158	37,17417299	-8,186431	137	Oxfordian	57	9
159	37,17557101	-8,180456	123	Oxfordian	228	10
160	37,17682804	-8,175002	100	Oxfordian	286	10
161	37,17859704	-8,195097	72	Oxfordian	240	13
162	37,171845	-8,191296	127	Oxfordian	208	15
163	37,16565899	-8,188726	119	Kimmeridgian	167	28
164	37,16516797	-8,186981	116	Kimmeridgian	132	35
165	37,16037302	-8,185143	102	Kimmeridgian	127	10
166	37,15780397	-8,182195	112	Kimmeridgian	47	19
167	37,15567597	-8,182289	125	Kimmeridgian	242	27
168	37,15302603	-8,181246	146	Kimmeridgian	228	20
169	37,13346996	-8,155671	88	Kimmeridgian	78	34
170	37,15000201	-8,126141	138	Kimmeridgian	312	24
171	37,151611	-8,115763	205	Kimmeridgian	154	29
172	37,15184997	-8,119764	189	Kimmeridgian	175	21
173	37,152014	-8,118333	191	Kimmeridgian	196	20
174	37,14456903	-8,269358	84	Kimmeridgian	309	22
175	37,15098102	-8,272646	68	Kimmeridgian	321	23
176	37,19687001	-8,286261	56	Lower Jurassic	19	12
177	37,23318896	-8,337121	148	Lower Jurassic	21	18

178	37,23172498	-8,347903	159	Quaternary	204	14
179	37,23056199	-8,353623	133	CVS	338	38
180	37,23208004	-8,35413	84	Triassic	175	35
181	37,23400402	-8,355173	66	Triassic	174	43
182	37,235367	-8,35196	70	Triassic	149	28
183	37,23855497	-8,346598	89	Triassic	131	16
184	37,24306896	-8,336543	114	Triassic	162	25
185	37,24335101	-8,333492	135	Hettangian	163	27
186	37,24128102	-8,333074	161	Contact Hettangian-CVS	169	36
187	37,25268401	-8,323299	191	Triassic	147	18
188	37,24877603	-8,329324	197	Triassic	141	15
189	37,24594303	-8,329197	201	Hettangian	130	26
190	37,26069703	-8,319932	149	Hettangian	135	32
191	37,25888897	-8,335583	119	Triassic	166	27
192	37,27219096	-8,312443	104	Carboniferous	331	19
193	37,264878	-8,312666	148	Triassic	254	11
194	37,26980497	-8,235547	165	Carboniferous	25	44
195	37,26812197	-8,23364	161	Triassic	191	25
196	37,178317	-8,221113	78	Hettangian	207	47
197	37,17832304	-8,221123	80	Oxfordian	208	20
198	37,17905704	-8,229357	132	Upper Jurassic	160	22
199	37,17856804	-8,233145	141	Upper Jurassic	164	48
200	37,17445504	-8,243766	159	Upper Jurassic	155	30
201	37,23803597	-8,174778	241	CVS	42	38
202	37,23882303	-8,173414	250	Lower Jurassic	58	13
203	37,24313702	-8,173702	320	Lower Jurassic	64	25
204	37,24735798	-8,172196	331	Hettangian	179	28
205	37,17464598	-7,896803	269	Triassic	213	19
206	37,17596898	-7,894828	267	Carboniferous	60	52
207	37,16105598	-7,899778	296	Oxfordian	137	42
208	37,13991003	-7,891184	184	Oxfordian	183	24
209	37,13534701	-7,89027	151	Oxfordian	150	21
210	37,13079203	-7,874549	161	Upper Jurassic	238	10
211	37,13861796	-7,867974	217	Upper Jurassic	152	26
212	37,13522103	-7,868732	180	Upper Jurassic	159	32
213	37,12664902	-7,894652	147	Oxfordian	46	10
214	37,08390903	-7,871815	128	Upper Jurassic	183	25
215	37,09918002	-7,848568	197	Upper Jurassic	272	46
216	37,10142402	-7,848076	184	Upper Jurassic	245	35
217	37,10532001	-7,846357	219	Oxfordian	353	46
218	37,10368303	-7,832872	309	Oxfordian	2	10
219	37,10124498	-7,826738	350	Oxfordian	7	53
220	37,10053998	-7,828898	365	Oxfordian	195	27
221	37,10980601	-7,858705	251	Oxfordian	259	10
222	37,10523301	-7,874322	213	Oxfordian	77	10

223	37,10046404	-7,883532	154	Oxfordian	4	19
224	37,13640497	-8,394754	85	Lower Cretaceous	278	19
225	37,136093	-8,396865	74	Lower Cretaceous	263	10
226	37,13510703	-8,404709	68	Lower Cretaceous	282	25
227	37,15530398	-8,531541	26	Middle Jurassic	116	47
228	37,17915804	-8,544619	66	Middle Jurassic		
229	37,19274804	-8,605407	28	Middle Jurassic	28	20
230	37,19173802	-8,604869	43	Middle Jurassic	12	36
231	37,19140199	-8,604856	47	Middle Jurassic	28	30
232	37,19125598	-8,604756	47	Contact Middle Jurassic-Hettangian		
233	37,19116696	-8,603745	78	Middle Jurassic		
234	37,19329203	-8,603964	69	Lower Cretaceous	168	14
235	37,19345002	-8,604016	72	Lower Cretaceous	118	33
236	37,19368899	-8,603995	62	Lower Cretaceous	200	22
237	37,19382503	-8,603837	57	Lower Cretaceous	172	40
238	37,19391899	-8,603592	52	Lower Cretaceous	139	51
239	37,19371699	-8,604823	31	Lower Cretaceous	158	33
240	37,16226197	-8,680131	32	Triassic	137	21
241	37,163936	-8,706228	74	Lower Jurassic	6	45
242	37,16448703	-8,706317	67	Lower Jurassic	156	48
243	37,16112697	-8,709752	62	Lower Jurassic	162	30
244	37,10327399	-8,723114	48	Lower Cretaceous	242	10
245	37,10463102	-8,719158	50	Lower Cretaceous	132	41
246	37,10095899	-8,741444	16	Lower Jurassic	334	33
247	37,10147498	-8,743335	45	Lower Jurassic	345	72
248	37,10134598	-8,742618	54	Lower Jurassic	344	68
249	37,11965198	-8,756011	62	Lower Jurassic		
250	37,11707002	-8,754479	65	Lower Jurassic	68	36
251	37,113544	-8,756091	50	Lower Jurassic	125	82
252	37,11341701	-8,759042	35	Lower Jurassic	152	37
253	37,15087197	-8,740685	40	Hettangian	146	30
254	37,15069897	-8,740699	50	Hettangian	168	12
255	37,14979598	-8,741912	74	Lower Jurassic	144	44
256	37,15144001	-8,733754	56	Lower Jurassic	133	47
257	37,15904399	-8,717901	31	Lower Jurassic	23	18
258	37,16251904	-8,711052	36	Triassic	144	38
259	37,16323402	-8,709909	41	Carboniferous	37	70
260	37,13825997	-8,781341	95	Carboniferous	104	11
261	37,09283299	-8,803103	59	Middle Jurassic	272	67
262	37,09198801	-8,789871	42	Middle Jurassic	112	34
263	37,08799697	-8,756754	84	Middle Jurassic	320	38
264	37,10677503	-8,70735	63	Lower Cretaceous	180	26
265	37,09263098	-8,725486	30	Lower Cretaceous	147	9
266	37,08668503	-8,723166	2	Lower Cretaceous	107	6

267	37,08606896	-8,720192	0	Lower Cretaceous	160	4
268	37,08565498	-8,718889	1	Lower Cretaceous	114	8
269	37,08550402	-8,717522	1	Lower Cretaceous	95	14
270	37,085947	-8,728492	2	Lower Cretaceous	136	10
271	37,08532196	-8,729282	2	Lower Cretaceous	104	7
272	37,084681	-8,730327	3	Lower Cretaceous	140	5
273	37,085644	-8,689643	3	Lower Cretaceous	71	41
274	37,08556898	-8,690497	3	Lower Cretaceous	91	26
275	37,085587	-8,691365	3	Lower Cretaceous	105	14
276	37,08521099	-8,693718	5	Lower Cretaceous	105	4
277	37,08500898	-8,695227	4	Lower Cretaceous	106	5
278	37,08487202	-8,696946	6	Lower Cretaceous	125	3
279	37,08431798	-8,700309	5	Lower Cretaceous	117	4
280	37,08428998	-8,702028	9	Lower Cretaceous	120	9
281	37,08524996	-8,685114	9	Lower Cretaceous	113	9
282	37,084595	-8,68278	9	Lower Cretaceous	85	8
283	37,08458	-8,732757	13	Lower Cretaceous	133	7
284	37,08371297	-8,735112	17	Lower Cretaceous	149	13
285	37,07175401	-8,773115	18	Lower Cretaceous	203	14
286	37,07191402	-8,771497	34	Lower Cretaceous	163	22
287	37,07753903	-8,751112	58	Lower Cretaceous	178	11
288	37,08562396	-8,778952	20	Lower Cretaceous	350	16
289	37,08284101	-8,817781	40	Hettangian	174	18
290	37,08222804	-8,820039	16	CVS		
291	37,08339798	-8,820934	17	Hettangian	47	32
292	37,08460297	-8,821224	29	Hettangian	6	29
293	37,06586497	-8,81027	13	Lower Cretaceous	78	12
294	37,06734002	-8,808074	14	Lower Cretaceous	50	22
295	37,06674599	-8,807681	11	Lower Cretaceous	359	19
296	37,06620201	-8,807736	18	Lower Cretaceous	14	23
297	37,08163996	-8,832267	34	Triassic	166	18
298	37,07557599	-8,83149	41	Middle Jurassic	309	21
299	37,07381797	-8,829881	32	Upper Jurassic	215	18
300	37,07224896	-8,828705	25	Upper Jurassic	343	21
301	37,071608	-8,827452	18	Upper Jurassic	326	31
302	37,06628901	-8,824084	18	Lower Cretaceous	270	12
303	37,06555702	-8,821048	9	Lower Cretaceous	142	40
304	37,065784	-8,819739	10	Lower Cretaceous	120	33
305	37,06571099	-8,818964	11	Lower Cretaceous		
306	37,06585198	-8,818009	9	Lower Cretaceous	122	28
307	37,06600796	-8,817366	10	Lower Cretaceous	115	18
308	37,06603303	-8,81674	9	Lower Cretaceous	113	12
309	37,06603303	-8,816497	7	Lower Cretaceous	329	14
310	37,06566699	-8,81473	7	Lower Cretaceous	209	16
311	37,06518897	-8,813867	7	Upper Jurassic	134	23

312	37,06489996	-8,825854	7	Lower Cretaceous	280	24
313	37,06426604	-8,826978	19	Lower Cretaceous	298	13
314	37,06372096	-8,828169	20	Lower Cretaceous	1	22
315	37,06383697	-8,827716	18	Lower Cretaceous	333	10
316	37,06837803	-8,823228	56	Upper Jurassic	23	7
317	37,06987596	-8,817205	79	Lower Cretaceous	240	22
318	37,07364002	-8,808876	21	Upper Jurassic	147	17
319	37,06678002	-8,803007	71	Upper Jurassic	311	18
320	37,06764202	-8,805612	82	Upper Cretaceous Basalt	120	16
321	37,06867701	-8,805953	80	Upper Jurassic	335	20
322	37,06767303	-8,796158	25	Upper Jurassic	173	21
323	37,06592004	-8,795841	6	Lower Cretaceous	152	15
324	37,04660696	-8,878423	7	Upper Jurassic	230	15
325	37,04542	-8,877785	2	Upper Jurassic	181	23
326	37,04530198	-8,876777	10	Upper Jurassic	125	23
327	37,04469304	-8,875017	14	Upper Jurassic	129	20
328	37,04489202	-8,873847	14	Upper Jurassic	193	16
329	37,04544296	-8,876098	22	Fault	313	77
330	37,04426296	-8,880288	10	Upper Jurassic	207	11
331	37,04667703	-8,871348	11	Upper Jurassic	179	20
332	37,06019503	-8,873644	28	Upper Jurassic	313	60
333	37,06614501	-8,85528	37	Triassic	255	21
334	37,06512602	-8,854667	42	Hettangian	119	34
335	37,064289	-8,855324	32	CVS	179	28
336	37,05747896	-8,854873	14	Middle Jurassic	229	20
337	37,05456499	-8,855388	12	Upper Jurassic	126	11
338	37,07067903	-8,851313	47	Upper Jurassic	156	26
339	37,070674	-8,851317	46	Triassic	140	20
340	37,07333098	-8,846722	35	Triassic	162	10
341	37,06368098	-8,841209	23	Upper Jurassic	153	44
342	37,06097899	-8,83899	16	Upper Jurassic	122	9
343	37,06098796	-8,838953	16	Lower Cretaceous	116	36
344	37,06106599	-8,837512	17	Lower Cretaceous	152	13
345	37,06078503	-8,840399	13	Upper Jurassic	237	16
346	37,06025404	-8,841316	10	Upper Jurassic	140	25
347	37,05887002	-8,886979	59	Middle Jurassic	329	16
348	37,04196104	-8,892615	25	Upper Jurassic	261	18
349	37,04219498	-8,893164	10	Upper Jurassic	290	27
350	37,04043997	-8,895124	10	Upper Jurassic	263	30
351	37,04390799	-8,895827	30	Upper Jurassic	249	10
352	37,04519402	-8,893298	40	Upper Jurassic	344	13
353	37,06980497	-8,893254	49	CVS	173	32
354	37,06762198	-8,892948	48	Lower Jurassic	103	34
355	37,06051103	-8,894875	32	Lower Jurassic	125	48
356	37,05389796	-8,897429	30	Lower Jurassic	113	45

357	37,04908398	-8,898125	12	Lower Jurassic	140	37
358	37,04809802	-8,896761	10	Middle Jurassic	170	13
359	37,08246399	-8,899993	80	Triassic	207	7
360	37,02373702	-8,93781	31	Upper Jurassic	148	24
361	37,02933697	-8,936267	41	Upper Jurassic	156	36
362	37,03064396	-8,93582	46	Upper Jurassic	155	9
363	37,039768	-8,932085	52	Upper Jurassic	180	25
364	37,053128	-8,924699	60	Middle Jurassic	52	22
365	37,06082803	-8,923088	71	Middle Jurassic	330	20
366	37,07457997	-8,917299	97	Lower Jurassic	299	26
367	37,07726402	-8,917453	105	Triassic	192	17
368	37,073751	-8,912875	88	Lower Jurassic	359	30
369	37,06974001	-8,91274	86	Lower Jurassic	149	39
370	37,06798199	-8,918844	75	Middle Jurassic	211	25
371	37,06242898	-8,940435	105	Lower Jurassic	181	32
372	37,06500004	-8,940996	94	Hettangian	142	36
373	37,07277903	-8,935327	95	Hettangian	178	22
374	37,072068	-8,934223	91	Hettangian	120	12
375	37,07339401	-8,927376	107	Quaternary	336	8
376	37,06640803	-8,928517	85	Lower Jurassic	172	14
377	37,06737497	-8,929632	86	CVS	141	30
378	37,02140903	-8,921772	27	Upper Jurassic	224	7
379	37,02183802	-8,920961	5	Upper Jurassic	174	13
380	37,02296002	-8,920022	20	Upper Jurassic	175	11
381	37,00424801	-8,947432	9	Upper Jurassic	179	16
382	37,00557402	-8,934673	14	Middle Jurassic	114	21
383	37,004981	-8,941403	18	Middle Jurassic	118	12
384	37,01458097	-8,95341	43	Middle Jurassic	50	9
385	37,02512003	-8,963122	10	Middle Jurassic	187	22
386	37,025963	-8,964643	10	Upper Jurassic	147	16
387	37,023259	-8,994914	76	Upper Jurassic	68	14
388	37,02240396	-8,993986	58	Upper Jurassic	164	13
389	37,02116503	-8,992266	51	Upper Jurassic	134	13
390	37,04632298	-8,978521	26	Hettangian	281	10
391	37,075089	-8,884536	114	Hettangian	162	30
392	37,08354098	-8,918726	95	Hettangian	181	16
393	37,05511602	-8,971691	84	Hettangian	155	42
394	37,05402402	-8,973116	77	Hettangian	161	42
395	37,02884302	-8,98721	69	Fault		
396	37,03006301	-8,987207	10	Lower Jurassic	44	29
397	37,03056199	-8,988268	26	Lower Jurassic	45	21
398	37,04894702	-8,983416	64	Triassic	254	20

APPENDIX 3

Well data

Well Name	X (WGS84)	Y (WGS84)	TD	Neogene-Quaternary thickness	Neogene-Quaternary lithology	Paleogene thickness	Top Paleogene	Paleogene lithology	AUGC/AWGC thickness	Top AUGC/AWGC	AUGC/AWGC lithology	Upper Cretaceous thickness	Top Upper Cretaceous	Upper Cretaceous lithology	Lower Cretaceous thickness	Top Lower Cretaceous	Lower Cretaceous lithology	Upper Jurassic thickness	Top Upper Jurassic	Upper Jurassic lithology	Middle Jurassic thickness	Top Middle Jurassic	Middle Jurassic lithology	Lower Jurassic thickness	Top Lower Jurassic	Lower Jurassic lithology	Hettangian thickness	Top Hettangian	Hettangian lithology	Triassic lithology	Triassic lithology	Triassic lithology	Top Paleozoic	Paleozoic lithology
ALGARVE-1	-7,566533	36,901261	-3597	811	-536	lime	-991	lime	0			0			946	-1346	sand	555	-2295	lime	>735	2862	lime											
ALGARVE-2	-7,515603	36,809642	-2242	1687	-540	clay	>675	-1560	sand																									
ALMONTE-1	-6,472194	37,263889	-1345	701	80	clay	0			0			0			0		0			0			112	-621	lime	414	-733	lime	0			-1184	slate
ASPERILLO-1	-6,647469	37,078575	-3310	1232	46	clay	0			0			0			353	-1182	lime	109	-1539	dolo	766	-1648	dolo	>847	-2414	salt							
ATLANTIDA-2	-7,187081	36,989203	-2610	2067	-78	clay	170	-1975	clay	0			360	-2145	clay	>105	-2505	dolo																
ATLANTIDA 2-2	-7,198961	36,990308	-1505	>1411	-79	clay																												
ATLANTIDA-3	-7,085922	36,842422	-2115	>1962	-139	clay																												
BAEZA-1	-3,542944	37,982194	-410	365	542	marls	0			0			0			0		0			0			0			>45	177	marls					
BAEZA-2	-3,542944	37,982194	-640	530	542	marls	0			0			0			0		0			0			0			>110	11	marls					
BAILEN-1	-3,745556	38,051028	-458	298	277	marls	0			0			0			0		0			0			0			17	-42	marls				-145	slate
BETICA 14 -1	-6,136817	37,022378	-3507	>273	3	marls	0			2623	-592	clay	0			>18	-3486	lime																
BETICA 18-1	-6,000850	36,779711	-4348	146	84	clay	0			0			491	-1557	clay	981	-2071	sil	387	-3035	lime	579	3439	lime	0			618	-3608	anhy	0			-4256	basic rock
BORNOS 1	-5,758333	36,683333	-3030	533	268	lime	0			0			0			0		0			0			0			>2497	-265	salt					
CARMONA-1	-5,701625	37,522725	-792	>792	93	marls																												
CARMONA-2	-5,614125	37,526342	-583	547	90	clay	0			0			0			0		0			0			0			0			0			-483	porphyry
CARMONA-3	-5,619128	37,482450	-908	675	93	clay	0			228	-582	clay	0			0		0			0			0			0			0			-810	porphyry
CARMONA-4	-5,598017	37,443283	-1232	424	93	clay	0			806	-307	clay	0			0		0			0			0			0			0			-1137	gneiss
CARMONA-5	-5,544939	37,411556	-1575	22	76	clay	0			1549	-54	clay	0			0		0			0			0			0			0			-1495	gneiss
CARMONA-6	-5,493306	37,374972	-1846	60	93	marls	0			1846	0	clay				0		0			0			0			0			0				
CASA NIEVES-1	-6,236106	37,193017	-1630	119	5	marls	0			0			0			0		0			0			0			0			0			-1615	schists
CASTILLEJA DE LA CUESTA-1	-6,061908	37,383847	-937	922	108	marls	0			0			0			0		0			0			0			0			0			-820	clay
CORDOBA A-1	-5,412150	37,533756	-1015	982	160	clay	0			0			0			0		0			0			0			0			0			-818	slate
CORDOBA A-2	-5,370497	37,579811	-707	690	147	clay	0			0			0			0		0			0			0			0			0			-539	granite
CORDOBA A-3	-5,449028	37,584297	-660	645	84	clay	0			0			0			0		0			0			0			0			0			-576	schist
CORDOBA A-5	-5,443922	37,571122	-794	794	102	clay																												
CORVINA-1	-7,786333	36,924944	-3083	780	-198	marls	240	-971	lime	0			0			680	-1195	sand	458	-1837	lime	>788	2295	lime										
ECIJA-1	-5,081625	37,572169	-354	>354	98	marls																												
ECIJA-2	-5,084111	37,571997	-1547	340	100	clay	0			1202	-219	clay	0			0		0			0			0			0			0			-1447	slate
ECIJA-3	-5,127736	37,626892	-994	993	85	clay	0			0			0			0		0			0			0			0			0			-908	gneiss
EL CIERVO-1	-5,825394	37,461275	-748	>748	54	sand																												
FUENSANTA DE MARTOS 1	-3,880222	37,670778	-1800	0			0			0			0			250	1060	lime	433	806	lime	215	-373	lime	>582	-424	lime							
GOLFO DE CADIZ 6-X-1	-7,209072	36,833883	-1800	1262	-339	clay	138	-1463	clay	0			>185	-1601	clay																			
GOLFO DE CADIZ 6Y-1BIS	-7,060742	36,706447	-3520	752	-452	clay	0			0			0			0			0			1222	-1204	lime	>445	-2426	lime	40	-3116	anhy	0			-3156	clay
GOLFO DE CADIZ B-1	-7,120931	36,980339	-4298	2685	-79	clay	1384	-1380	lime	0			371	-2764	clay	268	-3135	clay	498	-3403	dolo	300	-3902	silt	0			>96	-4202	salt					
GOLFO DE CADIZ B-2	-7,084092	36,939836	-2962	2862	-92	clay	1013	-1945	lime	0			>4	-2958	clay																			
GOLFO DE CADIZ B-3	-7,091261	36,850919	-2203	1303	-128	clay	0			0			0			>353	-1710	clay																
GOLFO DE CADIZ B-4	-7,089308	36,957878	-1980	>1896	-84	clay	>105	-1875	lime																									

GOLFO DE CADIZ B-5	-7,122278	36,986172	-2047	1906	-69	clay	493	-1482	lime	0			0			>72	-1975	clay																		
GOLFO DE CADIZ B-6	-7,078353	36,833883	-2491	>2367	-124	clay	0			0			>115	-2251	mud																					
GOLFO DE CADIZ C-1	-7,033433	36,826228	-2763	1594	-127	clay	0			0			0			0			0			0			0			>1042	-1721	anhy						
GOLFO DE CADIZ C-2	-7,048783	36,953908	-1979	>1877	-78	clay	>109	-1870	lime																											
GOLFO DE CADIZ C-3	-7,036553	36,872036	-2893	>2785	-108	clay	>213	-2680	clay																											
GOLFO DE CADIZ C-4	-7,032194	36,970889	-1863	>1784	-65	sand	>63	-1786	lime																											
GOLFO DE CADIZ D-1	-6,903569	36,969700	-4130	1953	-46	clay	0			0			405	-1999	clay	79	-2404	clay	>953	-2483	lime														
GOLFO DE CADIZ D-2	-6,891139	36,977056	-2737	2222	-43	clay	>202	-2062	lime	0			>472	-2265	clay	7	-2301	clay	>429	-2308															
GOLFO DE CADIZ D-3	-6,904933	36,883844	-1939	1867	-72	clay																													
GOLFO DE CADIZ D-4	-6,912183	36,886172	-2025	1976	-72	clay	0			>35	-1976	clay																							
GOLFO DE CADIZ E-1	-6,848706	36,688942	-1985	>1884	-101	clay	>140	-1845	clay	0																									
GOLFO DE CADIZ G-1	-6,662256	36,641481	-1591	975	-64	clay	0			>553	-975	clay																							
HUELVA-1	-6,783022	37,178306	-1431	662	56	clay	0			0			0			0			45	-603	dolo	343	648	dolo	>383	991	dolo								
IMPERADOR 1	-8,398278	36,786306	-2639	572	-370	clay	0			0			0			567	-943	dolo	>1107	1507	dolo	>1107	>1107	lime											
ISLA MAYOR 1	-6,147189	37,160517	-2373	1175	3	clay	0			1020	-673	clay	0			0			0			0			0			0			0			-2192	slate
MARISMAS A-1	-6,572581	37,091711	-1379	1357	15?	clay	0			0			0			0			>22	-1342	lime													
MARISMAS C-1	-6,188342	37,311272	-1136	1090	51	clay	0			0			0			0			0			0			0			0			0			-1039	slate
MEDINA SIDONIA-1	-5,916928	36,374964	-184	184	62	clay																													
MOGUER-1	-6,801072	37,157189	-2473	713	50	clay	0			0			0			0			80	-663	dolo	383	-743	dolo	728	-1126	dolo	434	-1854	anhy	46	-2288	sand	-2400	shale
NEPTUNO-1	-6,606936	36,461597	-1952	1575	-80	clay	0			0			>272	-1655	clay																				
NEPTUNO-2	-6,439286	36,479136	-2050	>1985	-51	clay																													
NUEVA CARTEYA-1	-4,393556	37,599111	-3750	40	445	clay	0			0			0			815	410	clay																	
Orion 2-1	-7,236278	36,858583	-1522	1040	-288	clay	0			0			0			0			0			0			0			>194	-1328	salt					
PALANCARES-1	-6,208611	37,320278	-1053	1028	74	clay	0			0			0			0			0			0			0			0						-947	slate
PUERTO DE OJEN-1	-5,632486	36,156081	-1751	0			>1751	105	clay																										
RIO GUADALQUIVIR N-1	-4,811389	37,738489	-998	968	255	clay	0			0			0			0			0			0			0			0						-709	igneus rock
RUIVO-1	-8,191278	36,886272	-2249	876	-91	sand	217	-750	lime	0			0			181	-967	sand	0			852	1148	lime	0			>224	-2025	anhy					
SALTERAS-1	-6,102461	37,417456	-665	644	160	marls	0			0			0			0			0			0			0			0						-497	schists
SAPO-1	-6,208583	37,064722	-971	835	3	clay	0			>136	-832	clay																							
TARIFA-1	-5,653039	36,127764	-3023	0			0						>3023	220	marls																				
TARIFA-2	-5,644711	36,130533	-1171	>1171	132	marls	600	-500	marls																										
VILLALBA DEL ALCOR-1	-6,490506	37,451069	-210	200	142	clay	0			0			0			0			0			0			0			0						58	slate
VILLAMANRIQUE-1	-6,308583	37,233889	-1341	1196	18	clay	0			0			0			0			0			0			0			121	-1178	clay	0			-1296	schists
VILLANUEVA DE LA REINA-1	-3,843583	37,985417	-322	230	354	marls	0			0			0			0			0			0			0			0			64	124	marls	60	slate

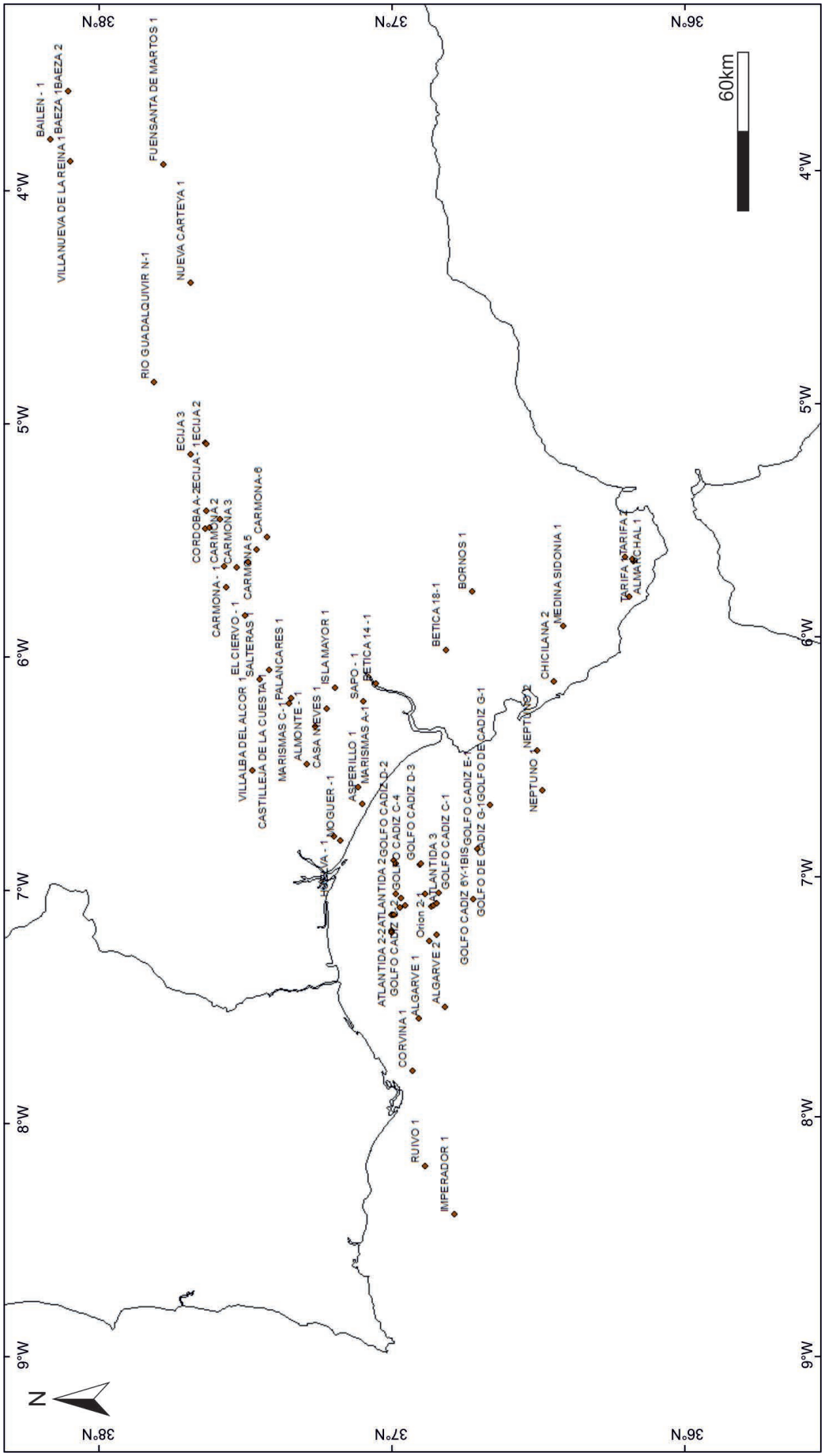
38°N
37°N
36°N
4°W
5°W
6°W
7°W
8°W
9°W
60km
N
BAILEN - 1
BAEZA 1
BAEZA 2
VILLANUEVA DE LA REINA 1
FUENSANTA DE MARTOS 1
NUEVA CARTEYA 1
RIO GUADALQUIVIR N-1
ECIJA 3
ECIJA 1
ECIJA 2
CORDOBA A-2
CARMONA 1
CARMONA 2
CARMONA 3
CARMONA 5
CARMONA-6
EL CIERVO - 1
SALTERAS
PALANCARES 1
VILLALBA DEL ALCOR 1
CASTILLEJA DE LA CUESTA
MARISMAS C-1
ALMONTE - 1
CASA NIEVES 1
ISLA MAYOR 1
SAPO - 1
BETICA 14 -1
MARISMAS A-1
ASPERILLO 1
MOGUER -1
HUELVA - 1
ATLANTIDA 2-2
GOLFO CADIZ C-2
GOLFO CADIZ C-4
GOLFO CADIZ D-2
GOLFO CADIZ D-3
ATLANTIDA 2
ATLANTIDA 3
Orion 2-1
GOLFO CADIZ C-1
ALGARVE 1
ALGARVE 2
CORVINA 1
RUIVO 1
IMPERADOR 1
GOLFO CADIZ 6Y-1BIS
GOLFO CADIZ E-1
GOLFO DE CADIZ G-1
GOLFO DE CADIZ DE
BETICA 18-1
BORNOS 1
NEPTUNO 1
NEPTUNO 2
CHICLANA 2
MEDINA SIDONIA 1
TARIFA
ALMARCHAL 1

Map 2.1. Location map of the wells present in the SW Iberian margin.

APPENDIX 4

Gegological map of the Algarve Basin